NEW APPROACHES TO STUDY CILIOPATHIES AND CENTRIOLES-RELATED GENETIC DISORDERS

EDITED BY: Carlo Iomini, Sonia Mulero Navarro and Jose Maria Carvajal-Gonzalez

PUBLISHED IN: Frontiers in Genetics

frontiers Research Topics

frontiers

ISSN 1664-8714
ISBN 978-2-88966-140-4
DOI 10.3389/978-2-88966-140-4

About Frontiers

Frontiers is more than just an open-access publisher of scholarly articles: it is a pioneering approach to the world of academia, radically improving the way scholarly research is managed. The grand vision of Frontiers is a world where all people have an equal opportunity to seek, share and generate knowledge. Frontiers provides immediate and permanent online open access to all its publications, but this alone is not enough to realize our grand goals.

Frontiers Journal Series

The Frontiers Journal Series is a multi-tier and interdisciplinary set of open-access, online journals, promising a paradigm shift from the current review, selection and dissemination processes in academic publishing. All Frontiers journals are driven by researchers for researchers; therefore, they constitute a service to the scholarly community. At the same time, the Frontiers Journal Series operates on a revolutionary invention, the tiered publishing system, initially addressing specific communities of scholars, and gradually climbing up to broader public understanding, thus serving the interests of the lay society, too.

Dedication to Quality

Each Frontiers article is a landmark of the highest quality, thanks to genuinely collaborative interactions between authors and review editors, who include some of the world's best academicians. Research must be certified by peers before entering a stream of knowledge that may eventually reach the public - and shape society; therefore, Frontiers only applies the most rigorous and unbiased reviews.
Frontiers revolutionizes research publishing by freely delivering the most outstanding research, evaluated with no bias from both the academic and social point of view. By applying the most advanced information technologies, Frontiers is catapulting scholarly publishing into a new generation.

What are Frontiers Research Topics?

Frontiers Research Topics are very popular trademarks of the Frontiers Journals Series: they are collections of at least ten articles, all centered on a particular subject. With their unique mix of varied contributions from Original Research to Review Articles, Frontiers Research Topics unify the most influential researchers, the latest key findings and historical advances in a hot research area! Find out more on how to host your own Frontiers Research Topic or contribute to one as an author by contacting the Frontiers Editorial Office: researchtopics@frontiersin.org

NEW APPROACHES TO STUDY CILIOPATHIES AND CENTRIOLES-RELATED GENETIC DISORDERS

Topic Editors:
Carlo Iomini, Wilmer Eye Institute, Johns Hopkins Medicine, United States
Sonia Mulero Navarro, University of Extremadura, Spain
Jose Maria Carvajal-Gonzalez, University of Extremadura, Spain

Citation: Iomini, C., Navarro, S. M., Carvajal-Gonzalez, J. M., eds. (2020). New Approaches to Study Ciliopathies and Centrioles-Related Genetic Disorders. Lausanne: Frontiers Media SA. doi: 10.3389/978-2-88966-140-4

Table of Contents

04 ***Survey of the Ciliary Motility Machinery of* Drosophila *Sperm and Ciliated Mechanosensory Neurons Reveals Unexpected Cell-Type Specific Variations: A Model for Motile Ciliopathies***
Petra zur Lage, Fay G. Newton and Andrew P. Jarman

24 ***Microscopy-Based Automated Live Cell Screening for Small Molecules That Affect Ciliation***
Peishan Zhang, Anna A. Kiseleva, Vladislav Korobeynikov, Hanqing Liu, Margret B. Einarson and Erica A. Golemis

39 ***Identification of Important Effector Proteins in the FOXJ1 Transcriptional Network Associated With Ciliogenesis and Ciliary Function***
Ishita Mukherjee, Sudipto Roy and Saikat Chakrabarti

55 ***Synchronizing Protein Traffic to the Primary Cilium***
Wladislaw Stroukov, Axel Rösch, Carsten Schwan, Abris Jeney, Winfried Römer and Roland Thuenauer

65 ***Opportunities and Challenges for Molecular Understanding of Ciliopathies–The 100,000 Genomes Project***
Gabrielle Wheway, Genomics England Research Consortium and Hannah M. Mitchison

86 ***Corrigendum: Opportunities and Challenges for Molecular Understanding of Ciliopathies–The 100,000 Genomes Project***
Gabrielle Wheway, Genomics England Research Consortium and Hannah M. Mitchison

88 ***The* Trp73 *Mutant Mice: A Ciliopathy Model That Uncouples Ciliogenesis From Planar Cell Polarity***
Margarita M. Marques, Javier Villoch-Fernandez, Laura Maeso-Alonso, Sandra Fuertes-Alvarez and Maria C. Marin

97 ***A Combined* in silico, in vitro *and Clinical Approach to Characterize Novel Pathogenic Missense Variants in PRPF31 in Retinitis Pigmentosa***
Gabrielle Wheway, Liliya Nazlamova, Nervine Meshad, Samantha Hunt, Nicola Jackson and Amanda Churchill

114 ***661W Photoreceptor Cell Line as a Cell Model for Studying Retinal Ciliopathies***
Gabrielle Wheway, Liliya Nazlamova, Dann Turner and Stephen Cross

128 ***Structural but not Functional Alterations in Cones in the Absence of the Retinal Disease Protein Retinitis Pigmentosa 2 (RP2) in a Cone-Only Retina***
Linjing Li, Kollu N. Rao and Hemant Khanna

135 ***Diminished Expression of Fat and Dachsous PCP Proteins Impaired Centriole Planar Polarization in Drosophila***
Sergio Garrido-Jimenez, Angel-Carlos Roman and Jose Maria Carvajal-Gonzalez

141 ***An Integrated Analysis of Radial Spoke Head and Outer Dynein Arm Protein Defects and Ciliogenesis Abnormality in Nasal Polyps***
Xiao-xue Zi, Wei-jie Guan, Yang Peng, Kai Sen Tan, Jing Liu, Ting-ting He, Yew-kwang Ong, Mark Thong, Li Shi and De-yun Wang

frontiers in Genetics

ORIGINAL RESEARCH
published: 01 February 2019
doi: 10.3389/fgene.2019.00024

Survey of the Ciliary Motility Machinery of *Drosophila* Sperm and Ciliated Mechanosensory Neurons Reveals Unexpected Cell-Type Specific Variations: A Model for Motile Ciliopathies

*Petra zur Lage, Fay G. Newton and Andrew P. Jarman**

Centre for Discovery Brain Sciences, Edinburgh Medical School, University of Edinburgh, Edinburgh, United Kingdom

OPEN ACCESS

Edited by:
Carlo Iomini, Icahn School of Medicine at Mount Sinai, United States

Reviewed by:
Colin Anfimov Johnson, University of Leeds, United Kingdom
Marek Mlodzik, Icahn School of Medicine at Mount Sinai, United States
Sunayna Best contributed to the review of Colin Anfimov Johnson

***Correspondence:**
Andrew P. Jarman
andrew.jarman@ed.ac.uk

Specialty section:
This article was submitted to Genetic Disorders, a section of the journal Frontiers in Genetics

Received: *22 June 2018*
Accepted: *15 January 2019*
Published: *01 February 2019*

Citation:
zur Lage P, Newton FG and Jarman AP (2019) Survey of the Ciliary Motility Machinery of Drosophila Sperm and Ciliated Mechanosensory Neurons Reveals Unexpected Cell-Type Specific Variations: A Model for Motile Ciliopathies. Front. Genet. 10:24. doi: 10.3389/fgene.2019.00024

The motile cilium/flagellum is an ancient eukaryotic organelle. The molecular machinery of ciliary motility comprises a variety of cilium-specific dynein motor complexes along with other complexes that regulate their activity. Assembling the motors requires the function of dedicated "assembly factors" and transport processes. In humans, mutation of any one of at least 40 different genes encoding components of the motility apparatus causes Primary Ciliary Dyskinesia (PCD), a disease of defective ciliary motility. Recently, *Drosophila* has emerged as a model for motile cilia biology and motile ciliopathies. This is somewhat surprising as most *Drosophila* cells lack cilia, and motile cilia are confined to just two specialized cell types: the sperm flagellum with a 9+2 axoneme and the ciliated dendrite of auditory/proprioceptive (chordotonal, Ch) neurons with a 9+0 axoneme. To determine the utility of *Drosophila* as a model for motile cilia, we survey the *Drosophila* genome for ciliary motility gene homologs, and assess their expression and function. We find that the molecules of cilium motility are well conserved in *Drosophila*. Most are readily characterized by their restricted cell-type specific expression patterns and phenotypes. There are also striking differences between the two motile ciliated cell types. Notably, sperm and Ch neuron cilia express and require entirely different outer dynein arm variants—the first time this has been clearly established in any organism. These differences might reflect the specialized functions for motility in the two cilium types. Moreover, the Ch neuron cilia lack the critical two-headed inner arm dynein (I1/f) but surprisingly retain key regulatory proteins previously associated with it. This may have implications for other motile 9+0 cilia, including vertebrate embryonic nodal cilia required for left-right axis asymmetry. We discuss the possibility that cell-type specificity in ciliary motility machinery might occur in humans, and therefore underlie some of the phenotypic variation observed in PCD caused by different gene mutations. Our work

lays the foundation for the increasing use of *Drosophila* as an excellent model for new motile ciliary gene discovery and validation, for understanding motile cilium function and assembly, as well as understanding the nature of genetic defects underlying human motile ciliopathies.

Keywords: cilium, flagellum, *Drosophila*, ciliopathy, dynein

INTRODUCTION

Motile cilia play important developmental and physiological roles concerned with the movement of fluid (e.g., airway cilia in mucociliary clearance, embryonic nodal cilia in left-right asymmetry determination) or movement through fluid (e.g., the sperm flagellum). Although many types of cilia are immotile and play a sensory role, the ancestral cilium is thought to have been motile, and the molecular machinery of ciliary motility is highly conserved. As such, a range of model organisms have been able to contribute much to our knowledge of motile cilia, from mammals to unicellular eukaryotes such as the biflagellate green alga, *Chlamydomonas reinhardtii* (King, 2016). From numerous studies over many years the structure and function of the motility apparatus is known in great detail, yet it is also bewilderingly complex with much remaining to be understood. In humans, the inherited disease, Primary Ciliary Dyskinesia (PCD) is caused by mutations in around 40 different genes encoding components of the motility apparatus. PCD is characterized by reduction or loss of ciliary motility, leading to defects in mucociliary clearance, organ left-right asymmetry, and male and female fertility (Mitchison and Valente, 2017). There is a continuing need to discover and validate new genes that may cause PCD when defective, as well as a need to understand the cellular and molecular functions of these genes. Model organisms can play a key role in advancing both these goals.

The motors of ciliary movement are the outer and inner dynein arms (ODA, IDA, see **Table 1** for abbreviations) that decorate the A tubules of the axonemal microtubule doublets (**Figure 1A**). These large multi-subunit complexes exist in several subtypes defined largely by their heavy chain (HC) constituents, which are likely required for different aspects of beat strength, frequency, and waveform (King, 2016). *Chlamydomonas* studies have shown that dynein activity is coordinated and modulated by several large "regulatory hub" complexes (Mitchell, 2017; Viswanadha et al., 2017; Porter, 2018), including: (a) the nexin–dynein regulatory complex (N-DRC), which both connects adjacent doublets and transmits information on interdoublet sliding (Bower et al., 2013); (b) the central pair-radial spoke (CP/RS) complex, which may transmit information between doublets to coordinate motor activity during bending to one side of axoneme only (Oda et al., 2014b); (c) the base of IDA subtype I1/f with the modifier of inner arms (MIA) complex, which may interface between the motors and the N-DRC/RS (Yamamoto et al., 2013). Several proteins are required for attachment (or docking) of these complexes along the axonemal microtubules in the correct periodicity. These include outer arm docking complex (ODA-DC) proteins and the "96 nm molecular ruler" proteins that guide spacing and attachment of IDA, RS, and N-DRC (Oda et al., 2014a). Tektins may also be required for IDA docking/attachment in addition to microtubule stability (Amos, 2008). As far as is known, the large variety of motile cilia in different organisms largely share this machinery, with the notable exception that some lack the CP/RS complexes, thereby having a 9+0 axonemal microtubule structure rather than 9+2. The most notable example of this exception is the nodal cilia of the vertebrate embryonic node that are required for left-right axis asymmetry.

Construction of the motility machinery during ciliogenesis is itself an intricate process requiring specialized pathways of protein assembly and transport. The various motility complexes appear to be pre-assembled in the cytoplasm before being transported into the cilium as whole complexes (Fok et al., 1994; Fowkes and Mitchell, 1998; Viswanadha et al., 2014). The process is best known for ODA/IDA for which assembly requires a set of at least 11 dedicated proteins known as dynein assembly factors (DNAAFs) (Mitchison and Valente, 2017). At the base of the cilium, pre-assembled complexes are transported into the cilium by intraflagellar transport (IFT), requiring a specialized set of kinesin and dynein motors along with adaptor proteins.

Ecdysozoans such as nematodes and insects have lost cilia from almost all cells, with the remaining ciliated cell types having specialized roles. Similarly to *C. elegans*, the only somatic cells bearing cilia in *Drosophila* are the Type I sensory neurons, in which the cilium forms the terminal sensory apparatus and is the site of sensory transduction. Unlike *C. elegans*, however, some of these sensory neurons retain ciliary motility, namely the chordotonal (Ch) neurons that are required for proprioception and auditory reception. The 9+0 axoneme of the Ch neuron cilium is decorated with ODA/IDA in its proximal region (**Figures 1B,C**; Kavlie et al., 2010; Newton et al., 2012). Dynein activity is required for sensory mechanotransduction, probably as adaptation motors that drive active amplification and frequency tuning (Newton et al., 2012; Senthilan et al., 2012; Moore et al., 2013; Diggle et al., 2014; Karak et al., 2015). Apart from Ch neurons, the only other *Drosophila* cell type with axonemal motility is the spermatozoan, whose flagellum has a 9+2 structure (**Figure 1D**). The flagellum is unusually long (1.9 mm), and flagellogenesis is unusual in that it does not depend on IFT, and instead proceeds by a pathway of cytoplasmic construction followed by extrusion during sperm individualization (Han et al., 2003; Sarpal et al., 2003). Mutation of genes required for dynein structure or assembly results in viable flies with proprioceptive/auditory defects and male infertility (Kavlie et al., 2010; Moore et al., 2013). This is the fly equivalent of human PCD.

As might be expected, in *Drosophila* the expression of known ciliary motility genes is highly cell-type-specific (Cachero et al., 2011; Newton et al., 2012). Indeed in differentiating Ch neurons, motility gene transcription was found to be regulated by a combination of two transcription factors: the ciliogenesis regulator, Rfx, and the Foxj1-related factor, Fd3F (Laurençon et al., 2007; Newton et al., 2012); the paired Rfx/Fd3F binding sites form a motile cilium "gene regulatory code" (Cachero et al., 2011; zur Lage et al., 2011; Newton et al., 2012). This very restricted distribution provides benefits for transcriptomic screening and genetic analysis of candidate ciliary motility genes. This has recently enabled *Drosophila* to contribute to characterization of several novel dynein assembly factors, thereby aiding PCD gene discovery and validation (Moore et al., 2013; Diggle et al., 2014; zur Lage et al., 2018). However, the highly specialized nature of *Drosophila* motile cilia/flagella raises questions of how much of the ancestral motile cilium machinery is retained in this organism, and how these conserved aspects are distributed across the two motile ciliated cell types: 9+0/IFT-dependent and 9+2/IFT-independent.

Here, we comprehensively characterize the molecular basis of ciliary motility in *Drosophila*. Based on homology to genes required for ciliary motility in other organisms (particularly *Chlamydomonas* and human), we show that *Drosophila* has an almost full complement of ciliary motility genes, including orthologs of almost all human genes that have been associated with PCD. Based on transcriptome analysis, the majority of these genes are uniquely expressed in the two motile ciliated cell types. Genetic analysis by targeted RNA interference confirms that knockdown of many motility genes results in impaired motility that can be detected by simple proprioception and fertility analyses. Strikingly, our analysis reveals major differences in the expression of ciliary motors and related components between Ch neurons and spermatocytes. Notably, the two cell types harbor distinct ODA complexes and differ in the expression of a key IDA motor subtype (I1/f). Our analysis lays the basis for further use of *Drosophila* as a motile ciliopathy model, as well as for the understanding of cell-type specializations of motile cilia.

TABLE 1 | Glossary of motile cilia proteins and complexes.

Name	Abbreviation
Microtubule	MT
Outer dynein arm	ODA
Inner dynein arm	IDA
Two-headed inner dynein arm	IDA I1/f
Single-headed inner dynein arm	IDA a–g
Dynein heavy chain	HC
Dynein intermediate chain	IC
Dynein light chain	LC
Dynein light-intermediate chain	LIC
Nexin-dynein regulatory complex	N-DRC
Tether/tetherhead complex	T/TH
Modifier of inner arms	MIA
Calmodulin-spoke complex	CSC
Radial spoke complexes (1, 2, 3)	RS (RS1, RS2, RS3)
Central pair complex	CP
Outer dynein arm docking complex	ODA-DC
Intraflagellar transport	IFT
Dynein pre-assembly factor	DNAAF
A-kinase anchoring protein	AKAP

MATERIALS AND METHODS

Gene Orthology

Eukaryotic ciliary motility genes were compiled from the literature, particularly of *Chlamydomonas* and human studies (Wickstead and Gull, 2007; King, 2016; Viswanadha et al., 2017). Orthology in *Drosophila* was assessed using DIOPT (Hu et al., 2011), with contributions from previous specific studies (Wickstead and Gull, 2007; Karak et al., 2015; Kollmar, 2016; Viswanadha et al., 2017; Neisch et al., 2018).

Fly Lines

RNAi lines were obtained from Vienna *Drosophila* Resource Center (GD and KK lines) as shown in **Table S1**. Flies were maintained on standard cornmeal-agar medium at 25°C. *UAS-Dcr2; scaGal4. BamGal4* was provided by Helen White-Cooper (Cardiff University). *cato*-GFP is described in zur Lage and Jarman (2010).

Transcriptome Analysis of Embryonic Ch Neurons

Transcriptome analysis was performed by fluoresence activated cell sorting (FACS) and microarray analysis using *cato*-GFP embryos similarly to previously described (Cachero et al., 2011). *cato*-GFP embryos were collected and aged at 25°C on grape juice agar plates. At 10:45–11:45 h age (stage 13/14 of embryonic development) embryos were dechorionated in 50% bleach for 2 min 30 s and washed thoroughly with water. The embryos were transferred to a Dounce homogeniser in dissociation medium [Shields and Sang M3 insect medium (Sigma) with 5% FBS (ThermoFisher)] and homogenized with 25 gentle strokes of a loose pestle avoiding foam formation. The cell suspension was then transferred to siliconised tubes previously rinsed in dissociation medium. After centrifugation at 1,000 g for 3 min at room temperature, the supernatant was discarded, and the pellet of cells was resuspended in 1 ml Trypsin (Sigma) in PBS. The suspension was incubated at room temperature for 7 min on a rotating wheel and after subsequent centrifugation at 1,000 g for 3 min at 4°C the supernatant was discarded. The cells were resuspended in 0.2 ml dissociation medium and transferred to a new tube containing 1 ml of dissociation buffer and centrifuged. This step was repeated once, before FACS was performed using a BD FACSAria cell sorter (Becton-Dickinson). The cells were collected into dissociation medium. Up to 300,000 GFP positive cells were sorted per tube and up to 1,000,000 GFP negative cells in a separate tube. Subsequently, the cells were spun at 1,000 g for 3 min at 4°C and the pellet was carefully resuspended in 300 µl of RLT lysis buffer (Qiagen) containing β-mercaptoethanol before storage at −80°C. mRNA from GFP-positive and -negative cells was hybridized to Affymetrix 2.0 microarrays

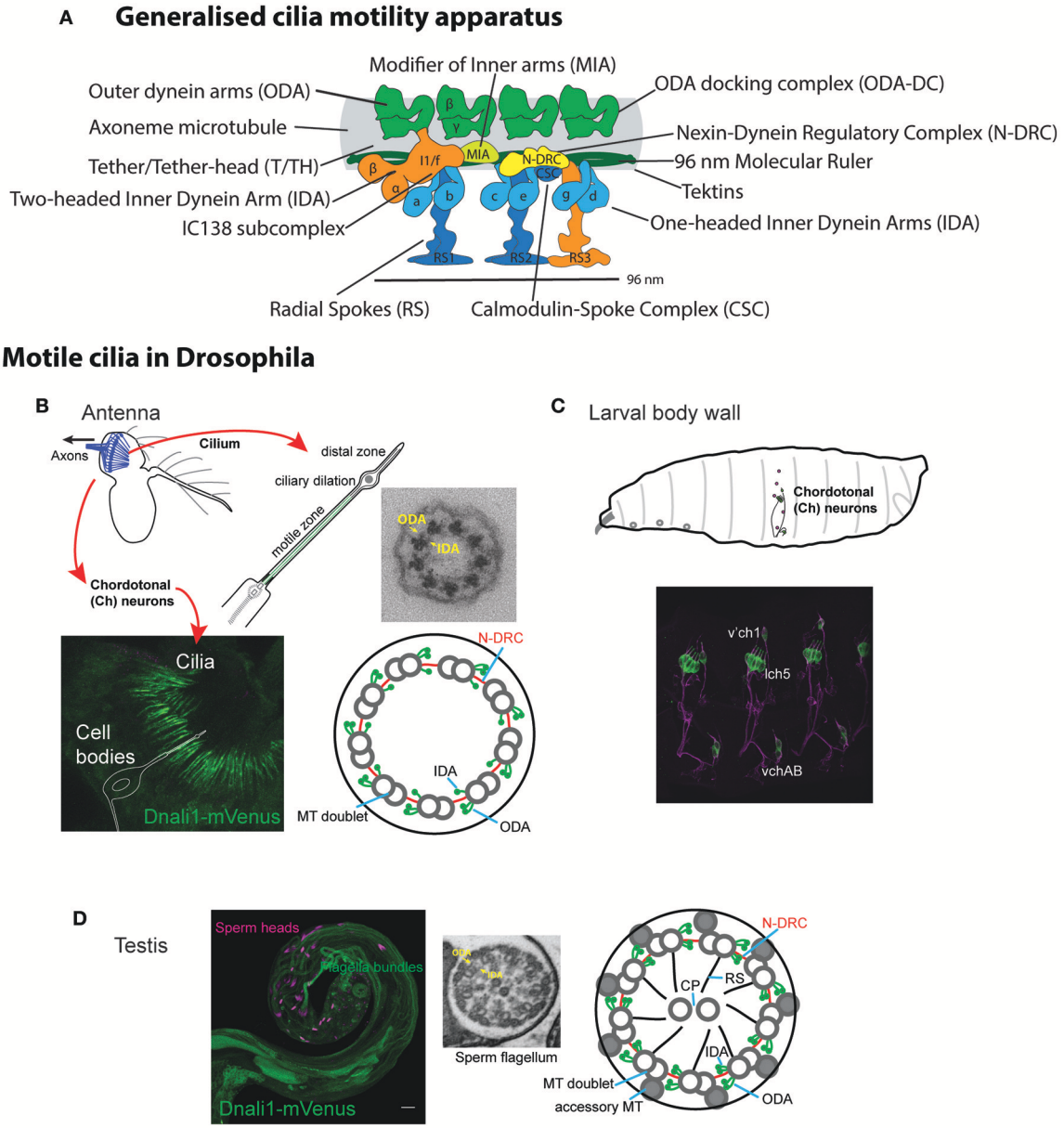

FIGURE 1 | Motile ciliated/flagellated cells in *Drosophila*. **(A)** Schematic diagram of ciliary motility apparatus in a generalized motile cilium (based on cryoEM of human respiratory cilia in Lin et al., 2015). Center of cilium would be toward the bottom. Single repeat unit shown spanning 96 nm with 4 ODA complexes spaced every 24 nm, while the periodicity of different IDA forms is 96 nm. See **Table 1** for glossary of terms. **(B,C)** *Drosophila* Ch neurons. **(B)** Auditory Ch neurons in the antenna. Each Ch neuron bears a terminal mechanosensory cilium with 9+0 axoneme structure. The proximal zone of the terminal cilium has dynein arms, marked in the image by *CG6971*-mVenus (*Dnali1*) (green). Ch neurons are also located in legs and wings (not shown), where they are proprioceptive. **(C)** Similar ciliated Ch neurons are present in the body wall of the larva, where they are both proprioceptive and auditory. **(D)** Sperm. Image shows sperm flagella bundles in testis marked with *CG6971*-mVenus (green), with sperm heads labeled with DAPI. In cross-section, the flagellum has a 9+2 axoneme structure and motile features. ODA, outer dynein arm; IDA, inner dynein arm; MT, microtubule; CP, central pair; RS, radial spoke, N-DRC, nexin-dynein regulatory complex.

by Glasgow Polyomics, University of Glasgow (3 replicates each). Differential expression was determined as a ratio of expression in GFP-positive vs. GFP-negative cells. Data analysis was performed in Partek Genomic Suite 6.6 with the dataset normalized using RMA normalization. One-way ANOVA was performed between positive and negative data with *P*-values then adjusted for multiple test correction using the FDR step-up method.

Drosophila Embryo *in situ* Hybridization

Embryos were harvested from a 24 h collection at 25°C. After dechorionating the embryos in 50% chlorine bleach for

5 min, they were fixed for 20 min in 1:1 mixture of 3.7% formaldehyde/PBS and heptane while shaking at 200 rpm. After removing the PBS formaldehyde lower phase, methanol was added for devitellinisation. Settled embryos were collected and washed twice with methanol. Subsequently, the embryos were rehydrated in a stepwise manner starting with a 3:1, 1:1, and 1:3 ratio of methanol and PBST (PBS plus 0.1% Tween-20), before postfixing them in 3.7% formaldehyde for 20 min. To remove all traces of the latter, the embryos were washed 5 × 5 min in PBST, before incubating them in a 1:1 mixture of hybridization buffer (RNA hybridization buffer: 50% formaldehyde, 5x SSC, 50 µg/ml heparin, 100 µg/ml tRNA, 0.1% Tween-20, pH6.5). After another 10 min of incubation in hybridization buffer at room temperature, prehybridisation was performed for at least 2 h at 70°C in hybridization buffer. After removal of the prehybridisation buffer, the probe was added and incubation took place overnight. Wash solutions were heated at 70°C and after removing the probe, six washes were carried out for 30 min each using initially hybridization buffer, then a 1:1 ratio with PBST, followed by four PBST washes. After a brief wash with PBST at room temperature, the embryos were incubated for 2 h in a 1:2,000 dilution of anti-DIG-AP (alkaline phosphatase) (Roche) while rotating. After three 20 min washes in PBT, they were rinsed in reaction solution (100 mM Tris, pH9.5 and 100 mM NaCl). The color reaction was carried out following the NBT/BCIP protocol (Roche). Once the color reaction had sufficiently developed, the embryos were washed 3x in PBST to stop the reaction before being mounted on slides in 70% glycerol/PBS. Slides were imaged on an Olympus Provis AX-70 microscope using an UPlanApo 20x/0.7 objective. Images were cropped and adjusted for contrast in FIJI.

RNA Probe Preparation

Antisense RNA probes were synthesized using the DIG RNA labeling kit (Roche) from a PCR product containing the T7 promoter on the right primer (**Table S1**). The DIG labeling reaction contained 100–200 ng purified PCR product in a final volume of 10 µl and was carried out for at least 2 h at 37°C. Subsequently, the probe was cleaned using the GeneJET RNA purification kit (ThermoFisher) and eluted in 30 µl of H_2O. The probe was usually used in a 1:200 dilution in hybridization buffer after heating for 5 min at 95°C.

RT-PCR Analysis

Total RNA was isolated from 120 pairs of adult antennae or 150 pairs of testes using the RNeasy Mini kit (Qiagen #74104). cDNA was synthesized using the ImProm-II™ Reverse Transcription system (Promega #A3800). Primers were designed to span at least one intron in order to distinguish mature mRNA from genomic DNA (**Table S1**). For genomic DNA control, DNA was isolated from adult flies using a standard *Drosophila* DNA extraction protocol. PCR amplification was carried out using Roche Taq polymerase (#4728874001).

Genetic Analysis

RNAi knockdown was performed as described previously (zur Lage et al., 2018) using fly lines harboring inducible UAS-hairpin constructs. Knockdown was performed in sensory neurons (driven by *UAS-Dcr2; scaGal4*) or testes (*BamGal4*). For controls we used progeny from each Gal4 line crossed to the appropriate parent strain for the RNAi line in question. Locomotory coordination (requiring Ch neuron function) was tested in an adult climbing assay. Batches of 15 UAS-*Dcr2/+; scaGal4/+*, *UAS-RNAi/+* flies were placed in a vertical sealed tube with gradations as 5, 10, and 15 cm. After banging down, flies were allowed to climb the tube for 30 s. At this point flies were scored according to their vertical location reached (1: <5 cm; 2: 5–10 cm; 3: 10–15 cm; 4: >15 cm). The average score constituted the Climbing Index for that batch ($n = 5$–10 batches per line). Average climbing index was transformed as a proportion of the climbing index achieved by the control flies (<1 represents defective climbing). Male fertility was tested by crossing individual UAS-RNAi/+; BamGal4/+ males ($n = 10$) to 2 OregonR females, allowing them to mate for 2 days, then transferring to new vials for two more days. The number of progeny (per male) from the latter vials were counted. In some cases, average number of progeny per male was determined and expressed as a ratio compared to the progeny produced by control males (<1 represents reduction in fertility). In cases where no or very few progeny were produced, infertility was recorded as the proportion of males yielding a complete lack of progeny. In some cases, production of motile sperm was assessed by examination of dissected and partially squashed testes by light microscopy. In all cases, significance was tested by ordinary 1-way ANOVA with Dunnetts *post-hoc* correction for multiple testing.

RESULTS

Ciliary Motility Genes in *Drosophila*: Identification, Expression, and Genetic Requirement

Ciliary motility genes are well conserved among eukaryotes. To survey the presence of such genes in *Drosophila*, we compiled a gene list of eukaryotic ciliary motility genes derived particularly from *Chlamydomonas* and human studies (Wickstead and Gull, 2007; King, 2016; Viswanadha et al., 2017). Orthology in *Drosophila* was assessed primarily using the DRSC Integrative Orthology Prediction Tool (DIOPT) (Hu et al., 2011). We concentrated on genes that are required exclusively for the structure, function, or generation of motile cilia, thereby excluding structures (e.g., transition zone proteins) and processes (e.g., IFT complexes) shared with immotile or primary cilia. The orthologs identified are compiled in **Tables 2**–**4**, **S2**. In summary, we find that *Drosophila* has orthologs of almost all genes associated with ciliary motility. Among these genes are orthologs of almost all human genes that have been associated with PCD (**Table 6**).

For the identified orthologs, we characterized expression in the two motile ciliated cell types. For testis expression we utilized FlyAtlas adult tissue microarray data (Robinson et al.,

2013). For Ch neurons, we determined the transcriptome of embryonic differentiating Ch neurons in a procedure similar to that which we previously reported (Cachero et al., 2011), but using later stage embryos in order to target terminal cellular differentiation and ciliogenesis. In short, we used a *cato*-GFP fly line, in which differentiating Ch neurons were marked by GFP expression (GFP is also expressed to a much lesser degree in other sensory neurons; zur Lage and Jarman, 2010). Embryos from timed egg collections were dissociated and GFP+ vs. GFP– cells were isolated by FACS. Gene expression was determined using Affymetrix 2.0 microarrays, and candidate Ch-enriched transcripts identified by ratio of expression in GFP+ cells vs. GFP– cells (i.e., the rest of the embryo) (data in **Table S3**). For selected genes, embryonic mRNA expression was confirmed by *in situ* hybridization or RT-PCR. In summary, the majority of orthologs were specifically expressed in one or both motile ciliated cell types (**Tables 2–4**), while a few were more widely expressed.

For further validation and to explore cell-type differences, the functional requirement of selected genes was tested by RNAi knockdown using UAS-hairpin lines. For Ch neuron function, flies with knockdown in sensory neurons (driven by *UAS-Dcr2; scaGal4*) were tested for defective locomotion in a climbing assay (which requires proprioceptive information from Ch neurons). For sperm function, male flies with testis-specific knockdown (driven by *BamGal4*) were tested their ability to produce offspring. Knockdown results are presented in **Table 5**.

In the following sections, we describe the *Drosophila* representation of ciliary motility genes and their expression starting with the dynein motors.

Drosophila Has an Almost Complete Repertoire of Axonemal Dyneins

Dynein motors comprise ODAs docked at 24 nm intervals along the axoneme and several subtypes of IDA docked in a 96-nm repeating pattern (**Figure 1A**). Motor activity is largely performed by their Heavy Chains (HCs) while Intermediate Chains (ICs) often contribute to stable assembly of the complexes (**Figure 2A**). A variety of Light Chains (LCs) have accessory and regulatory functions. Whilst HCs and ICs are largely specific to each dynein subtype, many LCs are shared. In the account below, we concentrate on HCs, ICs, and those LCs that can be assigned to specific motor subtypes. Previous reports have identified several *Drosophila* homologs of axonemal dynein genes (Rasmusson et al., 1994; Newton et al., 2012; Karak et al., 2015). In our homology searches based on human and *Chlamydomonas* dynein chains (Wickstead and Gull, 2007; Hom et al., 2011; Kollmar, 2016; Viswanadha et al., 2017), we found that despite the specialized nature of its motile ciliated cells, *Drosophila* retains genes for an almost complete repertoire of ODAs and IDAs (**Table 2**; **Figure 2A**). In our analysis, we follow the dynein taxonomy proposed by Kollmar (2016).

Outer Arm Dyneins: Different Forms in Ch Neurons and Sperm

In *Chlamydomonas*, ODA is thought to be the major motor for force generation (King, 2016). In metazoans, ODA is two-headed, containing HCs equivalent to beta and gamma HCs of *Chlamydomonas*. In humans, beta HCs are encoded by *DNAH9*, *DNAH11*, and *DNA17* while gamma HCs are encoded by *DNAH5* and *DNAH8* (unless otherwise stated, human gene designations are given hereafter). *Drosophila* has HC genes orthologous to each of these human chains (Kollmar, 2016; **Table 2**; **Figure 2A**). Interestingly, different gamma/beta gene pairs are exclusively expressed in each of the two cell types: *CG9492* and *Dhc93AB* in Ch neurons (corresponding to human *DNAH5/DNAH11*); *kl*-3 and *kl*-5 in sperm (corresponding to *DNAH8/DNAH17*). Consistent with this separation, both sperm-specific HCs are encoded by Y chromosome genes (Carvalho et al., 2000).

To corroborate these differences, we analyzed gamma HC expression by RT-PCR. This confirmed that *kl*-3 expression is exclusive to testis while *CG9492* expression appears exclusive to antennae (which contain a large array of Ch neurons, **Figures 1B**, **2B**). For comparison, an ODA LC (*CG8800/DNAL1*) was found to be expressed in both tissues (**Figures 2A,B**). *In situ* hybridization in embryos also confirms Ch-neuron specific expression of *Dhc93AB* and *CG9492*, although expression is quite weak, consistent with low transcription levels (**Figures 3A–C,J**; Newton et al., 2012). Further validation of cell-type specificity is provided by RNAi knockdown, which showed that the different ODA HCs yield phenotypes in only one or other cell type, thereby correlating with their expression patterns (**Table 5**).

A further beta HC (*CG3339*, corresponding to *DNAH9*), appears not to be highly expressed in either cell type by transcriptome analysis (**Table 2**). However, RT-PCR revealed that this HC is expressed in antennal Ch neurons (**Figure 2B**).

Human ODAs contain an IC heterodimer of DNAI1/DNAI2. *Drosophila* has a single *DNAI1* ortholog (*CG9313/Dnai1*), which is expressed in both motile ciliated cell types. RNAi knockdown confirms its requirement in both cell types (**Table 5**). In contrast, three *DNAI2* orthologs are present. One is Ch neuron-specific (*CG6053*) (**Table 2**; **Figure 3L**) and the other two are sperm-specific (*CG1571*, *CG10859*) (**Figure 2A**). RNAi knockdown of *CG6053* confirms that it is required for proprioception but not for male fertility (**Table 5**).

For LCs, *Drosophila* has homologs of all major families (Tctex1, Roadblock, and LC8 families) (**Table S2**). The distribution of LCs across dynein subtypes is not fully known, and indeed many subunits are not specific to axonemal dyneins. On current knowledge only DNAL1/LC1 is ODA-specific. *Drosophila* has two DNAL1 orthologs: as noted above, ortholog *CG8800* is expressed in both Ch neurons and testes, but *CG10839* is only expressed in testes (**Figures 2A,B**, **3K**). For the Roadblock family (shared with IDA I1/f, below), several homologs are strongly expressed in testes, while *robls54B* is strongly enriched in Ch neurons.

In conclusion, in *Drosophila* cell-type-specific ODA complexes exist characterized by different HCs, as well as some different ICs and LCs. This suggests divergence of ODA function in the two cell types (**Figures 2A**, **4A**).

Outer Dynein Arm Docking Complex (ODA-DC) Differs in Ch Neurons and Sperm

In *Chlamydomonas*, ODA-DC proteins are required to stabilize ODA docking on the axoneme (Oda et al., 2016). The human equivalent of ODA-DC is thought to consist of CCDC63,

TABLE 2 | Axonemal dynein HC and IC genes in *Drosophila*.

Gene	Name	Class/name	*Chlamydomonas*	Human	Dynein complex	Ch neuron expression	Testis expression	Expression summary	Expression corroboration
OUTER ARM DYNEIN									
CG45785	*kl-3*	HC, DHC3A	OADgamma	*DNAH8*	ODA	(not on chip)	15.20 (38)	Ch + Testis	RT-PCR
CG9492		HC, DHC3B	OADgamma	*DNAH5*	ODA	3.13	4.50 (9.2)	Ch only	ISH, RT-PCR
CG3723	*Dhc93AB*	HC, DHC4A	OADbeta	*DNAH11*	ODA	8.12	0.20 (1.9)	Ch only	Newton et al., 2012
CG45786	*kl-5*	HC, DHC4B	OADbeta	*DNAH17*	ODA	(not on chip)	3.2 (13)	Testis only	
CG3339		HC, DHC4C	OADbeta	*DNAH9*	ODA	1.02	1.3 (6)	Ch only	RT-PCR
CG9313		IC, IC78	DIC1/ODA9	*DNAI1*	ODA	5.61	10.6 (1106)	Ch + Testis	ISH (Karak et al., 2015)
CG6053	*Dnai2*	IC, IC70	DIC2/ODA6	*DNAI2*	ODA	2.04	0.80 (3.1)	Ch only	
CG10859		IC, IC70	DIC2/ODA6	*DNAI2*	ODA	−2.13	13.70 (1580.2)	Testis only	
CG1571		IC, IC70	DIC2/ODA6	*DNAI2*	ODA	1.12	18.30 (246)	Testis only	
INNER ARM DYNEIN, SINGLE-HEADED									
CG5526	*Dhc36C*	HC, DHC7A	DHC6	*DNAH7*	IDA a,b,c,e	4.47	9.5 (288.1)	Ch + Testis	ISH
CG17150	*Dnah3*	HC, DHC7B	DHC5	*DNAH3*	IDA a,b,c,e	4.32	21 (391)	Ch + Testis	Karak et al., 2015
CG15804	*Dhc62B*	HC, DHC7C	DHC9	*DNAH12*	IDA a,b,c,e	8.34	8.4 (98.8)	Ch + Testis	Newton et al., 2012
No ortholog		HC, DHC8	DHC2	*DNAH1*	IDA d	na	na	na	
CG7092	*Dhc16F*	HC, DHC9A	DHC7	*DNAH6*	IDA g	3.85	8.7 (163.9)	Ch + Testis	ISH
No ortholog		HC, DHC9B	DHC3	*DNAH14*	IDA g	na	na	na	
CG6971		IC, LIC1	p28	*DNALI1*	IDA a,c,d	6.29	13 (707.9)	Ch + Testis	Newton et al., 2012
CG31802		IC, Centrin	DLE2	*CENTRIN*	IDA b,e,g	1.03	11 (1250.7)	Widely expressed	
INNER ARM DYNEIN I1/F, TWO-HEADED									
CG1842	*Dhc98D*	HC, DHC5	DHC1	*DNAH10*	IDA I1/f	1.18	14.30 (67)	Testis only	
CG17866	*kl-2*	HC, DHC6	DHC10	*DNAH2*	IDA I1/f	1.15	7.10 (54)	Testis only	
CG14838		IC, IC140	IC140/DIC3	*WDR63*	IDA I1/f	1.1	12.0, (112.9)	Testis only	
CG13930		IC, IC138	IC138/DIC4	*WDR78*	IDA I1/f	5.08	1.30 (4.5)	Ch only	Newton et al., 2012
CG7051	*Dic61B*	IC, IC138	IC138/DIC4	*WDR78*	IDA I1/f	−1.36	18.00 (256.3)	Testis only	
CG15373		IC, IC97	IC97	*CASC1/LAS1*	IDA I1/f,	1.12	1.7 (13.7)	Testis only	

For HCs names, we follow the proposed nomenclature and relationships of Kollmar (2016). Ch expression: ratio of expression in differentiating Ch neurons from 12 h embryos relative to expression in rest of embryo. Testis expression: mRNA enrichment and expression signal (brackets) data from FlyAtlas. Expression summary: Ch expression (>2.0 differential expression) and testis expression (>1.5 enrichment, >10 signal). Expression corroboration: obtained from: ISH: mRNA in situ hybridization (this study), RT-PCR (this study), or from the reference cited. Where there is no ortholog, expression is not applicable (na).

CCDC114 (DC2 homologs), and ARMC4; mutation of these genes causes PCD with loss of ODA (Hjeij et al., 2013; Knowles et al., 2013; Onoufriadis et al., 2013, 2014). In *Drosophila*, ODA-DC orthologs show strong differences in expression between sperm and Ch neurons (**Table 3**). Sperm and Ch neurons express distinct orthologs of CCDC63/114 (*CG17083* and *CG14905* respectively, **Figure 3I**). Knockdown of *CG14905* confirms a specific function in Ch neurons (**Table 5**). In contrast, the ortholog of ARMC4 (*CG5155/gudu*) is expressed only in sperm. Interestingly, human ARMC4 seems to be required for correct CP structure (Hjeij et al., 2013; Onoufriadis et al., 2014), and so lack of *gudu* expression in Ch neurons correlates with their lack of the CP.

In humans, another protein, CCDC103, is independently required for ODA docking (Panizzi et al., 2012; King and Patel-King, 2015). The *Drosophila* ortholog (*CG13202*) differs from human CCDC103 in not possessing an RPAP3 domain, but it is nevertheless expressed in Ch neurons and testes. Knockdown of *CG13202* confirms at least a partial requirement in sperm and Ch neurons (**Table 5**).

Two-Headed Inner Arm Dynein I1/f: Present in Sperm but Lacking From Ch Neurons

IDA I1/f is thought to regulate movement by resisting other dyneins. It is two-headed with two HCs and three ICs. *Drosophila* genes characteristic of this complex include homologs of alpha and beta HC genes (DNAH10: *Dhc98D* and DNAH2: *kl-2*), and the three ICs (WDR78/IC138: *Dic61B*; WDR63/IC140: *CG14838*; LAS1/IC97: *CG15373*) (**Table 2**). Each of these genes is expressed in testes, suggesting that sperm have a functional I1/f motor and associated machinery (**Figure 2A**). In striking contrast, none of these sperm HCs and ICs are expressed in Ch neurons, which therefore lack the I1/f motor. RNAi knockdown of the I1/f HCs confirms that this subtype has a role in sperm but not in Ch neurons (**Table 5**). This is corroborated by male infertility of *Dic61B* mutants (Fatima, 2011). In *Chlamydomonas*

TABLE 3 | Other motility apparatus genes in *Drosophila*.

Gene	Name	*Chlamydomonas*	Human	Ch neuron expression	Testis expression	Expression summary	Expression corroboration
MIA COMPLEX							
CG17564		MIA2/FAP73	*CCDC43A/B*	78.21	12 (909)	Ch + Testis	
CG10750		MIA2/FAP73	*CCDC43B*	6.56	14 (783)	Ch + Testis	
No ortholog		MIA1/FAP100	*CCDC38*	na	na	na	
T/TH COMPLEX							
CG17687		CFAP43	*CFAP43*	3.2	204	Ch + Testis	
CG34124		CFAP44	*CFAP44*	Not on chip	Not on chip	Not detected	
ODA DOCKING COMPLEX (ODA-DC)							
CG14905		DCC2/ODA1	*CCDC63*	108.8	1.5 (6)	Ch only	ISH
CG17083		DCC2/ODA1	*CCDC114*	1.13	14 (980)	Testis only	
CG5155	*gudu*		*ARMC4*	1.07	11 (729)	Testis only	
ODA ADAPTOR							
CG13202			*CCDC103*	8.19	12 (257.3)	Ch + Testis	
96 NM MOLECULAR RULER							
CG17387			*CCDC39*	4.07	16 (316)	Ch + Testis	
CG41265	*l(2)41Ab*		*CCDC40*	4.06	14 (229)	Ch + Testis	
PROTOFILAMENT STABILITY AND IDA DOCKING							
CG10541	*Tektin-C*		*TEKT1*	3.6	15 (887)	Ch + Testis	ISH, Berkeley *Drosophila* Genome Project database
CG4767	*Tektin-A*		*TEKT4*	19.42	13 (1348)	Ch + Testis	ISH
CG3085			*TEKT2*	56.14	10 (1321)	Ch + Testis	ISH, Berkeley *Drosophila* Genome Project database
CG17450			*TEKT3/TEKT5*	3.69	14 (1054)	Ch + Testis	
NEXIN-DYNEIN REGULATORY COMPLEX (N-DRC)							
CG10958		DRC1	*DRC1/CCDC164*	4.81	12.1 (462)	Ch + Testis	Berkeley *Drosophila* Genome Project database
CG30259		DRC2	*CCDC65/CILD27*	1.67	0.9 (3)	(Ch only)	
CG13125	*TbCMF46*	DRC3	*LRRC48*	58.6	7.3 (89)	Ch + Testis	
CG14271	*Gas8*	DRC4	*GAS8*	3.2	12.5 (249)	Ch + Testis	ISH
CG14325		DRC5	*TCTE1*	1.7	0.2 (0)	(Ch only)	
CG8272		DRC6	*FBXL13*	1.2	1.5 (95)	Testis only	
CG34110	*lobo*	DRC7	*CCDC135*	34.2	11.1 (46)	Ch + Testis	
CG11041		DRC8	*EFCAB2*	9.9	0.4 (0)	Ch only	Berkeley *Drosophila* Genome Project database
CG13972		DRC9	*IQCG*	17.6	0.9 (0)	Ch only	
CG13168		DRC10	*IQCD*	1.99	13.6 (865)	Ch + Testis	
CG16789		DRC11	*IQCA*	30.7	1.6 (9)	Ch only	ISH, Berkeley *Drosophila* Genome Project database
RADIAL SPOKE							
CG32392		RSP3	*RSPH3/AKAP*	10.46	14 (801)	Ch + Testis	
CG5458		RSP1	*RSPH1*	1.03	14 (826)	Testis only	
CG31803			*RSPH9*	−1	11 (1011)	Testis only	
CG3121		RSP4/6	*RSPH4A*	1.08	16 (695)	Testis only	
CG2981	*TpnC41C*	RSP7	*CALML5*	−1.53	not detected	not detected	
CG10014		RSP11	*ROPN1L*	1.1	14 (811)	Testis only	
CG17266		RSP12	*PPIL6*	−1.45	0.6 (64)	Testis only	
CG8336		RSP12	*PPIL6*	1.4	3.5 (388)	Testis only	
CG13501		RSP14	*RTDR1*	−1.01	12 (278)	Testis only	
CG10578	*Dnaj-1*	RSP16	*DNAJB13*	1.64	2.0 (1378)	Widely expressed	
CG15547		RSP23	*NME5*	1.4	8.9 (242)	Testis only	

(Continued)

TABLE 3 | Continued

Gene	Name	*Chlamydomonas*	Human	Ch neuron expression	Testis expression	Expression summary	Expression corroboration
CALMODULIN-SPOKE COMPLEX (CSC)							
CG30275		FAP61	*C20orf26*	1	17 (396)	Testis only	
CG30268		FAP61	*C20orf26*	1	16 (254)	Testis only	
CG15143		FAP91/CaM-IP2	*MAATS1*	1.62	14 (158)	Testis only	
CG15144		FAP91/CaM-IP2	*MAATS1*	−1.05	14 (334)	Testis only	
CG15145		FAP91/CaM-IP2	*MAATS1*	−1.13	19 (284)	Testis only	
No ortholog		FAP251	*WDR66*	na	na	na	
OTHER							
CG17230			*CCDC11/CFAP53*	3.8	820	Ch + Testis	
No ortholog			*HYDIN*	na	na	na	

Columns and abbreviations as for ***Table 2.*** *CG17450 seems to be triplicated in Drosophila melanogaster (with CG32820, CG32819).*

it has been suggested that this dynein is intimately involved in receiving and responding to regulatory signals from the CP/RS system (Viswanadha et al., 2017). Thus, *Drosophila* seems to support this role in that the absence of functional IDA I1/f from Ch neurons correlates with their lack of CP/RS (**Figure 4A**).

Ch Neurons Retain Key Regulatory Subunits Associated With I1/f Dynein and Radial Spokes

In contradiction to their lack of HC expression for IDA I1/f, we found that Ch neurons surprisingly uniquely express *CG13930*, a second ortholog of the I1/f subunit, WDR78/IC138 (**Figures 2A**, **3G**). Although this is an IC of I1/f, it is also thought to form part of an "IC138 subcomplex" that mediates regulation of motor activity by signals emanating from the RS and CP (Viswanadha et al., 2017; **Figure 1A**). Knockdown of *CG13930* confirms that it is required in Ch neurons but not in testes, despite the lack of I1/f motor and CP/RS in Ch neurons (**Table 5**). In Ch neurons, *CG13930* is potentially in a subcomplex with several LCs including *robls54B*, but this is not certain because no LCs are specific to dynein I1/f (**Figure 2A**; **Table S2**).

Given this finding, we examined expression of other proteins thought to interact with IDA I1/f. The MIA complex is proposed mediate transmission of signals from CP/RS via phosphorylation of IC138 (Yamamoto et al., 2013; **Figure 1A**). *Drosophila* has two orthologs of MIA2/FAP73 (*CG17564* and *CG10750*), and these are expressed in both testes and Ch neurons (**Table 3**; **Figure 2A**). The MIA transcripts are particularly highly enriched in Ch neurons (**Tables 3**, **S1**). In *Chlamydomonas*, IDA I1/f HCs are also associated with and regulated by a "tether and tether-head" (T/TH) complex (CFAP43/CFAP44). Unexpectedly, the *Drosophila* homolog of CFAP43 (*CG17687*) is expressed not only in testes, but also in Ch neurons. A CFAP44 homolog also exists (*CG34124*) but it is not represented on the microarray used in our expression analysis.

Given that these regulatory subunits are thought to link to CP/RS function, we analyzed the presence and expression of RS proteins. These are not well characterized in metazoans, but many RS proteins of *Chlamydomonas* have orthologs in *Drosophila* (**Table 3**). As expected, most are expressed in testes and not in Ch neurons, confirming that the latter's 9+0 cilia lack RS complexes. However, the RSPH3 homolog, *CG32392*, is an interesting exception as it is highly expressed in both cell types (**Table 3**). Interestingly, although RSPH3 is an RS component, it is predicted to act as an A-kinase anchoring protein (AKAP) to regulate the IC138 phospho-regulator. *CG32392* may therefore have an RS-independent function linked to a Ch neuron-specific IC138/*CG13930* regulatory complex.

Radial spokes are associated with a Calmodulin and Spoke-associated Complex (CSC), which is required for RS2 assembly and modulating dynein activity, possibly by transmitting signals from the RS to dyneins via N-DRC (Dymek et al., 2011). CSC subunits FAP61 and FAP91 have *Drosophila* homologs that expressed in testes, but none are enriched in Ch neurons.

In conclusion, despite their lack of CP/RS complex and functional I1/f dynein, Ch neurons express several key proteins previously associated with transmitting signals from CP/RS to dynein motors (**Figures 2A**, **4A**), suggesting their cilia retain key parts of this regulatory axis for another purpose.

Single-Headed Inner Arm Dyneins: Shared in Both Sperm and Ch Neurons

Six single-headed dynein variants are thought to exist in *Chlamydomonas* and humans (a–e, g), as classified by their HC and IC constituents. These IDA forms are thought to function as dyad pairs with one DNALI1/p28-containing and one centrin-containing motor in each dyad—a/b, c/e, g/d (Hirose and Amos, 2012; **Figure 1A**). *Drosophila* has four HC genes that encode orthologs of chains found in IDA a, b, c, e, and g (Wickstead and Gull, 2007; **Table 2**; **Figure 2A**). However, no d-specific HC gene (ortholog of human *DNAH1*) is present in *Drosophila*. Curiously, however, *DNAH1* has an apparent ortholog in *Apis mellifera* (Kollmar, 2016). Single-headed IDAs contain either centrin (b, e, d) or DNALI1/p28 (a, c, g) (**Figure 2A**). In *Drosophila*, the

TABLE 4 | Genes for dynein motor assembly and transport in *Drosophila*.

Gene	Name	*Chlamydomonas*	Human	Ch neuron expression	Testis expression	Expression summary	Expression corroboration
ODA LATE ASSEMBLY COMPLEX							
CG14127		ODA10/ODA5	*CCDC151*	2.22	not detected	Ch only	
CG14185		ODA8	*LRRC56*	2.46	not detected	Ch only	
CG13502			*TTC25*	3.48	1 (9.2)	Ch only	
DYNEIN CYTOPLASMIC PREASSEMBLY FACTORS							
CG31623	*dtr*	ODA7	*DNAAF1/LRRC50*	2.38	16 (648)	Ch + Testis	
CG1553	*nop17l*	PF13?	*DNAAF2/KTU*	1.20	0.3 (74)	Widely expressed	ISH
CG5048		PF13?	*PIH1D3*	55.39	9.7 (1891)	Ch + Testis	ISH, Berkeley *Drosophila* Genome Project database
CG17669		PF22	*DNAAF3*	19.61	14 (347)	Ch + Testis	ISH, Berkeley *Drosophila* Genome Project database
CG14921		PF23	*DNAAF4/DYX1C1*	5.20	8.9 (294)	Ch + Testis	ISH, Berkeley *Drosophila* Genome Project database
CG14620	*tilB*		*LRRC6*	9.40	12 (191)	Ch + Testis	
CG11253	*Zmynd10*		*ZMYND10*	41.98	12 (503)	Ch + Testis	ISH (Newton et al., 2012)
CG31320	*Heatr2*		*HEATR2/DNAAF5*	12.26	7.8 (493)	Ch + Testis	ISH, Berkeley *Drosophila* Genome Project database (Newton et al., 2012)
CG18675			*C21orf59*	52.13	15 (871)	Ch + Testis	ISH
CG18472			*SPAG1*	17.31	12 (410)	Ch + Testis	ISH (zur Lage et al., 2018)
CG9750	*reptin*		*REPTIN/RUVBL2*	2.53	2.6 (700)	Widely expressed	ISH, Berkeley *Drosophila* Genome Project database
CG4003	*pontin*		*PONTIN/RUVBL1*	1.59	2.1 (477)	Widely expressed	ISH (zur Lage et al., 2018)
CG14353	*Wdr92*		*WDR92*	4.10	6.3 (376)	Ch + Testis	ISH (zur Lage et al., 2018)

Columns and abbreviations as for ***Table 2.***

DNALI1 ortholog, CG6971, is localized to Ch neuron cilia and sperm flagella (**Figure 3H**; Diggle et al., 2014).

In contrast to the other dyneins, none of the single-headed IDA HCs are unique to one or other motile ciliated cell type in *Drosophila*: all are expressed in Ch neurons and testes (**Table 2**; **Figures 2A**, **3D–F**). RT-PCR analysis of *CG17150* (*DNAH3*) confirmed that it is expressed in both antennae and testes. Interestingly, however, this analysis also revealed that the antennal transcript includes an extra penultimate 39-bp exon compared to testis (and not annotated in the *Drosophila* genome) (**Figure 2B**). Knockdown of *Dhc16F*, *Dhc36C*, and *Dhc62B* all result in full or partial reduction of fertility and climbing (**Table 5**).

Attachment of Inner Dynein Arms (the "Molecular Ruler" and Tektins)

In humans, CCDC39 and CCDC40 proteins associate, and mutation of either can cause PCD with loss of N-DRC, RS, and DNALI1-containing IDAs (Becker-Heck et al., 2011; Merveille et al., 2011; Antony et al., 2013). Work in *Chlamydomonas* suggests that an elongated CCDC39/40 complex (FAP59/FAP172) forms a 96 nm molecular ruler to guide periodicity of docking of RS, N-DRC, IDAs (Oda et al., 2014a; **Figure 1A**). *Drosophila* has orthologs of both genes (*CG17387* and *l(2)41Ab*) and each is expressed in Ch neurons and testes (**Table 3**). RNAi knockdown of *CG17387/CCDC39* causes a severe climbing phenotype as well as immotile sperm (**Table 5**).

Tektins appear to be required for IDA assembly on, or attachment to, the microtubule doublets, but it is not clear whether they also have other functions in both motile and non-motile cilia (Tanaka et al., 2004; Amos, 2008; Linck et al., 2014). *Drosophila* has four tektin genes, all of which are expressed in testes and enriched in Ch neurons. *In situ* hybridization confirmed that *Drosophila Tektin*-A, *Tektin*-C and *CG3085* are expressed in Ch neurons, but they are not expressed in sensory neurons with non-motile cilia (**Figures 3M–O**). Knockdown shows that these tektins have some function in fertility, but Ch neuron phenotypes are not observed, perhaps due to redundancy or compensation (**Table 5**).

Nexin–Dynein Regulatory Complex (N-DRC) Has Cell-Type-Specific Subunits

N-DRC is a large complex that bridges the microtubule doublets in motile cilia (**Figure 1A**). In *Chlamydomonas* it has at least 11 subunits and helps to maintain axonemal alignment and resistance to sliding (Bower et al., 2013). It is also an important regulatory hub that contacts ODA, IDA

TABLE 5 | Effects of gene knock down on ciliary motility functions.

Drosophila	Human	Fertility relative to wild type	*P*-value for fertility	Climbing index relative to wild type	*P*-value for climbing	Phenotype summary	Note
Dhc93AB	*DNAH11*	1.07	ns	0.62	<0.0001	Ch only	KK
CG9492	*DNAH5*	0/10 infertile		0.81	0.0096	Ch only	KK
Dhc16F	*DNAH6*	10/10 infertile		0.73	<0.0001	Ch + Testis	GD
Dhc62B	*DNAH12*	3/5 infertile		0.62	<0.0001	Ch + Testis	KK
Dhc36C	*DNAH7*	0.43	<0.0001	0.67	<0.0001	Ch + Testis	GD
Dhc98D	*DNAH10*	9/10 infertile		1.01	ns	Testis only	KK
CG13930	*WDR78/IC138*	1.19	ns	0.83	0.050	Ch only	GD
CG9313	*DNAI1*	10/10 infertile		0.63	<0.0001	Ch + Testis	KK
CG6053	*DNAI2*	0.95	ns	0.90	<0.0001	Ch only	KK
CG6971	*DNALI1*	9/10 infertile		0.83	0.0126	Ch + Testis	KK
CG14905	*CCDC63/114*	1.15	ns	0.59	<0.0001	Ch only	KK
Tektin-C	*TEKT1*	0.28	<0.0001	1.07	ns	Testis only	KK
Tektin-A	*TEKT4*	0.51	0.02	0.99	ns	Testis only	KK
CG3085	*TEKT2*	0.72	ns	0.99	ns	None	KK
CG14127	*CCDC151*	1.23	ns	0.81		Ch only	GD
CG13202	*CCDC103*	5/5 infertile		0.77	0.0002	Ch + Testis	KK
CG10958	*CCDC164*	9/10 infertile		0.64	<0.0001	Ch + Testis	KK
CG30259	*CCDC65*	1/5 infertile		0.73	<0.0001	Ch only	KK
Gas8	*GAS8*	5/5 infertile		0.65	<0.0001	Ch + Testis	KK
CG17387	*CCDC39*	0.07	<0.0001	0.62	<0.0001	Ch + Testis	KK
CG17564	*MIA2*	0.88	ns	0.81	<0.0001	Ch only	GD
dtr	*DNAAF1*	10/10 infertile		0.56	<0.0001	Ch + Testis	GD
nop17l	*DNAAF2*	0.08	<0.0001	0.72	<0.0001	Ch + Testis	GD
CG5048	*PIH1D3*	0.42	<0.0001	0.65	<0.0001	Ch + Testis	GD
CG17669	*DNAAF3*	0.50	0.0002	0.54	<0.0001	Ch + Testis	GD
CG14921	*DNAAF4*	0.31	<0.0001	0.87	0.0013	Ch + Testis	KK
tilB	*LRRC6*	10/10 infertile		0.44	<0.0001	Ch + Testis	KK (Kavlie et al., 2010)
Zmynd10	*ZMYND10*	Immotile sperm		Defective		Ch + Testis	Moore et al., 2013
Heatr2	*HEATR2*	Immotile sperm		Defective		Ch + Testis	Diggle et al., 2014
reptin	*REPTIN*	Immotile sperm		Lethal		?Ch + Testis	zur Lage et al., 2018
pontin	*PONTIN*	Immotile sperm		Lethal		?Ch + Testis	zur Lage et al., 2018
CG18675	*C21orf59*	10/10 infertile		0.60	<0.0001	Ch + Testis	KK
CG18472	*SPAG1*	0.20	<0.0001	0.49	<0.0001	Ch + Testis	KK
Wdr92	*WDR92*	Immotile sperm		Defective		Ch + Testis	zur Lage et al., 2018

*Fertility phenotype is summarized as number of progeny per male relative to control or as the number of completely infertile males. Proprioceptive phenotype is summarized as climbing assay index (height climbed) relative to control (therefore an index of 1 means no reduction). ns, not significantly decreased. RNAi lines used are from the GD and KK collections of the Vienna Drosophila Resource Center (**Table S1**). P-values are shown where a difference from control reaches significance (≤0.05) in ordinary 1-way ANOVA with Dunnetts post-hoc correction.*

I1/f, and RS2 (Viswanadha et al., 2017). Human homologs of some subunits cause PCD with only subtle defects of ciliary beating [DRC4/*GAS8* (Jeanson et al., 2016; Lewis et al., 2016), *DRC1*/*CCDC164* (Wirschell et al., 2013), *CCDC65* (Horani et al., 2013)] while in *Chlamydomonas*, *drc* mutants still retain 9+2 structure and motility (Bower et al., 2013). In *Drosophila*, orthologs of most human N-DRC subunits can be identified, and many are expressed in both Ch neurons and testis (**Table 3**). *Gas8* and *CG17689* expression in Ch neurons was confirmed by *in situ* hybridization (**Figures 3P,Q**). Despite subtle effects of mutation in N-DRC genes in human and *Chlamydomonas* cilium beating, knockdown of *Drosophila Gas8* and *CG10958* (*CCDC164*/*DRC1*) clearly impairs climbing and male fertility (**Table 5**). The expression of N-DRC components in Ch neurons but not in other sensory neurons that have non-motile cilia (**Figures 3P,Q**) supports the hypothesis that this complex is structurally and functionally important in both 9+2 and 9+0 motile cilia but not responsible for axoneme stability in non-motile cilia (Porter, 2018). Surprisingly homologs of some components that might be considered core subunits are expressed exclusively in Ch

neurons or in testes, suggesting cell-type specific variations in N-DRC (**Table 3**). Notably, *CG30259* (*CCDC65/DRC2*) appears to be absent from sperm. Consistent with this, knockdown of *CG30259* only affects Ch neuron function (**Table 5**).

Motile Ciliogenesis: ODA Late Assembly/Transport Genes Are Expressed Exclusively in Ch Neurons

In *Chlamydomonas*, ODA5 and ODA10 are related to ODA-DC proteins, but are thought to be required along with ODA8 for maturation of pre-assembled ODA complexes prior to association with IFT machinery (Mitchell, 2017). Human ODA10 homolog *CCDC151* is mutated in PCD, and is required for stable localization of ODA-DC proteins (CCDC114 and ARMC4) in human and zebrafish (Hjeij et al., 2014; Jerber et al., 2014). In *Drosophila*, *CG14127* (*CCDC151*) and *CG14185* (*ODA8/LRRC56*) are both expressed exclusively in Ch neurons, thus correlating with the only motile ciliated cell type that requires IFT (**Table 4**). As noted by Jerber et al. (2014), this supports a role in linking dynein complexes to IFT for transport through the cilium. In addition, human PCD-associated *TTC25* is also proposed to link *CCDC151* to IFT (Wallmeier et al., 2016). Consistent with this, the *Drosophila* ortholog *CG13502* is exclusively expressed in Ch neurons (**Table 4**).

Motile Ciliogenesis: Dynein Assembly Factors Are Shared Between Ch Neurons and Sperm

A cohort of some 11 proteins, largely identified through characterization of PCD mutations, are required for the cytoplasmic pre-assembly of axonemal dynein complexes (Mitchison and Valente, 2017). All known DNAAFs have clear orthologs in *Drosophila* (**Table 4**). Despite the cell-type-specific differences in motors, these orthologs are highly expressed in both testes and Ch neurons (**Table 4**; **Figures 3R–T**), and have clear defects in both cell types upon knock-down (**Table 5**).

Several PIH (Protein Interacting with Hsp90) domain proteins are involved in dynein assembly (Omran et al., 2008; Dong et al., 2014; Olcese et al., 2017; Paff et al., 2017), and *Drosophila* has functional homologs of each of these (**Tables 4**, **5**). Human *PIH1D3* and *DNAAF2/KTU* are both PCD-causative genes (Omran et al., 2008; Olcese et al., 2017; Paff et al., 2017). *PIH1D3* is represented in *Drosophila* by *CG5048*. This gene is highly expressed in Ch neurons and testes, consistent with a specific role in dynein assembly (**Table 4**; **Figure 3R**). In contrast *CG1553/nop17l* (the ortholog of *DNAAF2/KTU*) is expressed only moderately in testes and its expression is not specific to that tissue in adults (**Table 4**). It is not strongly enriched in Ch neurons either, with RNA *in situ* hybridization revealing widespread expression, but somewhat elevated in Ch neurons (**Figure 3S**). It seems likely that *nop17l* is not dedicated solely to dynein assembly in *Drosophila*.

DISCUSSION

We found in general that the entire ciliary motility apparatus is highly conserved in *Drosophila* (**Figure 4A**). This suggests that despite the restricted distribution and function of its motile cilia, *Drosophila* has great potential as a genetic model for metazoan motile cilia biology. Indeed, the fact that only two cell types have motile cilia can be turned to advantage: it aids gene discovery and characterization, and it also provides a simple model system for exploring how diversity of motile cilium structure and function might be explained by cell-type-specific differences in ciliary motility machinery. Our cell type-specific comparison is illuminating: we find interesting differences in expression of dynein motors and other components that can be related to differences in ciliary structure (9+2 vs. 9+0), function, and mode of ciliogenesis (IFT vs. cytoplasmic assembly) (**Figure 4A**).

Cell Type-Specific Differences in Axonemal Motors

For the dynein motor complexes, all expected metazoan outer and inner dynein subtypes are represented in the *Drosophila* genome except for the IDA d subtype (containing the DNAH1 HC in humans). Human *DNAH1* function (but not expression) appears restricted to sperm (Ben Khelifa et al., 2014). Single-headed IDAs work in pairs (dyads). In the absence of IDA d in *Drosophila*, it seems likely that this position on the axoneme is filled by another IDA form in order to complete the last IDA dyad (**Figures 2A**, **4A**).

Our analysis has revealed interesting differences between the two motile ciliated cell types. Notably, their ODA motors appear entirely distinct, being distinguished by different HC pairs, different IC DNAI2 variants and a sperm-specific LC DNAL1 variant (**Figures 2A**, **4A**). ODA motor differences presumably reflect the different functions of ciliary motility between the two cell types. In sperm, the motors must generate substantial force at a relatively low frequency for movement. In Ch neuron cilia, motors are required for the highly specialized process of auditory mechanotransduction, putatively for active mechanical amplification and probably also for sensory adaptation. In hearing, the whole antenna "quivers" in response to sound and it also generates spontaneous movements in the same frequency range in the absence of sound. It is known that these characteristics require axonemal dynein motor function within the Ch neurons (Göpfert and Robert, 2003; Newton et al., 2012; Karak et al., 2015), but the movement of Ch neuron cilia has not thus far been directly investigated. However, the Ch cilium motors must potentially respond with high temporal resolution (e.g., antennal Ch neurons are tuned to 100–300 Hz auditory stimuli; cf the ciliary beat frequency of human respiratory cilia of c.15 Hz). We propose that the Ch neuron ODA HCs (*CG9492* and *Dhc93AB*) are force generating for adaptation and amplification in mechanotransduction. Here we found that knockdown of either HC results in defective proprioception, consistent with defective Ch neuron mechanotransduction.

A second striking difference between the cell types is the presence in sperm but not Ch neuron cilia of a functional two-headed IDA I1/f dynein motor (based on the expression and

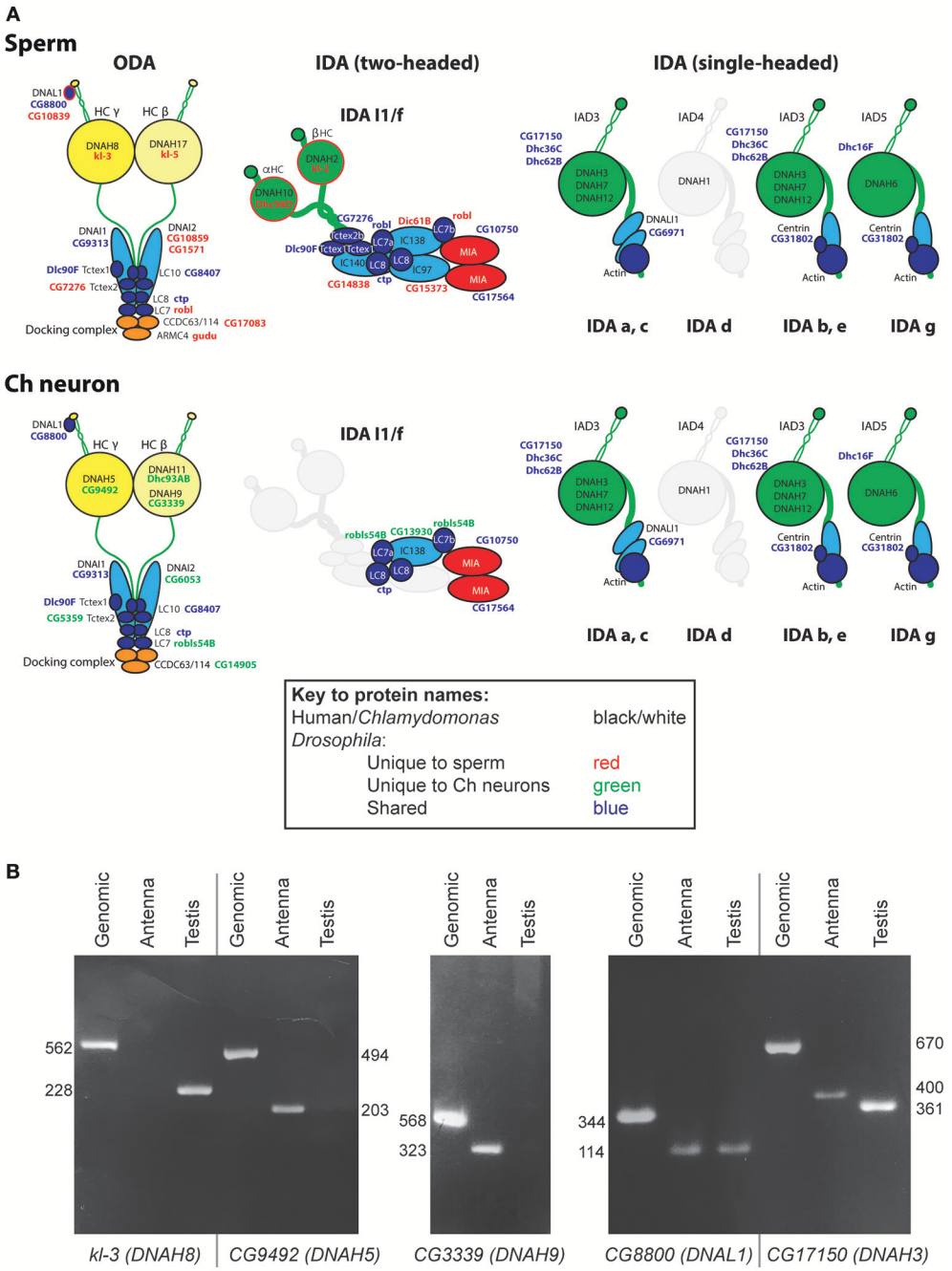

FIGURE 2 | Axonemal dyneins in *Drosophila* cell types. **(A)** Summary of dynein subunits and subtypes represented in *Drosophila* as determined by homology and transcriptome analyses. The information is mapped onto schematics representing human or *Chlamydomonas* data (gene names in black or white), with corresponding *Drosophila* gene names in blue, red or green. Blue gene names are *Drosophila* subunits that appear in common across both motile ciliated cell types; red/green gene names are *Drosophila* subunits that appear unique to one or other cell type. Only form IDA d appears to be completely missing in *Drosophila* (grayed out). The ODA complexes have some shared subunits but also many that are unique to one or other cell type (including HCs, IC2, some LCs, docking complex chains). IDA I1/f motor is largely absent from Ch neurons except for a unique homolog of IC138 (CG13930) and potentially LC7 (robls54B). In contrast, the associated MIA subunits CG10750/CG17564 are present in both sperm and Ch neurons. The association of I1/f LCs is speculative as they are largely not unique to this motor. In contrast to these motors, monomeric IDA motors seem to be common between the cell types. **(B)** RT-PCR analysis of dynein HC expression in antenna and testis. Fragment lengths are shown in base pairs.

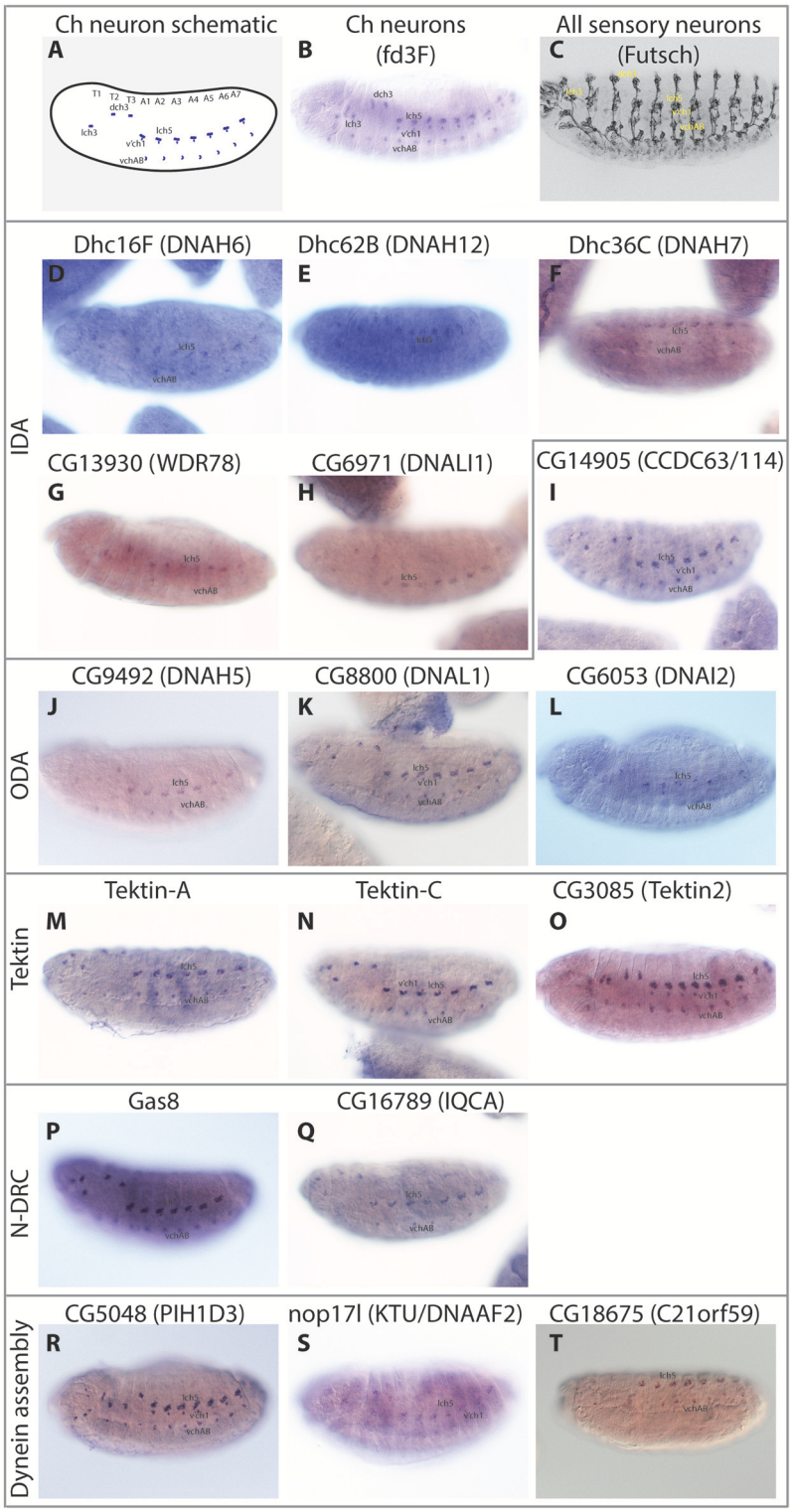

FIGURE 3 | Embryonic expression patterns of ciliary motility genes. RNA *in situ* hybridisations in stage 14–16 embryos. **(A)** Schematic of late stage embryo showing the locations of Ch neurons. **(B)** For comparison, mRNA of *fd3F*, known to be uniquely expressed in differentiating Ch neurons (Newton et al., 2012). **(C)** For comparison, expression of Futsch protein in sensory neurons. This protein is expressed in both Ch neurons and other sensory neurons with immotile cilia. **(D–T)** The remaining panels show RNA expression of selected genes. In general, all are uniquely expressed or at least enriched (*nop17l*) in a pattern consistent with the distribution of Ch neurons.

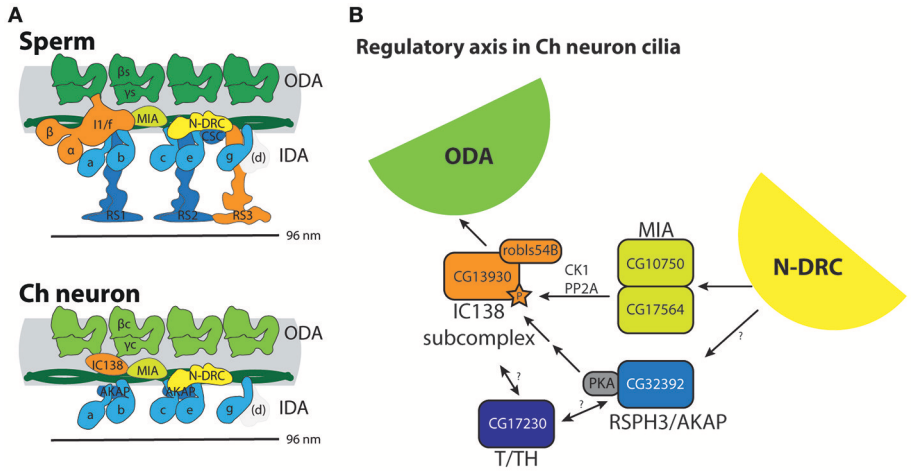

FIGURE 4 | Summary of molecular apparatus for ciliary motility in *Drosophila*, as inferred from transcriptome and genetic analysis. **(A)** The predicted complexes are mapped onto schematic representations of human motility complexes based on cryoEM (Lin et al., 2015; **Figure 1A**). **(B)** Model for a regulatory axis in Ch neuron cilia, building on functional and biochemical models proposed for *Chlamydomonas* (Gaillard et al., 2006; Wirschell et al., 2011; Yamamoto et al., 2013; Fu et al., 2018). Surprisingly, despite the lack of CP/RS and functional IDA I1/f motor, Ch neuron cilia express several factors thought to transmit regulatory information from CP/RS to I1/f as well as ODA motors.

genetic requirement of its HCs). In *Chlamydomonas* this dynein is thought to be important for regulating the size and shape of the axonemal bend, but clearly this motor function is dispensable in Ch neuron cilia.

In striking contrast to ODAs and IDA I1/f, Ch neurons and sperm appear to share the same single-headed IDA dynein subtypes. The DNAH3 homolog (CG17150) is required for hearing and male fertility (Karak et al., 2015) and we found that *Dhc16F*, *Dhc36C*, and *Dhc62B* are also required for normal proprioception and male fertility. Even for these single-headed IDAs, however, our limited expression analysis suggests that cell-type specific variations exist: we found that CG17150/DNAH3 exists as a different isoform in Ch neurons vs. sperm as a result of alternative splicing (**Figure 2B**). Therefore, dynein motor HCs vary between different cell types both in terms of presence/absence and also by the presence of cell-type specific isoforms.

Other Cell Type Differences: Differences in Function or Differences in Mode of Ciliogenesis?

Some cell type differences in motility proteins can be ascribed to their requirement for IFT during ciliogenesis, and therefore are not expressed in IFT-independent sperm. This includes the ODA late assembly proteins (*CG14127, CG14185*) and the *TTC25* homolog (*CG13502*), all of which are Ch neuron-specific and have previously been linked to IFT (Jerber et al., 2014). In addition, there are strong differences in ODA-DC proteins expressed in each cell type. This may reflect the different docking requirements of the different ODA motors in each cell type, or the need to interact with IFT machinery in Ch neuron ciliogenesis.

Interestingly, we find some differences in expression of N-DRC subunits between cell types: for example, the *DRC2* homolog, *CG30259* appears to be expressed and required only in Ch neurons. Whether this reflects cell type differences in N-DRC function or transport remains to be determined. N-DRC structure and function is only beginning to be understood in *Chlamydomonas* (Porter, 2018), and is very poorly known in other organisms. However, it has been noted that the *Chlamydomonas* homolog of *DRC2* is required for N-DRC assembly, perhaps due to its association with IFT? We suggest that *Drosophila* will be a useful model for exploring the possibility of cell type-specific differences in N-DRC.

Conversely, the observation that dynein pre-assembly factor (DNAAF) homologs are all required in both motile ciliated cell types corroborates the view that they are required for cytoplasmic pre-assembly of motors rather than for their IFT-dependent trafficking.

An Unusual Motor Regulatory Axis in Ch Neuron Cilia

In *Chlamydomonas*, part of the distinctive IDA I1/f motor forms the "IC138 regulatory subcomplex," which is thought to control motor activity and microtubule sliding based on signals transmitted from the CP/RS complex and N-DRC via the MIA complex (**Figure 1A**; Bower et al., 2009; Yamamoto et al., 2013; Hwang et al., 2018). Regulation of IC138 is partly through phosphorylation by kinases that are anchored to the axoneme via RSP3 [acting as A-kinase anchoring proteins (AKAP); Gaillard et al., 2006].

Given the absence of both CP/RS and a functional I1/f motor from Ch neuron cilia, it is highly intriguing that they express a cell-type-specific homolog of WDR78/IC138 (CG13930), as well as MIA subunits and the RSPH3/AKAP homolog. This does not appear to be an evolutionary remnant since knockdown of *CG13930* (IC138) and *CG32392* (RSPH3) each affects Ch neuron

TABLE 6 | PCD gene homologs in *Drosophila*.

Human gene	*Drosophila* gene	Expression summary	RNAi phenotype	
			Uncoordinated	Male infertile
ARMC4	*gudu*	Testis only	nd	nd
C21orf59	*CG18675*	Ch + Testis	+	+
CCDC103	*CG13202*	Ch + Testis	+	+
CCDC114	*CG17083*	Testis only	nd	nd
CCDC114	*CG14905*	Ch only	+	–
CCDC151	*CG14127*	Ch only	+	–
CCDC39	*CG17387*	Ch + Testis	+	+
CCDC40	*CG41265*	Ch + Testis	nd	nd
CCDC65	*CG30259*	Ch only	+	–
CCNO	No ortholog			
DNAAF1	*dtr*	Ch + Testis	+	+
DNAAF2/KTU	*CG1553*	Widely expressed	+	+
DNAAF3	*CG17669*	Ch + Testis	+	+
DNAH11	*Dhc93AB*	Ch only	+	–
DNAH5	*CG9492*	Ch only	+	–
DNAH8	*kl-3*	Testis only	nd	nd
DNAI1	*CG9313*	Ch + Testis	+	+
DNAI2	*CG6053*	Ch only	+	–
DNAI2	*CG10859*	Testis only	nd	nd
DNAI2	*CG1571*	Testis only	nd	nd
DNAJB13	*Dnaj-1*	Ch + Testis	nd	nd
DNAL1	*CG8800*	Ch + Testis	nd	nd
DNAL1	*CG10829*	Testis only	nd	nd
DRC1	*CG10958*	Ch + Testis	+	+
DYX1C1	*CG14921*	Ch + Testis	+	+
GAS8	*CG14271*	Ch + Testis	+	+
HEATR2	*CG31320*	Ch + Testis	+	+
HYDIN	No ortholog			
LRRC56/ODA8	*CG14185*	Ch only	nd	nd
LRRC6	*tilB*	Ch + Testis	+	+
NME8	*CG18130*	Testis only	nd	nd
RSPH1	*CG5458*	Testis only	nd	nd
RSPH3	*CG32392*	Ch + Testis	nd	nd
RSPH4A	*CG3121*	Testis only	nd	nd
RSPH9	*CG31803*	Testis only	nd	nd
SPAG1	*CG18472*	Ch + Testis	+	+
TTC25	*CG13502*	Ch + Testis	nd	nd
ZMYND10	*CG11253*	Ch + Testis	+	+

PCD gene list taken from National Health Service (NHS) gene panel v.2.0. Key to phenotypes: +, impaired; –, unaffected; nd, not determined.

function. In addition, Ch neurons express at least one homolog of T/TH complex proteins (CFAP43). Again, this is intriguing because the *Chlamydomonas* T/TH complex is associated with I1/f HCs and is proposed to provide mechanical feedback (Fu et al., 2018). However, T/TH complex is also required for IC138 phosphorylation and interacts with RSP3 (Fu et al., 2018).

Taken together, we propose that in Ch neuron cilia, IC138-RSPH3-MIA-T/TH might represent retention of this key regulatory axis for regulating ODA activity and/or the waveform of ciliary movement (**Figure 4B**). One caveat of this suggestion is that Ch neurons apparently do not express a homolog of IC140, which is required for assembly of the IC138 subcomplex in *Chlamydomonas*. However, there is evidence that IC138 also binds tubulin directly (Hendrickson et al., 2013). Further investigation would require showing that these proteins indeed localize to the Ch cilium. In *Chlamydomonas* the molecular mechanism of how dynein motor activity is regulated is very uncertain (Porter, 2018). Overall, Ch neuron cilia may provide a useful model for future analysis of this regulatory axis, and excitingly this may provide insight into the molecular mechanism

of mechanosensory amplification and frequency selectivity in these neurons.

Implications for Human Motile Cilia Biology and PCD Research

The disease PCD results from the mutation of any one of at least 40 different human genes encoding diverse components of the ciliary motility machinery (Mitchison and Valente, 2017). The high retention of ciliary motility genes in *Drosophila* is reflected in the fact that the majority of PCD-causative genes have functional *Drosophila* homologs (**Table 6**). This suggests that despite its specialized motile ciliated cell types, *Drosophila* will continue to be a useful metazoan model for PCD studies. Indeed, transcriptome and genetic analyses in *Drosophila* have recently been particularly useful to identify and validate new DNAAFs (*Zmynd10, Heatr2, Wdr92*) (Moore et al., 2013; Diggle et al., 2014; zur Lage et al., 2018). Whilst human ZMYND10 and HEATR2 are known PCD-causative genes, WDR92 remains highlighted as a PCD candidate gene based on the analysis of its *Drosophila* homolog.

As shown here, genetically supplied RNAi knockdown in developing sensory neurons (driven by *scaGal4*) and spermatocytes (driven by *BamGal4*) is quite efficient for validating the function of ciliary motility genes in *Drosophila*. RNAi analysis appears particularly effective in showing the function of genes expected to have a major effect on motility (DNAAFs, molecular ruler, etc). RNAi phenotypes as assayed in our study are less consistently clear for other structural proteins, where motility may be less severely affected by the loss of single components. Single-headed IDA HCs may fit this category: knockdown of *Dhc36C* and *Dhc62B* result in partial reduction of fertility and climbing. Similarly, mutation of *CG17150/Dnah3* caused deafness, but fertility appeared normal unless tested by a sperm competition assay (Karak et al., 2015). Of course, it is important to bear in mind that a lack of effect could also reflect incomplete effectiveness of RNAi knockdown for the lines tested rather than a partial requirement in ciliary motility. This could explain unexpectedly negative results of knockdown for some genes (e.g., *CG17564/MIA*). Follow up of specific genes identified in this study will require better characterization of knockdown efficiency, or more likely the generation of specific mutations. Nevertheless, as an initial screening tool transcriptome analysis followed by RNAi analysis is largely effective, and the conservation of ciliary machinery in *Drosophila* is such that it will continue to play a useful role in identification, validation and analysis of PCD genes.

Beyond gene discovery and validation, there is an urgent requirement for mechanistic analysis of known PCD genes. This is particularly true of DNAAFs because the possibility that they are co-chaperones for motor protein folding, stabilization and assembly raises the potential of therapeutic intervention in PCD such as "chaperone therapy." Indeed this is supported by our recent discovery in *Drosophila* that the Hsp90 co-chaperones, *Wdr92/CG14353* and *Pih1d1/CG5792* cause PCD when mutated in *Drosophila* (zur Lage et al., 2018). Neither gene is yet clearly linked to human PCD but they are strong candidates. In contrast, two other PIH domain proteins are known PCD-causative DNAAFs in humans—*KTU/DNAAF2* (Omran et al., 2008) and *PIH1D3* (Olcese et al., 2017; Paff et al., 2017). *CG5048* is the *Drosophila* ortholog of *PIH1D3*, and is highly expressed in Ch neurons and testes, and its knockdown causes strong motility phenotypes. *nop17l* is the ortholog of *DNAAF2/KTU*. Exceptionally, *nop17l* is not strongly enriched in Ch neurons and whilst expressed moderately in testes, it is also expressed strongly in other adult tissues. *nop17l* may have a broader function beyond dynein assembly in *Drosophila*. It is notable that *DNAAF2/KTU* mutations are a rare cause of PCD, suggesting that most human mutations may not be viable (Omran et al., 2008). Recent analysis in zebrafish suggests that different PIH-domain DNAAFs are required for assembly of different subsets of motors (Yamaguchi et al., 2018). We suggest that *Drosophila* will be a useful model system for understanding the complex and possibly overlapping roles of PIH-domain DNAAFs.

A major implication for PCD research stems from our clear demonstration of strong cell type specificity in dynein motor subunit expression and function. We found in *Drosophila* that dynein motor HCs vary between cell types both by their presence/absence and also in one case by presence of a cell-type specific isoforms. The severity of human PCD is variable in terms not only of the degree of impaired ciliary motility but also of co-presentation of different phenotypes. For instance, the prevalence of situs inversus varies between PCD gene mutations (Olbrich et al., 2015). How much does cell type specificity in motile gene expression/function underlie PCD phenotype variability? Given that the *Drosophila* cell-type-specific ODA HC variants correspond to specific human orthologs it is possible that cell-type-specific functional specialization of ODAs is also found in humans. However, the cell-type specific distribution and function of human dyneins is very poorly known. DNAH17 is expressed in both human and *Drosophila* sperm, but it is not known in humans whether it is restricted to sperm like it is in *Drosophila*. Human DNAH5/8/9/11 are all expressed in both respiratory cilia and sperm (Yagi and Kamiya, 2018). PCD mutations in these HC genes correlate with differences in phenotype and severity, which may reflect quantitative expression differences of these dyneins across cell-types, but so far there is no evidence for complete cell-type specificity (Yagi and Kamiya, 2018).

It is interesting that the three ODA HC genes that have been found to be mutated in PCD (DNAH5, DNAH9 and DNAH11) are orthologous to the three ODA HC genes that function in Ch neurons, despite the highly specialized nature of Ch cilium motility (Kollmar, 2016). This might suggest that Ch neurons may model human motile cilium biology better than *Drosophila* sperm.

The other major structural difference between Ch neuron cilia and sperm flagella is their 9+0 vs. 9+2 axonemal structures, and accordingly Ch neurons do not express most RS subunit genes. The absence from Ch neurons of the IDA I1/f motor complex is consistent with this, since in the *Chlamydomonas* flagellum it is regulated by signals transmitted from CP/RS and N-DRC (Viswanadha et al., 2017). It would therefore be interesting to determine whether the lack of I1/f motor is a

feature of 9+0 motile cilia more generally, including the nodal cilia of vertebrate embryos that are required for left-right axis asymmetry.

CONCLUSION

Drosophila retains almost all ciliary motility machinery, including homologs of almost all known PCD genes. There are notable differences between the two motile ciliated cell types, which might be usefully exploited in the future to further the understanding of ciliary motility. It will continue to be a useful genetic model in the future for validation and functional analysis of ciliary motility genes.

DATA AVAILABILITY STATEMENT

The microarray datasets generated for this study can be found in the Gene Expression Omnibus repository (accession: E-MTAB-7529).

AUTHOR CONTRIBUTIONS

PzL conducted most of the experiments and data analysis, contributed to experimental design, and edited the manuscript. FN carried out *in situ* hybridisations. AJ conducted data analysis, contributed to experimental design, and wrote the manuscript. All authors contributed to manuscript revision, read, and approved the submitted manuscript.

FUNDING

This research was funded by grants from the Medical Research Council of Great Britain (MR/K018558/1), Biotechnology and Biological Sciences Research Council of Great Britain (BB/M008533/1) and a Wellcome Trust ISSF3 award.

ACKNOWLEDGMENTS

We thank Panagiota Stefanopoulou, Kate Barr, Iain Savage for technical assistance. We thank the staff at Glasgow Polyomics, particularly Pavel Herzyk and Jing Wang, for the microarray analysis, and the staff of the QMRI Flow Cytometry Facility (University of Edinburgh). We are grateful to Stephen King (University of Connecticut) for comments on an early draft of this study.

SUPPLEMENTARY MATERIAL

The Supplementary Material for this article can be found online at: https://www.frontiersin.org/articles/10.3389/fgene.2019.00024/full#supplementary-material

REFERENCES

Amos, L. A. (2008). The tektin family of microtubule-stabilizing proteins. *Genome Biol.* 9:229. doi: 10.1186/gb-2008-9-7-229

Antony, D., Becker-Heck, A., Zariwala, M. A., Schmidts, M., Onoufriadis, A., Forouhan, M., et al. (2013). Mutations in CCDC39 and CCDC40 are the major cause of primary ciliary dyskinesia with axonemal disorganization and absent inner dynein arms. *Hum. Mutat.* 34, 462–472. doi: 10.1002/humu.22261

Becker-Heck, A., Zohn, I. E., Okabe, N., Pollock, A., Lenhart, K. B., Sullivan-Brown, J., et al. (2011). The coiled-coil domain containing protein CCDC40 is essential for motile cilia function and left-right axis formation. *Nat. Genet.* 43, 79–84. doi: 10.1038/ng.727

Ben Khelifa, M., Coutton, C., Zouari, R., Karaouzène, T., Rendu, J., Bidart, M., et al. (2014). Mutations in DNAH1, which encodes an inner arm heavy chain dynein, lead to male infertility from multiple morphological abnormalities of the sperm flagella. *Am. J. Hum. Genet.* 94, 95–104. doi: 10.1016/j.ajhg.2013.11.017

Bower, R., Tritschler, D., VanderWaal, K., Perrone, C. A., Mueller, J., Fox, L., et al. (2013). The N-DRC forms a conserved biochemical complex that maintains outer doublet alignment and limits microtubule sliding in motile axonemes. *Mol. Biol. Cell* 24, 1134–1152. doi: 10.1091/mbc.E12-11-0801

Bower, R., Vanderwaal, K., O 'toole, E., Fox, L., and Perrone, C., Mueller, J., et al. (2009). IC138 defines a subdomain at the base of the I1 dynein that regulates microtubule sliding and flagellar motility. *Mol. Biol. Cell* 20, 3055–3063. doi: 10.1091/mbc.E09

Cachero, S., Simpson, T. I., zur Lage, P. I., Ma, L., Newton, F. G., Holohan, E. E., et al. (2011). The gene regulatory cascade linking proneural specification with differentiation in Drosophila sensory neurons. *PLoS Biol.* 9:e1000568. doi: 10.1371/journal.pbio.1000568

Carvalho, A. B., Lazzaro, B. P., and Clark, A. G. (2000). Y chromosomal fertility factors kl-2 and kl-3 of *Drosophila melanogaster* encode dynein heavy chain polypeptides. *Proc. Natl. Acad. Sci. U.S.A.* 97, 13239–13244. doi: 10.1073/pnas.230438397

Diggle, C. P., Moore, D. J., Mali, G., zur Lage, P., Ait-Lounis, A., Schmidts, M., et al. (2014). HEATR2 plays a conserved role in assembly of the ciliary motile apparatus. *PLoS Genet.* 10:e1004577. doi: 10.1371/journal.pgen.1004577

Dong, F., Shinohara, K., Botilde, Y., Nabeshima, R., Asai, Y., Fukumoto, A., et al. (2014). Pih1d3 is required for cytoplasmic preassembly of axonemal dynein in mouse sperm. *J. Cell Biol.* 204, 203–213. doi: 10.1083/jcb.201304076

Dymek, E. E., Heuser, T., Nicastro, D., and Smith, E. F. (2011). The CSC is required for complete radial spoke assembly and wild-type ciliary motility. *Mol. Biol. Cell* 22, 2520–2531. doi: 10.1091/mbc.E11-03-0271

Fatima, R. (2011). Drosophila dynein intermediate chain gene, Dic61B, is required for spermatogenesis. *PLoS ONE* 6:e27822. doi: 10.1371/journal.pone.0027822

Fok, A. K., Wang, H., Katayama, A., Aihara, M. S., and Allen, R. D. (1994). 22S axonemal dynein is preassembled and functional prior to being transported to and attached on the axonemes. *Cell Motil. Cytoskeleton* 29, 215–224. doi: 10.1002/cm.970290304

Fowkes, M. E., and Mitchell, D. R. (1998). The role of preassembled cytoplasmic complexes in assembly of flagellar dynein subunits. *Mol. Biol. Cell* 9, 2337–47.

Fu, G., Wang, Q., Phan, N., Urbanska, P., Joachimiak, E., Lin, J., et al. (2018). The I1 dynein-associated tether and tether head complex is a conserved regulator of ciliary motility. *Mol. Biol. Cell* 29, 1003–1152. doi: 10.1091/mbc.E18-02-0142

Gaillard, A. A., Fox, L. A., Rhea, J. M., Craige, B., and Sale, W. S. (2006). Disruption of the A-kinase anchoring domain in flagellar radial spoke protein 3 results in unregulated axonemal cAMP-dependent protein kinase activity and abnormal flagellar motility. *Mol. Biol. Cell* 17, 2626–2635. doi: 10.1091/mbc.E06-02-0095

Göpfert, M. C., and Robert, D. (2003). Motion generation by Drosophila mechanosensory neurons. *Proc. Natl. Acad. Sci. U. S. A.* 100, 5514–5519. doi: 10.1073/pnas.0737564100

Han, Y. G., Kwok, B. H., and Kernan, M. J. (2003). Intraflagellar transport is required in drosophila to differentiate sensory cilia but not sperm. *Curr. Biol.* 13, 1679–1686. doi: 10.1016/j.cub.2003.08.034

Hendrickson, T. W., Goss, J. L., Seaton, C. A., and Rohrs, H. W. (2013). The IC138 and IC140 intermediate chains of the I1 axonemal dynein complex bind

directly to tubulin. *Biochim. Biophys. Acta Mol. Cell Res.* 1833, 3265–3271. doi: 10.1016/j.bbamcr.2013.09.011

Hirose, K., and Amos, L. (2012). *Handbook of Dynein*. Singapore: Pan Stanford Publishing Pte Ltd.

Hjeij, R., Lindstrand, A., Francis, R., Zariwala, M. A., Liu, X., Li, Y., et al. (2013). ARMC4 mutations cause primary ciliary dyskinesia with randomization of left/right body asymmetry. *Am. J. Hum. Genet.* 93, 357–367. doi: 10.1016/j.ajhg.2013.06.009

Hjeij, R., Onoufriadis, A., Watson, C. M., Slagle, C. E., Klena, N. T., Dougherty, G. W., et al. (2014). CCDC151 mutations cause primary ciliary dyskinesia by disruption of the outer dynein arm docking complex formation. *Am. J. Hum. Genet.* 95, 257–274. doi: 10.1016/j.ajhg.2014.08.005

Hom, E. F., Witman, G. B., Harris, E. H., Dutcher, S. K., Kamiya, R., Mitchell, D. R., et al. (2011). A unified taxonomy for ciliary dyneins. *Cytoskeleton* 68, 555–565. doi: 10.1002/cm.20533

Horani, A., Brody, S. L., Ferkol, T. W., Shoseyov, D., Wasserman, M. G., Tashma, A., et al. (2013). CCDC65 mutation causes primary ciliary dyskinesia with normal utrastructure and hyperkinetic cilia. *PLoS ONE* 8:e72299. doi: 10.1371/journal.pone.0072299

Hu, Y., Flockhart, I., Vinayagam, A., Bergwitz, C., Berger, B., Perrimon, N., et al. (2011). An integrative approach to ortholog prediction for disease-focused and other functional studies. *BMC Bioinformatics* 12:357. doi: 10.1186/1471-2105-12-357

Hwang, J., Hunter, E. L., Sale, W. S., and Wirschell, M. (2018). "Control of axonemal inner dynein arms," in *Dyneins: The Biology of Dynein Motors, 2nd Edn,* ed S. M. King (Cambridge, MA: Academic Press), 271–297. doi: 10.1016/B978-0-12-809471-6.00009-7

Jeanson, L., Thomas, L., Copin, B., Coste, A., Sermet-Gaudelus, I., Dastot-Le Moal, F., et al. (2016). Mutations in GAS8, a gene encoding a nexin-dynein regulatory complex subunit, cause primary ciliary dyskinesia with axonemal disorganization. *Hum. Mutat.* 37, 776–785. doi: 10.1002/humu.23005

Jerber, J., Baas, D., Soulavie, F., Chhin, B., Cortier, E., Vesque, C., et al. (2014). The coiled-coil domain containing protein CCDC151 is required for the function of IFT-dependent motile cilia in animals. *Hum. Mol. Genet.* 23, 563–577. doi: 10.1093/hmg/ddt445

Karak, S., Jacobs, J. S., Kittelmann, M., Spalthoff, C., Katana, R., Sivan-Loukianova, E., et al. (2015). Diverse roles of axonemal dyneins in drosophila auditory neuron function and mechanical amplification in hearing. *Sci. Rep.* 5:17085. doi: 10.1038/srep17085

Kavlie, R. G., Kernan, M. J., and Eberl, D. F. (2010). Hearing in drosophila requires TilB, a conserved protein associated with ciliary motility. *Genetics* 185, 177–188. doi: 10.1534/genetics.110.114009

King, S. M. (2016). Axonemal dynein arms. *Cold Spring Harb. Perspect. Biol.* 8:a028100. doi: 10.1101/cshperspect.a028100

King, S. M., and Patel-King, R. S. (2015). The oligomeric outer dynein arm assembly factor CCDC103 is tightly integrated within the ciliary axoneme and exhibits periodic binding to microtubules. *J. Biol. Chem.* 290, 7388–7401. doi: 10.1074/jbc.M114.616425

Knowles, M. R., Leigh, M. W., Ostrowski, L. E., Huang, L., Carson, J. L., Hazucha, M. J., et al. (2013). Exome sequencing identifies mutations in CCDC114 as a cause of primary ciliary dyskinesia. *Am. J. Hum. Genet.* 92, 99–106. doi: 10.1016/j.ajhg.2012.11.003

Kollmar, M. (2016). Fine-tuning motile cilia and flagella: Evolution of the dynein motor proteins from plants to humans at high resolution. *Mol. Biol. Evol.* 33, 3249–3267. doi: 10.1093/molbev/msw213

Laurençon, A., Dubruille, R., Efimenko, E., Grenier, G., Bissett, R., Cortier, E., et al. (2007). Identification of novel regulatory factor X (RFX) target genes by comparative genomics in Drosophila species. *Genome Biol.* 8:R195. doi: 10.1186/gb-2007-8-9-r195

Lewis, W. R., Malarkey, E. B., Tritschler, D., Bower, R., Pasek, R. C., Porath, J. D., et al. (2016). Mutation of growth arrest specific 8 reveals a role in motile cilia function and human disease. *PLoS Genet.* 12:e1006220. doi: 10.1371/journal.pgen.1006220

Lin, J., Yin, W., Smith, M. C., Song, K., Leigh, M. W., Zariwala, M. A., et al. (2015). Cryo-electron tomography reveals ciliary defects underlying human RSPH1 primary ciliary dyskinesia. *Nat. Commun.* 5:5727. doi: 10.1038/ncomms6727

Linck, R., Fu, X., Lin, J., Ouch, C., Schefter, A., Steffen, W., et al. (2014). Insights into the structure and function of ciliary and flagellar doublet microtubules: tektins, Ca2+-binding proteins, and stable protofilaments. *J. Biol. Chem.* 289, 17427–17444. doi: 10.1074/jbc.M114.568949

Merveille, A. C., Davis, E. E., Becker-Heck, A., Legendre, M., Amirav, I., Bataille, G., et al. (2011). CCDC39 is required for assembly of inner dynein arms and the dynein regulatory complex and for normal ciliary motility in humans and dogs. *Nat. Genet.* 43, 72–78. doi: 10.1038/ng.726

Mitchell, D. R. (2017). Evolution of cilia. *Cold Spring Harb. Perspect. Biol.* 9:a028290. doi: 10.1101/cshperspect.a028290

Mitchison, H. M., and Valente, E. M. (2017). Motile and non-motile cilia in human pathology: from function to phenotypes. *J. Pathol.* 241, 294–309. doi: 10.1002/path.4843

Moore, D. J., Onoufriadis, A., Shoemark, A., Simpson, M. A., Zur Lage, P. I., De Castro, S. C., et al. (2013). Mutations in ZMYND10, a gene essential for proper axonemal assembly of inner and outer dynein arms in humans and flies, cause primary ciliary dyskinesia. *Am. J. Hum. Genet.* 93, 346–356. doi: 10.1016/j.ajhg.2013.07.009

Neisch, A. L., Avery, A. W., Min-Gang, L., and Hays, T. S. (2018). "Drosophila cytoplasmic dynein: mutations, tools, and developmental functions," in *Dyneins: The Biology of Dynein Motors, 2nd Edn*, ed S. M. King (Cambridge, MA: Academic Press), 569–627. doi: 10.1016/B978-0-12-809471-6.00021-8

Newton, F. G., zur Lage, P. I., Karak, S., Moore, D. J., Göpfert, M. C., and Jarman, A. P. (2012). Forkhead transcription factor Fd3F cooperates with Rfx to regulate a gene expression program for mechanosensory cilia specialization. *Dev. Cell* 22, 1221–1233. doi: 10.1016/j.devcel.2012.05.010

Oda, T., Abe, T., Yanagisawa, H., and Kikkawa, M. (2016). Docking complex-independent alignment of outer dynein arms with 24-nm periodicity *in vitro*. *J. Cell Sci.* 103, 1547–1551. doi: 10.1242/jcs.184598

Oda, T., Yanagisawa, H., Kamiya, R., and Kikkawa, M. (2014a). A molecular ruler determines the repeat length in eukaryotic cilia and flagella. *Science* 346, 857–860. doi: 10.1126/science.1260214

Oda, T., Yanagisawa, H., Yagi, T., and Kikkawa, M. (2014b). Mechanosignaling between central apparatus and radial spokes controls axonemal dynein activity. *J. Cell Biol.* 204, 807–819. doi: 10.1083/jcb.201312014

Olbrich, H., Cremers, C., Loges, N. T., Werner, C., Nielsen, K. G., Marthin, J. K., et al. (2015). Loss-of-function GAS8 mutations cause primary ciliary dyskinesia and disrupt the nexin-dynein regulatory complex. *Am. J. Hum. Genet.* 97, 546–554. doi: 10.1016/j.ajhg.2015.08.012

Olcese, C., Patel, M. P., Shoemark, A., Kiviluoto, S., Legendre, M., Williams, H. J., et al. (2017). X-linked primary ciliary dyskinesia due to mutations in the cytoplasmic axonemal dynein assembly factor PIH1D3. *Nat. Commun.* 8:14279. doi: 10.1038/ncomms14279

Omran, H., Kobayashi, D., Olbrich, H., Tsukahara, T., Loges, N. T., Hagiwara, H., et al. (2008). Ktu/PF13 is required for cytoplasmic pre-assembly of axonemal dyneins. *Nature* 456, 611–616. doi: 10.1038/nature07471

Onoufriadis, A., Paff, T., Antony, D., Shoemark, A., Micha, D., Kuyt, B., et al. (2013). Splice-site mutations in the axonemal outer dynein arm docking complex gene CCDC114 cause primary ciliary dyskinesia. *Am. J. Hum. Genet.* 92, 88–98. doi: 10.1016/j.ajhg.2012.11.002

Onoufriadis, A., Shoemark, A., Munye, M. M., James, C. T., Schmidts, M., Patel, M., et al. (2014). Combined exome and whole-genome sequencing identifies mutations in ARMC4 as a cause of primary ciliary dyskinesia with defects in the outer dynein arm. *J. Med. Genet.* 51, 61–67. doi: 10.1136/jmedgenet-2013-101938

Paff, T., Loges, N. T., Aprea, I., Wu, K., Bakey, Z., Haarman, E. G., et al. (2017). Mutations in PIH1D3 Cause X-linked primary ciliary dyskinesia with outer and inner dynein arm defects. *Am. J. Hum. Genet.* 100, 160–168. doi: 10.1016/j.ajhg.2016.11.019

Panizzi, J. R., Becker-Heck, A., Castleman, V. H., Al-Mutairi, D. A., Liu, Y., Loges, N. T., et al. (2012). CCDC103 mutations cause primary ciliary dyskinesia by disrupting assembly of ciliary dynein arms. *Nat. Genet.* 44, 714–719. doi: 10.1038/ng.2277

Porter, M. E. (2018). "Ciliary and flagellar motility and the nexin-dynein regulatory complex," in *Dyneins: The Biology of Dynein Motors, 2nd Edn.*, ed S. M. King (Cambridge, MA: Academic Press), 299–335. doi: 10.1016/B978-0-12-809471-6.00010-3

Rasmusson, K., Serr, M., Gepner, J., Gibbons, I., and Hays, T. S. (1994). A family of dynein genes in *Drosophila melanogaster*. *Mol. Biol. Cell* 5, 45–55. doi: 10.1091/mbc.5.1.45

Robinson, S. W., Herzyk, P., Dow, J. A., and Leader, D. P. (2013). FlyAtlas: database of gene expression in the tissues of *Drosophila melanogaster*. *Nucleic Acids Res.* 41, D744–D750. doi: 10.1093/nar/gks1141.

Sarpal, R., Todi, S. V., Sivan-Loukianova, E., Shirolikar, S., Subramanian, N., Raff, E. C., et al. (2003). Drosophila KAP interacts with the kinesin II motor subunit KLP64D to assemble chordotonal sensory cilia, but not sperm tails. *Curr. Biol.* 13, 1687–1696. doi: 10.1016/j.cub.2003.09.025

Senthilan, P. R., Piepenbrock, D., Ovezmyradov, G., Nadrowski, B., Bechstedt, S., Pauls, S., et al. (2012). Drosophila auditory organ genes and genetic hearing defects. *Cell* 150, 1042–1054. doi: 10.1016/j.cell.2012.06.043

Tanaka, H., Iguchi, N., Toyama, Y., Kitamura, K., Takahashi, T., Kaseda, et al. (2004). Mice deficient in the axonemal protein Tektin-t exhibit male infertility and immotile-cilium syndrome due to impaired inner arm dynein function. *Mol. Cell. Biol.* 18, 7958–7964. doi: 10.1128/MCB.24.18.7958-7964.2004

Viswanadha, R., Hunter, E. L., Yamamoto, R., Wirschell, M., Alford, L. M., Dutcher, S. K., et al. (2014). The ciliary inner dynein arm, I1 dynein, is assembled in the cytoplasm and transported by IFT before axonemal docking. *Cytoskeleton* 71, 573–586. doi: 10.1002/cm.21192

Viswanadha, R., Sale, W. S., and Porter, M. E. (2017). Ciliary motility: regulation of axonemal dynein motors. *Cold Spring Harb. Perspect. Biol.* 9:a018325. doi: 10.1101/cshperspect.a018325

Wallmeier, J., Shiratori, H., Dougherty, G. W., Edelbusch, C., Hjeij, R., Loges, N. T., et al. (2016). TTC25 deficiency results in defects of the outer dynein arm docking machinery and primary ciliary dyskinesia with left-right body asymmetry randomization. *Am. J. Hum. Genet.* 99, 460–469. doi: 10.1016/j.ajhg.2016.06.014

Wickstead, B., and Gull, K. (2007). Dyneins across eukaryotes: a comparative genomic analysis. *Traffic* 8, 1708–1721. doi: 10.1111/j.1600-0854.2007.00646.x

Wirschell, M., Olbrich, H., Werner, C., Tritschler, D., Bower, R., Sale, W. S., et al. (2013). The nexin-dynein regulatory complex subunit DRC1 is essential for motile cilia function in algae and humans. *Nat. Genet.* 45, 262–268. doi: 10.1038/ng.2533

Wirschell, M., Yamamoto, R., Alford, L., Gokhale, A., Gaillard, A., and Sale, W. S. (2011). Regulation of ciliary motility: Conserved protein kinases and phosphatases are targeted and anchored in the ciliary axoneme. *Arch. Biochem. Biophys.* 510, 93–100. doi: 10.1016/j.abb.2011.04.003

Yagi, T., and Kamiya, R. (2018). "Genetic approaches to axonemal dynein function in Chlamydomonas and other organisms," in *Dyneins: The Biology of Dynein Motors, 2nd Edn*, ed S. M. King (Cambridge, MA: Academic Press). doi: 10.1016/B978-0-12-809471-6.00007-3

Yamaguchi, H., Oda, T., Kikkawa, M., and Takeda, H. (2018). Systematic studies of all PIH proteins in zebrafish reveal their distinct roles in axonemal dynein assembly. *Elife* 7:e36979. doi: 10.7554/eLife.36979

Yamamoto, R., Song, K., Yanagisawa, H. A., Fox, L., Yagi, T., Wirschell, M., et al. (2013). The MIA complex is a conserved and novel dynein regulator essential for normal ciliary motility. *J. Cell Biol.* 201, 263–278. doi: 10.1083/jcb.201211048

zur Lage, P. I., and Jarman, A. P. (2010). The function and regulation of the bHLH gene, cato, in *Drosophila neurogenesis*. *BMC Dev. Biol.* 10:34. doi: 10.1186/1471-213X-10-34

zur Lage, P. I., Simpson, T. I., and Jarman, A. (2011). Linking specification to differentiation: from proneural genes to the regulation of ciliogenesis. *Fly* 5, 322–326. doi: 10.4161/fly.5.4.16159

zur Lage, P. I., Stefanopoulou, P., Styczynska-Soczka, K., Quinn, N., Mali, G., von Kriegsheim, A., et al. (2018). Ciliary dynein motor preassembly is regulated by Wdr92 in association with HSP90 co-chaperone, R2TP. *J. Cell Biol.* 218:2583 doi: 10.1083/jcb.201709026

Conflict of Interest Statement: The authors declare that the research was conducted in the absence of any commercial or financial relationships that could be construed as a potential conflict of interest.

frontiers in Genetics

METHODS
published: 12 February 2019
doi: 10.3389/fgene.2019.00075

Microscopy-Based Automated Live Cell Screening for Small Molecules That Affect Ciliation

Peishan Zhang[1,2†], Anna A. Kiseleva[2,3†], Vladislav Korobeynikov[2,4], Hanqing Liu[1], Margret B. Einarson[2] and Erica A. Golemis[2*]*

[1] School of Pharmacy, Jiangsu University, Zhenjiang, China, [2] Molecular Therapeutics Program, Fox Chase Cancer Center, Philadelphia, PA, United States, [3] Department of Biochemistry and Biotechnology, Kazan Federal University, Kazan, Russia, [4] Department of Pathology and Cell Biology, Columbia University, New York, NY, United States

OPEN ACCESS

Edited by:
Sonia Mulero Navarro,
Universidad de Extremadura, Spain

Reviewed by:
Max Christoph Liebau,
Universitätsklinikum Köln, Germany
Frederic Becq,
University of Poitiers, France
Giovanni Vozzi,
University of Pisa, Italy

***Correspondence:**
Hanqing Liu
hanqing@ujs.edu.cn
Erica A. Golemis
Erica.Golemis@fccc.edu

[†] These authors have contributed equally to this work

Specialty section:
This article was submitted to Genetic Disorders, a section of the journal Frontiers in Genetics

Received: 30 August 2018
Accepted: 28 January 2019
Published: 12 February 2019

Citation:
Zhang P, Kiseleva AA, Korobeynikov V, Liu H, Einarson MB and Golemis EA (2019) Microscopy-Based Automated Live Cell Screening for Small Molecules That Affect Ciliation. Front. Genet. 10:75. doi: 10.3389/fgene.2019.00075

The primary monocilium, or cilium, is a single antenna-like organelle that protrudes from the surface of most mammalian cell types, and serves as a signaling hub. Mutations of cilia-associated genes result in severe genetic disorders termed ciliopathies. Among these, the most common is autosomal dominant polycystic kidney disease (ADPKD); less common genetic diseases include Bardet–Biedl syndrome, Joubert syndrome, nephronophthisis, and others. Important signaling cascades with receptor systems localized exclusively or in part at cilia include Sonic Hedgehog (SHH), platelet derived growth factor alpha (PDGFRα), WNTs, polycystins, and others. Changes in ciliation during development or in pathological conditions such as cancer impacts signaling by these proteins. Notably, ciliation status of cells is coupled closely to the cell cycle, with cilia protruding in quiescent (G0) or early G1 cells, declining in S/G2, and absent in M phase, and has been proposed to contribute to cell cycle regulation. Because of this complex biology, the elaborate machinery regulating ciliary assembly and disassembly receives input from many cellular proteins relevant to cell cycle control, development, and oncogenic transformation, making study of genetic factors and drugs influencing ciliation of high interest. One of the most effective tools to investigate the dynamics of the cilia under different conditions is the imaging of live cells. However, developing assays to observe the primary cilium in real time can be challenging, and requires a consideration of multiple details related to the cilia biology. With the dual goals of identifying small molecules that may have beneficial activity through action on human diseases, and of identifying ciliary activities of existing agents that are in common use or development, we here describe creation and evaluation of three autofluorescent cell lines derived from the immortalized retinal pigmented epithelium parental cell line hTERT-RPE1. These cell lines stably express the ciliary-targeted fluorescent proteins L13-Arl13bGFP, pEGFP-mSmo, and tdTomato-MCHR1-N-10. We then describe methods for use of these cell lines in high throughput screening of libraries of small molecule compounds to identify positive and negative regulators of ciliary disassembly.

Keywords: ciliary disassembly, high content imaging, drugs, ADPKD, targeted therapy, aurora kinase A, heat shock protein 90, screening

INTRODUCTION

Primary cilia, also known as monocilia, are evolutionarily conserved, antenna-like organelles that protrude from the cell surface of almost all types of mammalian cell types, with limited exceptions (e.g., lymphocytes). Ciliated cells were a topic of considerable interest as early as the first half of the 19th century (Sharpey, 1835). For much of the first part of the 20th century, cilia were considered vestigial organelles, of unclear functionality. Starting in 1960s, a growing number of studies noted variations in ciliation across distinct cell types, and in relationship to proliferative state of cells. These studies led to a focus on the machinery governing ciliation, and to investigation of whether ciliary state in turn could reciprocally affect proliferation or other aspects of cell signaling. Early and ongoing studies have defined the cilium as an organelle important for mechano- and chemosensation, with mechanisms of signal transduction in some cases well defined, and in other cases still unclear (Seeger-Nukpezah and Golemis, 2012; Delling et al., 2016; Nag and Resnick, 2017; Spasic and Jacobs, 2017). Signaling receptors concentrated or exclusively localized to cilia make this organelle an important platform for the signal transduction, associated with Hedgehog (HH), WNT, Notch, and platelet derived growth factor alpha (PDGFRα) signaling pathways (Goetz et al., 2009; Liu et al., 2018), among others.

Detailed studies of ciliation patterns led to the recognition that this organelle undergoes assembly and disassembly dependent on cell cycle phase. Mammalian cells undergoing mitosis are invariably unciliated. Assembly of the primary cilium initiates immediately after mitotic exit in early G1 phase, and is most notable in cells that become quiescent, entering G0. Ciliary disassembly or resorption commonly occurs in S or G2 phase, although there is variation dependent on specific cell backgrounds. This timing of ciliary assembly/protrusion and disassembly/resorption in part reflects the fact that the ciliary structure emanates from a basal body, that nucleates the nine paired microtubular bundles that constitute the core of the central ciliary axoneme. The basal body is derived from the mother centriole of the centriolar pair present in the cell following cytokinesis, based on a process of differentiation. In the early stages of ciliary assembly, Golgi-derived vesicles localize to the vicinity of the mother centriole, which associates with specific accessory proteins that form distal appendages associated with the nascent basal body. The recruitment of targeted vesicles contributes to the formation of new membrane and transport of ciliary localized proteins, organized around the axonemal shaft. Specific members of the intraflagellar transport (IFT) particle protein family traffic ciliary components along the axoneme, elongating the axoneme itself and concentrating specific cilia-associated proteins on the membrane of the mature cilium (Pedersen et al., 2008). This process is reversed during ciliary disassembly, releasing the basal body from distal appendages and other cilia-specific proteins. The centrioles then undergo a discrete differentiation process involving association with a distinct group of proteins that allow it to act as a centrosome, duplicate, nucleate cytoplasmic microtubules and signaling complexes during interphase, and act as a microtubule organizing center (MTOC) that anchors the bipolar spindle during mitosis.

Because of the need to exactly synchronize ciliary assembly/disassembly cycles with cell cycle, the process is highly regulated through the activity of protein kinases and other enzymes that modify the IFT proteins, the axonemal microtubules, the cargo to be transported to the cilia, and other relevant proteins. Mechanistic details of these processes have been extensively reviewed (Cao et al., 2009; Ishikawa and Marshall, 2017; Korobeynikov et al., 2017; Nachury, 2018). Additional sources of regulation relevant to cilia include control of ciliary length, which is partially but not completely linked to cell cycle status, and can influence the strength of response to extracellular stimuli with ciliary receptor systems (Chien et al., 2018; Drummond et al., 2018). Definition of the cellular signals regulating ciliation has been a topic of much interest. Activation of the Aurora-A (AURKA) kinase has been shown to be a proximal signal for ciliary disassembly, based on interactions with its partners HEF1/NEDD9, and other proteins (Pugacheva and Golemis, 2006; Pugacheva et al., 2007; Plotnikova et al., 2012). As cells emerge from G0/quiescence in response to the addition of growth factors, multiple upstream signaling systems transiently activate AURKA at the basal body; conversely, a separate set of signaling proteins restrains AURKA activity, and collaborates to promote ciliary protrusion, following cytokinesis (reviewed in Korobeynikov et al., 2017). As the knowledge of which proteins regulate ciliary formation and resorption has gradually become more detailed, it has become apparent that many of the proteins involved were first defined based on roles in other biological processes (**Figure 1**).

Disassembly of the primary cilium is associated with the cell cycle and starts when cells exit G1/G0 phase. At the early stages, in a response to growth factors stimuli, the disassembly of the primary cilium is associated with the de-polymerization of the axoneme microtubules, which is partially controlled by an activation of kinesin superfamily protein 2A (KIF2A) and polo-like kinase-1 (PLK1) (Seeger-Nukpezah et al., 2012; Miyamoto et al., 2015). Another key event in cilium disassembly is the activation of Aurora A kinase (AURKA) at the basal body by a scaffolding protein NEDD9, which in turn activates HDAC6 and promotes de-acetylation of the axoneme tubulins with following destabilization of the axoneme microtubules (Pugacheva et al., 2007). Activation of AURKA in disassembly is also promoted by trichoplein (TCHP; Inoko et al., 2012) and other proteins (Korobeynikov et al., 2017). Some of these proteins act continuously to inhibit cilia assembly during cell cycle, including TCHP and nuclear distribution gene E homolog 1 (NDE1); the latter is expressed at high levels during mitosis and suppresses retrograde IFT complexes movement to suppress cilia formation (Kim et al., 2011).

Further ciliary regulatory systems control the specific localization of components of discrete signaling systems to the cilia, which can profoundly influence the activity of signaling pathways. In one of the best studied examples, the extracellular factor Sonic Hedgehog (SHH) binds to a ciliary localized receptor, Patched (PTCH1). In the absence of SHH binding, ciliary PTCH1 normally represses the activity of a downstream signaling

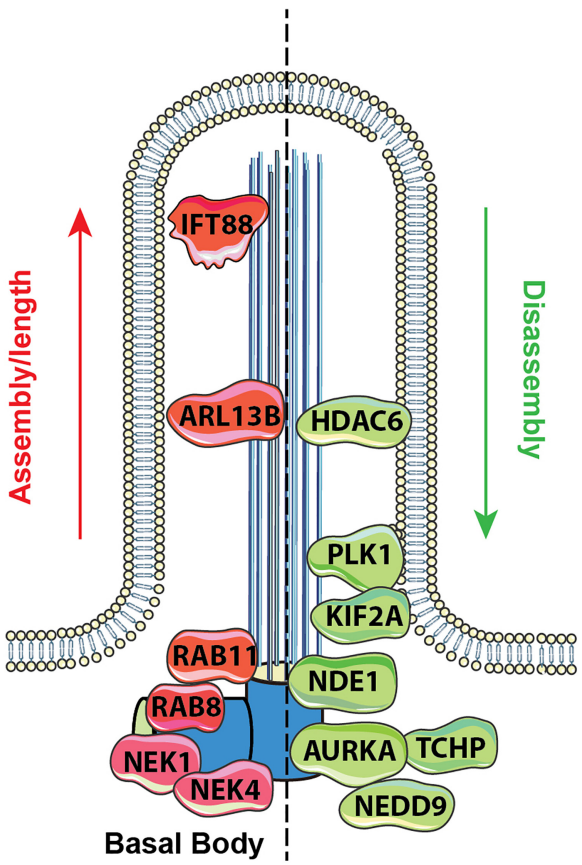

FIGURE 1 | Proteins regulating ciliary assembly and disassembly. Mechanisms of ciliary dynamics are complex and require the orchestrated action of numerous proteins. Some examples of proteins regulating ciliary protrusion (red) and resorption (green) are shown. The Rab GTPases (e.g., Rab8 and Rab11) are active at the early stages of cilia formation, promoting targeted vesicular trafficking required for the primary ciliogenesis (Knodler et al., 2010). Assembly of the primary cilium is highly dependent on the proper functioning of the IFT – a bidirectional movement throughout the axonemal microtubules which is essential for cilium elongation and maintenance. One of the key proteins controlling IFT-dependent ciliogenesis is IFT protein 88 homolog (IFT88); mutations inactivating IFT88 to an abnormally short cilia phenotype and development of polycystic kidney disease (Pazour et al., 2000). The movement of IFT particles along the microtubules is supported by a group of microtubule-based motors, which include kinesin family proteins (KIFs), providing anterograde transport (toward the cilia tip) and dynein family proteins (DYNs), providing retrograde transport (toward the cilia base). Cilia formation is also controlled by NIMA-related kinases (NRKs), namely, Nek1 and Nek4, which are often determined as mitotic kinases (Mahjoub et al., 2005; Coene et al., 2011). Additionally, ciliogenesis is regulated by small GTPases, including Arl13b, which localizes exclusively to the primary cilium, where it stabilizes the association between IFT-A and IFT-B complexes (Li et al., 2010).

cascade dependent on the GLI family of transcription factors; however, following SHH-PTCH1 interactions at cilia, PTCH1 translocates from the cilium, and Smoothened (SMO) enters, where it interacts with and activates GLI transcription factors (Bangs and Anderson, 2017). Because of this and other ciliary signaling receptor systems, control of ciliation is relevant to a number of clinically significant human pathological conditions (Pan et al., 2013).

Ciliopathies comprise a group of disorders associated with genetic mutations causing defects in ciliary structure or signaling, affect a significant number of individuals. Over 35 types of ciliopathy have been defined (Reiter and Leroux, 2017). The most common ciliopathy, autosomal dominant polycystic kidney disease (ADPKD), affects 1 in 500 people, and currently lacks effective treatments. Recent developments raise the possibility that targeting ciliation may be useful in slowing the course or alleviating the symptoms of at least some forms of this disease (Ma et al., 2013; Nikonova et al., 2018). Other less frequent ciliopathies associated with severe symptoms include Bardet–Biedl syndrome (BBS; Zaghloul and Katsanis, 2009), Meckel–Gruber syndrome, Joubert syndrome, and others (Mitchison and Valente, 2017); these also would benefit from better knowledge of, and tools to manipulate, ciliation. In other conditions, such as cancer, manipulation of ciliation has the potential to disrupt or intensify signaling axes relevant to disease formation, progression, and response to treatment (discussed extensively in Liu et al., 2018).

Of the mammalian proteins defined as regulating ciliation, a number have been shown to have causative or pro-oncogenic roles in cancer, and in some cases, targeted drugs designed to inhibit their activity have been developed. Notably, some of these drugs have been found to strongly influence either ciliation, or the trafficking of cellular signaling proteins to cilia. For example, the AURKA inhibitor alisertib increases cilia length and prevents ciliary resorption *in vitro* and *in vivo* (Pugacheva et al., 2007; Nikonova et al., 2014). Conversely, ganetespib, an inhibitor of heat shock protein 90 (HSP90) inhibits proteasomal degradation of NEK8 and the AURKA activator trichoplein, causing AURKA activation and promoting loss of ciliation, *in vitro* and *in vivo* (Seeger-Nukpezah et al., 2013; Nikonova et al., 2018). The control of ciliary dynamics remains far from completely defined; surprisingly, a recent study screening 1600 small molecule compounds in a human pancreatic cell line, CFPAC-1, identified 118 cilium-enhancing compounds for which no prior activity at cilia had been identified (Khan et al., 2016), suggesting modulation of ciliation status may not be an uncommon on-target or off-target effect of drugs of clinical interest. If so, it is considerable interest to be able to identify such compounds efficiently, as they may have unexpected "off-target" activities based on control of ciliary signaling systems such as SHH, which has important autocrine signaling in some cell types, and also plays an important role in paracrine signaling between various cell types, in both normal and pathogenic growth conditions (Lee et al., 2014; Tape et al., 2016; Bangs and Anderson, 2017). In one example particularly relevant to ciliopathies, treatment of a mouse model for ADPKD with an AURKA inhibitor under evaluation in the clinic blocked ciliary disassembly and significantly exacerbated disease symptoms (Nikonova et al., 2014), emphasizing the potential risks of perturbing ciliation with such genetic disorders.

There are many model systems that have been used for screening to detect modifiers of ciliation. Over the past

40 years, genetic and biochemical experiments performed in the unicellular alga *Chlamydomonas reinhardi* (Lefebvre and Rosenbaum, 1986), the nematode *Caenorhabditis elegans* (Muller et al., 2011), in *Danio rerio* (zebrafish) (Malicki et al., 2011), and others (Vincensini et al., 2011) have yielded critical information about genes regulating ciliary formation and length control. Our focus here is on the evaluation of small molecule agents relevant to humans and potentially other mammalian cancer models. For this purpose, to avoid potentially misleading results arising from imperfect conservation of drug targets across large evolutionary distances, it is optimal to develop a screening system based on the use of cultured cell lines. Cell lines that have been extensively exploited in studies of ciliation include hTERT1-immortalized human retinal pigmented epithelium cells (hTERT-RPE1 cells) (Bodnar et al., 1998), murine NIH3T3 fibroblasts, the murine inner medullary collecting duct cell line model (mIMCD3), and epithelial kidney cells.

We here describe a microscopy-based screening method that can be applied in high throughput to identify small molecules which affect ciliation. Numerous microscopic approaches are effective in low to moderate throughput for evaluating ciliation and ciliary dynamics in living or fixed cells, including differential interference contrast (DIC) microscopy, or confocal imaging of immunostained cilia. To minimize manipulation of cells and facilitate high throughput assessments, this procedure is based on the use of cell models stably expressing fluorescent proteins (e.g., EGFP, TdTomato) targeted to the cilia by fusion to a cilia-targeting moiety. We present data comparing the efficiency of visualization of cilia using targeting moieties provided by fusion of these fluorescent moieties to ADP-ribosylation factor-like protein 13b (ARL13b), SMO, and melanin-concentrating hormone receptor 1 (MCHR1) in the hTERT1-RPE1 cell line. We discuss relevant issues for optimizing analysis, and present an approach using an automated imaging system to visualize, quantify, and establish significance of ciliation data, using alisertib and ganetespib as examples of small molecules that influence ciliation.

MATERIALS AND METHODS

Development and Culture of Cell Models

Introduction, hTERT-RPE1 Cells

Although many cell lines could potentially be used for high throughput study of ciliation, a number of features have caused the hTERT-RPE1 (American Type Culture Collection, Manassas, VA, United States) (ATCC CRL4000) cell line to be a preferred model. hTERT-RPE1 cells were derived by transfecting primary human retinal pigmented epithelium cells with the catalytic component of human telomerase (hTERT; Bodnar et al., 1998). These cells are routinely maintained in DMEM/F-12 medium (Life Technologies, Carlsbad, CA, United States) with 10% FBS plus 1× penicillin/streptomycin, 1× Glutamax-I (Gibco/Thermo Fisher Scientific, Waltham, MA, United States), and 0.01 mg/ml hygromycin B (Life Technologies, Carlsbad, CA, United States). Using optimized culture conditions, it is possible to achieve ciliation of the substantial majority of the hTERT-RPE1 population (80–90% of cells), in contrast to other cell lines such as NIH3T3 in which maximum levels are closer to 60–70%. hTERT-RPE1 cells have a flat, spreading growth habit, and do not clump, which has supported their use not only for studies of ciliation, but also for studies of cell division and other processes requiring high resolution microscopy (e.g., Uetake and Sluder, 2004).

Although all protocols for generating cilia involve culture of cells at high density under conditions of little or no serum to induce quiescence, different cell lines become optimally ciliated under distinct growth regimens. In hTERT-RPE1 cells, for optimal induction of ciliation, cells are typically plated at 50–70% confluency, then maintained in serum free medium for 24–72 h. As a note of relevance to screening for regulation of ciliation, the longer cells are maintained under high density/low serum conditions, the longer it takes for them to respond to stimuli for ciliary resorption. With the goal of achieving maximally reproducible results, it is important to identify a single seeding density and timing for serum deprivation, and use this consistently.

Generation of Stable EGFP-Arl13b, EGFP-Smo, tdTomato-MCHR1 Expressing hTERT-RPE1 Cell Lines

A standard means of measuring ciliation is to fix cells with 4% paraformaldehyde (PFA), then use an antibody-based immunofluorescence approach to identify to proteins such as acetylated α-tubulin (Piperno and Fuller, 1985) to visualize the axoneme, in conjunction with an antibody to γ-tubulin (Muresan et al., 1993) to visualize the basal body. While this approach yields robust and highly quantifiable data, the need for fixation and staining with multiple antibodies results in slower throughput and higher costs than use of cilia-localizing fluorescent proteins. In this study, we have comparatively evaluated suitability of three fluorescent ciliary proteins, based on ciliary localization provided by ARL13b, SMO, and MCHR1 and autofluorescence provided by fused EGFP and tdTomato moieties.

Rationale for Choosing Arl13b, SMO, and MCHR1 as the Target Genes

Arl13b is a small guanosine (**Figure 2**)triphosphate (GTPase) which localizes exclusively to the primary cilium, where it controls ciliogenesis through stabilizing the coordination between IFT-A and IFT-B complexes (Li et al., 2010). Additionally, Arl13b regulates translocation of SMO receptor to the cilia (Larkins et al., 2011).

As noted above, the HH pathway is uniquely associated with the primary cilium (Bangs and Anderson, 2017). In the absence of HH ligands, PTCH1 accumulates at the ciliary membrane, preventing translocation of SMO to the cilia. When the HH ligand binds PTCH1, PTCH1 leaves the cilia, allowing SMO to translocate and activate the pathway.

Melanin-concentrating hormone receptor 1 is a protein which belongs to a class A of G-protein-coupled receptors (GPCRs) and localizes in neuronal cilia in the hypothalamus, where it plays an important role in controlling energy homeostasis potentially through modulating cAMP signaling (Green and Mykytyn, 2010; Schou et al., 2015).

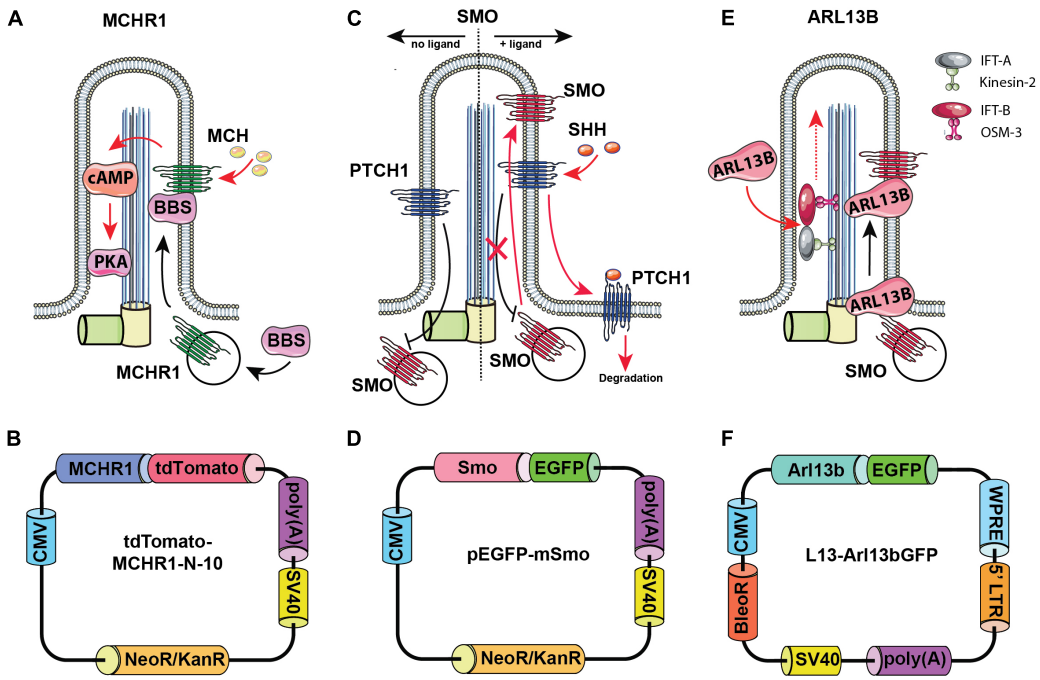

FIGURE 2 | Rationale for choosing Arl13b, SMO, and melanin-concentrating hormone receptor 1 (MCHR1) as cilia-targeting moieties. Mechanism of MCHR1 action **(A)** and a schematic **(B)** for tdTomato-MCHR1-N-10 plasmid. MCHR1 is a protein which belongs to a class A of G-protein-coupled receptors (GPCRs) and localizes in neuronal cilia in the hypothalamus (Green and Mykytyn, 2010). The translocation of MCHR1 to the ciliary membrane by the BBSome complex (Nachury, 2018) allows it to play an important role in controlling energy homeostasis potentially through modulating cAMP signaling (Schou et al., 2015). Mechanism of SMO action **(C)** and a schematic **(D)** for pEGFP-mSmo plasmid. Hedgehog (HH) pathway is uniquely associated with the primary cilium. Two key receptors for this pathway – Smoothened (SMO) and Patched (PTCH1) – localize within the ciliary membrane depending on the pathway's activation stage. In the absence of HH ligands, PTCH1 accumulates at the ciliary membrane preventing translocation of Smo to the cilia. When the ligand binds PTCH1, it leaves the cilia allowing SMO to translocate and activate the pathway. Mechanism of Arl13b action **(E)** and a schematic **(F)** for L13-Arl13bGFP plasmid. Arl13b is a small guanosine triphosphate (GTPase) which localizes exclusively to the primary cilium, where it controls ciliogenesis through stabilizing the coordination between IFT-A and IFT-B complexes (Li et al., 2010). Additionally, Arl13b regulates translocation of SMO receptor to the cilia (Larkins et al., 2011).

For each of these ciliary proteins, fusions to fluorescent proteins have been developed and are publicly available. The L13-Arl13bGFP (Larkins et al., 2011) (Addgene, plasmid #40879), pEGFP-mSMO (Chen et al., 2002) (Addgene, plasmid #25395), tdTomato-MCHR1-N-10 (Addgene, plasmid #58114; a gift of Michael Davidson) constructs, expressing the murine, full length coding sequences for Arl13b, SMO, and MCHR1 as fusions to small fluorescent proteins, were obtained from Addgene (Cambridge, MA, United States). hTERT-RPE1 cells with overexpression of tdTomato-MCHR1 and pEGFP-SMO were generated by transfection with the corresponding constructs using Lipofectamine 2000 transfection reagent (Life Technologies, Carlsbad, CA, United States), selection with G418 (500 μg/ml, for approximately 2 weeks), and further clonal selection by limiting dilution assay. Stable Arl13bGFP overexpression in the hTERT-RPE1 cell line was achieved via lentiviral delivery of L13-Arl13bGFP construct. Briefly, lentivirus was packaged by co-transfection of L13-Arl13bGFP construct with the packaging and envelope plasmids (psPAX2 and pMD2.G) by calcium phosphate transfection into HEK293T cells (Kingston et al., 2003). Medium was collected after 48 and 72 h, combined and filtered through a 0.45 μm filter, then applied to hTERT-RPE1 cells. At 72 h post-infection, hTERT-RPE1 cells were selected with 400 μg/ml zeocin for approximately 2 weeks and additionally selected by clonal selection by limiting dilution assay. All experiments with lentiviruses are conducted according to biosafety level 2 (BSL-2) guidelines.

Prior to using these models for screening, we evaluated the ciliary localization of the fluorescent marker and utility of the biomarker for measurement of disassembly using conventional low throughput methods. Figure 3 is a confocal image of cell lines selected for each of the three probes, maintained either under conditions of optimized ciliation (48 h starvation in serum free culture medium or Opti-MEM), or 2.5 h after the addition of 25% fetal bovine serum (FBS) to induce ciliary disassembly. All probes localized effectively to the cilium.

Protocols for Inducing Ciliary Assembly or Disassembly in a 96-Well Microtiter Plate Format

Growth Conditions to Induce Ciliation

High throughput screening (HTS) can be used both to identify compounds that induce ciliary disassembly, or block the ciliary disassembly caused by serum-encoded growth factors. In each case, it is important to optimize ciliation in a 96-well plate

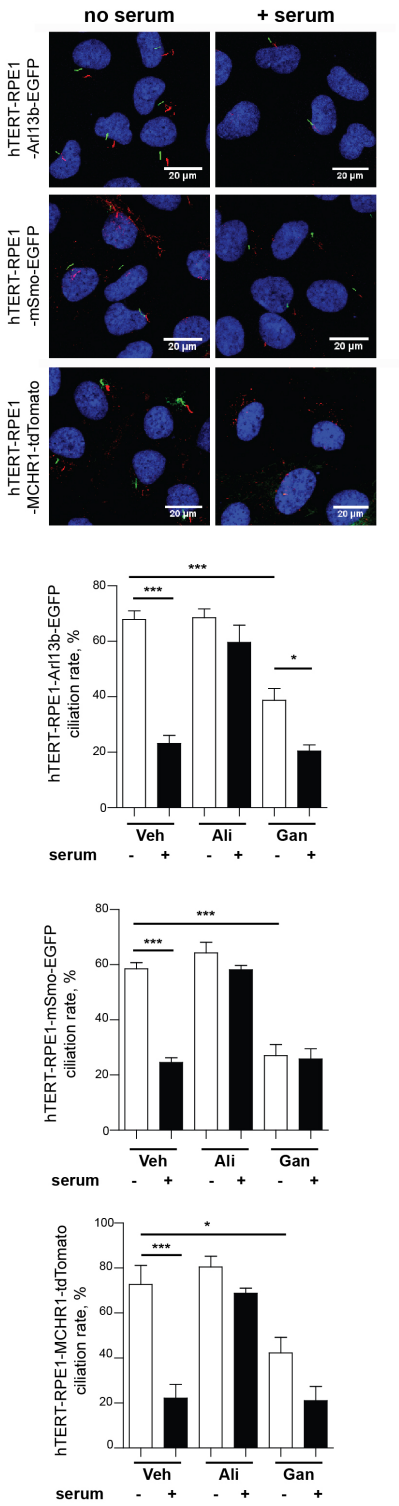

FIGURE 3 | Confocal images of tTERT-RPE1 cells expressing L13-Arl13bGFP, pEGFP-mSMO, and tdTomato-MCHR1-N-10. Top, representative images of RPE1-Arl13b-EGFP (green) pEGFP-mSMO (green), and tdTomato-MCHR1-N-10 (red) in cells also visualized with antibody to acetylated a-tubulin (red with Arl13b and SMO; green with MCHR1) and DAPI (blue). Images compare ciliation in cells with or without serum treatment.

(Continued)

FIGURE 3 | Continued

Bottom, quantification of data for L13-Arl13bGFP, pEGFP-mSmo, and tdTomato-MCHR1-N-10 from 250 cells, from three representative experiments; results following treatment with an inhibitor (alisertib) and a stimulator (ganetespib) of ciliary disassembly are also shown. Data are presented as mean ± SEM, $*p \leq 0.05$, $**p \leq 0.001$, $***p \leq 0.0001$ as compared to control.

format. *We note*, because edge effects (differences in growth pattern of cells located near the edge of a well), a 384-well format is generally not appropriate for experiments involving measurement of ciliation due to heterogeneity of growth habit. An additional key element of HTS is that it relies on analysis of a large number of cells to develop statistically meaningful data. Hence, it is necessary to screen at 20×. One factor to consider is that tagging an endogenous protein would be more physiological and help avoid the issue with overexpressed transgenes themselves affecting ciliary stability. However, we have observed that cell lines expressing low levels of the tagged proteins described here (ascertained by Western blot) are difficult or impossible to visualize at 20× (although resolvable at 60×). Hence, use of more than one tagged cell line, or a tagged cell line followed by use of untagged cells in low throughput/high magnification, is recommended.

Figures 4A,B provide a general experimental schematic and representative images, respectively. For cell plating, bulk reagent dispensers such as the Thermo Scientific Matrix WellMate (Thermo Fisher Scientific, Waltham, MA, United States) can be used. For drug addition, automated liquid handlers can add nanoliter quantities of compounds using pin tools (available from sources such as such as V&P Scientific, San Jose, CA, United States) or liquid dispenser systems [such as the Tecan D300e (Tecan, Switzerland)]. In addition, these steps can be performed manually using hand-held disposable pin tools compatible with a 96-well plate format (for example, from Scinomix, Earth City, MO, United States).

For the high throughput assessment of model cell lines bearing fluorescent ciliary tags, for best performance, earlier passage transfected cells (usually p3–p5) are seeded in black 96-well clear bottom microplates (Costar catalog #3603, Corning Inc., Corning, NY, United States) at a set density in 100 µl culture medium (DMEM/F-12 supplemented with 10% FBS, 1× penicillin/streptomycin, 1× Glutamax-I, and 0.01 mg/ml hygromycin B, noted above), then incubated overnight (16 h) in a humidified incubator (37°C and 5% CO_2). The second day, 100 µl of Opti-MEM medium without FBS and other supplements for 48 h to induce ciliation. This typically leads to robust ciliation (>80%) in these cell models. However, it is important to titrate the initial seeding density. **Figure 5** compares the ciliation as a factor of cells initially seeded (from 8000 to 20,000 cells) for the hTERT-Arl13b-EGFP and hTERT-SMO-EGFP cell model; in this case, 15,000–20,000 cells were needed to obtain robust ciliation.

Measurement of Drug Effect on Ciliary Dynamics

In general, images of cilia and nuclei are acquired simultaneously, before and after perturbation by serum or drugs. All the steps

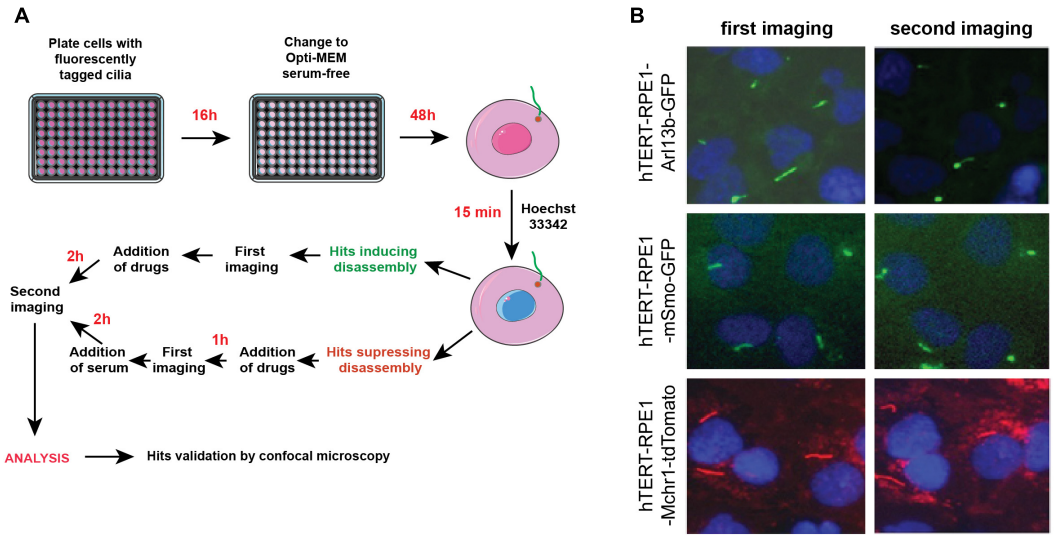

FIGURE 4 | Automated screening workflow and representative images from the ImageXpress microscope. **(A)** Steps for plating, imaging, drug/serum addition, and analysis. **(B)** Epifluorescent images acquired by ImageXpress from first (no serum) and second imaging (after addition of serum control), for the hTERT-RPE1-Arl13b-EGFP (green) hTERT-RPE1-pEGFP-mSMO (green), and hTERT-RPE1-MCHR1-tdTomato (red) models. Note higher background in hTERT-RPE1-MCHR1-tdTomato cells.

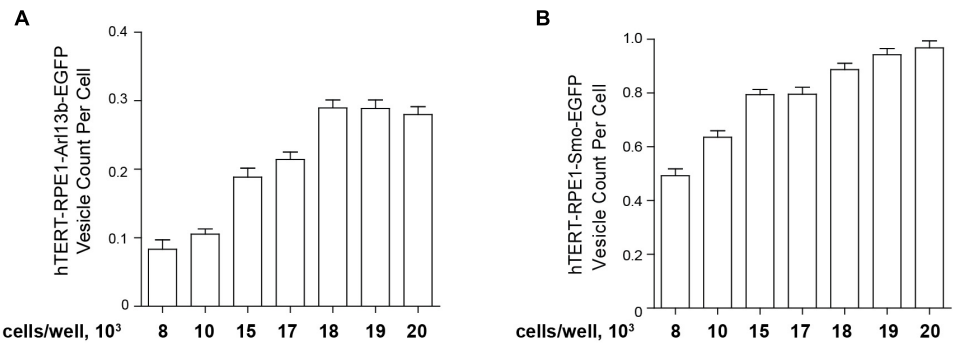

FIGURE 5 | Quantification of ciliation based on plating density. hTERT-RPE1-Arl13b-EGFP **(A)** and hTERT-RPE1-SMO-EGFP **(B)** cells were plated at concentrations shown under conditions described in text, and ciliation assessed after 48 h. Quantitation is based on use of "vesicle total count per cell" in the Transfluor module. Data are presented as mean ± SEM.

that require changing of medium or application of drugs can be accomplished using automated liquid handlers or manually, at the discretion of the user.

1. To allow visualization of nuclei as a reference for number of viable cells, medium is replaced with 100 μl of Hoechst-33342 (Life Technologies, Carlsbad, CA, United States) diluted 1:20,000 in Opti-MEM at the beginning of the experiment, and allowed to equilibrate for 15 min at 37°C in 5% CO_2. At this stage, a first imaging of cilia and nuclei is performed (see next section); these images represent the baseline for quantitation of ciliation prior to perturbation by serum or compounds.
2. To identify compounds that *induce* ciliary disassembly, compounds to be screened are added to the medium. Typically, compounds are prepared as 10 mg/ml stocks in DMSO which can be stored for up to 1 month at −20°C or 3 months at −80°C, then diluted to 1 or 5 μM in DMSO immediately before the experiment. For initial screening for activity in regulating cilia, evaluating drugs using at least two set concentrations between 200 nM and 2.5 μM (final concentration after addition) is a useful range. It is important to include appropriate negative and positive controls. Vehicle (0.01% DMSO) provides a negative control. Serum (25% FBS final volume) provides an essential positive control, which will typically define the maximum level of disassembly. For small molecules, alisertib (MedchemExpress, Monmouth Junction, NJ, United States) and ganetespib (Synta Pharmaceuticals, Bedford, MA, United States) provide useful reference compounds that cause ciliary stabilization and ciliary disassembly, respectively. Typically, compounds are diluted

in Opti-MEM and added in a volume of 100 μl per well. *We note*, best results are obtained if care is taken to add compounds to ciliated cells gently (that is, ensuring a low flow rate), to avoid the generation of mechanical shear forces that can independently influence ciliation (Iomini et al., 2004; Delaine-Smith et al., 2014), and to avoid dislodging cells. Cells are then incubated at 37°C in 5% CO_2 (an exact time should be selected based on initial optimization, then used consistently); subsequent to this incubation, a second set of images is acquired. For the models described here, we typically use 2.5–3 h as the imaging time point.

3. To identify compounds that *inhibit* ciliary disassembly experiment, after the initial imaging (step 1), compounds to be assessed are added immediately with controls in 100 μl Opti-MEM medium without serum (achieving a final volume in the wells of vehicle, 0.01% DMSO; alisertib 200 nM; and ganetespib 500 nM), and incubated at 37°C in 5% CO_2 for 0.5 h. This initial addition allows drugs time to interact with and inhibit relevant target proteins before initiation of disassembly. After 30 min of pre-treatment with drugs, a first imaging is performed. Subsequently, medium is replaced with 100 μl of Opti-MEM medium containing 25% FBS and drugs at the same concentration used for pre-incubation, and incubated for 2.5–3 h at 37°C in 5% CO_2. Subsequent to this incubation, a second set of images is acquired.

Protocols for Imaging Ciliation in High Throughput: Instrumentation, Settings, and Analysis

Options for Instrumentation

For the visualization and analysis of primary cilia, we typically use an ImageXpress micro automated microscope equipped with MetaXpress software (Molecular Devices, Sunnyvale, CA, United States). There are a number of alternative instruments available suitable for high throughput, high content imaging studies (reviewed in Buchser et al., 2012). These include the InCELL Analyzer (GE, Chicago, IL, United States) and associated software InCell Developer toolbox (see Dunn et al., 2018); the Thermofisher Cellinsight CX5 and associated Thermofisher HCS Studio Cell Analysis software (Pagliero et al., 2016) (Waltham, MA, United States); and the Operetta and associated Harmony software (Perkin Elmer, Waltham, MA, United States). In addition, any image acquisition technology can be coupled with multiple free image analysis software packages such as ImageJ (Schindelin et al., 2015) and Cell Profiler (Carpenter et al., 2006; Kamentsky et al., 2011).

Image Acquisition

Image acquisition is performed on an ImageXpress micro automated imaging system equipped with environmental control (Molecular Devices, Sunnyvale, CA, United States) driven by MetaXpress software. To capture as many cells as possible and to ensure data represent a homogeneous response across sample wells, nine images per well are taken, using two channels to capture matching signal from Hoechst-stained nuclei (DAPI channel, ex 377/50, em 447/60), and cilia tagged with fluorescing probes (ex 472/30 em 520/35 for EGFP, ex 525/40, em 585/40 for tdTomato). Epifluorescence images are acquired with a 20× objective (ELWD Plan Fluor, NA 0.45, WD 7.4), using laser autofocus with a z-offset. Nuclear images are acquired first, followed by cilia images at a set z-offset from the DAPI channel. The imaging routine was optimized for speed to minimize image acquisition time with live samples. The focus routine allows for one 96-well plate to be imaged in approximately 1 h. During optimization of the image acquisition routine, nine images per well represented the minimum number of images required to provide sufficient ciliated cells per well. Subsequent to this imaging of baseline ciliation, cells receive the next perturbation (serum addition and/or drug addition) and timed incubation prior to a second imaging. Automated imaging crucially allows for the first and second images to represent paired fields.

Image Analysis

In the primary analysis approach used for screening, acquired images were analyzed with MetaXpress software (Molecular Devices[1]) using the Transfluor module. The Transfluor module has been used successfully to identify various classes of intracellular vesicles and related signaling events (e.g., Wang et al., 2004; Garippa et al., 2006; Ross et al., 2008). Alternatively, image analysis methods to identify cilia can be developed using settings within the module MultiWavelength Scoring (MWS). As yet another approach, thresholding in ImageJ can be effective, and can be used to filter results for alternative parameters to those reported by a dot counting module such as Transfluor.

Within the Transfluor module, settings for "vesicle" generate a pixel mask or segmentation overlay that identifies objects within the image as either "nucleus" or "vesicle" (see example overlays in **Figure 6**). The "vesicle" settings are used to identify cilia using size minimum and maximum criteria in conjunction with intensity thresholds. Determination of appropriate settings for cilia automated counting are determined using the vehicle "no serum" and vehicle "plus serum" controls, to establish the intensity threshold. Minimum and maximum values for vesicle size are dependent on the cell model being utilized, due to varying intensities of the individual fluorescent tag in that cell model. For the three cell models analyzed here, the values for minimum vesicle size were in the range of 1–2 μm while the maximum varied from 8 to 11 μm. Representative images of L13-Arl13bGFP, tdTomato-MCHR1, and pEGFP-SMO expressing cells before and after serum addition, and the accompanying image segmentation overlay, are shown in **Figure 6**. L13-Arl13bGFP resulted in the best results from this automated analysis, based on the low occurrence of vesicles with GFP fluorescence in the cytoplasm. pEGFP-Smo expressing cells also yielded a signal suitable for statistically significant, consistent quantitation, albeit with a greater level of background signal (**Figure 6**). In contrast, tdTomato-MCHR1 contained too high a level of background labeled vesicles to be useful in high throughput approach. Hence, the L13-Arl13bGFP and

[1] www.moleculardevices.com

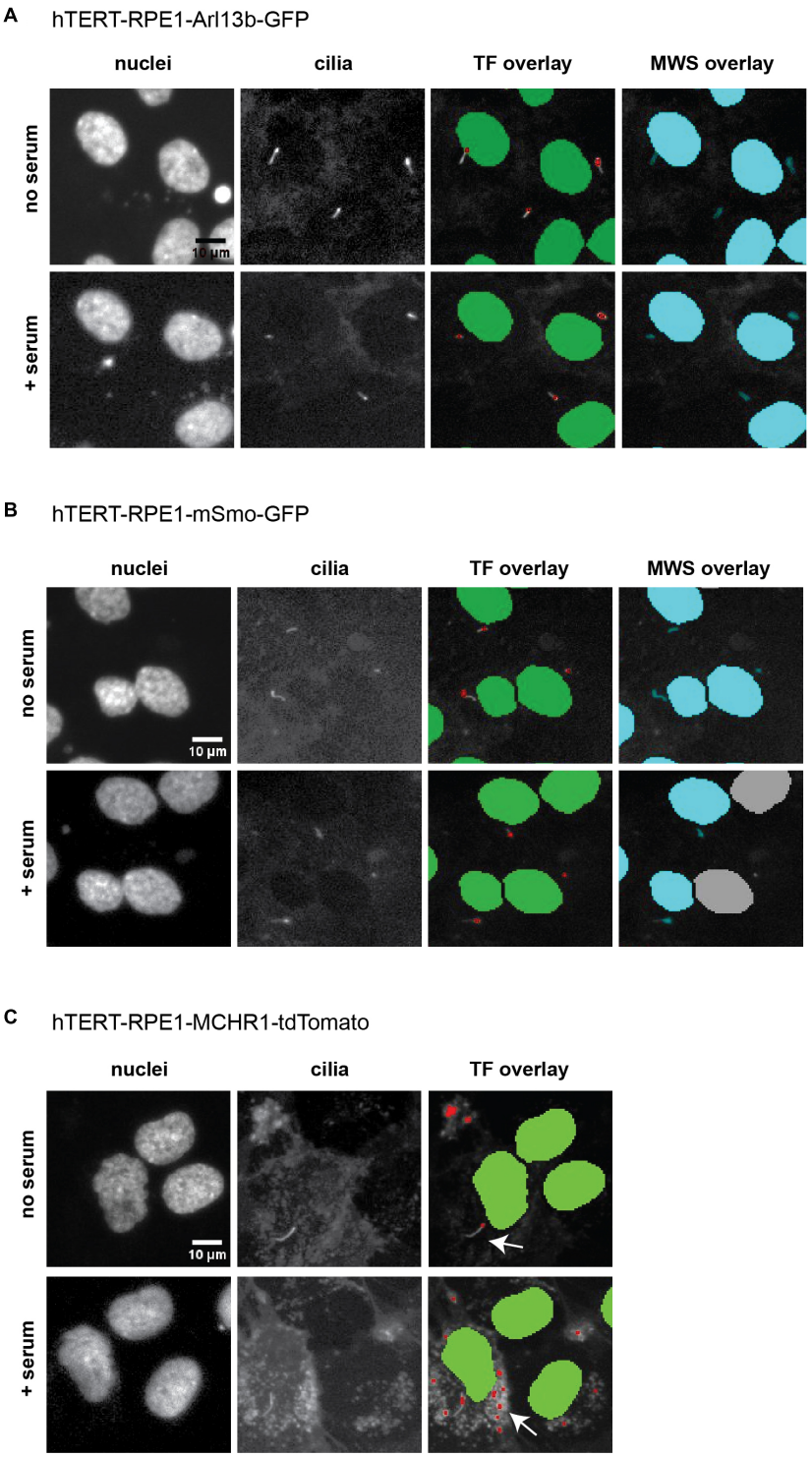

FIGURE 6 | ImageXpress images of cilia, emphasizing thresholding issues. Representative images of the three models of ciliation evaluated in this method, and typical image segmentation by MetaExpress software modules Transfluor (TF) and Multiwavelength Scoring (MWS). **(A)** hTERT-RPE1-Arl13b-EGFP. **(B)** hTERT-RPE1-SMO-EGFP. **(C)** hTERT-RPE1-tdTomato-MCHR1. Left panels show Hoechst stained nuclei, middle panels show labeled cilia, and right panels are representative image segmentation as recognized by the software (shown as an overlay of the cilia image. For TF, green is nuclear segmentation, red is the cilia segmentation; for MWS, nuclei and cilia are overlaid in cyan). For each cell model, no serum and + serum panels represent the same image field. In **A**, settings for both TF and MWS modules can be developed that discriminate between background and cilia; for **B**, settings for TF but not MWS can be used. The tdTomato-MCHR1 model, shown in **C**, has significant intracellular signal, particularly following addition of serum (see arrows in the right panel), which render automated counting unreliable by either TF or MWS approach.

pEGFP-SMO models are used for automated screening, while the tdTomato-MCHR1 models are used for subsequent validation by confocal analysis.

As an alternative to Transfluor, we have also used the MWS module, a standard image thresholding approach is used to segment nuclei utilizing images acquired in the DAPI channel (as in the Transfluor module), and to segment cilia as objects within the images acquired for visualization of cilia. The module for both nuclear segmentation and cilia segmentation requires the researcher to develop settings that successfully identify nuclei and cilia utilizing object minimum size (for cilia in our experiments, this ranges from 1 to 1.8 μm) and maximum size (which varies from 5 to 10 μm). It is also necessary to develop a minimum intensity (settings from 78 to 150 in the MWS module, dependent on the strength of the fluorescence signal) and a minimum stained area (settings from 1.5 to 3). The MWS captures more intracellular background than the Transfluor module, so that in our hands, only the L13-Arl13bGFP model was suitable for use with this approach, due to the low cytoplasmic staining in this line (**Figure 6**). However, if the cell line in use is suitable, MWS can provide a powerful tool to measure cilia parameters such as "positive stained area" or "% positive W2" (where W2 is wavelength utilized for cilia imaging; and % positive reflects the number of cells per image scoring within the segmentation metrics) allowing a more detailed phenotypic characterization than Transfluor analysis alone, permitting rough inference of ciliary length. As shown in **Figure 7**, the Transfluor module yielded statistically significant results for serum induced ciliary disassembly in both the L13-Arl13bGFP and pEGFP-SMO models, while the MWS module did so only in the L13-Arl13bGFP cell line.

It is important to note, additional parameters can be extracted from the MWS approach using custom software accessories (such as custom module developers, for example, Integrated Morphometry Analysis within MetaXpress). Utilization of these tools with the MWS module, in conjunction with a confocal imaging system, can yield more detailed cilia characteristics such as individual cilia length. A secondary application of the MWS module is to allow filtering of images prior to hit picking; for example, the metric "positive stained area" for the cilia channel can be used to identify images with excessive background; allowing the researcher to identify problematic images that require manual supervision prior to hit-picking.

Results from these types of analyses return multiparameter datasets quantitating each image. The parameters from Transfluor analysis used for this method include "vesicle count per cell" as shown in **Figure 5**, with cilia number normalized to number of nuclei. Other metrics reported, which can be used for some analyses, include "total vesicle area" and "vesicle area per cell," as shown in **Figure 7**. Data from image analysis can be returned to the investigator in two ways: (1) "summary" data representing the data from all nine images calculated as mean or sum and (2) "site" data which reports the metric of interest per image (or "site"). Therefore "summary" data represent a numerical quantitation of metrics at the level of the well, while the "site" data provide the same metric within each image. Importantly for this protocol, the automated imaging systems returns the plate to the same X,Y,Z coordinate, allowing the same fields to be acquired in both imaging runs. This is critical for the evaluation of cilia by this method; as this is an epifluorescence image and the cilia is changing in the Z dimension, the availability of the paired images allows for a critical quality control supervision without which this screening method would not be sufficiently robust to identify wells of interest.

With the Transfluor analysis, the first step in evaluation of wells for perturbation (drug, growth factor, serum) induction of cilia disassembly is to normalize all wells to the mean of all control wells for "vehicle and starved" (representative of maximal ciliation) using the metric "vesicle count per cell" (vesicle count per cell *sample* $^{\text{SUMMARY MEAN IR2}}$/vesicle count per cell *control* $^{\text{SUMMARY MEAN IR1}}$; where IR1 = image run1 or baseline and IR2 = image run 2 or post-perturbation). It is important to note that using an automated system based on epifluorescence, the change in ciliation rate induced by a strong stimulus such as 25% serum is in the range of ∼20–60%, compressing the dynamic range from that detectable by confocal microscopy. However, the ability to image large numbers of cells nevertheless results in highly significant data. In scale with this compressed dynamic range, small molecule hits of interest often first appear as differences of ∼10%, based on mean values; greater differences are detected in follow-up experiments, after optimization of dosing range and use of confocal scoring systems.

The second step, performed after this initial cutoff, is to review individually the nine imaged primary hit wells via comparison of individual paired images for image run 1 and image run 2 (total vesicle area *sample*$^{\text{SITE IR2}}$/total vesicle area *sample* $^{\text{SITE IR1}}$). This step allows the elimination of any "outlier images" including images that showed significant loss of cells or poor image quality. This typically improves the screening metric. Processing the resultant data allows selection of the two possible classes of ranked "screening hits" (for enhanced disassembly, or for resistance to disassembly). It is important to note that screen conditions must be optimized for either identification of cilia disassembly or resistance to disassembly; these hits are not identified concurrently in the same screen. The results are evaluated using standard statistical methods, and the significance usually is determined using *p*-values.

Confirmation of Cilia-Targeting Ability of Compounds Using Confocal Microscopy

All HTS approaches are useful for screening large numbers of specimens quickly, but are not ideal for generating high resolution data. Further, prudence in assigning activity to candidate hits requires measurement of effect using an alternative assay system to prioritize follow-up experiments. Although the screens described above are performed using duplicate wells for technical repetition, and at least two independent runs for biological repetition, before hit selection, we routinely confirm cilium-modulating activities of candidate drugs using a confocal fluorescence microscopy approach. In general, immunofluorescence protocols for analyzing cilia are well established, and have been used by many groups. For the novice,

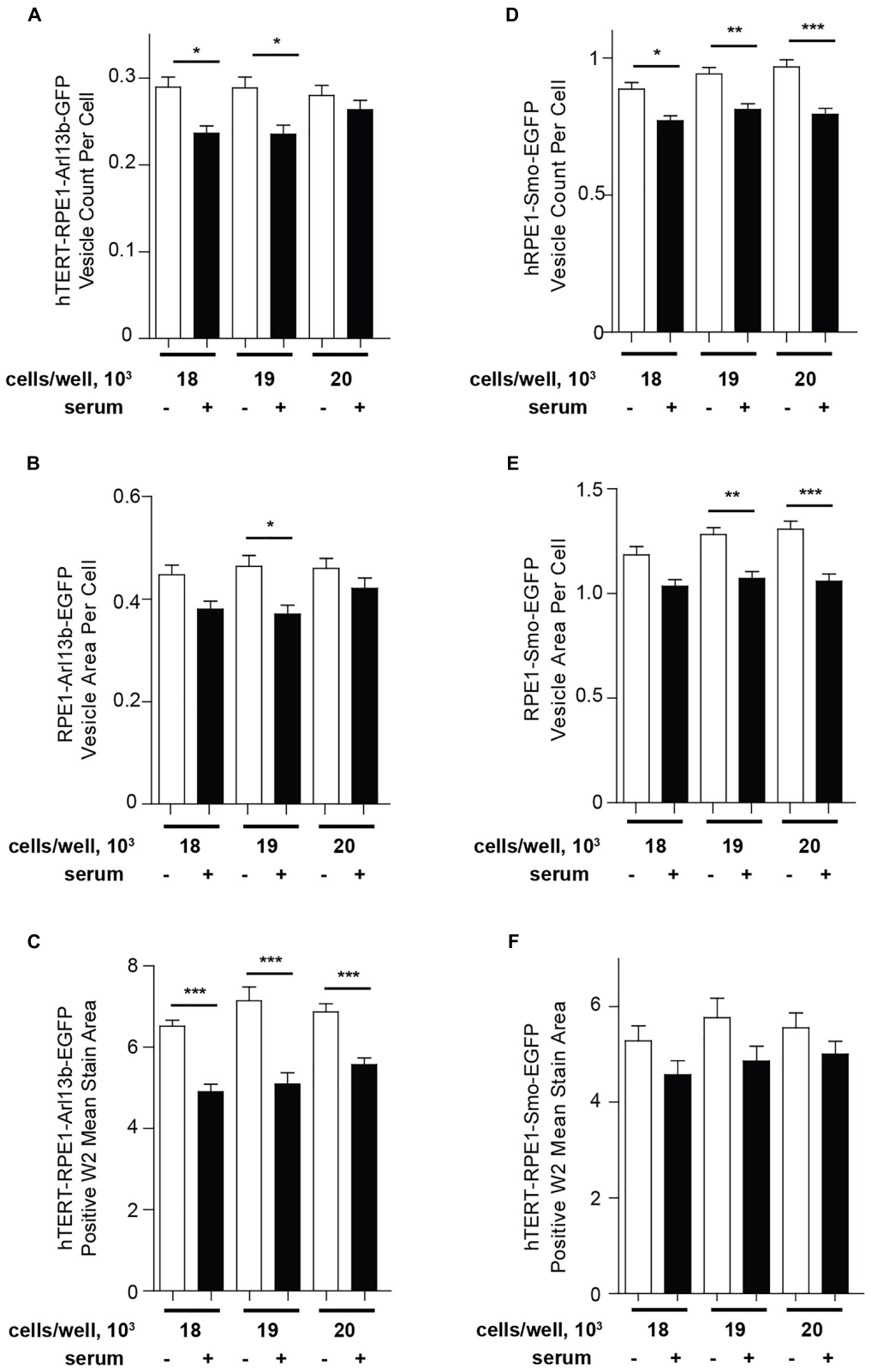

FIGURE 7 | Quantification of ciliation using Transfluor and MultiWavelength Scoring modules. **(A,B)** Analysis of ciliation in hTERT-RPE1-Arl13b-EGFP and hTERT-RPE1-Smo-EGFP cell lines based on "vesicle count per cell" and "vesicle per cell" in the TF module (**A,B** for Arl13b, **D,E** for SMO), and positive W2 mean stain area in the MWS module (**C** for Arl13b, **F** for SMO). Data are presented as mean ± SEM, $*p \leq 0.05$, $**p \leq 0.001$, $***p \leq 0.0001$ as compared to control.

several facts are important to note. First if it is intended to use a fluorescent protein as one of the markers for assessment in fixed cells, it is important to avoid methanol as a fixation method, as it will greatly reduce signal. Second, combined analysis of a probe localized to the cilium with a second probe localized to the basal body is extremely helpful in clarifying true from false positives. Third, one way in which a fixation-based protocol differs from the automated live-imaging approach is that imaging can only be performed at the end of the experiment. Hence, it is essential to perform sufficient controls to provide comparison sets for maximal and minimal ciliation under the conditions of the screen.

Protocol for Confirmation of Ciliation-Regulating Drug Hits by Standard Immunofluorescence

1. Cell lines bearing fluorescent ciliary marker proteins (RPE1-Arl13b-EGFP, RPE1-SMO-EGFP, or RPE1-MCHR1-tdTomato) are plated in 1 ml culture medium (DMEM/F-12) in a 24-well plate in which each well contains one sterile coverslip pre-coated with collagen (StemCell Technologies, Vancouver, BC, Canada). As with HTS, it is useful to perform preliminary tests to establish optimal plating density; we have found a density of 25,000 cells/well is typically appropriate. Incubate cells overnight (16 h) in a humidified incubator (37°C and 5% CO_2) to allow cells to attach tightly to the cover slips, and attain ∼60–70% confluency.
2. The second day, replace medium with Opti-MEM lacking serum, and incubate for another 48 h at 37°C and 5% CO_2. At this point, visual inspection of the plate by light microscope should indicate that cells are 90–100% confluent, but not overgrown. At this point, perform treatments with drug, control, and serum addition comparable to those used in HTS but omitting the step of Hoechst dye addition, scaled up to the larger medium volume.
3. At the experimental endpoint (∼2.5 h after the addition of drugs if measuring induced disassembly, or the addition of serum if measuring blockade of disassembly), fix cells with 250 μl 4% PBS-based PFA for 7 min. Next, remove PFA, wash one time in 1 ml PBS and add 250 μl 0.1% Triton X-100 in PBS for 10 min to permeabilize cells. Wash one time with 1 ml PBS and proceed to blocking.
4. Add PBS-based 3% bovine serum albumin solution for 30 min to block non-specific antibody interactions. Incubate cells with selected antibodies using standard protocols optimized for each reagent for immunofluorescence by the manufacturer[2]. In the human cell lines described here, useful primary antibodies for visualizing the ciliary basal body include rabbit anti-pericentrin (1:200 dilution; IHC-00264, Bethyl Laboratories, Inc., Montgomery, TX, United States) or anti-γ-tubulin (1:200 dilution; T5192, rabbit; Sigma–Aldrich Corp., St. Louis, MO, United States). The mouse anti-acetylated-α-tubulin (1:200 dilution; sc-23950, Santa Cruz Biotechnology, Inc., Santa Cruz, CA, United States) can be used for cilia visualization. Secondary antibodies include anti-rabbit conjugated to Alexa Fluor 488 or Alexa Fluor 568 (1:2000 dilution, Life Technologies, Carlsbad, CA, United States). Typical time of antibody incubation is 1 h at room temperature for primary, and 1 h at room temperature for secondary (with incubations performed in the dark), with three washes in PBS after each incubation. After the final wash, coverslips are removed from a plate and mounted using Prolong Gold with DAPI (Life Technologies, Carlsbad, CA, United States) to also visualize DNA.
5. All standard confocal microscope systems can be used to visualize cilia. In our hands, we image samples using the Leica SP8 advanced confocal system. Typically, we count 250 cells per condition at 63× magnification. Images were obtained by Leica Application Suite Advanced Fluorescence (LAS AF) software. An important issue to consider when imaging is the cell density; ideally, there should be 50–60 cells evenly distributed cells in the visual field when using these settings. Significant deviations from this number will increase variability due to overgrowth (uneven disassembly) or low density (low initial frequency of ciliation).
6. Hit confirmation of the phenotype scored in the screening environment is determined by a *p*-value determined by *t*-test to examine extent of ciliary loss, from quantitation of confocal images. Agents that were validated by these criteria were considered validated hits, and taken for further functional characterization.
7. *We note*, although both the RPE1-Arl13b-EGFP and RPE1-SMO-EGFP models are suitable for statistically significant quantitation using the methods described, RPE1-MCHR1-tdTomato model shows an accurate results only when analyzed using a low throughput confocal system, at higher magnification. Using two models for preliminary screening and one or more alternative model for confirmation has some advantages; most notably that it would eliminate hypothetical screening artifacts linked to drug effects on the Arl13b-EGFP or SMO-EGFP ciliary probes, by interfering with the biological regulation of Arl13b or SMO.

DISCUSSION

Because many genetic and sporadic diseases are now known to involve changes in ciliation, and because a growing number of drugs are appreciated as affecting ciliary structure and function, there is clear value in developing efficient tools and methodologies for high throughput profiling of ciliary phenotypes. In the method described here, we have used a live-cell imaging approach utilizing freely available fluorescent-cilia fusion proteins. As the methods and representative data above indicate, there are strengths and weaknesses associated with the use of fluorescent cilia-targeted proteins as a HTS modality to assess drug activity. As strengths, once a cell line

[2]https://www.abcam.com/protocols/immunocytochemistry-immunofluorescence-protocol

with an appropriate cilia-localized protein has been developed, screening involves a very limited number of steps, and costs of reagents are low, allowing the facile assessment of a large number of compounds. Data are read automatically, and quantified, removing potential sources of experimental bias. Multiple distinct modules are available for imaging systems, allowing the screener to adjust sensitivity level, and include or exclude partial phenotypes. Hits identified by this approach can rapidly be validated using an orthogonal fixation-based method, using the same or alternative ciliary proteins for antibody-based visualization.

Based on extensive practical experience, there are some limitations of HTS methods, which vary from model to model. As noted above, in some cases, the over-expressed tagged protein may be suitable for confocal analysis, where the *z*-axis can be readily modified and limited in depth; or for live cell imaging, but not for automatic counting, which is typically based on epifluorescence, and where it is impossible to exclude competing signal from the cytoplasm. Among the examples we test, the RPE1-MCHR1-tdTomato cell line has significant interfering background signal, and is not appropriate for high throughput analysis, although is suitable for confocal assessment. However, by carefully matching image analysis tool with cell line model, robust results can be achieved. As a particular strength, by utilizing biological and technical controls and development of appropriate settings in image analysis software, large number of images can be screened with the approach described herein. For automated approaches to be most effective, prior to commencement of large screening, it is important for researchers to invest the time at the beginning of experimentation to ensure that each metric returned by these software tools is validated by statistical analyses and manual supervision of images.

When using automated approaches for compound screening, it is important to be aware of potential confounding issues. One common issue is the inherent fluorescence of some compounds, which can affect the assay and final analysis. In our hands, some drugs we have worked with have a strong yellow color, which caused higher background in the GFP channel on the ImageXpress; such competing signal from compounds can compromise the use of automated image analysis. An additional technical issue to consider is the possibility that over-expressed autofluorescent proteins that localize in part or in sum to cilia may affect ciliary integrity and rate of resorption. For example, in our hands, cilia in the RPE1-Arl13b-EGFP cell line resorb at 3 h after treatment with serum, in contrast to the hTERT-RPE1 parental control, where resorption occurs at 2 h after treatment. In practice, this is a minor feature of screening that can be easily accommodated by adjustment of assay times. In principle, this may mean the expressed protein is affecting ciliary trafficking machinery in a manner that alters the spectrum of which drugs do or do not impact ciliation. If resources are available, such issues can be eliminated by performing parallel screening in two independent cell lines expressing different ciliary tags that have distinct biological activities. Whether or not parallel screening is performed, is important to confirm the activity of "hit" proteins during the validation process, in multiple cell lines lacking overexpressed ciliary proteins.

The protocols described above focus on the identification of small molecule compounds that regulate ciliary disassembly. It is also possible to study compounds that regulate ciliary assembly, using modifications of the described protocols. However, identification of such compounds is more challenging, because of several technical and biological considerations. Ciliary disassembly is performed over a short time period (2–3 h) in cells pre-synchronized by contact inhibition and serum starvation into quiescence. Ciliary assembly occurs over 24–72 h (depending on the cell model), in cell populations that are initially asynchronously growing. Hence, drugs to be assessed must be added at early time points, and maintained in the culture medium for at least 24 h. As a result, there is much more opportunity for "reduction in ciliation" due to confounding alternative drug activities to be made manifest. Drug actions resulting in non-specific reduction of ciliation would include general cell cycle arrest at a stage where cilia are already resorbed, induction of apoptosis or other forms of cell death, change in cell-cell attachment properties (so contact inhibition does not occur), and detachment from the plate, among others. Considerable care must be taken in designing controls if attempting such experiments.

The three model cell lines described here – RPE1-Arl13b-EGFP, RPE1-SMO-EGFP, and RPE1-MCHR1-tdTomato – use cilia-localization sequences provided by three very well-studied ciliary proteins that associate with the ciliary membrane. Over the past several years, large scale studies have defined the proteome of the ciliary membrane, axoneme, basal body, and associated structures (Ishikawa et al., 2012; Mick et al., 2015; Dean et al., 2016; Kohli et al., 2017). These studies provide a useful resource for identifying alternative ciliary tags, some of which can illuminate specific ciliary domains such as the ciliary tip or the ciliary transition zone. We view the use of autofluorescent visualization proteins associated with the ciliary membrane as likely to yield less problematic outcomes (e.g., disruption of ciliary transport) than those targeting core structures such as the IFT machinery, but for any new system, empirical assessment will be needed. Finally, other parameters of ciliary dynamics, such as ciliary beat frequencies for motile cilia (beyond the scope of this methods study) have been obtained through moderate-throughput, computational analysis of videos (Mantovani et al., 2010). Fluorescent tags can similarly augment such approaches.

AUTHOR CONTRIBUTIONS

PZ, AK, and VK contributed to experimental data. ME assisted during HTS procedures including development and execution of image acquisition and image analysis routines. EG and HL supervised the staff and ensured the quality of data analysis. PZ, AK, EG, and ME wrote and edited the manuscript.

FUNDING

The authors and work were supported by NIH R01 DK108195 (to EG); by the Russian Government Program for Competitive Growth of Kazan Federal University (to AK); by NIH R50

CA211479 (to ME); by the National Natural Science Foundation 81672582, the Natural Science Foundation of Jiangsu Province for Distinguished Young Scholars BK20160013, the Top Talent of Innovative Research Team of Jiangsu Province, and Six Talent Peak Project from Government of Jiangsu Province 2015-SWYY-019 (to HL); and by NIH Core Grant CA006927 (to Fox Chase Cancer Center).

ACKNOWLEDGMENTS

Figures 1, **2**, and **4** were created by modification of Servier Medical Art templates, licensed under a Creative Commons Attribution 3.0 Unported License[3].

[3] https://smart.servier.com

REFERENCES

Bangs, F., and Anderson, K. V. (2017). Primary cilia and mammalian hedgehog signaling. *Cold Spring Harb. Perspect. Biol.* 9:a028175. doi: 10.1101/cshperspect.a028175

Bodnar, A. G., Ouellette, M., Frolkis, M., Holt, S. E., Chiu, C. P., Morin, G. B., et al. (1998). Extension of life-span by introduction of telomerase into normal human cells. *Science* 279, 349–352. doi: 10.1126/science.279.5349.349

Buchser, W., Collins, M., Garyantes, T., Guha, R., Haney, S., Lemmon, V., et al. (2012). "Assay development guidelines for image-based high content screening, high content analysis and high content imaging," in *Assay Guidance Manual*, eds G. S. Sittampalam, N. P. Coussens, K. Brimacombe, A. Grossman, M. Arkin, D. Auld, et al. (Rockville, MD: Bethesda).

Cao, M., Li, G., and Pan, J. (2009). Regulation of cilia assembly, disassembly, and length by protein phosphorylation. *Methods Cell Biol.* 94, 333–346. doi: 10.1016/S0091-679X(08)94017-6

Carpenter, A. E., Jones, T. R., Lamprecht, M. R., Clarke, C., Kang, I. H., Friman, O., et al. (2006). CellProfiler: image analysis software for identifying and quantifying cell phenotypes. *Genome Biol.* 7:R100. doi: 10.1186/gb-2006-7-10-r100

Chen, J. K., Taipale, J., Cooper, M. K., and Beachy, P. A. (2002). Inhibition of Hedgehog signaling by direct binding of cyclopamine to Smoothened. *Genes Dev.* 16, 2743–2748. doi: 10.1101/gad.1025302

Chien, Y. H., Srinivasan, S., Keller, R., and Kintner, C. (2018). Mechanical strain determines cilia length, motility, and planar position in the left-right organizer. *Dev. Cell* 45:e314. doi: 10.1016/j.devcel.2018.04.007

Coene, K. L., Mans, D. A., Boldt, K., Gloeckner, C. J., Van Reeuwijk, J., Bolat, E., et al. (2011). The ciliopathy-associated protein homologs RPGRIP1 and RPGRIP1L are linked to cilium integrity through interaction with Nek4 serine/threonine kinase. *Hum. Mol. Genet.* 20, 3592–3605. doi: 10.1093/hmg/ddr280

Dean, S., Moreira-Leite, F., Varga, V., and Gull, K. (2016). Cilium transition zone proteome reveals compartmentalization and differential dynamics of ciliopathy complexes. *Proc. Natl. Acad. Sci. U.S.A.* 113, E5135–E5143. doi: 10.1073/pnas.1604258113

Delaine-Smith, R. M., Sittichokechaiwut, A., and Reilly, G. C. (2014). Primary cilia respond to fluid shear stress and mediate flow-induced calcium deposition in osteoblasts. *FASEB J.* 28, 430–439. doi: 10.1096/fj.13-231894

Delling, M., Indzhykulian, A. A., Liu, X., Li, Y., Xie, T., Corey, D. P., et al. (2016). Primary cilia are not calcium-responsive mechanosensors. *Nature* 531, 656–660. doi: 10.1038/nature17426

Drummond, M. L., Li, M., Tarapore, E., Nguyen, T. T. L., Barouni, B. J., Cruz, S., et al. (2018). Actin polymerization controls cilia-mediated signaling. *J. Cell Biol.* 217:jcb.201703196. doi: 10.1083/jcb.201703196

Dunn, M., Boltaev, U., Beskow, A., Pampou, S., Realubit, R., Meira, T., et al. (2018). Identification of fluorescent small molecule compounds for synaptic labeling by image-based, high-content screening. *ACS Chem. Neurosci.* 9, 673–683. doi: 10.1021/acschemneuro.7b00263

Garippa, R. J., Hoffman, A. F., Gradl, G., and Kirsch, A. (2006). High-throughput confocal microscopy for beta-arrestin-green fluorescent protein translocation G protein-coupled receptor assays using the Evotec Opera. *Methods Enzymol.* 414, 99–120. doi: 10.1016/S0076-6879(06)14007-0

Goetz, S. C., Ocbina, P. J., and Anderson, K. V. (2009). The primary cilium as a Hedgehog signal transduction machine. *Methods Cell Biol.* 94, 199–222. doi: 10.1016/S0091-679X(08)94010-3

Green, J. A., and Mykytyn, K. (2010). Neuronal ciliary signaling in homeostasis and disease. *Cell. Mol. Life Sci.* 67, 3287–3297. doi: 10.1007/s00018-010-0425-4

Inoko, A., Matsuyama, M., Goto, H., Ohmuro-Matsuyama, Y., Hayashi, Y., Enomoto, M., et al. (2012). Trichoplein and Aurora A block aberrant primary cilia assembly in proliferating cells. *J. Cell Biol.* 197, 391–405. doi: 10.1083/jcb.201106101

Iomini, C., Tejada, K., Mo, W., Vaananen, H., and Piperno, G. (2004). Primary cilia of human endothelial cells disassemble under laminar shear stress. *J. Cell Biol.* 164, 811–817. doi: 10.1083/jcb.200312133

Ishikawa, H., and Marshall, W. F. (2017). Intraflagellar transport and ciliary dynamics. *Cold Spring Harb. Perspect. Biol.* 9:a021998. doi: 10.1101/cshperspect.a021998

Ishikawa, H., Thompson, J., Yates, J. R. III, and Marshall, W. F. (2012). Proteomic analysis of mammalian primary cilia. *Curr. Biol.* 22, 414–419. doi: 10.1016/j.cub.2012.01.031

Kamentsky, L., Jones, T. R., Fraser, A., Bray, M. A., Logan, D. J., Madden, K. L., et al. (2011). Improved structure, function and compatibility for CellProfiler: modular high-throughput image analysis software. *Bioinformatics* 27, 1179–1180. doi: 10.1093/bioinformatics/btr095

Khan, N. A., Willemarck, N., Talebi, A., Marchand, A., Binda, M. M., Dehairs, J., et al. (2016). Identification of drugs that restore primary cilium expression in cancer cells. *Oncotarget* 7, 9975–9992. doi: 10.18632/oncotarget.7198

Kim, S., Zaghloul, N. A., Bubenshchikova, E., Oh, E. C., Rankin, S., Katsanis, N., et al. (2011). Nde1-mediated inhibition of ciliogenesis affects cell cycle re-entry. *Nat. Cell Biol.* 13, 351–360. doi: 10.1038/ncb2183

Kingston, R. E., Chen, C. A., and Rose, J. K. (2003). Calcium phosphate transfection. *Curr. Protoc. Mol. Biol.* 9:1. doi: 10.1002/0471142727.mb0901s63

Knodler, A., Feng, S., Zhang, J., Zhang, X., Das, A., Peranen, J., et al. (2010). Coordination of Rab8 and Rab11 in primary ciliogenesis. *Proc. Natl. Acad. Sci. U.S.A.* 107, 6346–6351. doi: 10.1073/pnas.1002401107

Kohli, P., Hohne, M., Jungst, C., Bertsch, S., Ebert, L. K., Schauss, A. C., et al. (2017). The ciliary membrane-associated proteome reveals actin-binding proteins as key components of cilia. *EMBO Rep.* 18, 1521–1535. doi: 10.15252/embr.201643846

Korobeynikov, V., Deneka, A. Y., and Golemis, E. A. (2017). Mechanisms for nonmitotic activation of Aurora-A at cilia. *Biochem. Soc. Trans.* 45, 37–49. doi: 10.1042/BST20160142

Larkins, C. E., Aviles, G. D., East, M. P., Kahn, R. A., and Caspary, T. (2011). Arl13b regulates ciliogenesis and the dynamic localization of Shh signaling proteins. *Mol. Biol. Cell* 22, 4694–4703. doi: 10.1091/mbc.E10-12-0994

Lee, J. J., Perera, R. M., Wang, H., Wu, D. C., Liu, X. S., Han, S., et al. (2014). Stromal response to Hedgehog signaling restrains pancreatic cancer progression. *Proc. Natl. Acad. Sci. U.S.A.* 111, E3091–E3100. doi: 10.1073/pnas.1411679111

Lefebvre, P. A., and Rosenbaum, J. L. (1986). Regulation of the synthesis and assembly of ciliary and flagellar proteins during regeneration. *Annu. Rev. Cell Biol.* 2, 517–546. doi: 10.1146/annurev.cb.02.110186.002505

Li, Y., Wei, Q., Zhang, Y., Ling, K., and Hu, J. (2010). The small GTPases ARL-13 and ARL-3 coordinate intraflagellar transport and ciliogenesis. *J. Cell Biol.* 189, 1039–1051. doi: 10.1083/jcb.200912001

Liu, H., Kiseleva, A. A., and Golemis, E. A. (2018). Ciliary signalling in cancer. *Nat. Rev. Cancer* 18, 511–524. doi: 10.1038/s41568-018-0023-6

Ma, M., Tian, X., Igarashi, P., Pazour, G. J., and Somlo, S. (2013). Loss of cilia suppresses cyst growth in genetic models of autosomal dominant polycystic kidney disease. *Nat. Genet.* 45, 1004–1012. doi: 10.1038/ng.2715

Mahjoub, M. R., Trapp, M. L., and Quarmby, L. M. (2005). NIMA-related kinases defective in murine models of polycystic kidney diseases localize to primary cilia and centrosomes. *J. Am. Soc. Nephrol.* 16, 3485–3489. doi: 10.1681/ASN.2005080824

Malicki, J., Avanesov, A., Li, J., Yuan, S., and Sun, Z. (2011). Analysis of cilia structure and function in zebrafish. *Methods Cell Biol.* 101, 39–74. doi: 10.1016/B978-0-12-387036-0.00003-7

Mantovani, G., Pifferi, M., and Vozzi, G. (2010). Automated software for analysis of ciliary beat frequency and metachronal wave orientation in primary ciliary dyskinesia. *Eur. Arch. Otorhinolaryngol.* 267, 897–902. doi: 10.1007/s00405-009-1161-y

Mick, D. U., Rodrigues, R. B., Leib, R. D., Adams, C. M., Chien, A. S., Gygi, S. P., et al. (2015). Proteomics of primary cilia by proximity labeling. *Dev. Cell* 35, 497–512. doi: 10.1016/j.devcel.2015.10.015

Mitchison, H. M., and Valente, E. M. (2017). Motile and non-motile cilia in human pathology: from function to phenotypes. *J. Pathol.* 241, 294–309. doi: 10.1002/path.4843

Miyamoto, T., Hosoba, K., Ochiai, H., Royba, E., Izumi, H., Sakuma, T., et al. (2015). The microtubule-depolymerizing activity of a mitotic kinesin protein KIF2A drives primary cilia disassembly coupled with cell proliferation. *Cell Rep.* doi: 10.1016/j.celrep.2015.01.003 [Epub ahead of print].

Muller, R. U., Zank, S., Fabretti, F., and Benzing, T. (2011). Caenorhabditis elegans, a model organism for kidney research: from cilia to mechanosensation and longevity. *Curr. Opin. Nephrol. Hypertens.* 20, 400–408. doi: 10.1097/MNH.0b013e3283471a22

Muresan, V., Joshi, H. C., and Besharse, J. C. (1993). Gamma-tubulin in differentiated cell types: localization in the vicinity of basal bodies in retinal photoreceptors and ciliated epithelia. *J. Cell Sci.* 104(Pt 4), 1229–1237.

Nachury, M. V. (2018). The molecular machines that traffic signaling receptors into and out of cilia. *Curr. Opin. Cell Biol.* 51, 124–131. doi: 10.1016/j.ceb.2018.03.004

Nag, S., and Resnick, A. (2017). Biophysics and biofluid dynamics of primary cilia: evidence for and against the flow-sensing function. *Am. J. Physiol. Renal. Physiol.* 313, F706–F720. doi: 10.1152/ajprenal.00172.2017

Nikonova, A. S., Deneka, A. Y., Kiseleva, A. A., Korobeynikov, V., Gaponova, A., Serebriiskii, I. G., et al. (2018). Ganetespib limits ciliation and cystogenesis in autosomal-dominant polycystic kidney disease (ADPKD). *FASEB J.* 32, 2735–2746. doi: 10.1096/fj.201700909R

Nikonova, A. S., Plotnikova, O. V., Serzhanova, V., Efimov, A., Bogush, I., Cai, K. Q., et al. (2014). Nedd9 restrains renal cystogenesis in Pkd1-/- mice. *Proc. Natl. Acad. Sci. U.S.A.* 111, 12859–12864. doi: 10.1073/pnas.1405362111

Pagliero, R. J., D'astolfo, D. S., Lelieveld, D., Pratiwi, R. D., Aits, S., Jaattela, M., et al. (2016). Discovery of small molecules that induce lysosomal cell death in cancer cell lines using an image-based screening platform. *Assay Drug Dev. Technol.* 14, 489–510. doi: 10.1089/adt.2016.727

Pan, J., Seeger-Nukpezah, T., and Golemis, E. A. (2013). The role of the cilium in normal and abnormal cell cycles: emphasis on renal cystic pathologies. *Cell. Mol. Life Sci.* 70, 1849–1874. doi: 10.1007/s00018-012-1052-z

Pazour, G. J., Dickert, B. L., Vucica, Y., Seeley, E. S., Rosenbaum, J. L., Witman, G. B., et al. (2000). Chlamydomonas IFT88 and its mouse homologue, polycystic kidney disease gene tg737, are required for assembly of cilia and flagella. *J. Cell Biol.* 151, 709–718. doi: 10.1083/jcb.151.3.709

Pedersen, L. B., Veland, I. R., Schroder, J. M., and Christensen, S. T. (2008). Assembly of primary cilia. *Dev. Dyn.* 237, 1993–2006. doi: 10.1002/dvdy.21521

Piperno, G., and Fuller, M. T. (1985). Monoclonal antibodies specific for an acetylated form of alpha-tubulin recognize the antigen in cilia and flagella from a variety of organisms. *J. Cell Biol.* 101, 2085–2094. doi: 10.1083/jcb.101.6.2085

Plotnikova, O. V., Nikonova, A. S., Loskutov, Y. V., Kozyulina, P. Y., Pugacheva, E. N., and Golemis, E. A. (2012). Calmodulin activation of Aurora-A kinase (AURKA) is required during ciliary disassembly and in mitosis. *Mol. Biol. Cell* 23, 2658–2670. doi: 10.1091/mbc.E11-12-1056

Pugacheva, E. N., and Golemis, E. A. (2006). HEF1-aurora A interactions: points of dialog between the cell cycle and cell attachment signaling networks. *Cell Cycle* 5, 384–391. doi: 10.4161/cc.5.4.2439

Pugacheva, E. N., Jablonski, S. A., Hartman, T. R., Henske, E. P., and Golemis, E. A. (2007). HEF1-dependent Aurora A activation induces disassembly of the primary cilium. *Cell* 129, 1351–1363. doi: 10.1016/j.cell.2007.04.035

Reiter, J. F., and Leroux, M. R. (2017). Genes and molecular pathways underpinning ciliopathies. *Nat. Rev. Mol. Cell Biol.* 18, 533–547. doi: 10.1038/nrm.2017.60

Ross, D. A., Lee, S., Reiser, V., Xue, J., Alves, K., Vaidya, S., et al. (2008). Multiplexed assays by high-content imaging for assessment of GPCR activity. *J. Biomol. Screen.* 13, 449–455. doi: 10.1177/1087057108317685

Schindelin, J., Rueden, C. T., Hiner, M. C., and Eliceiri, K. W. (2015). The imageJ ecosystem: an open platform for biomedical image analysis. *Mol. Reprod. Dev.* 82, 518–529. doi: 10.1002/mrd.22489

Schou, K. B., Pedersen, L. B., and Christensen, S. T. (2015). Ins and outs of GPCR signaling in primary cilia. *EMBO Rep.* 16, 1099–1113. doi: 10.15252/embr.201540530

Seeger-Nukpezah, T., and Golemis, E. A. (2012). The extracellular matrix and ciliary signaling. *Curr. Opin. Cell Biol.* 24, 652–661. doi: 10.1016/j.ceb.2012.06.002

Seeger-Nukpezah, T., Liebau, M. C., Hopker, K., Lamkemeyer, T., Benzing, T., Golemis, E. A., et al. (2012). The centrosomal kinase Plk1 localizes to the transition zone of primary cilia and induces phosphorylation of nephrocystin-1. *PLoS One* 7:e38838. doi: 10.1371/journal.pone.0038838

Seeger-Nukpezah, T., Proia, D. A., Egleston, B. L., Nikonova, A. S., Kent, T., Cai, K. Q., et al. (2013). Inhibiting the HSP90 chaperone slows cyst growth in a mouse model of autosomal dominant polycystic kidney disease. *Proc. Natl. Acad. Sci. U.S.A.* 110, 12786–12791. doi: 10.1073/pnas.1301904110

Sharpey, W. (1835). "Cilia," in *Cyclopoedia of Anatomy and Physiology*, ed. R. B. Todd (London: Longman, Brown, Green, Longman and Roberts), 606–638.

Spasic, M., and Jacobs, C. R. (2017). Primary cilia: cell and molecular mechanosensors directing whole tissue function. *Semin. Cell Dev. Biol.* 71, 42–52. doi: 10.1016/j.semcdb.2017.08.036

Tape, C. J., Ling, S., Dimitriadi, M., Mcmahon, K. M., Worboys, J. D., Leong, H. S., et al. (2016). Oncogenic KRAS regulates tumor cell signaling via stromal reciprocation. *Cell* 165, 910–920. doi: 10.1016/j.cell.2016.03.029

Uetake, Y., and Sluder, G. (2004). Cell cycle progression after cleavage failure: mammalian somatic cells do not possess a "tetraploidy checkpoint". *J. Cell Biol.* 165, 609–615. doi: 10.1083/jcb.200403014

Vincensini, L., Blisnick, T., and Bastin, P. (2011). 1001 model organisms to study cilia and flagella. *Biol. Cell* 103, 109–130. doi: 10.1042/BC20100104

Wang, T., Li, Z., Cvijic, M. E., Krause, C., Zhang, L., and Sum, C. S. (2004). "Measurement of beta-arrestin recruitment for GPCR targets," in *Assay Guidance Manual*, eds G. S. Sittampalam, N. P. Coussens, K. Brimacombe, A. Grossman, M. Arkin, D. Auld, et al. (Rockville, MD: Bethesda).

Zaghloul, N. A., and Katsanis, N. (2009). Mechanistic insights into Bardet-Biedl syndrome, a model ciliopathy. *J. Clin. Invest.* 119, 428–437. doi: 10.1172/JCI37041

Conflict of Interest Statement: The authors declare that the research was conducted in the absence of any commercial or financial relationships that could be construed as a potential conflict of interest.

frontiers in Genetics

ORIGINAL RESEARCH
published: 01 March 2019
doi: 10.3389/fgene.2019.00023

Identification of Important Effector Proteins in the FOXJ1 Transcriptional Network Associated With Ciliogenesis and Ciliary Function

Ishita Mukherjee[1], Sudipto Roy[2,3,4] and Saikat Chakrabarti[1]**

[1] Translational Research Unit of Excellence, Structural Biology and Bioinformatics Division, Council for Scientific and Industrial Research – Indian Institute of Chemical Biology, Kolkata, India, [2] Institute of Molecular and Cell Biology, Singapore, Singapore, [3] Department of Paediatrics, Yong Loo Lin School of Medicine, National University of Singapore, Singapore, Singapore, [4] Department of Biological Sciences, National University of Singapore, Singapore, Singapore

OPEN ACCESS

Edited by:
Jose Maria Carvajal-Gonzalez, Universidad de Extremadura, Spain

Reviewed by:
Angel Carlos Roman, Cajal Institute (CSIC), Spain
Georges Nemer, American University of Beirut, Lebanon

***Correspondence:**
Sudipto Roy
sudipto@imcb.a-star.edu.sg
Saikat Chakrabarti
saikat@iicb.res.in

Specialty section:
This article was submitted to Genetic Disorders, a section of the journal Frontiers in Genetics

Received: *27 July 2018*
Accepted: *15 January 2019*
Published: *01 March 2019*

Citation:
Mukherjee I, Roy S and Chakrabarti S (2019) Identification of Important Effector Proteins in the FOXJ1 Transcriptional Network Associated With Ciliogenesis and Ciliary Function. Front. Genet. 10:23. doi: 10.3389/fgene.2019.00023

Developmental defects in motile cilia, arising from genetic abnormalities in one or more ciliary genes, can lead to a common ciliopathy known as primary ciliary dyskinesia (PCD). Functional studies in model organisms undertaken to understand PCD or cilia biogenesis have identified 100s of genes regulated by Foxj1, the master regulator of motile ciliogenesis. However, limited systems based studies have been performed to elucidate proteins or network/s crucial to the motile ciliary interactome, although this approach holds promise for identification of multiple cilia-associated genes, which, in turn, could be utilized for screening and early diagnosis of the disease. Here, based on the assumption that FOXJ1-mediated regulatory and signaling networks are representative of the motile cilia interactome, we have constructed and analyzed the gene regulatory and protein–protein interaction network (PPIN) mediated by FOXJ1. The predicted FOXJ1 regulatory network comprises of 424 directly and 148 indirectly regulated genes. Additionally, based on gene ontology analysis, we have associated 17 directly and 6 indirectly regulated genes with possible ciliary roles. Topological and perturbation analyses of the PPIN (6927 proteins, 40,608 interactions) identified 121 proteins expressed in ciliated cells, which interact with multiple proteins encoded by FoxJ1 induced genes (FIG) as important interacting proteins (IIP). However, it is plausible that IIP transcriptionally regulated by FOXJ1 and/or differentially expressed in PCD are likely to have crucial roles in motile cilia. We have found 20 de-regulated topologically important effector proteins in the FOXJ1 regulatory network, among which some (PLSCR1, SSX2IP, ACTN2, CDC42, HSP90AA1, PIAS4) have previously reported ciliary roles. Furthermore, based on pathway enrichment of these proteins and their primary interactors, we have rationalized their possible roles in the ciliary interactome. For instance, 5 among these novel proteins that are involved in cilia associated signaling pathways (like Notch, Wnt, Hedgehog, Toll-like receptor etc.) could be 'topologically

important signaling proteins.' Therefore, based on this FOXJ1 network study we have predicted important effectors in the motile cilia interactome, which are possibly associated with ciliary biology and/or function and are likely to further our understanding of the pathophysiology in ciliopathies like PCD.

Keywords: FOXJ1, motile cilia, primary ciliary dyskinesia, ciliopathy, transcriptional network, protein–protein interaction, network analysis

INTRODUCTION

Cilia, microtubule based hair-like organelles, are primarily composed of a structural core, the axoneme, in addition to the basal body, transition zone, ciliary membrane and the ciliary tip (Fliegauf et al., 2007). Macromolecular synthesis and assembly of all of these ciliary structures is a complex and co-ordinately regulated process that involves intraflagellar transport (except cytosolic ciliogenesis), membrane trafficking and selective import of ciliary proteins through the transition zone (Ishikawa and Marshall, 2011). Based on their axonemal organization, 9+2 microtubular architecture with dynein arms or 9+0 without dynein, cilia can be either motile or non-motile, respectively. Both of these kinds of cilia have diverse tissue specific roles in different physiological and developmental processes like cellular motility, fluid clearance, sensory reception, and signaling (Bisgrove and Yost, 2006; Fliegauf et al., 2007). Given their complexity, mutation(s) or defect(s) in one or more proteins involved in the structural organization of cilia or regulation of their assembly can result in abnormalities in the formation or function of these organelles (Horani et al., 2016). These defects in cilia formation or function result in disrupted development of body pattern or physiology of multiple organ systems (Bisgrove and Yost, 2006; Ishikawa and Marshall, 2011) leading to a range of disorders collectively referred to as 'ciliopathies.' In particular, this spectrum of disorders could be associated with immotile/primary cilia like polycystic kidney diseases, nephronophthisis, Bardet-Biedl syndrome etc. or with motile cilia like primary ciliary dyskinesia (PCD) (Bisgrove and Yost, 2006).

PCD, the most prevalent of ciliopathies, is a genetically heterogeneous disorder, clinically associated with chronic respiratory infections, bronchiectasis, infertility and in certain cases, hydrocephalus or laterality defects (Zariwala et al., 2011). However, PCD exhibits variability in clinical phenotype, and further, mutations in all disease causing genes may not be exhibited as defects in ciliary ultrastructure. Thus, a genetic screening test for PCD causing genes could be helpful for disease diagnosis (Zariwala et al., 2011). In this respect, the genetic basis of PCD, which is usually inherited as an autosomal recessive trait, has been studied with the help of conventional family based, genome-wide linkage studies, candidate gene testing, homozygosity mapping as well as genome and exome sequencing studies to identify causative mutations (Zariwala et al., 2011; Horani et al., 2016). In addition, while identification of PCD causing genes with conventional studies (family based or genome-wide linkage analysis) has been challenging due to locus heterogeneity, nevertheless, different sequencing approaches have identified multiple disease causing genes in families of PCD patients during the last decade (Zariwala et al., 2011; Horani et al., 2016). At present, the OMIM database lists about 35 disease causing genes with mutations associated with PCD (McKusick, 1998; Amberger et al., 2015).

However, such disease causing variants identified with the help of sequencing could be family specific (Horani et al., 2016), and moreover, such approaches may only be useful to study certain cases that have been successfully diagnosed. Thus, other complementary approaches in model organisms, which explore cilia biogenesis to identify genes or proteins important in cilia formation or function, have also been undertaken (for example, May-Simera et al., 2016; Rao et al., 2016; Terré et al., 2016). In addition, some large scale studies have identified thousands of proteins in the ciliary proteome that co-ordinately interact to form these organelles (Ishikawa et al., 2012; Boldt et al., 2016), and such cascades of interactions are regulated by transcription factors like GemC1, McIdas, E2f4, E2f5, Myb, Rfx1, Rfx2, Rfx3, Rfx4, and FoxJ1 (Choksi et al., 2014b; Arbi et al., 2016; Danielian et al., 2016; Vladar and Mitchell, 2016). Further, while Rfx factors regulate both motile and immotile cilia genes, FoxJ1 specifically regulates motile cilia biogenesis, and appears to be its master regulator (Choksi et al., 2014b). This is because FoxJ1 regulates a set of genes known as FoxJ1 induced genes (FIG), which together are sufficient for motile cilia development and function (Stubbs et al., 2008; Yu et al., 2008; Choksi et al., 2014a).

In this study, our primary objective lay in studying the motile cilia interactome to identify possible essential proteins and their probable functions in this interactome. In this respect, we have studied two components of the motile cilia interactome, a probable transcriptional network and a probable signaling network. The transcriptional network in the motile cilia interactome that we have considered here is the FOXJ1 regulatory network. For this purpose, we have predicted the regulatory network of the motile cilia master regulator, FOXJ1 and annotated the network genes based on information from different ciliary reference databases. Based on this analysis, however, we found that while ∼83% of the regulatory network genes are expressed in multiple motile ciliated tissues, only ∼24% of them are presently annotated. Further, the annotated network genes mainly comprised of ciliary structural component proteins or motility associated proteins. As mentioned above, it has been established in previous studies that FoxJ1 over-expression is sufficient to drive the motile ciliogenic program and generate functional ectopic motile cilia (Stubbs et al., 2008; Yu et al., 2008; Choksi et al., 2014a). It is possible that the FIG encoded protein (FIGp) participate in motile cilia assembly or function in a co-ordinated manner in association with other

proteins (signaling) of the ciliary milieu. In this context, we next sought to study the representative motile cilia interactome comprised of the regulatory network proteins and their protein–protein interaction network (PPIN) with different graph theory metrics. This analysis was performed in order to identify the key connector proteins (regulatory network proteins) that relay the information onto the signaling component/s during motile cilia biogenesis. Further, the topological analysis has been complemented with a functional analysis to determine whether these proteins could indeed be essential for ciliogenesis or ciliary function. Traditionally, such essential proteins have been identified with the help of gene misexpression, targeted gene knock-out or knock-down studies in experimental model systems (Stubbs et al., 2008; Yu et al., 2008; Choksi et al., 2014a; May-Simera et al., 2016; Terré et al., 2016). By contrast, in this study we have utilized an *in silico* knock-out strategy, and determined the effects on the motile cilia interactome by deriving whether the effective change in a centrality measure as a result of the knock-out varied significantly. Moreover, in order to ascertain the relevance of these predicted essential proteins to ciliary biology, we have utilized literature-based evidences to determine whether some of the proteins have previously identified involvements in ciliary biology. Finally, to determine the likely functions of these proteins, we have utilized the concept of 'guilt by association' (which states that two proteins that are known to interact with one another, may usually participate in the same or similar cellular functions; Oliver, 2000; Schwikowski et al., 2000), and determined the enriched pathways or processes among the proteins of interest.

Thus, studying the PPIN associated with the FOXJ1 regulatory network might help us in elucidating the topologically important effector proteins that lie at the interface of the FOXJ1 regulatory network and the associated protein interaction network. These proteins might form a crucial link between the FOXJ1 regulatory and cilia biogenesis-associated signaling components in the motile cilium, and mediate some of the functions of FOXJ1 and its regulatory network. Importantly, such proteins identified in this manner could be crucial for ciliary development or maintenance of ciliary function, and one could screen for defects in this repertoire of proteins to determine possible causal or etiological genes for PCD.

MATERIALS AND METHODS

Collating an Information Resource Regarding Cilia Biogenesis

Genes experimentally probed and identified to be involved in ciliogenesis or ciliary function were collected from different studies and databases like the SysCilia gold standard database (van Dam et al., 2013), Reactome pathway database [R-HSA-5617833] (Croft et al., 2014; Fabregat et al., 2018), FIG study (Choksi et al., 2014a), cilliary proteome related studies (Gupta et al., 2015; Boldt et al., 2016) and OMIM database (McKusick, 1998; Amberger et al., 2015). This resource has been subsequently utilized to summarize the previously identified involvement(s) of the FOXJ1 transcriptional network genes. It has also been utilized as a preliminary validation resource to ascertain whether certain genes predicted to be involved in ciliogenesis or ciliary function by our computational approach are actually involved in the process.

Cilia Associated Expression Analysis

In order to prepare a set of disease (PCD) associated genes, we have considered a dataset available from a previous study that explored the expression profile of bronchial tissue of PCD patients (Geremek et al., 2014). Differentially expressed genes were determined with the help of limma (Ritchie et al., 2015) R package in Gene Expression Omnibus (GEO) series dataset (GSE25186) (Edgar et al., 2002; Barrett et al., 2013; Geremek et al., 2014). Genes having fold change ≥ 2 and p-value ≤ 0.05 were considered as differentially expressed and possibly associated with PCD based on the considered PCD case study. Databases or datasets [e.g., Choksi et al. (2014a) expression study, CilDB (Arnaiz et al., 2009; Arnaiz et al., 2014), PCD expression analysis case study (Geremek et al., 2014) and Human Protein Atlas (Uhlen et al., 2010; Uhlén et al., 2015; Thul et al., 2017)] providing evidence for RNA or protein expression abundance in ciliary cells were taken into consideration for 'cilia associated expression analysis.' For this, if genes had expression information in the 'cilia associated expression analysis,' they were considered to have possible associations with ciliary biology.

Constructing the FOXJ1 Regulatory Network

Transcription factor binding sites may generally be predicted by scanning a position weight matrix (PWM) against DNA using a pattern matching algorithm (Bulyk, 2004). Genes which are likely to be regulated transcriptionally by FOXJ1 were predicted with the help of Rsat (Turatsinze et al., 2008). An initial set of genes (FIG) to be studied was prepared based on their induction upon FoxJ1 over-expression in the zebrafish (Choksi et al., 2014a). With the help of the Ensembl Compara database we could determine that these FIG have high confidence orthologs in humans (*Homo sapiens*) and mice (*Mus musculus*) (Herrero et al., 2016). Further, for prediction of transcription factor binding motifs, pre-requisites include a PWM for the transcription factor and a background matrix representative of general base frequencies around the transcription start site (TSS) of genes. It is possible that orthologous transcription factors from human and mouse may share similar binding specificities (Jolma et al., 2013). Thus, a PWM for FoxJ1 (mouse) [PB0016.1] was collected from footprintDB database (Sebastian and Contreras-Moreira, 2014) since PWM for human FOXJ1 is unavailable. It was observed that these proteins are 92.6% identical, and moreover, the DNA binding domains are 100% identical (**Supplementary Figure 1A**), which further suggested that these proteins may share similar binding specificities. Further, a background model (Markov order), representative of ± 6 kb of random *Homo sapiens* genes, was prepared. These were then utilized to scan ± 6 kb of the FIG for the presence of FOXJ1 binding motif (Medina-Rivera et al., 2015). Predicted binding sites having p-value $\leq 1e^{-04}$ were considered to be genes directly regulated by FOXJ1. Further, a logoplot (R Core Team, 2016) representative of the binding specificity of FOXJ1 (human) was prepared from the multiple

sequence alignment of the predicted FOXJ1 binding sites among human orthologs of FIG.

Determining Ciliary Functional Associations of FOXJ1 Regulatory Network Genes Based on Gene Ontology (GO) Analysis

Based on the CCR dataset we could ascertain the ciliary roles of some of the FOXJ1 regulatoy network genes. However, we further performed GO analysis and GO enrichment analysis in order to assign probable functional relevance to the remaining genes. GO analysis was performed using DAVID web server (Huang da et al., 2009b), and with the help of FGNet (Aibar et al., 2015), certain GO based enriched clusters among the genes were determined. Functions of genes belonging to clusters having p-value $\leq 1e^{-02}$, cluster enrichment score ≥ 2, fold enrichment ≥ 4 could be predicted based on this analysis.

Constructing the FOXJ1 Associated Ciliary Interactome

In order to prepare a PPIN representative of proteins and connections important for cilia structure or function in relation to FOXJ1 activation, we considered the FIGp as seed proteins. In particular, a PPIN is comprised of proteins as nodes, and two proteins are connected by an edge if they are known to be interacting. Thus, a PPIN was constructed around these seed proteins by obtaining high confidence experimentally reported interactions between these proteins and other proteins from SysCilia (van Dam et al., 2013), Bioplex (Huttlin et al., 2015), STRING (Szklarczyk et al., 2015), and BioGrid (Stark et al., 2006; Chatr-aryamontri et al., 2017) databases. In this way, a network of primary interactors of FIGp was constructed, and the largest connected component of this network was extracted (FIG-sub-network). We then analyzed the degree distribution of the FIG-sub-network to determine whether the constructed network was a scale free network wherein the degree distribution follows a power law. The degree (k: number of proteins each protein is connected to) of each protein in the network was computed and a power law [$P(k) \sim k^{-\alpha}$ where α is the degree exponent] was fitted to the resulting distribution. A Kolmogorov–Smirnov test (which computes a p-value for the estimated power-law fit to the data) was used to determine the goodness of fit of the degree distributions to the power law (at 0.1 level of significance) (Clauset et al., 2009; R Core Team, 2016).

Identifying Topologically Important or Essential Proteins in the Representative Motile Cilia Interactome (FIG-sub-network)

Once we had a PPIN representative of motile cilia interactome in hand, we analyzed the FIG-sub-network based on a computationally faster implementation of a previously proposed methodology (Bhattacharyya and Chakrabarti, 2015). With the help of this analysis we have identified topologically important proteins in this network. For this purpose, we have considered different graph theory metrics like degree, shortest path and centrality to determine important interacting proteins (IIP) (combination of hub, bottleneck, central, local network perturbing, and global network perturbing proteins) in our FIG-sub-network as outlined below.

Node Perturbation Analysis of the FIG-sub-network

Previously, it has been found that removal of hub proteins has a significant effect on the topology of the PPIN, while they are extremely resilient toward the removal of random nodes (Barabási and Oltvai, 2004). Based on this observation, we have previously devised a centrality measure which tries to capture the change in the topology of the network on *in silico* node removal to identify topologically important proteins in a protein interaction network (Bhattacharyya and Chakrabarti, 2015). Thus, with the objective of identifying topologically important proteins, a node perturbation analysis of the global network and local sub-graphs in the FIG-sub-network was performed. The local sub-graphs comprised of proteins having degree higher than 2, and their 2nd level interactors and the local network centrality measures of the nodes before and after node removal in the local sub-graph were compared. It was assumed that higher the difference in the scores (LNCS), higher is the perturbation ability, and thus, proteins important for maintaining the integrity of the local sub-network determined in this manner were termed as local network perturbing proteins (LNPP). Similarly, global network perturbation was performed by removing a single node at a time and studying its effect on the global network centrality score (GNCS) before and after the perturbation. Proteins identified as crucial for maintaining the global sub-network integrity, based on the difference in the GNCS scores before and after perturbation, were termed as global network perturbing proteins (GNPP).

$$CS = \sum C(betweeness) + C(closeness) + C(clustering\ coeficient)$$

$$CCS = \sum_{1}^{n} CS$$

$$LNCS = 1/N \sum_{1}^{N} CCS$$

where n is the number of first degree interactors, CS is the combined score, CCS is the cumulative centrality score, $LNCS$ is the local network centrality score and N is the number of nodes in local sub graph. The LNCS scores were normalized into z-score and nodes having z-score ≥ 1 were considered as LNPP.

$$GNCS = 1/N \sum_{1}^{N} CCS$$

where $GNCS$ is the global network centrality score and N is the number of nodes in the global network. The GNCS scores were normalized into z-score and nodes having z-score ≥ 0.5 were considered as GNPP.

Identification of Hub and Bottleneck Proteins

Analyses of different biological PPINs have identified that hub and bottleneck proteins, which are determined by graph

theory calculations that measure inherent properties of scale free networks, could indeed be essential proteins (Barabási and Oltvai, 2004; Albert, 2005; Yu et al., 2007). For calculating hubs, the node degrees were normalized into z-scores and the fraction of degree population having z-score $\geq$2 was considered as having significantly higher degree than the rest of the population, and protein nodes having degree 57 or higher were considered as hub proteins. Additionally, bottleneck proteins which have a high betweenness centrality value (multiple "shortest paths" passing through them) could be key connector proteins (Yu et al., 2007). Herein, proteins having betweenness centrality indices higher than two standard deviations from the mean of the betweenness centrality distribution were considered as bottleneck proteins.

Centrality Analysis of the FIG-sub-network

Compactness of a network and capability of relaying information can be further assessed with the help of another graph theory based concept, for instance, centrality (Pavlopoulos et al., 2011). It is possible to identify proteins which could be of biological significance with the help of centrality analysis, since previous reports have suggested that the removal of central proteins by gene deletion may lead to lethal phenotypic consequences (Jeong et al., 2001). Thus herein, we have considered a range of centrality indices to identify central proteins with possible biological significance in our FIG-sub-network. Centrality indices like closeness, load, eigen centrality and clustering coefficient were evaluated and combined to derive an average centrality parameter (combined score, CS) for each node. The CS and the cumulative centrality score (CCS) were computed as shown below:

$$CS = \sum C(load) + C(closeness) + C(eigen\ vector) + C(clustering\ coeficient)$$

$$CCS = \sum_{1}^{n} CS$$

where n is the number of first degree interactors, CS is the combined score and CCS is the cumulative centrality score. The CCS scores were normalized into z-score and nodes having z-score $\geq$ 2 were considered as central proteins.

IIP in the FIG-sub-network

Based on the assumption that proteins identified as topologically important in two or more categories (hub, bottleneck, central, local network perturbing, and global network perturbing) could be essential proteins in the FIG-sub-network, we have categorized them as IIP. Only proteins with expression information support in ciliated cells based on 'cilia associated expression analysis' were retained as IIP. Additionally, any overlap between the IIP and the CCR dataset may be suggestive of their functional relevance in the ciliary milieu. Moreover, in order to ascertain the probable functional role(s) of these IIP in association with FIGp, we have estimated the enriched pathways among interacting FIGp, IIP and their direct interactors with the help of an R package (Yu and He, 2016).

Identifying Important Effector Proteins by Comparing FOXJ1 Associated Transcriptional and PPINs

IIP which could be associated with ciliogenesis or PCD based on their differential expression status upon ectopic FoxJ1 expression in zebrafish or in PCD were identified as important effectors in FOXJ1 regulatory network. Further, these topologically important effector proteins are likely to be involved in a range of cellular pathways particularly signaling pathways. Pathway enrichment analysis with p-value cut off of $1e^{-06}$ was performed in ReactomePA (Yu and He, 2016) considering the effectors and their primary interactors. Proteins participating in enriched 'cilia associated signaling pathways' were predicted to have possible ciliary association. In this analysis, we have considered 'cilia associated signaling pathways' such as cell cycle (Quarmby and Parker, 2005; Izawa et al., 2015), TGF-beta (Clement et al., 2013), FGF (Neugebauer et al., 2009), RHO GTPase (Kim et al., 2015), Hedgehog, PDGF, WNT (Goetz and Anderson, 2010), TLR signaling (Baek et al., 2017) and vesicle mediated transport (Nachury et al., 2010), since all of these are known to have an association with cilia. The pathway enrichment analysis was complemented with GO mapping in DAVID (Huang da et al., 2009b). Proteins associated with GO categories associated with cilia biology like cilium morphogenesis, cell cycle (Quarmby and Parker, 2005; Izawa et al., 2015), actin organization (cytoskeleton organization, actin filament organization), protein ubiquitination, centrosome cycle, protein folding (heat shock proteins) and establishment or maintenance of cell polarity (Stephens and Lemieux, 1999; Pan et al., 2007; Nachury et al., 2010; Bettencourt-Dias et al., 2011; Jones et al., 2012; Prodromou et al., 2012; Kasahara et al., 2014; May-Simera et al., 2016; Shearer and Saunders, 2016; Kohli et al., 2017) were predicted to have possible ciliary association.

Determining the Relevance of the Predicted IIP in the Ciliary Interactome to Ciliary Biology

Literature based evidences of the involvements of the IIP in ciliary biology or gene expression based association of the IIP with PCD were considered as preliminary supportive evidences toward the relevance of the computational predictions to ciliary biology. In order to determine the significance of the finding that some of the IIP were found to be differentially expressed in PCD patients, we have performed a randomization analysis. In each trial, a 121 proteins were randomly selected from the set of proteins in FIG-sub-network and matched to the set of differentially expressed PCD proteins in our network. Based on the number of matches obtained in a 1000 trials, a z-test was performed to determine whether the association between the IIP and PCD expression status that we had observed was significant. Additionally, a few of the IIP proteins have previously reported ciliary roles in literature. A similar randomization analysis was performed considering matches with the CCR and the significance of this association was also determined.

RESULTS

FOXJ1 Regulatory Network Governing Motile Cilia Biogenesis and Function

Functional genomics studies have identified the FoxJ1 protein as the master regulator of motile ciliogenesis, and it is crucial for ciliary axoneme assembly, basal body docking and ciliary motility (Stubbs et al., 2008; Yu et al., 2008; Choksi et al., 2014a). Over-expression of FoxJ1 in model systems such as the zebrafish and *Xenopus* appears to be necessary and sufficient for the development of motile cilia (Stubbs et al., 2008; Yu et al., 2008). Therefore, determining the predicted regulatory network of FOXJ1, might in turn, help us to better understand ciliogenesis and ciliopathies associated with abnormal ciliary differentiation and function in humans. In order to study the regulatory network that is essential in motile cilia development, we have predicted the genes that are likely to be transcriptionally regulated, directly or indirectly, by FOXJ1 and associated them with known or probable ciliary roles. Based on the presence of FOXJ1 *cis*-regulatory sites in upstream/downstream region of transcription start sites of FIG (Choksi et al., 2014a), we could identify that a large fraction of the FIG (424/572) are directly regulated by FOXJ1 (**Supplementary Figure 1B** and **Supplementary Table 1**). It is likely that the other 148 induced genes either contain FOXJ1 binding sites in distant enhancers or are indirectly regulated by FOXJ1 via other transcription factors directly activated by FOXJ1. Further, the FOXJ1 protein appears to have a binding preference toward the consensus sequence NNN[GA]TAAACAAANNNN (**Supplementary Figure 1C**). Additionally, functional annotations for these genes were retrieved from the CCR, and the identified known ciliary associations for genes directly and indirectly regulated by FOXJ1 were classified into functional cohorts (Assigned Ciliary Role) manually (**Supplementary Table 2**).

Additional Ciliary Association for FOXJ1 Regulatory Network Genes Based on GO Analysis

Functional enrichment analysis of proteins associating with one another under a particular context may provide an idea regarding the probable collective activities and the most likely functions that these proteins may have in this context. At the outset, GO mapping elucidated 20 transcription factors (associated with DNA binding or transcription factor ontology class) among the FIGp (**Supplementary Table 2**). Further, predicted ciliary associations were determined based on GO enrichment analysis (**Supplementary Table 3**). In the GO mapped data, we found groups of genes having similar functions (co-associated genes) (Huang da et al., 2009a,b) belonging to multiple GO annotation categories, and such co-associated genes from different annotation clusters were grouped and categorized into common 'GO based Ciliary Association(s)' (**Supplementary Table 3**).

In this manner, we were able to assign possible ciliary roles to 102 (directly) and 35 (indirectly) regulated genes based on the CCR dataset (**Supplementary Table 2**), and 17 (directly) and 6 (indirectly) regulated genes with the help of the GO analysis (**Table 1**). Based on the CCR dataset based annotation, we could assign ciliary associations such as participating in 'ciliary structural assembly or motility' for most of the directly (82) and indirectly (26) regulated FOXJ1 target genes (**Figure 1** and **Supplementary Figure 2**). Briefly, this analysis elucidated that FOXJ1 primarily influences 'ciliary structural assembly or motility' by regulating three classes of proteins. These classes include 'proteins that act as structural constituents of cilia' (axoneme assembly, IFT complex, centrosome component, basal body associated), 'proteins that regulate the structural assembly of cilia' (cilia assembly, ciliogenesis) and 'proteins that have a role in ciliary function' (like ciliary transport or motility)

TABLE 1 | Novel predicted functions of FOXJ1 regulated genes based on gene ontology analysis.

S. No	FOXJ1 Target Gene	[1]Effect	[2]Assigned Ciliary Role
1	RABGAP1L	Direct	Cilia associated by localization
2	DNAH8	Direct	Ciliary structure/motility
3	TPPP3	Direct	Ciliary structure/motility
4	NME9	Direct	Ciliary structure/motility
5	DNAH17	Direct	Ciliary structure/motility
6	TPGS1	Direct	Ciliary structure/motility
7	EML5	Direct	Ciliary structure/motility
8	SYBU	Direct	Ciliary structure/motility
9	HSBP1	Direct	Regulates genes involved in ciliary assembly/motility (Transcription factor)
10	MYCBP	Direct	Regulates genes involved in ciliary assembly/motility (Transcription factor)
11	ATXN1	Direct	Regulates genes involved in ciliary assembly/motility (Transcription factor)
12	BARHL2	Direct	Regulates genes involved in ciliary assembly/motility (Transcription factor)
13	LMX1A	Direct	Regulates genes involved in ciliary assembly/motility (Transcription factor)
14	MEOX2	Direct	Regulates genes involved in ciliary assembly/motility (Transcription factor)
15	PAX8	Direct	Regulates genes involved in ciliary assembly/motility (Transcription factor)
16	RXRB	Direct	Regulates genes involved in ciliary assembly/motility (Transcription factor)
17	ZBTB22	Direct	Regulates genes involved in ciliary assembly/motility (Transcription factor)
18	TUBA3D	Indirect	Ciliary structure/motility
19	NR1H2	Indirect	Regulates genes involved in ciliary assembly/motility (Transcription factor)
20	FOSB	Indirect	Regulates genes involved in ciliary assembly/motility (Transcription factor)
21	ATF5	Indirect	Regulates genes involved in ciliary assembly/motility (Transcription factor)
22	CHD4	Indirect	Regulates genes involved in ciliary assembly/motility (Transcription factor)
23	ELF3	Indirect	Regulates genes involved in ciliary assembly/motility (Transcription factor)

[1]Effect: Direct/Indirect depending on whether the gene is directly or indirectly regulated by FOXJ1. [2]Assigned Ciliary Role: Predicted ciliary role based on gene ontology analysis.

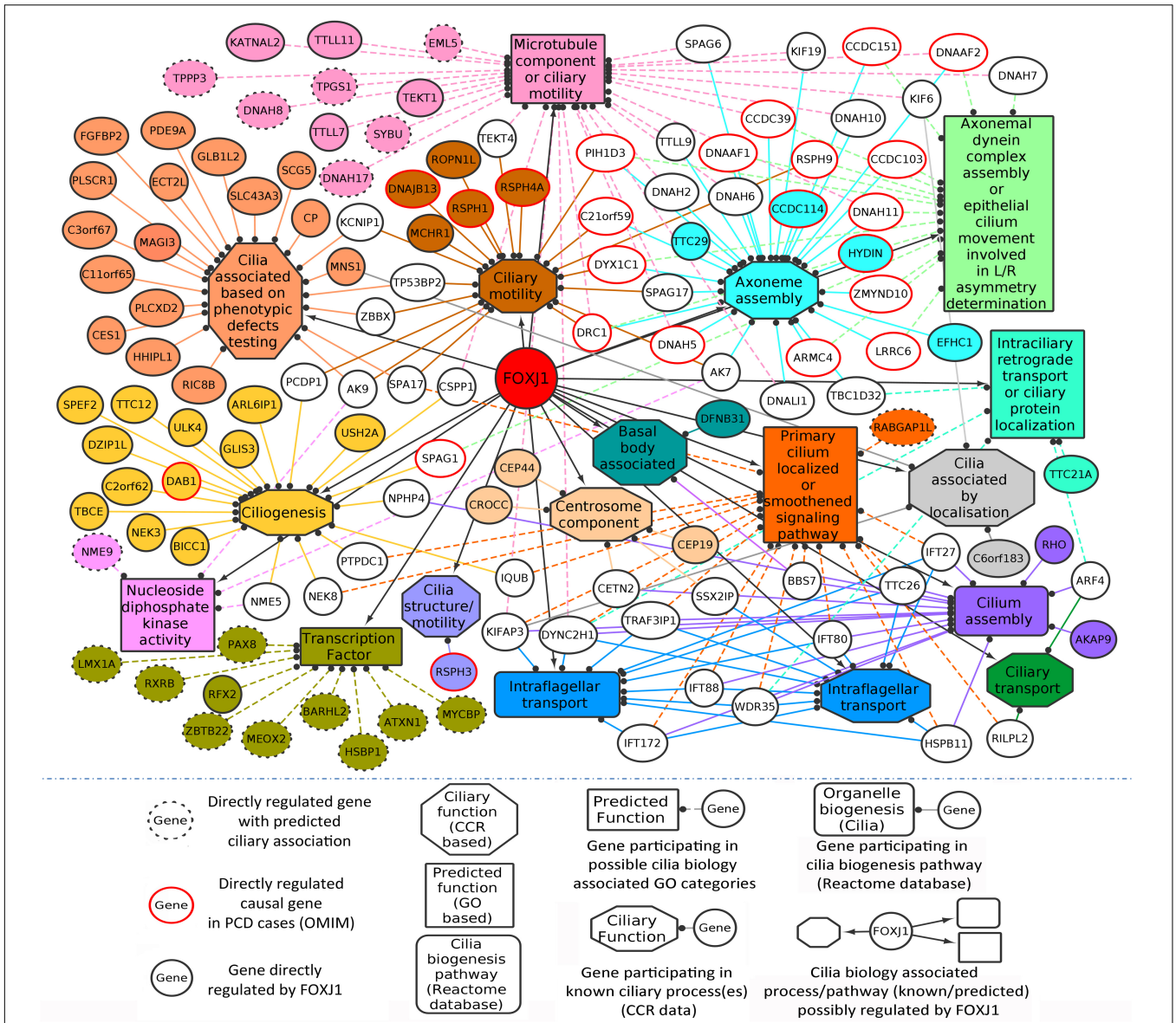

FIGURE 1 | Directly regulated genes in the predicted FOXJ1 gene regulatory network and possible ciliary processes mediated by them. FOXJ1 directly regulates genes that are involved in ciliary structure assembly and motility, as depicted here. Known ciliary associations were derived from the collated ciliary resource. Additionally, the probable roles of some genes predicted based on gene ontology analysis have also been included here. The genes and edges are color coded to indicate the processes the genes regulate or are involved in (genes associated with more than one process are not colored).

(**Figure 1**, **Supplementary Figure 2**, and **Supplementary Table 2**). A fraction of directly regulated (24.06%) and indirectly regulated (23.65%) FIG shared an overlap with the CCR dataset, and as such many FIG could not be associated with ciliary roles in this manner (**Supplementary Table 2**). Thus, having studied the FOXJ1 transcriptional network, it became apparent that the majority of genes that have been identified or extensively characterized are structural components of cilia. However, based on 'cilia associated expression analysis,' 84.67% of directly and 81.76% of indirectly regulated genes were found to be expressed in multiple motile ciliated tissues and some are differentially expressed in PCD (**Supplementary Figures 3A–C** and **Supplementary Table 2**). Further, it has been established that signaling pathways like Notch, Fgf and Wnt (Neugebauer et al., 2009; Lopes et al., 2010; Caron et al., 2012) are known to be involved in motile cilia biology. In this context, we were interested in studying the regulatory network proteins in a broader context including the associated protein–protein interactions, in order to identify the key connector proteins (regulatory network proteins) that relay the information onto the signaling component within the cell. Additionally, it is possible that disruptions in some of these network interactions or genes causing PCD may alter the motile cilia interactome, in turn leading to ciliopathies. Therefore, we were interested in

studying the probable signaling network/s acting concurrently or in response to FOXJ1 activation involved in this process. In order to achieve this, we have subsequently analyzed the PPIN associated with FOXJ1 and its induced proteins, and studied the probable role(s) of the identified essential or effector proteins in the network.

Essential or Important Interacting Proteins in Representative Motile Cilia Network

Identification of IIP in the FOXJ1 regulatory network or possible essential proteins in the motile cilia protein interactome may be achieved with extensive computational analysis of the PPIN likely to be associated with the FIGp. Scale free biological networks that follow a power law exhibit certain characteristic topological properties, which may be studied with different graph theory based metrics in pursuance of inferences regarding the PPIN (Barabási and Oltvai, 2004; Yook et al., 2004; Yu et al., 2007). Therefore, with the help of high confidence physical interaction data from different protein-protein interaction databases including cilia specific datasets, a re-constructed PPIN (FIG-sub-network) was prepared. The FIG-sub-network comprised of 6493 primary interactors of FIGp (434) and their first level interactors participating in 40,608 interactions (**Figure 2A**). Networks conforming to the power law must have *p*-value higher than 0.1 (Clauset et al., 2009), and the *p*-value of the estimated fit of the degree distribution to the power law determined herein was found to be 0.71. Thus, it was concluded that the re-constructed network was a scale free network (**Figure 2B**).

Network Analysis of Representative Motile Cilia Interactome (Primary Interaction Network of FIGp)

Topologically important proteins in a scale free PPIN like hub, bottleneck and central proteins, may be identified with the help of different graph theory based measures, and such proteins could be essential for the network integrity or function (Barabási and Oltvai, 2004; Yu et al., 2007; Pavlopoulos et al., 2011). In this respect, *in silico* node deletion that resulted in significant changes in network topology were studied as a measure of centrality, and 85 local network perturbing and 13 global network perturbing proteins were identified (**Figure 2C**). The overlap among these network perturbing proteins and other topologically important proteins [hub (243), bottleneck (86), and central (166)] was studied, and proteins identified as important in two or more metrics, were identified as IIP (122) (**Figure 2C** and **Supplementary Table 4**). Genes may be associated with cilia based on their expression, and such expression-based evidences from multiple studies might further strengthen our assumption that IIP possibly interact with FIGp in the ciliary interactome. We have taken into consideration expression information at the mRNA or protein levels in multiple motile ciliated tissues or differential expression (mRNA) information from studies exploring cilia biogenesis or ciliopathies as indicated in the 'cilia associated expression analysis' (**Figure 2D**). Further, the distribution pattern of the 121 cilia expressed IIP in multiple motile ciliated tissues elucidated that 114 among them were expressed in all ciliated tissues considered here (**Supplementary Figure 3D** and **Supplementary Table 4**). Moreover, among these proteins, 6 were found to be associated with PCD based on the differential expression analysis (**Supplementary Figure 3E**) [the randomization analysis indicated that this observation is significant at 10% level of significance]. Further, the observation that 33 IIP had established roles in ciliogenesis and/or cilia function suggested that the identified IIP could indeed have essential roles in motile cilia or PCD pathogenesis (**Supplementary Table 4**) [based on the randomization analysis this observation is significant at 1% level of significance].

IIP and Their Probable Essential Roles in Motile Cilia Interactome

Among the thousands of interacting proteins in the motile cilia interactome, 121 crucial interacting proteins were identified in the representative motile cilia interactome (primary interaction network of FIGp). These IIP form an inter-connected module in the ciliary interactome including 2060 interactions among FIGp (246), IIP (120) and their primary interactors (1666 motile cilia expressed proteins) (**Figure 3A**). Such IIP that have extensive interactions with FIGp could possibly be involved in the coordinated assembly of functional motile cilia in association with FIGp. Such interacting proteins namely FIGp and IIP, based on the concept of 'guilt by association' (Oliver, 2000; Schwikowski et al., 2000), may participate in the same or similar cellular pathways, possibly involved in ciliogenesis. In order to further determine the cellular pathways that the IIP might participate in together with FIGp, we have performed Reactome pathway enrichment analysis among the IIP and FIGp that were found to be interacting. Pathways such as signal transduction, developmental biology, cell cycle, generic transcription pathway, immune system etc. were found to be significantly enriched among these proteins (**Figure 3B** and **Supplementary Table 5**). This suggests that in addition to acting as structural components of the ciliary organelle, FIGp, in association with IIP, may participate in different signaling pathways, cell cycle and developmental biology associated processes or regulate transcription of other genes during motile cilia development.

Important Effector Proteins in the FOXJ1 Regulatory Network Possibly Involved in Ciliary Biology

As outlined above, by extensively analyzing the probable motile cilia interactome, we have determined topologically important proteins in the network. Further, we could identify a module comprised of 246 FIGp and topologically important proteins that are mainly signaling proteins. While such IIP may be essential in the ciliary milieu and possibly functionally relevant, another pertinent question is which proteins in the FOXJ1 regulatory network might act as essential modulators that relay the information onto the signaling component. To address this question, firstly we have considered whether genes that are induced upon FoxJ1 over-expression have been identified as

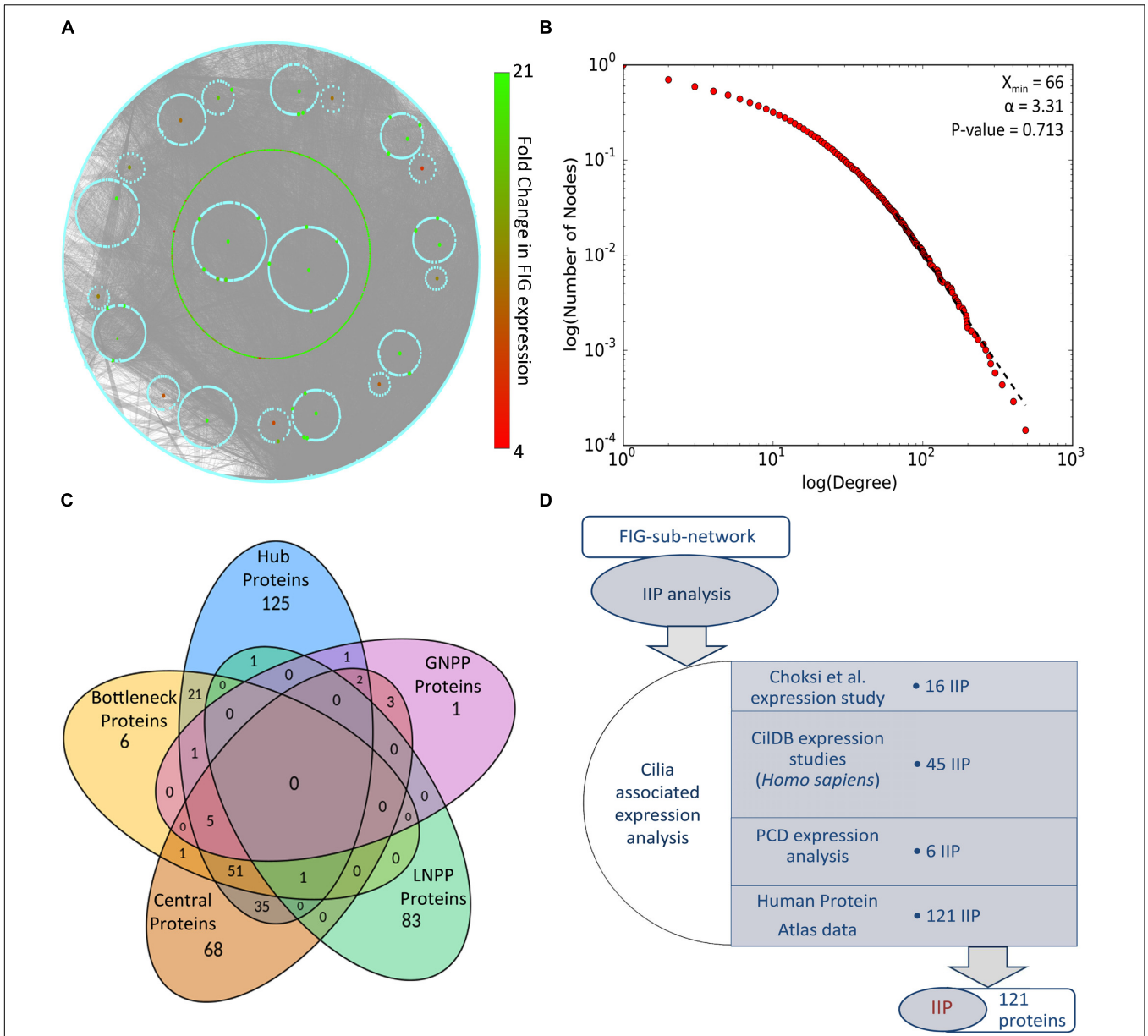

FIGURE 2 | PPIN analysis of primary interaction network of FIG-sub-network proteins. **(A)** The scale free network comprising of largest connected component of primary interaction network of FIGp considered for the IIP analysis is shown here. **(B)** The degree distribution plot and the p-value for goodness of fit of the power law to the degree distribution as determined by the Kolmogorov-Smirnov test is represented here. **(C)** The number of proteins identified in each category (hub, bottleneck, central, local network perturbing and global network perturbing protein) considered during IIP analysis are indicated in the Venn diagram. **(D)** The number of proteins that could be associated with cilia based on 'cilia associated expression analysis' that were considered as IIP is shown here. Abbreviations: FIG, FoxJ1 induced genes; FIGp, FIG encoded protein; IIP, Important interacting proteins; PPIN, protein-protein interaction network.

IIP. In this respect, we have found that in particular 16 IIP in the regulatory network interact with multiple other FIG (26), IIP (68) and other expression associated ciliary interactome proteins (1255) (**Figure 3A**). These FIGp that share extensive interactions with topologically important proteins in the motile cilia interactome are possibly key mediators acting downstream of FOXJ1 activation that in turn participate in ciliogenesis or maintenance of ciliary function. Moreover, genes may be associated with ciliogenesis or PCD based on their differential expression in respiratory epithelial cells of patients with PCD. Interestingly, an additional set of 4 IIP that were found to be differentially expressed in a PCD case study also had associations with multiple FIGp (**Figure 3A**). Thus, such IIP found to be directly involved in the FOXJ1 regulatory network have been classified as important interacting protein effector (IIP-effector) in the FOXJ1 regulatory network. In addition, IIP that have possible associations with PCD and the FOXJ1 regulatory network (via intermediate FIGp), have also been classified as

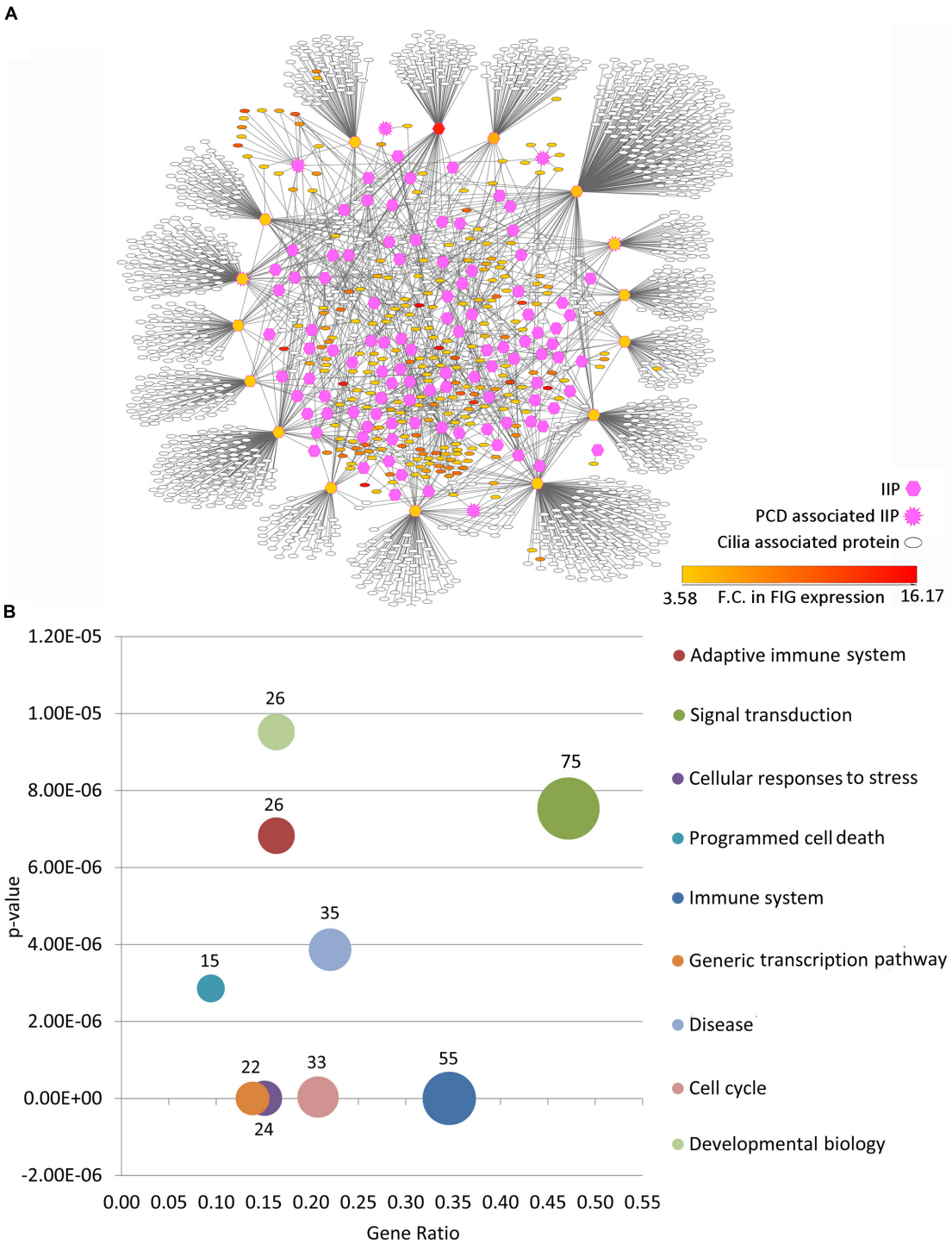

FIGURE 3 | Inter-relationship among IIP and FOXJ1 regulatory network proteins or FIGp. **(A)** The IIP (120) and their primary interactors form an inter-connected module with FIGp (246) within the motile cilia interactome as depicted here. **(B)** Cellular pathways that the inter-connected FOXJ1 regulatory network proteins and IIP (enriched pathways with p-value lower than $1e^{-05}$) are likely to be involved in are shown. Abbreviations: F.C., Fold change; FIG, FoxJ1 induced genes; FIGp, FIG encoded protein; IIP, Important interacting proteins; PCD, Primary ciliary dyskinesia.

IIP-effector in the FOXJ1 regulatory network (**Table 2**). While some of these effector proteins (HSP90AA1, CDC42, ACTN2, SSX2IP, PLSCR1, PIAS4) have previously documented roles in ciliogenesis (Choi et al., 2013; Choksi et al., 2014a; Croft et al., 2014; Klinger et al., 2014; Ramachandran et al., 2015; Kohli et al., 2017; Fabregat et al., 2018), we report here a set of 14

TABLE 2 | IIP-effector proteins in FOXJ1 regulatory network.

IIP-effector Category	Gene Name	[1]IIP category	[2]GO association (Ciliary)	[3]Comment
IIP directly regulated by FOXJ1	ATXN1	HUB and BP and CP		
	EEF1A1	HUB and BP and CP		Associated with BBSome proteins (**Figure 4**), could be involved in cargo trafficking to cilia
	FKBP5	HUB & BP	Protein folding (GO) [GO:0006457~protein folding]	
	PIAS4	HUB and CP		PIAS4 regulates SUMOylation of Glis2/NPHP7, which is a transcriptional regulator mutated in type 7 nephronophthisis (Ramachandran et al., 2015)
	PLSCR1	HUB and BP		Cilia phenotype defects occur upon knockdown (Choksi et al., 2014a)
	SOCS3	HUB and CP		
	SSX2IP	HUB and CP	Cilium morphogenesis (GO) [GO:0042384~cilium assembly, GO:0060271~ cilium morphogenesis, GO:0035735~intraciliary transport involved in cilium morphogenesis	SSX2IP targets Cep290 to the ciliary transition zone. Cep290 takes a central role in gating proteins to the ciliary compartment (Klinger et al., 2014)
	STOM	HUB and BP and CP		
	SYNCRIP	HUB and BP		
	MEOX2	HUB and BP and CP		
	NLGN3	HUB and BP		
	FAM19A3	HUB and BP		
IIP indirectly regulated by FOXJ1	APOE	HUB and CP	Cytoskeleton organization (GO)[GO:0007010~ cytoskeleton organization]	
	DLG4	HUB and BP	Establishment or maintenance of epithelial cell apical/basal polarity (GO) [GO:0045197]	
FOXJ1 directly regulated IIP showing differential expression (mRNA) in PCD	ACTN2	CP and GNPP	Actin filament organization (GO)[GO:0051695~actin filament uncapping, GO:0005884~actin filament], Cytoskeleton organization (GO) [GO:0005856~cytoskeleton]	RhoA dependent actin remodeling for establishment of an apical web-like structure of actin for basal body docking and axoneme growth (Kohli et al., 2017)
	CASP8	HUB and BP and CP		
IIP showing differential expression (mRNA) in PCD	BTRC	HUB and BP and CP	Protein ubiquitination (GO)[GO:0000209~protein polyubiquitination, GO:0006511~ubiquitin-dependent protein catabolic process, GO:0043161~proteasome-mediated ubiquitin-dependent protein catabolic process], Cell cycle (GO)[GO:0051726~regulation of cell cycle]	
	HSP90AA1	HUB and BP and CP	Protein folding (GO)[GO:0006457~protein folding]	Participates in cilium assembly according to Reactome database (Croft et al., 2014; Fabregat et al., 2018)
	TERF1	HUB and CP		
	CDC42	HUB & CP	Establishment or maintenance of cell polarity (GO)[GO:0007163~establishment or maintenance of cell polarity], Small GTPase mediated signal transduction (GO) [GO:0007264~small GTPase mediated signal transduction], Cytoskeleton organization (GO)[GO:0030036~actin cytoskeleton organization], Actin filament organization (GO) [GO:0051017~actin filament bundle assembly]	Cdc42 docks vesicles carrying ciliary proteins and localizes the exocyst to primary cilia. CDC42 deficiency results in deranged ciliogenesis and polycystic kidney disease (Choi et al., 2013).

The identified IIP-effector proteins that figure at the interface of the FOXJ1 regulatory network and the associated PPIN are listed here. The possible roles of some of these IIP-effectors and their primary interactors in cilia are also outlined. [1]IIP category: Different graph theory metric categories (e.g., hubs: HUB, central proteins: CP, bottleneck proteins: BP and global network perturbing proteins: GNPP) that have identified the protein as topologically important. [2]GO association (Ciliary): Predicted GO association of IIP-effector. [3]Comment: Reports whether this protein has been previously associated with cilia assembly or function.

novel proteins that may act as crucial mediators in the FOXJ1 regulatory network (**Table 2**).

Previously, we have determined that the regulatory network proteins forming a part of the inter-connected module interact primarily with signaling proteins in motile ciliated cells (**Figure 3B**). Therefore, in order to determine which cellular pathways/processes these IIP-effectors might be participating in within the ciliary interactome, we have again utilized the concept of 'guilt by association.' GO mapping suggested the involvement of DLG4 and CDC42 in maintenance of cell polarity (establishment or maintenance of epithelial cell apical/basal polarity [GO: 0045197], establishment or maintenance of cell polarity [GO: 0007163], respectively) (**Table 2** and **Figure 4**). Moreover, the pathway enrichment analysis revealed the probable existence of a number of 'cilia associated signaling pathways' among IIP-effectors and their primary interactors. Further, based on this analysis, we could identify topologically important signaling proteins in the FOXJ1 regulatory network which are essentially IIP-effectors that were found to be related to or had involvement in some 'cilia associated signaling pathways.' In this respect, FOXJ1 effector proteins SYNCRIP and BTRC participate in pathways that regulate motile cilium development like cell cycle, Fgfr, Wnt and Notch signaling (**Supplementary Table 6** and **Figure 4**). CASP8, SOCS3, BTRC, PIAS4 (IIP-effector) and their primary interactors might participate in pathways implicated in primary cilium development and function like TGF-beta, Hedgehog and Toll-like receptor signaling (**Supplementary Table 6** and **Figure 4**).

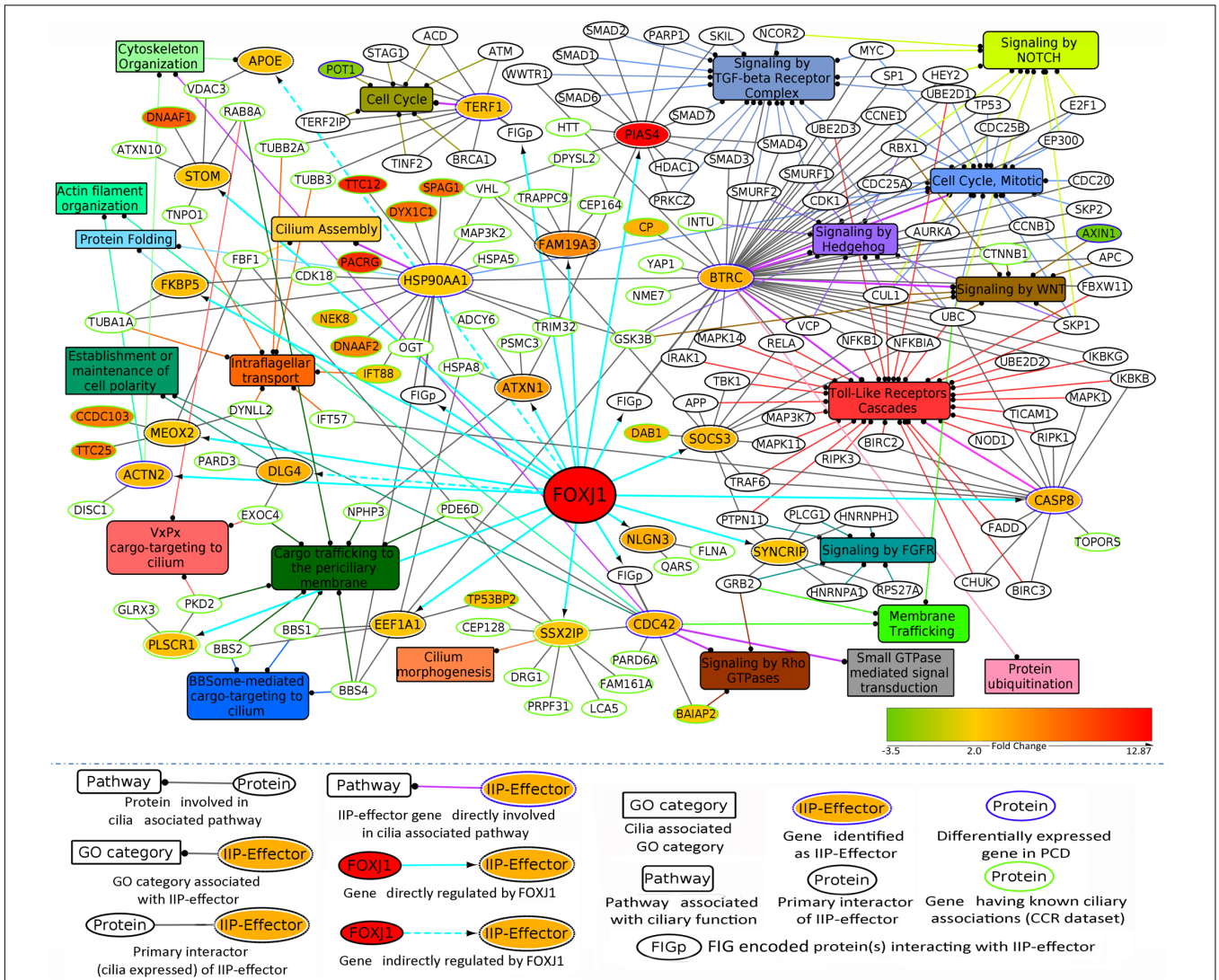

FIGURE 4 | IIP-effectors in FOXJ1 regulatory network and their probable ciliary associations. Probable cilia associated pathways or processes that the IIP-effectors and their network interactors may participate in were determined with the help of pathway enrichment and GO analysis and such possible ciliary role(s) of each IIP-effector is depicted. The edge color denotes the ciliary process(es) or pathway(s) the gene/protein is/are associated with. Fold changes in genes differentially expressed in Choksi et al. expression study (Choksi et al., 2014a) or PCD case study (Geremek et al., 2014) are mapped onto the protein nodes.

Thus, it appears that these pathways could also be important in motile cilia development and/or function. Importantly, different FOXJ1 regulatory network genes either code for topologically important signaling proteins (CASP8, SOCS3, SYNCRIP) or form extensive cross-talk with topologically important signaling proteins (BTRC, HSP90AA1, CDC42). Further, these 'protein-pathway' associations have not previously been studied in the context of ciliogenesis which may be analyzed in further studies.

DISCUSSION

Here, extensive computational analysis of the FOXJ1 regulatory network and the PPIN associated with it were undertaken to identify essential proteins in the motile cilia interactome and key effector proteins in the FOXJ1 regulatory network that possibly mediate the functional role(s) of FOXJ1. With the help of GO and enrichment analysis of FOXJ1 regulatory network genes, we could identify additional transcription factors and other proteins associated with ciliary structure or motility among FIGp. For instance, directly regulated transcription factors MYCBP and HSBP1 have predicted ciliary associations based on GO analysis, and additional literature studies also indicated that it is likely that MYCBP and HSBP1 may also play a role in ciliogenesis. This is because MYCBP is known to regulate Hedgehog signaling (Lin et al., 2014) and also interacts with A-kinase anchoring proteins (Rao et al., 2016) that are involved in regulating dynein-driven motility, and HSBP1 may be involved in Wnt signaling pathway (Eroglu et al., 2014). Similarly, indirectly regulated genes, ATF5 and CHD4 that participate in maintaining centrosome integrity (Sillibourne et al., 2007; Madarampalli et al., 2015), could also have additional ciliary roles as transcription factors in cilia [defects in centrosome structure or function may lead to ciliopathies; Bettencourt-Dias et al., 2011)]. We observed that the annotated transcriptionally regulated proteins (∼24% of FIGp) mainly comprised of ciliary structural component proteins, mutations in which may be associated with ciliary ultrastructure defects occurring in PCD. However, the other FIGp could also be involved in regulating the assembly or function of cilia in association with other proteins expressed in ciliating cells. In order to identify possible essential proteins for motile cilia development or function, we have studied the PPIN associated with FOXJ1 regulatory network proteins with the assumption that it represents the motile cilia interactome. A number of IIP (121) were identified with the help of an *in silico* node deletion analysis and standard graph theory measures computed based on degree, shortest path and centrality. Furthermore, 33 IIP had previously reported ciliary roles, and it is likely that such topologically important proteins participating in multiple signaling pathways, cell cycle, generic transcription, developmental biology etc. may act as essential proteins in cilia development or function.

Interestingly, 120 IIP along with 246 FIGp form an interconnected module in the ciliary interactome. Moreover, genes may be associated with a condition based on their differential expression under a diseased state. Thus, differentially expressed genes occurring in PCD patients may be considered as genes associated with motile cilia biogenesis or function. Similarly, genes that are differentially expressed in *in vitro* model systems wherein motile ciliogenesis is perturbed could also be associated with motile cilia biogenesis or function. We have mapped such associations based on expression analysis (Edgar et al., 2002; Choksi et al., 2014a; Geremek et al., 2014) onto our predicted motile cilia interactome. These associated genes (proteins) figure at the interface of the FOXJ1 regulatory network and the associated protein interaction network, and we have classified such IIP as important effector proteins in the FOXJ1 regulatory network. 16 FOXJ1 regulated IIP-effectors share extensive connections with the FOXJ1 regulatory network proteins and some cilia specific PPIN proteins. Subsequently, we have tried to establish the most likely roles of these IIP-effectors in ciliary biology based on the assumption that interacting proteins may share similar cellular functions ('guilt by association'). Pathway enrichment analysis elucidated that some of these IIP-effectors act as signaling proteins. The IIP-effectors and its interacting partners in the interaction module are particularly involved in Wnt, Notch, Fgfr, Hedgehog, Tgf-beta and Toll-like receptor signaling pathways downstream of FOXJ1 activation. This is in accordance with previous reports wherein Notch, Wnt and Fgf signaling pathways have been shown to regulate processes like left-right patterning, cilia length or number in motile cilia bearing cells (Neugebauer et al., 2009; Lopes et al., 2010; Caron et al., 2012). It is likely that the 'topologically important signaling proteins' form a crucial link between the FOXJ1 regulatory and cilia biogenesis associated signaling components in the motile cilium. In particular, BTRC and CASP8 (PCD associated IIP-effector), along with their primary interactors in the ciliary interactome, are possibly involved in mediating Toll-like receptor signaling. Moreover, PCD patients generally are susceptible to recurrent respiratory infections (Alanin et al., 2015) which have been attributed to impaired mucociliary clearance due to cilia motility defects. However, these patients may additionally have impaired TLR signaling that mediate innate immune responses (Kawasaki and Kawai, 2014) or innate immune response pathways due to defects in PCD associated IIP-effectors or their interactome. Other IIP and FIGp also have possible involvement in innate immune responses and Toll-like receptor signaling cascades. Further, IIP-effectors like EEF1A1 and DLG4 were found to be related to well-known processes involved in ciliary biology like maintenance of cell polarity and intra-flagellar transport. EEF1A1 (directly regulated IIP-effector), a small GTPase protein, is likely to be involved in intra-flagellar transport because of its interactions with multiple BBSome component proteins and it has also been reported as an intra-flagellar transport cargo protein (Engel et al., 2012). Likewise, the indirectly regulated IIP-effector DLG4 may be involved in establishing or maintaining apico-basal polarity of cells during ciliogenesis (as predicted by our GO mapping). Therefore, based on cilia associated expression analysis, literature studies, GO and pathway analysis we could rationalize the involvement of the identified topologically important effector proteins in cilia biogenesis or function. Additional experimental studies will help establish their causal link to PCD.

CONCLUSION

In conclusion, by analyzing the FOXJ1 associated motile cilia interactome comprised of predicted PPIN of the FOXJ1 regulatory network proteins, we have identified topologically important effector proteins in the motile cilia interactome and FOXJ1 regulatory network. Moreover, we have rationalized their possible roles in ciliary biology with the help of GO and enrichment analysis. We propose that defects in the function(s) of such essential genes may be associated with impaired ciliary development or function, and this list of genes will be useful for screening and diagnosis of novel PCD associated mutations in the future.

DATA AVAILABILITY

Expression analysis datasets are available in a publicly accessible repository. Choksi et al. (2014a) dataset utilized in this study can be found at Array Express (https://www.ebi.ac.uk/arrayexpress/) under accession number E-MTAB-2815 and the PCD case study dataset can be accessed at GEO (https://www.ncbi.nlm.nih.gov/geo/) under accession number GSE25186. The raw data [collated ciliary resource (prepared from ciliary reference databases and other literature studies)] supporting the conclusions of this manuscript will be made available by the authors, without undue reservation, to any qualified researcher. All other relevant data generated/analyzed for this study are included in the manuscript and the **Supplementary Files**.

AUTHOR CONTRIBUTIONS

SC, SR, and IM formulated the study design. IM performed the experiments. SC, IM, and SR analyzed and interpreted the results. IM, SR, and SC prepared the manuscript. All authors read and approved the final version of the manuscript.

FUNDING

This work was partly supported from the "BSC0121" fund of Council of Scientific and Industrial Research (CSIR), India and "HRR/2016/000093" from Department of Science and Technology (DST), India to SC and the Agency for Science, Technology and Research (A*STAR) of Singapore to SR. IM is grateful to the CSIR for her fellowship. The funders had no role in study design, data collection and analysis, decision to publish, or preparation of the manuscript.

ACKNOWLEDGMENTS

SC acknowledges CSIR-Indian Institute of Chemical Biology (IICB) for infrastructural support.

SUPPLEMENTARY MATERIAL

The Supplementary Material for this article can be found online at: https://www.frontiersin.org/articles/10.3389/fgene.2019.00023/full#supplementary-material

REFERENCES

Aibar, S., Fontanillo, C., Droste, C., and De Las Rivas, J. (2015). Functional gene networks: R/bioc package to generate and analyze gene networks derived from functional enrichment and clustering. *Bioinformatics* 31, 1686–1688. doi: 10.1093/bioinformatics/btu864

Alanin, M. C., Nielsen, K. G., von Buchwald, C., Skov, M., Aanaes, K., Høiby, N., et al. (2015). A longitudinal study of lung bacterial pathogens in patients with primary ciliary dyskinesia. *Clin. Microbiol. Infect.* 21, 1093.e1–1097.e1. doi: 10.1016/j.cmi.2015.08.020

Albert, R. (2005). Scale-free networks in cell biology. *J. Cell Sci.* 118, 4947–4957. doi: 10.1242/jcs.02714

Amberger, J. S., Bocchini, C. A., Schiettecatte, F., Scott, A. F., and Hamosh, A. (2015). OMIM.org: online mendelian inheritance in man (OMIM®), an online catalog of human genes and genetic disorders. *Nucleic Acids Res.* 43, D789–D798. doi: 10.1093/nar/gku1205

Arbi, M., Pefani, D., Kyrousi, C., Lalioti, M., Kalogeropoulou, A., Papanastasiou, A. D., et al. (2016). GemC1 controls multiciliogenesis in the airway epithelium. *EMBO Rep.* 17, 400–413. doi: 10.15252/embr.201540882

Arnaiz, O., Cohen, J., Tassin, A. M., and Koll, F. (2014). Remodeling Cildb, a popular database for cilia and links for ciliopathies. *Cilia* 3:9. doi: 10.1186/2046-2530-3-9

Arnaiz, O., Malinowska, A., Klotz, C., Sperling, L., Dadlez, M., Koll, F., et al. (2009). Cildb: a knowledgebase for centrosomes and cilia. *Database* 2009:ba022. doi: 10.1093/database/bap022

Baek, H., Shin, H. J., Kim, J.-J., Shin, N., Kim, S., Yi, M.-H., et al. (2017). Primary cilia modulate TLR4-mediated inflammatory responses in hippocampal neurons. *J. Neuroinflammation* 14:189. doi: 10.1186/s12974-017-0958-7

Barabási, A. L., and Oltvai, Z. N. (2004). Network biology: understanding the cell's functional organization. *Nat. Rev. Genet.* 5, 101–113. doi: 10.1038/nrg1272

Barrett, T., Wilhite, S. E., Ledoux, P., Evangelista, C., Kim, I. F., Tomashevsky, M., et al. (2013). NCBI GEO: archive for functional genomics data sets–update. *Nucleic Acids Res.* 41, D991–D995. doi: 10.1093/nar/gks1193

Bettencourt-Dias, M., Hildebrandt, F., Pellman, D., Woods, G., and Godinho, S. (2011). Centrosomes and cilia in human disease. *Trends Genet.* 27, 307–315. doi: 10.1016/j.tig.2011.05.004

Bhattacharyya, M., and Chakrabarti, S. (2015). Identification of important interacting proteins (IIPs) in *Plasmodium falciparum* using large-scale interaction network analysis and in-silico knock-out studies. *Malar. J.* 14:70. doi: 10.1186/s12936-015-0562-1

Bisgrove, B. W., and Yost, H. J. (2006). The roles of cilia in developmental disorders and disease. *Development* 133, 4131–4143. doi: 10.1242/dev.02595

Boldt, K., van Reeuwijk, J., Lu, Q., Koutroumpas, K., Nguyen, T. M., Texier, Y., et al. (2016). An organelle-specific protein landscape identifies novel diseases and molecular mechanisms. *Nat. Commun.* 7:11491. doi: 10.1038/ncomms11491

Bulyk, M. L. (2004). Computational prediction of transcription-factor binding site locations. *Genome Biol.* 5:201. doi: 10.1186/gb-2003-5-1-201

Caron, A., Xu, X., and Lin, X. (2012). Wnt/beta-catenin signaling directly regulates Foxj1 expression and ciliogenesis in zebrafish Kupffer's vesicle. *Development* 139, 514–524. doi: 10.1242/dev.071746

Chatr-aryamontri, A., Oughtred, R., Boucher, L., Rust, J., Chang, C., Kolas, N. K., et al. (2017). The BioGRID interaction database: 2017 update. *Nucleic Acids Res.* 45, D369–D379. doi: 10.1093/nar/gkw1102

Choi, S. Y., Chacon-Heszele, M. F., Huang, L., McKenna, S., Wilson, F. P., Zuo, X., et al. (2013). Cdc42 deficiency causes ciliary abnormalities and cystic kidneys. *J. Am. Soc. Nephrol.* 24, 1435–1450. doi: 10.1681/ASN.2012121236

Choksi, S. P., Babu, D., Lau, D., Yu, X., and Roy, S. (2014a). Systematic discovery of novel ciliary genes through functional genomics in the zebrafish. *Development* 141, 3410–3419. doi: 10.1242/dev.108209

Choksi, S. P., Lauter, G., Swoboda, P., and Roy, S. (2014b). Switching on cilia: transcriptional networks regulating ciliogenesis. *Development* 141, 1427–1441. doi: 10.1242/dev.074666

Clauset, A., Shalizi, C. R., and Newman, M. E. J. (2009). Power-law distributions in empirical data. *SIAM Rev.* 51, 661–703. doi: 10.1137/070710111

Clement, C. A., Ajbro, K. D., Koefoed, K., Vestergaard, M. L., Veland, I. R., Henriques de Jesus, M. P., et al. (2013). TGF-beta signaling is associated with endocytosis at the pocket region of the primary cilium. *Cell Rep.* 3, 1806–1814. doi: 10.1016/j.celrep.2013.05.020

Croft, D., Mundo, A. F., Haw, R., Milacic, M., Weiser, J., Wu, G., et al. (2014). The Reactome pathway knowledgebase. *Nucleic Acids Res.* 42, D472–D477. doi: 10.1093/nar/gkt1102

Danielian, P. S., Hess, R. A., and Lees, J. A. (2016). E2f4 and E2f5 are essential for the development of the male reproductive system. *Cell Cycle* 15, 250–260. doi: 10.1080/15384101.2015.1121350

Edgar, R., Domrachev, M., and Lash, A. E. (2002). Gene expression omnibus: NCBI gene expression and hybridization array data repository. *Nucleic Acids Res.* 30, 207–210. doi: 10.1093/nar/30.1.207

Engel, B. D., Ishikawa, H., Wemmer, K. A., Geimer, S., Wakabayashi, K., Hirono, M., et al. (2012). The role of retrograde intraflagellar transport in flagellar assembly, maintenance, and function. *J. Cell Biol.* 199, 151–167. doi: 10.1083/jcb.201206068

Eroglu, B., Min, J. N., Zhang, Y., Szurek, E., Moskophidis, D., Eroglu, A., et al. (2014). An essential role for heat shock transcription factor binding protein 1 (HSBP1) during early embryonic development. *Dev. Biol.* 386, 448–460. doi: 10.1016/j.ydbio.2013.12.038

Fabregat, A., Jupe, S., Matthews, L., Sidiropoulos, K., Gillespie, M., Garapati, P., et al. (2018). The reactome pathway knowledgebase. *Nucleic Acids Res.* 46, D649–D655. doi: 10.1093/nar/gkx1132

Fliegauf, M., Benzing, T., and Omran, H. (2007). When cilia go bad: cilia defects and ciliopathies. *Nat. Rev. Mol. Cell Biol.* 8, 880–893. doi: 10.1038/nrm2278

Geremek, M., Ziętkiewicz, E., Bruinenberg, M., Franke, L., Pogorzelski, A., Wijmenga, C., et al. (2014). Ciliary genes are down-regulated in bronchial tissue of primary ciliary dyskinesia patients. *PLoS One* 9:e88216. doi: 10.1371/journal.pone.0088216

Goetz, S. C., and Anderson, K. V. (2010). The primary cilium: a signalling centre during vertebrate development. *Nat. Rev. Genet.* 11, 331–344. doi: 10.1038/nrg2774

Gupta, G. D., Coyaud, E., Goncalves, J., Mojarad, B. A., Liu, Y., Wu, Q., et al. (2015). A dynamic protein interaction landscape of the human centrosome-cilium interface. *Cell* 163, 1484–1499. doi: 10.1016/j.cell.2015.10.065

Herrero, J., Muffato, M., Beal, K., Fitzgerald, S., Gordon, L., Pignatelli, M., et al. (2016). Ensembl comparative genomics resources. *Database* 2016:bav096. doi: 10.1093/database/bav096

Horani, A., Ferkol, T. W., Dutcher, S. K., and Brody, S. L. (2016). Genetics and biology of primary ciliary dyskinesia. *Paediatr. Respir. Rev.* 18, 18–24. doi: 10.1016/j.prrv.2015.09.001

Huang da, W., Sherman, B. T., and Lempicki, R. A. (2009a). Bioinformatics enrichment tools: paths toward the comprehensive functional analysis of large gene lists. *Nucleic Acids Res.* 37, 1–13. doi: 10.1093/nar/gkn923

Huang da, W., Sherman, B. T., and Lempicki, R. A. (2009b). Systematic and integrative analysis of large gene lists using DAVID bioinformatics resources. *Nat. Protoc.* 4, 44–57. doi: 10.1038/nprot.2008.211

Huttlin, E. L., Ting, L., Bruckner, R. J., Gebreab, F., Gygi, M. P., Szpyt, J., et al. (2015). The bioPlex network: a systematic exploration of the human interactome. *Cell* 162, 425–440. doi: 10.1016/j.cell.2015.06.043

Ishikawa, H., and Marshall, W. F. (2011). Ciliogenesis: building the cell's antenna. *Nat. Rev. Mol. Cell Biol.* 12, 222–234. doi: 10.1038/nrm3085

Ishikawa, H., Thompson, J., Yates, J. R., and Marshall, W. F. (2012). Proteomic analysis of mammalian primary cilia. *Curr. Biol.* 22, 414–419. doi: 10.1016/j.cub.2012.01.031

Izawa, I., Goto, H., Kasahara, K., and Inagaki, M. (2015). Current topics of functional links between primary cilia and cell cycle. *Cilia* 4:12. doi: 10.1186/s13630-015-0021-1

Jeong, H., Mason, S. P., Barabási, A. L., and Oltvai, Z. N. (2001). Lethality and centrality in protein networks. *Nature* 411, 41–42. doi: 10.1038/35075138

Jolma, A., Yan, J., Whitington, T., Toivonen, J., Nitta, K. R., Rastas, P., et al. (2013). DNA-binding specificities of human transcription factors. *Cell* 152, 327–339. doi: 10.1016/j.cell.2012.12.009

Jones, T. J., Adapala, R. K., Geldenhuys, W. J., Bursley, C., Abou Alaiwi, W. A., Nauli, S. M., et al. (2012). Primary cilia regulates the directional migration and barrier integrity of endothelial cells through the modulation of Hsp27 dependent actin cytoskeletal organization. *J. Cell Physiol.* 227, 70–76. doi: 10.1002/jcp.22704

Kasahara, K., Kawakami, Y., Kiyono, T., Yonemura, S., Kawamura, Y., Era, S., et al. (2014). Ubiquitin-proteasome system controls ciliogenesis at the initial step of axoneme extension. *Nat. Commun.* 5:5081. doi: 10.1038/ncomms6081

Kawasaki, T., and Kawai, T. (2014). Toll-Like receptor signaling pathways. *Front. Immunol.* 5:461. doi: 10.3389/fimmu.2014.00461

Kim, J., Jo, H., Hong, H., Kim, M. H., Kim, J. M., Lee, J. K., et al. (2015). Actin remodelling factors control ciliogenesis by regulating YAP/TAZ activity and vesicle trafficking. *Nat. Commun.* 6:6781. doi: 10.1038/ncomms7781

Klinger, M., Wang, W., Kuhns, S., Bärenz, F., Dräger-Meurer, S., Pereira, G., et al. (2014). The novel centriolar satellite protein SSX2IP targets Cep290 to the ciliary transition zone. *Mol. Biol. Cell* 25, 495–507. doi: 10.1091/mbc.E13-09-0526

Kohli, P., Hohne, M., Jungst, C., Bertsch, S., Ebert, L. K., Schauss, A. C., et al. (2017). The ciliary membrane-associated proteome reveals actin-binding proteins as key components of cilia. *EMBO Rep.* 18, 1521–1535. doi: 10.15252/embr.201643846

Lin, C., Yao, E., Wang, K., Nozawa, Y., Shimizu, H., Johnson, J. R., et al. (2014). Regulation of Sufu activity by p66beta and Mycbp provides new insight into vertebrate Hedgehog signaling. *Genes Dev.* 28, 2547–2563. doi: 10.1101/gad.249425.114

Lopes, S. S., Lourenço, R., Pacheco, L., Moreno, N., Kreiling, J., and Saúde, L. (2010). Notch signalling regulates left-right asymmetry through ciliary length control. *Development* 137, 3625–3632. doi: 10.1242/dev.054452

Madarampalli, B., Yuan, Y., Liu, D., Lengel, K., Xu, Y., Li, G., et al. (2015). ATF5 connects the pericentriolar materials to the proximal end of the mother centriole. *Cell* 162, 580–592. doi: 10.1016/j.cell.2015.06.055

May-Simera, H. L., Gumerson, J. D., Gao, C., Campos, M., Cologna, S. M., Beyer, T., et al. (2016). Loss of Macf1 abolishes ciliogenesis and disrupts apicobasal polarity establishment in the retina. *Cell Rep.* 17, 1399–1413. doi: 10.1016/j.celrep.2016.09.089

McKusick, V. A. (1998). *Mendelian Inheritance in Man. A Catalog of Human Genes and Genetic Disorders*, 12th Edn. Baltimore: Johns Hopkins University Press.

Medina-Rivera, A., Defrance, M., Sand, O., Herrmann, C., Castro-Mondragon, J. A., Delerce, J., et al. (2015). RSAT 2015: regulatory sequence analysis tools. *Nucleic Acids Res.* 43, W50–W56. doi: 10.1093/nar/gkv362

Nachury, M. V., Seeley, E. S., and Jin, H. (2010). Trafficking to the ciliary membrane: how to get across the periciliary diffusion barrier? *Annu. Rev. Cell Dev. Biol.* 26, 59–87. doi: 10.1146/annurev.cellbio.042308.113337

Neugebauer, J. M., Amack, J. D., Peterson, A. G., Bisgrove, B. W., and Yost, H. J. (2009). FGF signaling during embryo development regulates cilia length in diverse epithelia. *Nature* 458, 651–654. doi: 10.1038/nature07753

Oliver, S. (2000). Guilt-by-association goes global. *Nature* 403, 601–603. doi: 10.1038/35001165

Pan, J., You, Y., Huang, T., and Brody, S. L. (2007). RhoA-mediated apical actin enrichment is required for ciliogenesis and promoted by Foxj1. *J. Cell Sci.* 120, 1868–1876. doi: 10.1242/jcs.005306

Pavlopoulos, G. A., Secrier, M., Moschopoulos, C. N., Soldatos, T. G., Kossida, S., Aerts, J., et al. (2011). Using graph theory to analyze biological networks. *BioData Min.* 4:10. doi: 10.1186/1756-0381-4-10

Prodromou, N. V., Thompson, C. L., Osborn, D. P., Cogger, K. F., Ashworth, R., Knight, M. M., et al. (2012). Heat shock induces rapid resorption of primary cilia. *J. Cell Sci.* 125(Pt 18), 4297–4305. doi: 10.1242/jcs.100545

Quarmby, L. M., and Parker, J. D. K. (2005). Cilia and the cell cycle? *J. Cell Biol.* 169, 707–710. doi: 10.1083/jcb.200503053

R Core Team (2016). *R: A Language and Environment for Statistical Computing*. Available at: https://www.R-project.org

Ramachandran, H., Herfurth, K., Grosschedl, R., Schäfer, T., and Walz, G. (2015). SUMOylation blocks the ubiquitin-mediated degradation of the

nephronophthisis gene product Glis2/NPHP7. *PLoS One* 10:e0130275. doi: 10.1371/journal.pone.0130275

Rao, V. G., Sarafdar, R. B., Chowdhury, T. S., Sivadas, P., Yang, P., Dongre, P. M., et al. (2016). Myc-binding protein orthologue interacts with AKAP240 in the central pair apparatus of the *Chlamydomonas flagella*. *BMC Cell Biol.* 17:24. doi: 10.1186/s12860-016-0103-y

Ritchie, M. E., Phipson, B., Wu, D., Hu, Y., Law, C. W., Shi, W., et al. (2015). Limma powers differential expression analyses for RNA-sequencing and microarray studies. *Nucleic Acids Res.* 43:e47. doi: 10.1093/nar/gkv007

Schwikowski, B., Uetz, P., and Fields, S. (2000). A network of protein-protein interactions in yeast. *Nat. Biotechnol.* 18, 1257–1261. doi: 10.1038/82360

Sebastian, A., and Contreras-Moreira, B. (2014). footprintDB: a database of transcription factors with annotated cis elements and binding interfaces. *Bioinformatics* 30, 258–265. doi: 10.1093/bioinformatics/btt663

Shearer, R. F., and Saunders, D. N. (2016). Regulation of primary cilia formation by the ubiquitin-proteasome system. *Biochem. Soc. Trans.* 44, 1265–1271. doi: 10.1042/BST20160174

Sillibourne, J. E., Delaval, B., Redick, S., Sinha, M., and Doxsey, S. J. (2007). Chromatin remodeling proteins interact with pericentrin to regulate centrosome integrity. *Mol. Biol. Cell* 18, 3667–3680. doi: 10.1091/mbc.E06-07-0604

Stark, C., Breitkreutz, B.-J., Reguly, T., Boucher, L., Breitkreutz, A., and Tyers, M. (2006). BioGRID: a general repository for interaction datasets. *Nucleic Acids Res.* 34, D535–D539. doi: 10.1093/nar/gkj109

Stephens, R. E., and Lemieux, N. A. (1999). Molecular chaperones in cilia and flagella: implications for protein turnover. *Cell Motil. Cytoskeleton* 44, 274–283. doi: 10.1002/(SICI)1097-0169(199912)44:4<274::AID-CM5>3.0.CO;2-O

Stubbs, J. L., Oishi, I., Izpisua Belmonte, J. C., and Kintner, C. (2008). The forkhead protein Foxj1 specifies node-like cilia in *Xenopus* and zebrafish embryos. *Nat. Genet.* 40, 1454–1460. doi: 10.1038/ng.267

Szklarczyk, D., Franceschini, A., Wyder, S., Forslund, K., Heller, D., Huerta-Cepas, J., et al. (2015). STRING v10: protein–protein interaction networks, integrated over the tree of life. *Nucleic Acids Res.* 43, D447–D452. doi: 10.1093/nar/gku1003

Terré, B., Piergiovanni, G., Segura Bayona, S., Gil-Gómez, G., Youssef, S. A., and Attolini, C. S. (2016). GEMC1 is a critical regulator of multiciliated cell differentiation. *EMBO J.* 35, 942–960. doi: 10.15252/embj.201592821

Thul, P. J., Åkesson, L., Wiking, M., Mahdessian, D., Geladaki, A., and Ait Blal, H. (2017). A subcellular map of the human proteome. *Science* 356:eaal3321. doi: 10.1126/science.aal3321

Turatsinze, J. V., Thomas-Chollier, M., Defrance, M., and van Helden, J. (2008). Using RSAT to scan genome sequences for transcription factor binding sites and cis-regulatory modules. *Nat. Protoc.* 3, 1578–1588. doi: 10.1038/nprot.2008.97

Uhlén, M., Fagerberg, L., Hallström, B. M., Lindskog, C., Oksvold, P., Mardinoglu, A., et al. (2015). Tissue-based map of the human proteome. *Science* 347:1260419. doi: 10.1126/science.1260419

Uhlen, M., Oksvold, P., Fagerberg, L., Lundberg, E., Jonasson, K., and Forsberg, M. (2010). Towards a knowledge-based human protein atlas. *Nat. Biotechnol.* 28, 1248–1250. doi: 10.1038/nbt1210-1248

van Dam, T. J., Wheway, G., Slaats, G. G., Huynen, M. A., and Giles, R. H. (2013). The SYSCILIA gold standard (SCGSv1) of known ciliary components and its applications within a systems biology consortium. *Cilia* 2:7. doi: 10.1186/2046-2530-2-7

Vladar, E. K., and Mitchell, B. J. (2016). It's a family act: the geminin triplets take center stage in motile ciliogenesis. *EMBO J.* 35, 904–906. doi: 10.15252/embj.201694206

Yook, S. H., Oltvai, Z. N., and Barabasi, A. L. (2004). Functional and topological characterization of protein interaction networks. *Proteomics* 4, 928–942. doi: 10.1002/pmic.200300636

Yu, G., and He, Q. (2016). ReactomePA: an R/Bioconductor package for reactome pathway analysis and visualization. *Mol. Biosyst.* 12, 477–479. doi: 10.1039/c5mb00663e

Yu, H., Kim, P. M., Sprecher, E., Trifonov, V., and Gerstein, M. (2007). The importance of bottlenecks in protein networks: correlation with gene essentiality and expression dynamics. *PLoS Comput. Biol.* 3:e59. doi: 10.1371/journal.pcbi.0030059

Yu, X., Ng, C. P., Habacher, H., and Roy, S. (2008). Foxj1 transcription factors are master regulators of the motile ciliogenic program. *Nat. Genet.* 40, 1445–1453. doi: 10.1038/ng.263

Zariwala, M. A., Omran, H., and Ferkol, T. W. (2011). The emerging genetics of primary ciliary dyskinesia. *Proc. Am. Thorac. Soc.* 8, 430–433. doi: 10.1513/pats.201103-023SD

Conflict of Interest Statement: The authors declare that the research was conducted in the absence of any commercial or financial relationships that could be construed as a potential conflict of interest.

frontiers in Genetics

ORIGINAL RESEARCH
published: 08 March 2019
doi: 10.3389/fgene.2019.00163

Synchronizing Protein Traffic to the Primary Cilium

Wladislaw Stroukov[1,2†], *Axel Rösch*[1,2†], *Carsten Schwan*[3], *Abris Jeney*[1,4], *Winfried Römer*[1,4] *and Roland Thuenauer*[1,4*]

[1] Signalling Research Centres BIOSS and CIBSS, University of Freiburg, Freiburg, Germany, [2] Faculty of Chemistry and Pharmacy, University of Freiburg, Freiburg, Germany, [3] Medical Faculty, Institute of Experimental and Clinical Pharmacology and Toxicology, University of Freiburg, Freiburg, Germany, [4] Faculty of Biology, University of Freiburg, Freiburg, Germany

The primary cilium is able to maintain a specific protein composition, which is critical for its function as a signaling organelle. Here we introduce a system to synchronize biosynthetic trafficking of ciliary proteins that is based on conditional aggregation domains (CADs). This approach enables to create a wave of ciliary proteins that are transported together, which opens novel avenues for visualizing and studying ciliary import mechanisms. By using somatostatin receptor 3 (SSTR3) as model protein we studied intracellular transport and ciliary import with high temporal and spatial resolution in epithelial Madin-Darby canine kidney (MDCK) cells. This yielded the interesting discovery that SSTR3, besides being transported to the primary cilium, is also targeted to the basolateral plasma membrane. In addition, we found a similar behavior for another ciliary protein, nephrocystin-3 (NPHP3), thus suggesting a potential correlation between ciliary and basolateral trafficking. Furthermore, our CAD-based system allowed assembling a large dataset in which apical and basolateral surface SSTR3 signals could be compared to ciliary SSTR3 signals on a single cell level. This enabled to generate novel complementary evidence for the previously proposed lateral import mechanism of SSTR3 into the cilium along the plasma membrane.

Keywords: primary cilium, epithelial cells, protein trafficking, somatostatin receptor 3, nephrocystin-3

OPEN ACCESS

Edited by:
Jose Maria Carvajal-Gonzalez, Universidad de Extremadura, Spain

Reviewed by:
Raj Ladher, National Centre for Biological Sciences, India
Aparna Lakkaraju, University of California, San Francisco, United States

***Correspondence:**
Roland Thuenauer
roland.thuenauer@gmail.com

† These authors have contributed equally to this work

Specialty section:
This article was submitted to Systems Biology, a section of the journal Frontiers in Genetics

Received: *27 September 2018*
Accepted: *14 February 2019*
Published: *08 March 2019*

Citation:
Stroukov W, Rösch A, Schwan C, Jeney A, Römer W and Thuenauer R (2019) Synchronizing Protein Traffic to the Primary Cilium. Front. Genet. 10:163. doi: 10.3389/fgene.2019.00163

INTRODUCTION

The primary cilium is a cellular organelle that maintains a particular composition of proteins and lipids, although the ciliary membrane and the surrounding plasma membrane are continuous (Singla and Reiter, 2006). The capacity of the cilium to concentrate or exclude specific proteins is of critical importance for its function as a signaling organelle. Various ciliopathies, such as Joubert syndrome and nephronophthisis, show an altered concentration of signaling proteins at the primary cilium (Shi et al., 2017). The key structure controlling access to the cilium is a "ciliary gate" that is located at the base of the cilium. A presumable part of the ciliary gate is a membrane diffusion barrier that can hinder free diffusion of specific membrane proteins (Vieira et al., 2006; Hu and Nelson, 2011; Hu et al., 2012; Reales et al., 2015); thus assisting in the distinctive concentration of proteins at the cilium. However, alternative mechanisms that do not necessarily require a diffusion barrier have also been described: membrane proteins can be excluded from the cilium by anchoring to the actin cytoskeleton (Francis et al., 2011), and, *vice versa*, ciliary proteins could be selectively anchored within the cilium (Hu and Nelson, 2011). In addition, the anterograde intraflagellar transport machinery could actively drag proteins into the cilium, whereas proteins leaking from the

cilium could be rapidly endocytosed (Hu and Nelson, 2011). To distinguish between these different mechanisms, which might all be at work for different classes of ciliary proteins, novel methods are required that enable to directly image and quantify the biosynthetic transport of ciliary proteins toward the cilium and into the cilium.

Here, we applied an approach based on conditional aggregation domains (CADs) (Rivera et al., 2000; Thuenauer et al., 2014) to synchronize biosynthetic trafficking of ciliary proteins. The particular strength of synchronization is that it ensures that a cohort of a protein of interest is transported together and reaches the primary cilium only along biosynthetic trafficking routes. Hence, the synchronized movement of proteins makes it easier to distinguish and follow individual transport steps. This cannot be achieved with other techniques, such as ciliary fluorescence recovery after bleaching (FRAP), in which the cilium can be refilled with newly synthesized proteins and also with proteins recruited from recycling compartments. In addition, due to the basic limits of optical resolution, it is difficult to selectively bleach the primary cilium but not adjacent regions such as the periciliary membrane or subapical vesicles.

To demonstrate the capabilities of our approach we applied the CAD-based system to study ciliary trafficking in epithelial Madin-Darby canine kidney (MDCK) cells. MDCK cells form their primary cilium from a midbody remnant and therefore do not exhibit a ciliary pocket (Bernabe-Rubio et al., 2016). It is not well-understood if and how the presence of a ciliary pocket influences ciliary trafficking, since most studies on ciliary trafficking had been carried out in cells bearing a ciliary pocket. We analyzed the intracellular and ciliary trafficking of the ciliary model protein somatostatin receptor 3 (SSTR3) utilizing a CAD-tagged synchronizable version of SSTR3. SSTR3 has been reported to be expressed in kidney epithelial cells (Bates et al., 2003) and a recent study has identified a mechanism for ciliary import of SSTR3 via lateral transport along the periciliary membrane regulated by tubby-family proteins and the intraflagellar transport sub-complex A (IFT-A) (Badgandi et al., 2017). Surprisingly, our approach revealed that SSTR3 is also transported to the basolateral plasma membrane of MDCK cells. In addition, we found a similar behavior for another ciliary protein, nephrocystin-3 (NPHP3), thus suggesting a potential link between ciliary trafficking and basolateral trafficking. Finally, by analyzing the correlation between apical SSTR3 and ciliary SSTR3, and between basolateral SSTR3 and ciliary SSTR3, on a single cell level, we provide quantitative evidence for lateral import of SSTR3 from the apical plasma membrane into the ciliary membrane also in MDCK cells, which are devoid of a ciliary pocket.

RESULTS AND DISCUSSION

Design of a Synchronizable Version of SSTR3

SSTR3 is a rhodopsin-family G protein-coupled heptahelical receptor that is expressed in many tissues, including the nervous system and kidneys (Bates et al., 2003). It is imported into the primary cilium, presumably by binding the IFT-A complex in a manner coordinated by the tubby-family proteins TULP3 and TUB (Badgandi et al., 2017).

Motivated by the successful synchronization of another rhodopsin-family receptor, rhodopsin (Thuenauer et al., 2014), we reapplied the tagging strategy for generating a synchronizable version of SSTR3. The architecture of the resulting construct CAD4-FLAG-SSTR3-GFP is shown in **Figure 1A**. A signal sequence (SS) derived from the human growth hormone ensures insertion of the protein of interest into the endoplasmic reticulum (ER) membrane during synthesis. Four copies of CAD domains (4 X CAD) are responsible for synchronization: After expression, large CAD-mediated aggregates are formed (**Figure 1B**, step 1), which are retained at the ER. After addition of the membrane permeable small molecule D/D-solubilizer, the aggregates are dissolved, and a synchronous wave of the protein of interest is released from the ER (**Figure 1B**, step 2) and then trafficked to the plasma membrane (**Figure 1B**, step 3). The CAD domains are separated from the remaining construct by a furin cleavage site (FCS) enabling the trans-Golgi network (TGN)-resident protease furin to remove the CADs at the TGN (Thuenauer et al., 2014). In addition, a FLAG-tag is linked to the extracellular N-terminus of SSTR3 and thereby accessible at the plasma membrane from the extracellular medium, whereas a green fluorescent protein (GFP) is attached at the cytoplasmic C-terminus of SSTR3. In the lower row of **Figure 1B** it can be seen that the hybrid protein CAD4-FLAG-SSTR3-GFP formed intracellular clusters before release (0 h), but reached the primary cilium after 2 h of release. Interestingly, also a presumable basolateral localization of FLAG-SSTR3-GFP became evident after 2 h of release.

Taken together, the construct CAD4-FLAG-SSTR3-GFP is successfully retained at the ER after expression and is trafficked to the primary cilium after ER release upon addition of D/D-solubilizer.

Optimization of Transfection

In initial tests we used a plasmid encoding for CAD4-FLAG-SSTR3-GFP under the control of a constitutive CMV-promoter (pCMV-CAD4-FLAG-SSTR3-GFP). Transient transfection experiments with this plasmid showed that the major prerequisite for unbiased quantification of individual cells can be achieved: only single isolated cells within a polarized, transwell filter-grown MDCK monolayer were transfected using PEI as transfection reagent for 12 h (data not shown). However, we recognized that transfected cells rarely displayed cilia, which presumably resulted from cellular stress during transient transfection. Therefore, we made the plasmid pTet-CAD4-FLAG-SSTR3-GFP, for expressing the same construct under control of a tetracycline (tet)-inducible promoter, with the goal to separate the time point of transfection from the time point of the onset of expression. After establishing a cell line stably expressing a tet transactivator (tet-MDCK), we used the plasmid pTet-CAD4-FLAG-SSTR3-GFP to optimize conditions for best cilia expression (**Figure 2A**). Increasing the resting period between transfection with pTet-CAD4-FLAG-SSTR3-GFP and induction of CAD4-FLAG-SSTR3-GFP expression with doxycycline (dox) from 0 d to 2 d increased

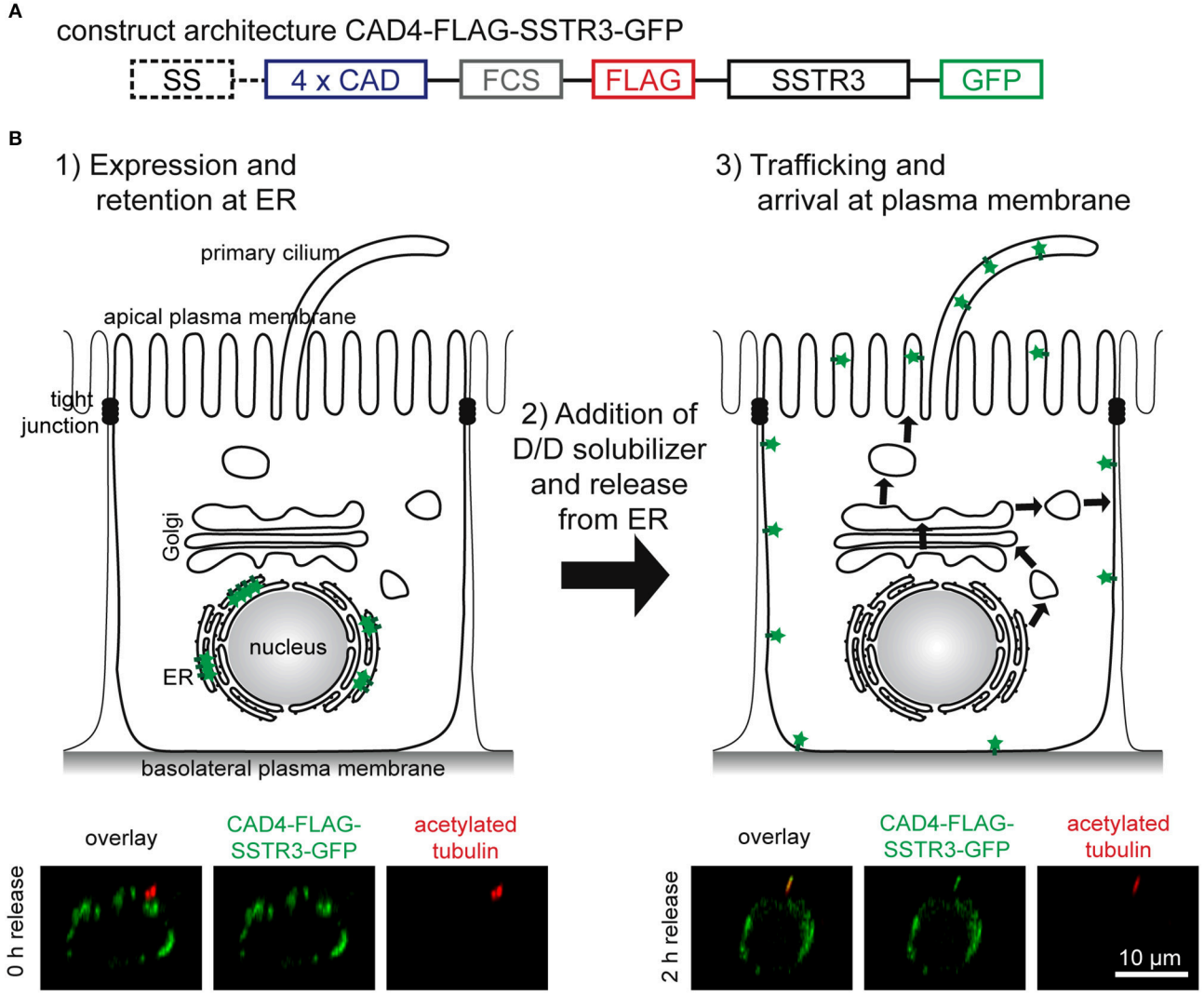

FIGURE 1 | Functional principle of CAD-mediated synchronized protein trafficking to the primary cilium of epithelial cells. **(A)** Architecture of the construct CAD4-FLAG-SSTR3-GFP. A signal sequence (SS) derived from the human growth hormone ensures insertion into the ER membrane during synthesis. This is followed by four copies of conditional aggregation domains (4 x CAD), a furin cleavage site (FCS) ensuring removal of the CAD-domains by furin in the trans-Golgi network, a FLAG-tag, SSTR3, and GFP. **(B)** After transient expression, the resulting proteins CAD4-FLAG-SSTR3-GFP are retained at the ER due to CAD-mediated formation of aggregates (1). The aggregates can be rapidly dissolved by addition of D/D-solubilizer (2). This generates a wave of proteins synchronously transported to the plasma membrane (3). Whereas, the upper images show schematic representations, the lower images display apico-basal cross-sections of representative cells expressing CAD4-FLAG-SSTR3-GFP (green) and cilia highlighted by anti-acetylated tubulin staining (red) derived from confocal image stacks.

the ratio of transfected cells bearing cilia from 9.1 to 38.1%, respectively. Reducing the PEI transfection dose by a factor of two only slightly improved the cilia expression ratio from 9.1 to 12.5%, respectively, for 0 d resting periods. Using Lipofectamine 2000 as transfection reagent completely failed and abolished virtually all cilia. Thus, using PEI as transfection reagent followed by a 2 d resting period appeared to be the best option.

However, the ratio of transfected cells expressing cilia was still low. To identify the cause, we compared cilia expression rates for untransfected tet-MDCK cells and wt MDCK cells, which revealed that more wt MDCK cells expressed cilia: 75% of polarized wt MDCK cells had cilia, compared to only 53% of polarized tet-MDCK cells. Hence, to further optimize CAD4-FLAG-SSTR3-GFP expression conditions, we chose an alternative strategy based on wt MDCK cells, which we co-transfected with a plasmid encoding a tet transactivator (pWHE644) and pTet-CAD4-FLAG-SSTR3-GFP. After 2 d of rest before dox induction, 53.7% of transfected cells expressed cilia as compared to 75% of all cells in the sample. To further analyze the contributions from resting periods vs. cell/clone type, we calculated to which extend cilia expression was lowered in transfected cells in comparison to all cells for the investigated conditions (**Figure 2B**). This verified again the positive effect of an increase of the resting period. Importantly, transfection

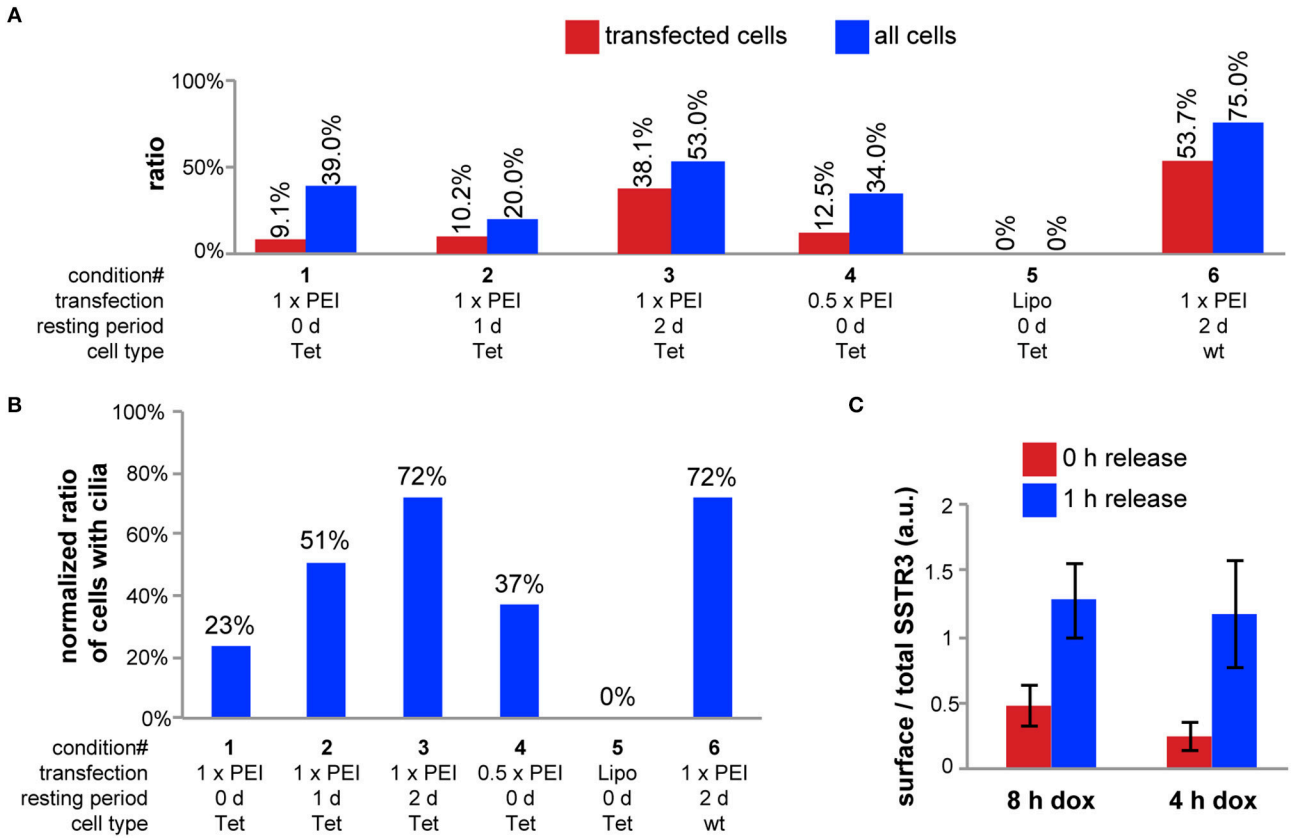

FIGURE 2 | Optimization of the transfection and induction. **(A)** For conditions 1-3, tet-MDCK cells grown on transwell filters were transfected using 1.5 μg pTet-CAD4-FLAG-SSTR3-GFP and 5 μl PEI stock solution for 12 h. For condition 4, only the half amount of DNA and PEI was used. For condition 5, tet-MDCK cells were transfected using 1.6 μg pTet-CAD4-FLAG-SSTR3-GFP and 4 μl Lipofectamine 2000. For condition 6, wt MDCK cells were transfected using 0.75 μg of pTet-CAD4-FLAG-SSTR3-GFP and 0.75 μg of pWHE644 (encoding a tet transactivator) and 5 μl PEI stock solution. After transfection, all samples were washed with medium and incubated at 37°C for the indicated resting periods. Then, in all samples CAD4-FLAG-SSTR3-GFP expression was induced by treatment with doxycycline for 8 h. To characterize cilia expression, cells were fixed, stained for α-tubulin, and imaged with a confocal microscope. The ratio of SSTR3-expressing cells and of all cells showing cilia (red and blue bars, respectively) were manually counted from n > 3 randomly chosen regions with lateral dimensions of 200 × 200 μm. **(B)** Ratio of CAD4-FLAG-SSTR3-GFP-transfected cells displaying cilia normalized to the ratio of all cells displaying cilia for the same conditions as in **(A)**. **(C)** Transwell filter grown wt MDCK cells were transfected using 0.75 μg of pTet-CAD4-FLAG-SSTR3-GFP and 0.75 μg of pWHE644 and 5 μl PEI stock solution for 12 h and then allowed to rest for 2 d. CAD4-FLAG-SSTR3-GFP expression was induced by treatment with doxycycline for 8 or 4 h. Next, D/D-solubilizer was either added for 1 h (1 h release) or not (0 h release) and FLAG-SSTR3-GFP that had arrived at the cell surface was stained by apical and basolateral addition of anti-FLAG antibodies. After fixation, cells were imaged with a confocal microscope. To assess the leakiness of the ER retention of CAD4-FLAG-SSTR3-GFP, the ratio of total surface signals from anti-FLAG staining and GFP signals representing the total CAD4-FLAG-SSTR3-GFP amount were determined for $n > 25$ single cells per condition and averaged.

lowered cilia expression in both, tet-MDCK and wt MDCK cells, to the same extend (reduction to 72%), which indicates that the parameters "resting period" and "cell/clone type" independently contribute to the cilia expression ratio.

Previous work with CAD-synchronized proteins in our group revealed that different proteins display varying degrees of leakiness during the period of ER retention (unpublished). Therefore, we sought to minimize the duration of dox-induced protein synthesis to lower leakiness from the ER. For quantification, we stained cell surface FLAG-SSTR3-GFP with apically and basolaterally applied FLAG-antibodies and then measured the SSTR3 cell surface to total SSTR3 signal ratios in cells induced for 8 or 4 h with dox and treated with D/D-solubilizer for 0 or 1 h (**Figure 2C**). This showed that induction for 4 h yields sufficient expression levels but results in lower leakiness. With these optimized conditions we verified by Western blot analysis that furin cleavage of CAD4-FLAG-SSTR3-GFP occurred (**Supplementary Figure 1**).

In summary, a dox-inducible strategy allowed for a 2 d resting period after transfection, which drastically increased the ratio of transfected cells expressing cilia. In addition, 4 h of dox induction resulted in sufficient expression levels together with a low ER leakiness of the construct CAD4-FLAG-SSTR3-GFP.

Quantification of Polarized Cell Surface and Ciliary Arrival

As released FLAG-SSTR3-GFP was found not only at the primary cilium, but also at the basolateral plasma membrane, we sought to further investigate its trafficking to the apical and basolateral cell surface in a time-dependent manner (**Figures 3A,B**). This

revealed that FLAG-SSTR3-GFP arrived at the basolateral plasma membrane at an ∼2-fold higher amount than at the apical plasma membrane throughout the tracked 2 h release period (**Figure 3B**). (Note: We use the term "apical plasma membrane" in this context to denominate the combination of the ciliary membrane and non-ciliary apical plasma membrane).

In addition, we found for another ciliary protein, NPHP3, that it was also partially targeted to the basolateral plasma membrane after ER release (**Supplementary Figure 2**). Interestingly, NPHP3 uses a different mechanism for ciliary import than SSTR3: NPHP3 can be anchored to the cytosolic leaflet of the plasma membrane via a myristoyl lipid anchor. This anchor can be masked by UNC119, thus creating a cytosolic complex and enabling import into the cilium via a cytosolic route. In the primary cilium UNC119 is removed with the help of the small GTPase ARL3 and NPHP3 can insert its lipid anchor into the ciliary membrane (Wright et al., 2011; Jaiswal et al., 2016). Our data suggests that basolateral localization in epithelial cells could be a feature of many ciliary proteins, and indeed, basolateral localization has been observed before for e.g., Smoothened (Corbit et al., 2005) and polycystin-1 (Roitbak et al., 2004; Su et al., 2015). These observations indicate a startling link between basolateral and ciliary trafficking. To further substantiate this hypothesis, we investigated the localization of the activated Smoothened mutant SmoA1 (Boehlke et al., 2010) during establishment of polarity in MDCK cells (**Supplementary Figure 3**). This revealed that SmoA1 remained intracellular in non-polarized MDCK cells. Only after polarization SmoA1 localized to the primary cilium and also to the basolateral plasma membrane. This indicates that polarity is essential for SmoA1 plasma membrane localization and that ciliary and basolateral localization seem to be established within the same timeframe.

One explanation for the coincidence between ciliary and basolateral localization could lie in the convergence or overlap between ciliary and basolateral trafficking mechanisms. For example, the small GTPase Rab8 and the clathrin adaptor AP-1 have been implicated in both, ciliary and basolateral membrane trafficking (Kaplan et al., 2010; Carvajal-Gonzalez et al., 2012; Rodriguez-Boulan and Macara, 2014). Another possibility could be the presence of a transcytotic delivery pathway from the basolateral plasma membrane to the primary cilium. This would be consistent with our observation (**Figure 3B**) that the arrival of SSTR3 at the basolateral plasma membrane peaked at 1 h, whereas the arrival at the apical plasma membrane peaked slightly later, at 1.5 h. To directly assess the existence of transcytotic delivery of SSTR3 we carried out an experiment in which we first released CAD4-FLAG-SSTR3-GFP for 1 h and then applied primary anti-FLAG antibodies to the basolateral medium to label FLAG-SSTR3-GFP at the basolateral surface. After further 1 or 4 h of incubation at 37°C, we probed for transcytosis with apically applied secondary antibodies recognizing the primary anti-FLAG antibodies. This showed that indeed transcytosis of SSTR3 occurred (**Supplementary Figure 4**). Therefore, we suggest that after ER release SSTR3 is trafficked to the apical and basolateral plasma membrane, and

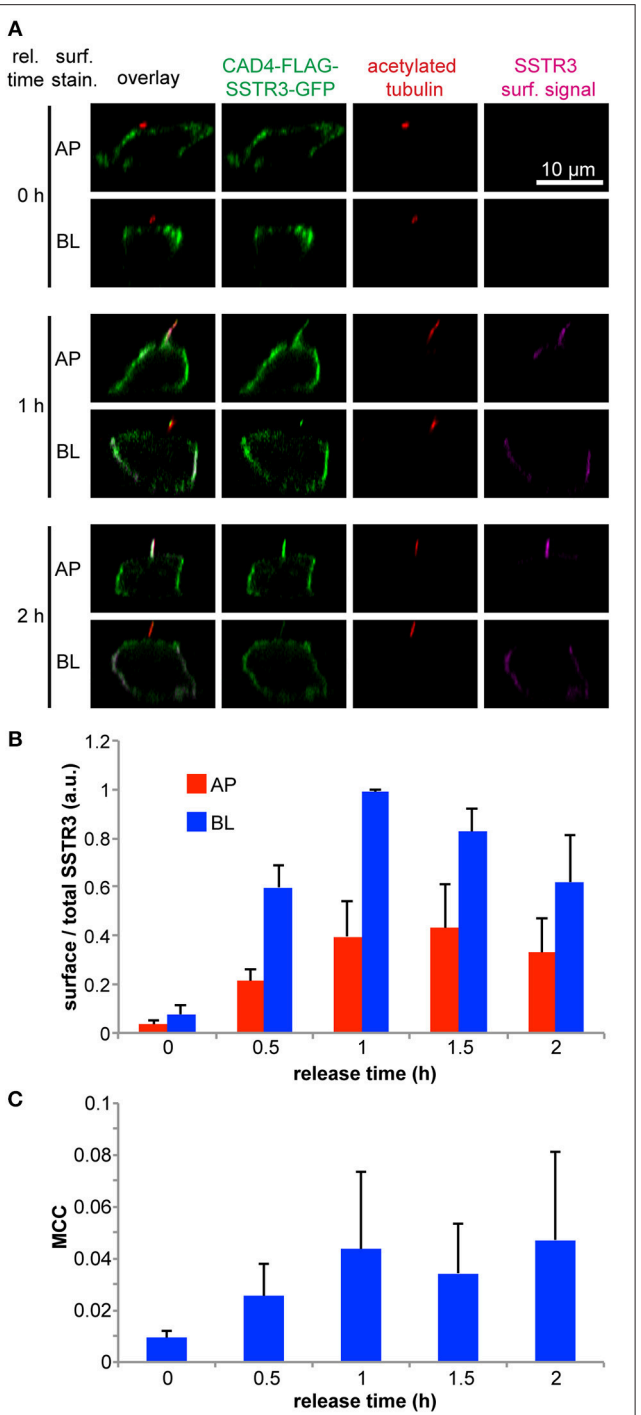

FIGURE 3 | Time-resolved arrival of SSTR3 at the apical and basolateral plasma membrane and at the primary cilium. **(A)** Transwell filter grown wt MDCK cells were transfected using 0.75 µg of pTet-CAD4-FLAG-SSTR3-GFP and 0.75 µg of pWHE644 and 5 µl PEI stock solution for 12 h and then allowed to rest for 2 d. CAD4-FLAG-SSTR3-GFP (green) expression was induced by treatment with doxycycline for 4 h followed by treatment with D/D-solubilizer to induce ER release for the indicated times. Afterwards FLAG-SSTR3-GFP that had arrived at the apical (AP) or basolateral (BL) cell surface (magenta) was stained using anti-FLAG antibodies administered only to apical or basolateral side, respectively. After fixation, the primary cilium was

(Continued)

FIGURE 3 | stained using anti-acetylated tubulin antibodies (red). **(B)** Quantification of FLAG-SSTR3-GFP apical (AP) and basolateral (BL) cell surface arrival after the indicated ER release periods. The mean values from three independent experiments are shown. In one experiment, the surface to total FLAG-SSTR3-GFP signal ratios were determined from $n > 50$ individual cells per condition, averaged, and normalized to the maximum value of the time series before the mean values for the repeated experiments were calculated. **(C)** Manders' co-localization coefficient (MCC) between FLAG-SSTR3-GFP and acetylated tubulin as ciliary marker in dependence of the CAD4-FLAG-SSTR3-GFP release time. The mean values from three independent experiments with each $n > 30$ cells per condition are displayed.

concomitantly transcytosis from the basolateral to the apical side takes place.

An open question is the physiological role of the basolateral pool of ciliary proteins. Is this pool capable of transducing signals to a similar extent as the ciliary pool? Or is it acting as a reservoir that can be rapidly recruited to the primary cilium if required? It will be highly interesting to investigate these hypotheses in future and our synchronization system offers a powerful experimental handle to approach these questions.

We further aimed to directly visualize and quantify the arrival of FLAG-SSTR3-GFP at the primary cilium. To this end we analyzed the co-localization of FLAG-SSTR3-GFP with the ciliary marker acetylated tubulin via a Manders' co-localization coefficient (MCC) in dependence of the ER release time (**Figure 3C**). Our analysis revealed that this approach requires several measures to quantify ciliary co-localization of FLAG-SSTR3-GFP correctly: (1) the threshold in the acetylated tubulin channel needs to be carefully set so that only signals directly from the primary cilium remain and other acetylated tubulin signals from within the cells are effectively cut off. (2) A co-localization analysis is inherently limited by the resolution of the used microscope. To minimize artifacts that derive from limited resolution, we only analyzed the MCC for cells that had clearly protruding cilia and not from cells where e.g., cilia were sharply tilted and were therefore localized in the same image plane as the surrounding apical plasma membrane.

Over the course of 2 h, we could observe an increase of FLAG-SSTR3-GFP in the primary cilium of MDCK cells, reaching saturation after approximately 1–1.5 h (**Figure 3C**). Since the MCC is defined as the sum of co-localizing signal normalized to the total signal (see equation (1) in section Quantification of Polarized Cell Surface Arrival and Ciliary Arrival), its value represents the fraction of SSTR3 localized in the primary cilium. It peaks around 0.05, meaning that 5% of the total SSTR3 protein is present in the primary cilium. This supports an active accumulation of SSTR3 in the primary cilium, because the ciliary volume is smaller by factor of 2,700–6,800 than the total cellular volume (Nachury, 2014) and hence random delivery of SSTR3 into the primary cilium could only account for MCC values of <0.0004.

A further strength of our system is that we are able to analyze ciliary arrival in populations of individual cells. To illustrate this, we plotted the distribution of MCC values vs. the normalized apical FLAG-SSTR3-GFP surface signal (**Figure 4A**) and vs. the normalized basolateral FLAG-SSTR3-GFP surface signal (**Figure 4B**) for individual cells after 1 h of release. First, no saturation effects were observable for cells with higher apical or basolateral surface signals, which indicates that we operated with expression levels that were low enough to not exhaust the transport machinery toward or into the primary cilium.

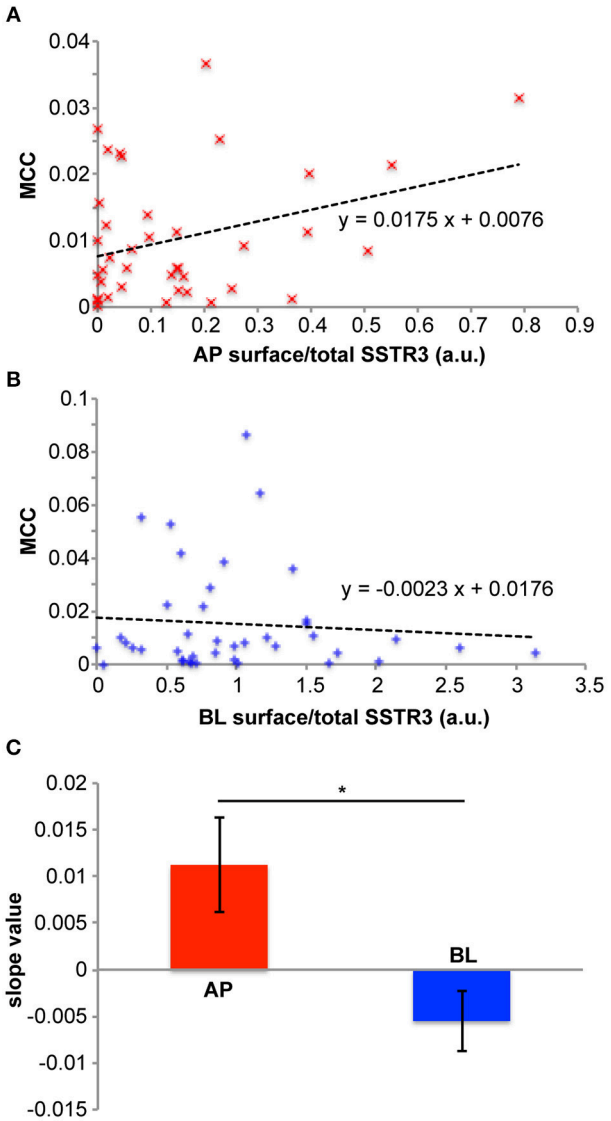

FIGURE 4 | Relations between SSTR3 ciliary arrival and SSTR3 apical and basolateral surface localization. **(A–C)** cells were treated as described in **Figure 3**. **(A)** depicts a representative diagram showing how the ciliary FLAG-SSTR3-GFP localization (measured by the Manders' co-localization coefficient (MCC) between FLAG-SSTR3-GFP and acetylated tubulin as ciliary marker) depends on apical (AP) FLAG-SSTR3-GFP (measured by the ratio of the apical surface FLAG-SSTR3-GFP staining signal to the total FLAG-SSTR3-GFP signal) in individual cells after 1 h of ER release (red ×). A linear fit to the data is displayed as black dashed line, together with the corresponding equation. **(B)** Same as in **(A)**, but for basolateral (BL) FLAG-SSTR3-GFP. **(C)** The slope values for linear fits of ciliary FLAG-SSTR3-GFP vs. apical (AP) or basolateral (BL) FLAG-SSTR3-GFP were averaged from three independent experiments. Statistical analysis was carried out with a two-tailed paired *t*-test, and * indicates $p < 0.05$.

Second, there exists a positive correlation between MCC and the normalized apical SSTR3 surface signal, i.e., in cells with higher apical signals also higher signals were found in the cilium. In contrast, the MCC and the normalized basolateral SSTR3 surface signal exhibited a negative correlation. For quantification, a linear fit to the data of **Figures 4A,B** was carried out and the slope of the resulting line was defined as measure for the correlation between MCC and surface signal. Analysis of three independent replicates revealed a significant difference between the slope for the apical side and the slope for the basolateral side (**Figure 4C**), with the apical slope always assuming positive values. This is consistent with the assumption that SSTR3 was imported into the primary cilium via lateral transport along the apical plasma membrane in MDCK cells, which corresponds to the proposed tubby-family and IFT-A-mediated mechanism for SSTR3 ciliary import (Badgandi et al., 2017). Since the tubby/IFT-A-mediated mechanism was established using cells bearing a ciliary pocket, our results suggest that in cells that do not possess a ciliary pocket, such as MDCK cells (Bernabe-Rubio et al., 2016), the same mechanism for SSTR3 ciliary import is employed.

Taken together, we showed that our CAD-based synchronization approach enables to quantify polarized cell surface arrival and ciliary import of proteins in a time-dependent manner on a single cell and population level. Furthermore, the synchronization system was instrumental for uncovering a potential link between ciliary and basolateral trafficking.

Live-Cell Imaging of Ciliary Targeting

To demonstrate the feasibility of monitoring transport into the primary cilium in live cells, we co-transfected cells with pCMV-CAD4-SSTR3-GFP and p5HT6-tdTomato as a ciliary marker (Berbari et al., 2008; Lesiak et al., 2018). As it can be seen in **Figure 5** and in **Supplementary Movie 1**, this enabled to image the gradual accumulation of SSTR3-GFP at the primary cilium by spinning disc confocal microscopy. To quantify the imaging data (**Figure 5A**), we measured the signal of SSTR3-GFP co-localizing with 5HT6-tdTomato over time (**Figure 5B**). The kinetics determined by the live cell imaging approach largely corresponded to the kinetics that was determined by the averaged values from multiple fixed single cells (**Figure 3C**), with an onset of ciliary localization at 30 min that increased until ∼1 h after release.

In summary, these experiments show that our system is capable to visualize and quantify the ciliary arrival of proteins in live cells.

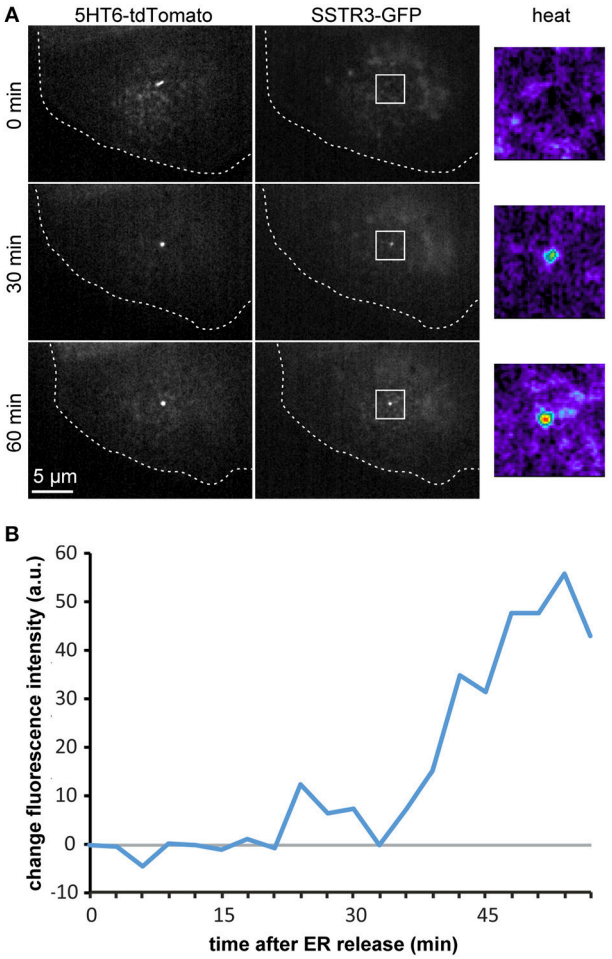

FIGURE 5 | Live-cell imaging and quantification of ciliary arrival. **(A)** Polarized MDCK cells were transfected with pCMV-CAD4-SSTR3-GFP and p5HT6-tdTomato as ciliary marker. 4 h after transfection, CAD4-SSTR3-GFP was released from the ER by addition of D/D-solubilizer ($t = 0$ min). Time lapse images from a single confocal image plane at the level of the primary cilium are displayed and increase of SSTR3-GFP fluorescence in selected areas (white boxes) is also shown in false-color magnifications (heat). **(B)** The cilium outlined by the signal from the 5HT6-tdTomato channel was used to mask the SSTR3-GFP channel in order to quantify the increase of SSTR3-GFP fluorescence intensity at the cilium in dependence of the time after addition of D/D-solubilizer.

CONCLUSIONS

Here we introduce an approach to synchronize the biosynthetic trafficking of ciliary proteins based on tagging with CADs. We show that this system is broadly applicable for proteins imported into the primary cilium by different mechanisms, as illustrated for SSTR3, which is imported via lateral transport along the plasma membrane, and NPHP3, which is imported via the cytosol in a state where its membrane anchor is masked. By using SSTR3 as model protein, we demonstrated that creating a synchronous wave of proteins targeted to the primary cilium is a fruitful approach to uncover mechanistic details of ciliary delivery. In particular, CAD-based synchronization facilitates direct observation of intracellular transport to the primary cilium starting from a state in which the cilium is free from the protein of interest. This allows a selective investigation of biosynthetic delivery to the primary cilium, which is not possible with other methods such as ciliary FRAP. In addition, many individual cells can be monitored in parallel and we present a framework to quantify the kinetics of polarized cell surface arrival and ciliary arrival in epithelial cells. This framework laid the foundation for the discovery that ciliary proteins, including SSTR3 and NPHP3, can exhibit also basolateral localization in epithelial cells. In

future, the synchronization system will be instrumental to study the relation between basolateral and ciliary trafficking mechanisms, including the characterization of a potential transcytotic route from the basolateral plasma membrane to the primary cilium. Furthermore, the data we generated allowed to investigate the correlation between apical SSTR3 and ciliary SSTR3 and between basolateral SSTR3 and ciliary SSTR3 on a single cell level. This yielded complementary quantitative evidence for lateral import of SSTR3 into the cilium along the plasma membrane. Finally, we demonstrated that CAD-based synchronization also allowed imaging and quantifying ciliary import in live cells, thus opening novel possibilities to monitor ciliary trafficking in real time with high resolution in time and space.

MATERIALS AND METHODS

Cell Culture and Protein Expression

MDCK strain II cells (wt MDCK) were a gift from Enrique Rodriguez-Boulan (Weill Cornell Medical College, NY, USA) and were maintained in Dulbecco's modified Eagle's medium (DMEM) supplemented with 5% fetal calf serum (FCS) at 37°C and 5% CO_2 in 10 cm culture dishes and passaged every 2–3 d.

For growing polarized monolayers, cells were cultured on transwell filters (#3401 from Corning-Costar) for 4 d. Transfections were carried out using polyethylenimine (PEI; linear, 25 kDa; Polysciences, stock concentration 1 μg/μl) or Lipofectamine 2000 (Thermo Fisher Scientific) using the dosages indicated in the main text. Doxycycline (Sigma Aldrich) was used at a concentration of 5 μg/ml and D/D-solubilizer (Clontech/Takara) at a concentration of 5 μM.

For generating the cell line stably expressing a tet-regulated transactivator, wt MDCK cells were transfected with the plasmid pWHE644 linearized with *Ahd I* (Herr et al., 2011) and afterwards clones were selected with puromycin (Sigma Aldrich). Six clones were selected and tested using a plasmid encoding for GFP under control of a tet-promoter. Two clones with the tightest repression and highest inducibility after treatment with doxycycline for 12 h were selected. They were further inspected for their capability to form well-polarized monolayers by culturing the cells on transwell filters for 4 d followed by immunofluorescence staining with antibodies directed against the basolateral marker β-catenin (ab32572 from Abcam), the apical marker podocalyxin (produced by the hybridoma cell line R26.4C obtained from the Developmental Studies Hybridoma Bank at the University of Iowa), and against α-tubulin to visualize cilia (T5168 from Sigma Aldrich) and the best clone was chosen for further experiments (tet-MDCK).

Plasmids

The plasmids pCMV-CAD4-FLAG-SSTR3-GFP, pTet-CAD4-FLAG-SSTR3-GFP, and pCMV-CAD4-SSTR3-GFP were cloned using Gibson assembly with a vector encoding pCMV-FM4-GFP (Thuenauer et al., 2014) as backbone and using the murine SSTR3 sequence from ptdTomato-SSTR3-N-17 (gift from Michael Davidson, Addgene plasmid # 58132). pWHE644 was obtained from TET Systems GmbH (Heidelberg, Germany). The plasmid p5HT6-tdTomato was cloned from pEGFPN3-5HT6 (gift from Kirk Mykytyn, Addgene plasmid # 35624).

Surface Staining and Immunofluorescence

Staining for CAD4-FLAG-SSTR3-GFP arrived at the cell surface was carried out with anti- DYKDDDDK/FLAG antibodies (637301 from BioLegend) that were diluted in medium 1:200 and applied to the apical or basolateral side of transwell filter-grown cells for 15 min at room temperature. After two washes with phosphate buffered saline (PBS), cells were fixed with a 4% formaldehyde solution for 15 min at room temperature.

For immunofluorescence (IF), cells were permeabilized with SAPO medium (PBS supplemented with 0.2% bovine serum albumin and 0.02% saponin) for 30 min at room temperature. Next secondary anti-rat Alexa647-tagged antibodies (A21247 from Thermo Fisher Scientific) directed against the primary anti-FLAG antibodies were applied for 1 h, followed by staining with anti-acetylated tubulin antibodies (T7451 from Sigma Aldrich) for 1 h, and then secondary anti-mouse Cy3-tagged antibodies (715-166-1500 from Jackson ImmunoResearch) directed against the anti-acetylated tubulin antibodies for 30 min. After excising filters with a scalpel, they were mounted in DABCO-medium (Müller et al., 2017).

Quantification of Polarized Cell Surface Arrival and Ciliary Arrival

Cells were imaged with a confocal microscope (Nikon A1R) equipped with a 60X oil immersion objective with a numerical aperture (N.A.) of 1.49 and lasers emitting at 405, 488, 561, and 641 nm. Image stacks covering complete cell heights were recorded and used for quantification with a custom-written Matlab program (Thuenauer et al., 2014; Müller et al., 2017). To ensure proper quantification at a single cell level, only cells that were surrounded by non-expressing cells were quantified. First, background signal levels were determined from regions covering non-expressing cells and subtracted from the images. For quantifying apical/basolateral cell surface arrival, the ratio of the intensities from apical/basolateral cell surface staining and GFP intensities representing total FLAG-SSTR3-GFP amounts were determined in individual cells and averaged.

Ciliary arrival was quantified via calculating the MCC (Dunn et al., 2011) between the FLAG-SSTR3-GFP signal above background and the signal above background from the ciliary marker acetylated tubulin according to the formula

$$MCC = \frac{\sum_i SSTR3_i^{coloc}}{\sum_j SSTR3_j} \quad (1)$$

where $SSTR3_i^{coloc}$ is the FLAG-SSTR3-GFP signal from voxels that were also positive for acetylated tubulin, and $SSTR3_j$ is the signal from voxels positive for FLAG-SSTR3-GFP. To minimize potential artifacts resulting from the limited resolution

of the confocal microscope, only cells with clearly visible and protruding cilia were measured.

Live Cell Imaging

Live cell imaging was carried out with a Zeiss Observer Z1 microscope equipped with a 100X N.A. 1.46 oil immersion objective, lasers emitting at 488 and 561 nm, a spinning disc unit (Yokogawa CSU-X1), and a Photometrics Prime sCMOS camera. MDCK cells were grown on glass bottom dishes for 5 d, starved for 48 h and then transfected with pCMV-CAD4-SSTR3-GFP and p5HT6-tdTomato as ciliary marker.

Statistics

If not indicated otherwise, mean values were determined from three independent experiments. Error bars represent the standard error of the mean. Statistical analysis was carried out with a two-tailed paired *t*-test, and * indicates $p < 0.05$.

DATA AVAILABILITY

The raw data supporting the conclusions of this manuscript will be made available by the authors, without undue reservation, to any qualified researcher.

AUTHOR CONTRIBUTIONS

WS performed experiments and wrote the manuscript. AR, AJ, and CS performed experiments. WR contributed to study design. RT contributed to study design, developed the methods, performed experiments, and wrote the manuscript. All authors proofread the manuscript.

FUNDING

RT and WR acknowledge funding from the German Research Foundation ([EXC 294] and [RO 4341/2-1]). RT acknowledges support from the Ministry of Science, Research and the Arts of Baden-Württemberg [Az: 7533-30-10/25/36]. WR acknowledges support from the Ministry of Science, Research and the Arts of Baden-Württemberg [Az: 33-7532.20]. CS was supported by the German Research Foundation [CRC/SFB 1140].

SUPPLEMENTARY MATERIAL

The Supplementary Material for this article can be found online at: https://www.frontiersin.org/articles/10.3389/fgene.2019.00163/full#supplementary-material

REFERENCES

Badgandi, H. B., Hwang, S. H., Shimada, I. S., Loriot, E., and Mukhopadhyay, S. (2017). Tubby family proteins are adapters for ciliary trafficking of integral membrane proteins. *J. Cell Biol.* 216, 743–760. doi: 10.1083/jcb.201607095

Bates, C. M., Kegg, H., Petrevski, C., and Grady, S. (2003). Expression of somatostatin receptors 3, 4, and 5 in mouse kidney proximal tubules. *Kidney Int.* 63, 53–63. doi: 10.1046/j.1523-1755.2003.00716.x

Berbari, N. F., Johnson, A. D., Lewis, J. S., Askwith, C. C., and Mykytyn, K. (2008). Identification of ciliary localization sequences within the third intracellular loop of G protein-coupled receptors. *Mol. Biol. Cell* 19, 1540–1547. doi: 10.1091/mbc.e07-09-0942

Bernabe-Rubio, M., Andrés, G., Casares-Arias, J., Fernández-Barrera, J., Rangel, L., Reglero-Real, N., et al. (2016). Novel role for the midbody in primary ciliogenesis by polarized epithelial cells. *J. Cell Biol.* 214, 259–273. doi: 10.1083/jcb.201601020

Boehlke, C., Bashkurov, M., Buescher, A., Krick, T., John, A. K., Nitschke, R., et al. (2010). Differential role of rab proteins in ciliary trafficking: Rab23 regulates smoothened levels. *J. Cell Sci.* 123(Pt 9), 1460–1467. doi: 10.1242/jcs.058883

Carvajal-Gonzalez, J. M., Gravotta, D., Mattera, R., Diaz, F., Perez Bay, A., Roman, A. C., et al. (2012). Basolateral sorting of the coxsackie and adenovirus receptor through interaction of a canonical YXX motif with the clathrin adaptors AP-1A and AP-1B. *Proc. Natl. Acad. Sci. U.S.A* 109, 3820–3825. doi: 10.1073/pnas.1117949109

Corbit, K. C., Aanstad, P., Singla, V., Norman, A. R., Stainier, D. Y., and Reiter, J. F. (2005). Vertebrate smoothened functions at the primary cilium. *Nature* 437, 1018–1021. doi: 10.1038/nature04117

Dunn, K. W., Kamocka, M. M., and McDonald, J. H. (2011). A practical guide to evaluating colocalization in biological microscopy. *Am. J. Physiol. Cell Physiol.* 300, C723–C742. doi: 10.1152/ajpcell.00462.2010

Francis, S. S., Sfakianos, J., Lo, B., and Mellman, I. (2011). A hierarchy of signals regulates entry of membrane proteins into the ciliary membrane domain in epithelial cells. *J. Cell Biol.* 193, 219–233. doi: 10.1083/jcb.201009001

Herr, R., Wöhrle, F. U., Danke, C., Berens, C., and Brummer, T. (2011). A novel MCF-10A line allowing conditional oncogene expression in 3D culture. *Cell Commun. Signal.* 9:17. doi: 10.1186/1478-811X-9-17

Hu, Q., Milenkovic, L., Jin, H., Scott, M. P., Nachury, M. V., Spiliotis, E. T., et al. (2012). A septin diffusion barrier at the base membrane protein distribution. *Science* 329, 436–439. doi: 10.1126/science.1191054

Hu, Q., and Nelson, W. J. (2011). Ciliary diffusion barrier: the gatekeeper for the primary cilium compartment. *Cytoskeleton* 68, 313–324. doi: 10.1002/cm.20514

Jaiswal, M., Fansa, E. K., Kösling, S. K., Mejuch, T., Waldmann, H., and Wittinghofer, A. (2016). Novel biochemical and structural insights into the interaction of myristoylated cargo with Unc119 protein and their release by Arl2/3. *J. Biol. Chem.* 291, 20766–20778. doi: 10.1074/jbc.M116.741827

Kaplan, O. I., Molla-Herman, A., Cevik, S., Ghossoub, R., Kida, K., Kimura, Y., et al. (2010). The AP-1 Clathrin adaptor facilitates cilium formation and functions with RAB-8 in *C. elegans* ciliary membrane transport. *J. Cell Sci.* 123(Pt 22), 3966–3977. doi: 10.1242/jcs.073908

Lesiak, A. J., Brodsky, M., Cohenca, N., Croicu, A. G., and Neumaier, J. F. (2018). Restoration of physiological expression of 5-HT6 receptor into the primary cilia of null mutant neurons lengthens both primary cilia and dendrites. *Mol. Pharmacol.* 94, 731–742. doi: 10.1124/mol.117.111583

Müller, S. K., Wilhelm, I., Schubert, T., Zittlau, K., Imberty, A., Madl, J., et al. (2017). Gb3-binding lectins as potential carriers for transcellular drug delivery. *Expert Opin. Drug Del.* 14, 141–153. doi: 10.1080/17425247.2017.1266327

Nachury, M. V. (2014). How do cilia organize signalling cascades? *Philosophical Trans. R. Soc. Lond. Ser. B. Biol. Sci.* 369:20130465. doi: 10.1098/rstb.2013.0465

Reales, E., Bernabé-Rubio, M., Casares-Arias, J., Rentero, C., Fernández-Barrera, J., Rangel, L., et al. (2015). The MAL protein is crucial for proper membrane condensation at the ciliary base, which is required for primary cilium elongation. *J. Cell Sci.* 128, 2261–2270. doi: 10.1242/jcs.164970

Rivera, V. M., Wang, X., Wardwell, S., Courage, N. L., Volchuk, A., Keenan, T., et al. (2000). Regulation of protein secretion through controlled aggregation in the endoplasmic reticulum. *Science* 287, 826–830. doi: 10.1126/science.287.5454.826

Rodriguez-Boulan, E., and Macara, I. G. (2014). Organization and execution of the epithelial polarity programme. *Nat. Rev. Mol. Cell Biol.* 15, 225–242. doi: 10.1038/nrm3775

Roitbak, T., Ward, C. J., Harris, P. C., Bacallao, R., Ness, S. A., and Wandinger-Ness, A. (2004). A Polycystin-1 multiprotein complex is disrupted in polycystic kidney disease cells. *Mol. Biol. Cell* 15, 1334–1346. doi: 10.1091/mbc.e03-05-0296

Shi, X., Garcia, G., III, Van De Weghe, J. C., McGorty, R., Pazour, G. J., Doherty, D., et al. (2017). Super-resolution microscopy reveals that disruption of ciliary transition-zone architecture causes joubert syndrome. *Nat. Cell Biol.* 19, 1178–1188. doi: 10.1038/ncb3599

Singla, V., and Reiter, J. F. (2006). The primary cilium as the cell's antenna: signaling at a sensory organelle. *Science* 313, 629–633. doi: 10.1126/science.1124534

Su, X., Wu, M., Yao, G., El-Jouni, W., Luo, C., Tabari, A., et al. (2015). Regulation of Polycystin-1 ciliary trafficking by motifs at its C-Terminus and Polycystin-2 but not by cleavage at the GPS site. *J. Cell Sci.* 128, 4063–4073. doi: 10.1242/jcs.160556

Thuenauer, R., Hsu, Y. C., Carvajal-Gonzalez, J. M., Deborde, S., Chuang, J. Z., Römer, W., et al. (2014). Four-dimensional live imaging of apical biosynthetic trafficking reveals a post-golgi sorting role of apical endosomal intermediates. *Proc. Natl. Acad. Sci. U.S.A* 111, 4127–4132. doi: 10.1073/pnas.1304168111

Vieira, O. V., Gaus, K., Verkade, P., Fullekrug, J., Vaz, W. L., and Simons, K. (2006). FAPP2, cilium formation, and compartmentalization of the apical membrane in polarized Madin-Darby Canine Kidney (MDCK) cells. *Proc. Natl. Acad. Sci. U.S.A.* 103, 18556–18561. doi: 10.1073/pnas.0608291103

Wright, K. J., Baye, L. M., Olivier-Mason, A., Mukhopadhyay, S., Sang, L., Kwong, M., et al. (2011). An ARL3-UNC119-RP2 GTPase cycle targets myristoylated NPHP3 to the primary cilium. *Genes Dev.* 25, 2347–2360. doi: 10.1101/gad.173443.111

Conflict of Interest Statement: The authors declare that the research was conducted in the absence of any commercial or financial relationships that could be construed as a potential conflict of interest.

frontiers in Genetics

REVIEW
published: 11 March 2019
doi: 10.3389/fgene.2019.00127

Opportunities and Challenges for Molecular Understanding of Ciliopathies–The 100,000 Genomes Project

Gabrielle Wheway[1†], *Genomics England Research Consortium and* *Hannah M. Mitchison*[2*]

[1] Human Development and Health, Faculty of Medicine, University of Southampton, Southampton General Hospital, Southampton, United Kingdom, [2] Genetics and Genomic Medicine, University College London, UCL Great Ormond Street Institute of Child Health, London, United Kingdom

Cilia are highly specialized cellular organelles that serve multiple functions in human development and health. Their central importance in the body is demonstrated by the occurrence of a diverse range of developmental disorders that arise from defects of cilia structure and function, caused by a range of different inherited mutations found in more than 150 different genes. Genetic analysis has rapidly advanced our understanding of the cell biological basis of ciliopathies over the past two decades, with more recent technological advances in genomics rapidly accelerating this progress. The 100,000 Genomes Project was launched in 2012 in the UK to improve diagnosis and future care for individuals affected by rare diseases like ciliopathies, through whole genome sequencing (WGS). In this review we discuss the potential promise and medical impact of WGS for ciliopathies and report on current progress of the 100,000 Genomes Project, reviewing the medical, technical and ethical challenges and opportunities that new, large scale initiatives such as this can offer.

Keywords: 100,000 Genome Project, ciliopathies, cilia, genomics, genetics

OPEN ACCESS

Edited by:
Carlo Iomini,
Icahn School of Medicine at Mount Sinai, United States

Reviewed by:
John Andrew Sayer,
Newcastle University, United Kingdom
Theodora Katsila,
University of Patras, Greece

***Correspondence:**
Hannah M. Mitchison
h.mitchison@ucl.ac.uk

[†]*Gabrielle Wheway*
orcid.org/0000-0002-0494-0783

Specialty section:
This article was submitted to Genetic Disorders, a section of the journal Frontiers in Genetics

Received: *22 November 2018*
Accepted: *05 February 2019*
Published: *11 March 2019*

Citation:
Wheway G, Genomics England Research Consortium and Mitchison HM (2019) Opportunities and Challenges for Molecular Understanding of Ciliopathies–The 100,000 Genomes Project. Front. Genet. 10:127. doi: 10.3389/fgene.2019.00127

THE 100,000 GENOMES PROJECT

The launch of the UK's 100,000 Genomes project was announced in December 2012 as part of the UK's Life Sciences Strategy. This ambitious £300 million national project aimed to sequence 100,000 complete genomes from 70,000 individuals with cancer or rare disease, and their unaffected family members (Turnbull et al., 2018). Unlike other population genomics studies such as those in Iceland, Japan, Finland, Sweden and the Netherlands (An, 2017), the 100,000 Genomes Project is a hybrid clinical/research initiative, with an aim to fully integrate genomic testing for eligible individuals within existing routine healthcare pathways in the UK National Health Service (NHS). Sequence data is linked to longitudinal patient records such as hospital admissions and responses to interventions, providing a rich resource of genomic medical information. In many respects, it is the first scheme of its kind in the world, and one of the largest.

The project built upon the legacy of successful population healthcare genetics studies in the UK, such as the Deciphering Developmental Disorders (DDD) study (Wright et al., 2015) and UK10K (Consortium et al., 2015) which built upon the Avon Longitudinal Study of Parents And Children (ALSPAC) (Boyd et al., 2013) and TwinsUK (Moayyeri et al., 2013). It aims to secure the UK's position as a world-leader in healthcare and genomics.

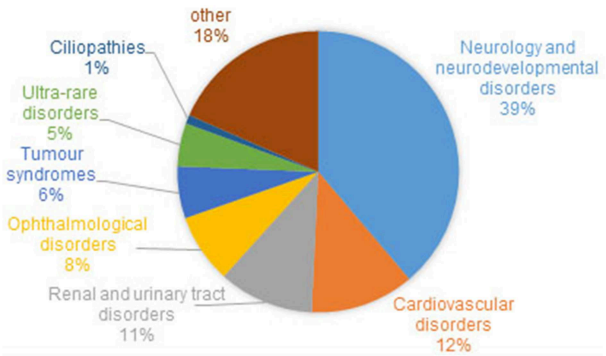

FIGURE 1 | Proportion of families and individuals with different disorders within the rare disease cohort of the 100,000 Genomes Project. Around 1% of recruited families/individuals have a ciliopathy. Cohort summary data courtesy of Genomics England, with permission.

Recruitment for the 100,000 Genome Project has been coordinated across 13 Genomic Medicine Centers set up across 85 NHS Trusts in England, Northern Ireland and Scotland. Of the estimated 8,000 rare diseases (Boycott et al., 2017), 190 were recruited to the Rare Disease pathway of the 100,000 Genomes Project, from 2015/16 until 31st September 2018. Eligible rare diseases were nominated by clinicians and researchers who felt there was an unmet clinical need, for example, diseases for which there are a sizeable proportion of patients with no known genetic diagnosis. The range of phenotypes and the proportion of patients with different disorders within the rare disease cohort is shown in **Figure 1**. Where possible, "trios" were recruited, i.e., the affected individual and both parents, with efforts made to recruit both affected and unaffected family members to allow effective variant filtration.

GENETIC BASIS OF CILIOPATHIES—DISEASES AFFECTING CILIA STRUCTURE AND FUNCTION

Ciliopathies represent one group of rare diseases recruited to the 100,000 Genomes project. The ciliopathies are a diverse grouping but have a common etiology, originating in ciliogenesis (growth and maintenance) and/or structural or functional defects of the cilium (Reiter and Leroux, 2017). Cilia are highly evolved, complex organelles with important roles in motility and signaling (Waters and Beales, 2011; Mitchison and Valente, 2017; Wheway et al., 2018). The extent of the overall medical impact of ciliopathies, which individually most often are rare conditions but collectively affect a large number of individuals, has emerged over the last 20 years as their functions have continued to be revealed through genetic analysis in animal models and human families (Fliegauf et al., 2007; Goetz and Anderson, 2010).

Cilia can broadly be divided into motile and non-motile (primary), each with separate functions, both of which form a unique cellular compartment distinct from the rest of the cell. Primary cilia are more ubiquitous, distributed across most cell types of the body, extending out from the cell surface into their external environment as a single projection with diverse mechanosensory and chemosensory signal transduction roles (Singla and Reiter, 2006). The photoreceptors of the eye have a modified cilium, the outer segment (Wright et al., 2010). In contrast, motile cilia are found only on specialized epithelial surfaces and usually as multiple motile cilia (perhaps 200 per cell). Motile cilia lining notably the respiratory airways, brain ventricles and fallopian tubes, move essential body fluids and gametes, with a structural composition related to that of sperm flagella in male gamete movement (Spassky and Meunier, 2017). Single motile nodal cilia that exist transiently in the embryonic left-right organizer function in laterality determination (Hamada, 2016).

Owing to the central role of the cilium in development and health, ciliopathies often include complex multi-organ developmental phenotypes. The most severe-lethal ciliopathies, Meckel-Gruber syndrome (MKS) (Wheway and Johnson, 2014; Hartill et al., 2017), Joubert syndrome (JBTS) (Parisi and Glass, 1993; Bachmann-Gagescu et al., 2015), orofacial digital syndrome (OFD) (Gurrieri et al., 2007) as well as Bardet-Biedl syndrome (BBS) (Forsythe and Beales, 2013), all include neurodevelopmental features. These are often present alongside other features such as retinal dystrophy, renal dysplasia and skeletal abnormalities (Waters and Beales, 2011). Skeletal ciliopathies range from lethal short-rib thoracic dysplasias to more mild phenotypes such as Jeune syndrome (Huber and Cormier-Daire, 2012; Mitchison and Valente, 2017; Schmidts and Mitchison, 2018). Renal ciliopathies are some of the most common conditions associated with cilia defects. Autosomal polycystic kidney disease (ADPKD) alone affects between 1:2,500 and 1:4,000 individuals in the EU, making it one of the most common genetic diseases in humans, and the most common cause of end–stage renal failure (Willey et al., 2017). Renal malformations can also take the form of nephronophthisis, characterized by chronic tubulointerstitial nephritis, in isolated conditions or part of multiorgan ciliopathies including Senior-Loken syndrome (Wolf and Hildebrandt, 2011). Due to the importance of the highly specialized photoreceptor cilium in the function of the retina, many syndromic ciliopathies include a retinal dystrophy phenotype. Furthermore, around one third of non-syndromic inherited retinal dystrophies, such as retinitiris pigmentosa (RP) and Leber congenital amaurosis (LCA), are associated with a retinal cilium defect (Estrada-Cuzcano et al., 2012). These are termed retinal ciliopathies (Bujakowska et al., 2017).

Rather than being distinct clinical entities, ciliopathies are considered to form a spectrum of disorders, with considerable phenotypic and genotypic overlap between different conditions. In addition to this, there is also extensive phenotypic and genetic heterogeneity amongst ciliopathies (Mitchison and Valente, 2017; Oud et al., 2017). There are currently at least 190 known ciliopathy disease genes causing defects of the primary cilia (**Table 1**), and mutations in many of the same genes can cause strikingly different phenotypes. A classic example is *CEP290*, mutations in which can cause perinatal lethal MKS, severe JBTS, or non-syndromic LCA, which only affects the retina (Coppieters et al., 2010; Drivas and Bennett, 2014).

TABLE 1 | Overview of genes mutated in ciliopathies showing the heterogeneity of certain ciliopathies.

Gene	OMIM	Description
NEURODEVELOPMENTAL CILIOPATHIES		
AHI1	608894	JBTS
ARL3	604695	JBTS, RP?
ARL13B	608922	JBTS
ARMC9	NA	JBTS
ATXN10	611150	JBTS-like
B9D1	614144	MKS
B9D2	611951	MKS
C5orf42	614571	JBTS, OFDS
CC2D2A	612013	JBTS, MKS
CELSR2	604265	JBTS-like
CEP104	616690	JBTS
CEP120	613446	JBTS, SRTD
CEP290	610142	JBTS, SLSN, LCA, MKS, BBS
CEP41	610523	JBTS
CEP55	610000	MKS-like
CLUAP1	616787	JBTS, OFDS
CPLANE1	614571	JBTS
CSPP1	611654	JBTS
EXOC4	608185	MKS
EXOC8	615283	JBTS
HYLS1	610693	MKS-like
ICK	612325	ECO
IFT81	605489, 617895	JBTS-like, SRTD
INPP5E	613037	JBTS
KIAA0556	616650	JBTS
KIAA0586	610178, 616546	JBTS, SRTD
KIF14	611279	MKS, microcephaly with kidney defects
KIF7	611254	JBTS, MKS-like, ACLS
MKS1	609883	MKS, BBS, JBTS
NPHP1	607100	JBTS, NPHP, SLSN
NPHP3	608002	MKS, NPHP
OFD1	300170	JBTS, OFDS
PDE6D	602676	JBTS
PIBF1	607532	JBTS
RPGRIP1L	610937	JBTS, MKS
SUFU	607035	JBTS
TCTN1	609863	JBTS
TCTN2	613846	JBTS
TCTN3	613847	JBTS, OFDS
TMEM107	616183	MKS, OFDS
TMEM138	614459	JBTS
TMEM216	613277	JBTS, MKS
TMEM231	614949	JBTS, MKS
TMEM237	614423	JBTS
TMEM67	609884	MKS, JBTS, NPHP, BBS
TTBK2	611695	JBTS-like
ZNF423	604557	JBTS, NPHP
CILIOPATHIES WITH MAJOR SKELETAL INVOLVEMENT		
C2CD3	615944	OFDS
CEP120	613446	SRTD
C21ORF2	603191	JATD
DDX59	615464	OFDS
DYNC2LI1	617083	SRTD
DYNC2H1	603297	JATD, SRTD
EVC	604831	EVC, WAD
EVC2	607261	EVC, WAD
IFT122	606045	CED
IFT140	614620	SRTD, RP
IFT172	607386	JATD, MZSDS, SRTD, RP
IFT43	614068	CED, SRTD, RP
IFT52	617094	SRTD +/− polydactyly +/− LCA
IFT80	611177	JATD, SRTD +/− retinal dystrophy
INTU	610621	OFDS? SRTD + polydactyly?
KIAA0753	617112	OFDS? JBTS?
NEK1	604588	SRTD
OFD1	300170	OFDS, SGBS, JBTS
SCLT1	611399	OFDS
TBC1D32	615867	OFDS
TCTEX1D2	617353	JATD, SRTD
TTC21B	612014	JATD, NPHP
WDR19	608151	JATD, CED, NPHP, SLSN
WDR34	613363	JATD, SRTD
WDR35	613602	EVC, CED, SRTD
WDR60	615462	JATD, SRTD
ISOLATED AND SYNDROMIC OBESITY		
ALMS1	606844	ALMS
ARL6	608845	BBS, RP
BBIP1	613605	BBS
BBS1	209901	BBS
BBS10	610148	BBS
BBS12	610683	BBS
BBS2	606151	BBS, RP
BBS4	600374	BBS
BBS5	603650	BBS
BBS7	607590	BBS
BBS9 (PTHB1)	607968	BBS
C8orf37	614477	BBS, CORD, RP
CCDC28B	610162	BBS
CEP19	615586	MOSPGF
IFT27	615870	BBS, unclassified lethal ciliopathy with renal involvement
IFT74	608040	BBS
LZTFL1	606568	BBS

(Continued)

TABLE 1 | Continued

Gene	OMIM	Description
MKKS	604896	BBS, MKKS
TRIM32	602290	BBS
TTC8	608132	BBS, RP
WDPCP	613580	BBS
RENAL CILIOPATHIES		
ANKS6	615370	NPHP
CEP164	614848	NPHP
CEP83	615847	NPHP
DCDC2	605755	NPHP
GLIS2	608539	NPHP
INVS	243305	NPHP
IQCB1	609237	SLSN
MAPKBP1	616786	NPHP
NEK8	609799	NPHP
NPHP4	607215	NPHP, SLSN
PKD1	601313	ADPKD
PKD2	173910	ADPKD
PKHD1	606702	ARPKD
SDCCAG8	613524	SLSN, BBS
TRAF3IP1	607380	SLSN
VHL	608537	VHL
XPNPEP3	613553	NPHP-like
ISOLATED RETINAL CILIOPATHY		
C21orf71	613425	RP
CDHR1	609502	RP, CORD
CLRN1 (USH3A)	606397	RP, USH
EYS	612424	RP
LCA5	611408	LCA
MAK	154235	RP
PRPF3	607301	
PRPF31	606419	RP
PRPF4	607795	RP
PRPF6	613979	RP
PRPF8	607300	RP
RP1	603937	RP
RPGR	312610	RP, PCD
RPGRIP1	605446	LCA
SNRNP200	601664	RP
SPATA7	609868	RP, LCA
TOPORS	609507	RP
TULP1	602280	RP, LCA
USH2A	608400	RP, USH
RETINAL DYSTROPHY WITH SENSORINEURAL HEARING LOSS		
ADGRV1	602851	USH
ARSG	610008	USH
CDH23	605516	USH
CEP78	617110	CORD + deafness
CIB2	605564	USH
HARS	142810	USH
MYO7A	276903	USH
PCDH15	605514	USH
PDZD7	612971	USH
SANS	607696	USH
TUBB4B	602662	LCA with early-onset hearing loss
USH1C	605242	USH
USH1E	602097	USH
USH1H	612632	USH
USH1K	614990	USH
WHRN	607928	USH
OTHER CILIOPATHIES		
CENPF	600236	Microcephaly, agenesis of corpus callosum
CCDC11	614759	Laterality defects
CDK10	603464	Suspected complex multisystem ciliopathy affecting development, speech with agenesis of corpus callosum, sensorineural deafness, retinitis pigmentosa, vertebral anomalies, patent ductus arteriosus, facial dysmorphism
SPAG17	616554	Brain malformations, CED-like skeletal dysplasia
WDR11	606417	congenital hypogonadotropic hypogonadism, Kallmann syndrome
PRIMARY CILIARY DYSKINESIA		
ARMC4	615408	PCD
C21orf59	615494	PCD
CCDC103	614677	PCD
CCDC114	615038	PCD
CCDC151	615956	PCD
CCDC39	613798	PCD
CCDC40	613799	PCD
CCDC65	611088	PCD
CCNO	607752	PCD
CFAP300	618058	PCD
DNAAF1	613190	PCD
DNAAF2	612517	PCD
DNAAF3	614566	PCD
DNAAF4	608706	PCD
DNAAF5	614864	PCD
DNAH1	603332	Male infertility, PCD association
DNAH11	603339	PCD
DNAH5	603335	PCD
DNAH9	603330	PCD
DNAI1	604366	PCD
DNAI2	605483	PCD
DNAJB13	610263	PCD

(Continued)

TABLE 1 | Continued

Gene	OMIM	Description
DNAL1	610062	PCD
DRC1	615288	PCD
GAS8	605179	PCD
HYDIN	610812	PCD
LRRC6	614930	PCD
LRRC56	N/A	Mucociliary clearance and laterality defects
MCIDAS	614086	PCD
MNS1	610766	Male infertility, laterality defects
NME8	607421	PCD
PIH1D3	300933	PCD
RSPH1	609314	PCD
RSPH3	615876	PCD
RSPH4A	612647	PCD
RSPH9	612648	PCD
SPAG1	603395	PCD
STK36	607652	PCD
TTC25	617095	PCD
ZMYND10	607070	PCD

Modified from Oud et al. (2017).
ACLS, acrocallosal syndrome; ADPKD, autosomal dominant polycystic kidney disease; ALMS, Alström syndrome; ARPKD, autosomal recessive polycystic kidney disease; BBS, Bardet-Biedl syndrome; CED, cranioectodermal dysplasia syndrome; CORD, cone-rod dystrophy; ECO, endocrine-cerebro-osteodysplasia syndrome; EVC, Ellis-van Creveld syndrome; JATD, Jeune asphyxiating thoracic dysplasia; JBTS, Joubert syndrome; LCA, Leber congenital amaurosis; MKKS, McKusick-Kaufman syndrome; MKS, Meckel-Gruber syndrome; MOSPGF, morbid obesity and spermatogenic failure; NPHP, nephronophthisis; OFDS, oral-facial-digital syndrome; PCD, primary ciliary dyskinesia; RP, retinitis pigmentosa; SGBS, Simpson-Golabi-Behmel syndrome; SLSN, Senior-Løken syndrome; SRTD, short-rib thoracic dysplasia; USH, Usher syndrome; VHL, von Hippel-Lindau syndrome; WAD, Weyers acrodental dysostosis. OMIM: ID number in Online Mendelian Inheritance in Man (https://omim.org/). NA: OMIM number is not available.

Motile ciliopathies are grouped under the name primary ciliary dyskinesia (PCD). A component of PCD manifests with left-right axis abnormalities and this association is also called Kartagener's syndrome, which affects around 50% of PCD patients; additionally there is a more rare disease component arising from defects of ciliogenesis affecting cilia numbers, which is also being called reduced generation of multiple motile cilia (RGMC) (Boon et al., 2014; Lucas et al., 2014; Knowles et al., 2016). Apart from laterality defects that may be linked to cardiac disease (Best et al., 2018), PCD disease features include chronic respiratory infections from earliest life, progressive upper respiratory problems and loss of lung function (bronchiectasis), conductive hearing problems, subfertility, and infrequent hydrocephalus. The same as for the nonmotile ciliopathies, PCD is a genetically and clinically heterogeneous condition, with mutations in around 40 different motile cilia genes currently recognized to cause disease (**Table 1**). Similarly to the primary ciliopathies, a wider than previously suspected spectrum of motile ciliopathy disease is starting to emerge with greater genetic understanding of these conditions. Gene mutations causing more severe (Davis et al., 2015; Amirav et al., 2016; Irving et al., 2018) and more mild (Knowles et al., 2014; Lucas et al., 2017b; Best et al., 2018; Irving et al., 2018; Shoemark et al., 2018) disease have more recently been recognized, as well as subtypes with features that overlap with the primary ciliopathies such as retinitis pigmentosa and developmental delay (Budny et al., 2006; Moore et al., 2006). These syndromic disease subtypes e.g. Simpson-Golabi-Behmel type 2 syndrome, expand our understanding of the extent of the motile ciliopathy disease spectrum (Mitchison and Shoemark, 2017).

CHALLENGES OF DIAGNOSING CILIOPATHIES USING GENOMICS

Despite advances in genetic understanding of these conditions with the advent of next generation sequencing, ciliopathies remain under-diagnosed and poorly recognized due to insensitive and non-specific aspects of available diagnostic tests, compounded by variable disease features. Genetic diagnostic rates of severe primary ciliopathies remain around 62% using targeted gene panel sequencing (Bachmann-Gagescu et al., 2015; Knopp et al., 2015) and 44% using whole exome sequencing (Sawyer et al., 2016). The diagnostic rate of the arguably more uniform motile ciliopathies disease grouping is higher, using well-characterized cohorts, at up to 67% using targeted gene panels (Boaretto et al., 2016; Paff et al., 2018) and 76% using whole exome sequencing with targeted copy number variation (CNV) analysis (Marshall et al., 2015). For both the primary and motile ciliopathies, many genetic causes of these conditions remain unknown. There remain very few, if any, treatment options for the vast majority of these conditions (Lucas et al., 2014, 2017a; Molinari and Sayer, 2017). Thus, there is a pressing clinical need to advance genetic understanding for the purpose of diagnostics, prognostics and development of novel targeted therapies. Clinical genome data from the 100,000 Genomes Project presents exciting opportunities to offer patients genetic diagnoses, gain novel insights into etiology of disease, and uncover new targets for therapies.

Ciliopathy patients and family members account for around 1% of the rare disease cohort recruited to the UK 100,000 Genomes Project (**Figure 1**). In the majority of cases, patients recruited to the ciliopathy pathway have had the relevant ciliopathy disease genes sequenced and excluded as the cause of their disease. Such testing is provided as a genetic diagnostic service by accredited NHS genomics labs, and involves sequencing the exons and intron/exon boundaries of a panel of currently 123 genes known to be mutated in ciliopathies.

At the time of writing, genomes have been sequenced and analyzed from 274 patients and family members with respiratory ciliopathies (126 PCD patients, 148 non-cystic fibrosis (CF) bronchiectasis patients and family members) and 81 patients and family members with congenitial malformations caused by ciliopathies (45 BBS, 14 JBTS, 22 rare multisystem ciliopathy disorders). These numbers will increase as sequencing and analysis is ongoing. However, it is likely that a much larger number of ciliopathy patients have been recruited to the

project within other categories such as "renal and urinary tract disorders," which includes phenotypic descriptor "cystic kidney disease" which accounts for 1,516 individuals alone. Furthermore, within the "ophthalmological disorders" category there are likely to be many undiagnosed retinal ciliopathy patients. One thousand two hundred and sixty individuals with a diagnosis of rod-cone dystrophy or LCA)/early onset severe retinal dystrophy have been recruited. It can be estimated that around one third of these patients have a retinal dystrophy owing to a retinal photoreceptor cilium defect (Estrada-Cuzcano et al., 2012). There are many patients in the project with other dysmorphic and congenital abnormalities with features overlapping ciliopathy phenotypes, which may be undiagnosed ciliopathies. This includes 19 patients with unexplained monogenic fetal disorders. Similarly, there are more than 6,000 patients (39% of the total rare disease patient cohort, **Figure 1**) with a general neurology or neurodevelopmental disorder. These include patients with intellectual disability, holoprosencephaly and hereditary ataxia, all of which are ciliopathy phenotypes seen in syndromic ciliopathies. A subset of these patients could also have undiagnosed ciliopathies. Numbers will increase as data from more patients is made available in upcoming data releases. The 100,000 Genomes Project may thus represent a unique opportunity to discover and diagnose orphan ciliopathies in patients whose phenotype does not currently easily fit into existing disease categories.

The success of the project may lie in the accuracy and thoroughness of phenotyping information provided i.e., the consistent use of Human Phenotype Ontology (HPO) terms. The HPO system was developed to annotate clinical disease terms and definitions with a standardized phenotypic vocabulary (Robinson et al., 2008; Köhler et al., 2017). A particular difficulty with ciliopathies is that they are extremely heterogeneous conditions and it has been suggested that clinicians should be encouraged to actively involve patients in describing their own phenotype (Gainotti et al., 2018). There is great power in larger collections of well-defined patient cohorts to support better clinical research and diagnostics, with the development of rare disease patient registries being a key component supporting the activities of European Reference Networks (ERNs) on rare diseases (Kodra et al., 2018). The European Organization for Rare Diseases (EURORDIS) has developed recommendations on ethical and responsible international data sharing to help inform a clinical diagnosis (Gainotti et al., 2018).

A wide range of phenotypes of different severities are associated with the ciliopathies, demonstrating their complexity (Lee and Gleeson, 2011; Arts and Knoers, 2013; Mitchison and Valente, 2017). **Figure 2** is not exhaustive but shows selected clinical features of the ciliopathies, highlighting those relevant to recruitment criteria for 100,000 Genomes Project. This is a constantly expanding spectrum, with motile and non-motile cilia recently implicated in the etiology of congenital heart disease (You et al., 2015; Best et al., 2018). *Situs inversus* and associated cardiac malformations found in common between motile and some nonmotile ciliopathies suggest an influence on laterality determination at the embryonic left-right organizer during development from non-motile as well as motile cilia, or else that there are shared motile cilia defects, or a mixture of both. There is growing evidence for respiratory involvement in the non-motile primary ciliopathies, but the molecular basis of these findings remains unclear (Mitchison and Shoemark, 2017).

In terms of genetic heterogeneity, interpreting large volumes of genetic variants from all of the ciliopathy patients in order to identify the truly pathogenic disease-causing variant in each individual represents a major challenge. In addition to primary causal variants, modifier genes and variable mutational load have been proposed to play roles in determining the genetic spectrum for both primary ciliopathies (Katsanis et al., 2001; Davis et al., 2011; Zaki et al., 2011; Lindstrand et al., 2016) and motile ciliopathies (Li et al., 2016). Different mutation types can be expected in different ciliopathies, for example motile cilia disease tends to arise from high impact pathogenicity mutations, most often single base substitutions, small insertions and deletions or larger CNVs, that result in protein frameshifts, premature stop codons, missense changes, or splicing defects giving rise to null alleles effects. In contrast, for the non-motile primary ciliopathies lethality frequently arises as a consequence of such alleles, whilst surviving patients would carry only one or no copies of this type of high impact allele, but instead carry one or two hypomorphic alleles such as milder effect missense changes (Davis et al., 2011; Hildebrandt et al., 2011; Schmidts et al., 2013; Reiter and Leroux, 2017). Some specific mutations may be expected, for example splicing mutations and CNVs are common in retinal degeneration caused by *PRPF31* mutations (Buskin et al., 2018). With the superior detection of many mutations through whole genome sequencing, the genetic landscape is expected to greatly expand and may significantly change with implementation of large scale whole genome sequencing (Belkadi et al., 2015). For example the 100,000 Genome Project has already detected a deep intronic mutation in *DNAH11* causing PCD which would not have been detected by other current clinical screening methods (Ellingford et al., 2018).

CILIOPATHY GENOMICS DATA ANALYSIS IN THE 100,000 GENOMES PROJECT

Genomics England Clinical Interpretation Partnerships (GeCIPs) currently coordinate a crowdsourcing approach to data analysis, building on the success of aggregate consortia such as the Exome Aggregation Consortium (ExAc) (Karczewski et al., 2017) and Genome Aggregation Database (GnomAD) (Lek et al., 2016), and public databases such as ClinVar (Landrum and Kattman, 2018), Human Gene Mutation Database HGMD (Stenson et al., 2017) and the Leiden Open-source Variation Database LOVD (Fokkema et al., 2011). In addition to GeCIPs, formed of individuals from not-for-profit organizations, such as academics and clinicians who must apply for access to anonymized data, private commercial companies also have access to the anonymized data. The project is achieved through public-private partnerships (PPPs) between Genomics England Limited, owned by the UK Government's Department of Health & Social Care, and private companies including Illumina Inc. Illumina is a partner both in sequencing and bioinformatics data analysis (https://www.genomicsengland.co.uk/bioinformatics-

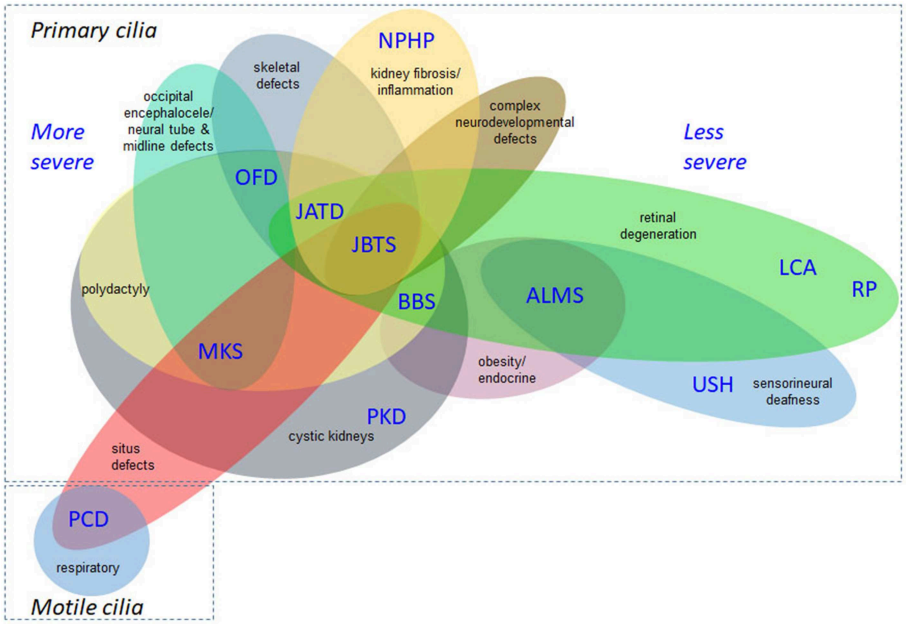

FIGURE 2 | Overlapping disease features of the ciliopathies. This is not an exhaustive list but illustrates the complex phenotypes and overlapping clinical features of ciliopathies. The severe/lethal diseases tend to have more complex combinations of disease features, compared to diseases at the milder end of the clinical spectrum. Situs inversus and associated cardiac malformations are found in common between non-motile and motile ciliopathies and the former can also display respiratory defects. ALMS, Alström syndrome; BBS, Bardet-Biedl syndrome; JATD, Jeune asphyxiating thoracic dysplasia; JBTS, Joubert syndrome; LCA, Leber congenital amaurosis; MKS, Meckel-Gruber syndrome; NPHP, nephronophthisis; OFD, oral-facial-digital syndrome; PCD, primary ciliary dyskinesia; PKD, polycystic kidney disease; RP, retinitis pigmentosa; USH, Usher syndrome.

partnership-with-illumina/). Other "interpretation partners" include Congenica, ICON, Fabric Genomics and WuxiNextCode (https://www.genomicsengland.co.uk/the-100000-genomes-project/data/current-research/). Further to this, industrial companies have been invited to engage with the project and access data by joining the Genomics Expert Network for Enterprises (GENE) for a fee.

Currently, novel or rare variants identified in rare disease patients in the 100,000 Genomes Project are "tiered" according to predicted pathogenicity, following the Association for Clinical Genetic Science's Best Practice Guidelines for Variant Classification (https://www.acgs.uk.com/quality/best-practice-guidelines/) which builds upon Standards and Guidelines for the Interpretation and Reporting of Sequence Variants in Cancer published by the Association for Molecular Pathology (Li et al., 2017). This allows classification of variants into Tier 1, variants with strong clinical significance; Tier 2, variants with potential clinical significance; Tier 3, variants of unknown clinical significance; and Tier 4, variants deemed benign or likely benign. Tiering is achieved using information from PanelApp, an online resource in which clinicians, academic researchers and laboratory scientists pool information about known disease genes, and pathogenic variants within them (https://panelapp.genomicsengland.co.uk/). This crowdsourcing tool enables a "virtual gene panel" approach to the analysis of genomic data; focusing on known or predicted pathogenic genes and variants. Patients' genomes are first analyzed against a panel of genes most closely associated with their disease phenotype (i.e., ciliopathy gene panels), then against other suitable gene panels with features overlapping the phenotype e.g., retinal dystrophy gene panel, neurology panel. Tier 1 variants are protein truncating (frameshift, stop gain, stop loss, splice acceptor variant, or splice donor variant) or *de novo* (protein truncating, missense, or splice region) variants in at least one transcript of a gene on the diagnostic grade "green" gene list in the virtual gene panel for the disorder in question. Tier 2 variants are protein altering variants, such as missense and splice region variants, in at least one transcript of a gene on the diagnostic grade "green" gene list in the virtual gene panel for the disorder in question. Tier 1 and 2 variants are not commonly found in the general healthy population, the allelic state matches the known mode of inheritance for the gene and disorder, and segregates with disease (where applicable). Protein truncating, *de novo* or protein altering variants affecting genes not in the virtual gene panel are Tier 3. If a variant does not meet any of these criteria it is untiered[1].

To provide some sense of scale of the challenge faced, at the time of going to press, there were 2,605 Tier 3 variants in probands with the phenotype "primary ciliary disorders;" primary ciliary dyskinesia' and "primary ciliary dyskinesia::primary ciliary disorders." Of these, 174 are frameshift/stop gain/stop loss/splice donor variant/splice

[1]For further information we direct readers to https://panelapp.genomicsengland.co.uk/

acceptor variants i.e., presumed loss-of function, and 1,829 are missense variants, in around 115 genes. Similarly, at the time of going to press, there were 4,518 Tier 3 variants in probands with phenotype "Bardet-Biedl syndrome;" "Joubert syndrome" or "rare multisystem ciliopathy disorders." Of these, 506 are frameshift/stop gain/stop loss/splice donor variant/splice acceptor variant i.e., presumed loss-of function, and 3,028 are missense variants. Characterizing the effect of these mutations poses a significant challenge in terms of computing power, manpower and bioinformatics expertise.

MOLECULAR MODELING OF CILIOPATHIES

Traditional approaches to modeling non-motile ciliopathies involve 2D ciliated cell line cultures (**Table 2**) or whole animal studies, typically zebrafish (Marshall and Osborn, 2016; Song et al., 2016), mice (Norris and Grimes, 2012), *Xenopus* (Walentek and Quigley, 2017; Blum and Ott, 2018), chick (Schock et al., 2016) and *C.elegans* (Mok and Héon, 2012). Study of motile ciliopathies usually involves studying cells *in vivo*, or on *ex vivo* cultures such as mouse tracheal explants or nasal brush samples from patients with PCD, grown at the air-liquid interface (ALI) (Hirst et al., 2010). There are no adherent immortalized cell lines which can grow motile cilia, although a recent paper reported the immortalization of a multiciliated cell line with dyskinetic cilia (Kuek et al., 2018) which is unlikely to be useful as a control for studying motile ciliopathies. Much understanding of motile cilia has been achieved using single celled flagellated organisms such as *Chlamydomonas reinhardtii* (Harris et al., 2009) and *Trypanosoma brucei* (Langousis and Hill, 2014) which possess one and two flagella, respectively. More recent models include multiciliates planaria and paramecia (King and Patel-King, 2016; Fassad et al., 2018). These model systems offer numerous advantages, including ease of culture and biochemical purification of motile cilia and ease of genetic manipulation. For a useful review of cilia model organisms, see (Vincensini et al., 2011).

3D organoids derived from human embryonic stem (ES) cells or induced pluripotent stem cell (iPSCs) are increasingly replacing animals in ciliopathy research. These can be derived from patient fibroblasts, or can be genetically engineered to harbor patient mutations, to study effect of mutation and efficacy of possible treatments. In the past decade, techniques have particularly advanced in culture methods for producing *in vitro* 3D cell culture models to study cilia and ciliopathies. These include urine-derived renal epithelial cells (URECs) (Ajzenberg et al., 2015) and models of mammalian retina for studying retinal ciliopathies. Robust protocols for culture of retinal organoids from human embryonic stem (ES) cells and induced pluripotent stem cells (iPSCs) have been published and refined (Meyer et al., 2011; Kuwahara et al., 2015). These organoids form laminated neural retina with mature photoreceptor cells, which can be selectively isolated using specific cell surface markers (Lakowski et al., 2018). This provides a highly relevant human-derived model for studying retinal development and retinal degeneration. This is particularly useful for studying human retinal dystrophies which are not recapitulated in genetic mouse models, such as knock-in and knock-out mice models of RP associated with pre-mRNA splicing factor 31 mutations, which do show photoreceptor degeneration (Bujakowska et al., 2009). Similarly, culture techniques are advancing toward the ability to grow motile ciliated cells from iPSCs and ES cells, including in 3D spheroids (Firth et al., 2014; Konishi et al., 2016).

Techniques for genetically editing these ciliated cell models are also advancing, where primary patient cells are not suitable or available for research. This field is moving toward a point where investigators can replicate a potentially pathogenic variant of unknown clinical significance in a human ES cell or iPSC, and differentiate these cells toward a cell type relevant to the primary disease tissue to study the effect of mutation and evaluate methods of genetic correction. Since the development of zinc finger nucleases (ZFNs) (Bibikova et al., 2003) and transcription activator-like effector nucleases (TALENs) (Wood et al., 2011) it has been possible to edit the genome with a high degree of accuracy, to introduce DNA double strand breaks at specific genomic locations, which are generally repaired by error-prone non-homologous end joining (NHEJ) introducing small insertions or deletions, in order to create specific genetic knockouts. However, design and production of such zinc finger nucleases was slow and laborious. It is now possible to introduce such specific breaks with one common nuclease; Cas9 nuclease, significantly increasing throughput. Cas9 is targeted to the genome using a specific guide RNA, in a process termed Clustered Regularly Interspaced Short Palindromic Repeats (CRISPR)/Cas9 genome editing (Cong et al., 2013). The development of the "dual nickase" approach increases specificity and reduces off-target effects (Ran et al., 2013) but off-target effects remain one of the major challenges of scientists using CRISPR. Whilst knockouts can be generated at high efficiency, relying on NHEJ, the introduction of specific insertions, deletions, transitions or transversions using a specific repair template via homology directed repair (HDR), occurs at significantly lower frequency.

In response to this, investigators have now developed base editing, a modified form of CRISPR/Cas9 genome editing, in which Cas9 nickase (Cas9n) is tethered to a cytidine deaminase enzyme which catalyzes the efficient conversion of C●G>T●A changes within a specific window of activity (Komor et al., 2016; Koblan et al., 2018). This refined genetic system can be used to study specific dominant, recessive and compound heterozygous mutations in relevant cells, or animal models. Recently, new adenine base editing tools have been developed, which enable engineering of specific A●T>G●C changes in cell lines (Gaudelli et al., 2017; Koblan et al., 2018). Both technologies have been optimized for mutation in mammalian systems (Koblan et al., 2018). C●G>T●A and A●T>G●C changes can now be efficiently engineered into cells and animals to model dominant disease. However, there is a restricted window of activity 4–8 nucleotides from the first nucleotide of the guide RNA, and guides can only be designed immediately upstream of a relevant protospacer adjacent motif (PAM). Engineering of Cas9 is enabling wider application of this base editing

technology by adjusting the PAM sequence recognized by Cas9, so that with the newly engineered Cas9-cytidine deaminase fusions, approximately 2.5x more variants in ClinVar can be targeted using the technology (Kim et al., 2017) (**Figure 3**). Despite these current limitations, the technology is rapidly advancing and a "double hit" approach provides an efficient new method for modeling compound heterozygous mutations in cell systems. As most ciliopathies are recessive disorders, and compound heterozygosity is common in individuals from non-consanguineous unions, this provides a valuable tool for characterizing variants of unknown significance from the 100,000 Genomes Project.

Characterizing the genetics of ciliopathies may be a larger challenge than in other rare diseases, due to more complex genetics, for example the putative oligogenic inheritance in BBS (Katsanis et al., 2001) and modifier allele effects in multiple ciliopathies (Khanna et al., 2009; Davis et al., 2011; Cardenas-Rodriguez et al., 2013), but novel genome editing technologies provide solutions to these challenges. In order to process the large volume of variants, high-throughput approaches will need to be employed, for example high-content imaging screens such as previously published screens including a whole genome siRNA knockdown screen in ciliated mouse kidney cell line IMCD3 (Wheway et al., 2015) and a druggable genome siRNA knockdown screen in ciliated human retinal cell line hTERT-RPE1 (Kim et al., 2010).

HEALTH POTENTIAL AND FUTURE OPPORTUNITIES OF THE 100,000 GENOMES PROJECT

Despite the challenges, there are undoubtedly enormous opportunities provided by this rich, varied and comprehensively phenotyped dataset. The project represents one of the greatest opportunities for novel disease gene discovery, especially in the case of very rare genes/genetic mutations. The aggregation of many families into the dataset allows multiple families with mutations in the same gene to be identified, leading to disease gene identification. One recent example is *PRPS1*, a gene in which heterozygous missense mutations were found to be carried by retinal dystrophy patients from 5 families

TABLE 2 | Immortalized cell lines used for modeling ciliopathy mutations.

Cell line name	Species origin	Tissue origin	Ciliation *in vitro*	Transfection	ATCC ref	References	Notes
A6	*Xenopus laevis*, frog, South African clawed	Kidney	**	?	CCL-102	Rafferty and Sherwin, 1969	Requires growth on porous collagen-coated filters to allow underside of cells to contact growth media. Grow very long cilia (up to 50 microns long). Can grow motile cilia.
ARPE-19	*Homo sapiens*	Retina—pigmented epithelium	**	*	CRL-2302	Dunn et al., 1998	
HEK293(T)	*Homo sapiens*	Embryonic kidney	*?	****	CRL-1573; CRL-6216	Graham et al., 1977	Often used as an exemplary transfection host cell line. Not well-characterized as being ciliated in culture, but cilia have been described on these cells. Requires growth on porous filters to allow underside of cells to contact growth media
HeLa	*Homo sapiens*	Cervix - adenocarcinoma	*	***	CCL-2	Jones et al., 1971	These are not well-characterized as being ciliated in culture, but cilia have been described on these cells.
hTERT-RPE1	*Homo sapiens*	Retina—pigmented epithelium	**	**	CRL-4000	Rambhatla et al., 2002	
LLC-PK1	*Sus scrofa* (pig)	Kidney—proximal tubule	**	?	CL-101	Perantoni and Berman, 1979	
mIMCD-3	*Mus musculus*	Kidney—inner medullary collecting duct	***	***	CRL-2123	Rauchman et al., 1993	
MDCK	*Canis familiaris*	Kidney—distal tubule/collecting duct	**	**	CCL-34	Gaush et al., 1966	Requires growth on porous filters to allow underside of cells to contact growth media.
NIH/3T3	*Mus musculus*	Fibroblast	***	***	CRL-1658	Jainchill et al., 1969	

ATCC, American Type Culture Collection; ?, no information available. Asterisks indicate degree of ciliation achieved and ease of transfection in different cell lines.

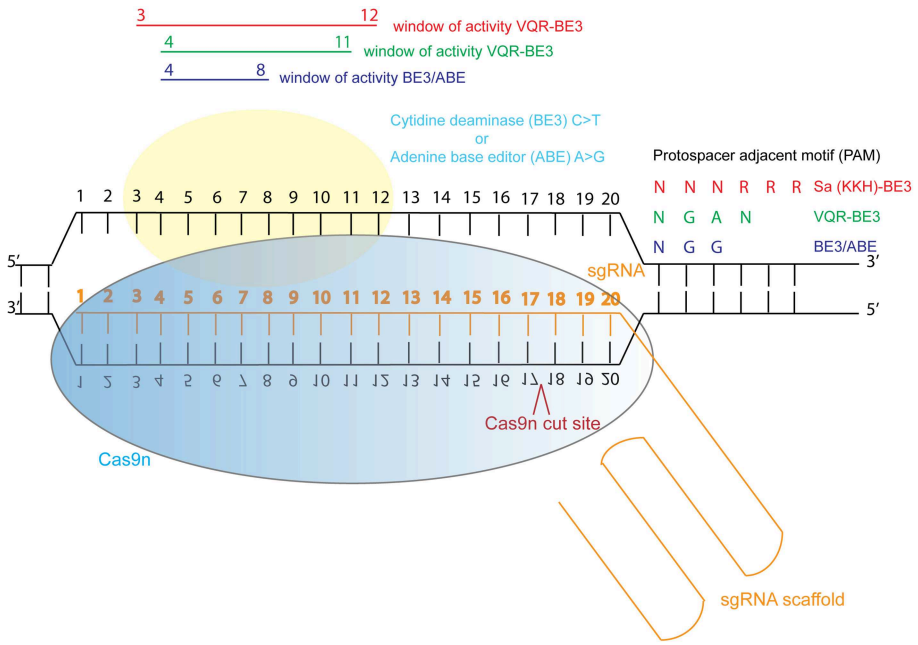

FIGURE 3 | Schematic illustration of cytidine deaminase and adenine base editing of the genome. Abbreviations: sgRNA, single guide RNA; BE3, third generation base editor; ABE, adenine base editor.

in the 100,000 Genomes Project, providing robust genetic evidence for the cause of this condition. Mutations in *PRPS1* are normally found in the more severe Arts syndrome, Charcot-Marie Tooth, and nonsyndromic sensorineural deafness, so if mutations in this gene had only been identified in one family, this may have been disregarded as the pathogenic cause of disease (Fiorentino et al., 2018).

Furthermore, the aggregation of all rare disease patient data into one database may enable diagnosis of novel orphan ciliopathies in a way that was not previously possible. The extensive phenotypic and genotypic heterogeneity of ciliopathies raises the likelihood that there exist individuals or groups of individuals who have a disorder arising from a defect in cilia, but have not had their condition defined as a ciliopathy. The collection of all 60,000 rare disease individuals in the 100,000 Genomes Project may enable identification of novel, previously unrecognized ciliopathies.

In addition to novel disease gene discovery, the project offers many opportunities to gain novel insights into even the most basic gene functions. Around 35% of human genes still have no known function (pantherdb.org) (**Figure 4**). Functional genetics studies investigating genes and variants of interest from the 100,000 Genomes Project may uncover many novel developmental pathways and gene functionalities.

Such disease gene discoveries and new biological insights may provide opportunities for developing targeted therapies for ciliopathies, which currently have very few, if any, treatment options. A number of studies have investigated the efficacy and safety of gene therapy for treatment of ciliopathies, particularly in retinal ciliopathies. *RPGR*, mutations in which cause up to 60% of cases of X-linked RP (Vervoort et al., 2000) has been a particular focus for gene therapy development, including tested in large mammalian models, which have shown to be effective in preventing onset of degeneration (Beltran et al., 2012; Deng et al., 2015; Wu et al., 2015) and also successful in preventing progression of established disease (Beltran et al., 2015). More recently, *RPGR* gene editing approaches have been developed in addition to existing gene augmentation approaches (Deng et al., 2018). However, more than 20 years after the discovery of RPGR, there is still no gene therapy in clinic, although there are three clinical trials currently recruiting, at the time of writing (https://clinicaltrials.gov/ct2/results?cond=&term=rpgr&cntry=&state=&city=&dist=). There are now several more genes being targeted for gene therapy in retinal ciliopathies including *CEP290* (mutations in which cause LCA10) (Estrada-Cuzcano et al., 2012; Burnight et al., 2014; Zhang et al., 2018); and *LCA5* (Song et al., 2018). Gene therapy is also being investigated as a possible treatment for syndromic ciliopathies. Gene augmentation has been demonstrated to be effective and safe in *Bbs4* genetic mouse models of BBS; (McIntyre et al., 2012, 2013; Chamling et al., 2013), but the only clinical phenotype which was rescued was the olfactory sensory defect. It is clear that we need to look beyond gene therapy for treatment options for ciliopathies. The extensive genetic heterogeneity underlying these conditions is a hinderance to development of personalized medicines, but many recurrent and founder effect mutations are also found to underlie the ciliopathies. The future of effective drug development for ciliopathies requires an understanding of the molecular mechanism of disease, which requires genetic and cell biology studies that the 100,000 Genomes Project can accelerate. Much added value will arise from integration of genomics with multi-omics data (proteomics, transcriptomics, metabolomics,

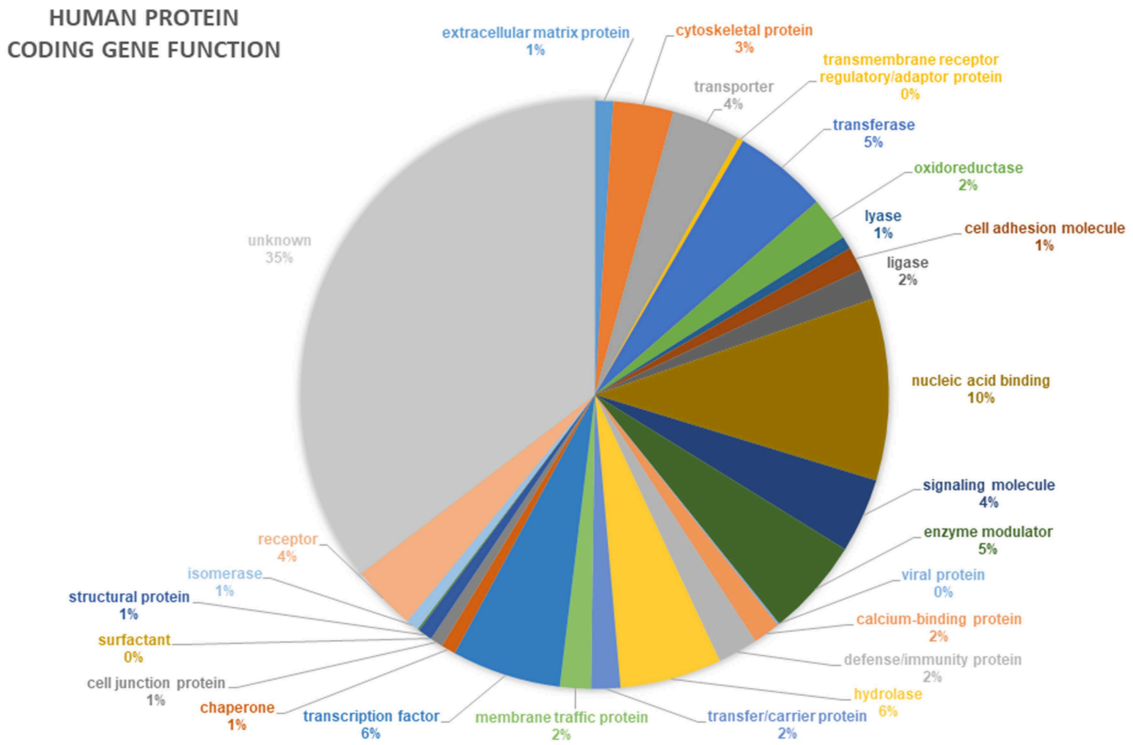

FIGURE 4 | Proportion of annotated human protein coding genes with specific functions. Data from pantherdb.org. Thirty-five percentage of human genes have an unknown function.

epigenomics) and deep phenotyping of ciliopathies, as recently discussed (Kenny et al., 2017).

Re-purposing and re-licensing of FDA-approved drugs could be the most rapid way to bring clinical therapeutics to patients. For example, it has been suggested that re-purposing of cyclin dependent kinase inhibitors could be an appropriate treatment option for a broad range of ciliopathies which have a common basis in replication stress (Slaats et al., 2015). Treatment with CDK inhibitors such as roscovitine has been shown to be effective in rescuing cilia defects in cells derived from patients with Joubert syndrome (Srivastava et al., 2017). Patients with mutations in *NEK1*, a DNA damage response gene mutated in patients with the ciliopathy short rib polydactyly syndrome (Thiel et al., 2011), could potentially be treated in this manner. NEK1 interacts with other ciliopathy proteins C21orf2 and SPATA7 (Wheway et al., 2015), suggesting that other ciliopathies could likewise be treated with CDK inhibitors. As a center for Hh signaling, cilia defects can also be potentially treated with Hh agonists (Hynes et al., 2014), for example purmorphamine, which has been shown to be effective in rescuing cilia defects in cells derived from patients with Joubert syndrome (Srivastava et al., 2017). Uncovering novel mechanisms of disease through functional characterization of variants in the 100,000 Genomes project ciliopathy patient dataset may well identify common pathways of disease which can be targeted to provide therapies for many individuals. Furthermore, if and when any potential therapies reach clinical trials, the national genomic registry provided by the 100,000 Genomes Project will allow rapid identification of individuals suitable for entering the trial.

Until treatments are developed, perhaps the main advantage of insights provided by the 100,000 Genomes Project is the ability to provide genetic diagnosis, for the purposes of better disease monitoring and management, carrier testing, and family planning. This is a particularly pressing need for rare, poorly recognized and difficult to diagnose conditions such as the ciliopathies. If a genetic diagnosis is made, family members can undergo carrier testing which can also inform marriage planning (Nouri et al., 2017; Komlosi et al., 2018). This is especially useful in communities practicing first cousin marriage (consanguinity) in which ciliopathies are at higher risk. One of the aims of the Human Genome Project in Saudi Arabia, where rates of first cousin marriage are around 40%, is to establish a service whereby every engaged couple can undergo whole genome sequencing to test for pathogenic alleles. Worldwide, couples carrying pathogenic variants can make informed decisions about planning pregnancies, including options for pre-implantation diagnosis (PGD). Genetic diseases require robust genetic information before they will be approved by the Human Fertilization and Embryology Authority (HFEA) for PGD. Many genetic subtypes of ciliopathies are now approved for PGD by HFEA, including BBS1, BBS10 and most genetic subtypes of Joubert syndrome (https://www.hfea.gov.uk/pgd-conditions/).

FUTURE PERSPECTIVES FOR UK MEDICAL GENOMICS

On 31st September 2018, recruitment to the rare disease pathway of the 100,000 Genomes Project closed. DNA samples from 61,282 rare disease patients and family members have been deposited in the UK Biobank and 87,231 whole genome sequences have been produced, from rare disease and cancer patients.

Data from the project will continue to provide diagnoses and uncover novel biological insights for years to come. But what of the future of genomic testing in the NHS? In place of the project, from 1st October 2018 the new National Genomic Medicine Service was established, with an aim to provide consistent and equitable access to genomic testing services across the NHS. Genetic testing will now be conducted across a Genomic Laboratory Network of seven hubs, with choice of tests available dictated by the National Genomic Test Directory (https://www.england.nhs.uk/publication/national-genomic-test-directories/). Of the 190 rare diseases recruited into the project, neurological, neurodevelopmental conditions and complex congenital malformations, such as ciliopathies, are those most likely to continue to benefit from genome testing. There are now 22 indications for frontline WGS, 12 of which include ciliopathy phenotypes (**Table 3**). Bardet-Biedl syndrome and respiratory ciliopathies will be initially tested using WES or a large panel test, followed by WGS in year 3 if no results are found (**Table 3**).

This represents the largest restructuring of genetic testing in the history of the NHS and serves as a model for other countries embarking on similar initiatives. These clinical advances will be of enormous benefit to patients with complex syndromic conditions such as ciliopathies. The aim is that WGS will now be the standard, frontline diagnostic test for many of these families, and hopefully increases in diagnostic rates beyond 60% will be start to be achieved. The medical benefits to families of achieving a rapid diagnosis through WGS for rare diseases like ciliopathies and the costs saved to the NHS can be calculated (Mestek-Boukhibar et al., 2018). Studies in the USA have shown that WGS is by far the most time- and cost-effective way to achieve a diagnosis for complex, heterogeneous disorders such as ciliopathies. In the case of general neurodevelopmental disorders, which are also extensively heterogeneous, WGS can reduce time to diagnosis by 77 months, reduce cost of diagnosis by $11,460, and improve clinical care (Soden et al., 2014). For extremely genetically heterogeneous conditions such as neurodevelopmental disorders and ciliopathies, WGS provides an opportunity to allow families to circumvent the traditional "diagnostic odyssey" (Sawyer et al., 2016). Genomics England now plan to sequence 5 million genomes over next 5 years.

GLOBAL PERSPECTIVE AND FUTURE CHALLENGES

There are many other national genome projects around the world, including many with a focus on understanding rare disease, cancer, and genomics for precision medicine. Launched just after the UK's 100,000 Genomes Project, in December 2013, the Saudi Human Genome Program aims to sequence 100,000 individuals, with a specific focus on understanding rare inherited disease, common in Saudi Arabia where first-cousin marriage is common. Two of the largest national genome projects at the time of writing are the USA's $215 million Precision Medicine Initiative announced in January 2015, which aims to sequence 1 million genomes (https://www.nature.com/news/us-precision-medicine-proposal-sparks-questions-1.16774) and China's genomic medicine initiative, launched in 2016, which also aims to sequence 1 million genomes, as part of its 13th five-year plan. Two of the longest running are the Estonia Genome Project (since 2001) and DeCODE project in Iceland, which has been running since 1996 and has sequenced 160,000 individuals, a large proportion of the entire Icelandic population. Others include Genome Russia Project, Proyecto Genoma Navarra (NAGEN) (Spain), Qatar Genome Programme, Belgian Medical Genomics Inititative. More recently, in 2016, France announced its Genomic Medicine Plan 2025 "Médecine Génomique 2025' which involves cooperation with Genomics England, to co-fund analysis of genomes. More local efforts which are large-scale in terms of numbers, but are not nationwide include Geisinger MyCode (Pennsylvania and New Jersey) which has recruited 190,000 patients, and the Utah Genome Project. Transnational efforts include GenomeAsia100K and international efforts include the Personal Genome Project. Transnational and international collaborative efforts may become more commonplace in the future, to increase the power of shared resources.

As well as state-funded clinical and research genomics projects, there also exist privately funded genomics projects, including Craig Venter's "Human Longevity," which aims to sequence 1 million genomes by 2020. AstraZeneca's genomics initiative (in partnership with Human Longevity, Genomics England, Montreal Heart Institute, Sanger Institute and University of Helsinki) uses retrospective patient data from clinical trials over the past 10 years, and will continue to collect data until 2026. In total, up to 2 million genomes will be sequenced, including 500,000 from patients who have taken part in AstraZeneca clinical trials, to significantly enhance drug development for precision medicine approaches.

Each project has different specific aims but they each share many similarities. They all use Illumina short-read sequencing technologies, although it seems likely that in the future at least some will couple these with longer-read sequencing using platforms such as Pacific Biosciences (PacBio) and Oxford Nanopore. Most projects are driven by the same financial initiatives. Since 2008, there has been a global concerted effort to reduce national spending on healthcare, which in developed countries typically accounts for spending equivalent to 10–15% of national GDP (http://www.abpi.org.uk/facts-and-figures/global-pharmaceutical-market/global-health-expenditure-as-a-share-of-gdp/). The Saudi Human Genome Program estimates the total global annual cost of treating rare inherited disease at around US$27 billion (Project Team, 2015). A substantial reduction in children born with genetic disabilities, as a result

TABLE 3 | Conditions indicated for WGS diagnosis in the UK NHS.

Clinical indication	Optimal family structure	Test method year 1	Test method year 2	Test method year 3
Acutely unwell infants with a likely monogenic disorder	Trio	WGS	WGS	WGS
Ultra-rare and atypical monogenic disorders	Trio or singleton	WGS	WGS	WGS
Congenital malformation and dysmorphism syndromes—likely monogenic	Trio	WGS	WGS	WGS
Moderate, severe or profound intellectual disability	Trio	WGS	WGS	WGS
Floppy infant with a likely central cause	Trio	WGS	WGS	WGS
Skeletal dysplasia	Trio	WGS	WGS	WGS
Rare syndromic craniosynostosis or isolated multisuture synostosis	Trio	WGS	WGS	WGS
Neonatal diabetes	Trio	WGS	WGS	WGS
Likely inborn error of metabolism—targeted testing not possible	Trio	WGS	WGS	WGS
Hereditary ataxia with onset in adulthood	Singleton	WGS	WGS	WGS
Hereditary ataxia with onset in childhood	Trio or singleton	WGS	WGS	WGS
Early onset or syndromic epilepsy	Trio	WGS	WGS	WGS
Childhood onset hereditary spastic paraplegia	Trio or singleton	WGS	WGS	WGS
Arthrogryposis	Trio	WGS	WGS	WGS
Other rare neuromuscular disorders	Trio or singleton	WGS	WGS	WGS
Cerebellar anomalies	Trio	WGS	WGS	WGS
Holoprosencephaly—NOT chromosomal	Trio	WGS	WGS	WGS
Hydrocephalus	Trio	WGS	WGS	WGS
Cerebral malformation	Trio	WGS	WGS	WGS
Severe microcephaly	Trio	WGS	WGS	WGS
Childhood onset leukodystrophy	Trio	WGS	WGS	WGS
Cystic renal disease	Singleton	WGS	WGS	WGS
Parental sequencing for lethal autosomal recessive disorders	Parents only	WES	WES	WGS
Bardet-Biedl syndrome	Singleton	WES or large panel	WES or large panel	WGS
Fetal anomalies with a likely genetic cause	Singleton	WES or large panel	WES or large panel	WGS
Hypertrophic cardiomyopathy—teen and adult	Singleton	WES or large panel	WES or large panel	WES or large panel
Dilated cardiomyopathy—teen and adult	Singleton	WES or large panel	WES or large panel	WES or large panel
Molecular autopsy	Singleton	WES or large panel	WES or large panel	WES or large panel
Progressive cardiac conduction disease	Singleton	WES or large panel	WES or large panel	WES or large panel
Thoracic aortic aneurysm or dissection	Singleton	WES or large panel	WGS	WGS
Pediatric or syndromic cardiomyopathy	Singleton	WES or large panel	WES or large panel	WGS
Primary lymphoedema	Singleton	WES or large panel	WES or large panel	WGS
Non-syndromic hearing loss	Singleton	WES or large panel	WES or large panel	WGS
Monogenic diabetes	Singleton	WES or large panel	WES or large panel	WES or large panel
Growth failure in early childhood	Singleton	WES or large panel	WGS	WGS
Bilateral congenital or childhood onset cataracts	Singleton	WES or large panel	WGS	WGS
Retinal disorders	Singleton	WES or large panel	WES or large panel	WGS
Structural eye disease	Singleton	WES or large panel	WES or large panel	WGS
Cholestasis	Singleton	WES or large panel	WES or large panel	WES or large panel
Disorders of sex development	Singleton	WES or large panel	WGS	WGS
Possible X-linked retinitis pigmentosa	Singleton	WES or large panel	WES or large panel	WGS
Sorsby retinal dystrophy	Singleton	WES or large panel	WES or large panel	WGS

(Continued)

TABLE 3 | Continued

Clinical indication	Optimal family structure	Test method year 1	Test method year 2	Test method year 3
Doyne retinal dystrophy	Singleton	WES or large panel	WES or large panel	WGS
Polycystic liver disease	Singleton	WES or large panel	WES or large panel	WES or large panel
Infantile inflammatory bowel disease	Singleton	WES or large panel	WES or large panel	WES or large panel
Bleeding and platelet disorders	Singleton	WES or large panel	WES or large panel	WGS
Rare anemia	Singleton	WES or large panel	WES or large panel	WGS
Cytopenia—NOT Fanconi anemia	Singleton	WES or large panel	WES or large panel	WGS
Cytopenia—Fanconi breakage testing indicated	Singleton	WES or large panel	WES or large panel	WGS
Thrombophilia with a likely monogenic cause	Singleton	WES or large panel	WES or large panel	WES or large panel
Primary immunodeficiency	Singleton	WES or large panel	WGS	WGS
Glycogen storage disease	Singleton	WES or large panel	WES or large panel	WES or large panel
Lysosomal storage disorder	Singleton	WES or large panel	WES or large panel	WES or large panel
Mitochondrial DNA maintenance disorder	Singleton	WES or large panel	WGS	WGS
Mitochondrial disorder with complex I deficiency	Singleton	WES or large panel	WGS	WGS
Mitochondrial disorder with complex II deficiency	Singleton	WES or large panel	WGS	WGS
Mitochondrial disorder with complex III deficiency	Singleton	WES or large panel	WGS	WGS
Mitochondrial disorder with complex IV deficiency	Singleton	WES or large panel	WGS	WGS
Mitochondrial disorder with complex V deficiency	Singleton	WES or large panel	WGS	WGS
Possible mitochondrial disorder—nuclear genes	Singleton	WES or large panel	WGS	WGS
Ehlers Danlos syndrome with a likely monogenic cause	Singleton	WES or large panel	WES or large panel	WES or large panel
Osteogenesis imperfecta	Singleton	WES or large panel	WES or large panel	WES or large panel
Adult onset dystonia, chorea or related movement disorder	Singleton	WES or large panel	WES or large panel	WGS
Childhood onset dystonia, chorea or related movement disorder	Singleton	WES or large panel	WES or large panel	WGS
Adult onset neurodegenerative disorder	Singleton	WES or large panel	WGS	WGS
Adult onset hereditary spastic paraplegia	Singleton	WES or large panel	WGS	WGS
Adult onset leukodystrophy	Singleton	WES or large panel	WGS	WGS
Paroxysmal neurological disorders, pain disorders and sleep disorders	Singleton	WES or large panel	WES or large panel	WGS
Hereditary neuropathy—NOT PMP22 copy number	Singleton	WES or large panel	WGS	WGS
Congenital muscular dystrophy	Singleton	WES or large panel	WGS	WGS
Congenital myaesthenic syndrome	Singleton	WES or large panel	WGS	WGS
Congenital myopathy	Singleton	WES or large panel	WGS	WGS
Limb girdle muscular dystrophy	Singleton	WES or large panel	WGS	WGS
Neuromuscular arthrogryposis	Singleton	WES or large panel	WGS	WGS
Cerebral vascular malformations	Singleton	WES or large panel	WES or large panel	WES or large panel
Renal tubulopathies	Singleton	WES or large panel	WES or large panel	WES or large panel
Nephrocalcinosis or nephrolithiasis	Singleton	WES or large panel	WES or large panel	WES or large panel
Unexplained pediatric onset end-stage renal disease	Singleton	WES or large panel	WES or large panel	WES or large panel
Proteinuric renal disease	Singleton	WES or large panel	WGS	WGS
Laterality disorders and isomerism	Singleton	WES or large panel	WES or large panel	WES or large panel
Respiratory ciliopathies including non-CF bronchiectasis	Singleton	WES or large panel	WES or large panel	WES or large panel
Epidermolysis bullosa and congenital skin fragility	Singleton	WES or large panel	WES or large panel	WES or large panel
Neonatal erythroderma	Singleton	WES or large panel	WES or large panel	WES or large panel

of improved genetic diagnostics through understanding gained from genome projects, could immediately save over US$270 million. Furthermore, most governments cite the importance of remaining, or becoming, internationally competitive in the nascent field of genome-guided drug development as reasons behind their investment in large-scale genomics projects. The pharmaceutical industry is one of the world's largest industries, worth in excess of $800,000 million annually (http://www.abpi.org.uk/facts-and-figures/global-pharmaceutical-market/top-10-pharmaceutical-markets-by-value-usd/).

In order to achieve the greatest global health benefits from the information in these multiple genomics projects, responsible and secure data sharing is essential. Achieving this whilst maintaining patient confidentiality and data security is a global challenge. The Global Alliance for Genomics and Health (GA4GH) was established in 2013 to develop best-practice guidelines, and develop tools for genome data sharing. Most recently, GA4GH have developed the application programming interface (API) Beacon, which allows organizations to share genomic and health data in a way which preserves patient confidentiality and data anonymity. Through Beacon, individuals who are not registered and approved users of individual genomics datasets, such as a GeCIP member, can still query these datasets to retrieve information about specific alleles. This saves time; there is no need to go through an often lengthy database access protocol and it actually preserves patient confidentiality since no raw genome data is accessed. Beacon is part of the new interoperability standards, contributing to the Framework for Responsible Sharing of Genomic and Health-Related Data developed by GA4GH (https://www.ga4gh.org/genomic-data-toolkit/regulatory-ethics-toolkit/framework-for-responsible-sharing-of-genomic-and-health-related-data/). Congenica and Genomics England are members of the GA4GH and contribute to the Steering Committee of GA4GH, so it seems likely that at some point in the future data will become more widely available for exploitation for the benefit of human health.

Meaningful and effective sharing of data from many genome projects also poses a practical challenge in terms of interoperability of analytical platforms. Whilst all large scale genome projects predominantly use Illumina sequence technologies, each program has bespoke data standards, analytical pipelines, storage and access protocols which are potentially incompatible with each other. There may also be variations in the standards applied to use of phenotypic terms, variant calling and descriptions of pathogenicity of alleles. GA4GH develops tools and defines standards to harmonize data generation, analysis, storage and access. Recently, GA4GH developed a set of standards for variant calling, which allows stratification of performance by variant type and genome context (Krusche et al., 2018). Furthermore, GA4GH develops standards for workflow development, and APIs for packaging of workflows to support their application within multiple different environments. This will allow researchers to run the same analysis workflow on data in multiple clouds and environments in order to standardize data analysis across projects.

Ensuring interoperability of platforms will becoming increasingly important as more genome projects incorporate long-read sequence technologies to complement short-read sequence technologies. This approach allows resolution and alignment of repetitive regions, including regions with many short tandem repeats, or genes with many pseudogenes, phasing of compound heterozygous mutations and provides information about epigenetic marks (Simpson et al., 2017; Pollard et al., 2018). This has clinical relevance in ciliopathies; ADPKD associated with *PKD1* mutations is difficult to diagnose genetically due to 6 pseudogenes of *PKD1* on chromosome 16 with 97.7% sequence identity (Eisenberger et al., 2015). Similarly, in the X-linked retinal ciliopathy retinitis pigmentosa, diagnostic yields are low due to the fact that most patients have a mutation in the highly repetitive region of *RPGR* ORF15, which is difficult to amplify by PCR and Sanger sequencing, and difficult to align with Illumina short read sequencing (Vervoort et al., 2000; Branham et al., 2012).

As well as ensuring integration of different sequencing analysis platforms, it is essential to ensure that platforms for sequence storage and analysis integrate properly with electronic clinical data management systems. This is particularly important for reporting and genetic counseling, and clinical management of patients in receipt of a genetic diagnosis (Welch et al., 2018). It is also crucial to the meaningful analysis of genome data, in the context of detailed medical records including family history, phenotype (using standard HPO terms) and treatment history. GA4GH have developed best practice guidelines for using Family Health History patient record systems with genomics data.

Complex challenges remain, including standardizing a definition of what constitutes a pathogenic allele across all genomics projects. The Association for Clinical Genetic Science's Best Practice Guidelines for Variant Classification 2017 (Ellard et al., 2017) forms the basis of the standard for the 100,000 Genomes Project, based upon Standards and Guidelines for the Interpretation and Reporting of Sequence Variants in Cancer published by the Association for Molecular Pathology (Li et al., 2017). However, it must be acknowledged that we remain relatively naïve in our understanding of pathogenicity, particularly with regard to variants affecting splicing. It has been calculated that 35-40% of pathogenic variants in non-canonical splice site positions are missing from public databases, suggesting that we currently under-diagnose pathogenic causes of disease associated with splicing (Lord et al., 2018). We do not yet know enough about the functional effect of non-coding variants, subtle missense variants and variants in exonic splice enhancers to be able to report these back to patients without functional validation. This is likely to be the significant bottleneck in exploitation of the expanding wealth of genome and population-genetics data. Most *in silico* predictors of pathogenicity are notoriously unreliable, and will only improve with machine learning aided by robust *in vitro* data from functional experiments. This is time-consuming and expensive work. Beyond simple monogenic disorders, we also need frameworks for consistently assigning pathogenicity based on polygenic risk scores, and combined total gene variation scores (Khera et al., 2018; Mossotto et al., 2018). For these reasons, it seems appropriate that this remains an ongoing area of development by GA4GH's Variation Annotation Task Team.

GLOBAL SOCIAL CHALLENGES

The UK, USA and China all strive to be global leaders in this area, and as a result, have each launched ambitious genome sequencing projects such as the 100,000 Genomes Project, arguably before the necessary skills, understanding or, importantly, public appetite, to manage these projects effectively is in place. Public understanding and trust of genomics remains a global challenge

to the success of all genomics projects. Lack of understanding or confidence in genomics in the workforce and the patient population poses a barrier to effective implementation and recruitment to genomics projects. This requires an entire "Workforce transformation" (https://www.genomicseducation.hee.nhs.uk/news/item/357-transforming-healthcare-the-impact-of-genomics-on-the-nhs/). Health Education England, (HEE) is a key delivery partner in the 100,000 Genomes Project and has developed a Genomics Education Programme delivered by higher education providers around the UK as a postgraduate masters (MSc) in Genomic Medicine. Parts of this programme are also possible to study, with a shorter training period, awarded as a PGCert and PGDip, or as standalone modules available as part of continuing professional development (CPD). Courses are designed to fit around work, or to be attended part-time, by staff within the NHS and a One-day Primer In Genomic Medicine is currently offered by University of Southampton (https://www.southampton.ac.uk/medicine/primer-in-genomic-medicine-web-form.page; https://www.genomicseducation.hee.nhs.uk/taught-courses/courses/primer-genomic-medicine/.

Patient education and education of the general public in genomics remains a barrier to greater success and higher recruitment, and impacts on truly "*informed* consent." Furthermore, the nature of a consent process in which all individuals must consent to the research element of the project, which includes sharing of information with commercial companies, raises issues around autonomy and consent (Dheensa et al., 2018). The public outreach initiative "Socializing the Genome," developed by West of England Genomic Medicine Center, reached 19,000 people across the south-west, now launched across Manchester region (https://www.genomicseducation.hee.nhs.uk/news/item/347-how-lego-pro-bots-are-bringing-genomics-to-life-in-the-classroom/). At a time when public understanding, including in the workforce, remains low, there is concern that mainstreaming of genomics services at this point in time may be premature (Ormondroyd et al., 2018). Ethical implications of incidental findings, data security and anonymity, and intellectual property of findings resulting from genome studies also remain unresolved issues across all projects. Many professionals currently believe incidental findings should be reported with caution, with an "approach that is responsive to accumulating evidence." These issues present a significant challenge (Ormondroyd et al., 2018). The general consensus is that there is not enough evidence to form a robust policy regarding secondary findings yet, so data should be interpreted with caution (Ormondroyd et al., 2018). Similarly, decisions about how often to reanalyze data and the mechanism for reporting data back to patients still requires resolution.

It is of utmost importance for healthcare professionals, researchers, and policymakers to be open and honest about the challenges, in order to avoid "genohype" and setting unrealistic expectations. In the past there has been a tendency to overstate the opportunities and understate the risks associated with genetic testing (Samuel and Farsides, 2017) and this has led to some loss of public confidence in genetics. Time taken to return findings remains a significant issue in genomic testing (Moss and Wernham, 2018). Transparency, clear and ongoing communication between healthcare professionals and patients is essential (Dheensa et al., 2018), communicating the possibility of no certain findings either now, or in the near future. We also need to reconsider our concept of the need for fully informed consent, which may not be possible in genomics. Rather, we must consider the general social contract around healthcare provision in the UK, and commitments to public education in the area of genomics.

CONCLUDING REMARKS

The 100,000 Genomes Project provides many opportunities and challenges to improve our understanding of ciliopathies. Perhaps the real power in this dataset will be realized through aggregation of this information with other genome projects worldwide. For this to be a success, data security, regulation and ethics must be at the center of such efforts, to establish and maintain public trust in genome testing. There must be a truly global effort to standardize phenotypic descriptions, data standards, analysis pipelines and mechanisms for data sharing and discovery. Perhaps then, with global cooperation, we can finally increase diagnostic yields, inform better clinical management and translate new understanding into targeted therapies for ciliopathy patients.

DATA AVAILABILITY

All datasets generated for this study are included in the manuscript and/or the supplementary files.

AUTHOR CONTRIBUTIONS

GERC provided essential data for this publication. All authors listed have made a substantial, direct and intellectual contribution to the work, and approved it for publication.

ACKNOWLEDGMENTS

GW was supported by a Wellcome Trust Seed Award in Science (204378/Z/16/Z) and a University of Southampton Faculty of Medicine Research Management Committee Research Project Award. HM was supported by Great Ormond Street Children's Charity grant Leadership awards (V1299, V2217), the NIHR Biomedical Research Center at Great Ormond Street Hospital for Children NHS Foundation Trust and University College London and the COST Action BEAT-PCD: Better Evidence to Advance Therapeutic options for PCD network (BM1407). This research was made possible through access to the data and findings generated by the 100,000 Genomes Project. The 100,000 Genomes Project is managed by Genomics England Limited (a wholly owned company of the Department of Health). The 100,000 Genomes Project is funded by the National Institute for Health Research and NHS England. The Wellcome Trust, Cancer Research UK and the Medical Research Council have also funded research infrastructure. The 100,000 Genomes Project uses data

provided by patients and collected by the National Health Service as part of their care and support.

THE MEMBERS OF THE GENOMICS ENGLAND RESEARCH CONSORTIUM

Ambrose J. C.[1], Baple E. L.[1], Bleda M.[1], Boardman-Pretty F.[1,2], Boissiere J. M.[1], Boustred C. R.[1], Caulfield M. J.[1,2], Chan G. C.[1], Craig C. E. H.[1], Daugherty L. C.[1], de Burca A.[1], Devereau, A.[1], Elgar G.[1,2], Foulger R. E.[1], Fowler T.[1], Furió-Tarí P.[1], Hackett J. M.[1], Halai D.[1], Holman J. E.[1], Hubbard T. J. P.[1], Jackson R.[1], Kasperaviciute D.[1,2], Kayikci M.[1], Lahnstein L.[1], Lawson K.[1], Leigh S. E. A.[1], Leong I. U. S.[1], Lopez F. J.[1], Maleady-Crowe F.[1], Mason J.[1], McDonagh E. M.[1,2], Moutsianas L.[1,2], Mueller M.[1,2], Murugaesu N.[1], Need A. C.[1,2], Odhams C. A.[1], Patch C.[1,2], Perez-Gil D.[1], Polychronopoulos D.[1], Pullinger J.[1], Rahim T.[1], Rendon A.[1], Riesgo-Ferreiro P.[1], Rogers T.[1], Ryten M.[1], Savage K.[1], Sawant K.[1], Scott R. H.[1], Siddiq A.[1], Sieghart A.[1], Smedley D.[1,2], Smith K. R.[1,2], Sosinsky A.[1,2], Spooner W.[1], Stevens H. E.[1], Stuckey A.[1], Sultana R.[1], Thomas E. R. A.[1,2], Thompson S. R.[1], Tregidgo C.[1], Tucci A.[1,2], Walsh E.[1], Watters, S. A.[1], Welland M. J.[1], Williams E.[1], Witkowska K.[1,2], Wood S. M.[1,2], Zarowiecki M.[1]. (1) Genomics England, London, UK. (2) William Harvey Research Institute, Queen Mary University of London, London, EC1M 6BQ, UK.

REFERENCES

Ajzenberg, H., Slaats, G. G., Stokman, M. F., Arts, H. H., Logister, I., Kroes, H. Y., et al. (2015). Non-invasive sources of cells with primary cilia from pediatric and adult patients. *Cilia* 4:8. doi: 10.1186/s13630-015-0017-x

Amirav, I., Wallmeier, J., Loges, N. T., Menchen, T., Pennekamp, P., Mussaffi, H., et al. (2016). Systematic analysis of CCNO variants in a defined population: implications for clinical phenotype and differential diagnosis. *Hum. Mutat.* 37, 396–405. doi: 10.1002/humu.22957

An, J. Y. (2017). National human genome projects: an update and an agenda. *Epidemiol. Health* 39:e2017045. doi: 10.4178/epih.e2017045

Arts, H. H., and Knoers, N. V. (2013). Current insights into renal ciliopathies: what can genetics teach us? *Pediatr. Nephrol.* 28, 863–874. doi: 10.1007/s00467-012-2259-9

Bachmann-Gagescu, R., Dempsey, J. C., Phelps, I. G., O'Roak, B. J., Knutzen, D. M., Rue, T. C., et al. (2015). Joubert syndrome: a model for untangling recessive disorders with extreme genetic heterogeneity. *J. Med. Genet.* 52, 514–522. doi: 10.1136/jmedgenet-2015-103087

Belkadi, A., Bolze, A., Itan, Y., Cobat, A., Vincent, Q. B., Antipenko, A., et al. (2015). Whole-genome sequencing is more powerful than whole-exome sequencing for detecting exome variants. *Proc. Natl. Acad. Sci. U.S.A.* 112, 5473–5478. doi: 10.1073/pnas.1418631112

Beltran, W. A., Cideciyan, A. V., Iwabe, S., Swider, M., Kosyk, M. S., McDaid, K., et al. (2015). Successful arrest of photoreceptor and vision loss expands the therapeutic window of retinal gene therapy to later stages of disease. *Proc. Natl. Acad. Sci. U.S.A.* 112, E5844–E5853. doi: 10.1073/pnas.1509914112

Beltran, W. A., Cideciyan, A. V., Lewin, A. S., Iwabe, S., Khanna, H., Sumaroka, A., et al. (2012). Gene therapy rescues photoreceptor blindness in dogs and paves the way for treating human X-linked retinitis pigmentosa. *Proc. Natl. Acad. Sci. U.S.A.* 109, 2132–2137. doi: 10.1073/pnas.1118847109

Best, S., Shoemark, A., Rubbo, B., Patel, M. P., Fassad, M. R., Dixon, M., et al. (2018). Risk Factors for Situs Defects and congenital heart disease in primary ciliary dyskinesia. *Thorax* 74, 203–205. doi: 10.1136/thoraxjnl-2018-212104

Bibikova, M., Beumer, K., Trautman, J. K., and Carroll, D. (2003). Enhancing gene targeting with designed zinc finger nucleases. *Science* 300:764. doi: 10.1126/science.1079512

Blum, M., and Ott, T. (2018). Xenopus: an undervalued model organism to study and model human genetic disease. *Cells Tissues Organs.* 9, 1–11. doi: 10.1159/000490898

Boaretto, F., Snijders, D., Salvoro, C., Spalletta, A., Mostacciuolo, M. L., Collura, M., et al. (2016). Diagnosis of primary ciliary dyskinesia by a targeted next-generation sequencing panel: molecular and clinical findings in italian patients. *J. Mol. Diagn.* 18, 912–922. doi: 10.1016/j.jmoldx.2016.07.002

Boon, M., Wallmeier, J., Ma, L., Loges, N. T., Jaspers, M., Olbrich, H., et al. (2014). MCIDAS mutations result in a mucociliary clearance disorder with reduced generation of multiple motile cilia. *Nat. Commun.* 5:4418. doi: 10.1038/ncomms5418

Boycott, K. M., Rath, A., Chong, J. X., Hartley, T., Alkuraya, F. S., Baynam, G., et al. (2017). International cooperation to enable the diagnosis of all rare genetic diseases. *Am. J. Hum. Genet.* 100, 695–705. doi: 10.1016/j.ajhg.2017.04.003

Boyd, A., Golding, J., Macleod, J., Lawlor, D. A., Fraser, A., Henderson, J., et al. (2013). Cohort Profile: the 'children of the 90s'–the index offspring of the avon longitudinal study of parents and children. *Int. J. Epidemiol.* 42, 111–127. doi: 10.1093/ije/dys064

Branham, K., Othman, M., Brumm, M., Karoukis, A. J., Atmaca-Sonmez, P., Yashar, B. M., et al. (2012). Mutations in RPGR and RP2 account for 15% of males with simplex retinal degenerative disease. *Invest. Ophthalmol. Vis. Sci.* 53, 8232–8237. doi: 10.1167/iovs.12-11025

Budny, B., Chen, W., Omran, H., Fliegauf, M., Tzschach, A., Wisniewska, M., et al. (2006). A novel X-linked recessive mental retardation syndrome comprising macrocephaly and ciliary dysfunction is allelic to oral-facial-digital type I syndrome. *Hum. Genet.* 120, 171–178. doi: 10.1007/s00439-006-0210-5

Bujakowska, K., Maubaret, C., Chakarova, C. F., Tanimoto, N., Beck, S. C., Fahl, E., et al. (2009). Study of gene-targeted mouse models of splicing factor gene Prpf31 implicated in human autosomal dominant retinitis pigmentosa (RP). *Invest. Ophthalmol. Vis. Sci.* 50, 5927–5933. doi: 10.1167/iovs.08-3275

Bujakowska, K. M., Liu, Q., and Pierce, E. A. (2017). Photoreceptor cilia and retinal ciliopathies. *Cold Spring Harb. Perspect. Biol.* 9:a028274. doi: 10.1101/cshperspect.a028274

Burnight, E. R., Wiley, L. A., Drack, A. V., Braun, T. A., Anfinson, K. R., Kaalberg, E. E., et al. (2014). CEP290 gene transfer rescues Leber congenital amaurosis cellular phenotype. *Gene Ther.* 21, 662–672. doi: 10.1038/gt.2014.39

Buskin, A., Zhu, L., Chichagova, V., Basu, B., Mozaffari-Jovin, S., Dolan, D., et al. (2018). Disrupted alternative splicing for genes implicated in splicing and ciliogenesis causes PRPF31 retinitis pigmentosa. *Nat. Commun.* 9:4234. doi: 10.1038/s41467-018-06448-y

Cardenas-Rodriguez, M., Osborn, D. P., Irigoín, F., Graña, M., Romero, H., Beales, P. L., et al. (2013). Characterization of CCDC28B reveals its role in ciliogenesis and provides insight to understand its modifier effect on Bardet-Biedl syndrome. *Hum. Genet.* 132, 91–105. doi: 10.1007/s00439-012-1228-5

Chamling, X., Seo, S., Bugge, K., Searby, C., Guo, D. F., Drack, A. V., et al. (2013). Ectopic expression of human BBS4 can rescue Bardet-Biedl syndrome phenotypes in Bbs4 null mice. *PLoS ONE* 8:e59101. doi: 10.1371/journal.pone.0059101

Cong, L., Ran, F. A., Cox, D., Lin, S., Barretto, R., Habib, N., et al. (2013). Multiplex genome engineering using CRISPR/Cas systems. *Science* 339, 819–823. doi: 10.1126/science.1231143

Consortium, U. K., Walter, K., Min, J. L., Huang, J., Crooks, L., Memari, Y., et al. (2015). The UK10K project identifies rare variants in health and disease. *Nature* 526, 82–90. doi: 10.1038/nature14962

Coppieters, F., Lefever, S., Leroy, B. P., and De Baere, E. (2010). CEP290, a gene with many faces: mutation overview and presentation of CEP290base. *Hum. Mutat.* 31, 1097–1108. doi: 10.1002/humu.21337

Davis, E. E., Zhang, Q., Liu, Q., Diplas, B. H., Davey, L. M., Hartley, J., et al. (2011). TTC21B contributes both causal and modifying alleles across the ciliopathy spectrum. *Nat. Genet.* 43, 189–196. doi: 10.1038/ng.756

Davis, S. D., Ferkol, T. W., Rosenfeld, M., Lee, H. S., Dell, S. D., Sagel, S. D., et al. (2015). Clinical features of childhood primary ciliary dyskinesia by genotype

and ultrastructural phenotype. *Am. J. Respir. Crit. Care Med.* 191, 316–324. doi: 10.1164/rccm.201409-1672OC

Deng, W. L., Gao, M. L., Lei, X. L., Lv, J. N., Zhao, H., He, K. W., et al. (2018). Gene correction reverses ciliopathy and photoreceptor loss in iPSC-derived retinal organoids from retinitis pigmentosa patients. *Stem Cell Rep*. 10, 1267–1281. doi: 10.1016/j.stemcr.2018.05.012

Deng, W. T., Dyka, F. M., Dinculescu, A., Li, J., Zhu, P., Chiodo, V. A., et al. (2015). Stability and safety of an AAV vector for treating RPGR-ORF15 X-linked retinitis pigmentosa. *Hum. Gene Ther.* 26, 593–602. doi: 10.1089/hum.2015.035

Dheensa, S., Samuel, G., Lucassen, A. M., and Farsides, B. (2018). Towards a national genomics medicine service: the challenges facing clinical-research hybrid practices and the case of the 100,000 genomes project. *J. Med. Ethics* 44, 397–403. doi: 10.1136/medethics-2017-104588

Drivas, T. G. B., and Bennett, J. (2014). "CEP290 and the primary cilium," in *Retinal Degenerative Diseases,* eds J. Ash, C. Grimm, J. Hollyfield, R. Anderson, M. LaVail, and C. Bowes Rickman (New York, NY: Springer), 519–525.

Dunn, K. C., Marmorstein, A. D., Bonilha, V. L., Rodriguez-Boulan, E., Giordano, F., and Hjelmeland, L. M. (1998). Use of the ARPE-19 cell line as a model of RPE polarity: basolateral secretion of FGF5. *Invest. Ophthalmol. Vis. Sci.* 39, 2744–2749.

Eisenberger, T., Decker, C., Hiersche, M., Hamann, R. C., Decker, E., Neuber, S., et al. (2015). An efficient and comprehensive strategy for genetic diagnostics of polycystic kidney disease. *PLoS ONE,* 10:e0116680. doi: 10.1371/journal.pone.0116680

Ellard, S., Baple, E. L., Owens, M., Eccles, D. M., Abbs, S., Deans, Z. C., et al. (2017). *ACGS Best Practice Guidelines for Variant Classification 2017.* Association for Clinical Genetic Science. Available online at: http://www.acgs.uk.com/media/1059605/uk_practice_guidelines_for_variant_classification_2017_24_05_17.pdf

Ellingford, J. M., Beaman, G., Webb, K., Callaghan, C., Hirst, R. A., Black, G. C. M., et al. (2018). Whole genome sequencing enables definitive diagnosis of cystic fibrosis and primary ciliary Dyskinesia. *bioRxiv[Preprint]:438838*. doi: 10.1101/438838

Estrada-Cuzcano, A., Roepman, R., Cremers, F. P., den Hollander, A. I., and Mans, D. A. (2012). Non-syndromic retinal ciliopathies: translating gene discovery into therapy. *Hum. Mol. Genet.* 21, R111–R124. doi: 10.1093/hmg/dds298

Fassad, M. R., Shoemark, A., Legendre, M., Hirst, R. A., Koll, F., le Borgne, P., et al. (2018). Mutations in outer dynein arm heavy chain DNAH9 cause motile cilia defects and situs inversus. *Am. J. Hum. Genet.* 103, 984–994. doi: 10.1016/j.ajhg.2018.10.016

Fiorentino, A., Fujinami, K., Arno, G., Robson, A. G., Pontikos, N., Arasanz Armengol, M., et al. (2018). Missense variants in the X-linked gene PRPS1 cause retinal degeneration in females. *Hum. Mutat.* 39, 80–91. doi: 10.1002/humu.23349

Firth, A. L., Dargitz, C. T., Qualls, S. J., Menon, T., Wright, R., Singer, O., et al. (2014). Generation of multiciliated cells in functional airway epithelia from human induced pluripotent stem cells. *Proc. Natl. Acad. Sci. U.S.A.* 111, E1723–E1730. doi: 10.1073/pnas.1403470111

Fliegauf, M., Benzing, T., and Omran, H. (2007). When cilia go bad: cilia defects and ciliopathies. *Nat. Rev. Mol. Cell Biol.* 8, 880–893. doi: 10.1038/nrm2278

Fokkema, I. F., Taschner, P. E., Schaafsma, G. C., Celli, J., Laros, J. F., and den Dunnen, J. T. (2011). LOVD v.2.0: the next generation in gene variant databases. *Hum. Mutat.* 32, 557–563. doi: 10.1002/humu.21438

Forsythe, E., and Beales, P. L. (2013). Bardet-Biedl syndrome. *Eur. J. Hum. Genet.* 21, 8–13. doi: 10.1038/ejhg.2012.115

Gainotti, S., Mascalzoni, D., Bros-Facer, V., Petrini, C., Floridia, G., Roos, M., et al. (2018). Meeting patients' right to the correct diagnosis: ongoing international initiatives on undiagnosed rare diseases and ethical and social issues. *Int. J. Environ. Res. Public Health* 15:E2072. doi: 10.3390/ijerph15102072

Gaudelli, N. M., Komor, A. C., Rees, H. A., Packer, M. S., Badran, A. H., Bryson, D. I., et al. (2017). Programmable base editing of A*T to G*C in genomic DNA without DNA cleavage. *Nature* 551, 464–471. doi: 10.1038/nature24644

Gaush, C. R., Hard, W. L., and Smith, T. F. (1966). Characterization of an established line of canine kidney cells (MDCK). *Proc. Soc. Exp. Biol. Med.* 122, 931–935. doi: 10.3181/00379727-122-31293

Goetz, S. C., and Anderson, K. V. (2010). The primary cilium: a signalling centre during vertebrate development. *Nat. Rev. Genet.* 11, 331–344. doi: 10.1038/nrg2774

Graham, F. L., Smiley, J., Russell, W. C., and Nairn, R. (1977). Characteristics of a human cell line transformed by DNA from human adenovirus type 5. *J. Gen. Virol.* 36, 59–74. doi: 10.1099/0022-1317-36-1-59

Gurrieri, F., Franco, B., Toriello, H., and Neri, G. (2007). Oral-facial-digital syndromes: review and diagnostic guidelines. *Am. J. Med. Genet. A* 143A, 3314–3323. doi: 10.1002/ajmg.a.32032

Hamada, H. (2016). "Roles of motile and immotile cilia in left-right symmetry breaking," in *Etiology and Morphogenesis of Congenital Heart Disease: From Gene Function and Cellular Interaction to Morphology*, eds T. Nakanishi, R. R. Markwald, H. S. Baldwin, B. B. Keller, D. Srivastava, and H. Yamagishi (Tokyo: Springer), 57–65.

Harris, E. H., Witman, G. B., and Stern, D. (2009). *The Chlamydomonas Sourcebook, 2nd Edn, Vol. 1–3*. Oxford: Academic Press, Elsevier.

Hartill, V., Szymanska, K., Sharif, S. M., Wheway, G., and Johnson, C. A. (2017). Meckel-gruber syndrome: an update on diagnosis, clinical management, and research advances. *Front. Pediatr.* 5:244. doi: 10.3389/fped.2017.00244

Hildebrandt, F., Benzing, T., and Katsanis, N. (2011). Ciliopathies. *N. Engl. J. Med.* 364, 1533–1543. doi: 10.1056/NEJMra1010172

Hirst, R. A., Rutman, A., Williams, G., and O'Callaghan, C. (2010). Ciliated air-liquid cultures as an aid to diagnostic testing of primary ciliary dyskinesia. *Chest* 138, 1441–1447. doi: 10.1378/chest.10-0175

Huber, C., and Cormier-Daire, V. (2012). Ciliary disorder of the skeleton. *Am. J. Med. Genet. C Semin. Med. Genet.* 160C, 165–174. doi: 10.1002/ajmg.c.31336

Hynes, A. M., Giles, R. H., Srivastava, S., Eley, L., Whitehead, J., Danilenko, M., et al. (2014). Murine Joubert syndrome reveals Hedgehog signaling defects as a potential therapeutic target for nephronophthisis. *Proc. Natl. Acad. Sci. U.S.A.* 111, 9893–9898. doi: 10.1073/pnas.1322373111

Irving, S., Dixon, M., Fassad, M. R., Frost, E., Hayward, J., Kilpin, K., et al. (2018). Primary ciliary dyskinesia due to microtubular defects is associated with worse lung clearance index. *Lung* 196, 231–238. doi: 10.1007/s00408-018-0086-x

Jainchill, J. L., Aaronson, S. A., and Todaro, G. J. (1969). Murine sarcoma and leukemia viruses: assay using clonal lines of contact-inhibited mouse cells. *J. Virol.* 4, 549–553.

Jones, H. W., McKusick, V. A., Harper, P. S., and Wuu, K. D. (1971). George Otto Gey. (1899-1970). The HeLa cell and a reappraisal of its origin. *Obstet Gynecol.* 38, 945–949.

Karczewski, K. J., Weisburd, B., Thomas, B., Solomonson, M., Ruderfer, D. M., Kavanagh, D., et al. (2017). The ExAC browser: displaying reference data information from over 60,000 exomes. *Nucleic Acids Res.* 45, D840–D845. doi: 10.1093/nar/gkw971

Katsanis, N., Ansley, S. J., Badano, J. L., Eichers, E. R., Lewis, R. A., Hoskins, B. E., et al. (2001). Triallelic inheritance in Bardet-Biedl syndrome, a Mendelian recessive disorder. *Science* 293, 2256–2259. doi: 10.1126/science.1063525

Kenny, J., Forsythe, E., Beales, P., and Bacchelli, C. (2017). Toward personalized medicine in Bardet-Biedl syndrome. *Per. Med.* 14, 447–456. doi: 10.2217/pme-2017-0019

Khanna, H., Davis, E. E., Murga-Zamalloa, C. A., Estrada-Cuzcano, A., Lopez, I., den Hollander, A. I., et al. (2009). A common allele in RPGRIP1L is a modifier of retinal degeneration in ciliopathies. *Nat. Genet.* 41, 739–745. doi: 10.1038/ng.366

Khera, A. V., Chaffin, M., Aragam, K. G., Haas, M. E., Roselli, C., Choi, S. H., et al. (2018). Genome-wide polygenic scores for common diseases identify individuals with risk equivalent to monogenic mutations. *Nat. Genet.* 50, 1219–1224. doi: 10.1038/s41588-018-0183-z

Kim, J., Lee, J. E., Heynen-Genel, S., Suyama, E., Ono, K., Lee, K., et al. (2010). Functional genomic screen for modulators of ciliogenesis and cilium length. *Nature* 464, U1048–U1114. doi: 10.1038/nature08895

Kim, Y. B., Komor, A. C., Levy, J. M., Packer, M. S., Zhao, K. T., and Liu, D. R. (2017). Increasing the genome-targeting scope and precision of base editing with engineered Cas9-cytidine deaminase fusions. *Nat. Biotechnol.* 35, 371–376. doi: 10.1038/nbt.3803

King, S. M., and Patel-King, R. S. (2016). Planaria as a model system for the analysis of ciliary assembly and motility. *Methods Mol. Biol.* 1454, 245–254. doi: 10.1007/978-1-4939-3789-9_16

Knopp, C., Rudnik-Schoneborn S., Eggermann, T., Bergmann, C., Begemann, M., Schoner, K., et al. (2015). Syndromic ciliopathies: from single gene to multi gene analysis by SNP arrays and next generation sequencing. *Mol. Cell. Probes* 29, 299–307. doi: 10.1016/j.mcp.2015.05.008

Knowles, M. R., Ostrowski, L. E., Leigh, M. W., Sears, P. R., Davis, S. D., Wolf, W. E., et al. (2014). Mutations in RSPH1 cause primary ciliary dyskinesia with a unique clinical and ciliary phenotype. *Am. J. Respir. Crit. Care Med.* 189, 707–717. doi: 10.1164/rccm.201311-2047OC

Knowles, M. R., Zariwala, M., and Leigh, M. (2016). Primary ciliary Dyskinesia. *Clin. Chest Med.* 37, 449–461. doi: 10.1016/j.ccm.2016.04.008

Koblan, L. W., Doman, J. L., Wilson, C., Levy, J. M., Tay, T., Newby, G. A., et al. (2018). Improving cytidine and adenine base editors by expression optimization and ancestral reconstruction. *Nat. Biotechnol.* 36, 843–846. doi: 10.1038/nbt.4172

Kodra, Y., Weinbach, J., Posada-de-la-Paz, M., Coi, A., Lemonnier, S. L., van Enckevort, D., et al. (2018). Recommendations for improving the quality of rare disease registries. *Int. J. Environ. Res. Public Health* 15:E1644. doi: 10.3390/ijerph15081644

Köhler, S., Vasilevsky, N. A., Engelstad, M., Foster, E., McMurry, J., Ayme, S., et al. (2017). The human phenotype ontology in 2017. *Nucleic Acids Res.* 45, D865–D876. doi: 10.1093/nar/gkw1039

Komlosi, K., Diederich, S., Fend-Guella, D. L., Bartsch, O., Winter, J., Zechner, U., and Schweiger, S. (2018). Targeted next-generation sequencing analysis in couples at increased risk for autosomal recessive disorders. *Orphanet J. Rare Dis.* 13:23. doi: 10.1186/s13023-018-0763-0

Komor, A. C., Kim, Y. B., Packer, M. S., Zuris, J. A., and Liu, D. R. (2016). Programmable editing of a target base in genomic DNA without double-stranded DNA cleavage. *Nature* 533, 420–424. doi: 10.1038/nature17946

Konishi, S., Gotoh, S., Tateishi, K., Yamamoto, Y., Korogi, Y., Nagasaki, T., et al. (2016). Directed induction of functional multi-ciliated cells in proximal airway epithelial spheroids from human pluripotent stem cells. *Stem Cell Rep.* 6, 18–25. doi: 10.1016/j.stemcr.2015.11.010

Krusche, P., Trigg, L., Boutros, P. C., Mason, C. E., De La Vega, F. M., Moore, B. L., et al. (2018). Best practices for benchmarking germline small variant calls in human genomes. *bioRXiv[Preprnt]:270157*. doi: 10.1101/270157

Kuek, L. E., Griffin, P., Martinello, P., Graham, A. N., Kalitsis, P., Robinson, P. J., et al. (2018). Identification of an immortalized human airway epithelial cell line with dyskinetic cilia. *Am. J. Respir. Cell Mol. Biol.* 59, 375–382. doi: 10.1165/rcmb.2017-0188OC

Kuwahara, A., Ozone, C., Nakano, T., Saito, K., Eiraku, M., and Sasai, Y. (2015). Generation of a ciliary margin-like stem cell niche from self-organizing human retinal tissue. *Nat. Commun.* 6:6286. doi: 10.1038/ncomms7286

Lakowski, J., Welby, E., Budinger, D., Di Marco, F., Di Foggia, V., Bainbridge, J. W. B., et al. (2018). Isolation of human photoreceptor precursors via a cell surface marker panel from stem cell-derived retinal organoids and fetal retinae. *Stem Cells* 36, 709–722. doi: 10.1002/stem.2775

Landrum, M. J., and Kattman, B. L. (2018). ClinVar at five years: delivering on the promise. *Hum. Mutat.* 39, 1623–1630. doi: 10.1002/humu.23641

Langousis, G., and Hill, K. L. (2014). Motility and more: the flagellum of Trypanosoma brucei. *Nat. Rev. Microbiol.* 12, 505–518. doi: 10.1038/nrmicro3274

Lee, J. E., and Gleeson, J. G. (2011). A systems-biology approach to understanding the ciliopathy disorders. *Genome Med.* 3:59. doi: 10.1186/gm275

Lek, M., Karczewski, K. J., Minikel, E. V., Samocha, K. E., Banks, E., Fennell, T., et al. (2016). Analysis of protein-coding genetic variation in 60,706 humans. *Nature* 536, 285–291. doi: 10.1038/nature19057

Li, M. M., Datto, M., Duncavage, E. J., Kulkarni, S., Lindeman, N. I., Roy, S., et al. (2017). Standards and guidelines for the interpretation and reporting of sequence variants in cancer: a joint consensus recommendation of the association for molecular pathology. American society of clinical oncology, and college of American pathologists. J. Mol. Diagn. 19, 4–23. doi: 10.1016/j.jmoldx.2016.10.002

Li, Y., Yagi, H., Onuoha, E. O., Damerla, R. R., Francis, R., Furutani, Y., et al. (2016). DNAH6 and its interactions with PCD genes in heterotaxy and primary ciliary dyskinesia. *PLoS Genet.* 12:e1005821. doi: 10.1371/journal.pgen.1005821

Lindstrand, A., Frangakis, S., Carvalho, C. M., Richardson, E. B., McFadden, K. A., Willer, J. R., et al. (2016). Copy-number variation contributes to the mutational load of bardet-biedl syndrome. *Am. J. Hum. Genet.* 99, 318–336. doi: 10.1016/j.ajhg.2015.04.023

Lord, J., Gallone, G., Short, P. J., McRae, J. F., Ironfield, H., Wynn, E. H., et al. (2018). Pathogenicity and selective constraint on variation near splice sites. *Genome Res.* 29:159–170. doi: 10.1101/256636

Lucas, J. S., Alanin, M. C., Collins, S., Harris, A., Johansen, H. K., Nielsen, K. G., et al. (2017a). Clinical care of children with primary ciliary dyskinesia. *Expert Rev. Respir. Med.* 11, 779–790. doi: 10.1080/17476348.2017.1360770

Lucas, J. S., Barbato, A., Collins, S. A., Goutaki, M., Behan, L., Caudri, D., et al. (2017b). European respiratory society guidelines for the diagnosis of primary ciliary dyskinesia. *Eur. Respir. J.* 49:1601090. doi: 10.1183/13993003.01090-2016

Lucas, J. S., Burgess, A., Mitchison, H. M., Moya, E., Williamson, M., Hogg, C., et al. (2014). Diagnosis and management of primary ciliary dyskinesia. *Arch. Dis. Child.* 99, 850–856. doi: 10.1136/archdischild-2013-304831

Marshall, C. R., Scherer, S. W., Zariwala, M. A., Lau, L., Paton, T. A., Stockley, T., et al. (2015). Whole-exome sequencing and targeted copy number analysis in primary ciliary dyskinesia. *G3 (Bethesda).* 5, 1775–1781. doi: 10.1534/g3.115.019851

Marshall, R. A., and Osborn, D. P. (2016). Zebrafish: a vertebrate tool for studying basal body biogenesis, structure, and function. *Cilia* 5:16. doi: 10.1186/s13630-016-0036-2

McIntyre, J. C., Davis, E. E., Joiner, A., Williams, C. L., Tsai, I. C., Jenkins, P. M., et al. (2012). Gene therapy rescues cilia defects and restores olfactory function in a mammalian ciliopathy model. *Nat. Med.* 18, 1423–1428. doi: 10.1038/nm.2860

McIntyre, J. C., Williams, C. L., and Martens, J. R. (2013). Smelling the roses and seeing the light: gene therapy for ciliopathies. *Trends Biotechnol.* 31, 355–363. doi: 10.1016/j.tibtech.2013.03.005

Mestek-Boukhibar, L., Clement, E., Jones, W. D., Drury, S., Ocaka, L., Gagunashvili, A., et al. (2018). Rapid Paediatric Sequencing (RaPS): comprehensive real-life workflow for rapid diagnosis of critically ill children. *J. Med. Genet.* 55, 721–728. doi: 10.1136/jmedgenet-2018-105396

Meyer, J. S., Howden, S. E., Wallace, K. A., Verhoeven, A. D., Wright, L. S., Capowski, E. E., et al. (2011). Optic vesicle-like structures derived from human pluripotent stem cells facilitate a customized approach to retinal disease treatment. *Stem Cells* 29, 1206–1218. doi: 10.1002/stem.674

Mitchison, H. M., and Shoemark, A. (2017). Motile cilia defects in diseases other than primary ciliary dyskinesia: The contemporary diagnostic and research role for transmission electron microscopy. *Ultrastruct. Pathol.* 41, 415–427. doi: 10.1080/01913123.2017.1370050

Mitchison, H. M., and Valente, E. M. (2017). Motile and non-motile cilia in human pathology: from function to phenotypes. *J. Pathol.* 241, 294–309. doi: 10.1002/path.4843

Moayyeri, A., Hammond, C. J., Valdes, A. M., and Spector, T. D. (2013). Cohort Profile: TwinsUK and healthy ageing twin study. *Int. J. Epidemiol.* 42, 76–85. doi: 10.1093/ije/dyr207

Mok, C. A., and Héon, E. (2012). Caenorhabditis elegans as a model organism for ciliopathies and related forms of photoreceptor degeneration. *Adv. Exp. Med. Biol.* 723, 533–538. doi: 10.1007/978-1-4614-0631-0_67

Molinari, E., and Sayer, J. A. (2017). Emerging treatments and personalised medicine for ciliopathies associated with cystic kidney disease. *Exp. Opin. Orph. Drugs* 5, 785–798. doi: 10.1080/21678707.2017.1372282

Moore, A., Escudier, E., Roger, G., Tamalet, A., Pelosse, B., Marlin, S., et al. (2006). RPGR is mutated in patients with a complex X linked phenotype combining primary ciliary dyskinesia and retinitis pigmentosa. *J. Med. Genet.* 43, 326–333. doi: 10.1136/jmg.2005.034868

Moss, C., and Wernham, A. (2018). The 100 000 Genomes Project: feeding back to patients. *BMJ* 361:k2441. doi: 10.1136/bmj.k2441

Mossotto, E., Ashton, J. J., Pengelly, R. J., Beattie, R. M., MacArthur, B. D., and Ennis, S. (2018). GenePy - a score for estimating gene pathogenicity in individuals using next-generation sequencing data. *bioRXiv[Preprint]:336701*. doi: 10.1101/336701

Norris, D. P., and Grimes, D. T. (2012). Mouse models of ciliopathies: the state of the art. *Dis. Model. Mech.* 5, 299–312. doi: 10.1242/dmm.009340

Nouri, N., Nouri, N., Tirgar, S., Soleimani, E., Yazdani, V., Zahedi, F., et al. (2017). Consanguineous marriages in the genetic counseling centers of Isfahan and the ethical issues of clinical consultations. *J. Med. Ethics Hist. Med.* 10:12.

Ormondroyd, E., Mackley, M. P., Blair, E., Craft, J., Knight, J. C., Taylor, J. C., et al. (2018). "Not pathogenic until proven otherwise": perspectives of UK clinical

genomics professionals toward secondary findings in context of a Genomic Medicine Multidisciplinary Team and the 100,000 Genomes Project. *Genet. Med.* 20, 320–328. doi: 10.1038/gim.2017.157

Oud, M. M., Lamers, I. J., and Arts, H. H. (2017). Ciliopathies: genetics in pediatric medicine. *J. Pediatr. Genet.* 6, 18–29. doi: 10.1055/s-0036-1593841

Paff, T., Kooi, I. E., Moutaouakil, Y., Riesebos, E., Sistermans, E. A., Daniels, H., et al. (2018). Diagnostic yield of a targeted gene panel in primary ciliary dyskinesia patients. *Hum. Mutat.* 39, 653–665. doi: 10.1002/humu.23403

Parisi, M., and Glass, I. (1993). "Joubert syndrome," in *GeneReviews((R))*, eds M. P. Adam, H. H. Ardinger, R. A. Pagon, S. E. Wallace, L. J. H. Bean, K. Stephens, and A. Amemiya. (Seattle, WA: University of Washington, Seattle), 1–59.

Perantoni, A., and Berman, J. J. (1979). Properties of Wilms' tumor line (TuWi) and pig kidney line (LLC-PK1) typical of normal kidney tubular epithelium. *In Vitro* 15, 446–454. doi: 10.1007/BF02618414

Pollard, M. O., Gurdasani, D., Mentzer, A. J., Porter, T., and Sandhu, M. S. (2018). Long reads: their purpose and place. *Hum. Mol. Genet.* 27, R234–R241. doi: 10.1093/hmg/ddy177

Project Team, S. G. (2015) The saudi human genome program: an oasis in the desert of Arab medicine is providing clues to genetic disease. *IEEE Pulse* 6, 22–26 doi: 10.1109/MPUL.2015.2476541

Rafferty, K. A., and Sherwin, R. W. (1969). The length of secondary chromosomal constrictions in normal individuals and in a nucleolar mutant of Xenopus laevis. *Cytogenetics* 8, 427–438. doi: 10.1159/000130054

Rambhatla, L., Chiu, C. P., Glickman, R. D., and Rowe-Rendleman, C. (2002). *In vitro* differentiation capacity of telomerase immortalized human RPE cells. *Invest. Ophthalmol. Vis. Sci.* 43, 1622–1630.

Ran, F. A., Hsu, P. D., Lin, C. Y., Gootenberg, J. S., Konermann, S., Trevino, A. E., et al. (2013). Double nicking by RNA-guided CRISPR Cas9 for enhanced genome editing specificity. *Cell* 154, 1380–1389. doi: 10.1016/j.cell.2013.08.021

Rauchman, M. I., Nigam, S. K., Delpire, E., and Gullans, S. R. (1993). An osmotically tolerant inner medullary collecting duct cell line from an SV40 transgenic mouse. *Am. J. Physiol.* 265(3 Pt 2), F416–424. doi: 10.1152/ajprenal.1993.265.3.F416

Reiter, J. F., and Leroux, M. R. (2017). Genes and molecular pathways underpinning ciliopathies. *Nat. Rev. Mol. Cell Biol.* 18, 533–547. doi: 10.1038/nrm.2017.60

Robinson, P. N., Köhler, S., Bauer, S., Seelow, D., Horn, D., and Mundlos, S. (2008). The Human Phenotype Ontology: a tool for annotating and analyzing human hereditary disease. *Am. J. Hum. Genet.* 83, 610–615. doi: 10.1016/j.ajhg.2008.09.017

Samuel, G. N., and Farsides, B. (2017). The UK's 100,000 Genomes Project: manifesting policymakers' expectations. *New Genet. Soc.* 36, 336–353. doi: 10.1080/14636778.2017.1370671

Sawyer, S. L., Hartley, T., Dyment, D. A., Beaulieu, C. L., Schwartzentruber, J., Smith, A., et al. (2016). Utility of whole-exome sequencing for those near the end of the diagnostic odyssey: time to address gaps in care. *Clin. Genet.* 89, 275–284. doi: 10.1111/cge.12654

Schmidts, M., Arts, H. H., Bongers, E. M., Yap, Z., Oud, M. M., Antony, D., et al. (2013). Exome sequencing identifies DYNC2H1 mutations as a common cause of asphyxiating thoracic dystrophy (Jeune syndrome) without major polydactyly, renal or retinal involvement. *J. Med. Genet.* 50, 309–323. doi: 10.1136/jmedgenet-2012-101284

Schmidts, M. M., and Mitchison, H. M. (2018). "Severe skeletal abnormalities caused by defects in retrograde intraflagellar transport dyneins," in *Dyneins: Structure, Biology and Disease*, ed S.M. King (Academic Press, Elsevier Inc.), 356–401.

Schock, E. N., Chang, C. F., Youngworth, I. A., Davey, M. G., Delany, M. E., and Brugmann, S. A. (2016). Utilizing the chicken as an animal model for human craniofacial ciliopathies. *Dev. Biol.* 415, 326–337. doi: 10.1016/j.ydbio.2015.10.024

Shoemark, A., Moya, E., Hirst, R. A., Patel, M. P., Robson, E. A., Hayward, J., et al. (2018). High prevalence of CCDC103 p.His154Pro mutation causing primary ciliary dyskinesia disrupts protein oligomerisation and is associated with normal diagnostic investigations. *Thorax* 73, 157–166. doi: 10.1136/thoraxjnl-2017-209999

Simpson, J. T., Workman, R. E., Zuzarte, P. C., David, M., Dursi, L. J., and Timp, W. (2017). Detecting DNA cytosine methylation using nanopore sequencing. *Nat. Methods* 14:407. doi: 10.1038/nmeth.4184

Singla, V., and Reiter, J. F. (2006). The primary cilium as the cell's antenna: signaling at a sensory organelle. *Science* 313, 629–633. doi: 10.1126/science.1124534

Slaats, G. G., Saldivar, J. C., Bacal, J., Zeman, M. K., Kile, A. C., Hynes, A. M., et al. (2015). DNA replication stress underlies renal phenotypes in CEP290-associated Joubert syndrome. *J. Clin. Invest.* 125, 3657–3666. doi: 10.1172/JCI80657

Soden, S. E., Saunders, C. J., Willig, L. K., Farrow, E. G., Smith, L. D., Petrikin, J. E., et al. (2014). Effectiveness of exome and genome sequencing guided by acuity of illness for diagnosis of neurodevelopmental disorders. *Sci. Transl. Med.* 6:265ra168. doi: 10.1126/scitranslmed.3010076

Song, J. Y., Aravand, P., Nikonov, S., Leo, L., Lyubarsky, A., Bennicelli, J. L., et al. (2018). Amelioration of neurosensory structure and function in animal and cellular models of a congenital blindness. *Mol. Ther.* 26, 1581–1593. doi: 10.1016/j.ymthe.2018.03.015

Song, Z., Zhang, X., Jia, S., Yelick, P. C., and Zhao, C. (2016). Zebrafish as a model for human ciliopathies. *J. Genet. Genomics* 43, 107–120. doi: 10.1016/j.jgg.2016.02.001

Spassky, N., and Meunier, A. (2017). The development and functions of multiciliated epithelia. *Nat. Rev. Mol. Cell Biol.* 18, 423–436. doi: 10.1038/nrm.2017.21

Srivastava, S., Ramsbottom, S. A., Molinari, E., Alkanderi, S., Filby, A., White, K., et al. (2017). A human patient-derived cellular model of Joubert syndrome reveals ciliary defects which can be rescued with targeted therapies. *Hum. Mol. Genet.* 26, 4657–4667. doi: 10.1093/hmg/ddx347

Stenson, P. D., Mort, M., Ball, E. V., Evans, K., Hayden, M., Heywood, S., et al. (2017). The human gene mutation database: towards a comprehensive repository of inherited mutation data for medical research, genetic diagnosis and next-generation sequencing studies. *Hum. Genet.* 136, 665–677. doi: 10.1007/s00439-017-1779-6

Thiel, C., Kessler, K., Giessl, A., Dimmler, A., Shalev, S. A., von der Haar, S., et al. (2011). NEK1 mutations cause short-rib polydactyly syndrome type majewski. *Am. J. Hum. Genet.* 88, 106–114. doi: 10.1016/j.ajhg.2010.12.004

Turnbull, C., Scott, R. H., Thomas, E., Jones, L., Murugaesu, N., Pretty, F. B., et al. (2018). The 100,000 genomes project: bringing whole genome sequencing to the NHS. *BMJ* 361:k1687. doi: 10.1136/bmj.k1687

Vervoort, R., Lennon, A., Bird, A. C., Tulloch, B., Axton, R., Miano, M. G., et al. (2000). Mutational hot spot within a new RPGR exon in X-linked retinitis pigmentosa. *Nat. Genet.* 25, 462–466. doi: 10.1038/78182

Vincensini, L., Blisnick, T., and Bastin, P. (2011). 1001 model organisms to study cilia and flagella. *Biol. Cell* 103, 109–130. doi: 10.1042/BC20100104

Walentek, P., and Quigley, I. K. (2017). What we can learn from a tadpole about ciliopathies and airway diseases: using systems biology in Xenopus to study cilia and mucociliary epithelia. *Genesis* 55, 1–2. doi: 10.1002/dvg.23001

Waters, A. M., and Beales, P. L. (2011). Ciliopathies: an expanding disease spectrum. *Pediatr. Nephrol.* 26, 1039–1056. doi: 10.1007/s00467-010-1731-7

Welch, B. M., Wiley, K., Pflieger, L., Achiangia, R., Baker, K., Hughes-Halbert, C., et al. (2018). Review and comparison of electronic patient-facing family health history tools. *J. Genet. Couns.* 27, 381–391. doi: 10.1007/s10897-018-0235-7

Wheway, G., Johnson, C. A. (2014). "Meckel-Gruber syndrome," in *Ciliopathies,* ed T. D. Kenny and P. L. Beales (Oxford: Oxford University Press), 132–149.

Wheway, G., Nazlamova, L., and Hancock, J. T. (2018). Signaling through the primary cilium. *Front. Cell Dev. Biol.* 6:8. doi: 10.3389/fcell.2018.00008

Wheway, G., Schmidts, M., Mans, D. A., Szymanska, K., Nguyen, T. M., Racher, H., et al. (2015). An siRNA-based functional genomics screen for the identification of regulators of ciliogenesis and ciliopathy genes. *Nat. Cell Biol.* 17, 1074–1087. doi: 10.1038/ncb3201

Willey, C. J., Blais, J. D., Hall, A. K., Krasa, H. B., Makin, A. J., and Czerwiec, F. S. (2017). Prevalence of autosomal dominant polycystic kidney disease in the European Union. *Nephrol. Dial. Transpl.* 32, 1356–1363. doi: 10.1093/ndt/gfw240

Wolf, M. T., and Hildebrandt, F. (2011). Nephronophthisis. *Pediatr. Nephrol.* 26, 181–194. doi: 10.1007/s00467-010-1585-z

Wood, A. J., Lo, T. W., Zeitler, B., Pickle, C. S., Ralston, E. J., Lee, A. H., et al. (2011). Targeted genome editing across species using ZFNs and TALENs. *Science* 333:307. doi: 10.1126/science.1207773

Wright, A. F., Chakarova, C. F., Abd El-Aziz, M. M., and Bhattacharya, S. S. (2010). Photoreceptor degeneration: genetic and mechanistic dissection of a complex trait. *Nat. Rev. Genet.* 11, 273–284. doi: 10.1038/nrg2717

Wright, C. F., Fitzgerald, T. W., Jones, W. D., Clayton, S., McRae, J. F., van Kogelenberg, M., et al. (2015). Genetic diagnosis of developmental disorders in the DDD study: a scalable analysis of genome-wide research data. *Lancet* 385, 1305–1314. doi: 10.1016/S0140-6736(14)61705-0

Wu, Z., Hiriyanna, S., Qian, H., Mookherjee, S., Campos, M. M., Gao, C., et al. (2015). A long-term efficacy study of gene replacement therapy for RPGR-associated retinal degeneration. *Hum. Mol. Genet.* 24, 3956–3970. doi: 10.1093/hmg/ddv134

You, L., Klena, N. T., Gabriel, G. C., Liu, X., Kim, A. J., Lemke, K., et al. (2015) Global genetic analysis in mice unveils central role for cilia in congenital heart disease. *Nature* 521, 520–524. doi: 10.1038/nature14269

Zaki, M. S., Sattar, S., Massoudi, R. A., and Gleeson, J. G. (2011). Co-occurrence of distinct ciliopathy diseases in single families suggests genetic modifiers. *Am. J. Med. Genet. A* 155A, 3042–3049. doi: 10.1002/ajmg.a.34173

Zhang, W., Li, L., Su, Q., Gao, G., and Khanna, H. (2018). Gene therapy using a miniCEP290 fragment delays photoreceptor degeneration in a mouse model of leber congenital amaurosis. *Hum. Gene Ther.* 29, 42–50. doi: 10.1089/hum.2017.049

Conflict of Interest Statement: The authors declare that the research was conducted in the absence of any commercial or financial relationships that could be construed as a potential conflict of interest.

frontiers in Genetics

CORRECTION
published: 13 August 2019
doi: 10.3389/fgene.2019.00569

Corrigendum: Opportunities and Challenges for Molecular Understanding of Ciliopathies–The 100,000 Genomes Project

Gabrielle Wheway[1†], *Genomics England Research Consortium and* *Hannah M. Mitchison*[2*]

[1] Human Development and Health, Faculty of Medicine, University of Southampton, Southampton General Hospital, Southampton, United Kingdom, [2] Genetics and Genomic Medicine, University College London, UCL Great Ormond Street Institute of Child Health, London, United Kingdom

Keywords: 100,000 Genome Project, ciliopathies, cilia, genomics, genetics

A Corrigendum on

Opportunities and Challenges for Molecular Understanding of Ciliopathies–The 100,000 Genomes Project

by Wheway, G., Genomics England Research Consortium and Mitchison, H. M. (2019). Front. Genet. 10:127. doi: 10.3389/fgene.2019.00127

In the original article, there was an error. We incorrectly stated that 'If a predicted pathogenic variant is found in the primary [gene] panel [on PanelApp], this will be classified as Tier 1. If a predicted pathogenic variant is found in another associated panel, this will be classified as Tier 2. If a predicted pathogenic variant in any other gene is found, this will be classified as Tier 3'.

A correction has been made to the article section **Ciliopathy Genomics Data Analysis in the 100,000 Genomes Project**, Paragraph 2.

"Currently, novel or rare variants identified in rare disease patients in the 100,000 Genomes Project are "tiered" according to predicted pathogenicity, following the Association for Clinical Genetic Science's Best Practice Guidelines for Variant Classification (https://www.acgs.uk.com/quality/best-practice-guidelines/) which builds upon Standards and Guidelines for the Interpretation and Reporting of Sequence Variants in Cancer published by the Association for Molecular Pathology (Li et al., 2017). This allows classification of variants into Tier 1, variants with strong clinical significance; Tier 2, variants with potential clinical significance; Tier 3, variants of unknown clinical significance; and Tier 4, variants deemed benign or likely benign. Tiering is achieved using information from PanelApp, an online resource in which clinicians, academic researchers and laboratory scientists pool information about known disease genes, and pathogenic variants within them (https://panelapp.genomicsengland.co.uk/). This crowdsourcing tool enables a "virtual gene panel" approach to the analysis of genomic data; focusing on known or predicted pathogenic genes and variants. Patients' genomes are first analyzed against a panel of genes most closely associated with their disease phenotype (i.e., ciliopathy gene panels), then against other suitable gene panels with features overlapping the phenotype e.g., retinal dystrophy gene panel, neurology panel. Tier 1 variants are protein truncating (frameshift, stop gain, stop loss, splice acceptor variant, or splice donor variant) or *de novo* (protein truncating, missense, or splice region) variants in at least one transcript of a gene on the diagnostic grade "green" gene list in

Approved by:
Frontiers Editorial Office, Frontiers Media SA, Switzerland

***Correspondence:**
Hannah M. Mitchison
h.mitchison@ucl.ac.uk

†Gabrielle Wheway
orcid.org/0000-0002-0494-0783

Specialty section:
This article was submitted to Genetic Disorders, a section of the journal Frontiers in Genetics

Received: *28 May 2019*
Accepted: *29 May 2019*
Published: *13 August 2019*

Citation:
Wheway G, Genomics England Research Consortium and Mitchison HM (2019) Corrigendum: Opportunities and Challenges for Molecular Understanding of Ciliopathies–The 100,000 Genomes Project. Front. Genet. 10:569. doi: 10.3389/fgene.2019.00569

the virtual gene panel for the disorder in question. Tier 2 variants are protein altering variants, such as missense and splice region variants, in at least one transcript of a gene on the diagnostic grade "green" gene list in the virtual gene panel for the disorder in question. Tier 1 and 2 variants are not commonly found in the general healthy population, the allelic state matches the known mode of inheritance for the gene and disorder, and segregates with disease (where applicable). Protein truncating, *de novo* or protein altering variants affecting genes not in the virtual gene panel are Tier 3. If a variant does not meet any of these criteria it is untiered."

For further information we direct readers to https://panelapp.genomicsengland.co.uk/.

We wish to extend our thanks to Prof Sian Ellard, South West NHS Genomic Medicine Centre, for bringing this to our attention.

Additionally, in the original article there was another error. Genomics England was not included as an author in the published article. The corrected Author Contributions Statement appears below.

"GERC provided essential data for this publication. All authors listed have made a substantial, direct and intellectual contribution to the work, and approved it for publication."

Additionally, the consortium members have now been added to the Acknowledgments. The corrected Acknowledgment section appear below:

"GW was supported by a Wellcome Trust Seed Award in Science (204378/Z/16/Z) and a University of Southampton Faculty of Medicine Research Management Committee Research Project Award. HM was supported by Great Ormond Street Children's Charity grant Leadership awards (V1299, V2217), the NIHR Biomedical Research Center at Great Ormond Street Hospital for Children NHS Foundation Trust and University College London and the COST Action BEAT-PCD: Better Evidence to Advance Therapeutic options for PCD network (BM1407). This research was made possible through access to the data and findings generated by the 100,000 Genomes Project. The 100,000 Genomes Project is managed by Genomics England Limited (a wholly owned company of the Department of Health). The 100,000 Genomes Project is funded by the National Institute for Health Research and NHS England. The Wellcome Trust, Cancer Research UK and the Medical Research Council have also funded research infrastructure. The 100,000 Genomes Project uses data provided by patients and collected by the National Health Service as part of their care and support.

THE MEMBERS OF THE GENOMICS ENGLAND RESEARCH CONSORTIUM

Ambrose J. C.[1], Baple E. L.[1], Bleda M.[1], Boardman-Pretty F.[1,2], Boissiere J. M.[1], Boustred C. R.[1], Caulfield M. J.[1,2], Chan G. C.[1], Craig C. E. H.[1], Daugherty L. C.[1], de Burca A.[1], Devereau, A.[1], Elgar G.[1,2], Foulger R. E.[1], Fowler T.[1], Furió-Tarí P.[1], Hackett J. M.[1], Halai D.[1], Holman J. E.[1], Hubbard T. J. P.[1], Jackson R.[1], Kasperaviciute D.[1,2], Kayikci M.[1], Lahnstein L.[1], Lawson K.[1], Leigh S. E. A.[1], Leong I. U. S.[1], Lopez F. J.[1], Maleady-Crowe F.[1], Mason J.[1], McDonagh E. M.[1,2], Moutsianas L.[1,2], Mueller M.[1,2], Murugaesu N.[1], Need A. C.[1,2], Odhams C. A.[1], Patch C.[1,2], Perez-Gil D.[1], Polychronopoulos D.[1], Pullinger J.[1], Rahim T.[1], Rendon A.[1], Riesgo-Ferreiro P.[1], Rogers T.[1], Ryten M.[1], Savage K.[1], Sawant K.[1], Scott R. H.[1], Siddiq A.[1], Sieghart A.[1], Smedley D.[1,2], Smith K. R.[1,2], Sosinsky A.[1,2], Spooner W.[1], Stevens H. E.[1], Stuckey A.[1], Sultana R.[1], Thomas E. R. A.[1,2], Thompson S. R.[1], Tregidgo C.[1], Tucci A.[1,2], Walsh E.[1], Watters, S. A.[1], Welland M. J.[1], Williams E.[1], Witkowska K.[1,2], Wood S. M.[1,2], Zarowiecki M.[1]. (1) Genomics England, London, UK. (2) William Harvey Research Institute, Queen Mary University of London, London, EC1M 6BQ, UK."

The authors apologize for this error and state that this does not change the scientific conclusions of the article in any way. The original article has been updated.

REFERENCES

Li, M. M., Datto, M., Duncavage, E. J., Kulkarni, S., Lindeman, N. I., Roy, S., et al. (2017). Standards and guidelines for the interpretation and reporting of sequence variants in cancer: a joint consensus recommendation of the association for molecular pathology. American society of clinical oncology, and college of American pathologists. *J. Mol. Diagn.* 19, 4–23. doi: 10.1016/j.jmoldx.2016.10.002

frontiers in Genetics

MINI REVIEW
published: 15 March 2019
doi: 10.3389/fgene.2019.00154

The *Trp73* Mutant Mice: A Ciliopathy Model That Uncouples Ciliogenesis From Planar Cell Polarity

*Margarita M. Marques[1], Javier Villoch-Fernandez[2], Laura Maeso-Alonso[2], Sandra Fuertes-Alvarez[2] and Maria C. Marin[2]**

[1]*Departamento de Producción Animal, Laboratorio de Diferenciación Celular y Diseño de Modelos Celulares, Instituto de Desarrollo Ganadero y Sanidad Animal, Universidad de León, León, Spain,* [2]*Departamento de Biología Molecular, Laboratorio de Diferenciación Celular y Diseño de Modelos Celulares, Instituto de Biomedicina, Universidad de León, León, Spain*

p73 transcription factor belongs to one of the most important gene families in vertebrate biology, the p53-family. *Trp73* gene, like the other family members, generates multiple isoforms named TA and DNp73, with different and, sometimes, antagonist functions. Although p73 shares many biological functions with p53, it also plays distinct roles during development. *Trp73* null mice (p73KO from now on) show multiple phenotypes as gastrointestinal and cranial hemorrhages, rhinitis and severe central nervous system defects. Several groups, including ours, have revisited the apparently unrelated phenotypes observed in total p73KO and revealed a novel p73 function in the organization of ciliated epithelia in brain and trachea, but also an essential role as regulator of ependymal planar cell polarity. Unlike p73KO or TAp73KO mice, tumor-prone *Trp53*−/− mice (p53KO) do not present ependymal ciliary or planar cell polarity defects, indicating that regulation of ciliogenesis and PCP is a p73-specific function. Thus, loss of ciliary biogenesis and epithelial organization might be a common underlying cause of the diverse p73KO-phenotypes, highlighting *Trp73* role as an architect of the epithelial tissue. In this review we would like to discuss the data regarding p73 role as regulator of ependymal cell ciliogenesis and PCP, supporting the view of the *Trp73*-mutant mice as a model that uncouples ciliogenesis from PCP and a possible model of human congenital hydrocephalus.

Keywords: TAp73, DNp73, ependymal cells, ciliogenesis, planar cell polarity, microtubules, actin cytoskeleton, hydrocephalus

OPEN ACCESS

Edited by:
Jose Maria Carvajal-Gonzalez, Universidad de Extremadura, Spain

Reviewed by:
David R. Kaplan, Hospital for Sick Children, Canada
Nuria Moreno Marin, Instituto Gulbenkian de Ciência (IGC), Portugal

****Correspondence:***
Maria C. Marin
carmen.marin@unileon.es

Specialty section:
This article was submitted to Genetic Disorders, a section of the journal Frontiers in Genetics

Received: *20 November 2018*
Accepted: *13 February 2019*
Published: *15 March 2019*

Citation:
Marques MM, Villoch-Fernandez J, Maeso-Alonso L, Fuertes-Alvarez S and Marin MC (2019) The Trp73 Mutant Mice: A Ciliopathy Model That Uncouples Ciliogenesis From Planar Cell Polarity. Front. Genet. 10:154. doi: 10.3389/fgene.2019.00154

INTRODUCTION

The p53-family is constituted by the transcription factors p53, p63 and p73. The tumor suppressive function of p53 largely resides in its capacity to sense potentially oncogenic and genotoxic stress conditions, and to coordinate a complex set of molecular events leading to growth restraining responses and, ultimately, to senescence and/or apoptosis. Thus, p53 is a central node in the molecular network controlling cell proliferation and death in response to pathological and physiological conditions, a network in which p73 and p63 are also entangled (Pflaum et al., 2014). Emerging evidence reveals the role of the p53-family in other biological processes like stem cell self-renewal, cell metabolism, fertility or inflammation

(Gebel et al., 2017; Napoli and Flores, 2017; Nemajerova et al., 2018). Despite its function in the maintenance of genomic integrity, the initial analysis of p53KO mice suggested that there were developmentally normal (Donehower et al., 1992). However, posterior in-depth analysis revealed that p53 was essential for normal development (reviewed by Donehower et al., 1992; Shin et al., 2013; Jain and Barton, 2018). *Trp63* and *Trp73* gene targeting studies showed that both genes are also required during embryogenesis (Mills et al., 1999; Yang et al., 2000; Tomasini et al., 2009; Wang et al., 2017). Thus, the emerging picture is that of an interconnected pathway, in which p63 and p73 share many functional properties with p53 but they also claim distinct and unique biological roles (Van Nostrand et al., 2017; Wang et al., 2017).

Moreover, *Trp73* generates functionally different TA and DNp73 isoforms (Candi et al., 2014). Dependent upon the presence of the N-terminal transcriptionally active TA-domain, TAp73 variants exhibit p53-like transcriptional activities and tumor suppressive functions. Conversely, N-terminally truncated DN-isoforms act as dominant-negative inhibitor of p53 and TAp73 and thus, have oncogenic properties (Engelmann and Pützer, 2014). It is noteworthy that the p53 family members not only induce several common target-genes (Grob et al., 2001) but can also regulate each other's expression and function (Fatt et al., 2014). In agreement with all these complex interactions, compensatory mechanisms in the p53 family knockout models have been reported. Examples of this are the elevated levels of DNp73 mRNA in the constitutive TAp73KO and p63KO mice (Tomasini et al., 2008; Cancino et al., 2015).

Trp73 AND ITS ROLE IN CNS DEVELOPMENT

p73 fundamental role in brain development and homeostasis was highlighted by the central nervous system (CNS) defects in the p73KO mice. These included third ventricle enlargement, congenital hydrocephalus, hippocampal dysgenesis with abnormalities in the CA1–CA3 pyramidal cell layers and the dentate gyrus, loss of Cajal–Retzius neurons and abnormalities of the pheromone sensory pathway (Killick et al., 2011).

Identification of the predominant p73-isoform in the brain has proven complicated and the compiled data suggest a differential regulation of p73-isoforms expression during development that varies among cell types. Initial studies indicated that DNp73-isoforms were the predominant isoforms detected in sympathetic neurons *in vivo*, where they act as a survival factor (Pozniak et al., 2000, 2002; Yang et al., 2000); they were also expressed in Cajal–Retzius cells and in the choroid plexus (Meyer et al., 2004; Tissir et al., 2009; Hernández-Acosta et al., 2011). The analysis of DNp73-specific KO mice (DNp73KO) (Tissir et al., 2009; Wilhelm et al., 2010) confirmed the neuroprotective role of DNp73 and attributed most of the neurological phenotypes to its loss. However, DNp73KO mice did not develop striking hippocampal abnormalities like the p73KO, nor hydrocephalus, indicating that TAp73-isoforms may contribute to the development of the CNS. Nevertheless, in one of the DNp73KO models (Wilhelm et al., 2010), mutant mice had enlarged ventricles (Killick et al., 2011), suggesting a possible role of DNp73.

Expression of TAp73 appears to be restricted to specific brain areas. TAp73 was detected in the cortical hem, where it has a role in brain cortical patterning and in mature ependymal cells (ECs) of wild-type ventricles, which strongly express p73 (Medina-Bolívar et al., 2014; Fujitani et al., 2017). DNp73 has not been detected in these cells or in in its precursors, the radial glial cells (RGC) (Tissir et al., 2009). In addition, TAp73 is the predominant isoform expressed in embryonic neural stem cells (NSCs) (Tissir et al., 2009; Agostini et al., 2010; Medina-Bolívar et al., 2014) and has been shown to regulate NSCs stemness and brain neurogenic niche maintenance and cytoarchitecture (Agostini et al., 2010; Fujitani et al., 2010; Gonzalez-Cano et al., 2010, 2016; Talos et al., 2010). In agreement, TAp73KO mice show hippocampal dysgenesis with loss of the lower blade of the dentate gyrus like that in p73KO, but do not have ventricle enlargement or hydrocephalus (Tomasini et al., 2008), altogether posing the possibility of compensatory mechanisms in the absence of one of the isoforms.

Trp73 IS REQUIRED FOR RADIAL GLIAL TO EPENDYMAL CELL FATE DETERMINATION

The subventricular zone (SVZ) is one of the prominent regions of neurogenesis in the adult rodent brain and is located along the walls of the lateral ventricles next to the ependyma. The adult SVZ is a highly organized microenvironment comprised by multiciliated ECs that wrap around monociliated NSCs, forming organized neurogenic structures denominated pinwheels, which play a fundamental role in the maintenance of neurogenesis (Mirzadeh et al., 2010). In rodents, the walls of the lateral ventricles at birth maintain many similarities to the ventricular zone of the immature neuroepithelium but will change dramatically during postnatal development. The ECs that layer the wall of the lateral ventricle are derived from monociliated radial glial cells (RGCs) (**Figure 1A**). During perinatal development, a special subset of RGCs will lose their morphology and will give raise to multiciliated ECs (Spassky et al., 2005; Kriegstein and Alvarez-Buylla, 2009). This transformation requires RGC cell fate determination and EC differentiation (Merkle et al., 2004; Guirao et al., 2010). While specification of RGCs begins around E16, EC differentiation is initiated after birth and completed by P20, following a multistep process that includes multiciliogenesis and PCP (Ohata and Alvarez-Buylla, 2016; Kyrousi et al., 2017) (**Figure 1A**).

The hydrocephalus phenotype of p73KO suggested a possible p73 role in ependymal ciliary function that might be linked to its regulation of the neurogenic environment. Indeed, RGCs express p73 (Fujitani et al., 2017) and in its absence RGCs transition to ECs is altered generating immature cells with abnormal identities and morphology (Gonzalez-Cano et al., 2016). The specification of RGCs towards NSCs or ECs is identified

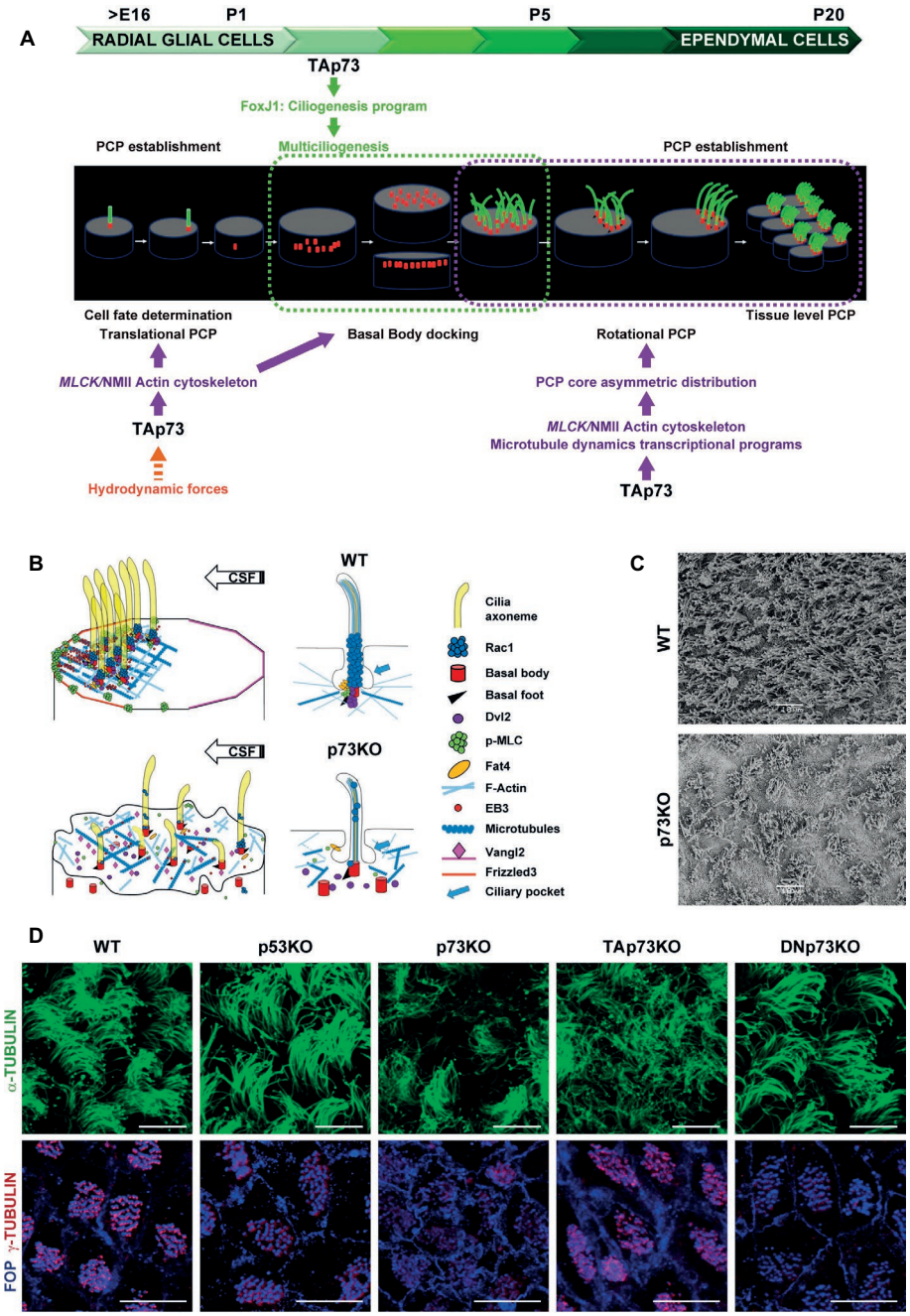

FIGURE 1 | *Trp73* deficiency affects ciliogenesis and the planar polarization of microtubule and actin networks resulting in lack of PCP and cilia disarrangement in ependymal cells. **(A)** Schematic representation of TAp73 regulation of PCP and ciliogenesis during the development from RGCs to ECs cells in rodent brain ventricular epithelia. Translational PCP begins by embryonic day E16, when RGCs primary cilium is displaced towards the anterior apical surface instructed by mechanosensory signaling. At this stage, TAp73 regulation of NMII activation is required for proper actin cytoskeleton dynamics, essential for tPCP establishment. Multiciliogenesis starts postnatally (P2) during the initial steps of ECs differentiation. TAp73 plays a central role activating transcriptional multiciliogenesis programs, but it is possible that p73-regulation of actin networks impinge on basal body (BB) docking. Around P5 motile cilia of immature ECs are randomly distributed on the apical surface. TAp73 regulation of polarized microtubules dynamics is important for the asymmetric localization of PCP-core proteins at opposite sides of the apical membrane at MT anchoring points at cell junctions. Asymetric PCP-core complexes instruct BBs to become aligned as the ependymal layer matures and rotational polarity is established with the formation of signaling complexes at the BBs, including Dvl and Rac1. At later stages (P15) TAp73 function is required for the establishment of tPCP in ECs which will be coordinated at tissular level. **(B)** Schematic representation of the subcellular localization of PCP-regulatory proteins and the effects of p73 deficiency in ependymal cells. The polarized distribution of activated NMII puncta at apical cell-junctions, and its association with the BBs (red) of crescents-BB clusters, sustains the establishment of polarized actin lattices (light blue). Activated NMII is depicted by p-MLC (green). Polarized cortical MT networks (dark blue) grew asymmetrically (EB3, red solid circle) from the center of the cell towards the anterior region contacting the plasma membrane at MT-anchoring

(Continued)

FIGURE 1 | points. These actin and microtubule networks allow the junctional localization of PCP-core protein complexes [Vangl2 (pink) and Frizzled (orange)] and the formation of signaling complexes at BB-clusters and at the base of cilia axoneme [Dvl2 (purple), Rac1 (blue) and Fat4 (yellow)]. p73 deficiency results in severe defects in ciliogenesis and the loss of apical cytoskeleton dynamics in ECs, which correlates with impaired BB docking, lack of asymmetric localization PCP-proteins and the disassembly of the signaling complexes associated with the cilia BB, resulting in lack of translational and rotational polarity in these cells and disorganization of cilia. **(C)** Representative scanning electron microscopy (SEM) images of WT and p73KO lateral ventricle wall (LW) whole-mounts (WMs) at P15. Scale bar 10 μm. **(D)** Regulation of ciliogenesis and PCP is a p73-specific function. Representative confocal images of WT, p53KO, p73KO, TAp73KO and DNp73KO LWs stained with α-tubulin to visualize the ciliary axoneme, or combined staining of FOP, which localized at the base of cilia, and γ-tubulin for the basal feet, to delineate the orientation of each cilium (rPCP). BBs from WT, p53KO and DNp73KO ECs were aligned in parallel rows that contained similar numbers of regularly spaced BBs, while in p73KO and TAp73KO cells the stereotypic arrangement of cilia (spacing and number of cilia per row) was severely impaired. The figure includes original images that reflect previously demonstrated data (Fuertes-Alvarez et al., 2018). Scale bar 10 μm.

by either GFAP or *GemC1* and *Mcidas* expression, respectively (Kyrousi et al., 2015). Interestingly, in the SVZ of p73KO brains, aberrant S100β^{+}-ECs that also expressed GFAP were detected (Gonzalez-Cano et al., 2016), indicating that lack of p73 results in alterations in cell fate determination transcriptional program of RGCs. Moreover, Fujitani and colleagues proposed that embryonic primary ciliogenesis may be regulated by p73, since they found that disruption of p73 (both TA and DNp73) during early postnatal EC development (P1-P5) did not cause hydrocephalus (Fujitani et al., 2017). The compiled data strongly support the idea that p73 functions at several stages during RGCs transformation into EC (**Figure 1A**), beginning at an earlier developmental stage before activation of *Mcidas* and *FoxJ1*, master regulatory genes of multiciliogenesis.

p73 function in MCC fate specification in tracheal epithelium is controversial. p73 fate specification function was proposed in a subset of basal cells that co-express p73 and p63, where p73 expression identified them to undergo MCC differentiation (Marshall et al., 2016). However, a second research group, using tracheal epithelium cultures (MTEC), concluded that p73 is downstream of *Mcidas* and functions mainly after MCC fate specification (Nemajerova et al., 2016). Both groups identified over 100 putative p73 target genes that regulate MCC differentiation and homeostasis and demonstrated that *Foxj1* is a direct target of TAp73, supporting a model in which p73 acts as a regulator of multiciliogenesis through direct and indirect regulation of key genes (Marshall et al., 2016; Nemajerova et al., 2016). Altogether, it was confirmed that TAp73 is at the center of the regulatory network of multiciliogenesis and that it is necessary and sufficient to activate the multiciliogenesis program in tracheal cells, and required in MCC from brain ventricles, oviduct, middle ear, sinus mucosa and flagella of sperm in the testis (Gonzalez-Cano et al., 2016; Marshall et al., 2016; Nemajerova et al., 2016; Fujitani et al., 2017). However, it is plausible that p73 acts, at least in brain, at more of one stage of the MCC generation process.

Trp73 IS REQUIRED FOR MULTICILIOGENESIS OF ECS

After birth, the initial steps of ECs differentiation imply a massive production of Basal Bodies (BBs) and their migration and docking to the apical membrane where they will nucleate motile cilia (Spassky and Meunier, 2017). Centriolar amplification requires the initial aggregation of immature centrioles into procentriole organizers, named deuterosomes. At the last stages, the centrioles will disengage from the deuterosome platforms, migrate to the apical membrane and the deuterosomes will disappear (Spassky and Meunier, 2017). In the absence of p73, BBs aggregate into deuterosomes, but these structures do not completely disappear and are detected in ECs from young (P15) and adult (P30) p73KO mice, suggesting the process is halted or defective (Gonzalez-Cano et al., 2016). Following their amplification, centrioles migrate to the apical surface where they become BBs (**Figure 1A**). p73KO ECs, as well as TAp73KO, have higher number of BBs scattered and deep into the cytoplasm, confirming the required role of TAp73 in centriolar amplification and docking in ECs (**Figure 1B**) (Fuertes-Alvarez et al., 2018). These defects might be due to TAp73 regulation of the MCC factors, *Foxj1* and *Myb*, both downstream of TAp73 (Marshall et al., 2016; Nemajerova et al., 2016), but also due to defects in actin-cytoskeleton dynamics (Fuertes-Alvarez et al., 2018).

ECs motile cilia directly emerge from the apical membrane in mature tissues (**Figures 1A,B**) following the extracellular ciliogenesis pathway (Mirzadeh et al., 2008). Thus, defects in BB docking could result in defective axoneme elongation. As expected, p73KO-ECs with total lack of p73 have severe ciliary defects, with many cells lacking ciliary axoneme and others displaying disorganized cilia of different lengths (Gonzalez-Cano et al., 2016) (**Figures 1B–D**). It is noteworthy, that cells that only lack the TAp73 isoform (TAp73KO) had defective BB docking and showed ciliary defects like disorganized cilia with a "disheveled" appearance (Fuertes-Alvarez et al., 2018). This suggested defects in BB organization and phenocopied the *Celsr2/3* mutant mice where the unidirectional orientation of the BB of their motile cilia, named rotational Planar Cell Polarity (rPCP), was not established (Tissir et al., 2010). However, most of the TAp73KO-ECs, although not all, have ciliary axoneme, displaying a milder ciliary-phenotype than p73KO-ECs (Fuertes-Alvarez et al., 2018) (**Figure 1D**). Nevertheless, additional studies are required to determine the extent of the effect of these alterations in ciliary function. On the other hand, and consistent with the lack of DNp73 expression in ECs (Tissir et al., 2009), DNp73KO-ECs do not display any cilia defects (Fuertes-Alvarez et al., 2018) indicating that, in the presence of TAp73, DNp73 is not necessary for ciliogenesis regulation. These data suggest that compensatory and redundant ciliary programs are induced in the absence of TAp73 when DNp73 is present, but not with total p73 deficiency. Thus, one might speculate that, in this

scenario, compensatory DNp73 upregulation could induce, directly or indirectly, key ciliogenesis regulators, downstream of TAp73 function, suggesting a requirement for DNp73.

Centriolar migration, docking and spacing require the organization of the actin cytoskeleton. BBs are transported, *via* an actin-myosin-based mechanism, to the apical surface (Boisvieux-Ulrich et al., 1990; Meunier and Azimzadeh, 2016). *Trp73* deficiency profoundly affects actin cytoskeleton in ECs, resulting in lack of the apical and subapical actin networks and scattered disposition of the BBs in the apical surface (**Figure 1B**). Subapical actin networks are required for BB spacing, establishment of global coordination of cilia polarity and metachronal synchrony (Werner et al., 2011). Our group have recently discovered that TAp73, in addition of its regulation of the ciliary programs, can regulate the activity and localization of the actin-binding protein non-muscle myosin II (NMII) (Vicente-Manzanares et al., 2009; Kishimoto and Sawamoto, 2012), via the transcriptional activation of its regulatory kinase gene: the myosin light polypeptide kinase *MLCK* (Fuertes-Alvarez et al., 2018). Thus, TAp73 regulation of *MLCK* directly links p73 with actin microfilament dynamics, ciliogenesis and the mechanisms that orchestrate cellular polarity.

p73 REGULATION OF PLANAR CELL POLARITY

Cilia maturation during EC differentiation requires the polarization and organization of the BBs for the cilia to beat in a synchronized manner and create directional fluid flow. This polarization, orthogonal to the apico-basal axis, is known as Planar Cell Polarity (PCP) and is acquired by ECs during their differentiation in a simultaneous process to multiciliogenesis (Ohata and Alvarez-Buylla, 2016) (**Figure 1A**). ECs display two types of PCP: the asymmetric localization of the cilia cluster at the anterior apical surface following the cerebral spinal fluid (CSF) flow, named translational polarity (tPCP), and rotational polarity (rPCP) (Mirzadeh et al., 2010). Combined staining of the centriolar satellite protein FOP (FGFR1 Oncogene Partner) and γ-tubulin is a frequently used indicator to delineate BB orientation and rPCP (Boutin et al., 2014) (**Figure 1D**). Unlike p73KO or TAp73KO mice, tumor-prone p53 KO mice do not present ependymal ciliary PCP defects, indicating that regulation of ciliogenesis and PCP is a p73-specific function (**Figure 1D**).

tPCP is first observed in RGCs as early as E16, when primary cilia become asymmetrically displaced in their apical surface (Mirzadeh et al., 2010). *Trp73* is necessary for the efficient establishment of tPCP in RGC and in immature ECs, and in the absence of p73, or TAp73, tPCP fails to be established (Gonzalez-Cano et al., 2016; Fujitani et al., 2017; Fuertes-Alvarez et al., 2018). Actin microfilament remodeling and NMII activity are essential to establish tPCP (Hirota et al., 2010). NMII is activated (p-MLC) by phosphorylation of its associated regulatory light chain by MLCK and ROCK kinases, but only MLCK activation regulates tPCP (Hirota et al., 2010). NMII activation and its polarized membrane localization in puncta at membrane junctions correlates with anterior migration of the crescent-shaped BB clusters and tPCP establishment (**Figure 1B**). TAp73 regulates tPCP through the modulation of NMII activity and localization, which are impaired in the absence of p73 (Fuertes-Alvarez et al., 2018).

PCP is regulated by asymmetric signaling through core and global regulatory modules. PCP-core module includes Frizzled (Fzd3–6), Van Gogh-like (Vangl1/2), cadherin epidermal growth factor (EGF)-like laminin G-like seven-pass G-type receptor (Celsr1–3), Dishevelled (Dvl1–3), and Prickle (Pk1–4). In ECs, asymmetric localization of the PCP-core complexes at opposite sides of the apical membrane is required for the rotational and translational-PCP (Boutin et al., 2014; Ohata et al., 2014). Adaptor proteins Dvl2, is detected in close association with BBs following a polarized distribution, highlighting its role in instructing polarization to the BBs and coupling BBs-associated information with the rest of the cell (Ohata and Alvarez-Buylla, 2016; Fuertes-Alvarez et al., 2018) (**Figure 1B**). Molecular complexes formed by Dvl and Daple at the base of the BBs may regulate ependymal PCP by activating effectors like aPKC, Rac1, and RhoA, leading to reorganization of the actin cytoskeleton (Ohata et al., 2014). Rac1 is localized on top of the BBs, at the base of the axoneme (Fuertes-Alvarez et al., 2018), which probably corresponds to the ciliary pocket, a proposed interface with the actin cytoskeleton and a platform for vesicle trafficking (**Figure 1B**) (Molla-Herman et al., 2010).

In ECs, mutations of the PCP-core genes *Celsr2/3, Vangl2* and *Dvl2* affect BB-docking and rPCP (Guirao et al., 2010; Hirota et al., 2010; Tissir et al., 2010), while alterations in *Celsr1, Fzd3* and *Vangl2* impair tPCP (Boutin et al., 2014). In this context, ablation of *Trp73* or TAp73, results in the absence of PCP-asymmetric complexes formation (**Figure 1B**) and lack of both, translational and rotational PCP (**Figure 1D**), suggesting that p73 might regulates early up-stream events of PCP establishment. Microtubules crosstalk with PCP at two stages: at the initial polarization establishment and as the downstream-effector of PCP (Vladar et al., 2012; Werner and Mitchell, 2012; Matis et al., 2014; Carvajal-Gonzalez et al., 2016b). Polarized microtubules (MTs) lay the tracks for PCP-core polarized trafficking and are required for rPCP establishment prior to PCP-core-module dissymmetry (Shimada et al., 2006; Harumoto et al., 2010).

In Drosophila the global module formed by the protocadherin Fat and its ligand Dachsous (Fat/Ds), acts by controlling the alignment and asymmetry of MT dynamics, promoting an initial polarization of the apical junctional MT which induces the asymmetric distribution of PCP-core complexes (Harumoto et al., 2010; Matis et al., 2014). As described in MTEC (Dau et al., 2016; Ohata and Alvarez-Buylla, 2016), in ECs Fat4 is located at the base of the cilia associated with the BBs (**Figure 1B**) (Fuertes-Alvarez et al., 2018). p73 deficiency blunts the formation of polarized MT-anchoring points at cell junctions, marked by EB3 staining (Boutin et al., 2014; Takagishi et al., 2017) (**Figure 1B**), suggesting that MT-dynamics impairment is at the root of the defect in p73-deficient cells (Boutin et al., 2014; Takagishi et al., 2017).

CAUSAL RELATIONSHIP BETWEEN OF PCP AND CILIOGENESIS AND p73 REGULATION

The causal relationship between ciliogenesis and PCP signaling is not fully deciphered (Wallingford, 2010). In ECs, PCP coordinately orients the cilia within cells and across the tissue and disruption in PCP establishment results in dysfunctions of ependymal cilia, implicating PCP signaling upstream of ciliogenesis (Boutin et al., 2014). However, elimination of motile cilia by conditional ablation of the ciliogenesis gene *Kif3a* (Kozminski et al., 1995) disrupted rotational orientation, but not tPCP (Mirzadeh et al., 2010). Moreover, in airway epithelia PCP depends on multiciliated cell differentiation and ciliogenesis (Vladar et al., 2016), indicating that cilia may regulate PCP.

Another point of discrepancy is whether PCP-proteins play a role orienting ciliary positioning or if there is also a crosstalk with ciliogenesis. Compiled data on *Vangl* mutants in mice and zebrafish strongly argue for a role of PCP-signaling upstream of ciliary positioning, but not in ciliogenesis *per se* [reviewed in (Carvajal-Gonzalez et al., 2016a)]. However, several PCP-mutants, like *Celsr2/3*-mutant mice, display ciliogenesis defects, linking the PCP-core factors to the ciliogenesis process (Tissir et al., 2010). New studies in *Drosophila* in non-ciliated epithelium establish that PCP-core signaling is an evolutionary conserved module, that acts upstream of centriole positioning independently of ciliogenesis (Carvajal-Gonzalez et al., 2016b).

The results regarding *Trp73* function in ciliogenesis and PCP situates this gene at the epicenter of this conundrum. TAp73 is a master regulator of ciliogenesis and *Trp73* total loss results in dramatic ciliary defects in oviduct, middle ear, respiratory tract and ECs, among others (Gonzalez-Cano et al., 2016; Marshall et al., 2016; Nemajerova et al., 2016; Fujitani et al., 2017). *Trp73* also regulates PCP through TAp73-regulation of actin and MT cytoskeleton dynamics (Fuertes-Alvarez et al., 2018). Moreover, TAp73 is necessary and sufficient for PCP-core protein membrane localization in a non-ciliated cellular model, indicating that p73-regulation of PCP is independent of its function in multiciliogenesis (**Figure 1A**). Interestingly, lack of TAp73 in ECs results in defective actin and MT networks and loss of PCP, but has mild effect on axonemal growth (Fuertes-Alvarez et al., 2018) (**Figure 1D**). Therefore, we propose that the *Trp73*-mutant mice (p73KO, TAp73KO and DNp73KO) represent a model that uncouples ciliogenesis from PCP.

Trp73 MUTANT MICE AS A MODEL OF HUMAN CONGENITAL HYDROCEPHALUS

p73KO mice exhibit congenital hydrocephalus that, in some cases, can progress to a severe communicating form (Yang et al., 2000). Considering the profound ependymal defects observed in the absence of p73, it feasible to hypothesize that the constitutive and inducible *Trp73* mutant mice could be useful models to increase our understanding of certain ciliopathies, in particular the ones that are accompanied by hydrocephalus (Fujitani et al., 2017). Hydrocephalus is a condition that can be caused by a variety of factors; thus, it is possible that the lack of total *Trp73* generates more that one of these situations. As proposed by Pozniak et al. (2002), cellular loss due to p53-induced apoptosis in the absence of DNp73 is probably one of the reasons of the hydrocephalus observed in p73KO mice. However, it is unlikely that this would be the only cause, since the double mutant p53KO/p73KO (DKO) mice, which lacks both apoptotic inducers, p53 and TAp73, developed ventriculomegaly shortly after birth (Gonzalez-Cano et al., 2016). Thus, other p73-dependent functions, different from DNp73-cell survival, should also be implicated in the development of p73KO-hydrocephalus. Both mutant mice, p73KO and DKO, have defects in PCP establishment and an abnormal ependymal layer with ECs that does not establish appropriate cell–cell contacts (Gonzalez-Cano et al., 2016). Interestingly, previous work had reported that loss of cell adhesion due to defective Non muscle myosin II, a tPCP regulator, can cause hydrocephalus (Ma et al., 2007). Other groups have shown that defects in tPCP in radial glia progenitors and in tissue polarity result in hydrocephalus (Hirota et al., 2010; Boutin et al., 2014; Takagishi et al., 2017). In that regard, our group and others have demonstrated that TAp73 is required for the establishment of tPCP (Gonzalez-Cano et al., 2016; Fujitani et al., 2017; Fuertes-Alvarez et al., 2018), a process that begins during late embryonic stages and determines primary cilia displacement and future positioning of mature ependymal cilia-tufts. Thus, it is feasible to hypothesize that embryonic p73-function in the establishment of tPCP in RGCs is crucial for hydrocephalus. In agreement with this, Fujitani and colleagues, using a conditional mutant, found that disruption of *Trp73* (both TA and DNp73) during early postnatal ependymal cells development (P1-P5) did not cause hydrocephalus and proposed that embryonic primary ciliogenesis may be regulated by p73 and this would be critical for hydrocephalus (Fujitani et al., 2017). Nevertheless, it is important to keep in mind that TAp73 central and required role for multiciliogenesis and *Foxj1* expression may also be fundamental for hydrocephalus (Marshall et al., 2016; Nemajerova et al., 2016), since disruption of *Foxj1* expression in ECs induces EC transformation, ventricular breakdown, and hydrocephalus (Abdi et al., 2018).

Congenital hydrocephalus (CH) is a major cause of childhood morbidity and mortality, affecting 4.65 per 10,000 births (Shaheen et al., 2017). Despite its prevalence, the etiology of this abnormal accumulation of CSF in the brain remains largely uncharacterized. Although it is known that the genetic component plays an important role in the development of the disease, only few genes have been identified as the primary cause of CH including: *L1CAM, AP1S2, MPDZ, CCDC88C, EML1,* and *WDR81* (Tully and Dobyns, 2014; Kousi and Katsanis, 2016; Shaheen et al., 2017). Recently, four neurogenesis-associated genes: *TRIM71, SMARCC1, PTCH1,* and *SHH*, have been added to this list, attracting attention to the fact that some communicating forms of CH may be related to impaired neurogenesis (Furey et al., 2018). Under this scenario, p73 mutant mice could also be a relevant model,

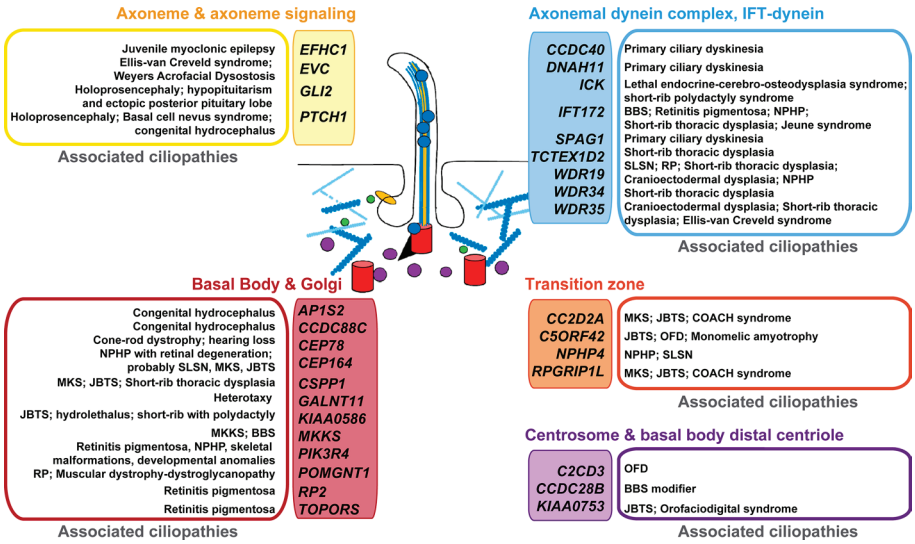

FIGURE 2 | Putative p73 transcriptional target genes and their association with ciliopathies. Human genes with established or likely roles in cilia were compared with genes that were differentially expressed in TAp73β-expressing Saos-2 cells and which contain TAp73 binding sites within 25 kb of the transcription start site (as identified by ChIP-seq analysis, Koeppel et al., 2011). Colors are used to differentiate the protein localization or functional categorization of the candidate p73 target-"ciliopathy-genes". The established ciliopathies linked to these genes (Reiter and Leroux, 2017) are grouped and shown beside. BBS: Bardet-Biedl syndrome; JBTS: Joubert syndrome; MKS: Meckel syndrome; MKKS: McKusick-Kaufman syndrome; NPHP: nephronophthisis; OFD: Orofaciodigital syndrome; RP: retinitis pigmentosa; SLSN: Senior-Loken syndrome.

since p73 deficient mice display a defective neurogenic capacity (Gonzalez-Cano et al., 2010, 2016).

Hydrocephalus can also be linked to primary ciliary dyskinesia (PCD), an autosomal recessive disorder of cilia ultrastructure and function. Although this clinical manifestation of PCD is not frequently diagnosed in humans, it is highly prevalent in mice and therefore, mouse models could help to understand the differences in susceptibility to this pathology (Norris and Grimes, 2012; Lee, 2013). Mutations in five genes (*DNAH5, DNAH11, DNAI1, CCDC39, CCDC40*) encoding proteins necessary for motile cilia function are the most common in PCD (Knowles et al., 2016), some of which were identified as direct TAp73-transcriptional targets by Nemajerova et al. (2016) in MTEC cultures.

Using a compiled list of human cilium-related genes linked to ciliopathies (Reiter and Leroux, 2017), we performed a cross-analysis with potential p73 target genes (**Figure 2**) identified in TAp73β-expressing Saos-2 cells (Koeppel et al., 2011). Supporting our hypothesis, the comparison uncovered some of the above mentioned genes as putative p73 transcriptional targets. These include genes encoding the adaptor protein complex 1- AP1S2, the primary receptor for Hedgehog ligands-PTCH1, the dynein axonemal heavy chain DNAH11, or the trafficking component SNX27. Of particular interest is the emergence of *CCDC88C* (encoding DAPLE) as candidate target for p73 regulation, since Daple-KO mice not only have hydrocephalus but also show defects in cell polarity and microtubule dynamics (Takagishi et al., 2017).

Considering the recent body of work regarding p73 role in ciliogenesis and the growing interest in ciliopathies, p73 mutant mice could become a prominent model system for studying the molecular genetics of cilia-associated disorders and, in particular, the possible crosstalk with PCP deregulation in the pathogenesis of these diseases.

DATA AVAILABILITY

Publicly available datasets were analyzed in this study. This data can be found here: https://academic.oup.com/nar/article/39/14/6069/1369723#supplementary-data.

AUTHOR CONTRIBUTIONS

MMM and MCM took the lead in writing and editing the review. JV-F and SF-A obtained data, crafted figures and drafted the work and LM-A performed data analysis. All authors provided critical feedback and revised the manuscript.

FUNDING

This work was supported by Grants SAF2015-71381-R from Spanish Ministerio de Economía y Competitividad co-financed by FEDER funds (to MCM) and LE021P17 from Junta de Castilla y Leon. JV-F and SF-A are holders of predoctoral fellowships from the Junta de Castilla y León. LM-A is supported by a pre-doctoral scholarship from the Asociación Española contra el Cáncer (AECC).

REFERENCES

Abdi, K., Lai, C. -H., Paez-Gonzalez, P., Lay, M., Pyun, J., and Kuo, C. T. (2018). Uncovering inherent cellular plasticity of multiciliated ependyma leading to ventricular wall transformation and hydrocephalus. *Nat. Commun.* 9:1655. doi: 10.1038/s41467-018-03812-w

Agostini, M., Tucci, P., Chen, H., Knight, R. A., Bano, D., Nicotera, P., et al. (2010). p73 regulates maintenance of neural stem cell. *Biochem. Biophys. Res. Commun.* 403, 13–17. doi: 10.1016/j.bbrc.2010.10.087

Boisvieux-Ulrich, E., Laine, M. C., and Sandoz, D. (1990). Cytochalasin D inhibits basal body migration and ciliary elongation in quail oviduct epithelium. *Cell Tissue Res.* 259, 443–454. doi: 10.1007/BF01740770

Boutin, C., Labedan, P., Dimidschstein, J., Richard, F., Cremer, H., Andre, P., et al. (2014). A dual role for planar cell polarity genes in ciliated cells. *Proc. Natl. Acad. Sci. U. S. A.* 111, E3129–E3138. doi: 10.1073/pnas.1404988111

Cancino, G. I., Fatt, M. P., Miller, F. D., and Kaplan, D. R. (2015). Conditional ablation of p63 indicates that it is essential for embryonic development of the central nervous system. *Cell Cycle* 14, 3270–3281. doi: 10.1080/15384101.2015.1087618

Candi, E., Agostini, M., Melino, G., and Bernassola, F. (2014). How the TP53 family proteins TP63 and TP73 contribute to tumorigenesis: regulators and effectors. *Hum. Mutat.* 35, 702–714. doi: 10.1002/humu.22523

Carvajal-Gonzalez, J. M., Mulero-Navarro, S., and Mlodzik, M. (2016a). Centriole positioning in epithelial cells and its intimate relationship with planar cell polarity. *BioEssays* 38, 1234–1245. doi: 10.1002/bies.201600154

Carvajal-Gonzalez, J. M., Roman, A. -C., and Mlodzik, M. (2016b). Positioning of centrioles is a conserved readout of Frizzled planar cell polarity signalling. *Nat. Commun.* 7:11135. doi: 10.1038/ncomms11135

Dau, C., Fliegauf, M., Omran, H., Schlensog, M., Dahl, E., Van Roeyen, C. R., et al. (2016). The atypical cadherin Dachsous1 localizes to the base of the ciliary apparatus in airway epithelia. *Biochem. Biophys. Res. Commun.* 473, 1177–1184. doi: 10.1016/j.bbrc.2016.04.036

Donehower, L. A., Harvey, M., Slagle, B. L., Mcarthur, M. J., Montgomery, C. A. Jr., Butel, J. S., et al. (1992). Mice deficient for p53 are developmentally normal but susceptible to spontaneous tumours. *Nature* 356, 215–221. doi: 10.1038/356215a0

Engelmann, D., and Pützer, B. M. (2014). Emerging from the shade of p53 mutants: N-terminally truncated variants of the p53 family in EMT signaling and cancer progression. *Sci. Signal.* 7:re9. doi: 10.1126/scisignal.2005699

Fatt, M. P., Cancino, G. I., Miller, F. D., and Kaplan, D. R. (2014). p63 and p73 coordinate p53 function to determine the balance between survival, cell death, and senescence in adult neural precursor cells. *Cell Death Differ.* 21, 1546–1559. doi: 10.1038/cdd.2014.61

Fuertes-Alvarez, S., Maeso-Alonso, L., Villoch-Fernandez, J., Wildung, M., Martin-Lopez, M., Marshall, C., et al. (2018). p73 regulates ependymal planar cell polarity by modulating actin and microtubule cytoskeleton. *Cell Death Dis.* 9:1183. doi: 10.1038/s41419-018-1205-6

Fujitani, M., Cancino, G. I., Dugani, C. B., Weaver, I. C., Gauthier-Fisher, A., Paquin, A., et al. (2010). TAp73 acts via the bHLH Hey2 to promote long-term maintenance of neural precursors. *Curr. Biol.* 20, 2058–2065. doi: 10.1016/j.cub.2010.10.029

Fujitani, M., Sato, R., and Yamashita, T. (2017). Loss of p73 in ependymal cells during the perinatal period leads to aqueductal stenosis. *Sci. Rep.* 7:12007. doi: 10.1038/s41598-017-12105-z

Furey, C. G., Choi, J., Jin, S. C., Zeng, X., Timberlake, A. T., Nelson-Williams, C., et al. (2018). De novo mutation in genes regulating neural stem cell fate in human congenital hydrocephalus. *Neuron* 99, 302–314.e304. doi: 10.1016/j.neuron.2018.06.019

Gebel, J., Tuppi, M., Krauskopf, K., Coutandin, D., Pitzius, S., Kehrloesser, S., et al. (2017). Control mechanisms in germ cells mediated by p53 family proteins. *J. Cell Sci.* 130, 2663–2671. doi: 10.1242/jcs.204859

Gonzalez-Cano, L., Fuertes-Alvarez, S., Robledinos-Anton, N., Bizy, A., Villena-Cortes, A., Farinas, I., et al. (2016). p73 is required for ependymal cell maturation and neurogenic SVZ cytoarchitecture. *Dev. Neurobiol.* 76, 730–747. doi: 10.1002/dneu.22356

Gonzalez-Cano, L., Herreros-Villanueva, M., Fernandez-Alonso, R., Ayuso-Sacido, A., Meyer, G., Garcia-Verdugo, J. M., et al. (2010). p73 deficiency results in impaired self renewal and premature neuronal differentiation of mouse neural progenitors independently of p53. *Cell Death Dis.* 1:e109. doi: 10.1038/cddis.2010.87

Grob, T. J., Novak, U., Maisse, C., Barcaroli, D., Lüthi, A. U., Pirnia, F., et al. (2001). Human ΔNp73 regulates a dominant negative feedback loop for TAp73 and p53. *Cell Death Differ.* 8, 1213–1223. doi: 10.1038/sj.cdd.4400962

Guirao, B., Meunier, A., Mortaud, S., Aguilar, A., Corsi, J. -M., Strehl, L., et al. (2010). Coupling between hydrodynamic forces and planar cell polarity orients mammalian motile cilia. *Nat. Cell Biol.* 12, 341–350. doi: 10.1038/ncb2040

Harumoto, T., Ito, M., Shimada, Y., Kobayashi, T. J., Ueda, H. R., Lu, B., et al. (2010). Atypical cadherins Dachsous and Fat control dynamics of noncentrosomal microtubules in planar cell polarity. *Dev. Cell* 19, 389–401. doi: 10.1016/j.devcel.2010.08.004

Hernández-Acosta, N. C., Cabrera-Socorro, A., Morlans, M. P., Delgado, F. J. G., Suárez-Solá, M. L., Sottocornola, R., et al. (2011). Dynamic expression of the p53 family members p63 and p73 in the mouse and human telencephalon during development and in adulthood. *Brain Res.* 1372, 29–40. doi: 10.1016/j.brainres.2010.11.041

Hirota, Y., Meunier, A., Huang, S., Shimozawa, T., Yamada, O., Kida, Y. S., et al. (2010). Planar polarity of multiciliated ependymal cells involves the anterior migration of basal bodies regulated by non-muscle myosin II. *Development* 137, 3037–3046. doi: 10.1242/dev.050120

Jain, A. K., and Barton, M. C. (2018). p53: emerging roles in stem cells, development and beyond. *Development* 145:dev158360. doi: 10.1242/dev.158360

Killick, R., Niklison-Chirou, M., Tomasini, R., Bano, D., Rufini, A., Grespi, F., et al. (2011). p73: a multifunctional protein in neurobiology. *Mol. Neurobiol.* 43, 139–146. doi: 10.1007/s12035-011-8172-6

Kishimoto, N., and Sawamoto, K. (2012). Planar polarity of ependymal cilia. *Differentiation* 83, S86–S90. doi: 10.1016/j.diff.2011.10.007

Knowles, M. R., Zariwala, M., and Leigh, M. (2016). Primary ciliary dyskinesia. *Clin. Chest Med.* 37, 449–461. doi: 10.1016/j.ccm.2016.04.008

Koeppel, M., Van Heeringen, S. J., Kramer, D., Smeenk, L., Janssen-Megens, E., Hartmann, M., et al. (2011). Crosstalk between c-Jun and TAp73alpha/beta contributes to the apoptosis-survival balance. *Nucleic Acids Res.* 39, 6069–6085. doi: 10.1093/nar/gkr028

Kousi, M., and Katsanis, N. (2016). The genetic basis of hydrocephalus. *Annu. Rev. Neurosci.* 39, 409–435. doi: 10.1146/annurev-neuro-070815-014023

Kozminski, K. G., Beech, P. L., and Rosenbaum, J. L. (1995). The Chlamydomonas kinesin-like protein FLA10 is involved in motility associated with the flagellar membrane. *J. Cell Biol.* 131, 1517–1527. doi: 10.1083/jcb.131.6.1517

Kriegstein, A., and Alvarez-Buylla, A. (2009). The glial nature of embryonic and adult neural stem cells. *Annu. Rev. Neurosci.* 32, 149–184. doi: 10.1146/annurev.neuro.051508.135600

Kyrousi, C., Arbi, M., Pilz, G. -A., Pefani, D. -E., Lalioti, M. -E., Ninkovic, J., et al. (2015). Mcidas and GemC1 are key regulators for the generation of multiciliated ependymal cells in the adult neurogenic niche. *Development* 142, 3661–3674. doi: 10.1242/dev.126342

Kyrousi, C., Lygerou, Z., and Taraviras, S. (2017). How a radial glial cell decides to become a multiciliated ependymal cell. *Glia* 65, 1032–1042. doi: 10.1002/glia.23118

Lee, L. (2013). Riding the wave of ependymal cilia: genetic susceptibility to hydrocephalus in primary ciliary dyskinesia. *J. Neurosci. Res.* 91, 1117–1132. doi: 10.1002/jnr.23238,

Ma, X., Bao, J., and Adelstein, R. S. (2007). Loss of cell adhesion causes hydrocephalus in nonmuscle myosin II-B-ablated and mutated mice. *Mol. Biol. Cell* 18, 2305–2312. doi: 10.1091/mbc.e07-01-0073

Marshall, C. B., Mays, D. J., Beeler, J. S., Rosenbluth, J. M., Boyd, K. L., Santos Guasch, G. L., et al. (2016). p73 is required for multiciliogenesis and regulates the Foxj1-associated gene network. *Cell Rep.* 14, 2289–2300. doi: 10.1016/j.celrep.2016.02.035

Matis, M., Russler-Germain, D. A., Hu, Q., Tomlin, C. J., and Axelrod, J. D. (2014). Microtubules provide directional information for core PCP function. *elife* 3:e02893. doi: 10.7554/eLife.02893

Medina-Bolívar, C., González-Arnay, E., Talos, F., González-Gómez, M., Moll, U. M., and Meyer, G. (2014). Cortical hypoplasia and ventriculomegaly of p73-deficient mice: developmental and adult analysis. *J. Comp. Neurol.* 522, 2663–2679. doi: 10.1002/cne.23556

Merkle, F. T., Tramontin, A. D., García-Verdugo, J. M., and Alvarez-Buylla, A. (2004). Radial glia give rise to adult neural stem cells in the subventricular zone. *Proc. Natl. Acad. Sci. U. S. A.* 101, 17528–17532. doi: 10.1073/pnas.0407893101

Meunier, A., and Azimzadeh, J. (2016). Multiciliated cells in animals. *Cold Spring Harb. Perspect. Biol.* 8:a028233. doi: 10.1101/cshperspect.a028233

Meyer, G., Socorro, A. C., Garcia, C. G. P., Millan, L. M., Walker, N., and Caput, D. (2004). Developmental roles of p73 in Cajal-Retzius cells and cortical patterning. *J. Neurosci.* 24, 9878–9887. doi: 10.1523/JNEUROSCI.3060-04.2004

Mills, A. A., Zheng, B., Wang, X. -J., Vogel, H., Roop, D. R., and Bradley, A. (1999). p63 is a p53 homologue required for limb and epidermal morphogenesis. *Nature* 398, 708–713. doi: 10.1038/19531

Mirzadeh, Z., Han, Y. G., Soriano-Navarro, M., Garcia-Verdugo, J. M., and Alvarez-Buylla, A. (2010). Cilia organize ependymal planar polarity. *J. Neurosci.* 30, 2600–2610. doi: 10.1523/JNEUROSCI.3744-09.2010

Mirzadeh, Z., Merkle, F. T., Soriano-Navarro, M., Garcia-Verdugo, J. M., and Alvarez-Buylla, A. (2008). Neural stem cells confer unique pinwheel architecture to the ventricular surface in neurogenic regions of the adult brain. *Cell Stem Cell* 3, 265–278. doi: 10.1016/j.stem.2008.07.004

Molla-Herman, A., Ghossoub, R., Blisnick, T., Meunier, A., Serres, C., Silbermann, F., et al. (2010). The ciliary pocket: an endocytic membrane domain at the base of primary and motile cilia. *J. Cell Sci.* 123, 1785–1795. doi: 10.1242/jcs.059519

Napoli, M., and Flores, E. R. (2017). The p53 family orchestrates the regulation of metabolism: physiological regulation and implications for cancer therapy. *Br. J. Cancer* 116, 149–155. doi: 10.1038/bjc.2016.384

Nemajerova, A., Amelio, I., Gebel, J., Dötsch, V., Melino, G., and Moll, U. M. (2018). Non-oncogenic roles of TAp73: from multiciliogenesis to metabolism. *Cell Death Differ.* 25, 144–153. doi: 10.1038/cdd.2017.178

Nemajerova, A., Kramer, D., Siller, S. S., Herr, C., Shomroni, O., Pena, T., et al. (2016). TAp73 is a central transcriptional regulator of airway multiciliogenesis. *Genes Dev.* 30, 1300–1312. doi: 10.1101/gad.279836.116

Norris, D. P., and Grimes, D. T. (2012). Mouse models of ciliopathies: the state of the art. *Dis. Model. Mech.* 5, 299–312. doi: 10.1242/dmm.009340

Ohata, S., and Alvarez-Buylla, A. (2016). Planar organization of multiciliated ependymal (E1) cells in the brain ventricular epithelium. *Trends Neurosci.* 39, 543–551. doi: 10.1016/j.tins.2016.05.004

Ohata, S., Nakatani, J., Herranz-Perez, V., Cheng, J., Belinson, H., Inubushi, T., et al. (2014). Loss of Dishevelleds disrupts planar polarity in ependymal motile cilia and results in hydrocephalus. *Neuron* 83, 558–571. doi: 10.1016/j.neuron.2014.06.022

Pflaum, J., Schlosser, S., and Müller, M. (2014). p53 family and cellular stress responses in cancer. *Front. Oncol.* 4:285. doi: 10.3389/fonc.2014.00285

Pozniak, C. D., Barnabé-Heider, F., Rymar, V. V., Lee, A. F., Sadikot, A. F., and Miller, F. D. (2002). p73 is required for survival and maintenance of CNS neurons. *J. Neurosci.* 22, 9800–9809. doi: 10.1523/JNEUROSCI.22-22-09800.2002

Pozniak, C. D., Radinovic, S., Yang, A., Mckeon, F., Kaplan, D. R., and Miller, F. D. (2000). An anti-apoptotic role for the p53 family member, p73, during developmental neuron death. *Science* 289, 304–306. doi: 10.1126/science.289.5477.304

Reiter, J. F., and Leroux, M. R. (2017). Genes and molecular pathways underpinning ciliopathies. *Nat. Rev. Mol. Cell Biol.* 18, 533–547. doi: 10.1038/nrm.2017.60

Shaheen, R., Sebai, M. A., Patel, N., Ewida, N., Kurdi, W., Altweijri, I., et al. (2017). The genetic landscape of familial congenital hydrocephalus. *Ann. Neurol.* 81, 890–897. doi: 10.1002/ana.24964

Shimada, Y., Yonemura, S., Ohkura, H., Strutt, D., and Uemura, T. (2006). Polarized transport of Frizzled along the planar microtubule arrays in Drosophila wing epithelium. *Dev. Cell* 10, 209–222. doi: 10.1016/j.devcel.2005.11.016

Shin, M. H., He, Y., and Huang, J. (2013). Embryonic stem cells shed new light on the developmental roles of p53. *Cell Biosci.* 3:42. doi: 10.1186/2045-3701-3-42

Spassky, N., Merkle, F. T., Flames, N., Tramontin, A. D., Garcia-Verdugo, J. M., and Alvarez-Buylla, A. (2005). Adult ependymal cells are postmitotic and are derived from radial glial cells during embryogenesis. *J. Neurosci.* 25, 10–18. doi: 10.1523/JNEUROSCI.1108-04.2005

Spassky, N., and Meunier, A. (2017). The development and functions of multiciliated epithelia. *Nat. Rev. Mol. Cell Biol.* 18, 423–436. doi: 10.1038/nrm.2017.21

Takagishi, M., Sawada, M., Ohata, S., Asai, N., Enomoto, A., Takahashi, K., et al. (2017). Daple coordinates planar polarized microtubule dynamics in ependymal cells and contributes to hydrocephalus. *Cell Rep.* 20, 960–972. doi: 10.1016/j.celrep.2017.06.089

Talos, F., Abraham, A., Vaseva, A. V., Holembowski, L., Tsirka, S. E., Scheel, A., et al. (2010). p73 is an essential regulator of neural stem cell maintenance in embryonal and adult CNS neurogenesis. *Cell Death Differ.* 17, 1816–1829. doi: 10.1038/cdd.2010.131

Tissir, F., Qu, Y., Montcouquiol, M., Zhou, L., Komatsu, K., Shi, D., et al. (2010). Lack of cadherins Celsr2 and Celsr3 impairs ependymal ciliogenesis, leading to fatal hydrocephalus. *Nat. Neurosci.* 13, 700–707. doi: 10.1038/nn.2555

Tissir, F., Ravni, A., Achouri, Y., Riethmacher, D., Meyer, G., and Goffinet, A. M. (2009). DeltaNp73 regulates neuronal survival in vivo. *Proc. Natl. Acad. Sci. U. S. A.* 106, 16871–16876. doi: 10.1073/pnas.0903191106

Tomasini, R., Tsuchihara, K., Tsuda, C., Lau, S. K., Wilhelm, M., Rufini, A., et al. (2009). TAp73 regulates the spindle assembly checkpoint by modulating BubR1 activity. *Proc. Natl. Acad. Sci. U. S. A.* 106, 797–802. doi: 10.1073/pnas.0812096106

Tomasini, R., Tsuchihara, K., Wilhelm, M., Fujitani, M., Rufini, A., Cheung, C. C., et al. (2008). TAp73 knockout shows genomic instability with infertility and tumor suppressor functions. *Genes Dev.* 22, 2677–2691. doi: 10.1101/gad.1695308

Tully, H. M., and Dobyns, W. B. (2014). Infantile hydrocephalus: a review of epidemiology, classification and causes. *Eur. J. Med. Genet.* 57, 359–368. doi: 10.1016/j.ejmg.2014.06.002

Van Nostrand, J. L., Bowen, M. E., Vogel, H., Barna, M., and Attardi, L. D. (2017). The p53 family members have distinct roles during mammalian embryonic development. *Cell Death Differ.* 24, 575–579. doi: 10.1038/cdd.2016.128

Vicente-Manzanares, M., Ma, X., Adelstein, R. S., and Horwitz, A. R. (2009). Non-muscle myosin II takes centre stage in cell adhesion and migration. *Nat. Rev. Mol. Cell Biol.* 10, 778–790. doi: 10.1038/nrm2786

Vladar, E. K., Bayly, R. D., Sangoram, A. M., Scott, M. P., and Axelrod, J. D. (2012). Microtubules enable the planar cell polarity of airway cilia. *Curr. Biol.* 22, 2203–2212. doi: 10.1016/j.cub.2012.09.046

Vladar, E. K., Nayak, J. V., Milla, C. E., and Axelrod, J. D. (2016). Airway epithelial homeostasis and planar cell polarity signaling depend on multiciliated cell differentiation. *JCI Insight* 1:e88027. doi: 10.1172/jci.insight.88027

Wallingford, J. B. (2010). Planar cell polarity signaling, cilia and polarized ciliary beating. *Curr. Opin. Cell Biol.* 22, 597–604. doi: 10.1016/j.ceb.2010.07.011

Wang, Q., Zou, Y., Nowotschin, S., Kim, S. Y., Li, Q. V., Soh, C. -L., et al. (2017). The p53 family coordinates wnt and nodal inputs in mesendodermal differentiation of embryonic stem cells. *Cell Stem Cell* 20, 70–86. doi: 10.1016/j.stem.2016.10.002

Werner, M. E., Hwang, P., Huisman, F., Taborek, P., Yu, C. C., and Mitchell, B. J. (2011). Actin and microtubules drive differential aspects of planar cell polarity in multiciliated cells. *J. Cell Biol.* 195, 19–26. doi: 10.1083/jcb.201106110

Werner, M. E., and Mitchell, B. J. (2012). Understanding ciliated epithelia: the power of *Xenopus*. *Genesis* 2000, 176–185. doi: 10.1002/dvg.20824

Wilhelm, M. T., Rufini, A., Wetzel, M. K., Tsuchihara, K., Inoue, S., Tomasini, R., et al. (2010). Isoform-specific p73 knockout mice reveal a novel role for delta Np73 in the DNA damage response pathway. *Genes Dev.* 24, 549–560. doi: 10.1101/gad.1873910

Yang, A., Walker, N., Bronson, R., Kaghad, M., Oosterwegel, M., Bonnin, J., et al. (2000). p73-deficient mice have neurological, pheromonal and inflammatory defects but lack spontaneous tumours. *Nature* 404, 99–103. doi: 10.1038/35003607

Conflict of Interest Statement: The authors declare that the research was conducted in the absence of any commercial or financial relationships that could be construed as a potential conflict of interest.

frontiers in Genetics

ORIGINAL RESEARCH
published: 22 March 2019
doi: 10.3389/fgene.2019.00248

A Combined *in silico*, *in vitro* and Clinical Approach to Characterize Novel Pathogenic Missense Variants in PRPF31 in Retinitis Pigmentosa

Gabrielle Wheway[1]†, Liliya Nazlamova[1]†, Nervine Meshad[2], Samantha Hunt[2], Nicola Jackson[3] and Amanda Churchill[2]**

[1] Centre for Research in Biosciences, University of the West of England, Bristol, United Kingdom, [2] Bristol Eye Hospital, University Hospitals Bristol NHS Foundation Trust, Bristol, United Kingdom, [3] Clinical Genetics Service, University Hospitals Bristol NHS Foundation Trust, Bristol, United Kingdom

OPEN ACCESS

Edited by:
Jose Maria Carvajal-Gonzalez, Universidad de Extremadura, Spain

Reviewed by:
Diana M. Horrigan, Brown University, United States
Angel Carlos Roman, Universidad de Extremadura, Spain

***Correspondence:**
Gabrielle Wheway
g.wheway@soton.ac.uk
Amanda Churchill
a.j.churchill@bristol.ac.uk

†Present address:
Gabrielle Wheway and Liliya Nazlamova, Human Development and Health, University of Southampton, Southampton, United Kingdom

Specialty section:
This article was submitted to Genetic Disorders, a section of the journal Frontiers in Genetics

Received: 23 October 2018
Accepted: 05 March 2019
Published: 22 March 2019

Citation:
Wheway G, Nazlamova L, Meshad N, Hunt S, Jackson N and Churchill A (2019) A Combined in silico, in vitro and Clinical Approach to Characterize Novel Pathogenic Missense Variants in PRPF31 in Retinitis Pigmentosa. Front. Genet. 10:248. doi: 10.3389/fgene.2019.00248

At least six different proteins of the spliceosome, including PRPF3, PRPF4, PRPF6, PRPF8, PRPF31, and SNRNP200, are mutated in autosomal dominant retinitis pigmentosa (adRP). These proteins have recently been shown to localize to the base of the connecting cilium of the retinal photoreceptor cells, elucidating this form of RP as a retinal ciliopathy. In the case of loss-of-function variants in these genes, pathogenicity can easily be ascribed. In the case of missense variants, this is more challenging. Furthermore, the exact molecular mechanism of disease in this form of RP remains poorly understood. In this paper we take advantage of the recently published cryo EM-resolved structure of the entire human spliceosome, to predict the effect of a novel missense variant in one component of the spliceosome; PRPF31, found in a patient attending the genetics eye clinic at Bristol Eye Hospital. Monoallelic variants in *PRPF31* are a common cause of autosomal dominant retinitis pigmentosa (adRP) with incomplete penetrance. We use *in vitro* studies to confirm pathogenicity of this novel variant *PRPF31* c.341T > A, p.Ile114Asn. This work demonstrates how *in silico* modeling of structural effects of missense variants on cryo-EM resolved protein complexes can contribute to predicting pathogenicity of novel variants, in combination with *in vitro* and clinical studies. It is currently a considerable challenge to assign pathogenic status to missense variants in these proteins.

Keywords: genetic disease, modeling, pathogenicity, missense, pre-mRNA splicing factor, retinitis pigmentosa, retinal ciliopathy

INTRODUCTION

Retinitis pigmentosa (RP) is a progressive retinal degeneration characterized by night blindness and restriction of peripheral vision. Later in the course of the disease, central and color vision can be lost. Many patients experience the first signs of RP between 20 and 40 years but there is much phenotypic variability from age of onset and speed of deterioration to severity of visual impairment (Hartong et al., 2006).

Retinitis pigmentosa, whilst classified as a rare disease, is the most common cause of inherited blindness worldwide. It affects between 1:3500 and 1:2000 people (Golovleva et al., 2010; Sharon and Banin, 2015), and can be inherited in an autosomal dominant (adRP), autosomal recessive (arRP), or X-linked (xlRP) manner. It may occur in isolation (non-syndromic RP) (Verbakel et al., 2018), or with other features (syndromic RP) as in Bardet–Biedl syndrome, Joubert syndrome and Usher syndrome (Mockel et al., 2011).

The condition is extremely heterogeneous, with 64 genes identified as causes of non-syndromic RP, and more than 50 genes associated with syndromic RP (RetNet[1]). Even with current genetic knowledge, diagnostic detection rate in adRP cohorts remains between 40% (Mockel et al., 2011) and 66% (Zhang et al., 2016), suggesting that many disease genes remain to be identified, and many mutations within known genes require characterization to ascribe pathogenic status. Detection rates are as low as 14% in cohorts of simplex cases (single affected individuals) and multiplex cases (several affected individuals in one family but unclear pattern of inheritance) (Jin et al., 2008). Such cases account for up to 50% of RP cases, so this presents a significant challenge to diagnosis (Greenberg et al., 1993; Haim, 1993; Najera et al., 1995).

The second most common genetic cause of adRP is *PRPF31*, accounting for 6% of United States cases (Sullivan et al., 2013) 8% of Spanish cases (Martin-Merida et al., 2018), 8% of French Canadian cases (Coussa et al., 2015), 8% of French cases (Audo et al., 2010), 8.9% of cases in North America (Daiger et al., 2014), 11.1% in small Chinese cohort (Lim et al., 2009), 10% in a larger Chinese cohort (Xu et al., 2012) and 10.5% of Belgian cases (Van Cauwenbergh et al., 2017). However, this is likely to be an underestimate due to variable penetrance of this form of RP, complicating attempts to co-segregate the variant with clinical disease, making genetic diagnosis difficult.

Whilst the majority of reported variants in *PRPF31* are indels, splice site variants and nonsense variants, large-scale deletions or copy number variations (Martin-Merida et al., 2018), which are easily ascribed pathogenic status, at least eleven missense variants in *PRPF31* have been reported in the literature (**Table 1**). Missense variants are more difficult to characterize functionally than nonsense or splicing mutations (Cooper and Shendure, 2011) and it is likely that there are false negative diagnoses in patients carrying missense mutations due to lack of confidence in prediction of pathogenicity of such variants. This is reflected in the enrichment of *PRPF31* missense variants labeled 'uncertain significance' in ClinVar, a public repository for clinically relevant genetic variants (Landrum et al., 2014, 2016). Furthermore, work has shown that some variants annotated as missense *PRPF31* variants may in fact be affecting splicing of *PRPF31*, introducing premature stop codons leading to nonsense mediated decay (NMD), a common disease mechanism in RP11 (Rio Frio et al., 2008). One example is c.319C > G, which, whilst originally annotated as p.Leu107Val, actually affects splicing rather than an amino acid substitution (Rio Frio et al., 2008). The presence of exonic splice enhancers is often overlooked by genetics researchers.

PRPF31 is a component of the spliceosome, the huge macromolecular ribonucleoprotein (RNP) complex which catalyzes the splicing of pre-messenger RNAs (pre-mRNAs) to remove introns and produce mature mRNAs (Will and Luhrmann, 2011). The spliceosome is composed of 5 small nuclear RNAs (snRNAs), U1–U5, and many proteins including pre-mRNA splicing factors PRPF3, PRPF4, PRPF6, PRPF8, and SNRNP200, all of which are also genetic causes of RP (Ruzickova and Stanek, 2016). It is unclear whether variants in these proteins have an effect on splicing of specific retinal transcripts (Deery et al., 2002; Yuan et al., 2005; Mordes et al., 2007; Wilkie et al., 2008). Some papers have failed to find any evidence for a generalized RNA splicing defects (Rivolta et al., 2006). Pre-mRNA splicing factors may have additional roles beyond splicing in the nucleus, after a study recently found that PRPF6, PRPF8, and PRPF31 are all localized to the base of the retinal photoreceptor connecting cilium and are essential for ciliogenesis, suggesting that this form of RP is a ciliopathy (Wheway et al., 2015). Missense variants in these proteins are, collectively, a common cause of adRP. This presents significant challenges in providing accurate diagnosis for patients with missense variants in these genes. Developing tools to provide accurate genetic diagnoses in these cases is a significant clinical priority.

The most commonly used *in silico* predictors of pathogenicity of missense variants, PolyPhen2 (Adzhubei et al., 2010) and CADD (Kircher et al., 2014), which use combined sequence conservation, structural and machine learning techniques only have around 15–20% success rate in predicting truly pathogenic variants (Miosge et al., 2015). Use of simple tools has around the same success rate (Gnad et al., 2013), and use of several tools in combination increases reliability (Gonzalez-Perez and Lopez-Bigas, 2011). Insight from structural biologists and molecular cell biologists is essential to make accurate predictions.

In this study we take advantage of the recently elucidated structure of the in-tact spliceosome to model the effect of a novel variant in *PRPF31*, found in a patient attending the genetics eye clinic at Bristol Eye Hospital. We combine this *in silico* analysis with *in vitro* studies to characterize this novel variant. We show that analysis of protein complexes *in silico* can complement clinical and laboratory studies in predicting pathogenicity of novel genetic variants.

MATERIALS AND METHODS

Genetic Testing

The study was conducted in accordance with the Declaration of Helsinki. Informed consent for diagnostic testing was obtained from the proband in clinic. Genomic DNA was extracted from a peripheral blood sample by Bristol Genetics Laboratory and tested against the retinal dystrophy panel of 176 genes in the NHS accredited Genomic Diagnostics Laboratory at Manchester Centre for Genomic Medicine, United Kingdom.

[1]https://sph.uth.edu/retnet/sum-dis.htm

TABLE 1 | Summary of published missense mutations in *PRPF31*.

cDNA variant	protein variant	Found in family or singleton?	Original reference(s)
c.413C > A	Thr138Lys	Large family	Waseem et al., 2007
c.581C > A	Ala194Glu	Single affected individual (SP42)	Vithana et al., 2001
c.590T > C	Leu197Pro	Large generation	Bryant et al., 2018
c.646G > C	Ala216Pro	Huge family (AD29)	Vithana et al., 2001
c.781G > C	Gly261Arg	Single affected individual	Xiao et al., 2017
c.862C > T	Arg288Trp	Single affected individual	Coussa et al., 2015
c.871G > C	Ala291Pro	Single affected individual	Sullivan et al., 2006
c.895T > C	Cys299Arg	3 independent families	Sullivan et al., 2006; Xu et al., 2012; Martin-Merida et al., 2018
c.896G > A	Cys299Tyr	Large family	Bhatia et al., 2018
c.1222C > T	Arg408Trp	Single affected individual	Xiao et al., 2017
c.1373A > T	Gln458Leu	Single affected individual	Xiao et al., 2017

Splicing Analysis

We used Human Splicing Finder (Desmet et al., 2009) to identify and predict the effect of variants on splicing motifs, including the acceptor and donor splice sites, branch point and auxiliary sequences known to enhance or repress splicing. This program uses 12 different algorithms to make a comprehensive prediction of the effect of variants on splicing.

3D Structural Protein Analysis

PyMol (Schrodinger Ltd.) program was used to characterize the effect of missense variants in human *PRPF31* protein. Missense variants were modeled on PRPF31 in the pre-catalytic spliceosome primed for activation (PDB file 5O9Z) (Bertram et al., 2017).

Variant Construct Cloning

Full-length, sequence-validated *PRPF31* ORF clone with C-terminal myc tag was obtained from OriGene. c.341T > A or c.581C > A variant was introduced using NEB Q5 site-directed mutagenesis kit. The entire wild-type and mutant clone sequence was verified by Sanger sequencing (Source Bioscience).

Cell Culture

HEK293 cells and 661W cells were cultured in DMEM high glucose + 10% FCS at 37°C, 5% CO_2, and split at a ratio of 1:8 once per week. hTERT-RPE1 cells (ATCC CRL-4000) were cultured in DMEM/F12 (50:50 mix) + 10% FCS at 37°C, 5% CO_2, and split at a ratio of 1:8 once per week.

Cell Transfection

The construct was transfected into HEK293 cells using PEI, and into hTERT-RPE1 and 661W cells using the Lonza Nucleofector.

Inhibition of Protein Translation

Cells were grown for 72 h, and treated with 30 μg/ml cycloheximide in DMSO. Untreated cells were treated with the equivalent volume of DMSO.

Protein Extraction

Total protein was extracted from cells using 1% NP40 lysis buffer and scraping. Insoluble material was pelleted by centrifugation at 10,000 × *g*. Cell fractionation was carried out by scraping cells into fractionation buffer containing 1 mM DTT, and passed through a syringe 10 times. Nuclei were pelleted at 720 × *g* for 5 min and separated from the cytoplasmic supernatant. Insoluble cytoplasmic material was pelleted using centrifugation at 10,000 × *g* for 5 min. Nuclei were washed, and lysed with 0.1% SDS and sonication. Insoluble nuclear material was pelleted using centrifugation at 10,000 × *g* for 5 min.

SDS-PAGE and Western Blotting

20 μg of total protein per sample with 2 × SDS loading buffer was loaded onto pre-cast 4–12% Bis-Tris gels (Life Technologies) alongside Spectra Multicolor Broad range Protein ladder (Thermo Fisher). Samples were separated by electrophoresis. Protein was transferred to PVDF membrane. Membranes were incubated with blocking solution [5% (w/v) non-fat milk/PBS], and incubated with primary antibody overnight at 4°C. After washing, membranes were incubated with secondary antibody for 1 h at room temperature and exposed using 680 nm and/or 780 nm laser, or incubated with SuperSignal West Femto reagent (Pierce) and exposed using Chemiluminescence settings on Li-Cor Odyssey imaging system (Li-Cor).

Primary Antibodies for WB

Mouse anti β-actin clone AC-15. 1:4000. Sigma-Aldrich A1978.
Goat anti-PRPF31 primary antibody 1:1000 (Abnova).
Mouse anti-c myc 1:5000 (Sigma).
Mouse anti PCNA-HRP conjugated 1:1000 (Bio-Rad).

Secondary Antibodies for WB

Donkey anti mouse 680 1:20,000 (Li-Cor).
Donkey anti goat 800 1:20,000 (Li-Cor).

Immunocytochemistry

Cells were fixed 24, 48, and 72 h after nucleofection. Cells were fixed in ice-cold methanol at −20°C for 5 min, immediately washed with PBS, and incubated with blocking solution (1% w/v non-fat milk powder/PBS). Coverslips were incubated with primary antibodies at

4°C overnight and with secondary antibodies and DAPI for 1 h at room temperature. Cells were mounted onto slides with Mowiol.

Primary Antibodies for IF

Goat anti-PRPF31 primary antibody 1:200 (Abnova).
Mouse anti-c myc 1:1000 (Sigma).
Rabbit anti-caspase 3 1:500 (Abcam).

Secondary Antibodies for IF

Donkey anti mouse IgG Alexa Fluor 488 1:500.
Donkey anti goat IgG Alexa Fluor 633 1:500.
Goat anti rabbit IgG Alexa Fluor 488 1:1000.
Goat anti mouse IgG Alexa Fluor 568 1:1000.

Confocal Imaging

Confocal images were obtained at the Centre for Research in Biosciences Imaging Facility at UWE Bristol, using a HC PL APO 63×/1.40 oil objective CS2 lens on a Leica DMi8 inverted epifluorescence microscope, attached to a Leica SP8 AOBS laser scanning confocal microscope, or in the Bioimaging Unit of University of Southampton, using a HC PL APO 63×/1.30 glycerol objective lens on a Leica DMi8 inverted epifluorescence microscope, attached to a Leica SP5 laser scanning confocal microscope. For publication, images were captured using LASX or LAS Af software, assembled in Adobe Photoshop, and figures prepared using Adobe Illustrator. For image analysis, images were captured using LASX software, assembled in Adobe Photoshop and randomized for analysis by an independent researcher blinded to the identity of samples.

RESULTS

Clinical Description of c.341T > A p.Ile114Asn Patient

A 39 years old female presented to the Genetic Eye clinic at Bristol Eye Hospital in 2013 complaining of some difficulty with dark adaptation, driving at night and a reduction in her field of vision (having to turn her head to see her children). Her general health was otherwise good. Over a 4 years period her best corrected visual acuity remained good at 6/6-3 right eye and 6/7.5 left eye (Snellen equivalent using a LogMar chart) whilst her peripheral vision deteriorated from an isolated mid-peripheral scotoma to tunnel vision by 2017 (**Figure 1A**). Fundoscopy showed widespread bilateral bone spicule pigmentation, attenuated retinal vessels and pale optic nerves typical of RP (**Figure 1B**). There was no evidence of lens opacities or macula oedema in either eye.

Variant Analysis of c.341T > A p.Ile114Asn

The patient described other family members having similar symptoms and losing their sight at a relatively young age (**Figure 2A**). A heterozygous *PRPF31* change, c.341T > A p.Ile114Asn was identified in the patient and her asymptomatic father, which was confirmed by bidirectional Sanger sequencing. All affected members of the family were on the father's side. We were not able to contact any other affected relatives for testing. Pathogenic variants in *PRPF31* are associated with a form of RP which shows incomplete penetrance, consistent with the pattern of inheritance seen in this family. The PRPF31 c.341T > A p.Ile114Asn variant is not present in the heterozygous or homozygous state in any individuals within the gnomAD database, nor are any other variants affecting Ile114, suggesting that this is a highly conserved residue. Analysis by PolyPhen2 suggested this change was probably damaging, with a score of 0.963 (**Figure 2B**) and SIFT concurred with this prediction with a score of 0.0. Comparative genomic alignment shows the residue to be conserved from humans to amphibia, within a highly conserved region, conserved across diverse metazoa including sponges (**Figure 2B**). The Grantham score (Grantham, 1974) is 149, where 0–50 is conservative, 51–100 is moderately conservative, 101–150 is moderately radical and >151 is radical (Li et al., 1984).

Splicing Analysis of Genetic Single Nucleotide Variants in *PRPF31*

We undertook *in silico* splicing analysis of our novel variant of interest c.341T > A p. Ile114Asn and found that it was not predicted to affect splicing. We also studied the nine published variants in *PRPF31* annotated as missense, and interestingly, five were predicted to potentially alter splicing, and one [c.1373A > T, p. Gln458Leu (Xiao et al., 2017)] was predicted to be highly likely to affect splicing (**Table 2**). This suggests that either this splice predictor should be used with caution, or that p.Gln458Leu may be mis-annotated as a missense variant, when it actually affects splicing. We suggest that this variant should be a priority for further functional characterization *in vitro*.

3D Structural Analysis of Missense Variants in PRPF31

We mapped all published missense variants onto the PRPF31 protein structure in the pre-catalytic spliceosome. For simplicity, we only show PRPF31 in complex with U4 snRNA and 15.5K (SNU13) protein (**Figure 3**) and (in complex with PRPF6 in **Supplementary Figure S1**; in complex with PRPF8 in **Supplementary Figure S2**). This showed that variants are located throughout the protein, but concentrated in several key domains. Three variants (Arg288Trp, Ala291Pro, and Cys299Arg), are located in α-helix 12 of the protein, in the Nop domain which interacts with RNA and the 15.5K (SNU13) protein. Three variants are in α-helix 6 of the coiled-coil domain (Ala194Glu, Leu197Pro, and Ala216Pro) and one variant is in α-helix 3 of the protein in the coiled-coil tip (Thr138Lys). Gly261Arg is within the flexible loop between the Nop and coiled-coil domains and Arg408Trp alone is in the C-terminal domain.

Analysis of interactions within 4 Å of each amino acid show that in most cases (Thr138Lys, Ala194Glu, Gly261Arg, Arg288Trp, Ala291Pro, and Cys299Arg), these substitutions are predicted to affect hydrogen (H) bonding in PRPF31.

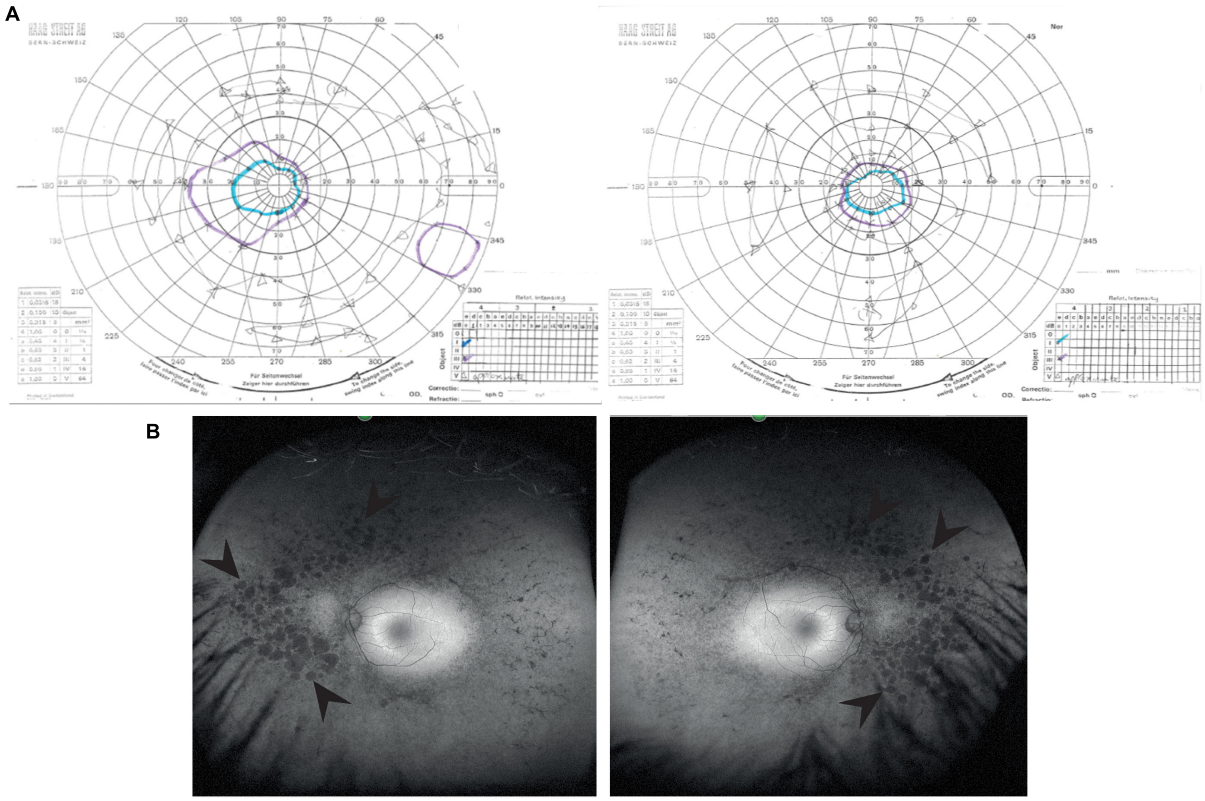

FIGURE 1 | Clinical characteristics of patient at visit in 2017. **(A)** Goldmann visual field images show bilateral tunnel vision with a small island of peripheral vision in the right eye. Both the I4e (turquoise line) and III4e (purple line) targets were used to plot the visual fields. Using the commonly used III4e target in both eyes, the visual fields extend from 10 degrees temporally to 40 degrees nasally along the horizontal and 15 degrees above and below fixation in the right eye with a peripheral island of vision in the inferotemporal quadrant. The peripheral fields in the left eye are constricted to the central 15 degrees. **(B)** Red-free fundus photographs show extensive bilateral retinal pigment disruption. Arrowheads point to areas of pigment defects in the periphery of the fundus for both eyes. Areas of defects are larger and more confluent in the nasal compared to temporal periphery.

H bonds with donor-acceptor distances of 2.2–2.5 Å are strong and mostly covalent; 2.5–3.2 Å are moderate mostly electrostatic and 3.2–4 are weak electrostatic interactions and can be predicted to be affecting protein folding and solubility (Jeffrey, 1997). In the case of Arg408Trp, the substitution does not affect H bonding within PRPF31, but does introduce a new interaction with neighboring PRPF6 (**Figure 4A** and **Supplementary Figures S1**, **S2**). Gly261Arg also introduces a new interaction with neighboring PRPF8 (**Figure 4B** and **Supplementary Figure S2**). Of the three small substitutions which do not affect H bonding, we discovered that in all cases the variant amino acid was proline, which introduces a new kink in the amino acid chain. Each of these substitutions also resulted in the loss of a polar contact (**Figures 4C–E**).

We next mapped the variant found in our patient attending the genetics eye clinic at Bristol Eye Hospital; Ile114Asn (**Figure 5A**). Ile114Asn is in the coiled-coil domain of the protein, in close proximity to published pathogenic variants Thr138Lys and Ala194Glu (**Figure 5B**). The substitution introduces new H bonds between this residue and Ala190 of an adjacent α-helix, and is predicted to affect protein folding and solubility, and be pathogenic (**Figure 5C**).

The effect of missense variants is summarized in **Table 3**.

To test the accuracy of our predictions, we took on c.341T > A p.Ile114Asn for further *in vitro* characterization.

In vitro Analysis of c.341T > A p.Ile114Asn Variant

To investigate whether c.341T > A p.Ile114Asn caused mislocalization of the protein, we transfected hTERT-RPE1 cells, an immortalized cell line derived from human retinal pigment epithelium, with plasmids expressing either wild-type (WT) PRPF31 or PRPF31 341T > A, both tagged with c-myc epitope tag. We used the Lonza nucleofector to ensure high transfection efficiency. We assayed the cells after 24, 48, and 72 h by immunofluorescence confocal microscopy using an anti-cmyc antibody. At 24 h we saw mid- to high-level expression of the WT protein exclusively in the nucleus of, on average, 52.5% of cells (**Figure 6A**). This gradually reduced at 48 h (44.0% of cells), and 72 h (34.4%) (**Figure 6A**). We did not observe the same pattern in cells expressing the mutant protein. In these cells, only 9.11% of cells showed nuclear c-myc staining at 24 h, and it was very intense, and also observed in the cytoplasm (**Figure 6A**). This was

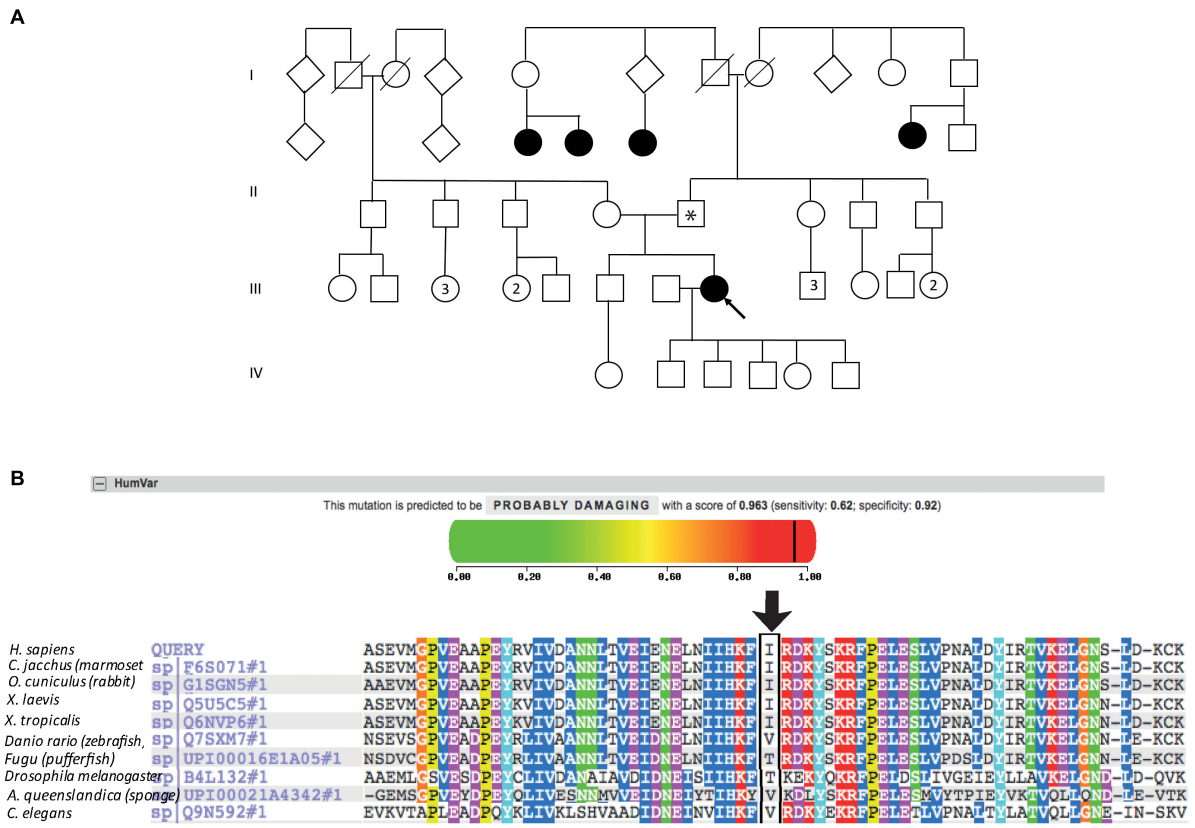

FIGURE 2 | Pedigree, PolyPhen2 and conservation analysis of *PRPF31* c.341T > A Ile114Asn variant. **(A)** Family pedigree. Affected individuals in generation II had visual symptoms suggestive of retinitis pigmentosa and appear on both sides of the paternal grandparents of the proband. Arrow = proband. Asterisk = father of proband, also found to possess heterozygous *PRPF31* c.341T > A Ile114Asn variant. **(B)** PolyPhen2 score predicts this variant is probably damaging with a score of 0.963 (top), alignment of PRPF31 sequence showing conservation of Ile114 and surrounding amino acids (bottom). Ile114 identity is conserved across tetrapods, from human to *Xenopus tropicalis*, and non-polar hydrophobic similarity is conserved from yeast to human, with variations in highly derived insects (*Drosophila melanogaster*) and fish (*Fugu*).

TABLE 2 | Mutations in PRPF31 annotated as missense, and their predicted impact on splicing.

cDNA variant	Protein variant	Predicted effect on splicing (Human Splicing Finder)	Notes	Summary - effect on splicing?	Estimate of pathogenicity
c.413C > A	Thr138Lys	Potential alteration of splicing		Maybe	Pathogenic
c.581C > A	Ala194Glu	Potential alteration of splicing	Functional characterization shows functional effect of missense change	No	Pathogenic
c.590T > C	Leu197Pro	Potential alteration of splicing	Functional characterization shows functional effect of missense change	No	Pathogenic
c.646G > C	Ala216Pro	Potential alteration of splicing	Functional characterization shows functional effect of missense change	No	Pathogenic
c.781G > C	Gly261Arg	No impact on splicing		No	Pathogenic
c.862C > T	Arg288Trp	Potential alteration of splicing		Maybe	Pathogenic
c.871G > C	Ala291Pro	No impact on splicing		No	Pathogenic
c.895T > C	Cys299Arg	No impact on splicing		No	Pathogenic
c.896G > A	Cys299Tyr	Potential alteration of splicing		Maybe	Pathogenic
c.1222C > T	Arg408Trp	Potential alteration of splicing		No	Pathogenic
c.1373A > T	Gln458Leu	Most probably affecting splicing		Yes	Pathogenic

All published missense mutations in PRPF31, and their predicted impact on splicing, according to Human Splicing Finder.

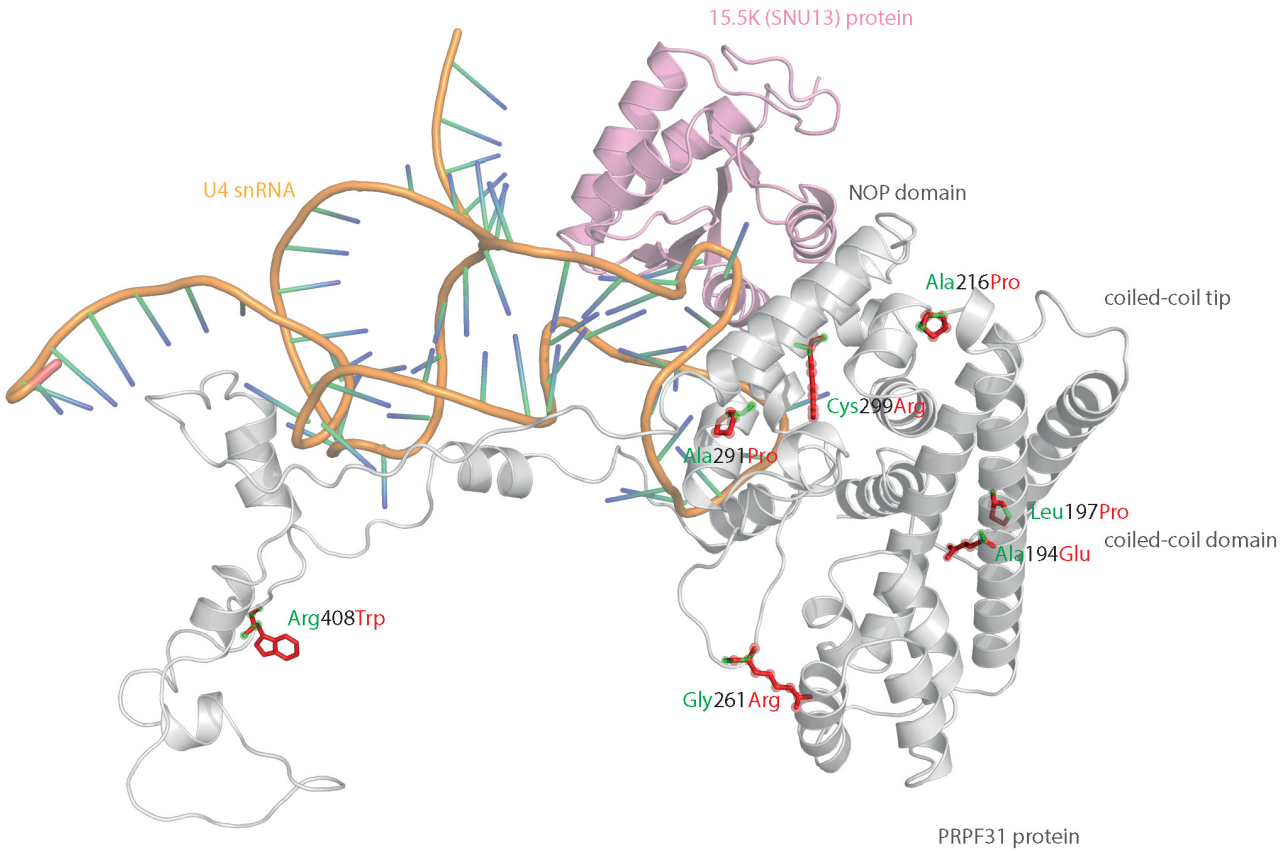

FIGURE 3 | 3D cartoon representation of PRPF31, including published missense mutations. Cartoon representation of alpha helical structure of PRPF31 (gray) and 15.5K/SNU13 (pink) with U4 snRNA (orange backbone), with published missense mutations mapped onto the physical structure, with wild-type amino acid structure in green, and mutant amino acid structure overlaid in red.

maintained at 48 h (11.9%), but dropped to 7.5% of cells at 72 h (**Figure 6A**). The difference in c-myc staining, in terms of % of cells with nuclear staining and % of cells with cytoplasmic staining, was statistically significant at all time points with the exception of cytoplasmic staining at 48 h (*t*-test, $p < 0.05$, $n = 4$ independent biological replicates) (**Figure 6B**). At each time point, many cells transfected with mutant PRPF31 showed abnormal nuclear morphology, with some micronuclei present (**Figure 6C**). There were statistically significantly more abnormal nuclei and micronuclei in the mutant cells compared to WT at 48 and 72 h (paired *t*-test, $p < 0.05$, $n = 4$ independent biological replicates) (**Figure 6D**). To confirm these findings, we compared these findings to cells transfected with PRPF31 c.581C > A p.Ala194Glu, and observed a similar pattern of staining and nuclear changes, although we were not able to calculate the statistical significance of these observations ($n = 2$) (**Supplementary Figure S3**). We also repeated these experiments in the 661W cell line, which is derived from mouse cone photoreceptor cells (Tan et al., 2004). Although we achieved lower transfection efficiency, we observed the same pattern of c-myc staining as we saw in the hTERT-RPE1 experiments. At 24 h we saw mid- to high-level expression of the WT protein exclusively in the nucleus of around 16.2% of cells (**Figure 7A**). We did not observe the same pattern in cells expressing the mutant protein. In these cells, at 24 h, only around 7.9% of cells showed c-myc staining in the nucleus, and it was very intense and also throughout the cytoplasm (**Figure 7A**). The difference in c-myc staining, in terms of % of cells with nuclear staining, was statistically significant at all time points (*t*-test, $p < 0.05$, $n = 3$ independent biological replicates) (**Figure 7B**). Again, we saw more abnormal nuclei and micronuclei in cells transfected with mutant PRPF31 compared to WT after 48 and 72 h (**Figure 7C**). The number of micronuclei was significantly higher in mutant cells at 48 and 72 h (*t*-test, $p < 0.05$, $n = 3$ independent biological replicates) (**Figure 7D**). In keeping with previously published studies (Yuan et al., 2005) we hypothesized that the mutant PRPF31 protein was aggregating in the nuclei and causing cell death by apoptosis. However, co-immunostaining of cells at each timepoint with caspase-3, a marker of apoptosis, did not confirm this. We consider two alternative possible hypotheses to explain the observation of nuclear abnormalities; that expression of mutant PRPF31 has an effect on centrosomal stability, affecting separation of nuclear material in mitosis, or that expression of mutant PRPF31 causes genome instability.

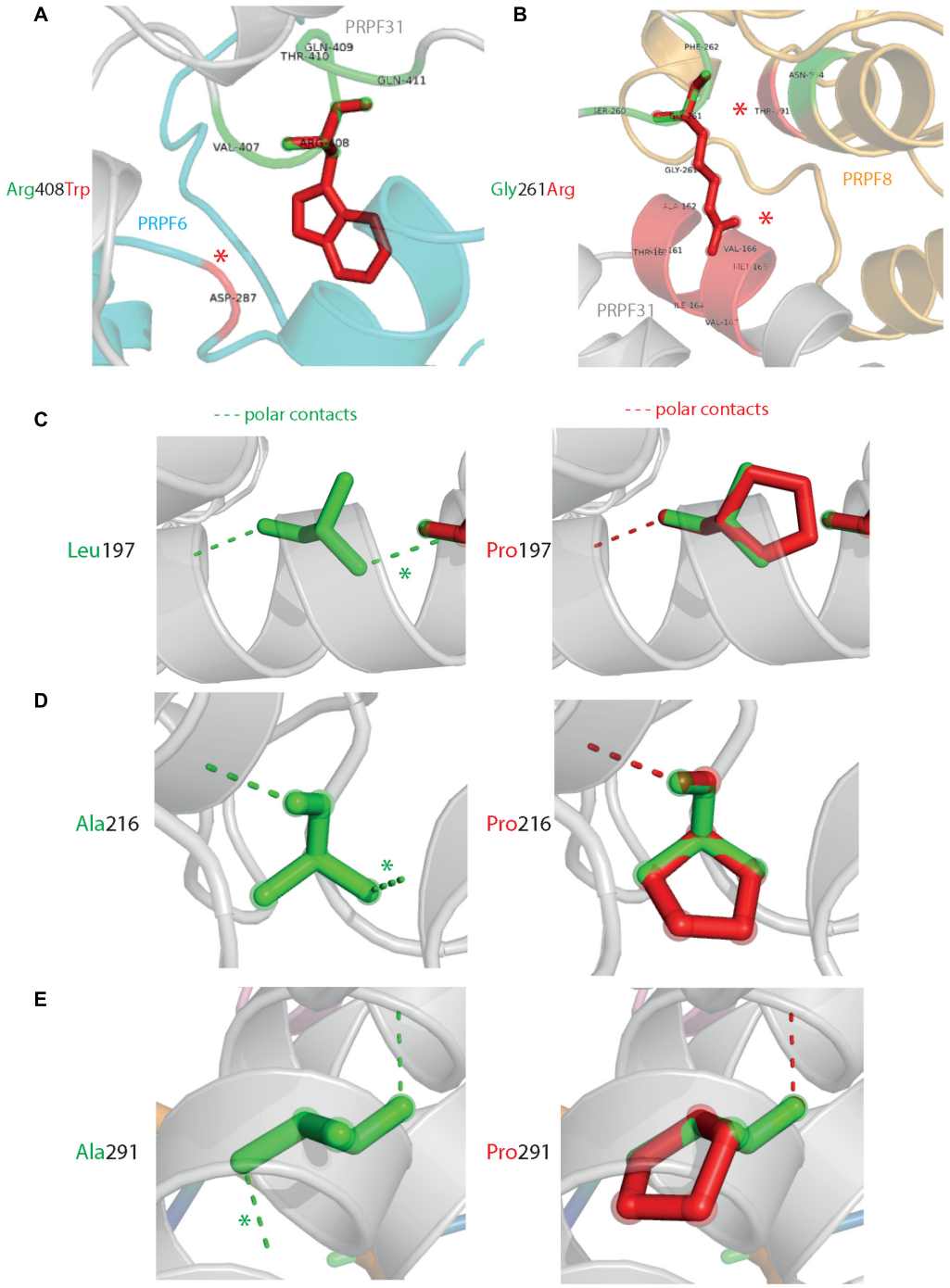

FIGURE 4 | 3D cartoon representation of regions of PRPF31 with published missense mutations and their interactions with other molecules within 4 Å, and their polar contacts. Cartoon representation of alpha helical structure of regions of PRPF31 (gray), with published missense mutations **(A)** Arg408Trp showing how this affects interaction with PRPF6 (blue) and **(B)** Gly261Arg showing how this affects interaction with PRPF8 (orange). Red asterisks are used to label where missense mutations introduce new H bonding. Cartoon representation of alpha helical structure of regions of PRPF31 (gray), with published missense mutations **(C)** Leu197, **(D)** Ala216Pro, and **(E)** Ala291Pro showing effect of these missense mutation on loss of polar contacts within PRPF31. Wild-type amino acid structure is shown in green, and mutant amino acid structure overlaid in red. Green asterisk shows polar contacts which are lost upon missense mutation.

The first hypothesis is consistent with recent findings that PRPF31 localizes to the primary cilium's basal body, which is derived from the centrosome (Wheway et al., 2015). The second hypothesis is consistent with the recent findings that the splicing machinery plays an important role in DNA damage response sensing, in association with the transcription machinery

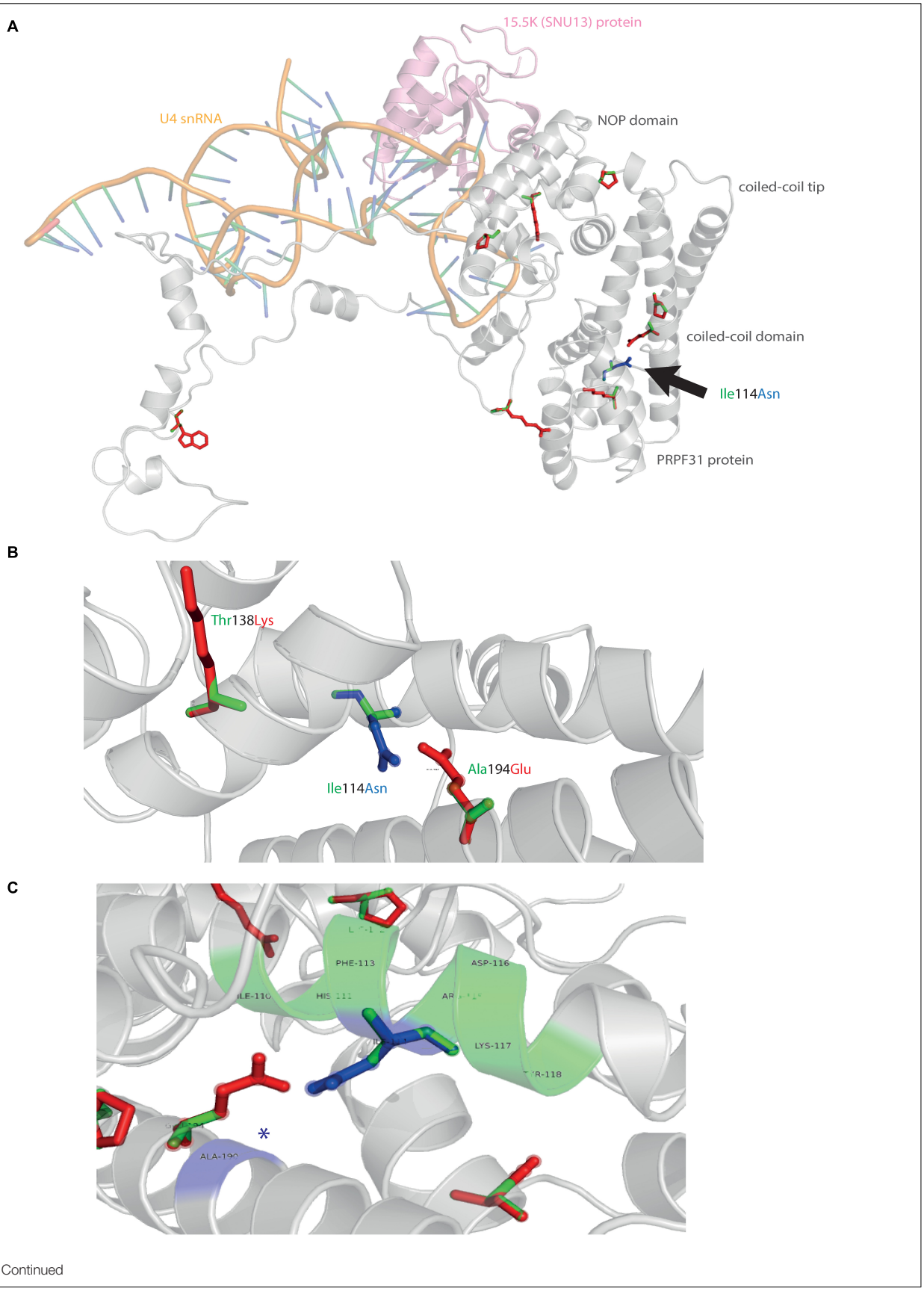

FIGURE 5 | Continued

FIGURE 5 | 3D cartoon representation of PRPF31 and variant Ile114Asn. **(A)** Cartoon representation of alpha helical structure of PRPF31 (gray) and 15.5K/SNU13 (pink) with U4 snRNA (orange backbone), with published missense mutations mapped onto the physical structure, with wild-type amino acid structure in green, and mutant amino acid structure overlaid in red. Ile114Asn (black arrow) is mapped onto the structure with wild-type amino acid structure in green, and mutant amino acid structure overlaid in blue. **(B)** Cartoon representation of alpha helical structure of subregion of PRPF31 (gray), with Ile114Asn, showing proximity to Thr138 and Ala194, both of which are published sites of mutation in RP patients. **(C)** Ile114Asn mapped onto the physical structure of PRPF31 with wild-type amino acid structure in green, and mutant amino acid structure overlaid in blue, and interactions within 4 Å, predicted to affect H bonding within PRPF31. Green regions of the alpha helix denote normal H bonding by Ile114, blue regions of the alpha helix denote novel H bonds of Asn114. Blue asterisks are used to label where missense mutation introduces new H bonding.

(Tresini et al., 2015). This will require further investigation beyond the scope of this project.

In order to investigate whether c.341T > A p.Ile114Asn affected protein stability in a similar way, we transfected HEK293 cells, a human embryonic kidney cell line which is useful for expressing protein at high levels for protein extraction experiments, with plasmids expressing either wild-type PRPF31 or PRPF31 341T > A, both tagged with c-myc epitope tag. We treated the transfected cells with cycloheximide protein translation inhibitor over a time course of 6 h, and assayed protein concentration over this period via western blotting.

Following our usual method for total protein extraction from cells using 1% NP40 detergent, we had difficulty extracting any mutant protein from the transfected cells (**Figure 8A**). This was despite the fact that we could observe protein expression in both cell types via immunofluorescent staining with anti-PRPF31 and anti-cmyc antibodies. We proceeded to repeat the experiment using cell fractionation, to selectively extract protein from the nuclear fraction using 0.1% SDS. This yielded a small amount of mutant protein (**Figure 8B**). Based on our observations, we hypothesized that the mutant protein was in the insoluble nuclear fraction. Once again, we fractionated the cells and lysed the nuclei with 0.1% SDS, but this time we did not remove the insoluble material by centrifugation, instead loading both soluble and insoluble nuclear protein on the gel. This revealed mutant protein, and confirms that the mutant protein is expressed in cells, but is insoluble (**Figure 8C**). No difference in protein stability was observable in the course of cycloheximide treatment (**Figure 8C**). Once we had optimized protein extraction from these cells, we were able to confirm our finding from immunofluorescent imaging that both the WT and mutant protein localized to the nucleus, not the cytoplasm (**Figure 8D**).

In summary, our findings suggest that c.341T > A p.Ile114Asn variant in *PRPF31* results in protein insolubility, with downstream effects on nuclear morphology, and is likely the pathogenic cause of RP in this individual. *In silico* structural analysis of this variant complemented existing techniques for predicting pathogenicity of this variant.

DISCUSSION

PRPF31 is a component of the major and minor spliceosome, the huge macromolecular ribonucleoprotein (RNP) complex which catalyzes the splicing of pre-messenger RNAs (pre-mRNAs) to remove introns and produce mature mRNAs. More than 90% of human genes undergo alternative splicing (Wang et al., 2008), and splicing is a core function of cells, remarkably well conserved from yeast to man. The spliceosome is composed of at least 43 different proteins, and 5 small nuclear RNAs (snRNAs), U1–U5 (Will and Luhrmann, 2011).

PRPF31 is essential for the assembly of the U4/U6.U5 tri-snRNP complex (Makarova et al., 2002), which, when combined with U1 and U2, forms the 'B complex'. After large rearrangements, the activated B complex is able to initiate the first step of splicing. In the absence of PRPF31, U4/U6 di-snRNP accumulates in the splicing-rich Cajal bodies in the nucleus, preventing formation of the tri-snRNP, and subsequently efficient splicing (Schaffert et al., 2004).

PRPF31 performs its function through several important protein domains; the flexible loop, Nop domain, coiled-coil domain and tip. The flexible loop (residues 256–265) protects the exposed C4' atoms of residues 37 and 38 from attack by free radicals, to protect the RNA without directly contacting it (Liu et al., 2007). The Nop domain is a conserved RNP-binding domain, with regions for binding protein and RNA. Although the sequence conservation of the Nop domain is relaxed in PRPF31, its specificity for binding U4 or U4atac and 15.5K protein is high (Liu et al., 2007). The protein also has several phosphorylation sites, clustered in the C-terminus (Liu et al., 2007).

Pathogenic variants in *PRPF31* were discovered as a cause of autosomal dominant RP with incomplete penetrance in 2001 (Vithana et al., 2001). Since then, more than 100 different variants have been reported in *PRPF31* in Human Gene Mutation Database[2], and *PRPF31* has been identified as one of the most common genetic causes of adRP (Lim et al., 2009; Audo et al., 2010; Xu et al., 2012; Sullivan et al., 2013; Daiger et al., 2014; Coussa et al., 2015; Van Cauwenbergh et al., 2017; Martin-Merida et al., 2018). Most of these pathogenic variants are nonsense, frameshift insertions and deletions and large-scale copy number variants, which are easy to clinically characterize. However, the pathogenicity of missense variants in *PRPF31* is much more difficult to predict, and many missense variants in *PRPF31* remain in variant databases such as ClinVar, under the category of 'unknown clinical significance.' This is made difficult by several factors. Firstly, predictions of pathogenicity based on conservation level of specific residues is unreliable in

[2]http://www.hgmd.cf.ac.uk/ac/index.php

TABLE 3 | Summary of *in silico* analysis of missense mutations in PRPF31.

cDNA mutation	Protein mutation	Original reference(s)	Predicted effect on splicing (Human Splicing Finder)	Location in protein	SIFT score	PolyPhen score	Grantham score	Affects H bonding within PRPF31?	Affects H bonding with other proteins?	Affects polar contacts in PRPF31?
c.319C > G	Leu107Val	Rio Frio et al., 2008	IMPACTS SPLICING - confirmed *in vitro*	Coiled coil domain alpha helix 1	0.04 (affects protein function)	0.074 (benign)	32	–	–	–
c.341T > A	Ile114Asn	This paper	No impact on splicing	Coiled coil domain alpha helix 1	0.00 (affects protein function)	0.963	149	Y	N	N
c.413C > A	Thr138Lys	Waseem et al., 2007	Potential alteration of splicing	Coiled coil tip alpha helix 3	0.05 (tolerated)	1	78	Y	N	N
c.581C > A	Ala194Glu	Vithana et al., 2001	Potential alteration of splicing	Coiled coil domain alpha helix 6	0.02 (affects protein function)	1	91	Y	N	N
c.590T > C	Leu197Pro	Bryant et al., 2018	Potential alteration of splicing	Coiled coil domain alpha helix 6	0.00 (affects protein function)	1	98	N	N	Y
c.646G > C	Ala216Pro	Vithana et al., 2001	Potential alteration of splicing	Coiled coil domain alpha helix 6	0.00 (affects protein function)	1	27	N	N	Y
c.781G > C	Gly261Arg	Xiao et al., 2017	No impact on splicing	Flexible loop	0.01 (affects protein function)	0.999	125	Y	Y (PRPF8)	N
c.862C > T	Arg288Trp	Coussa et al., 2015	Potential alteration of splicing	Nop domain alpha helix 12	0.00 (affects protein function)	1	101	Y	N	N
c.871G > C	Ala291Pro	Sullivan et al., 2006	No impact on splicing	Nop domain alpha helix 12	0.09 (tolerated)	1	27	Y	N	Y
c.895T > C	Cys299Arg	Sullivan et al., 2006; Xu et al., 2012; Martin-Merida et al., 2018	No impact on splicing	Nop domain alpha helix 12	0.00 (affects protein function)	1	180	Y	N	N
c.896G > A	Cys299Tyr	Bhatia et al., 2018	Potential alteration of splicing	Nop domain alpha helix 12	0.00 (affects protein function)	0.997	194	Y	N	N
c.1222C > T	Arg408Trp	Xiao et al., 2017	Potential alteration of splicing	C-terminal domain	0.00 (affects protein function). Low confidence prediction	1	101	N	Y (PRPF6)	N
c.1373A > T	Gln458Leu	Xiao et al., 2017	Most probably affecting splicing	C-terminal domain	0.00 (affects protein function). Low confidence prediction	0.931 (possibly damaging)	113	–	–	–

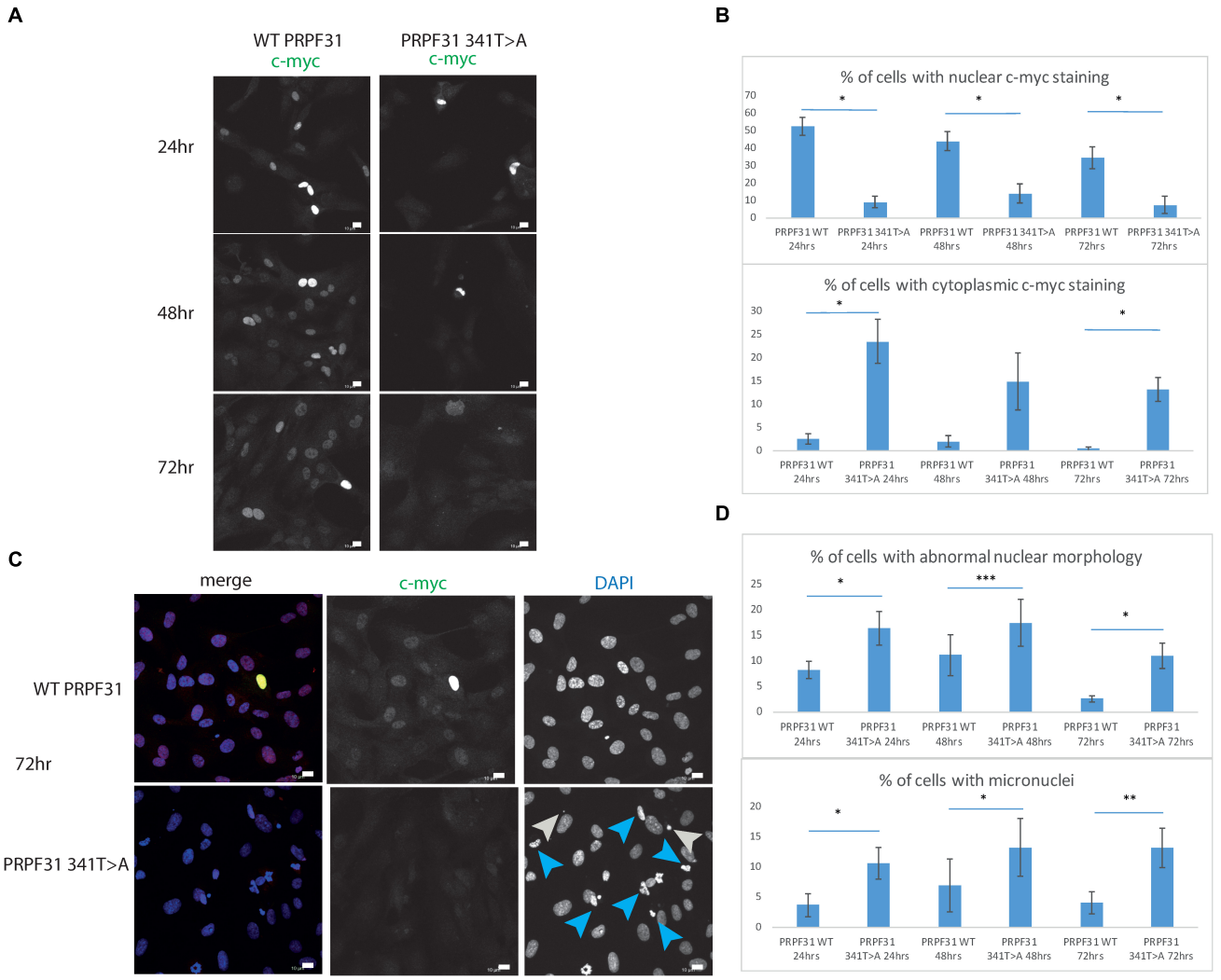

FIGURE 6 | *In vitro* characterization of *PRPF31* c.341T > A Ile114Asn variant in hTERT-RPE1 cells. **(A)** Immunofluorescence confocal images of RPE1 cells transfected with c-myc-tagged wild-type or mutant PRPF31, showing expression and localization of PRPF31-cmyc over 24, 48, and 72 h. c-myc PRPF31 is evenly distributed throughout the nuclei of cells transfected with WT plasmid at each time point, but is concentrated in the nuclei of a few cells in RPE cells transfected with the mutant plasmid, with some cytoplasmic staining. Scale bars = 10 μm. **(B)** Graphs and statistical significance of proportions of cells with nuclear and cytoplasmic c-myc staining after transfection with WT and 341T > A mutant PRPF31. *$p < 0.05$, $n = 4$. Error bars show standard error of the mean. **(C)** At 72 h, nuclei staining shows many micronuclei (gray arrows) and nuclei with abnormal morphology (blue arrows) in the cells transfected with mutant PRPF31. Scale bars = 10 μm. **(D)** Graphs and statistical significance of proportions of cells with abnormal nuclei morphology and micronuclei. *$p < 0.05$, **$p < 0.01$, ***$p < 0.001$, $n = 4$.

PRPF31. Whilst PRPF31 is a highly conserved protein, even the most important functional domains in the PRPF31 show relaxed sequence conservation whilst still maintaining high specificity for protein interactions (Liu et al., 2007). Indeed, several pathogenic missense variants in PRPF31 are at residues which are not highly conserved, such as Ala194Glu, and Ala291Pro which is predicted to be tolerated by SIFT (**Table 3**). Thus, conservation of 2D protein structure (i.e., amino acid sequence), which is the basis for the tool SIFT, may not be an accurate predictor of pathogenicity of missense variants in this protein. Our study illustrates the importance and utility of using *in silico* 3D spliceosome protein complex analysis (Bertram et al., 2017) for predicting novel pathogenic missense variants in PRPF31. 3D complex analysis is particularly useful in the case of PRPF31, in which 2D conservation is a poor predictor of pathogenicity, and which has been resolved in complex in high resolution. It is important to note that the spliceosome is a highly dynamic structure, and our 3D structural complex analysis only studies PRPF31 in one specific conformation, in the spliceosome primed for splicing (Bertram et al., 2017). For truly accurate predictions of pathogenicity, the 3D structure of the spliceosome at different stages of activity will need to be studied, preferably using Molecular dynamic simulation (MDS) with a package such as GROMACS (Berendsen et al., 1995) to provide deepest insights into effects of missense mutations. The publication of

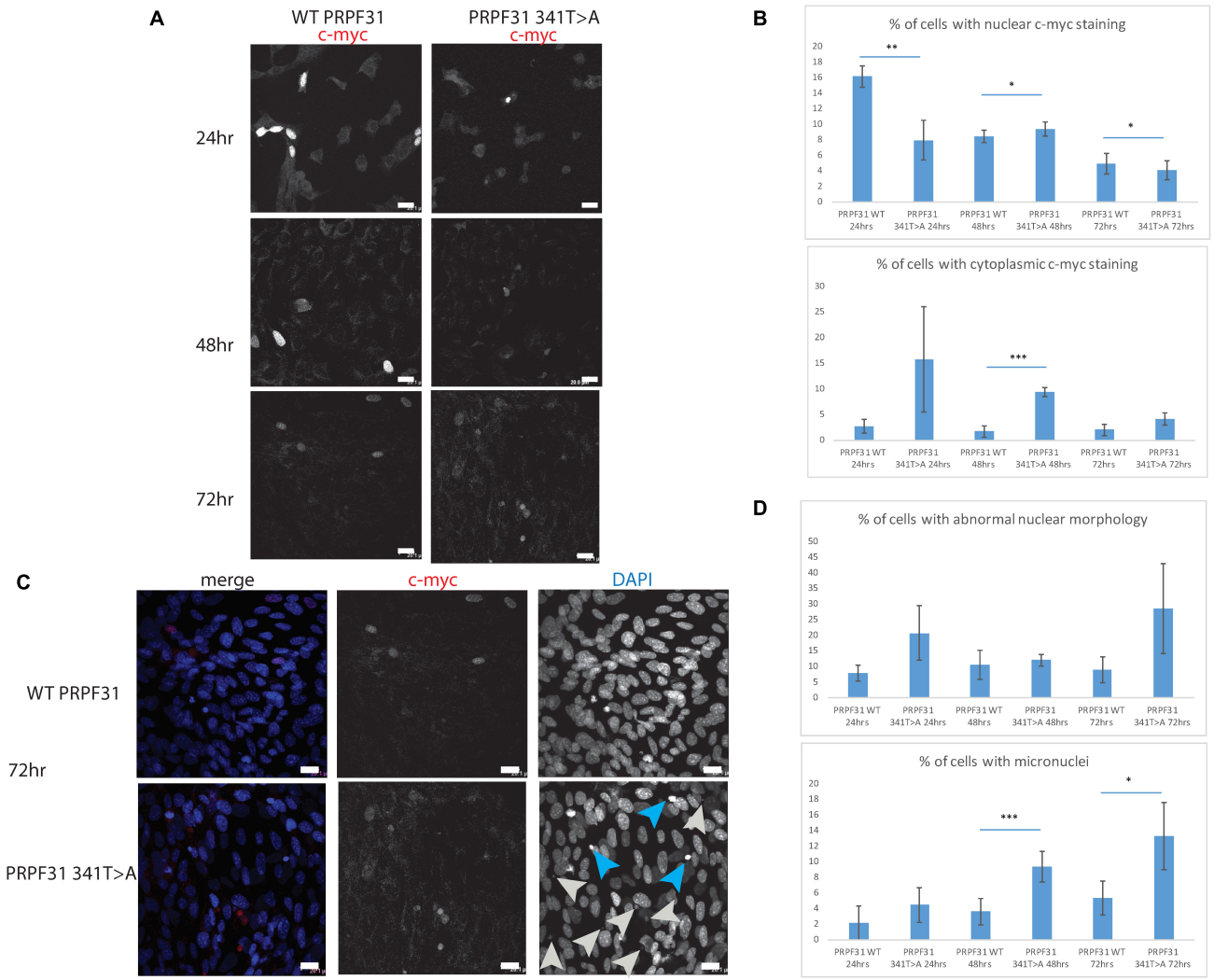

FIGURE 7 | *In vitro* characterisation of *PRPF31* c.341T > A Ile114Asn variant in 661W photoreceptor-like cells. **(A)** Immunofluorescence confocal images of 661W photoreceptor-like cells transfected with c-myc-tagged wild-type or mutant PRPF31, showing expression and localization of PRPF31-cmyc over 24, 48, and 72 h. c-myc PRPF31 is evenly distributed throughout the nuclei of cells transfected with WT plasmid at each time point, but is concentrated in the nuclei of a few cells in 661W cells transfected with the mutant plasmid, with some cytoplasmic staining. Scale bars = 20 μm. **(B)** Graphs and statistical significance of proportions of cells with nuclear and cytoplasmic c-myc staining after transfection with WT and 341T > A mutant PRPF31. $*p < 0.05$, $**p < 0.01$, $***p < 0.001$, $n = 3$. Error bars show standard error of the mean. **(C)** At 72 h, nuclear staining shows many micronuclei (gray arrows) and nuclei with abnormal morphology (blue arrows) in the cells transfected with mutant PRPF31. Scale bars = 20 μm. **(D)** Graphs and statistical significance of proportions of cells with abnormal nuclei morphology and micronuclei. $*p < 0.05$, $***p < 0.001$, $n = 3$.

more cryo-EM resolved complexes relevant to development of ciliopathies, such as the intraflagellar transport (IFT) complexes (Jordan et al., 2018) will further enhance our understanding of such conditions, and allow more accurate computational prediction of pathogenicity of variants.

Assessments of pathogenicity of variants in PRPF31 are also limited by the fact that only three missense variants in PRPF31 have been characterized in *in vitro* studies; Ala194Glu and Ala216Pro (Deery et al., 2002) and more recently Leu197Pro (Bryant et al., 2018), meaning that there is little confidence in ascribing pathogenic status to variants outside this region. Earlier studies described these residues as being contained within the Nop domain (Deery et al., 2002), leading to conclusions that variants in the Nop domain are more likely to be pathogenic, but recent studies suggest that this is not accurate. Resolution of the crystal structure of PRPF31 has shown that these variants are in alpha helix 6 of the coiled-coil domain, rather than the Nop domain (Liu et al., 2007). Published missense variants are found throughout the protein, and our study illustrates that missense changes toward the N-terminal of the protein are also pathogenic.

We suggest that all rare missense variants in PRPF31 should be considered as potentially pathogenic, irrespective of their

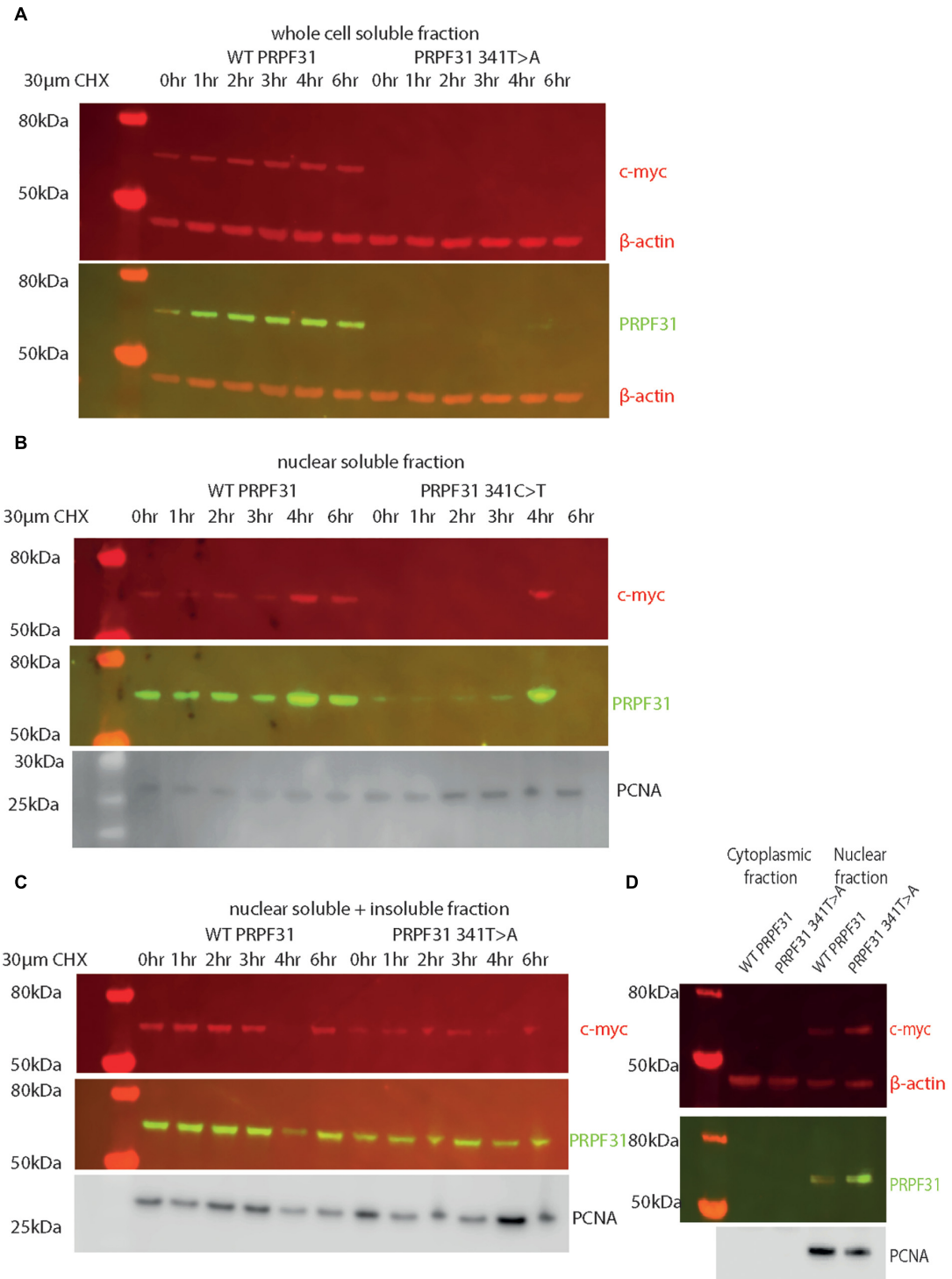

FIGURE 8 | Western blots of protein extracted from HEK293 cells transfected with wild-type or c.341T > A PRPF31 tagged with c-myc. **(A)** Cells treated with 30 µM cycloheximide (CHX) over 6 h, and soluble protein extracted from the whole cell showed stable levels of wild-type protein expression across the time course, and complete absence of mutant protein in the soluble whole cell fraction. β-actin is cytoplasmic loading control. **(B)** Cells treated with 30 µM cycloheximide (CHX) over 6 h, and soluble protein extracted from the nucleus showed stable levels of wild-type protein expression across the time course, and extremely low levels of mutant protein in the soluble nuclear fraction, except where some insoluble protein was accidentally loaded (4 h). β-actin is cytoplasmic loading control. PCNA is nuclear loading control. **(C)** Cells treated with 30 µM cycloheximide (CHX) over 6 h, and both soluble and insoluble protein extracted nucleus showed similar levels of wild-type and mutant protein expression and stability. PCNA is nuclear loading control marker. **(D)** Fractionation shows that both mutant and wild-type PRPF31 are localized to the nucleus. β-actin is cytoplasmic loading control, PCNA is nuclear loading control.

location within the protein. Constraint metrics, which provide quantitative measures of the extent to which a gene can tolerate change, indicate that *PRPF31* gene as a whole has an extremely low tolerance to missense variants (Z = 3.27) (Lek et al., 2016). *PRPF31* is particularly intolerant to missense changes even when compared to the other most common causes of adRP; *RPGR*, (Z = 1.51) and *Rho* (Z = 0.33). Despite the fact that Rho is more tolerant to missense changes, nearly all reported pathogenic changes in Rho are missense changes. This suggests that missense variants in PRPF31 are likely to be pathogenic even in residues with poor conservation, low Grantham score, or low PolyPhen/SIFT scores, if they are observed at low frequency in population variant databases. However, it is important to bear in mind incomplete penetrance associated with PRPF31, so presence of variant alleles in control population databases should not exclude particular variants as a cause of disease.

As well as providing data which can aid interpretation of *PRPF31* genetic findings in patients, our study provides deeper insights into the cell biology associated with pathogenic PRPF31 variants. Consistent with previous studies of Ala194Glu variant PRPF31 (Deery et al., 2002), we show that Ile114Asn variant PRPF31 does not prevent translocation of PRPF31 to the nucleus, but reduces the solubility of the protein in the nucleus. We hypothesize that this prevents normal PRPF31 protein function, effectively removing one copy of the protein from cells. This supports previous suggestions that haploinsufficiency is the common disease mechanism in RP11 rather than any dominant negative effects of missense variants (Abu-Safieh et al., 2006; Sullivan et al., 2006; Wilkie et al., 2008). Our novel observation that expression of mutant PRPF31 in cells results in abnormal nuclei supports a growing body of evidence that pre-mRNA splicing factors have multiple roles beyond splicing, including in cilia function and DNA damage sensing. It will be important to investigate this further, as it may offer novel insights into why variants in pre-mRNA splicing factors lead to retinal degeneration.

In summary, we highlight the potential pathogenicity of missense variants in PRPF31, irrespective of their location in the protein. We show the power of a combined approach to variant classification which considers clinical information, *in silico* modeling of 3D protein complex structure and *in vitro* studies for this protein. A combined approach is required to characterize the effect of missense variants in this protein which is both highly conserved, yet has regions of functional importance but surprising relaxation of conservation. We advise caution in disregarding missense variants in PRPF31 as unlikely to be pathogenic, particularly if those conclusions are based upon lack of sequence conservation. We suggest it is more important to study the effect of a missense variant on 3D protein structure rather than 2D amino acid sequence. We provide novel insights into the effect of missense variants in PRPF31 on retinal cell biology; we confirm previous findings that missense variants reduce solubility but find no evidence that leads to apoptosis of cells in the first 72 h of expression, in contrast to previously published data. We observe novel changes in nuclear morphology as a result of PRPF31 mutation which have not been reported previously, and warrant further investigation.

Considerable further work is required to elucidate why haploinsufficiency of PRPF31 causes retinal cells to degenerate, whether specific or global pre-mRNA splicing is affected, and why other tissues outside the retina are not affected by loss of protein.

DATA AVAILABILITY

All datasets generated for this study are included in the manuscript and/or the **Supplementary Files**.

AUTHOR CONTRIBUTIONS

GW and AC conceived of and designed the study. NM, SH, NJ, and AC examined the patient, coordinated genetic testing, and analyzed patient genetic data. GW and LN carried out *in silico* and *in vitro* experiments. GW, LN, NM, and AC prepared figures. GW and AC wrote the manuscript. SH reviewed the manuscript.

FUNDING

LN and GW are supported by National Eye Research Centre Small Award SAC019, Wellcome Trust Seed Award in Science 204378/Z/16/Z, and UWE Bristol Quality Research funds.

SUPPLEMENTARY MATERIAL

The Supplementary Material for this article can be found online at: https://www.frontiersin.org/articles/10.3389/fgene.2019.00248/full#supplementary-material

FIGURE S1 | 3D cartoon representation of PRPF31, including published missense mutations, in complex with U4 snRNA, 15.5K and PRPF6. **(A)** Cartoon representation of alpha helical structure of PRPF31 (gray) and 15.5K/SNU13 (pink) with U4 snRNA (dark orange backbone), and PRPF6 (blue) with published missense mutations mapped onto the physical structure, with wild-type amino acid structure in green, and mutant amino acid structure overlaid in red. This shows that only Arg408Trp is in interacting proximity with PRPF6. **(B)** An alternative view of the same complex, highlighting that variants in the NOP domain (black arrow) and coiled-coil domain do not appear to interact with PRPF6 in this conformation.

FIGURE S2 | 3D cartoon representation of PRPF31, including published missense mutations, in complex with U4 snRNA, 15.5K, PRPF6 and PRPF8. **(A)** Cartoon representation of alpha helical structure of PRPF31 (gray) and 15.5K/SNU13 (pink) with U4 snRNA (dark orange backbone), PRPF6 (blue), and PRPF8 (light orange) with published missense mutations mapped onto the physical structure, with wild-type amino acid structure in green, and mutant amino acid structure overlaid in red. This shows that only Gly261Arg is in interacting proximity with PRPF8. **(B)** An alternative view of the same complex, highlighting that only this Gly261Arg variant (black arrow) appears to interact with PRPF8 in this conformation.

FIGURE S3 | *In vitro* characterization of *PRPF31* c.581C > A Ala194Glu variant in hTERT-RPE1 cells. Immunofluorescence confocal images of RPE1 cells transfected with c-myc-tagged 581C > A mutant PRPF31, showing expression and localization of PRPF31-cmyc over 24, 48, and 72 h. c-myc PRPF31 is intensely expressed in the nuclei of cells transfected with the mutant plasmid at 24 h, and this becomes restricted to micronuclei and abnormal nuclei over time. A number of micronuclei and abnormal nuclei can be seen at each time point, most noticeably at 72 h (blue and gray arrows). Scale bars = 20 μm.

REFERENCES

Abu-Safieh, L., Vithana, E. N., Mantel, I., Holder, G. E., Pelosini, L., Bird, A. C., et al. (2006). A large deletion in the adRP gene PRPF31: evidence that haploinsufficiency is the cause of disease. *Mol. Vis.* 12, 384–388.

Adzhubei, I. A., Schmidt, S., Peshkin, L., Ramensky, V. E., Gerasimova, A., Bork, P., et al. (2010). A method and server for predicting damaging missense mutations. *Nat. Methods* 7, 248–249. doi: 10.1038/nmeth0410-248

Audo, I., Bujakowska, K., Mohand-Said, S., Lancelot, M. E., Moskova-Doumanova, V., Waseem, N. H., et al. (2010). Prevalence and novelty of PRPF31 mutations in french autosomal dominant rod-cone dystrophy patients and a review of published reports. *BMC Med. Genet.* 11:145. doi: 10.1186/1471-2350-11-145

Berendsen, H. J. C., van der Spoel, D., and van Drunen, R. (1995). GROMACS: a message-passing parallel molecular dynamics implementation. *Comp. Phys. Commun.* 91, 43–56. doi: 10.1016/0010-4655(95)00042-E

Bertram, K., Agafonov, D. E., Dybkov, O., Haselbach, D., Leelaram, M. N., Will, C. L., et al. (2017). Cryo-EM structure of a pre-catalytic human spliceosome primed for activation. *Cell* 170, 701.e11–713.e11. doi: 10.1016/j.cell.2017.07.011

Bhatia, S., Goyal, S., Singh, I. R., Singh, D., and Vanita, V. (2018). A novel mutation in the *PRPF31* in a North Indian adRP family with incomplete penetrance. *Doc. Ophthalmol.* 137, 103–119. doi: 10.1007/s10633-018-9654-x

Bryant, L., Lozynska, O., Marsh, A., Papp, T. E., van Gorder, L., Serrano, L. W., et al. (2018). Identification of a novel pathogenic missense mutation in *PRPF31* using whole exome sequencing: a case report. *Br. J. Ophthalmol.* doi: 10.1136/bjophthalmol-2017-311405

Cooper, G. M., and Shendure, J. (2011). Needles in stacks of needles: finding disease-causal variants in a wealth of genomic data. *Nat. Rev. Genet.* 12, 628–640. doi: 10.1038/nrg3046

Coussa, R. G., Chakarova, C., Ajlan, R., Taha, M., Kavalec, C., Gomolin, J., et al. (2015). Genotype and phenotype studies in autosomal dominant retinitis pigmentosa (adrp) of the french canadian founder population. *Invest. Ophthalmol. Vis. Sci.* 56, 8297–8305. doi: 10.1167/iovs.15-17104

Daiger, S. P., Bowne, S. J., and Sullivan, L. S. (2014). Genes and mutations causing autosomal dominant retinitis pigmentosa. *Cold Spring Harb. Perspect. Med.* 5:a017129. doi: 10.1101/cshperspect.a017129

Deery, E. C., Vithana, E. N., Newbold, R. J., Gallon, V. A., Bhattacharya, S. S., Warren, M. J., et al. (2002). Disease mechanism for retinitis pigmentosa (RP11) caused by mutations in the splicing factor gene PRPF31. *Hum. Mol. Genet.* 11, 3209–3219. doi: 10.1093/hmg/11.25.3209

Desmet, F. O., Hamroun, D., Lalande, M., Collod-Beroud, G., Claustres, M., and Beroud, C. (2009). Human splicing finder: an online bioinformatics tool to predict splicing signals. *Nucleic Acids Res.* 37:e67. doi: 10.1093/nar/gkp215

Gnad, F., Baucom, A., Mukhyala, K., Manning, G., and Zhang, Z. (2013). Assessment of computational methods for predicting the effects of missense mutations in human cancers. *BMC Genomics* 14(Suppl. 3):S7. doi: 10.1186/1471-2164-14-S3-S7

Golovleva, I., Kohn, L., Burstedt, M., Daiger, S., and Sandgren, O. (2010). Mutation spectra in autosomal dominant and recessive retinitis pigmentosa in northern sweden. *Adv. Exp. Med. Biol.* 664, 255–262. doi: 10.1007/978-1-4419-1399-9-29

Gonzalez-Perez, A., and Lopez-Bigas, N. (2011). Improving the assessment of the outcome of nonsynonymous SNVs with a consensus deleteriousness score, condel. *Am. J. Hum. Genet.* 88, 440–449. doi: 10.1016/j.ajhg.2011.03.004

Greenberg, J., Bartmann, L., Ramesar, R., and Beighton, P. (1993). Retinitis pigmentosa in southern africa. *Clin. Genet.* 44, 232–235. doi: 10.1111/j.1399-0004.1993.tb03888.x

Haim, M. (1993). Retinitis pigmentosa: problems associated with genetic classification. *Clin. Genet.* 44, 62–70. doi: 10.1111/j.1399-0004.1993.tb03848.x

Hartong, D. T., Berson, E. L., and Dryja, T. P. (2006). Retinitis pigmentosa. *Lancet* 368, 1795–1809. doi: 10.1016/S0140-6736(06)69740-7

Jeffrey, G. A. (1997). *An Introduction to Hydrogen Bonding*. Oxford: Oxford University Press.

Jin, Z. B., Mandai, M., Yokota, T., Higuchi, K., Ohmori, K., Ohtsuki, F., et al. (2008). Identifying pathogenic genetic background of simplex or multiplex retinitis pigmentosa patients: a large scale mutation screening study. *J. Med. Genet.* 45, 465–472. doi: 10.1136/jmg.2007.056416

Jordan, M. A., Diener, D. R., Stepanek, L., and Pigino, G. (2018). The cryo-EM structure of intraflagellar transport trains reveals how dynein is inactivated to ensure unidirectional anterograde movement in cilia. *Nat. Cell Biol.* 20, 1250–1255. doi: 10.1038/s41556-018-0213-1

Kircher, M., Witten, D. M., Jain, P., O'Roak, B. J., Cooper, G. M., and Shendure, J. (2014). A general framework for estimating the relative pathogenicity of human genetic variants. *Nat. Genet.* 46, 310–315. doi: 10.1038/ng.2892

Landrum, M. J., Lee, J. M., Benson, M., Brown, G., Chao, C., Chitipiralla, S., et al. (2016). ClinVar: public archive of interpretations of clinically relevant variants. *Nucleic Acids Res.* 44, D862–D868. doi: 10.1093/nar/gkv1222

Landrum, M. J., Lee, J. M., Riley, G. R., Jang, W., Rubinstein, W. S., Church, D. M., et al. (2014). ClinVar: public archive of relationships among sequence variation and human phenotype. *Nucleic Acids Res.* 42, D980–D985. doi: 10.1093/nar/gkt1113

Lek, M., Karczewski, K. J., Minikel, E. V., Samocha, K. E., Banks, E., Fennell, T., et al. (2016). Analysis of protein-coding genetic variation in 60,706 humans. *Nature* 536, 285–291. doi: 10.1038/nature19057

Li, W. H., Wu, C. I., and Luo, C. C. (1984). Nonrandomness of point mutation as reflected in nucleotide substitutions in pseudogenes and its evolutionary implications. *J. Mol. Evol.* 21, 58–71. doi: 10.1007/BF02100628

Lim, K. P., Yip, S. P., Cheung, S. C., Leung, K. W., Lam, S. T., and To, C. H. (2009). Novel PRPF31 and PRPH2 mutations and co-occurrence of PRPF31 and RHO mutations in chinese patients with retinitis pigmentosa. *Arch. Ophthalmol.* 127, 784–790. doi: 10.1001/archophthalmol.2009.112

Liu, S., Li, P., Dybkov, O., Nottrott, S., Hartmuth, K., Luhrmann, R., et al. (2007). Binding of the human Prp31 Nop domain to a composite RNA-protein platform in U4 snRNP. *Science* 316, 115–120. doi: 10.1126/science.1137924

Makarova, O. V., Makarov, E. M., Liu, S., Vornlocher, H. P., and Luhrmann, R. (2002). Protein 61K, encoded by a gene (PRPF31) linked to autosomal dominant retinitis pigmentosa, is required for U4/U6*U5 tri-snRNP formation and pre-mRNA splicing. *EMBO J.* 21, 1148–1157. doi: 10.1093/emboj/21.5.1148

Martin-Merida, I., Aguilera-Garcia, D., Fernandez-San Jose, P., Blanco-Kelly, F., Zurita, O., Almoguera, B., et al. (2018). Toward the mutational landscape of autosomal dominant retinitis pigmentosa: a comprehensive analysis of 258 spanish families. *Invest. Ophthalmol. Vis. Sci.* 59, 2345–2354. doi: 10.1167/iovs.18-23854

Miosge, L. A., Field, M. A., Sontani, Y., Cho, V., Johnson, S., Palkova, A., et al. (2015). Comparison of predicted and actual consequences of missense mutations. *Proc. Natl. Acad. Sci. U.S.A.* 112, E5189–E5198. doi: 10.1073/pnas.1511585112

Mockel, A., Perdomo, Y., Stutzmann, F., Letsch, J., Marion, V., and Dollfus, H. (2011). Retinal dystrophy in Bardet-Biedl syndrome and related syndromic ciliopathies. *Prog. Retin. Eye Res.* 30, 258–274. doi: 10.1016/j.preteyeres.2011.03.001

Mordes, D., Yuan, L., Xu, L., Kawada, M., Molday, R. S., and Wu, J. Y. (2007). Identification of photoreceptor genes affected by PRPF31 mutations associated with autosomal dominant retinitis pigmentosa. *Neurobiol. Dis.* 26, 291–300. doi: 10.1016/j.nbd.2006.08.026

Najera, C., Millan, J. M., Beneyto, M., and Prieto, F. (1995). Epidemiology of retinitis pigmentosa in the valencian community (Spain). *Genet. Epidemiol.* 12, 37–46. doi: 10.1002/gepi.1370120105

Rio Frio, T., Wade, N. M., Ransijn, A., Berson, E. L., Beckmann, J. S., and Rivolta, C. (2008). Premature termination codons in PRPF31 cause retinitis pigmentosa via haploinsufficiency due to nonsense-mediated mRNA decay. *J. Clin. Invest.* 118, 1519–1531. doi: 10.1172/JCI34211

Rivolta, C., McGee, T. L., Rio Frio, T., Jensen, R. V., Berson, E. L., and Dryja, T. P. (2006). Variation in retinitis pigmentosa-11 (PRPF31 or RP11) gene expression between symptomatic and asymptomatic patients with dominant RP11 mutations. *Hum. Mutat.* 27, 644–653. doi: 10.1002/humu.20325

Ruzickova, S., and Stanek, D. (2016). Mutations in spliceosomal proteins and retina degeneration. *RNA Biol.* 14, 544–552. doi: 10.1080/15476286.2016.1191735

Schaffert, N., Hossbach, M., Heintzmann, R., Achsel, T., and Luhrmann, R. (2004). RNAi knockdown of hPrp31 leads to an accumulation of U4/U6 di-snRNPs in Cajal bodies. *EMBO J.* 23, 3000–3009. doi: 10.1038/sj.emboj.7600296

Sharon, D., and Banin, E. (2015). Nonsyndromic retinitis pigmentosa is highly prevalent in the jerusalem region with a high frequency of founder mutations. *Mol. Vis.* 21, 783–792.

Sullivan, L. S., Bowne, S. J., Birch, D. G., Hughbanks-Wheaton, D., Heckenlively, J. R., Lewis, R. A., et al. (2006). Prevalence of disease-causing mutations in families with autosomal dominant retinitis pigmentosa: a screen of known genes in 200 families. *Invest. Ophthalmol. Vis. Sci.* 47, 3052–3064. doi: 10.1167/iovs.05-1443

Sullivan, L. S., Bowne, S. J., Reeves, M. J., Blain, D., Goetz, K., Ndifor, V., et al. (2013). Prevalence of mutations in eyeGENE probands with a diagnosis of autosomal dominant retinitis pigmentosa. *Invest. Ophthalmol. Vis. Sci.* 54, 6255–6261. doi: 10.1167/iovs.13-12605

Tan, E., Ding, X. Q., Saadi, A., Agarwal, N., Naash, M. I., and Al-Ubaidi, M. R. (2004). Expression of cone-photoreceptor-specific antigens in a cell line derived from retinal tumors in transgenic mice. *Invest. Ophthalmol. Vis. Sci.* 45, 764–768. doi: 10.1167/iovs.03-1114

Tresini, M. D., Warmerdam, O., Kolovos, P., Snijder, L., and Vrouwe, M. G. (2015). The core spliceosome as target and effector of non-canonical ATM signalling. *Nature* 523, 53–58. doi: 10.1038/nature14512

Van Cauwenbergh, C., Coppieters, F., Roels, D., De Jaegere, S., Flipts, H., De Zaeytijd, J., et al. (2017). Mutations in splicing factor genes are a major cause of autosomal dominant retinitis pigmentosa in belgian families. *PLoS One* 12:e0170038. doi: 10.1371/journal.pone.0170038

Verbakel, S. K., van Huet, R. A. C., Boon, C. J. F., den Hollander, A. I., Collin, R. W. J., Klaver, C. C. W., et al. (2018). Non-syndromic retinitis pigmentosa. *Prog. Retin. Eye Res.* 66, 157–186. doi: 10.1016/j.preteyeres.2018.03.005

Vithana, E. N., Abu-Safieh, L., Allen, M. J., Carey, A., Papaioannou, M., Chakarova, C., et al. (2001). A human homolog of yeast pre-mRNA splicing gene, *PRP31*, underlies autosomal dominant retinitis pigmentosa on chromosome 19q13.4 (*RP11*). *Mol. Cell.* 8, 375–381. doi: 10.1016/S1097-2765(01)00305-7

Wang, E. T., Sandberg, R., Luo, S., Khrebtukova, I., Zhang, L., Mayr, C., et al. (2008). Alternative isoform regulation in human tissue transcriptomes. *Nature* 456, 470–476. doi: 10.1038/nature07509

Waseem, N. H., Vaclavik, V., Webster, A., Jenkins, S. A., Bird, A. C., and Bhattacharya, S. S. (2007). Mutations in the gene coding for the pre-mRNA splicing factor, *PRPF31*, in patients with autosomal dominant retinitis pigmentosa. *Invest. Ophthalmol. Vis. Sci.* 48, 1330–1334. doi: 10.1167/iovs.06-0963

Wheway, G., Schmidts, M., Mans, D. A., Szymanska, K., Nguyen, T. M., Racher, H., et al. (2015). An siRNA-based functional genomics screen for the identification of regulators of ciliogenesis and ciliopathy genes. *Nat. Cell Biol.* 17, 1074–1087. doi: 10.1038/ncb3201

Wilkie, S. E., Vaclavik, V., Wu, H., Bujakowska, K., Chakarova, C. F., Bhattacharya, S. S., et al. (2008). Disease mechanism for retinitis pigmentosa (RP11) caused by missense mutations in the splicing factor gene PRPF31. *Mol. Vis.* 14, 683–690.

Will, C. L., and Luhrmann, R. (2011). Spliceosome structure and function. *Cold Spring Harb. Perspect. Biol.* 3:a003707. doi: 10.1101/cshperspect.a003707

Xiao, X., Cao, Y., Zhang, Z., Xu, Y., Zheng, Y., Chen, L. J., et al. (2017). Novel mutations in PRPF31 causing retinitis pigmentosa identified using whole-exome sequencing. *Invest. Ophthalmol. Vis. Sci.* 58, 6342–6350. doi: 10.1167/iovs.17-22952

Xu, F., Sui, R., Liang, X., Li, H., Jiang, R., and Dong, F. (2012). Novel PRPF31 mutations associated with chinese autosomal dominant retinitis pigmentosa patients. *Mol. Vis.* 18, 3021–3028.

Yuan, L., Kawada, M., Havlioglu, N., Tang, H., and Wu, J. Y. (2005). Mutations in PRPF31 inhibit pre-mRNA splicing of rhodopsin gene and cause apoptosis of retinal cells. *J. Neurosci.* 25, 748–757. doi: 10.1523/JNEUROSCI.2399-04.2005

Zhang, Q., Xu, M., Verriotto, J. D., Li, Y., Wang, H., Gan, L., et al. (2016). Next-generation sequencing-based molecular diagnosis of 35 Hispanic retinitis pigmentosa probands. *Sci. Rep.* 6:32792. doi: 10.1038/srep32792

Conflict of Interest Statement: The authors declare that the research was conducted in the absence of any commercial or financial relationships that could be construed as a potential conflict of interest.

frontiers in Genetics

ORIGINAL RESEARCH
published: 05 April 2019
doi: 10.3389/fgene.2019.00308

661W Photoreceptor Cell Line as a Cell Model for Studying Retinal Ciliopathies

Gabrielle Wheway[1,2,3], Liliya Nazlamova[1,2,3], Dann Turner[1] and Stephen Cross[4]*

[1] Centre for Research in Biosciences, University of the West of England, Bristol, Bristol, United Kingdom, [2] Human Development and Health, Faculty of Medicine, University of Southampton, Southampton, United Kingdom, [3] Human Development and Health, Southampton General Hospital, Southampton, United Kingdom, [4] Wolfson Bioimaging Facility, University of Bristol, Bristol, United Kingdom

The retina contains several ciliated cell types, including the retinal pigment epithelium (RPE) and photoreceptor cells. The photoreceptor cilium is one of the most highly modified sensory cilia in the human body. The outer segment of the photoreceptor is a highly elaborate primary cilium, containing stacks or folds of membrane where the photopigment molecules are located. Perhaps unsurprisingly, defects in cilia often lead to retinal phenotypes, either as part of syndromic conditions involving other organs, or in isolation in the so-called retinal ciliopathies. The study of retinal ciliopathies has been limited by a lack of retinal cell lines. RPE1 retinal pigment epithelial cell line is commonly used in such studies, but the existence of a photoreceptor cell line has largely been neglected in the retinal ciliopathy field. 661W cone photoreceptor cells, derived from mouse, have been widely used as a model for studying macular degeneration, but not described as a model for studying retinal ciliopathies such as retinitis pigmentosa. Here, we characterize the 661W cell line as a model for studying retinal ciliopathies. We fully characterize the expression profile of these cells, using whole transcriptome RNA sequencing, and provide this data on Gene Expression Omnibus for the advantage of the scientific community. We show that these cells express the majority of markers of cone cell origin. Using immunostaining and confocal microscopy, alongside scanning electron microscopy, we show that these cells grow long primary cilia, reminiscent of photoreceptor outer segments, and localize many cilium proteins to the axoneme, membrane and transition zone. We show that siRNA knockdown of cilia genes Ift88 results in loss of cilia, and that this can be assayed by high-throughput screening. We present evidence that the 661W cell line is a useful cell model for studying retinal ciliopathies.

Keywords: retina, photoreceptor, cilia, ciliopathy, cell model, retinitis pigmentosa

OPEN ACCESS

Edited by:
Carlo Iomini, Icahn School of Medicine at Mount Sinai, United States

Reviewed by:
Bo Chen, Icahn School of Medicine at Mount Sinai, United States
Hemant Khanna, University of Massachusetts Medical School, United States

****Correspondence:***
Gabrielle Wheway
G.wheway@soton.ac.uk

Specialty section:
This article was submitted to Genetic Disorders, a section of the journal Frontiers in Genetics

Received: *29 August 2018*
Accepted: *21 March 2019*
Published: *05 April 2019*

Citation:
Wheway G, Nazlamova L, Turner D and Cross S (2019) 661W Photoreceptor Cell Line as a Cell Model for Studying Retinal Ciliopathies. Front. Genet. 10:308. doi: 10.3389/fgene.2019.00308

INTRODUCTION

The sensory primary cilium is an important non-motile cellular organelle, responsible for detecting changes in the extracellular environment and transducing signals to allow the cell to respond accordingly. The retina contains several ciliated cell types, including the retinal pigment epithelium (RPE) and photoreceptor cells. There are two types of photoreceptors; rods and cones, which

differ in their shape and the photopigment they contain. Both cell types contain an inner segment, where the nuclei and other organelles are located. Extending from the apical surface of this inner segment is the connecting cilium, which contains a proximal region analogous to the transition zone of primary cilia on other cell types, and a distal region which is unique to the photoreceptor connecting cilia (Dharmat et al., 2018). At the end of the connecting cilium is a huge elaboration of stacks of membrane where the photopigment molecules are located; termed the outer segment (Sjöstrand, 1953). Rods have a long, thin rod-like outer segment containing rhodopsin (Wheway et al., 2014), and cones have a shorter conical outer segment containing opsins which absorb different wavelengths to allow color vision (**Figure 1**). Cone outer segments are often described as having folds of membrane continuous with the plasma membrane rather than disks separate from the plasma membrane but this is only true in lower vertebrates (Pearring et al., 2013; May-Simera et al., 2017).

Proteins are moved from the site of production, in the inner segment, to the site of light absorption, in the outer segment, along the connecting cilium via a process known as intraflagellar transport (IFT; Ishikawa and Marshall, 2017). The connecting cilium consists of an axoneme of nine microtubule doublets nucleated at the base by a triplet microtubule structure named the basal body. This structure is derived from the mother centriole, at the apical surface of the inner segment. The axoneme extends into the outer segment, converting to singlet microtubules toward the distal end, often reaching near the distal tip of the cone outer segment and at least half-way along the rod outer segment (Roof et al., 1991). The proximal region of the axoneme is stabilized by posttranslational modifications such as glutamylation and acetylation, and is turned over at the distal end as membranes are replaced at the distal end of the outer segment, particularly in cones (Eckmiller, 1996).

Collectively, the connecting cilium and outer segment are termed the photoreceptor cilium, and this is the most highly modified and specialized sensory cilium in the human body (Wheway et al., 2014).

Perhaps unsurprisingly, defects in cilia often lead to retinal phenotypes, either as part of syndromic conditions involving other organs, or in isolation in the so-called retinal ciliopathies (Bujakowska et al., 2017). Non-syndromic retinal ciliopathies include several genetic subtypes of retinitis pigmentosa (RP), Leber Congenital Amaurosis (LCA) and cone-rod dystrophy (CORD).

Retinitis pigmentosa is the most common cause of inherited blindness, affecting up to 1:2000 people worldwide (Golovleva et al., 2010; Sharon and Banin, 2015), and is characterized by night blindness and loss of peripheral vision due to degeneration of rod photoreceptor cells, often progressing to loss of central high acuity vision as cone receptors are also affected (Verbakel et al., 2018). It is normally diagnosed in the third or fourth decade of life, although age of onset and severity vary widely. It can occur in isolation, or as part of syndromes such as Usher syndrome, Bardet Biedl syndrome and Joubert syndrome. The condition is extremely genetically heterogeneous, with 64 genes identified as causes of non-syndromic RP, and more than 50 genes associated with syndromic RP (RetNet[1]) and can be inherited in an autosomal dominant, autosomal recessive, or X-linked manner.

Of the genetic causes of X-linked non-syndromic RP, OFD1, RP2 and RPGR encode cilia proteins. Within autosomal dominant non-syndromic RP (ADRP), RP1 and TOPORS (RP31) encode known cilia proteins. At least 13 genetic causes of autosomal recessive non-syndromic RP (ARRP) encode cilia proteins, including FAM161A (RP28), TTC8 (RP51), C2orf71 (RP54), ARL6 (RP55), MAK (RP62), NEK2 (RP67), BBS2 (RP74), IFT140 (RP80), ARL2BP, RP1L1, C8orf37, CC2D2A and IFT172.

Leber congenital amaurosis is the most common genetic cause of childhood blindness, with an estimated worldwide incidence between 1:33,000 (Alstrom, 1957) and 1:81,000 live births (Stone, 2007). It accounts for 20% of eye disease in children attending schools for the blind (Schappert-kimmijser et al., 1959). Patients with LCA are born with severe visual impairment which is normally diagnosed within a few months of birth by greatly reduced or non-recordable electroretinogram results. Alongside poor vision is nystagmus (involuntary movement of the eyes) and slow to no pupillary response. Although born with already poor eyesight, some patients with LCA undergo further deterioration of vision in adult life, with retinal pigmentary changes often occurring later in life (Heher et al., 1992). It can occur in isolation, or as part of syndromes such as Senior-Loken syndrome. LCA is also genetically heterogeneous, with 13 known genes associated with autosomal recessive LCA, and one gene associated with autosomal dominant LCA (RetNet see footnote 1).

Five genetic subtypes of LCA are known retinal ciliopathies. *LCA5* encodes lebercilin, a ciliary transport protein (den Hollander et al., 2007), *LCA6* encodes RPGRIP1, a ciliary transition zone protein (Dryja et al., 2001), *LCA10* encodes CEP290, a transition zone protein which is also mutated in numerous syndromic ciliopathies (den Hollander et al., 2006) and *LCA15* encodes IQCB1/NPHP5 which interacts with CEP290, localizes to the transition zone and is required for outer segment formation (Estrada-Cuzcano et al., 2010; Ronquillo et al., 2016). All of these proteins localize to the connecting cilium of photoreceptor cells. CLUAP1 (IFT38) is also a cause of LCA (Soens et al., 2016), and plays a central role in photoreceptor ciliogenesis (Lee et al., 2014).

Cone-rod dystrophies (CRD) are rare degenerative conditions with an estimated incidence of 1:40,000 (Hamel et al., 2000). The condition is characterized by loss of cone photoreceptors, leading to loss of central, high acuity vision, disruption of color vision (dyschromatopsia) and photophobia, sometimes followed by degeneration of rod photoreceptors, causing night blindness and tunnel vision. It is normally diagnosed in the first decade of life (Hamel, 2007). It can occur as an isolated condition or as part of the syndromic ciliopathy Alström syndrome (Hearn et al., 2002; Collin et al., 2012). CRDs are also genetically heterogeneous, with 16 autosomal recessive and five autosomal dominant genes having been identified as causing CRD (see footnote 1). Of these, at least seven encode cilia proteins (RAB28 (CORD18), C8orf37 (CORD16), CEP78, POC1B, IFT81, RPGRIP1, and TTLL5).

[1]https://sph.uth.edu/retnet/sum-dis.htm

In total, at least 30 cilia genes have been identified as genetic causes of non-syndromic retinal dystrophies, and this number continues to grow. New ciliary causes of retinal dystrophies continue to be discovered, and new links are made between cilia and retinal conditions not previously considered to be retinal ciliopathies. For example, a recent whole genome siRNA knockdown screen in a ciliated cell line identified PRPF6, PRPF8 and PRPF31, known causes of RP, as cilia proteins (Wheway et al., 2015), offering new perspectives on a poorly understood form of RP.

Clearly, the cilium is of central importance to retinal development and function, with defects in large numbers of cilia proteins leading to various inherited retinal dystrophies. Retinal dystrophies remain extremely difficult to treat, with very few, if any, treatment options for the vast majority of patients, with the exception of RPE65, CEP290, and GUY2D gene therapy in LCA (DiCarlo et al., 2018). In order for this situation to improve, better understanding of the cell biology and molecular genetics of retinal dystrophies, including retinal ciliopathies, is required.

This requires robust, easily genetically manipulated cell models of retinal cells. ARPE19 (ATCC CRL-2302; Dunn et al., 1996), a spontaneously arising male retinal pigment epithelial cell line, and hTERT RPE-1 (ATCC CRL-4000) an hTERT immortalized female retinal pigment epithelial cell line are routinely used in molecular biology studies of retinal ciliopathies, owing to their retinal origin and ability to ciliate upon serum starvation and during late G1 (Spalluto et al., 2013). However, these cells are morphologically and functionally different from photoreceptors, and a dedicated photoreceptor cell line would be of enormous value in this area. Induced pluripotent stem cells (iPSCs) can be reliably differentiated into retinal photoreceptor cells following a 60-day differentiation protocol (Mellough et al., 2012). However, rapid loss of cells committed to a photoreceptor fate (CRX^+/$OPSIN^+$/$RHODOPSIN^+$) is seen over days 45–60. The same phenomenon is observed in retinal progenitor cells from mice (Mansergh et al., 2010).

As an alternative to this, optic cups derived from mouse embryonic stem cells (Eiraku et al., 2011), human embryonic stem cells (Nakano et al., 2012) and human iPSCs (Meyer et al., 2011; Reichman et al., 2014) have become popular 3D models for retinal research. These take just 14–18 days to differentiate, and self-assemble in non-adherent culture. The resultant structures are homologous to embryonic retinal cups seen in vertebrate eye development, and include photoreceptors, but are not ideal models of mature retina. These also present problems associated with epigenetic effects, and the spheroid nature of optic cups which prevents access to the center of these organoids for testing or analysis. Attempts to grow and differentiate ESCs and retinal progenitor cells into retinal sheets in custom matrices have been successful, but showed poor lamination (Worthington et al., 2016; Singh et al., 2018).

661W is an immortalized cone photoreceptor cell line derived from the retinal tumor of a mouse expressing SV40 T antigen (Tan et al., 2004). These cells have largely been used as a cell model for studying photo-oxidative stress and apoptosis, but not for studying inherited retinal dystrophies.

Here, we characterize the 661W cell line as a model for studying retinal ciliopathies.

MATERIALS AND METHODS

Cell Culture

661W cells (Tan et al., 2004) were the kind gift of Prof Muayyad Al-Ubaidi, University of Houston. Cells were cultured in DMEM high glucose + 10% FCS at 37°C, 5% CO_2, and split at a ratio of 1:5 once per week. hTERT-RPE1 cells (ATCC CRL-4000) were cultured in DMEM/F12 (50:50 mix) + 10% FCS at 37°C, 5% CO_2, and split at a ratio of 1:8 once per week.

Immunocytochemistry

Cells were seeded at 1×10^5 per mL on sterile glass coverslips in complete media, and after 48 h media was changed to serum-free media, and cells grown for a further 72 h. Cells were rinsed in warm Dulbecco's phosphate buffered saline (DPBS) and fixed in ice-cold methanol at –20°C for 5 min. Cells were then immediately washed with PBS, and incubated with blocking solution (1% w/v non-fat milk powder/PBS) for 15 min at room temperature. Coverslips were inverted onto primary antibodies in blocking solution in a humidity chamber and incubated at 4°C overnight. After three washes with PBS, cells were incubated with secondary antibodies and DAPI for 1 h at room temperature in the dark. After three PBS washes and one dH_2O wash, cells were mounted onto slides with Mowiol.

Antibodies

Primary Antibodies for IF

Mouse anti Polyglutamylated tubulin (GT335) 1:1000. Adipogen Life Sciences AG-20B-0020.
Rabbit anti Gamma-tubulin 1:500. Abcam ab11317.
Rabbit anti Arl13b 1:500. Proteintech 17711-1-AP.
Rabbit anti Ift88 1:500. Proteintech 13967-1-AP.
Rabbit anti Rpgrip1l 1:100. Proteintech 55160-1-AP.
Mouse anti Cep164 1:100. Santa Cruz sc-515403.

Secondary Antibodies for IF

Goat anti rabbit IgG AlexaFluor 488 1:1000.
Goat anti mouse IgG AlexaFluor 568 1:1000.
Donkey anti mouse IgG AlexaFluor 488 1:500.
Donkey anti rabbit IgG AlexaFluor 568 1:500.

Primary Antibodies for WB

Mouse anti beta actin clone AC-15. 1:4000. Sigma-Aldrich A1978.
Rabbit anti Ift88 1:500. Proteintech 13967-1-AP.

Secondary Antibodies for WB

Donkey anti mouse 680 1:20,000 (LiCor).
Donkey anti rabbit 800 1:20,000 (LiCor).

High Resolution Confocal Imaging

Confocal images were obtained at the Centre for Research in Biosciences Imaging Facility at UWE Bristol, using a HC

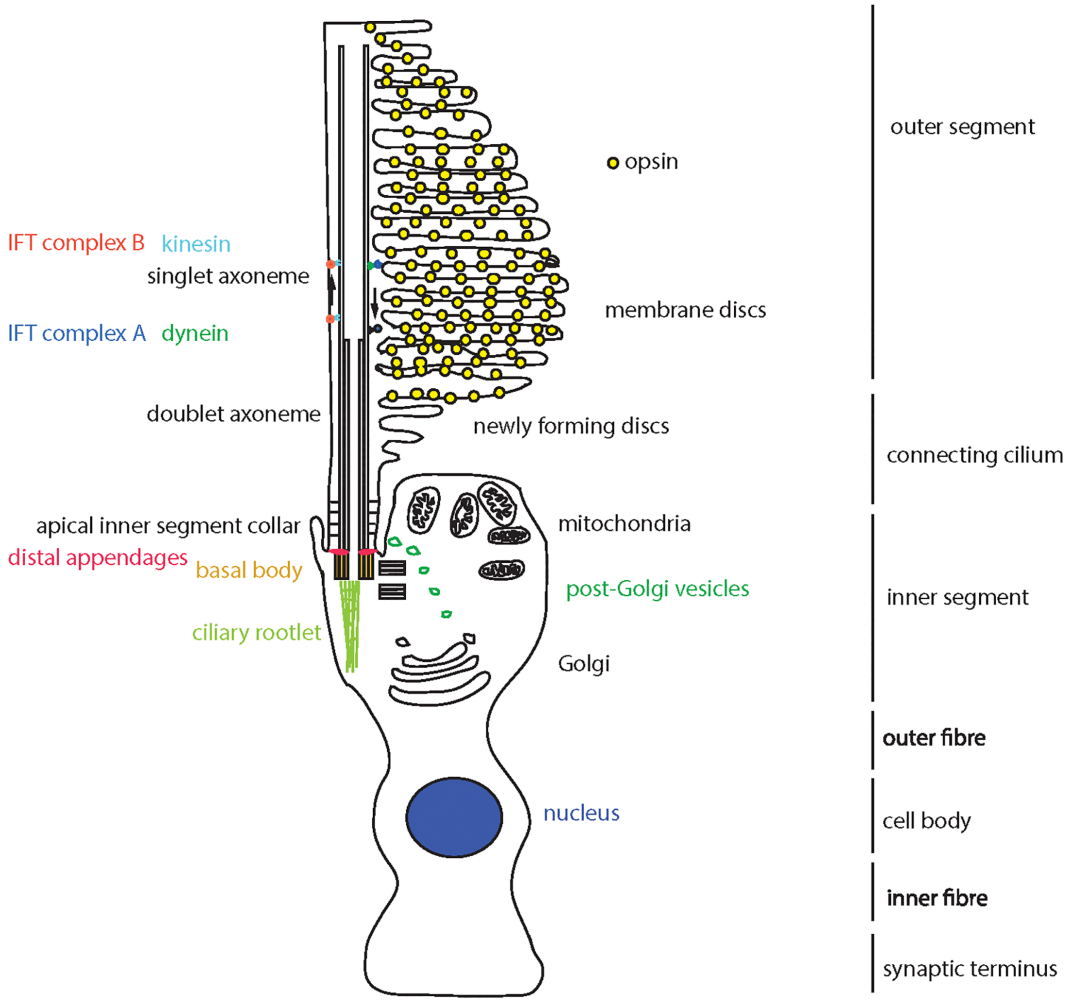

FIGURE 1 | Schematic representation of a cone photoreceptor cell and localization of ciliary proteins. The schematic represents the cone photoreceptor cell outer segment, connecting cilium, inner segment, outer fiber, cell body, inner fiber and synaptic terminus. A number of key components of the ciliary apparatus are color coded and indicated. The IFT complex A (blue) and complex B (red) are represented in the magnified inset.

PL APO 63x/1.40 oil objective CS2 lens on a Leica DMi8 inverted epifluorescence microscope, attached to a Leica SP8 AOBS laser scanning confocal microscope with four solid state AOTF supported lasers (405 nm/50 mW, 488 nm/20 mW, 552 nm/20 mW, and 638 nm/30 mW), two standard PMTs and two high sensitivity HyD hybrid SMD GaAsP detectors. Images were captured using LASX software with Hyvolution II, with automated settings for highest resolution imaging, with pinhole set at 0.5 AU. Images were deconvolved using Huygens Classic Maximum Likelihood Estimation (CMLE) algorithm (Scientific Volume Imaging). Images were assembled in Adobe Photoshop, and figures prepared using Adobe Illustrator.

Manual Cilium Counting and Length Measurements

Cells immunostained with Arl13b, which labels a larger length of the cilium than our alternative marker, GT335, were imaged at x63, and three fields of view taken to count number of whole nuclei (nuclei at edges of fields of view excluded) and number of cilia. Cilium length was measured using the scale bar as reference. Mean cilium length and percentage of ciliated cells was calculated per experiment. This was repeated in five independent biological replicates. Mean percentage of ciliated cells, and mean cilium length were calculated from the means of all experiments.

High-Throughput Confocal Imaging

Images were obtained at Wolfson Bioimaging Facility University of Bristol, using the Perkin Elmer OperaLX high-throughput imager, using a 60× water objective lens, 405, 488, and 561 nm lasers. PerkinElmer Opera Adjustment Plate containing multicolour beads was used to define the skewcrop and reference parameters. Cells were grown, fixed and immunostained in 96-well optical bottomed Cell Carrier plates (Perkin Elmer), and images were captured using OperaDB software. Individual z slices were exported as.flex files and assembled into maximum intensity projection z-stacks in Fiji ImageJ (Schindelin et al., 2012). These

z-stacks were exported as 16-bit TIFFs, which were imported into CellProfiler for analysis using custom analysis protocols (Carpenter et al., 2006; Kamentsky et al., 2011). Alternatively, z-stacks were constructed in OperaDB, and images analyzed using PerkinElmer Acapella scripts, including algorithms "Find nuclei," "Find cytoplasm," and "Find spots" (to find cilia).

SDS-PAGE and Western Blotting

Total protein was extracted from cells using NP40 lysis buffer and scraping. Insoluble material was pelleted by centrifugation at 10,000 × *g* for 5 min and the total protein concentration of the supernatant was assayed using detergent compatible protein assay kit (BioRad). 20 μg of total protein per sample was mixed with 2 × SDS loading buffer, boiled at 95°C for 5 min, and loaded onto pre-cast 4–12% NuPAGE Novex Bis-Tris gels (Life Technologies) alongside Spectra Multicolor Broad Range Protein ladder (Thermo Fisher). Samples were separated by electrophoreses in MES-SDS running buffer (Life Technologies) at 200 V for 45 min. Protein was transferred to PVDF membrane using wet transfer at 40 V for 2 h. Membranes were incubated with 5% (w/v) non-fat milk/PBS to saturate non-specific binding, and incubated with primary antibody overnight at 4°C. After washing in PBST, membranes were incubated with secondary antibody for 1 h at room temperature and exposed using 680 nm and/or 780 nm laser, or membrane was incubated with SuperSignal West Femto reagent (Pierce) and exposed using Chemiluminescence settings on LiCor Odyssey imaging system (LiCor).

Scanning Electron Microscopy (SEM)

Scanning electron microscopy images were obtained using a FEI Quanta FEG 650 field emission SEM at UWE Bristol Centre for Research in Biosciences Imaging Facility, using 20 μs dwell, 30.00 kV HV, 3.45 μm HFW. 8.33e–7 Torr pressure, 60,000× magnification.

RNA Sequencing

Total RNA was extracted from tissue using TRI reagent (Sigma-Aldrich). RNA samples were treated with a TURBO DNA-free™ Kit (Ambion Inc.) using conditions recommended by the manufacturers, and then cleaned with an RNA Clean & Concentrator™-5 spin column (Zymo Research Corp.). RNA was tested for quality and yield using a NanoDrop 1000 spectrophotometer and an Agilent 2100 Bioanalyzer.

Six total RNA samples were supplied and prepared into sequencing libraries from ∼500 ng by Bristol Genomics Facility using the Illumina TruSeq Stranded mRNA kit. Briefly, RNA was polyA-selected, chemically fragmented to about 200 nt in size (4-min fragmentation time), and cDNA synthesized using random hexamer primers. Each individual library received a unique Illumina barcode.

Quality of starting total RNA (diluted 1:100 to be within the limits of the assay) and the final libraries were also assessed using the Agilent TapeStation.

RNA-seq was performed on an Illumina NextSeq500 instrument with six libraries multiplexed and run across four lanes per flow-cell using 75 bp single end reads in high output mode. This resulted in more than 400 million reads per flow cell (651Mill, 590Mill PF), with an average of 94 million reads per sample.

Raw reads from four lanes per sample (four FASTQ files) were aligned to the mouse (*Mus musculus*) full genome (GRCm38, UCSC mm10) using STAR, a splice-aware aligner (Dobin et al., 2013), with UCSC mm10.gtf gene model for splice junctions and the resultant BAM files were merged.

Again, using UCSC mm10.gtf file, raw gene counts were estimated on merged BAM files using HTSeq, using the union method and –stranded = reverse options (Anders et al., 2015). Differential gene expression was analyzed using DESeq2 (Love et al., 2014) with statistical significance expressed as a *p*-value adjusted for a false discovery rate of 0.01 using Benjamini-Hochberg correction for multiple-testing.

Gene ontology (GO) Enrichment Analysis was carried out on the genes found to be differentially expressed between unstarved and starved cells using DAVID (Huang da et al., 2009).

For comparison to hTERT-RPE1 cell expression, we downloaded RNA sequence data from untreated and serum starved hTERT-RPE1 cells from the Sequence Read Archive (SRA; SRR2895378 and SRR2895380). These samples were selected for comparison to our 661 W samples, because the same protocols were followed for serum starvation, RNA extraction and purification, library preparation and sequencing. However, the sequencing read length for hTERT-RPE1 samples was shorter than for 661 Ws (50 bp single-end reads) and at lower depth (21 million reads and 26 million reads per sample). This data has been previously published in Wheway et al. (2015). Raw hTERT-RPE1 reads were aligned to the human (*Homo sapiens*) full genome (GRCh38.92, UCSC hg38) using STAR (Dobin et al., 2013), with UCSC hg38.gtf gene model for splice junctions.

Cufflinks tool (Trapnell et al., 2012) was used to calculate transcripts per kilobase of exon per million reads mapped (TPKM) for all assembled transcripts for all 661W samples and hTERT-RPE1 samples, and comparisons made between genes of interest between hTERT-RPE1 cell expression and 661W cell expression.

RESULTS

To confirm the cone photoreceptor origin of this cell line, and to fully characterize the expression profile of these cells, we performed whole transcriptome RNA sequencing on 661W cells, with and without exposure to serum starvation (GEO Accession: GSE119190; SRA Accession: SRP159075) and compared these to expression in hTERT-RPE cells subjected to the same growth conditions (SRA Accession: SRR2895378 and SRR2895380; **Supplementary Table 1**). Cells were starved of serum for 72 h to induce the cells to exit the cell cycle and form post-mitotic cilia (Santos and Reiter, 2008). We filtered the data to specifically study 47 genes which show characteristic expression in cone photoreceptor cells (Sharon et al., 2002; Corbo et al., 2007; **Figure 2A** and **Supplementary Table 2**). The data shows that 661W cells express a range of cone markers. Surprisingly, our data seemed to suggest that OPN1SW was expressed in the

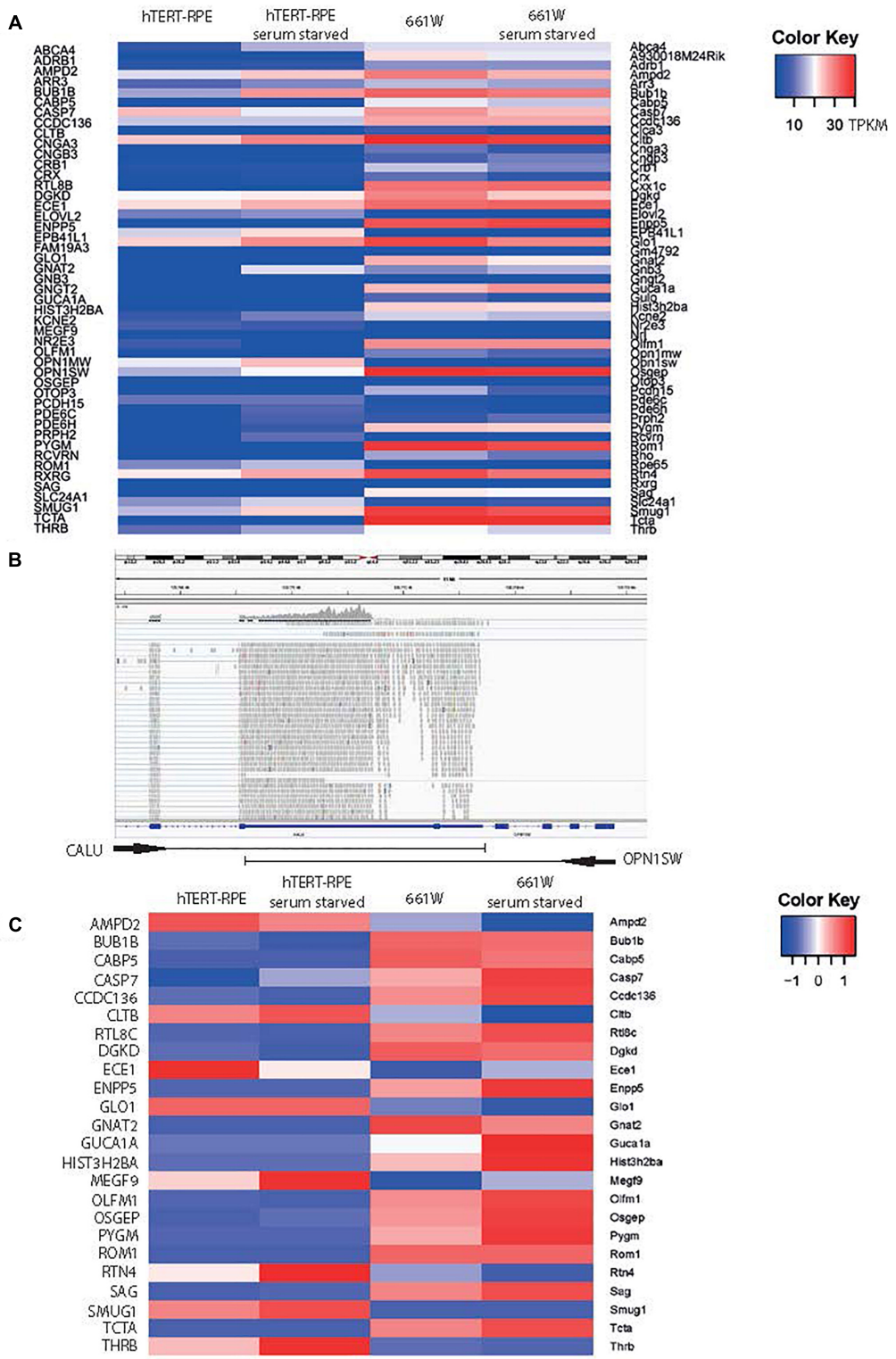

FIGURE 2 | 661W cells express markers of photoreceptor fate. **(A)** Heat map of expression of 48 genes characteristic of cone photoreceptors (Corbo et al., 2007) in hTERT-RPE1 cells and 661W cells in conditions of serum and serum starvation. Scale bar shows intensity of color relative to TPKM. **(B)** IGV screenshot of OPN1SW genomic location in human genome hg38, with one shared exon with CALU, which accounts for the mapping of reads to OPN1SW in the hTERT-RPE1 cell line. **(C)** Heat map showing expression level of all cone cell genes expressed in 661W cells, relative to the expression these genes in hTERT-RPE1 cells. Scale bar shows intensity of color relative to scaled expression value from –1 to 1 across each row.

hTERT-RPE1 cells with a TPKM of around 4, but analysis in Integrative Genomics Viewer (IGV; Robinson et al., 2011), showed that this was based upon alignment of many reads to one exon of OPN1SW which is shared with the neighboring gene CALU, which is highly expressed in these cells (**Figure 2B**). Based on our analysis of other alignments in IGV we decided to exclude any gene with an abundance estimate of less than 0.1 TPKM, and consider these as being not expressed. **Figure 2C** shows all markers of cone cell origin which are expressed in 661W cells, but are generally not expressed in hTERT-RPE1 cells, including cone alpha transducin (Gnat2) and Rom1. The data suggests that expression of most of these genes increase upon serum starvation, suggesting that the cells are induced toward a more cone-like fate upon serum starvation (**Figure 2C**). Short wave and medium wave opsin (Opn1sw and Opn1mw) and cone arrestin (Arr3) were not expressed in either cell type. This is in contrast to previously published papers showing expression of these cone markers in the 661W cell line. Earlier publications studied early passages of this cell type, whereas we studied cells between passage 24 and 27. This suggests that expression of these cone markers is not sustained over many passages.

To investigate expression of cilia genes in this cell line, we extracted TPKM transcript abundance estimates data from our RNAseq data for Syscilia Gold Standard (SCGS) genes (van Dam et al., 2013) in starved and unstarved hTERT-RPE1 and 661W cells. Again, excluding any genes with an abundance estimate of less than 0.1 TPKM, the 661W cells showed robust expression of 213 SCGS genes in unstarved and starved cells, including markers such as Cep164, Rpgrip1l and Ift88 (**Supplementary Table 3**). The cells also expressed numerous alpha- beta- and gamma-tubulin genes, as well as enzymes involved in post-translational modification of ciliary axonemal microtubules, such as Ttll9, which is involved in polyglutamylation of tubulin. Furthermore, 661W cells expressed 33 genes which are either not expressed in hTERT-RPE1 cells, or expressed at a low level in hTERT-RPE1 cells (**Figure 3A**). This includes many disease genes associated with a retinal ciliopathy phenotype, including Joubert disease genes Ahi1, Arl13b, Pde6b, Tmem138, and Tmem231; Bardet-Biedl disease genes Arl6, Bbs12, Bbs5, Bbs9, Ift74, Lztfl1, and Trim32; Senior-Loken syndrome gene Iqcb1; retinitis pigmentosa disease genes Arl3, Nek2, Rp2, and Topors; Leber congenital amaurosis disease gene Lca5 and; Usher syndrome gene Iqcb1 (**Figure 3A**). In addition to this, 661W cells express several syndromic ciliopathy disease genes which are not expressed at all in hTERT-RPE1 cells, including B9d1, B9d2, Evc2, Pkd1, and Tmem138 (**Figure 3B**). For the study of these disease genes, 661W cells are a valuable resource, as studies in the widely used retinal cell line hTERT-RPE1 will not be effective.

Of the 213 SCGS genes expressed in 661W cells, there is a statistically significant ($p < 0.05$) up or down regulation of 22/213 (10.3%) of these genes upon serum starvation. suggesting that the cells are induced toward a more differentiated state upon serum starvation (**Figure 3B**).

We then used HTSeq and DESeq2 to identify all genes differentially expressed in different conditions (starved vs. unstarved), controlling for batch-effects, and performed enrichment analysis on all hits with an adjusted p-value of >0.01 using DAVID (Huang da et al., 2009; **Supplementary Table 4**). This identified a number of enriched annotation clusters, including those with the GO terms "neuron differentiation" (enrichment score 2.22), "eye development" (enrichment score 0.16) and "sensory perception" (enrichment score 0.52), "GPCR, rhodopsin-like superfamily" (enrichment score 0.25) and "centrosome" (enrichment score 0.010; **Supplementary Table 4**).

Immunostaining and confocal microscopy of these cells shows that on average, 30.2% of serum starved cells grow a primary cilium (st. error 2.49, $n = 5$ independent replicates), with a mean cilium length of 3.01 μm (st. error 0.45, $n = 5$ independent replicates). The cells localize many cilium proteins to the axoneme (polyglutamylated tubulin, Ift88), ciliary transition zone (Rpgrip1l), cilium membrane (Arl13b) and basal body (gamma tubulin; **Figures 4A–D**). The cells can grow primary cilia up to almost 15 μm in length (**Figure 4B**). The ability to form long cilia is consistent with the long axonemes of cones seen *in vivo*. Whilst the axoneme of rod photoreceptors only extends along a portion of the outer segment, it extends along the entirety of the cone outer segment in *Xenopus laevis* toads *in vivo* (Eckmiller, 1996). The axoneme of most primary cilia tend to be extensively post-translationally modified, but in 661W cells only a small portion of the proximal axoneme is polyglutamylated (**Figures 4A–D**), consistent with a similar observation in cones in mice, which show extensive glutamylation and glycation in the connecting cilium region of the photoreceptor, but none along the axoneme of the outer segment of the cones (Bosch Grau et al., 2017). This level of post-translational modification is tightly regulated in mouse cones, and disruption of glycylation leading to hyperglutamylation leads to retinal degeneration (Bosch Grau et al., 2017). SEM shows these cilia grow in characteristic ciliary pits in the cell membrane (**Figure 4E**).

To further resolve the ultrastructure of this cilium, we used confocal microscopy with deconvolution to analyze the relative localisation of a centrosomal and basal body marker (gamma tubulin), distal centriolar appendage marker (Cep164), axonemal marker (Arl13b) and transition zone marker (Rpgrip1l) along the cilium (**Figures 5A–C**). This revealed an Arl13b cilium membrane extending from a ring of Cep164, lying distal to a ring of gamma tubulin of the mother centriole-derived basal body. A second gamma tubulin ring, of the daughter centriole, lies at approximately right-angles to this basal body. Rpgrip1l, a transition zone marker, extends from within the ring of Cep164 beyond this ring, presumably along the axoneme of the cilium. This differs from descriptions of Rpgrip1l localisation within the transition zone in primary cilia, where it is normally seen to reside in a tight ring narrower in diameter to Cep164, but more distal to Cep164 (Yang et al., 2015). However, it is known that transition zone assembly is highly cell-type specific, and Rpgrip1l plays a key role in this process (Wiegering et al., 2018). Extension of Rpgrip1l further beyond the distal appendages in this cell line is reminiscent of RPGR1P1L localisation in photoreceptors *in vivo*, where it is localized along the connecting cilium (Dharmat et al., 2018).

Non-coding RNA data from RNA sequencing of this cell line identifies a number of novel RNAs not previously linked to

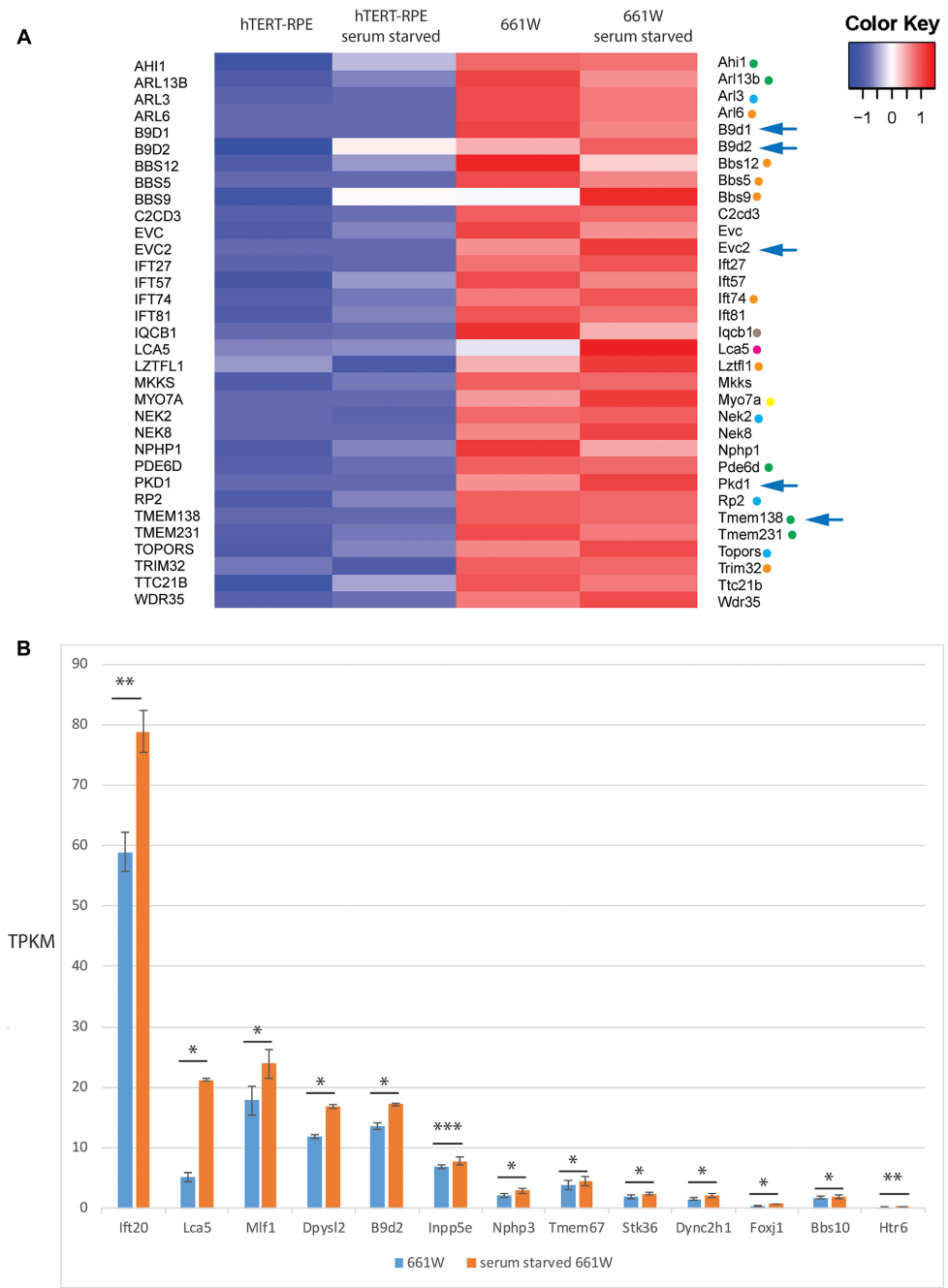

FIGURE 3 | 661W cells express markers of ciliated cell fate. **(A)** Heat map showing expression level of 33 Syscilia Gold Standard (SCGS) genes expressed in 661W cells which are either not expressed in hTERT-RPE1 cells, or are expressed at a low level in hTERT-RPE1 cells. Green dots indicate Joubert syndrome disease genes, blue dots indicate retinitis pigmentosa disease genes, orange dots indicate Bardet-Biedl syndrome disease genes, borwon dot indicates Senior-Loken syndrome disease gene, pink dot indicates Leber congenital amaurosis disease gene, yellow dot indicates Usher syndrome disease gene. Arrows indicate syndromic disease genes which are expressed in 661W cells but not expressed at all in hTERT-RPE1 cells. **(B)** Graph showing mean TPKM of selected SCGS genes in unstarved and serum starved cells, to show upregulation of these genes upon serum starvation to induce cilium formation. ***$p < 0.005$; **$p < 0.01$; *$p < 0.05$.

photoreceptor fate (**Supplementary Table 5**). Most noteworthy is mmu-mir-6236, which was expressed at very high levels in starved and unstarved cells. This miRNA has not been previously linked to photoreceptor fate or function. These cells were also found to express miR-17-hg, which has been previously linked to neuronal differentiation (Bian et al., 2013; Mao et al., 2016), and may contribute to neuronal photoreceptor differentiation in these cells. Interestingly, expression of this microRNA has been shown to promote cyst growth in polycystic kidney disease, a common ciliopathy (Patel et al., 2013). It could be hypothesized

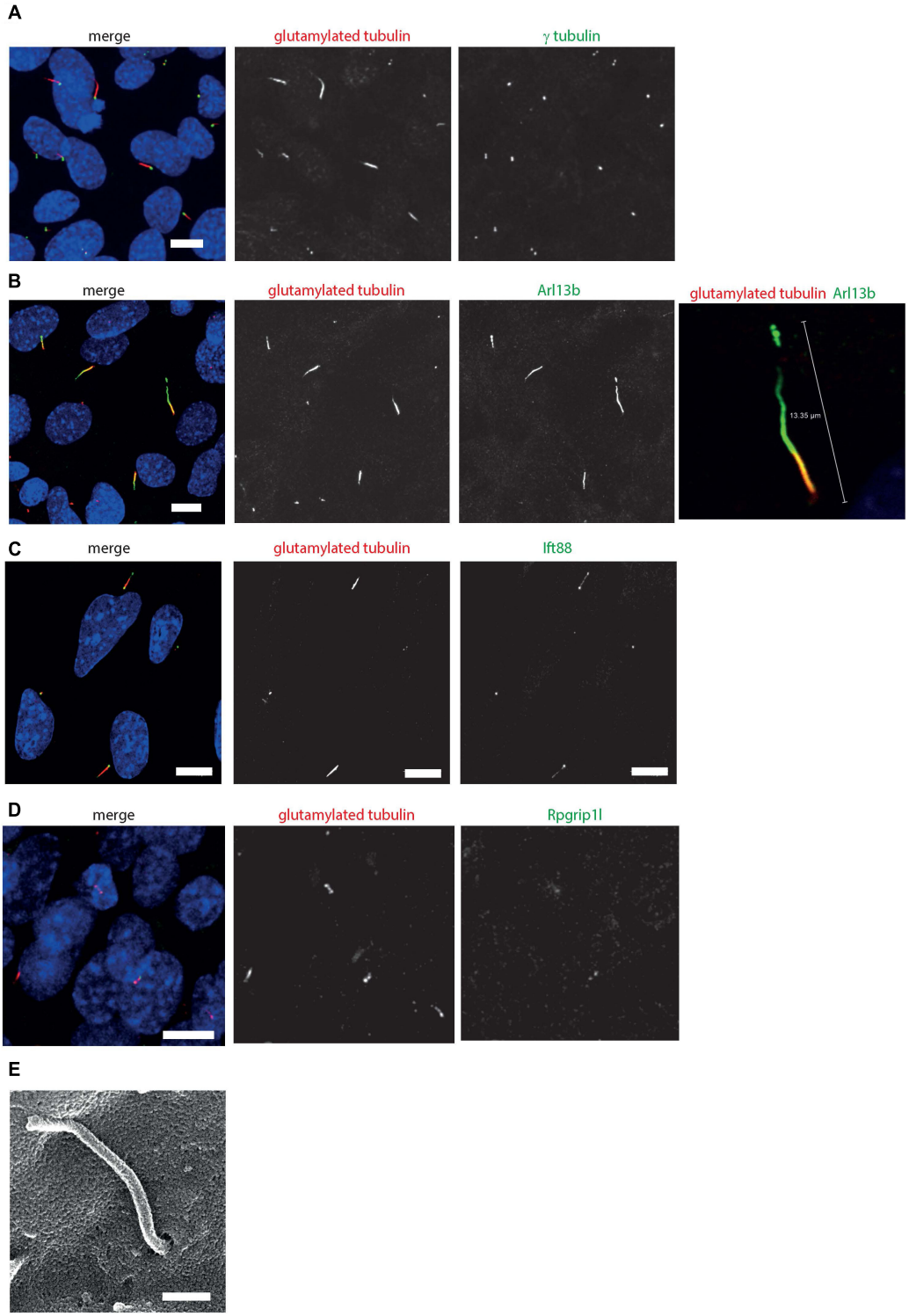

FIGURE 4 | 661W cells grow long primary cilia. **(A)** 661W stained with proximal axonemal marker polyglutamylated tubulin (red), basal body marker γ tubulin (green) show that many cells grow primary cilia. Cells counterstained with DAPI (blue). Scale bar 10 μm. **(B)** Staining with cilium membrane marker Arl13b (green) shows that these cells grow cilia up to approx. 15 μm long, with only the proximal portion of the axoneme polyglutamylated. Scale bar 10 μm **(C)** Staining with Ift88 antibody (green) shows that this IFT protein localizes along the cilium, with more concentrated localisation at the base and tip of the cilium. Scale bar 10 μm. **(D)** Staining with Rpgrip1l antibody (green) shows that this transition protein colocalises with polyglutamylated tubulin, with more concentrated localisation at the base of this region of polyglutamylated tubulin. Scale bar 10 μm. **(E)** Scanning electron microscope image of 661 W cell, showing cilium in ciliary pit. Scale bar = 500 nm.

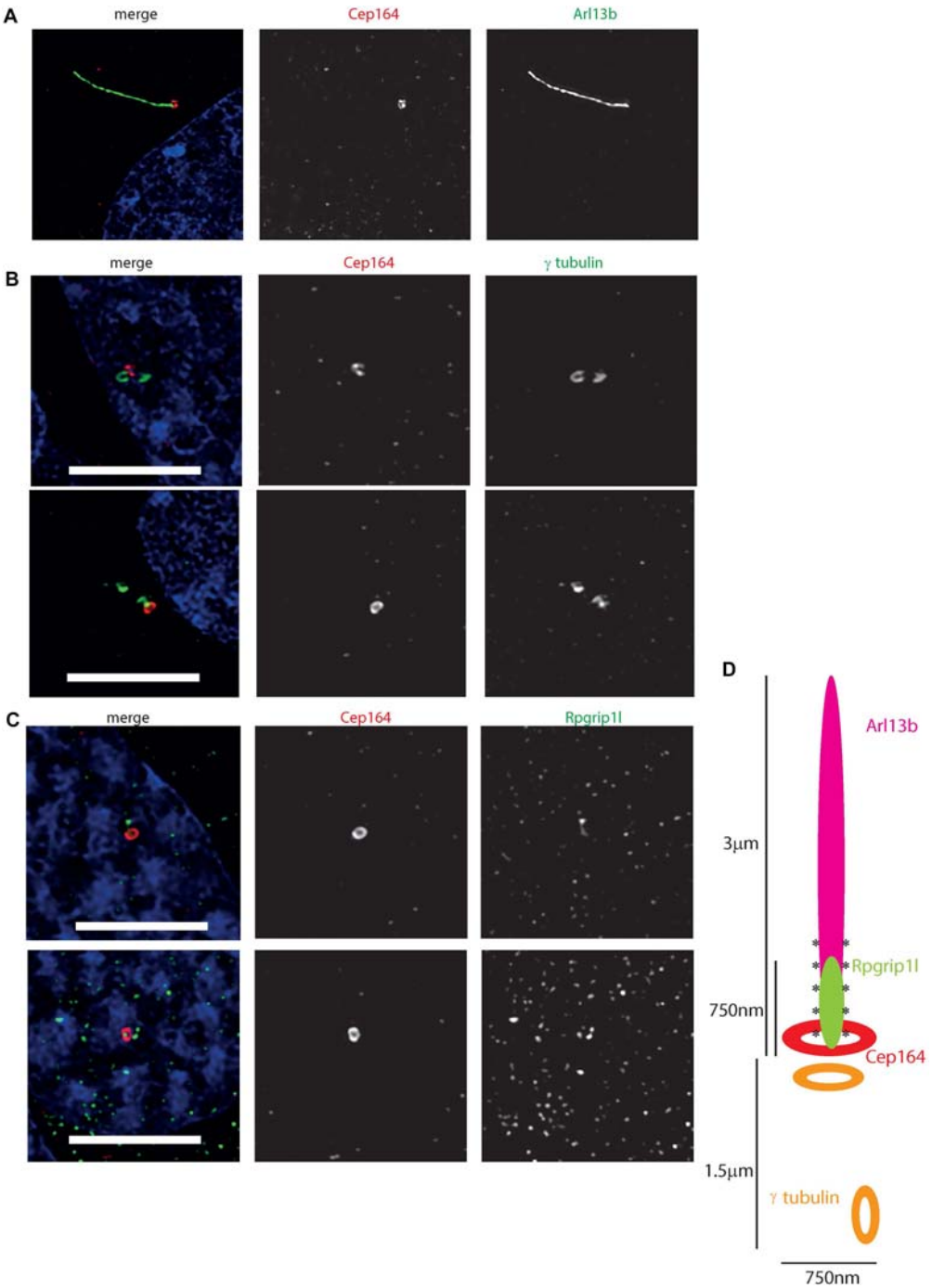

FIGURE 5 | Ultrastructure of the 661 W cilium. **(A)** Hyvolution imaging of distal centriolar appendage marker Cep164 (red), which localizes specifically to the mature mother centriole of the basal body, and cilium membrane protein Arl13b (green). **(B)** Hyvolution imaging of distal centriolar appendage marker Cep164 (red), which localizes specifically to the mature mother centriole of the basal body, and γ tubulin (green) which labels both mother and daughter centrioles. Scale bar = 5 μm. **(C)** Hyvolution imaging of distal centriolar appendage marker Cep164 (red), and transition zone protein Rpgrip1l (green). Scale bar = 5 μm. **(D)** Schematic representation of protein localisation in 661W cilia, with scale bars, labeled. Asterisks symbolize region of polyglutamylation of the axoneme.

that this miRNA plays a role in ciliogenesis in both the kidney and the photoreceptor.

Finally, in order to evaluate the utility of 661 W cells for high-throughput screening, we performed siRNA knockdown of cilia protein Ift88 in 661 W cells in 96 well optical-bottom culture plates, and assayed cell number and cilia number by high-content imaging, using Arl13b and polygutamylated tubulin as cilia markers (**Figure 6A**). Nuclei were identified using DAPI,

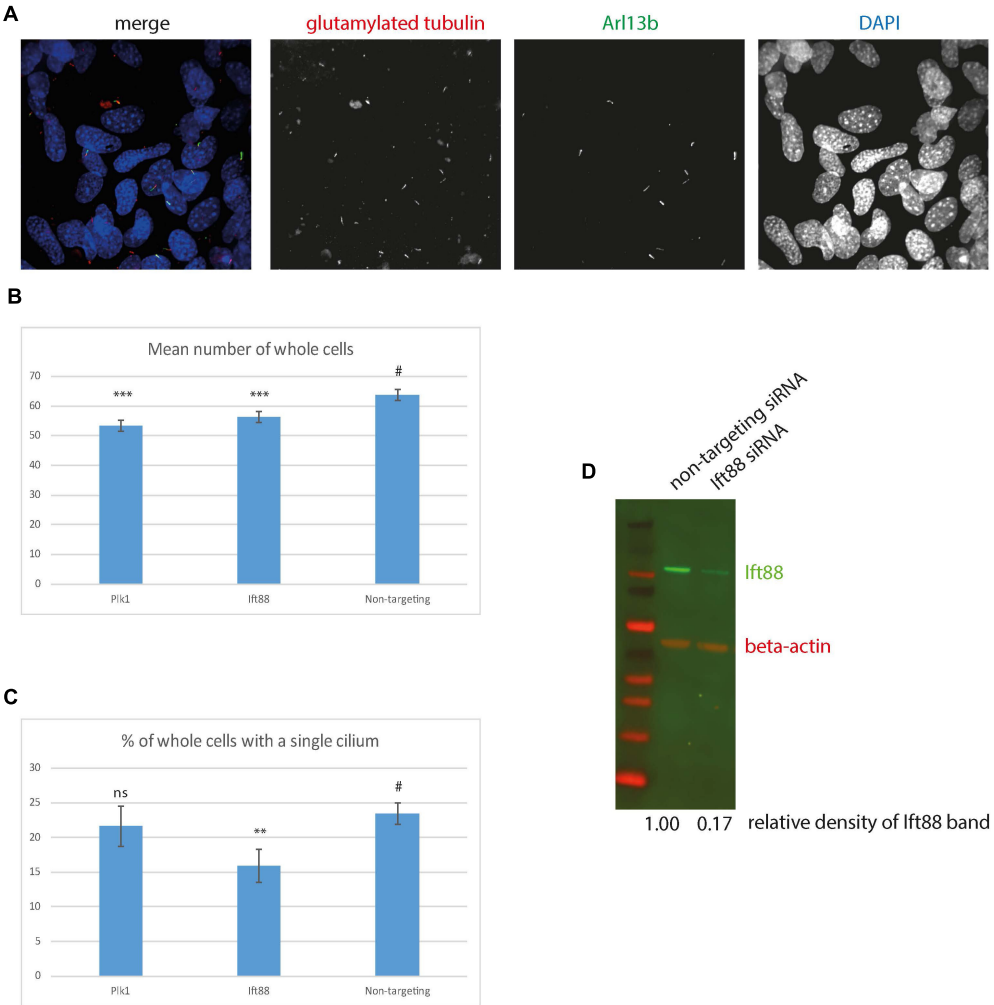

FIGURE 6 | High content imaging of 661 W cells. **(A)** Example images from the Perkin Elmer Opera, showing 661W cells stained with glutamylated tubulin (red), Arl13b (green) and DAPI (blue). **(B)** Mean number of whole cells per field of view is statistically significantly reduced after 72 h Plk1 and Ift88 siRNA knockdown compared to cells treated with non-targeting control, $^{***}p < 0.0001$. **(C)** % of cells with a single cilium per field of view is statistically significantly reduced after 72 h Ift88 siRNA knockdown compared to cells treated with non-targeting control, $^{**}p < 0.001$, $^{\#}$ is control experiment to which the statistical significance of the knockdowns are compared. **(D)** western blotting confirms reduction in Ift88 protein level (green) after 72 h Ift88 siRNA knockdown, compared to non-targeting control. Red shows beta actin loading control.

and cilia were detected using a modified "find spots" Perkin Elmer image analysis algorithm. This showed that knockdown of positive control Plk1 induced a statistically significant reduction in cell number (**Figure 6B**), and Ift88 knockdown induced a statistically significant reduction in the number of cells with a single cilium (**Figures 6B,C**). Western blotting confirmed knockdown of Ift88 (**Figure 6D**). The automated image analysis showed good agreement with our manual measurements of cilia number; around 22% of cells using manual counting.

DISCUSSION

Our comprehensive deep sequencing of total mRNA and selected non-coding RNAs in the 661 W cell line confirms its cone photoreceptor origin, and ability to grow a photoreceptor-like cilium in culture after serum starvation (**Figures 2–4** and **Supplementary Table 1**). A recent paper described the 661 W cell line as a retinal ganglion-like cell line, owing to its expression of markers specific to retinal ganglion cells, such as Rbpms, Pouf2, Pouf3, Thy1, and γ-synuclein (Sayyad et al., 2017). Our whole transcriptome RNA sequence data confirms that this cell line expresses Rbpms, Thy1, and Sncg at low levels, but does not express Pouf2 or Pouf3 (**Supplementary Table 1**). This suggests that this cell line does indeed have some features of retinal ganglion cells, but also expresses markers of cone photoreceptor fate. Our data supports the conclusion of Sayyad et al. (2017), that this cell line shows properties of both retinal ganglion and photoreceptor cells, and is a useful *in vitro* photoreceptor model.

Immunofluorescence confocal microscopy and deconvolution of images of these cells reveals a cilium similar in structure to cone photoreceptor cilia *in vivo*. After serum starvation in culture, around a third of cells extend a cilium of around three microns in length which is only post-translationally modified at the proximal end, and localizes Rpgrip1l along this proximal region (**Figures 4**, **5**). The cell line expresses many *bona fide* cilia genes, including many mutated in retinal ciliopathies, and expression of many of these increases upon serum starvation of the cells (**Figure 3** and **Supplementary Table 3**). Knockdown of key cilia gene Ift88 results in robust reduction in percentage of whole cells with a single cilium, which can be readily assayed by high-content imaging (**Figure 6**).

Our demonstration of high-content imaging of 661 W cells illustrates the potential utility of this cell line for high-throughput screening. A recent high-throughput small molecule screen in hTERT-RPE1 cells successfully identified eupatilin as a small molecule which rescued transition zone defects in CEP290 knockout RPE1 cells (Kim et al., 2018). A similar approach using 661 W cells could be an even more clinically relevant method for identifying small molecules which could be used for treating retinal ciliopathies. Similarly, the cell line could be useful for reverse genetics functional genomics screening to identify novel retinal cilia genes and retinal ciliopathy candidate genes, similar to previous screens (Wheway et al., 2015). These methods are of enormous importance in a field where effective treatments are so limited.

The 661 W cell line can be particularly useful for studying ciliopathy disease genes which are not expressed in hTERT-RPE1 cells, or are only expressed at a low level in this cell line (**Figure 3A**).

In summary, we provide evidence that 661 W cells are a useful *in vitro* model for studying retinal ciliopathies.

AUTHOR CONTRIBUTIONS

GW conceived the study, performed the experiments, carried out the data analysis, imaging, image analysis, bioinformatics analysis, and wrote the paper. LN performed the experiments, carried out the data analysis, imaging, and image analysis. DT contributed to bioinformatics analysis. SC provided support in high-throughput imaging and image analysis.

FUNDING

LN and GW are supported by National Eye Research Council Small Award SAC019, Wellcome Trust Seed Award in Science (Grant No. 204378/Z/16/Z), and UWE Bristol Quality Research funds. SC was supported by the Elizabeth Blackwell Institute, through its Wellcome Trust ISSF Award.

ACKNOWLEDGMENTS

We would like to thank Dr. David Patton for assistance with SEM. We would like to thank Prof. Muayyad Al-Ubaidi for the gift of the 661 W cells, and Prof. Jeremy Nathans for the gift of the opsin antibodies. We would like to thank all at Scientific Volume Imaging for assistance with Huygens deconvolution. GW would like to thank Prof. David Stephens and Prof. Catherine Nobes for providing access to the laboratories at University of Bristol School of Biochemistry.

SUPPLEMENTARY MATERIAL

The Supplementary Material for this article can be found online at: https://www.frontiersin.org/articles/10.3389/fgene.2019.00308/full#supplementary-material

TABLE S1 | Transcript abundance estimates in transcripts per kilobase of exon per million reads mapped (TPKM) for all genes in all repeats of starved and unstarved 661W cells (tab 1) and hTERT-RPE1 cells (tab 2).

TABLE S2 | Transcript abundance estimates in transcripts per kilobase of exon per million reads mapped (TPKM) for 47 cone photoreceptor genes in all repeats of starved and unstarved 661W cells and hTERT-RPE1 cells.

TABLE S3 | Transcript abundance estimates in transcripts per kilobase of exon per million reads mapped (TPKM) for 277 Syscilia Gold Standard (SCGS) genes in all repeats of starved and unstarved 661W cells and hTERT-RPE1 cells.

TABLE S4 | Results of differential gene expression analysis of starved and unstarved 661W cells (tab 1) and DAVID functional annotation cluster analysis of differentially expressed genes (tab 2).

TABLE S5 | Transcript abundance estimates in transcripts per kilobase of exon per million reads mapped (TPKM) for non-coding RNAs in all repeats of starved and unstarved 661W cells.

REFERENCES

Alstrom, C. H. (1957). Heredo-retinopathia congenitalis - monohybrida recessiva autosomalis. *Hereditas* 43, 1–77.

Anders, S., Pyl, P. T., and Huber, W. (2015). HTSeq–a Python framework to work with high-throughput sequencing data. *Bioinformatics* 31, 166–169. doi: 10.1093/bioinformatics/btu638

Bian, S., Hong, J., Li, Q., Schebelle, L., Pollock, A., Knauss, J. L., et al. (2013). MicroRNA cluster miR-17-92 regulates neural stem cell expansion and transition to intermediate progenitors in the developing mouse neocortex. *Cell Rep.* 3, 1398–1406. doi: 10.1016/j.celrep.2013.03.037

Bosch Grau, M., Masson, C., Gadadhar, S., Rocha, C., Tort, O., Marques Sousa, P., et al. (2017). Alterations in the balance of tubulin glycylation and glutamylation in photoreceptors leads to retinal degeneration. *J. Cell Sci.* 130, 938–949. doi: 10.1242/jcs.199091

Bujakowska, K. M., Liu, Q., and Pierce, E. A. (2017). Photoreceptor cilia and retinal ciliopathies. *Cold Spring Harb. Perspect. Biol.* 9:a028274. doi: 10.1101/cshperspect.a028274

Carpenter, A. E., Jones, T. R., Lamprecht, M. R., Clarke, C., Kang, I. H., Friman, O., et al. (2006). CellProfiler: image analysis software for identifying and quantifying cell phenotypes. *Genome Biol.* 7:R100. doi: 10.1186/gb-2006-7-10-r100

Collin, G. B., Marshall, J. D., King, B. L., Milan, G., Maffei, P., Jagger, D. J., et al. (2012). The Alstrom syndrome protein, ALMS1, interacts with alpha-actinin and components of the endosome recycling pathway. *PLoS One* 7:e37925. doi: 10.1371/journal.pone.0037925

Corbo, J. C., Myers, C. A., Lawrence, K. A., Jadhav, A. P., and Cepko, C. L. (2007). A typology of photoreceptor gene expression patterns in the mouse. *Proc. Natl. Acad. Sci. U.S.A.* 104, 12069–12074. doi: 10.1073/pnas.0705465104

den Hollander, A. I., Koenekoop, R. K., Mohamed, M. D., Arts, H. H., Boldt, K., Towns, K. V., et al. (2007). Mutations in LCA5, encoding the ciliary protein lebercilin, cause Leber congenital amaurosis. *Nat. Genet.* 39, 889–895. doi: 10.1038/ng2066

den Hollander, A. I., Koenekoop, R. K., Yzer, S., Lopez, I., Arends, M. L., Voesenek, K. E. J., et al. (2006). Mutations in the CEP290 (NPHP6) gene are a frequent cause of leber congenital amaurosis. *Am. J. Hum. Genet.* 79, 556–561. doi: 10.1086/507318

Dharmat, R., Eblimit, A., Robichaux, M. A., Zhang, Z., Nguyen, T. T., Jung, S. Y., et al. (2018). SPATA7 maintains a novel photoreceptor-specific zone in the distal connecting cilium. *J. Cell Biol.* 217:2851. doi: 10.1083/jcb.201712117

DiCarlo, J. E., Mahajan, V. B., and Tsang, S. H. (2018). Gene therapy and genome surgery in the retina. *J. Clin. Invest.* 128, 2177–2188. doi: 10.1172/JCI120429

Dobin, A., Davis, C. A., Schlesinger, F., Drenkow, J., Zaleski, C., Jha, S., et al. (2013). STAR: ultrafast universal RNA-seq aligner. *Bioinformatics* 29, 15–21. doi: 10.1093/bioinformatics

Dryja, T. P., Adams, S. M., Grimsby, J. L., McGee, T. L., Hong, D., Li, T., et al. (2001). Null RPGRIP1 alleles in patients with leber congenital amaurosis. *Am. J. Hum. Genet.* 68, 1295–1298. doi: 10.1086/320113

Dunn, K. C., Aotaki-Keen, A. E., Putkey, F. R., and Hjelmeland, L. M. (1996). ARPE-19, a human retinal pigment epithelial cell line with differentiated properties. *Exp. Eye Res.* 62, 155–169. doi: 10.1006/exer.1996.0020

Eckmiller, M. S. (1996). Renewal of the ciliary axoneme in cone outer segments of the retina of *Xenopus laevis*. *Cell Tissue Res.* 285, 165–169. doi: 10.1007/s004410050632

Eiraku, M., Takata, N., Ishibashi, H., Kawada, M., Sakakura, E., Okuda, S., et al. (2011). Self-organizing optic-cup morphogenesis in three-dimensional culture. *Nature* 472, 51–56. doi: 10.1038/nature09941

Estrada-Cuzcano, A., Koenekoop, R., and Kohl, C. F. (2010). IQCB1 mutations in patients with Leber congenital amaurosis. *Invest. Ophthalmol. Vis. Sci.* 52, 834–839. doi: 10.1167/iovs.10-5221

Golovleva, I., Kohn, L., Burstedt, M., Daiger, S., and Sandgren, O. (2010). Mutation spectra in autosomal dominant and recessive retinitis pigmentosa in northern Sweden. *Adv. Exp. Med. Biol.* 664, 255–262. doi: 10.1007/978-1-4419-1399-9_29

Hamel, C. P. (2007). Cone rod dystrophies. *Orphanet J. Rare Dis.* 2:7. doi: 10.1186/1750-1172-2-7

Hamel, C. P., Griffoin, J. M., Bazalgette, C., Lasquellec, L., Duval, P. A., Bareil, C., et al. (2000). Molecular genetics of pigmentary retinopathies: identification of mutations in CHM, RDS, RHO, RPE65, USH2A and XLRS1 genes. *J. Fr. Ophtalmol.* 23, 985–995.

Hearn, T., Renforth, G. L., Spalluto, C., Hanley, N. A., Piper, K., Brickwood, S., et al. (2002). Mutation of ALMS1, a large gene with a tandem repeat encoding 47 amino acids, causes alstrom syndrome. *Nat. Genet.* 31, 79–83. doi: 10.1038/ng874

Heher, K. L., Traboulsi, E. I., and Maumenee, I. H. (1992). The natural history of Lebers Congenital Amaurosis - age-related findings in 35 patients. *Ophthalmology* 99, 241–245. doi: 10.1016/S0161-6420(92)31985-2

Huang da, W., Sherman, B. T., and Lempicki, R. A. (2009). Systematic and integrative analysis of large gene lists using DAVID bioinformatics resources. *Nat. Protoc.* 4, 44–57. doi: 10.1038/nprot.2008.211

Ishikawa, H., and Marshall, W. F. (2017). Intraflagellar transport and ciliary dynamics. *Cold Spring Harb. Perspect. Biol.* 9:a021998. doi: 10.1101/cshperspect.a021998

Kamentsky, L., Jones, T. R., Fraser, A., Bray, M. A., Logan, D. J., Madden, K. L., et al. (2011). Improved structure, function and compatibility for Cell profiler: modular high-throughput image analysis software. *Bioinformatics* 27, 1179–1180. doi: 10.1093/bioinformatics/btr095

Kim, Y. J., Kim, S., Jung, Y., Jung, E., Kwon, H. J., and Kim, J. (2018). Eupatilin rescues ciliary transition zone defects to ameliorate ciliopathy-related phenotypes. *J. Clin. Invest.* 128, 3642–3648. doi: 10.1172/JCI99232

Lee, C., Wallingford, J. B., and Gross, J. M. (2014). Cluap1 is essential for ciliogenesis and photoreceptor maintenance in the vertebrate eye. *Invest. Ophthalmol. Vis. Sci.* 55, 4585–4592. doi: 10.1167/iovs.14-14888

Love, M. I., Huber, W., and Anders, S. (2014). Moderated estimation of fold change and dispersion for RNA-seq data with DESeq2. *Genome Biol.* 15:550. doi: 10.1186/s13059-014-0550-8

Mansergh, F. C., Vawda, R., Millington-Ward, S., Kenna, P. F., Haas, J., Gallagher, C., et al. (2010). Loss of photoreceptor potential from retinal progenitor cell cultures, despite improvements in survival. *Exp. Eye Res.* 91, 500–512. doi: 10.1016/j.exer.2010.07.003

Mao, S., Li, X., Wang, J., Ding, X., Zhang, C., and Li, L. (2016). miR-17-92 facilitates neuronal differentiation of transplanted neural stem/precursor cells under neuroinflammatory conditions. *J. Neuroinflammation* 13:208. doi: 10.1186/s12974-016-0685-5

May-Simera, H., Nagel-Wolfrum, K., and Wolfrum, U. (2017). Cilia - The sensory antennae in the eye. *Prog. Retin. Eye Res.* 60, 144–180. doi: 10.1016/j.preteyeres.2017.05.001

Mellough, C. B., Sernagor, E., Moreno-Gimeno, I., Steel, D. H., and Lako, M. (2012). Efficient stage-specific differentiation of human pluripotent stem cells toward retinal photoreceptor cells. *Stem Cells* 30, 673–686. doi: 10.1002/stem.1037

Meyer, J. S., Howden, S. E., Wallace, K. A., Verhoeven, A. D., Wright, L. S., Capowski, E. E., et al. (2011). Optic vesicle-like structures derived from human pluripotent stem cells facilitate a customized approach to retinal disease treatment. *Stem Cells* 29, 1206–1218. doi: 10.1002/stem.674

Nakano, T., Ando, S., Takata, N., Kawada, M., Muguruma, K., Sekiguchi, K., et al. (2012). Self-formation of optic cups and storable stratified neural retina from human ESCs. *Cell Stem Cell* 10, 771–785. doi: 10.1016/j.stem.2012.05.009

Patel, V., Williams, D., Hajarnis, S., Hunter, R., Pontoglio, M., Somlo, S., et al. (2013). miR-17∼92 miRNA cluster promotes kidney cyst growth in polycystic kidney disease. *Proc. Natl. Acad. Sci. U.S.A.* 110, 10765–10770. doi: 10.1073/pnas.1301693110

Pearring, J. N., Salinas, R. Y., Baker, S. A., and Arshavsky, V. Y. (2013). Protein sorting, targeting and trafficking in photoreceptor cells. *Prog. Retin. Eye Res.* 36, 24–51. doi: 10.1016/j.preteyeres.2013.03.002

Reichman, S., Terray, A., Slembrouck, A., Nanteau, C., Orieux, G., Habeler, W., et al. (2014). From confluent human iPS cells to self-forming neural retina and retinal pigmented epithelium. *Proc. Natl. Acad. Sci. U.S.A.* 111, 8518–8523. doi: 10.1073/pnas.1324212111

Robinson, J. T., Thorvaldsdóttir, H., Winckler, W., Guttman, M., Lander, E. S., Getz, G., et al. (2011). Integrative genomics viewer. *Nat. Biotechnol.* 29:24. doi: 10.1038/nbt.1754

Ronquillo, C. C., Hanke-Gogokhia, C., Revelo, M. P., Frederick, J. M., Jiang, L., and Baehr, W. (2016). Ciliopathy-associated IQCB1/NPHP5 protein is required for mouse photoreceptor outer segment formation. *FASEB J.* 30, 3400–3412. doi: 10.1096/fj.201600511R

Roof, D., Adamian, M., Jacobs, D., and Hayes, A. (1991). Cytoskeletal specializations at the rod photoreceptor distal tip. *J. Comp. Neurol.* 305, 289–303. doi: 10.1002/cne.903050210

Santos, N., and Reiter, J. F. (2008). Building it up and taking it down: the regulation of vertebrate ciliogenesis. *Dev. Dyn.* 237, 1972–1981. doi: 10.1002/dvdy.21540

Sayyad, Z., Sirohi, K., Radha, V., and Swarup, G. (2017). 661W is a retinal ganglion precursor-like cell line in which glaucoma-associated optineurin mutants induce cell death selectively. *Sci. Rep.* 7:16855. doi: 10.1038/s41598-017-17241-0

Schappert-kimmijser, J., Henkes, H. E., and Van den Bosch, J. (1959). Amaurosis congenita (Leber). *Arch. Ophthalmol.* 1959, 211–218. doi: 10.1001/archopht.1959.00940090213003

Schindelin, J., Arganda-Carreras, I., Frise, E., Kaynig, V., Longair, M., Pietzsch, T., et al. (2012). Fiji: an open-source platform for biological-image analysis. *Nat. Methods* 9, 676–682. doi: 10.1038/nmeth.2019

Singh, D., Wang, S. B., Xia, T., Tainsh, L., Ghiassi-Nejad, M., Xu, T., et al. (2018). A biodegradable scaffold enhances differentiation of embryonic stem cells into a thick sheet of retinal cells. *Biomaterials* 154, 158–168. doi: S0142-9612(17)30717-2

Sharon, D., and Banin, E. (2015). Nonsyndromic retinitis pigmentosa is highly prevalent in the Jerusalem region with a high frequency of founder mutations. *Mol. Vis.* 21, 783–792.

Sharon, D., Blackshaw, S., Cepko, C. L., and Dryja, T. P. (2002). Profile of the genes expressed in the human peripheral retina, macula, and retinal pigment

epithelium determined through serial analysis of gene expression (SAGE). *Proc. Natl. Acad. Sci. U.S.A.* 99, 315–320. doi: 10.1073/pnas.012582799

Sjöstrand, F. S. (1953). The ultrastructure of the outer segments of rods and cones of the eye as revealed by the electron microscope. *J. Cell Comp. Physiol.* 42, 15–44. doi: 10.1002/jcp.1030420103

Soens, Z. T., Li, Y., Zhao, L., Eblimit, A., Dharmat, R., Li, Y., et al. (2016). Hypomorphic mutations identified in the candidate Leber congenital amaurosis gene CLUAP1. *Genet. Med.* 18, 1044–1051. doi: 10.1038/gim.2015.205

Spalluto, C., Wilson, D. I., and Hearn, T. (2013). Evidence for reciliation of RPE1 cells in late G1 phase, and ciliary localisation of cyclin B1. *FEBS Open Bio* 3, 334–340. doi: 10.1016/j.fob.2013.08.002

Stone, E. M. (2007). Leber congenital amaurosis - A model for efficient genetic testing of heterogeneous disorders: LXIV Edward Jackson memorial lecture. *Am. J. Ophthalmol.* 144, 791–811. doi: 10.1016/j.ajo.2007.08.022

Tan, E., Ding, X. Q., Saadi, A., Agarwal, N., Naash, M. I., and Al-Ubaidi, M. R. (2004). Expression of cone-photoreceptor-specific antigens in a cell line derived from retinal tumors in transgenic mice. *Invest. Ophthalmol. Vis. Sci.* 45, 764–768. doi: 10.1167/iovs.03-1114

Trapnell, C., Roberts, A., Goff, L., Pertea, G., Kim, D., Kelley, D. R., et al. (2012). Differential gene and transcript expression analysis of RNA-seq experiments with TopHat and Cufflinks. *Nat. Protoc.* 7:562. doi: 10.1038/nprot.2012.016

van Dam, T. J., Wheway, G., Slaats, G. G., SYSCILIA Study Group, Huynen, M. A., and Giles, R. H. (2013). The SYSCILIA gold standard (SCGSv1) of known ciliary components and its applications within a systems biology consortium. *Cilia* 2:7. doi: 10.1186/2046-2530-2-7

Verbakel, S. K., van Huet, R. A. C., Boon, C. J. F., den Hollander, A. I., Collin, R. W. J., Klaver, C. C. W., et al. (2018). Non-syndromic retinitis pigmentosa. *Prog. Retin. Eye Res.* 66, 157–186. doi: 10.1016/j.preteyeres.2018.03.005

Wheway, G., Parry, D. A., and Johnson, C. A. (2014). The role of primary cilia in the development and disease of the retina. *Organogenesis* 10, 69–85. doi: 10.4161/org.26710

Wheway, G., Schmidts, M., Mans, D. A., Szymanska, K., Nguyen, T. M., Racher, H., et al. (2015). An siRNA-based functional genomics screen for the identification of regulators of ciliogenesis and ciliopathy genes. *Nat. Cell Biol.* 17, 1074–1087. doi: 10.1038/ncb3201

Wiegering, A., Dildrop, R., Kalfhues, L., Spychala, A., Kuschel, S., Lier, J. M., et al. (2018). Cell type-specific regulation of ciliary transition zone assembly in vertebrates. *EMBO J.* 37:e97791. doi: 10.15252/embj.201797791

Worthington, K. S., Green, B. J., Rethwisch, M., Wiley, L. A., Tucker, B. A., Guymon, C. A., et al. (2016). Neuronal differentiation of induced pluripotent stem cells on surfactant templated chitosan hydrogels. *Biomacromolecules* 17, 1684–1695. doi: 10.1021/acs.biomac.6b00098

Yang, T. T., Su, J., Wang, W. J., Craige, B., Witman, G. B., Tsou, M. F., et al. (2015). Superresolution pattern recognition reveals the architectural map of the ciliary transition zone. *Sci. Rep.* 5:14096. doi: 10.1038/srep14096

Conflict of Interest Statement: The authors declare that the research was conducted in the absence of any commercial or financial relationships that could be construed as a potential conflict of interest.

frontiers in Genetics

ORIGINAL RESEARCH
published: 05 April 2019
doi: 10.3389/fgene.2019.00323

Structural but Not Functional Alterations in Cones in the Absence of the Retinal Disease Protein Retinitis Pigmentosa 2 (RP2) in a Cone-Only Retina

*Linjing Li†, Kollu N. Rao† and Hemant Khanna**

Department of Ophthalmology and Visual Sciences, University of Massachusetts Medical School, Worcester, MA, United States

X-linked retinitis pigmentosa 2 (XLRP2) patients and *Rp2*^{null} mice exhibit severe cone photoreceptor degeneration. However, due to the paucity of cones in mammalian model systems, it is not clear how cones respond to the loss of RP2. Here we have used the *Nrl*$^{-/-}$ mice, which develop a rodless and short wavelength (S) opsin-containing cone-only retina, to generate *Rp2*^{null}::*Nrl*$^{-/-}$ double knock out (*Rp2*-DKO) mice. We found that the ciliary axoneme and the outer segments (OSs) of the cones were significantly longer with disorganized membrane infoldings as compared to the *Nrl*$^{-/-}$ mice. Additionally, we found misregulation in the expression of the genes related to ophthalmic disease, cell trafficking, and stress-response in the *Rp2*-DKO mice prior to the onset of cone degeneration. Surprisingly, the loss of RP2 did not affect progressive photoreceptor dysfunction of the *Nrl*$^{-/-}$ mice and the trafficking of S opsin. Our data suggest that RP2 is a negative regulator of cone OS length but does not affect S-opsin trafficking and S-cone function. Our studies also provide a cone-only platform to design cone-targeted therapeutic strategies for X-linked RP2.

Keywords: retinal degeneration, cilia, ciliopathies, photoreceptors, opsin, cone

OPEN ACCESS

Edited by:
Carlo Iomini,
Icahn School of Medicine at Mount Sinai, United States

Reviewed by:
Yang Sun,
Stanford University, United States
Wolfgang Baehr,
The University of Utah, United States

***Correspondence:**
Hemant Khanna
hemant.khanna@umassmed.edu

†Present address:
Linjing Li,
Shire, Lexington, MA, United States
Kollu N. Rao,
Sanofi, Framingham, MA, United States

Specialty section:
This article was submitted to Genetic Disorders, a section of the journal Frontiers in Genetics

Received: *15 November 2018*
Accepted: *22 March 2019*
Published: *05 April 2019*

Citation:
Li L, Rao KN and Khanna H (2019) Structural but Not Functional Alterations in Cones in the Absence of the Retinal Disease Protein Retinitis Pigmentosa 2 (RP2) in a Cone-Only Retina. Front. Genet. 10:323. doi: 10.3389/fgene.2019.00323

INTRODUCTION

Cilia are evolutionarily conserved microtubule-based antennae involved in regulating a myriad of cellular signaling cascades (Singla and Reiter, 2006; Gerdes et al., 2009). During cilia formation, the basal body (mother centriole) docks at the apical plasma membrane and initiates the nucleation of ciliary microtubules in the form of transition zone and distal axoneme (Inglis et al., 2006). The light-sensing outer segment (OS) of the rod and cone photoreceptors is a modified sensory cilium. Although the machinery involved in the generation of the photosensory cilia is conserved, the photoreceptors develop an elaborate distal cilium in the form of multiple membranous disks loaded with billions of opsin molecules and lipids involved in the phototransduction cascade (Rosenbaum et al., 1999; Rosenbaum and Witman, 2002; Besharse et al., 2003; Pazour and Witman, 2003; Insinna et al., 2009; Kennedy and Malicki, 2009). Even subtle defects in the formation or function of the photoreceptor cilia are associated with retinal degenerative diseases (Besharse et al., 2003; Anand and Khanna, 2012; Deretic and Wang, 2012; Yildiz and Khanna, 2012).

The cone and rod OSs are morphologically and physiologically different from each other (Kandel, 2013), indicating that they have developed unique pathways to generate and maintain

the sensory cilia. Functionally, the rods are sensitive to very low light intensities whereas cones mediate majority of our vision due to their ability to function in high light intensities. Hence, in retinal degenerative diseases, it is the loss of cones that affects the quality of life of patients (Kandel, 2013). Whereas the rod OSs are loaded with rhodopsin, two types of cone opsins are expressed in mice: red/green (medium wave-length, M)-opsin or short wave-length S-opsin. Moreover, the rod OSs have discrete disks independent of the OS (ciliary) plasma membrane loaded with rhodopsin, the cone OS invaginates and is continuous with the plasma membrane (Deretic and Wang, 2012).

We previously showed that the deletion of the retinal ciliopathy protein retinitis pigmentosa 2 (RP2) (Schwahn et al., 1998) results in hyperelongation of the ciliary microtubules and defective OS structure and function of M-opsin expressing cones but not rod photoreceptors in mice (Li et al., 2013, 2015). However, due to the paucity of cones in the mammalian retina, it has been difficult to understand how the loss of RP2 specifically modulates cone OS extension in mice and leads to cone dysfunction. To tackle this roadblock, we have used the $Nrl^{-/-}$ mice, which develop a rodless and cone-enriched retina. The cones of the $Nrl^{-/-}$ mice express cone-specific genes and exhibit morphological and physiological features of wild type (WT) cones (Mears et al., 2001; Daniele et al., 2005). These mice have been previously used to assess cone-related pathogenesis in retinal degenerative diseases (Chakraborty et al., 2010; Cideciyan et al., 2011; Thapa et al., 2012; Rajala et al., 2013; Rao et al., 2016). The $Nrl^{-/-}$ mouse platform can also be used to understand the responses of foveal cones that are present in a rodless environment in the primates (Roger et al., 2012). The aim of the current study was to understand how cones respond to the loss of RP2 in a rodless environment.

MATERIALS AND METHODS

Mice

All animal experiments were performed in accordance with the approved procedures of the Institutional Animal Care and Use Committee. All mice were maintained in the same conditions of 12-h light to 12-h dark, with unrestricted access to food and water. Lighting conditions were kept constant in all cages with illumination of 10 to 15 lux at the level of the cages.

The *Rp2*-DKO mice were generated by breeding the homozygous $Nrl^{-/-}$ with the previously reported $Rp2^{null}$ mice (Mears et al., 2001; Li et al., 2013). Male mice of appropriate genotypes were used in these studies. All mice were genotyped to confirm the absence of the *rd8* allele.

Antibodies

Antibodies against β-tubulin, actin and acetylated α-tubulin were obtained from Sigma-Aldrich (St. Louis, MO, United States). Peanut agglutinin (PNA) was procured from Vector Labs (Burlingame, CA, United States); Rhodopsin and S-opsin antibodies were purchased from Millipore (Billerica, MA, United States) and SantaCruz, respectively.

Fundus Examination and Electroretinography (ERG)

The fundus and ERG recordings were performed essentially as described earlier (Chang et al., 2006; Rao et al., 2016). Only photopic (cone-mediated) ERGs were recorded as the $Nrl^{-/-}$ mice develop a cone-only retina.

Immunofluorescence and Transmission Electron Microscopy (TEM)

For immunofluorescence analyses, mouse eyes were enucleated and then fixed in 4% paraformaldehyde in PBS (pH 7.4) followed by cryosectioning and staining as recently described (Li et al., 2013). Primary antibodies were prepared in blocking solution and slides were further incubated overnight at 4°C. Sections were then washed three times with PBS and incubated for 1 h with goat anti-rabbit (or mouse) Alexa Fluor 488, 546, or 647 nm secondary antibody (1:500) at RT. Hoechst 33342 (Life Technologies, Corp.) was used to label the nuclei. The sections were then visualized using a scanning confocal microscope (Leica TCS SP5 II laser; Leica Microsystems).

For transmission electron microscopy (TEM), mouse eyes were enucleated and fixed in 2% glutaraldehyde, 2% paraformaldehyde in 0.1 M sodium cacodylate buffer (pH 7.2) overnight at RT. The anterior portion was removed on the next morning and processed as described (Li et al., 2013). Ultrathin sections were observed in a Zeiss EM900 electron microscope and pictures were taken with a coupled digital camera using the ImageSP software.

Transcriptomic Analysis

Total RNA from the $Nrl^{-/-}$ and *Rp2*-DKO mice was extracted using the RNeasy plus mini kit (Qiagen, United States) according to manufacturer's instructions. The sample from neuroretina plus RPE was isolated from six retinas of each genotype in triplicates. The transcriptomic profile and data analysis of the differentially expressed transcripts were analyzed at Beijing Genomics Institute (Hong Kong), as described. Subsequent bioinformatic analysis was performed using the RPKM (reads per kilo base mapped) values, and the data were analyzed as $\log_2$ ratio from the RPKM values. We selected genes that were significantly altered at least 1.5-fold. Pathway analysis was performed using the IPA system (Ingenuity Systems, Redwood City, CA, United States). The differentially expressed genes were validated by qRT-PCR, as described (Rao et al., 2016).

RESULTS

Characterization of the *Rp2*-DKO Mice

We previously showed that the ablation of *Rp2* in mice ($Rp2^{null}$) results in cone OS extension and progressive cone dysfunction (Li et al., 2015). However, due to the overwhelming majority of rods in the mouse retina, it is difficult to investigate how cones respond to the loss of RP2. We therefore, generated $Rp2^{null}$:$Nrl^{-/-}$ double knockout (*Rp2*-DKO) mice and confirmed the absence of RP2 by immunoblotting using an anti-RP2 antibody. We detected the

RP2-immunoreactive band in the WT and the $Nrl^{-/-}$ mice but not in the $Rp2^{null}$ or the *Rp2*-DKO mice (**Figure 1A**). We also tested whether the loss of RP2 in cones resulted in alterations in the expression of other cone-specific phototransduction genes. We did not detect any differences in the expression of cone phosphodiesterase and S- opsin between the *Rp2*-DKO and $Nrl^{-/-}$ mouse retinas. As predicted, rhodopsin expression was undetectable in these retinas (**Figure 1B**).

We next assessed the retinal morphology of the *Rp2*-DKO mice. Whereas the fundus examination of the $Nrl^{-/-}$ mice at 1 and 3 months of age revealed the presence of white spots, which represent whorls and rosettes present in the outer nuclear layer (Roger et al., 2012), the *Rp2*-DKO mice did not exhibit such structures (**Figure 1C**). These findings were corroborated in the flat mounted retinas stained with peanut agglutinin (PNA; marker of cone extracellular matrix; red) (**Figure 1D**).

Cone Function and Morphology in the *Rp2*-DKO Mice

It was previously reported that the $Nrl^{-/-}$ mice exhibit cone-mediated supranormal photopic b-wave responses up to ∼3 months of age (Roger et al., 2012). We therefore, analyzed the effect of loss of RP2 on cone function in these mice. We found that the loss of RP2 did not affect the supranormal responses of the $Nrl^{-/-}$ mice. Moreover, the rate of age-dependent decline in photopic responses of the $Nrl^{-/-}$ mice was indistinguishable from the *Rp2*-DKO mice (**Figure 2A**). These data indicated that the previously reported cone dysfunction observed in the $Rp2^{null}$ mice or in the mice in which the *Rp2* gene was conditionally ablated specifically in M-opsin expressing cones was largely due to their dysfunction (Li et al., 2013, 2015). The *Rp2*-DKO mice have an overwhelming majority of short wave-length S-opsin expressing cones, which could mask the effect on the M-opsin expressing cones.

As the *Rp2*-DKO mice did not exhibit major changes in photoreceptor dysfunction, we next assessed whether the long cone OS phenotype of the $Rp2^{null}$ mice is phenocopied by the *Rp2*-DKO mice. Immunostaining of the *Rp2*-DKO mouse retinas with acetylated α-tubulin (microtubules) and S-opsin antibodies (outer segment marker) revealed the presence of elongated cone OS at 3 months of age as compared to the $Nrl^{-/-}$ mice (**Figure 2B**). Furthermore, we did not detect significant differences in the localization of S-opsin between the $Nrl^{-/-}$ and the *Rp2*-DKO retinas. The elongated OSs were detectable even at earlier stages (data not shown).

These results suggested that the longer cone OSs are functional in the S-cone rich *Rp2*-DKO mice. Thus, we predicted that the

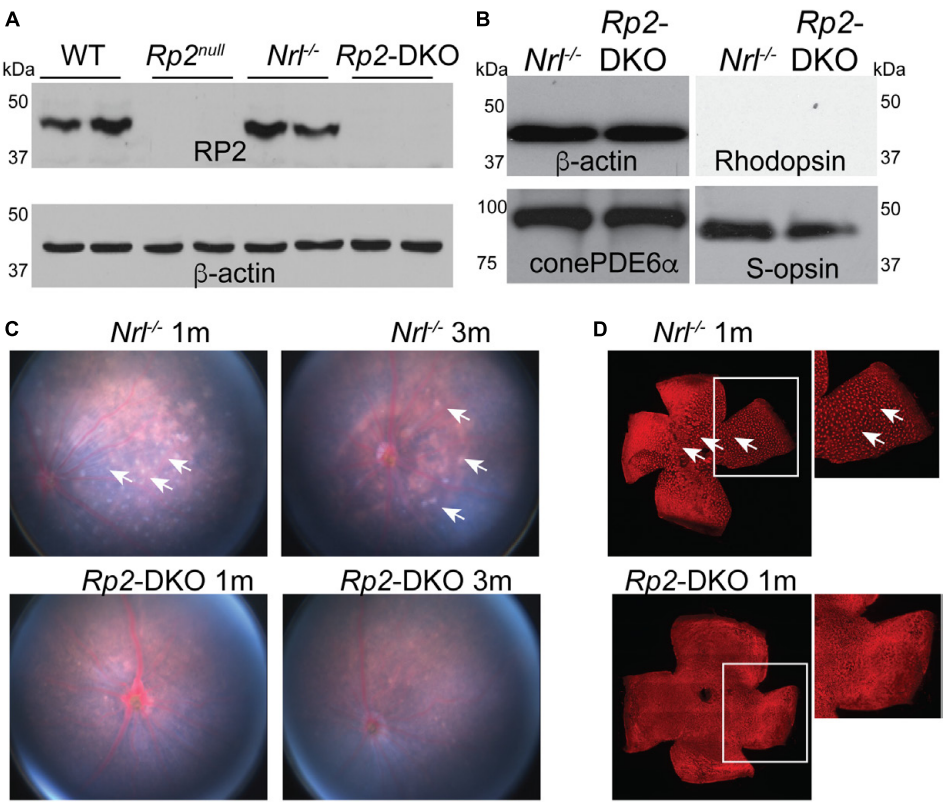

FIGURE 1 | Characterization of the *Rp2*-DKO mice. **(A,B)** Retinal extracts (100 μg) from the mice of the indicated genotypes were analyzed by SDS-PAGE and immunoblotting using anti-RP2, rhodopsin, S-opsin, cone PDE6α, and β-actin (loading control) antibodies. Fundus **(C)** and flat mounted retinal staining **(D)** of the $Nrl^{-/-}$ and *Rp2*-DKO mice was performed. Arrows point to the white spots in the fundus photograph that correspond to the whorls and rosettes observed in the PNA (red; peanut agglutinin) stained flat mounted retinas of the $Nrl^{-/-}$ mice. Such spots are undetectable in the *Rp2*-DKO mouse retinas.

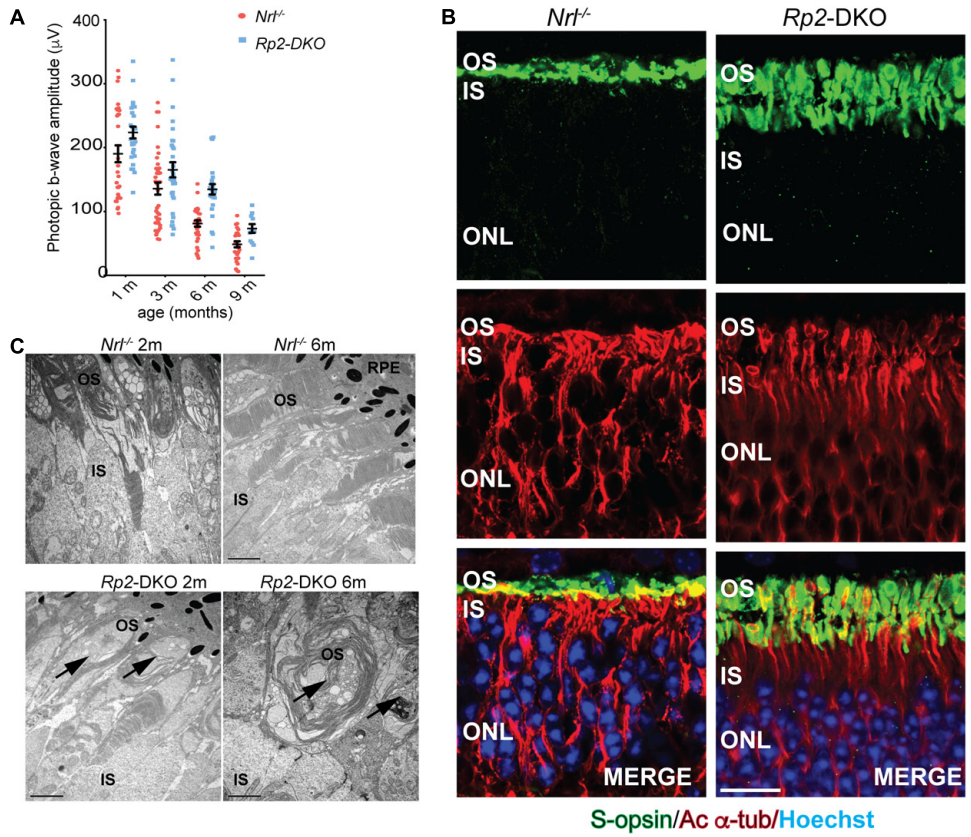

FIGURE 2 | Phenotypic analysis of the *Rp2*-DKO mice: **(A)** Photopic b-wave analysis of the $Nrl^{-/-}$ and *Rp2*-DKO mice at the indicated ages did not reveal statistically significant differences. The data represent Standard Error of Mean. **(B)** Immunofluorescence analysis of the cryosections of 3 months old $Nrl^{-/-}$ and *Rp2*-DKO mouse retinas was performed using anti-S-opsin (green) and acetylated α-tubulin (red) antibodies. Nuclei were stained with Hoechst (blue). OS, outer segment; IS, inner segment; ONL, outer nuclear layer. Scale bar: 25 μm. **(C)** TEM analysis of $Nrl^{-/-}$ and *Rp2*-DKO mouse retinas at 2 and 6 months of age was performed. Arrows indicate the irregular outer segment morphology in the *Rp2*-DKO mice. RPE, retinal pigment epithelium. Scale bar: 2 μm.

morphology of these cones would also be comparable to the $Nrl^{-/-}$ mice. However, ultrastructural analysis demonstrated the presence of abnormal OS membrane vesicles in the OSs in 2 months old *Rp2*-DKO mice (**Figure 2C**). As previously described, the $Nrl^{-/-}$ mice showed membranous vesicles in the OSs over wide areas of the retina and shorter OSs but with still discernible OS infoldings at 6 months of age (Roger et al., 2012). In contrast, the 6 months old *Rp2*-DKO mice exhibited abnormal infoldings loaded with membranous vesicles (**Figure 2C**). The connecting cilium appeared normal in the micrographs (data not shown).

Retinal Gene Expression Profile of *Rp2*-DKO Mice

The absence of rods in the $Nrl^{-/-}$ mice provides a unique opportunity to investigate pure cone responses to the loss of a retinal disease gene. To delineate the cellular responses underlying the intriguing phenotypes of elongated cone OSs, we performed comparative transcriptomic analysis of the retinas from the *Rp2*-DKO and $Nrl^{-/-}$ mice at 1 month of age. We chose this age to avoid degeneration-associated artifacts. We compared six retinas from each genotype and repeated the experiment three times. Our analysis revealed 154 differentially expressed genes (>1.5 fold) in the *Rp2*-DKO mice as compared to the $Nrl^{-/-}$ mice (**Supplementary Table S1**). These genes represented major biological pathways, including developmental and ophthalmic disorders, cellular movement/trafficking, and stress responses (**Figure 3A** and **Supplementary Table S2**). We identified several crystallin subunits whose expression was downregulated in the *Rp2*-DKO mice (**Figure 3B**). The crystallin subunits belong to the chaperone family of proteins, respond to stress and inflammation and are known to be upregulated during retinal disease (Fort and Lampi, 2011). On the other hand, *Lrat* (lecithin retinol acyltransferase) *Rpe65* (retinal pigment epithelium 65), *Dcdc2a* (Doublecortin domain containing protein), and *Dnahc8* (dynein axonemal heavy chain 8) were the major representative genes of the ophthalmic disease and cilia length regulation and cell trafficking pathways (Redmond et al., 1998; Ruiz et al., 1999; Moiseyev et al., 2005; Samant et al., 2005; Grati et al., 2015). We therefore validated the expression of these genes by qRT-PCR. As shown in **Figure 3C**, whereas the expression of *CryαA* subunit was diminished in the *Rp2*-DKO mice, *Dnahc8* exhibited ∼16-fold increase in expression. *Lrat* and *Rpe65*

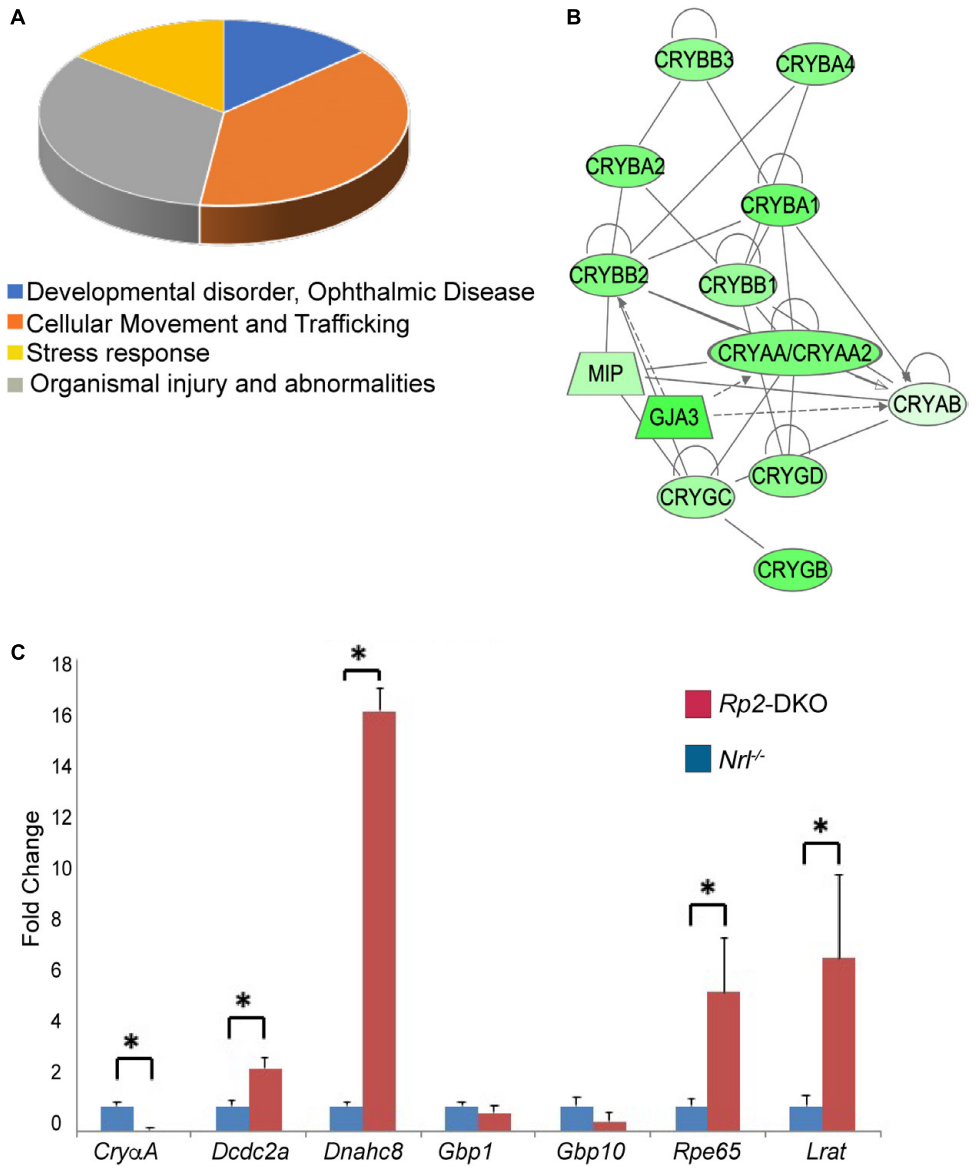

FIGURE 3 | Pathways dysregulated in the *Rp2*-DKO mice. **(A)** Pie chart representation of the major pathways that are represented by the genes with altered expression in the *Rp2*-DKO mice as compared to the $Nrl^{-/-}$ mice. **(B)** Network construction using IPA revealed the crystallin subunits as the major representative altered network in the *Rp2*-DKO mice. **(C)** qRT-PCR analysis of the indicated genes was performed using three independent samples each with six retinas. $^{*}p < 0.0001$.

expression was also elevated by ∼5 and 7 fold, respectively. As control, Gbp1 (guanylate binding protein 1) and Gbp10 did not show any change in the expression levels in the RNAseq and qRT-PCR analyses.

DISCUSSION

The mechanisms by which cones respond to the loss of a retinal disease genes have remained elusive. We had previously reported that the loss of RP2 results in OS elongation specifically of cones. Here we report that the elongation of the cone OSs is associated with an upregulation of the genes involved in the phototransduction cascade and microtubule-associated and intracellular trafficking and cell migration pathways. Significant decrease in the stress response related genes with reduction of the whorls and rosette formation in the $Nrl^{-/-}$ mice was also observed in the absence of RP2. However, no effect on the progression of the age-dependent decline in photoreceptor function of the $Nrl^{-/-}$ mice or the localization of S-opsin was observed in the absence of RP2. Given that the majority of cones in the $Nrl^{-/-}$ mice are S-cones, our data suggest that elongation of the S-cone OSs is independent of the localization of S opsin,

indicating a distinct regulation of the structural and functional pathways of the cones.

The whorls and rosettes are believed to be formed due to the structural collapse of the retina in the absence of rods. This leads to a detachment of the cones from the retinal pigment epithelium (RPE) (Roger et al., 2012). Our data suggest that the elongation of the cone OSs led to the dissolution of the whorls and rosettes due to their renewed contact with the RPE. However, the lack of the whorls and rosettes and a reduction in the stress response pathways in the *Rp2*-DKO mice did not perturb the age-dependent decline in photoreceptor function, further indicating a distinction between the structure of the cone OS and ERG outcomes. Additional studies are needed to investigate this intriguing observation.

Not much is known about the mechanism of cone OS extension. It is possible that RP2 is involved in modulating the turnover of tubulin required for the extension of the axoneme. Support of this hypothesis comes from the analysis of the primary structure of RP2. RP2 shows homology to tubulin-binding cofactor C and was found to stimulate the activity of tubulin as well as another small GTPase ARL3 (Arf-GTPase like-3) (Bartolini et al., 2002; Grayson et al., 2002; Kuhnel et al., 2006). Moreover, the upregulation of *Dnahc8, Dnai1,* and *Dcdc2a* (**Figure 3C** and **Supplementary Table S1**), microtubule-associated protein encoding genes suggests a possible role of RP2 in structural regulation of the cilia. Although DNAHC8 is known to be involved in modulating motile cilia function (Samant et al., 2005), it may play a different and as yet unknown role in the retina. An alternative explanation for long cone OS is that RP2 regulates the turnover of the OS components in cones. Our observations that the elongated OSs show deformed membrane extensions suggest that RP2 is potentially involved in the availability of the proteins involved in facilitating cone OS shedding by regulating their trafficking to the OS.

It was previously reported that the $Nrl^{-/-}$ mice exhibit Müller cell activation, retinal vasculature defects, and RPE atrophy (Roger et al., 2012). These pathways may still be contributing to the observed decline in photoreceptor function in the *Rp2*-DKO mice. Additional investigations are necessary to determine the involvement of these pathways in cone dysfunction in RP2-associated as well as other retinopathies.

ETHICS STATEMENT

All animal experiments were performed in accordance with the approved procedures of the Institutional Animal Care and Use Committee.

AUTHOR CONTRIBUTIONS

LL and KR performed the research. HK designed the research and wrote the manuscript.

FUNDING

This work was supported by grants from Foundation Fighting Blindness (to HK) and National Eye Institute (EY022372 to HK).

ACKNOWLEDGMENTS

We thank Wei Zhang, Manisha Anand, and other members of the Khanna lab for assistance with data gathering and helpful discussions during the preparation of this manuscript.

SUPPLEMENTARY MATERIAL

The Supplementary Material for this article can be found online at: https://www.frontiersin.org/articles/10.3389/fgene.2019.00323/full#supplementary-material

TABLE S1 | Differentially expressed genes in the *Rp2*-DKO mice.

TABLE S2 | Representative pathways that are altered in the *Rp2*-DKO mice.

REFERENCES

Anand, M., and Khanna, H. (2012). Ciliary transition zone (TZ) proteins RPGR and CEP290: role in photoreceptor cilia and degenerative diseases. *Expert Opin. Ther. Targets* 16, 541–551. doi: 10.1517/14728222.2012.680956

Bartolini, F., Bhamidipati, A., Thomas, S., Schwahn, U., Lewis, S. A., and Cowan, N. J. (2002). Functional overlap between retinitis pigmentosa 2 protein and the tubulin-specific chaperone cofactor C. *J. Biol. Chem.* 277, 14629–14634. doi: 10.1074/jbc.m200128200

Besharse, J. C., Baker, S. A., Luby-Phelps, K., and Pazour, G. J. (2003). Photoreceptor intersegmental transport and retinal degeneration: a conserved pathway common to motile and sensory cilia. *Adv. Exp. Med. Biol.* 533, 157–164. doi: 10.1007/978-1-4615-0067-4_20

Chakraborty, D., Conley, S. M., Stuck, M. W., and Naash, M. I. (2010). Differences in RDS trafficking, assembly and function in cones versus rods: insights from studies of C150S-RDS. *Hum. Mol. Genet.* 19, 4799–4812. doi: 10.1093/hmg/ddq410

Chang, B., Khanna, H., Hawes, N., Jimeno, D., He, S., Lillo, C., et al. (2006). In-frame deletion in a novel centrosomal/ciliary protein CEP290/NPHP6 perturbs its interaction with RPGR and results in early-onset retinal degeneration in the rd16 mouse. *Hum. Mol. Genet.* 15, 1847–1857. doi: 10.1093/hmg/ddl107

Cideciyan, A. V., Rachel, R. A., Aleman, T. S., Swider, M., Schwartz, S. B., Sumaroka, A., et al. (2011). Cone photoreceptors are the main targets for gene therapy of NPHP5 (IQCB1) or NPHP6 (CEP290) blindness: generation of an all-cone Nphp6 hypomorph mouse that mimics the human retinal ciliopathy. *Hum. Mol. Genet.* 20, 1411–1423. doi: 10.1093/hmg/ddr022

Daniele, L. L., Lillo, C., Lyubarsky, A. L., Nikonov, S. S., Philp, N., Mears, A. J., et al. (2005). Cone-like morphological, molecular, and electrophysiological features of the photoreceptors of the Nrl knockout mouse. *Invest. Ophthalmol. Vis. Sci.* 46, 2156–2167. doi: 10.1167/iovs.04-1427

Deretic, D., and Wang, J. (2012). Molecular assemblies that control rhodopsin transport to the cilia. *Vis. Res.* 75, 5–10. doi: 10.1016/j.visres.2012.07.015

Fort, P. E., and Lampi, K. J. (2011). New focus on alpha-crystallins in retinal neurodegenerative diseases. *Exp. Eye Res.* 92, 98–103. doi: 10.1016/j.exer.2010.11.008

Gerdes, J. M., Davis, E. E., and Katsanis, N. (2009). The vertebrate primary cilium in development, homeostasis, and disease. *Cell* 137, 32–45. doi: 10.1016/j.cell.2009.03.023

Grati, M., Chakchouk, I., Ma, Q., Bensaid, M., Desmidt, A., Turki, N., et al. (2015). A missense mutation in DCDC2 causes human recessive deafness DFNB66, likely by interfering with sensory hair cell and supporting cell cilia length regulation. *Hum. Mol. Genet.* 24, 2482–2491. doi: 10.1093/hmg/ddv009

Grayson, C., Bartolini, F., Chapple, J. P., Willison, K. R., Bhamidipati, A., Lewis, S. A., et al. (2002). Localization in the human retina of the X-linked retinitis pigmentosa protein RP2, its homologue cofactor C and the RP2 interacting protein Arl3. *Hum. Mol. Genet.* 11, 3065–3074. doi: 10.1093/hmg/11.24.3065

Inglis, P. N., Boroevich, K. A., and Leroux, M. R. (2006). Piecing together a ciliome. *Trends Genet.* 22, 491–500. doi: 10.1016/j.tig.2006.07.006

Insinna, C., Humby, M., Sedmak, T., Wolfrum, U., and Besharse, J. C. (2009). Different roles for KIF17 and kinesin II in photoreceptor development and maintenance. *Dev. Dyn.* 238, 2211–2222. doi: 10.1002/dvdy.21956

Kandel, E. R. (2013). *Principles of Neural Science*. New York, NY: McGraw-Hill. doi: 10.1002/dvdy.21956

Kennedy, B., and Malicki, J. (2009). What drives cell morphogenesis: a look inside the vertebrate photoreceptor. *Dev. Dyn.* 238, 2115–2138. doi: 10.1002/dvdy.22010

Kuhnel, K., Veltel, S., Schlichting, I., and Wittinghofer, A. (2006). Crystal structure of the human retinitis pigmentosa 2 protein and its interaction with Arl3. *Structure* 14, 367–378. doi: 10.1016/j.str.2005.11.008

Li, L., Khan, N., Hurd, T., Ghosh, A. K., Cheng, C., Molday, R., et al. (2013). Ablation of the X-linked retinitis pigmentosa 2 (Rp2) gene in mice results in opsin mislocalization and photoreceptor degeneration. *Invest. Ophthalmol. Vis. Sci.* 54, 4503–4511. doi: 10.1167/iovs.13-12140

Li, L., Rao, K. N., Zheng-Le, Y., Hurd, T. W., Lillo, C., and Khanna, H. (2015). Loss of retinitis pigmentosa 2 (RP2) protein affects cone photoreceptor sensory cilium elongation in mice. *Cytoskeleton* 72, 447–454. doi: 10.1002/cm.21255

Mears, A. J., Kondo, M., Swain, P. K., Takada, Y., Bush, R. A., Saunders, T. L., et al. (2001). Nrl is required for rod photoreceptor development. *Nat. Genet.* 29, 447–452. doi: 10.1038/ng774

Moiseyev, G., Chen, Y., Takahashi, Y., Wu, B. X., and Ma, J. X. (2005). RPE65 is the isomerohydrolase in the retinoid visual cycle. *Proc. Natl. Acad. Sci. U.S.A.* 102, 12413–12418. doi: 10.1073/pnas.0503460102

Pazour, G. J., and Witman, G. B. (2003). The vertebrate primary cilium is a sensory organelle. *Curr. Opin. Cell Biol.* 15, 105–110. doi: 10.1016/s0955-0674(02)00012-1

Rajala, A., Dighe, R., Agbaga, M. P., Anderson, R. E., and Rajala, R. V. (2013). Insulin receptor signaling in cones. *J. Biol. Chem.* 288, 19503–19515. doi: 10.1074/jbc.M113.469064

Rao, K. N., Li, L., Zhang, W., Brush, R. S., Rajala, R. V., and Khanna, H. (2016). Loss of human disease protein retinitis pigmentosa GTPase regulator (RPGR) differentially affects rod or cone-enriched retina. *Hum. Mol. Genet.* 25, 1345–1356. doi: 10.1093/hmg/ddw017

Redmond, T. M., Yu, S., Lee, E., Bok, D., Hamasaki, D., Chen, N., et al. (1998). Rpe65 is necessary for production of 11-cis-vitamin A in the retinal visual cycle. *Nat. Genet.* 20, 344–351. doi: 10.1038/3813

Roger, J. E., Ranganath, K., Zhao, L., Cojocaru, R. I., Brooks, M., Gotoh, N., et al. (2012). Preservation of cone photoreceptors after a rapid yet transient degeneration and remodeling in cone-only Nrl-/- mouse retina. *J. Neurosci.* 32, 528–541. doi: 10.1523/JNEUROSCI.3591-11.2012

Rosenbaum, J. L., Cole, D. G., and Diener, D. R. (1999). Intraflagellar transport: the eyes have it. *J. Cell Biol.* 144, 385–388. doi: 10.1083/jcb.144.3.385

Rosenbaum, J. L., and Witman, G. B. (2002). Intraflagellar transport. *Nat. Rev. Mol. Cell Biol.* 3, 813–825. doi: 10.1038/nrm952

Ruiz, A., Winston, A., Lim, Y. H., Gilbert, B. A., Rando, R. R., and Bok, D. (1999). Molecular and biochemical characterization of lecithin retinol acyltransferase. *J. Biol. Chem.* 274, 3834–3841. doi: 10.1074/jbc.274.6.3834

Samant, S. A., Ogunkua, O. O., Hui, L., Lu, J., Han, Y., Orth, J. M., et al. (2005). The mouse t complex distorter/sterility candidate, Dnahc8, expresses a gamma-type axonemal dynein heavy chain isoform confined to the principal piece of the sperm tail. *Dev. Biol.* 285, 57–69. doi: 10.1016/j.ydbio.2005.06.002

Schwahn, U., Lezner, S., Dong, J., Feil, S., Hinzmann, B., van Duijnhoven, G., et al. (1998). Positional cloning of the gene for X-linked retinitis pigmentosa 2. *Nat. Genet.* 19, 327–332. doi: 10.1038/1214

Singla, V., and Reiter, J. F. (2006). The primary cilium as the cell's antenna: signaling at a sensory organelle. *Science* 313, 629–633. doi: 10.1126/science.1124534

Thapa, A., Morris, L., Xu, J., Ma, H., Michalakis, S., Biel, M., et al. (2012). Endoplasmic reticulum stress-associated cone photoreceptor degeneration in cyclic nucleotide-gated channel deficiency. *J. Biol. Chem.* 287, 18018–18029. doi: 10.1074/jbc.M112.342220

Yildiz, O., and Khanna, H. (2012). Ciliary signaling cascades in photoreceptors. *Vis. Res.* 75, 112–116. doi: 10.1016/j.visres.2012.08.007

Conflict of Interest Statement: The authors declare that the research was conducted in the absence of any commercial or financial relationships that could be construed as a potential conflict of interest.

frontiers in Genetics

BRIEF RESEARCH REPORT
published: 12 April 2019
doi: 10.3389/fgene.2019.00328

Diminished Expression of Fat and Dachsous PCP Proteins Impaired Centriole Planar Polarization in Drosophila

Sergio Garrido-Jimenez[1†], Angel-Carlos Roman[2†] and Jose Maria Carvajal-Gonzalez[1]*

[1] Departamento de Bioquímica, Biología Molecular y Genética, Facultad de Ciencias, Universidad de Extremadura, Badajoz, Spain, [2] Champalimaud Neuroscience Programme, Lisbon, Portugal

OPEN ACCESS

Edited by:
Xiaogang Wu,
University of Nevada, Las Vegas,
United States

Reviewed by:
Nathan Weinstein,
National Autonomous University of Mexico, Mexico
Patricio Olguin,
Universidad de Chile, Chile
Giuliano Callaini,
University of Siena, Italy

***Correspondence:**
Jose Maria Carvajal-Gonzalez
jmcarvaj@unex.es

[†] These authors have contributed equally to this work

Specialty section:
This article was submitted to Systems Biology, a section of the journal Frontiers in Genetics

Received: 09 November 2018
Accepted: 28 March 2019
Published: 12 April 2019

Citation:
Garrido-Jimenez S, Roman A-C and Carvajal-Gonzalez JM (2019) Diminished Expression of Fat and Dachsous PCP Proteins Impaired Centriole Planar Polarization in Drosophila. Front. Genet. 10:328. doi: 10.3389/fgene.2019.00328

Proper ciliary basal body positioning within a cell is key for cilia functioning. Centriole and basal body positioning depends on signaling pathways such as the planar cell polarity pathway (PCP) governed by Frizzled (Fz-PCP). There have been described two PCP pathways controlled by different protein complexes, the Frizzled-PCP and the Fat-PCP pathway. Centriole planar polarization in non-dividing cells is a dynamic process that depends on the Fz-PCP pathway to properly occur during development from flies to humans. However, the function of the Ft-PCP pathway in centrioles polarization is elusive. Here, we present a descriptive initial analysis of centrioles polarization in Fat-PCP loss of function (LOF) conditions. We found that Fat (Ft) and Dachsous (Ds) LOF showed a marked centrioles polarization defect similar to what we have previously reported in Fz-PCP alterations. Altogether, our data suggest that centriole planar polarization in Drosophila wings depends on both Ft-PCP and Fz-PCP pathways. Further analyses in single and double mutant conditions will be required to address the functional connection between PCP and centriole polarization in flies.

Keywords: centrioles, planar cell polarity, fat and dachsous, actin polymerization, planar cell polarity effectors

INTRODUCTION

Cilium is an organelle projected at the cell surface with several crucial functions during development and in adult organs. Cells use their cilia to communicate with the environment or to physically interact with the surrounding media (Satir and Christensen, 2007; Goetz and Anderson, 2010; Ishikawa and Marshall, 2011; Malicki and Johnson, 2017). An example of signaling associated with cilia is its vastly known function on Sonic hedgehog signaling (Briscoe and Therond, 2013). On the other hand, a mechanical function for cilia could be found in the choroid plexus lining the brain ventricles, where the beating of the cilium at their apical membranes generates the proper directional fluid flow of the cerebrospinal fluid (CSF) (Brooks and Wallingford, 2014). Based on these two types of cilia functions (signaling and/or mechanical), many genetic disorders or diseases underlying cilia miss-functioning have been described. These diseases are included and named as ciliopathies, and most of them are initiated during early development (Hildebrandt et al., 2011; Novarino et al., 2011; Braun and Hildebrandt, 2017; Reiter and Leroux, 2017).

Structurally, cilia consist of membrane surrounding a cytoskeletal structure known as the axoneme, which is anchored to the basal bodies. In ciliopathies, cilium miss-functioning is usually associated to defective assembly or placement in a group of cells (Hildebrandt et al., 2011; Braun and Hildebrandt, 2017). Cilia assembly is controlled by structural proteins linked to the cytoskeleton like tubulin but also to trafficking related proteins and organelles like endosomes (Bernabe-Rubio and Alonso, 2017; Mirvis et al., 2018). Cilia positioning is also associated to the cytoskeleton, but in this case, it depends on the cell polarity pathways controlling the three-dimensional distribution of organelles and plasma membrane composition at the single cell level. In polarized epithelial cells, cilia are projected from the apical membrane and in some specialized tissues are restricted to sub-areas at that apical membrane, named translational polarity, and/or their basal bodies orient their basal foot to the same direction, named rotational polarity (Carvajal-Gonzalez et al., 2016a; Adler and Wallingford, 2017).

This positioning of cilia needs also to be coordinated within the tissue to produce a global response like coordinated ciliary beating. A key pathway involved in coordinating cells during tissue development is the Planar cell polarity (PCP) pathway, a conserved pathway from Drosophila to humans. PCP is established and maintained by two signaling cascades, the Frizzled PCP (Fz-PCP) and the Fat PCP (Ft-PCP) pathways. Fz-PCP pathway is governed by two protein complexes, the Frizzled/Disheveled/Flamingo/Diego (Fz/Dsh/Fmi/Dgo) complex and Vang/Prickle/Flamingo (Vang/Pk/Fmi) complex (Goodrich and Strutt, 2011; Adler, 2012; Peng and Axelrod, 2012; Singh and Mlodzik, 2012; Carvajal-Gonzalez and Mlodzik, 2014; Devenport, 2014). The Ft-PCP pathway is based on the interaction between Fat (Ft) and Dachsous (Ds). The interaction across adjacent membranes of these proto-cadherins is coordinated by the Golgi resident kinase Four-jointed (Fj) (Zeidler et al., 1999, 2000; Matakatsu and Blair, 2004, 2006; Simon, 2004; Brittle et al., 2010, 2012; Simon et al., 2010; Mao et al., 2011). Fz-PCP has been shown to control the orientation of the cilia by controlling the docking of the basal body including the mother and daughter centrioles. This connection between Fz-PCP and basal bodies/centriole positioning is a well-conserved function in different organs across species. On the contrary, the function of Ft-PCP in ciliary basal bodies/centriole positioning is not clarified yet. It has been shown that in *Fat4* knock-out mice, hair cells are mis-orientated throughout the cochlea when looking at stereocilia (Saburi et al., 2008), however, the kinocilium basal body positioning was not assessed.

We have recently found that centriole positioning was also controlled by the Fz-PCP pathway in Drosophila epithelial cells where cilia are absent (Carvajal-Gonzalez et al., 2016a,b). In Drosophila pupal wings, we were able to show that centrioles polarization (off-centered movement of centrioles at the apical planes) was a dynamic process that occurs during trichomes formation, and that this polarization was abnormal when Fz-PCP signaling was defective using loss or gain of function experimental conditions (Carvajal-Gonzalez et al., 2016a,b). Since Ft-PCP is also important during morphogenesis in Drosophila pupal wings, here we decided to test the connection between Ft-PCP and centriole positioning in this model system.

MATERIALS AND METHODS

Fly Strains

To analyze the role of Ft-PCP in centriole polarization in Drosophila pupal wings we first tested all the available RNAi lines targeting the known components of the Fat-PCP pathway including, Fat (Ft), Dachsous (Ds), Dachs and Four jointed (Fj). All culture and cross of fly lines were performed on standard medium and maintained at indicated temperatures (25 or 29°C). Following fly lines were used in this study: Ft-IR (9396/GD and 108863/KK VDRC stocks), Ds-IR (36219/DG and 4316/GD VDRC stocks), Dachs-IR (12555/GD; 32142/GD and 102504/GD VDRC stocks), Fj-IR (6774/GD VDRC stock). GAL4/UAS system was used to direct UAS-RNAi constructs to *decapentaplegic* (*dpp*) wing compartment, a stripe between L3 and L4. In our experimental conditions, we found that only two lines (Ft and Ds) produced robust PCP phenotypes (**Figures 1A,B** and **Supplementary Figure S1F**). These phenotypes in adult wings corresponded to hair mis-orientation in the proximal part of the wing near the L3 vein (**Figures 1A,B**). None of the tested lines for Fj generates PCP phenotypes under our experimental conditions (**Supplementary Figures S1D,E**) and out of the three lines tested for Dachs (**Supplementary Figures S1A–C**), only 1 line showed hair mis-orientation phenotypes but not in all the wings analyzed (**Supplementary Figure S1C**).

Adult Wing Analyses

For adult trichomes analyses, wings were removed, washed in PBS 0.1% Triton X-100 (PBS-t) and mounted on a slide in 80% glycerol in PBS. Adult wings were imaged on a BX51 direct microscope (Olympus). Images acquisition was performed with a camera (DP72, Olympus) and CellD software (Olympus).

Immunohistochemistry

Fly pupae at white stage were collected and cultured at 29°C for 25 or 28.5 h. Wings were dissected in PBS-t and fixed for 1 h with 4% paraformaldehyde (PFA). Pupae were washed in PBS-t three times for 5 min and blocked in PBS-t with 2% bovine serum albumin (BSA) for 45 min. Dissected pupae were incubated overnight with primary antibody at room temperature in PBS-t-BSA. After incubation, samples were washed five times in PBS-t and incubated in fluorescent phalloidin and fluorescent secondary antibodies for 90 min, both diluted in PBS-t-BSA. Five additional washes were performed in PBS-t, and pupal wings were detached from the pupal cage and mounted on slides with medium for fluorescence (Vectashield, Vector Laboratories). To stain the cellular membrane was used anti-Fmi (from DSHB). Secondary antibody conjugated with the fluorophore Alexa-405 (Invitrogen) and Alexa 594-phalloidin (Invitrogen) were used at 1:200.

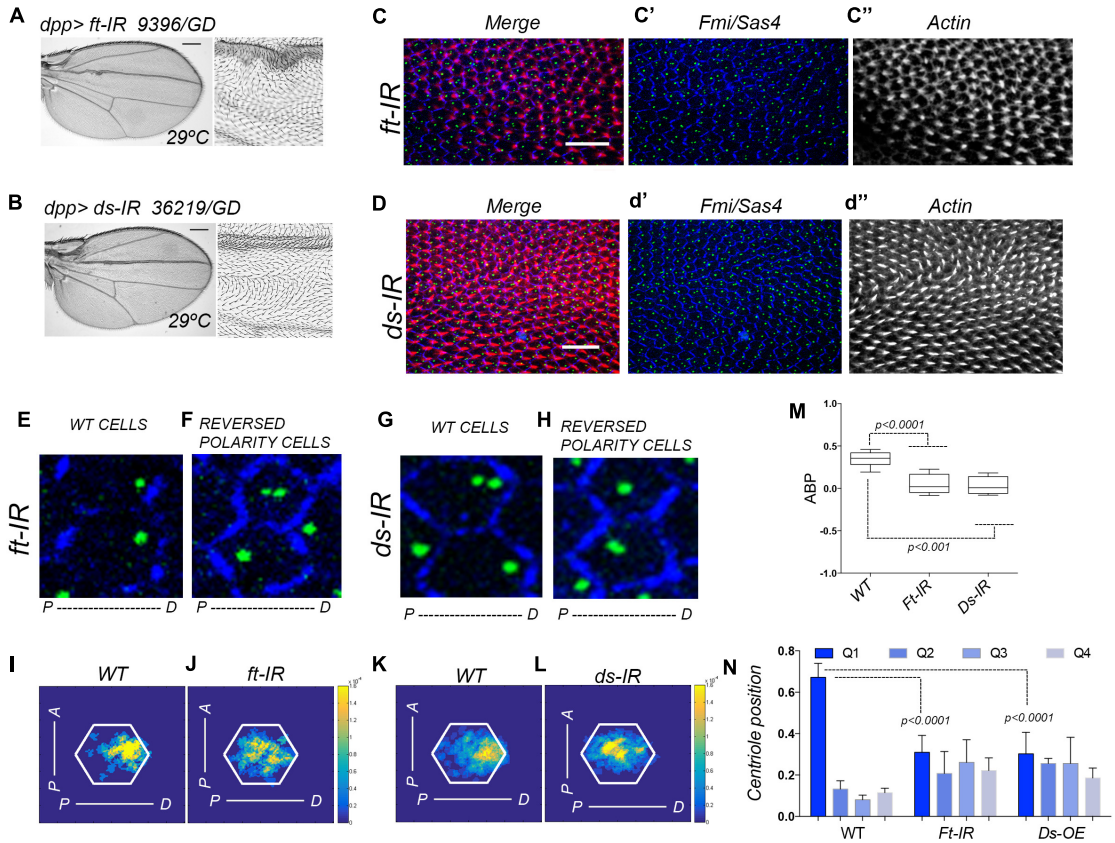

FIGURE 1 | Ft-PCP pathway LOF conditions affect centriole polarity. **(A,B)** In adult wings, single knock-down for Ft or Ds using *dpp>ft-IR or dpp>ds-IR* generates hair mis-orientation phenotypes and rounded wing shape. Both phenotypes have been previously observed in Ft and Ds mutants. **(C,D)** In *dpp>ft-IR or dpp>ds-IR* pupal wing hair mis-orientation phenotype are also presented in the dpp domain (actin-based hair labeled with phalloidin in red, *Sas4* coupled to GFP in green to mark centrioles, *Fmi* in blue for cell junctions). **(E–H)** Cells with WT orientation of hairs showed proper centriole localization at the distal side of the cell **(E,G)**. On the other hand, neighbor cells knocked-down for Ft or Ds with reversed polarity (reversed hair orientation) did not localize centrioles to the distal side of the cell **(F,H)**. **(I–L)** Centriole distribution visualization in density maps showed that both, *dpp>ds-IR* and *dpp>ft-IR*, centriole positioning is affected when compare to WT areas of the same wings. **(M,N)** Quantification of centriole polarization using the ABP method **(M)** or the Q method **(N)** showed that cells knocked-down for Ft or Ds failed to polarized centriole to the level of WT cells. Statistical analyses among experimental groups: *t*-test. Scale bars in **(A,B)** represent 25 mm Scale bars in **(C,D)** represent 10 μm.

Image Acquisition and Processing

To orientate pupal wings, the distal part was always pointed to the right side. Images were acquired using FV 1000 confocal microscope (Olympus). After acquisition, images were processed using Fiji, to generate the cell borders mask (Tissue Analyzer plugin), and Adobe Photoshop CC 2015 to create the color-coded mask based on the phenotype.

Heat (Density) Maps

We used density maps in order to visualize relative centriole positioning from a set of cells. Briefly, we modeled each cell to a regular hexagon with its area being the pixel numbers of the cell, and then we normalized all the modeled hexagon cells to the same size. Afterward, we normalized the position of the centriole relative to the centroid of its cell to the model cell. We have found that every cell in the Drosophila pupal wing has two centrioles but in many cases these two centrioles are too close to be separated, many times they are sitting one on top of the other. Our method compute each centriole individually. Finally, we represented the centriole density in the set of cells, so each pixel in the density map represents the probability of finding a centriole in that set of cells.

ABP Method

Average Basal Body Position (ABP) for each sample was calculated following Hashimoto et al. (2010) protocol. Briefly, the score of each cell represented the normalized position of the centriole along the anterior-posterior axis (being − 1.0 the minimal anterior coordinate of the cell, 0 the cell centroid and 1.0 the maximal posterior coordinate of the cell). Then, the ABP score was calculated as the average value of the cells in an image.

Q Method

Each centriole was assigned to a specific Quartile (Q) depending on their relative position to the anterior-posterior axis of the

cell that crosses the cell centroid (Taniguchi et al., 2011). If the centriole was located between $-\pi/4$ and $\pi/4$, then it was assigned to Q1. If the centriole was located between $\pi/4$ and $3\pi/4$, it was assigned to Q2. In the case of being located between $-\pi/4$ and $-3\pi/4$, then it was assigned to Q3, and finally the rest of centrioles were assigned to Q4.

Statistical Analyses

Data were analyzed using *t*-test (GraphPad Prism) for Q and ABP methods.

RESULTS

We have previously described that centrioles polarization is a dynamic process that occurred during hair formation in Drosophila pupal wings. In wild type (WT) conditions, centrioles move from centered positions at the most apical part of pupal wing epithelial cells and as the actin-based hair is forming centrioles move off center toward the base of the hairs (Carvajal-Gonzalez et al., 2016b; Garrido-Jimenez et al., 2018). To analyze the polarization of centrioles in Ft-PCP deficient conditions, we combined hair staining with phalloidin to assess those wings with well-formed hairs, while using GFP-Sas4 fluorescent expression to visualize centrioles and immunolabeled Fmi to delimit each epithelial cell (**Figures 1C–H** for higher magnifications). To visualize the centriole population distribution, we employed a heat (density) map for a WT or its RNAi neighbor field (**Figures 1I–L**). To properly quantify centriole polarization, we used two different standard methods, the ABP method and the Q method. Briefly, the ABP method measures the anterior or posterior positions of centrioles relative to the center of the cell (visualized from the top). On the other hand, the Q method quantify the distribution of centrioles in 45 degrees' quartiles (Q1, Q2, Q3, and Q4). In regions with hair mis-orientation phenotypes generated by knock-down of Ft or Ds we found that centrioles fail to properly polarize toward the distal side at the apical planes, as shown in density maps for Ds or Ft knocked-down cells compared to near WT cells (**Figures 1I–L**). Looking at the Q1-4 values, similar percentages of centrioles are found in each of them in Ft-IR and Ds-IR conditions. In contrast above 60% of centrioles are found in Q1 for WT cells (**Figure 1N**). In addition, the ABP quantification in Ft-IR and Ds-IR conditions showed that centriole remained at more centered position in the cell when compared to centriole polarization in WT areas of the same wings (**Figure 1M**). Altogether, these results support the hypothesis that centriole polarization is also controlled by the Fat and Dachsous PCP pathway.

DISCUSSION

This article together with the previously published data on cilia and PCP in vertebrates pushes forward the idea that PCP is a well-conserved regulator of centriole positioning. It also highlighted for the first time the importance of Ft-PCP

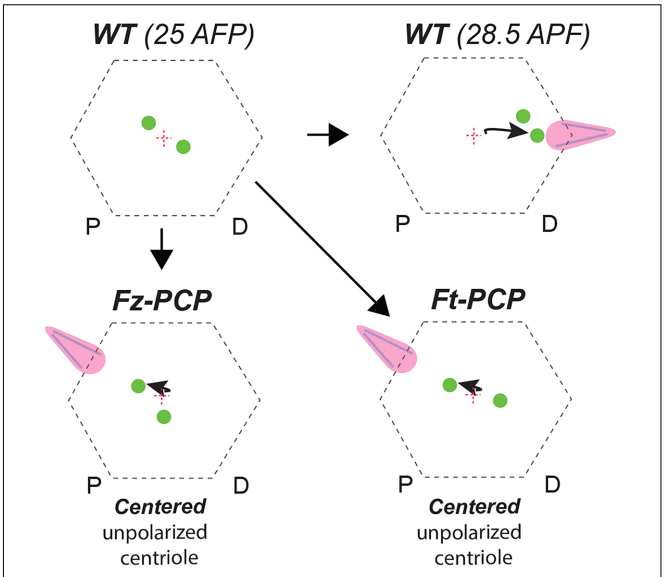

FIGURE 2 | Centriole positioning illustration in WT and Fz-PCP or Ft-PCP deficient conditions. Schematic representation of the phenotypes described. In WT Drosophila wing epithelial cells aged to 28.5 APF (after puparium formation) centrioles migrate to base of the actin-hairs. Under the same experimental conditions, in Ft-PCP LOF conditions centrioles failed in this polarized movement. This phenotype resembled the one found in Fz-PCP LOF conditions already published (Carvajal-Gonzalez et al., 2016b).

in centriole positioning independently of cell division. In vertebrates, there are four Fat homologs (Fat1–4), two Ds homologs (Ds1 and Ds2), and one Fj ortholog (Fjx1) (Rock et al., 2005). *Fat4* knock-out mice have been described to have dilated tubules and cysts formation in their kidneys. This phenotype is connected to randomization of spindle orientation affecting oriented cell division, which is important for tubule elongation and single lumen formation (Saburi et al., 2008). In addition, it has been shown that PCP proteins such as Fat4 and Vangl2 localize to the base of cilia in cultured cells. Interestingly, Fat4 is localized to the primary cilium. Furthermore, Dchs1 knock-out mice showed mild defects in early uroteric bud branching morphogenesis, resulting in kidneys that are reduced in size (Mao et al., 2011).

Moreover, over-expression of the Sple isoform of *pk* in developing wings has recently been reported to reverse PCP orientation, resulting in actin hair formation being moved to the proximal cellular vertex without affecting Vang or Dsh localization (Ayukawa et al., 2014; Olofsson et al., 2014). We have previously published that Pk over-expression in Drosophila pupal wings cause centriole positioning defects concomitant with reversed actin-based hair formation (Carvajal-Gonzalez et al., 2016a,b). In addition, Sple-OE was shown to modulate coupling between the Fz-PCP and Ft-PCP pathway (Merkel et al., 2014). As a whole, we can envision a system where centriole positioning is a global output controlled by both PCP pathways (**Figure 2**). Hence, this new role for Ft-PCP could be linked to Fz-PCP rather than independent of it. Future experiments are required

to confirm or rule out this long-standing conflict about the interdependency of these two PCP pathways.

AUTHOR CONTRIBUTIONS

SG-J performed all of the experiments. A-CR designed and performed the data analysis. JC-G designed the experiments, analyzed data, and wrote the manuscript.

FUNDING

JC-G was a recipient of an "Atraccion y Retencion de talento" contract from the GOBEX (Extremadura Government) and was recipient of a Ramón y Cajal contract (RYC-2015-17867). This work was supported by BFU2014-54699-P, BFU2017-85547-P grants from the Ministry of Economy to JC-G and GR15164 from Junta de Extremadura. A-CR was a recipient of a FEBS Long-Term Postdoctoral Fellowship. SG-J was a recipient of a Fellowship from the Universidad de Extremadura. All Spanish funding was co-sponsored by the European Union FEDER program.

ACKNOWLEDGMENTS

We are most grateful to Jordan Raff for many reagents and all members of the Carvajal lab for helpful suggestions, comments, and discussions during the development and execution of the project. We thank the Bloomington and VDRC Stock Centers for fly strains, and the DSHB for antibodies. Confocal microscopy was performed at the UEX microscopy core facility (Servicio de Técnicas Aplicadas a Biociencias, STAB).

SUPPLEMENTARY MATERIAL

The Supplementary Material for this article can be found online at: https://www.frontiersin.org/articles/10.3389/fgene.2019.00328/full#supplementary-material

FIGURE S1 | Fat-PCP pathway related RNAi lines used in adult screening that do not cause strong hair mis-orientation phenotypes. **(A–F)** Images from adult wing aged at 29°C and knock-down for single Ft-PCP components using *dpp>gal4 as a driver* that do not generate hair mis-orientation phenotypes. Scale bars represent 250 mm.

REFERENCES

Adler, P. N. (2012). The frizzled/stan pathway and planar cell polarity in the drosophila wing. *Curr. Top. Dev. Biol.* 101, 1–31. doi: 10.1016/B978-0-12-394592-1.00001-6

Adler, P. N., and Wallingford, J. B. (2017). From planar cell polarity to ciliogenesis and back: the curious tale of the PPE and CPLANE proteins. *Trends Cell Biol.* 27, 379–390. doi: 10.1016/j.tcb.2016.12.001

Ayukawa, T., Akiyama, M., Mummery-Widmer, J. L., Stoeger, T., Sasaki, J., Knoblich, J. A., et al. (2014). Dachsous-dependent asymmetric localization of spiny-legs determines planar cell polarity orientation in Drosophila. *Cell Rep.* 8, 610–621. doi: 10.1016/j.celrep.2014.06.009

Bernabe-Rubio, M., and Alonso, M. A. (2017). Routes and machinery of primary cilium biogenesis. *Cell Mol. Life Sci.* 74, 4077–4095. doi: 10.1007/s00018-017-2570-5

Braun, D. A., and Hildebrandt, F. (2017). Ciliopathies. *Cold Spring Harb. Perspect. Biol.* 9:a028191. doi: 10.1101/cshperspect.a028191

Briscoe, J., and Therond, P. P. (2013). The mechanisms of hedgehog signalling and its roles in development and disease. *Nat. Rev. Mol. Cell Biol.* 14, 416–429. doi: 10.1038/nrm3598

Brittle, A., Thomas, C., and Strutt, D. (2012). Planar polarity specification through asymmetric subcellular localization of Fat and Dachsous. *Curr. Biol.* 22, 907–914. doi: 10.1016/j.cub.2012.03.053

Brittle, A. L., Repiso, A., Casal, J., Lawrence, P. A., and Strutt, D. (2010). Four-jointed modulates growth and planar polarity by reducing the affinity of dachsous for fat. *Curr. Biol.* 20, 803–810. doi: 10.1016/j.cub.2010.03.056

Brooks, E. R., and Wallingford, J. B. (2014). Multiciliated cells. *Curr. Biol.* 24, R973–R982. doi: 10.1016/j.cub.2014.08.047

Carvajal-Gonzalez, J. M., and Mlodzik, M. (2014). Mechanisms of planar cell polarity establishment in Drosophila. *F1000Prime Rep.* 6:98. doi: 10.12703/P6-98

Carvajal-Gonzalez, J. M., Mulero-Navarro, S., and Mlodzik, M. (2016a). Centriole positioning in epithelial cells and its intimate relationship with planar cell polarity. *Bioessays* 38, 1234–1245. doi: 10.1002/bies.201600154

Carvajal-Gonzalez, J. M., Roman, A. C., and Mlodzik, M. (2016b). Positioning of centrioles is a conserved readout of frizzled planar cell polarity signalling. *Nat. Commun.* 7:11135. doi: 10.1038/ncomms11135

Devenport, D. (2014). The cell biology of planar cell polarity. *J. Cell Biol.* 207, 171–179. doi: 10.1083/jcb.201408039

Garrido-Jimenez, S., Roman, A. C., Alvarez-Barrientos, A., and Carvajal-Gonzalez, J. M. (2018). Centriole planar polarity assessment in Drosophila wings. *Development* 145:dev.169326. doi: 10.1242/dev.169326

Goetz, S. C., and Anderson, K. V. (2010). The primary cilium: a signalling centre during vertebrate development. *Nat. Rev. Genet.* 11, 331–344. doi: 10.1038/nrg2774

Goodrich, L. V., and Strutt, D. (2011). Principles of planar polarity in animal development. *Development* 138, 1877–1892. doi: 10.1242/dev.054080

Hashimoto, M., Shinohara, K., Wang, J., Ikeuchi, S., Yoshiba, S., Meno, C., et al. (2010). Planar polarization of node cells determines the rotational axis of node cilia. *Nat. Cell Biol.* 12, 170–176. doi: 10.1038/ncb2020

Hildebrandt, F., Benzing, T., and Katsanis, N. (2011). Ciliopathies. *N. Engl. J. Med.* 364, 1533–1543. doi: 10.1056/NEJMra1010172

Ishikawa, H., and Marshall, W. F. (2011). Ciliogenesis: building the cell's antenna. *Nat. Rev. Mol. Cell Biol.* 12, 222–234. doi: 10.1038/nrm3085

Malicki, J. J., and Johnson, C. A. (2017). The cilium: cellular antenna and central processing unit. *Trends Cell Biol.* 27, 126–140. doi: 10.1016/j.tcb.2016.08.002

Mao, Y., Mulvaney, J., Zakaria, S., Yu, T., Morgan, K. M., Allen, S., et al. (2011). Characterization of a Dchs1 mutant mouse reveals requirements for Dchs1-Fat4 signaling during mammalian development. *Development* 138, 947–957. doi: 10.1242/dev.057166

Matakatsu, H., and Blair, S. S. (2004). Interactions between Fat and Dachsous and the regulation of planar cell polarity in the Drosophila wing. *Development* 131, 3785–3794. doi: 10.1242/dev.01254

Matakatsu, H., and Blair, S. S. (2006). Separating the adhesive and signaling functions of the Fat and Dachsous protocadherins. *Development* 133, 2315–2324. doi: 10.1242/dev.02401

Merkel, M., Sagner, A., Gruber, F. S., Etournay, R., Blasse, C., Myers, E., et al. (2014). The balance of prickle/spiny-legs isoforms controls the amount of coupling between core and fat PCP systems. *Curr. Biol.* 24, 2111–2123. doi: 10.1016/j.cub.2014.08.005

Mirvis, M., Stearns, T., and James Nelson, W. (2018). Cilium structure, assembly, and disassembly regulated by the cytoskeleton. *Biochem. J.* 475, 2329–2353. doi: 10.1042/BCJ20170453

Novarino, G., Akizu, N., and Gleeson, J. G. (2011). Modeling human disease in humans: the ciliopathies. *Cell* 147, 70–79. doi: 10.1016/j.cell.2011.09.014

Olofsson, J., Sharp, K. A., Matis, M., Cho, B., and Axelrod, J. D. (2014). Prickle/spiny-legs isoforms control the polarity of the apical microtubule

network in planar cell polarity. *Development* 141, 2866–2874. doi: 10.1242/dev.105932

Peng, Y., and Axelrod, J. D. (2012). Asymmetric protein localization in planar cell polarity: mechanisms, puzzles, and challenges. *Curr. Top. Dev. Biol.* 101, 33–53. doi: 10.1016/B978-0-12-394592-1.00002-8

Reiter, J. F., and Leroux, M. R. (2017). Genes and molecular pathways underpinning ciliopathies. *Nat. Rev. Mol. Cell Biol.* 18, 533–547. doi: 10.1038/nrm.2017.60

Rock, R., Schrauth, S., and Gessler, M. (2005). Expression of mouse dchs1, fjx1, and fat-j suggests conservation of the planar cell polarity pathway identified in Drosophila. *Dev. Dyn.* 234, 747–755. doi: 10.1002/dvdy.20515

Saburi, S., Hester, I., Fischer, E., Pontoglio, M., Eremina, V., Gessler, M., et al. (2008). Loss of Fat4 disrupts PCP signaling and oriented cell division and leads to cystic kidney disease. *Nat. Genet.* 40, 1010–1015. doi: 10.1038/ng.179

Satir, P., and Christensen, S. T. (2007). Overview of structure and function of mammalian cilia. *Annu. Rev. Physiol.* 69, 377–400. doi: 10.1146/annurev.physiol.69.040705.141236

Simon, M. A. (2004). Planar cell polarity in the Drosophila eye is directed by graded Four-jointed and Dachsous expression. *Development* 131, 6175–6184. doi: 10.1242/dev.01550

Simon, M. A., Xu, A., Ishikawa, H. O., and Irvine, K. D. (2010). Modulation of fat:dachsous binding by the cadherin domain kinase four-jointed. *Curr. Biol.* 20, 811–817. doi: 10.1016/j.cub.2010.04.016

Singh, J., and Mlodzik, M. (2012). Planar cell polarity signaling: coordination of cellular orientation across tissues. *Wiley Interdiscip. Rev. Dev. Biol.* 1, 479–499. doi: 10.1002/wdev.32

Taniguchi, K., Maeda, R., Ando, T., Okumura, T., Nakazawa, N., Hatori, R., et al. (2011). Chirality in planar cell shape contributes to left-right asymmetric epithelial morphogenesis. *Science* 333, 339–341. doi: 10.1126/science.1200940

Zeidler, M. P., Perrimon, N., and Strutt, D. I. (1999). The four-jointed gene is required in the Drosophila eye for ommatidial polarity specification. *Curr. Biol.* 9, 1363–1372. doi: 10.1016/S0960-9822(00)80081-0

Zeidler, M. P., Perrimon, N., and Strutt, D. I. (2000). Multiple roles for four-jointed in planar polarity and limb patterning. *Dev. Biol.* 228, 181–196. doi: 10.1006/dbio.2000.9940

Conflict of Interest Statement: The authors declare that the research was conducted in the absence of any commercial or financial relationships that could be construed as a potential conflict of interest.

frontiers in Genetics

ORIGINAL RESEARCH
published: 13 November 2019
doi: 10.3389/fgene.2019.01083

An Integrated Analysis of Radial Spoke Head and Outer Dynein Arm Protein Defects and Ciliogenesis Abnormality in Nasal Polyps

Xiao-xue Zi[1,2†], Wei-jie Guan[2,3†], Yang Peng[2,3], Kai Sen Tan[2], Jing Liu[2], Ting-ting He[2], Yew-kwang Ong[4], Mark Thong[4], Li Shi[1] and De-yun Wang[2*]*

[1] Department of Otolaryngology-Head and Neck Surgery, Shandong Provincial ENT Hospital Affiliated to Shandong University, Jinan, China, [2] Department of Otolaryngology, Yong Loo Lin School of Medicine, National University of Singapore, Singapore, Singapore, [3] State Key Laboratory of Respiratory Disease, National Clinical Research Center for Respiratory Disease, Guangzhou Institute of Respiratory Health, First Affiliated Hospital of Guangzhou Medical University, Guangzhou Medical University, Guangzhou, Guangdong, China, [4] Department of Otolaryngology-Head and Neck Surgery, National University Hospital System (NUHS), Singapore, Singapore

OPEN ACCESS

Edited by:
Sonia Mulero Navarro,
University of Extremadura, Spain

Reviewed by:
Mark Philipp Kühnel,
Hannover Medical School, Germany
Raj Ladher,
National Centre for Biological Sciences, India
Angel Carlos Roman,
University of Extremadura, Spain

***Correspondence:**
Li Shi
shili126@sina.com
De-yun Wang
entwdy@nus.edu.sg

†These authors have contributed equally to this work

Specialty section:
This article was submitted to Genetic Disorders, a section of the journal Frontiers in Genetics

Received: 16 August 2018
Accepted: 09 October 2019
Published: 13 November 2019

Citation:
Zi X-x, Guan W-j, Peng Y, Tan KS, Liu J, He T-t, Ong Y-k, Thong M, Shi L and Wang D-y (2019) An Integrated Analysis of Radial Spoke Head and Outer Dynein Arm Protein Defects and Ciliogenesis Abnormality in Nasal Polyps. Front. Genet. 10:1083. doi: 10.3389/fgene.2019.01083

Background: Nasal polyp (NP) is a chronic upper airway inflammatory disease that is frequently triggered by defective host-defense. However, the mechanisms underlying the impaired barrier function such as cilia-mediated mucociliary clearance remain poorly understood.

Objective: To assess ciliary ultrastructural and ciliogenesis marker expression and the phenotypes of ciliated cells in NP.

Methods: NP biopsy samples were obtained from 97 NP patients and inferior turbinate from 32 healthy controls. Immunofluorescence staining, quantitative polymerase chain reaction, and single-cell cytospin staining were performed. We classified the patterns of radial spoke head protein (*RSPH*) 1, 4A (*RSPH4A*), 9 (*RSPH9*), and dynein axonemal heavy chain 5 (*DNAH5*) localization. A semi-quantitative scoring system was developed to assess their expression patterns and associations with ciliogenesis markers [centrosomal protein 110 (*CP110*) and forkhead box j1 (*FOXJ1*)].

Results: Median scores of *RSPH1*, *RSPH4A*, *RSPH9,* and *DNAH5* were significantly higher in NP than in healthy controls, particularly in eosinophilic NPs. Expression pattern scores of *RSPH1*, *RSPH4A*, *RSPH9,* and *DNAH5* correlated positively with each other in both groups. In primary-cell specimens, abnormal expression patterns were significantly more common in NP. The total fluorescence intensity of *CP110* and *FOXJ1* was significantly higher in NPs and correlated positively with expression pattern scores of *RSPH1*, *RSPH4A*, *RSPH9,* and *DNAH5*. A trend towards lengthened cilia was observed in NP.

Conclusion: In the chronic airway inflammatory milieu, the up-regulated ciliogenesis correlates with the abnormal expression of ciliary ultrastructural markers (i.e., *DNAH5*) in NP (particularly eosinophilic NP).

Keywords: abnormal ciliary ultrastructure, inflammation, inferior turbinate, nasal polyps, mucociliary clearance, up-regulated ciliogenesis

INTRODUCTION

Nasal polyp (NP) is a common chronic upper airway inflammatory disorder that frequently co-exists with lower airway inflammatory diseases such as asthma (Fokkens et al., 2012). In Asian population, NP is mostly characterized by prominent epithelial remodeling and mixed inflammatory phenotypes (Hao et al., 2006). Physiologically, the respiratory cilia maintain proper clearance of pathogens and allergens (Li et al., 2012). We have previously demonstrated the poorly proliferated basal cells and up-regulation of ciliogenesis markers [centrosomal protein 110 (*CP110*), and fork-head box J1 (*FOXJ1*)] in the aberrantly remodeled epithelium of NP (Li et al., 2014; Zhao et al., 2017). Furthermore, abnormal ciliary morphology (i.e., overly dense and lengthened cilia), abnormal expression of dynein axonemal heavy chain 5 (*DNAH5*, the marker crucial to microtubule sliding), and the significantly reduced ciliary beat frequency (CBF) have also been observed in NP (Lai et al., 2011; Li et al., 2014; Qiu et al., 2018). Therefore, abnormal ciliogenesis and/or ultrastructure might be critical drivers of impaired mucociliary clearance (MCC), contributing to the chronic inflammation in NPs.

Physiologically, ciliary motility is mainly regulated by the outer dynein arms and radial spoke (RS) complexes (Smith and Yang, 2004; Frommer et al., 2015). Abnormal expression of *DNAH5* (which has previously been linked to genetic defects) has been implicated in chronic lower airway inflammatory diseases such as primary ciliary dyskinesia (PCD), Kartagener syndrome, bronchiectasis, and chronic obstructive pulmonary disease (Hornef et al., 2006; Failly et al., 2009; Leigh et al., 2009; Lee et al., 2014; Chen et al., 2018; Qiu et al., 2018). RSs are important ultrastructural proteins that are aligned between the central and peripheral microtubules (Shinohara et al., 2015). Mutations of RS head protein 1 (*RSPH1*), 4A (*RSPH4A*), and 9 (*RSPH9*) could have significantly affected the interactions between RS head and central microtubules (Frommer et al., 2015). Intriguingly, RS defects have been identified among 19% of patients with ciliary ultrastructural abnormalities (Plesec et al., 2008), and reportedly account for ~6% of patients with PCD (Ibanez-Tallon et al., 2003).

To ensure proper ciliary motility, ciliogenesis is crucial to the formation of axonemes where ciliary ultrastructural proteins are assembled. *CP110* reportedly regulated centrosome duplication and centriole conversion to basal bodies (Chen et al., 2002; Yadav et al., 2016). Inflammation-mediated up-regulation of *CP110* contributed to defective cilia assembly and decreased motility in CRS (Lai et al., 2011; Li et al., 2014). Additionally, increased FOXJ1-positive cell count correlated with longer and denser cilia in NP (Li et al., 2014). Collectively, abnormal expression of *CP110* and *FOXJ1* may have resulted in disrupted cilia assembly in NP.

Currently, most reports focused on isolated ciliogenesis or ciliary ultrastructural marker. The association between ciliogenesis or ciliary ultrastructural marker expression remains understudied. Furthermore, abnormal expression of some ultrastructural markers (i.e. *DNAH5*) was reportedly present in congenital diseases such as PCD. Because secondary ciliary dyskinesia (SCD) is common among various chronic inflammatory diseases (Al-Rawi et al., 1998), we hypothesized that the inflammatory milieu might be the critical driver of the defective ciliogenesis and abnormality of ultrastructural markers in NP. Building on our previous research, we sought to systematically investigate the expression patterns of four ciliary ultrastructural markers (*RSPH1*, *RSPH4A*, *RSPH9,* and *DNAH5*) and two ciliogenesis markers (*CP110* and *FOXJ1*) for their manifestation of ciliary impairment in NPs. Our findings might help elucidate the roles of ciliogenesis and ciliary ultrastructural markers in NP pathogenesis, and whether chronic airway inflammation is responsible for the abnormal expression of ciliary ultrastructural markers.

METHODS

Study Population

Surgical samples from 97 patients with NP and inferior turbinate (IT) mucosa from 32 control subjects were obtained from The Second Affiliated Hospital of Shandong University (China) and National University Hospital of Singapore (Singapore). Patients were diagnosed as having chronic rhinosinusitis with NP (grade 2 or 3) according to European Position Paper on Rhinosinusitis and Nasal Polyps 2012 criteria and NP was histologically confirmed post-operatively. (Fokkens et al., 2012). Patients with upper respiratory tract infections within four weeks and who were highly suspicious of having PCD were excluded. Atopy was evaluated with skin prick testing, and asthma was diagnosed based on physician's diagnosis. Control subjects were scheduled for septum plastic surgery and remaining free of sinus symptoms. Primary single-cell specimens for cytospin were obtained from NP (n = 20) and healthy controls (n = 11). Due to the limited sizes of the tissue, not all specimens were used for each analysis.

Our study was carried out in accordance with The Declaration of Helsinki. Ethics approval was obtained from the institutional review boards of the two participating hospitals. All participants signed written informed consent.

Cytospin Preparation

Single-cell suspensions were obtained from fresh nasal specimens by using enzymatic digestion and mechanical dissociation. Sample was treated in 10 mg/ml of Dispase II (Sigma-Aldrich Inc., USA) followed by gentle shaking for 4°C overnight incubation. We treated samples with 1× trypsin/ethylene diaminetetraacetic acid at 37°C for 15 min. The dissociated cells were fixed in 4% formaldehyde at room temperature for 10 min, and washed twice with 1× Dulbecco's phosphate-buffered saline. Cytospin ($1\text{-}2\times10^4$ cells/slide) was prepared at 500 rpm for 5 min by using Shandon Cytospin 3 Cytocentrifuge (Thermo Fisher Scientific, Waltham, MA).

Immunohistochemistry (IHC) and Immunofluorescence (IF) Assays

Paraffin tissue sections and cytospin samples were used to perform the IHC and IF assay. See **Online Supplementary Text** for details.

Evaluation of IHC and Immunofluorescence Assays

Eosinophil and Neutrophil Count

All cases were assessed in a blinded fashion by independent researchers. Eosinophil infiltration was evaluated based on haemotoxylin-eosin (H&E) staining, while neutrophil infiltration by IHC staining. Eosinophils and neutrophils were enumerated at five high-power fields (HPF, 400× magnification) with the infiltration of inflammatory cell. Eosinophilia or neutrophilia denoted eosinophils or neutrophils exceeding 10% of the total leucocyte count (Gao et al., 2016).

Measurement of Cilia Length

Primary single cells from 20 patients with NP and 11 healthy controls were subject to cytospin slide preparations. Cilia length assessment was based on alpha-tubulin staining. We randomly selected five areas of images at 400× magnification. Cilia length was measured with ImageJ software and 20 measurements for each area were recorded. Scores of individual measurements were averaged before analysis.

RSPH1, RSPH4A, RSPH9, and DNAH5 Expression Patterns

Merged images were used for analyzing expression patterns of ciliary ultrastructural and ciliogenesis markers. Based on previous publications, immunofluorescence imaging of *RSPH1*, *RSPH4A*, *RSPH9,* and *DNAH5* shared three patterns (Shoemark et al., 2017; Qiu et al., 2018): (i) Pattern A, markers located throughout the entire axoneme; (ii) Pattern B, markers partly missing at distal axoneme. (iii) Pattern C, markers completely missing throughout the axoneme. To determine the magnitude of abnormality of ciliary ultrastructural markers, we developed a semi-quantitative scoring system for which 0 denoted pattern A > 70%, 1 denoted patterns A + B > 70%, and 2 denoted pattern C ≥ 30% to assess co-localization. Three to five areas of merged images at 400× magnifications were selected randomly, and scores of individual measurements were averaged (Shoemark et al., 2017; Qiu et al., 2018). In cytospin slides, 10 single cilia cells were randomly selected from each sample and the expression patterns of single cells were graded by using oil-immersion lens at 1,000× magnifications.

Evaluation of CP110 and FOXJ1 Expression

The total fluorescence intensity (TFI, presented in arbitrary units) measurements were performed to evaluate *CP110* and *FOXJ1* expression. The IF images on tissue sections were captured with 40× objective lens of fluorescence microscope (Olympus IX51; Olympus, Nagano, Japan). The positively stained area and mean fluorescence intensity (MFI) of each marker were recorded using ImageJ software. The TFI was calculated as the product of the positively stained area and the MFI (Li et al., 2014).

RNA Extraction and Quantitative Real-Time Polymerase Chain Reaction (qRT-PCR)

Total RNA was extracted from NP and IT in RNAlater (Ambion, Austin, TX, USA) with mirVana™ isolation kit. Expression of markers was evaluated by performing qRT-PCR (9StepOnePlusTM System, Applied Biosystems Inc., USA). Relative gene expression was calculated using the $2^{-\Delta\Delta Ct}$ algorithm with glyceraldehyde-3-phosphate dehydrogenase as the reference. Details are presented in **Online Supplementary Text**.

Transmission Electron Microscopy (TEM)

Tissue samples from patients with NP and controls were prepared according to the standardized protocol of performing the TEM. The cilia ultrastructure was evaluated with the JEOL instrument (Model: JEM 1010, Jeol Co. Ltd., Japan). Further details are presented in the **Online Supplementary Text**.

Statistical Analysis

Analyses were conducted using SPSS 22.0 (SPSS Inc., USA) and GraphPad Prism 6.0 (GraphPad Inc., USA). Differences in categorical variables (e.g., epithelial hyperplasia and eosinophilia/neutrophilia), *RSPH1*, *RSPH4A*, *RSPH9,* and *DNAH5* expression patterns of single-cell cytospin preparations between two groups were compared with chi-square test or Fisher's exact test as appropriate. The between-group difference in ciliary marker expression was analyzed with Mann-Whitney U test. The correlation analysis was performed by Spearman's correlation model and bootstrapping analysis. Linear mixed models were applied to compare the cilia length from primary cytospin preparations. $P \leq 0.05$ was considered significant for all analyses.

RESULTS

Demographic and Clinical Characteristics

The demographic and clinical characteristics are summarized in **Table 1**. Despite a trend towards the greater age in patients

TABLE 1 | Demographic and clinical characteristics of study participants.

Parameters	Controls	CRSwNP	*P* value
Nasal tissue (No.)	32	97	–
Paraffin specimens for staining (No.)	32	97	–
RNA for qRT-PCR (No.)	28	62	–
Cytospin preparations for staining (No.)	11	20	–
Age, yr [mean ± SD]	33.8 ± 14.3	40.2 ± 16.5	0.057
Male [N (%)]	22 (68.8)	67 (69.1)	0.973
Atopy [N (%)]	7 (21.9)	20 (20.6)	0.880
Asthma [N (%)]	2 (6.3)	18 (18.6)	0.157
Epithelial hyperplasia†	**3 (9.4)**	**82 (84.5)**	**<0.001**
Inflammatory cells [N (%)]‡			
Eosinophilia (No., %)	**2 (6.3)**	**44 (45.4)**	**<0.001**
Neutrophilia (No., %)	**3 (9.4)**	**58 (59.8)**	**<0.001**

CRSwNP, Chronic rhinosinusitis with nasal polyps; NA, not applicable; SD, standard deviation; yr, year; RNA, ribonucleic acid; qRT-PCR, quantitative reverse transcriptase polymerase chain reaction

Differences in categorical variables between the two groups were compared using chi-square test or Fisher's exact test. The difference of age was compared with independent t-test.

†Epithelium with more than 4 layers was defined as epithelial hyperplasia.

‡The percentage of eosinophils and neutrophil exceeding 10% was categorized as eosinophilia or neutrophilia.

P < 0.05 was considered statistically significant unless otherwise stated. Data in bold indicated the statistical analysis with significance.

with NP, the percentage of males and participants with atopy and asthma was comparable. Compared with IT, eosinophilic and neutrophilic infiltration was markedly more prevalent in patients with NP (6.3% vs. 45.4%; 9.4% vs. 59.8%, both $P < 0.001$). Epithelial hyperplasia was more common among patients with NP (84.5% vs. 9.4%, $P < 0.001$).

Aberrant Expression of Ciliary Ultrastructural Markers in NPs

We initially determined the co-localization of *RSPH1*, *RSPH4A*, *RSPH9*, *DNAH5,* and acetylated alpha-tubulin. Consistent with our previous reports, three patterns (Pattern A-C) of *RSPH1*, *RSPH4A*, *RSPH9,* and *DNAH5* were observed in both paraffin sections and primary single-cell cytospin slides (**Figure 1**).

Based on our semi-quantitative scoring system, the median (the 1st and 3rd quartile) scores of *RSPH1*, *RSPH4A*, *RSPH9,* and *DNAH5* were 0.2 (0.2, 0.5), 0.2 (0, 0.6), 0.2 (0, 0.8), and 0.4 (0.2, 0.7) in IT for paraffin sections, respectively. Conversely, the median (the 1st and 3rd quartile) scores of *RSPH1*, *RSPH4A*, *RSPH9,* and *DNAH5* were significantly higher [1.0 (0.6, 1.5), 1.2 (0.8, 1.6), 1.3 (0.8, 1.8), and 1.2 (0.8, 1.6)] in patients with NPs (all $P < 0.001$). In addition, mRNA expression levels of *RSPH4A* ($P < 0.001$), *RSPH9* ($P = 0.017$), and *DNAH5* ($P < 0.001$) were significantly higher in NP than in IT, although mRNA expression of *RSPH1* was comparable ($P = 0.965$) (**Figure 2**).

In single-cell cytospin slides, the percentage of pattern A-C was 50.0%, 22.0%, and 28.0% for *RSPH1*, 58.0%, 12.0%, and 30.0% for *RSPH4A*, 48.0%, 18.0%, and 34.0% for *RSPH9*, and 51.5%, 13.5%, and 35.0% for *DNAH5* in patients with NP, respectively. Conversely, the percentage of patterns A-C among control subjects was 72.0%, 18.0%, and 10.0% for *RSPH1*, 88.0%, 6.0%, and 6.0% for *RSPH4A*, 72.0%, 12.0%, and 16.0% for *RSPH9*, and 74.0%, 14.0%, and 12.0% for *DNAH5*, respectively (all $P < 0.05$). (**Table 2**)

Ciliogenesis Marker Expression

The IF staining patterns and the intensity of *CP110* in patients with NP differed considerably from those in IT tissues in control subjects. *CP110* staining showed a localized and thin pattern in control subjects, while a diffuse and thick pattern was seen in NP. The median (the 1st and 3rd quartile) of TFI for *CP110* was significantly higher in NP than in IT [1.3 (1.1, 1.6) vs. 0.7 (0.5, 0.9) $\times 10^6$ arbitrary units, $P < 0.01$]. Consistently, *CP110* mRNA levels were considerably higher in NP biopsy tissues than in IT ($P = 0.001$) (**Figure 3**).

FOXJ1 was stained within the nucleus of ciliated and non-ciliated epithelial cells. Compared with control subjects, the TFI for *FOXJ1* staining was markedly greater in NP than in IT [2.7

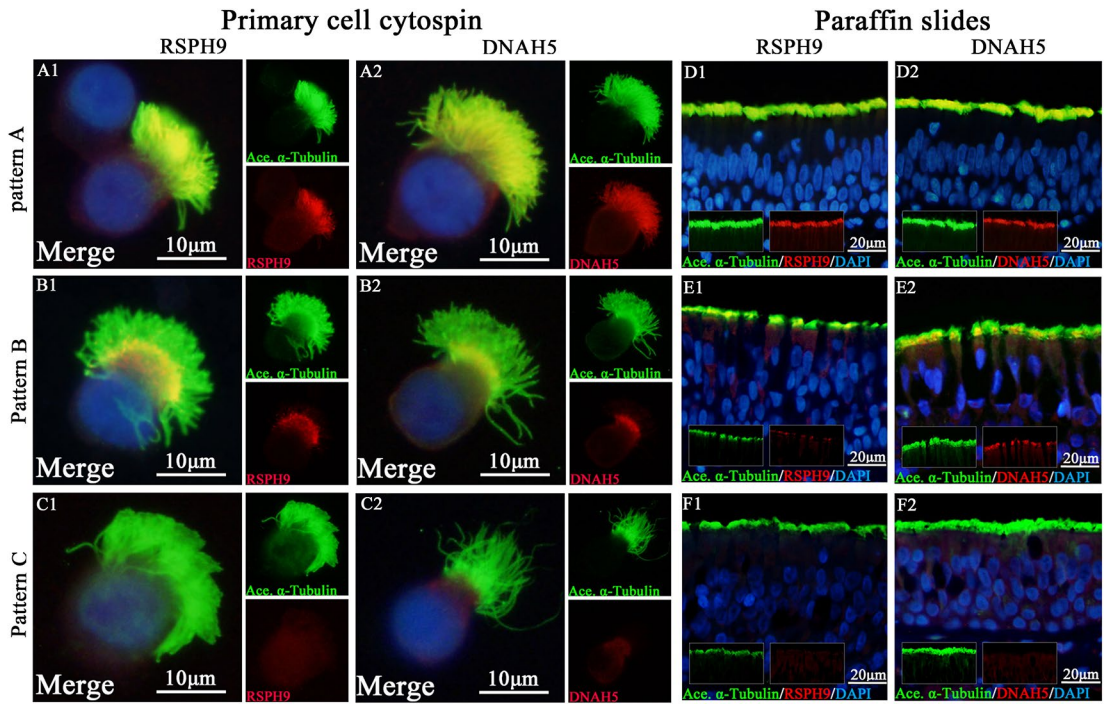

FIGURE 1 | Expression patterns of *RSPH9* and *DNAH5* in primary single-cell cytospin slides and paraffin slides. *RSPH1*, *RSPH4A*, *RSPH9,* and *DNAH5* shared three patterns based on our previous report, which were defined as Pattern **(A)**, markers located throughout the entire axoneme (A1-A2, D1-D2); Pattern **(B)**, markers partly missing at the distal parts of axoneme (B1-B2, E1-E2). Pattern **(C)**, markers completely missing throughout the entire axoneme (C1-C2, F1-F2). The expression patterns of RSPH1 and RSPH4A have been demonstrated in **Figure S1**. *RSPH9* and *DNAH5, Red*; *alpha-tubulin*, Green; DAPI, Blue; Co-localization of *RSPH1*, *RSPH4A*, *RSPH9,* and *DNAH5* with alpha-tubulin, Yellow. RSPH, Radial spoke head protein; DNAH5, Dynein arm heavy chain 5; DAPI, 4', 6-diamidino-2-phenylindole.

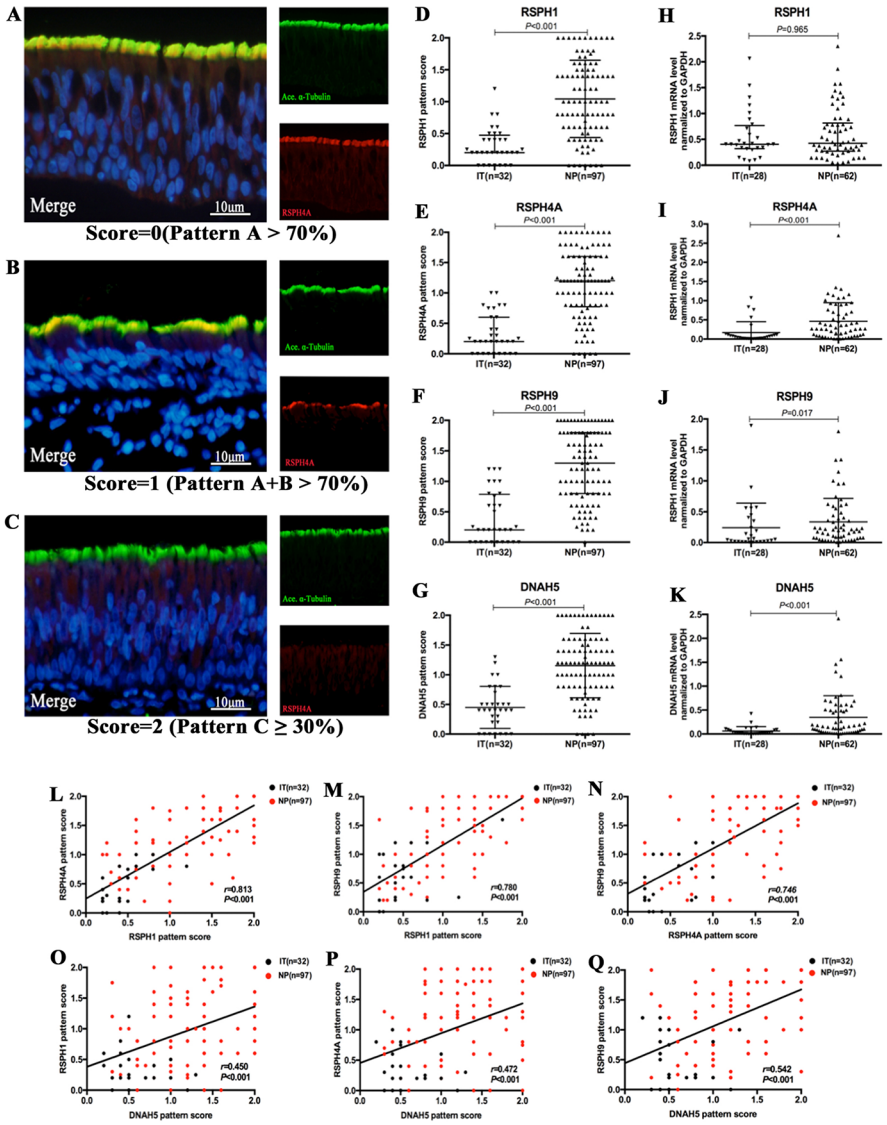

FIGURE 2 | The semi-quantitative grading system for paraffin specimens, the abnormal expressions of ciliary ultrastructural markers and their association in nasal epithelial specimens. **(A–C)** A semi-quantitative scoring system for which 0 = pattern A > 70% **(A)**; 1 = patterns A + B > 70% **(B)**; and 2 = pattern C ≥ 30% **(C)** to assess the co-localizations in paraffin. **(D–K)** The pattern scores **(D–G)** and the mRNA expressions **(H–K)** of *RSPH1*, *RSPH4A*, *RSPH9,* and *DNAH5*. **(L–Q)** Correlation between the pattern scores of *RSPH1*, *RSPH4A*, *RSPH9,* and *DNAH5. RSPH1*, *RSPH4A*, *RSPH9,* and *DNAH5, Red*; *alpha-tubulin*, Green; DAPI, Blue; Co-localization of *RSPH1*, *RSPH4A*, *RSPH9,* and *DNAH5* with alpha-tubulin, Yellow. RSPH, Radial spoke head protein; DNAH5, Dynein arm heavy chain 5; DAPI, 4',6-diamidino-2-phenylindole.

(2.1, 3.7) vs. 1.7 (1.3, 2.1) $\times 10^6$ arbitrary units, $P < 0.01$]. However, mRNA expression of *FOXJ1* was non-significantly greater in NP ($P = 0.468$) (**Figure 3**).

Association Between Ciliary Ultrastructural and Ciliogenesis Markers

The IF expression pattern scores of *RSPH1*, *RSPH4A*, *RSPH9,* and *DNAH5* correlated positively with each other in biopsy tissues of both groups (all $P < 0.001$) (**Figure 2**). Similarly, the mRNA expression levels showed similar correlation to the pattern scores (all $P < 0.01$) (**Figure S2**). The same trends were found in the NP-only groups (all $P < 0.05$) (**Figure S3**). The correlations were further confirmed based on the chi-square analysis that showed no significant difference between the normal/abnormal distribution among different ciliary markers. Similar findings were also observed using the bootstrapping analysis (**Tables S3** and **S4**).

Both protein expression levels (assessed with TFI) and mRNA expression of *CP110* and *FOXJ1* were correlated positively in biopsy samples ($r = 0.311$, $P < 0.001$; $r = 0.383$, $P < 0.001$, **Figures 3** and **S2**). We further investigated the associations of the expression levels between ciliary ultrastructural markers and ciliogenesis markers. The TFI of *CP110* and *FOXJ1* correlated

TABLE 2 | The expression patterns of ciliary ultrastructural markers in primary cell specimens.

Immunofluorescence staining patterns	Controls	CRSwNP	*P* value
Ciliary markers staining (No.)	5	5	–
Single ciliated cells evaluated (No.) [#]	50	50	–
RSPH1 staining patterns [No. (%)]	–	–	**0.040**
Pattern A	36 (72.0)	25 (50.0)	–
Pattern B	9 (18.0)	11 (22.0)	–
Pattern C	5 (10.0)	14 (28.0)	–
RSPH4A staining patterns [No. (%)]	–	–	**0.002**
Pattern A	44 (88.0)	29 (58.0)	–
Pattern B	3 (6.0)	6 (12.0)	–
Pattern C	3 (6.0)	15 (30.0)	–
RSPH9 staining patterns [No. (%)]	–	–	**0.044**
Pattern A	36 (72.0)	24 (48.0)	–
Pattern B	6 (12.0)	9 (18.0)	–
Pattern C	8 (16.0)	17 (34.0)	–
Ciliary markers staining (No.) [§]	5	20	–
Single ciliated cells evaluated (No.) [#]	50	200	–
DNAH5 staining patterns [No. (%)]	–	–	**0.005**
Pattern A	37 (74.0)	103(51.5)	–
Pattern B	7 (14.0)	27(13.5)	–
Pattern C	6 (12.0)	70(35.0)	–

The number of patient's samples for immunostaining of different ultrastructural markers was variable because of the limited cell count for performing assays. Priority was assigned to DNAH5 staining.

[#]Primary cells were obtained from 5 patients, and 10 single ciliated cells were randomly selected for assessment from each sample.

[§]Primary cells were obtained from 5 healthy controls and 20 patients with nasal polyps, 10 single ciliated cells were randomly selected for assessment from each sample.

P value in bold indicated the statistical analysis with significance.

RSPH, Radial spoke head protein; DNAH5, Dynein axonemal heavy chain 5.

positively with the pattern scores of *RSPH1*, *RSPH4A*, *RSPH4A*, and *DNAH5* (all $P < 0.05$, **Figure 4**). Similarly, the mRNA levels of *CP110* also correlated positively with those of ultrastructural markers (all $P < 0.001$). *FOXJ1* mRNA expression also correlated positively with that of *RSPH1* and *DNAH5* ($r = 0.706$, $P < 0.001$; $r = 0.213$, $P = 0.044$), but not *RSPH4A* and *RSPH9* ($r = 0.131$, $P = 0.218$; $r = 0.046$, $P = 0.667$) (**Figure S2**). In the NP-only groups, the TFI of *CP110* correlated significantly with the pattern score of *RSPH1, RSPH4A, RSPH9,* and *DNAH5* (all $P < 0.05$), but not the TFI of *FOXJ1* ($P > 0.05$, **Figure S4**).

Cilia Length of Primary Single Cells and Cilia Ultrastructure Assessment Under TEM

Among single-cell cytospin preparations, the mean of cilia length was significantly greater in NP than in IT (6.5 ± 0.9μm vs. 4.65 ± 0.7μm, $P < 0.05$) (**Figure 4**). Non-significantly greater cilia length was observed in eosinophilic NP compared with non-eosinophilic NP (6.6 ± 1.0μm vs. 6.4 ± 0.9μm, $P = 0.481$). Neutrophilia did not contribute to significantly different cilia length (**Figure S6**).

Because TEM has been applied as the standardized diagnostic tool for ciliary disorders in clinical settings, we have further evaluated the IT and NP samples with TEM to provide objective evidence that the insults of airway inflammation could have predisposed the epithelium to secondary ciliary disorders with an IF staining-independent technique. Indeed, under TEM, normal cilia ultrastructure was found in control epithelium,

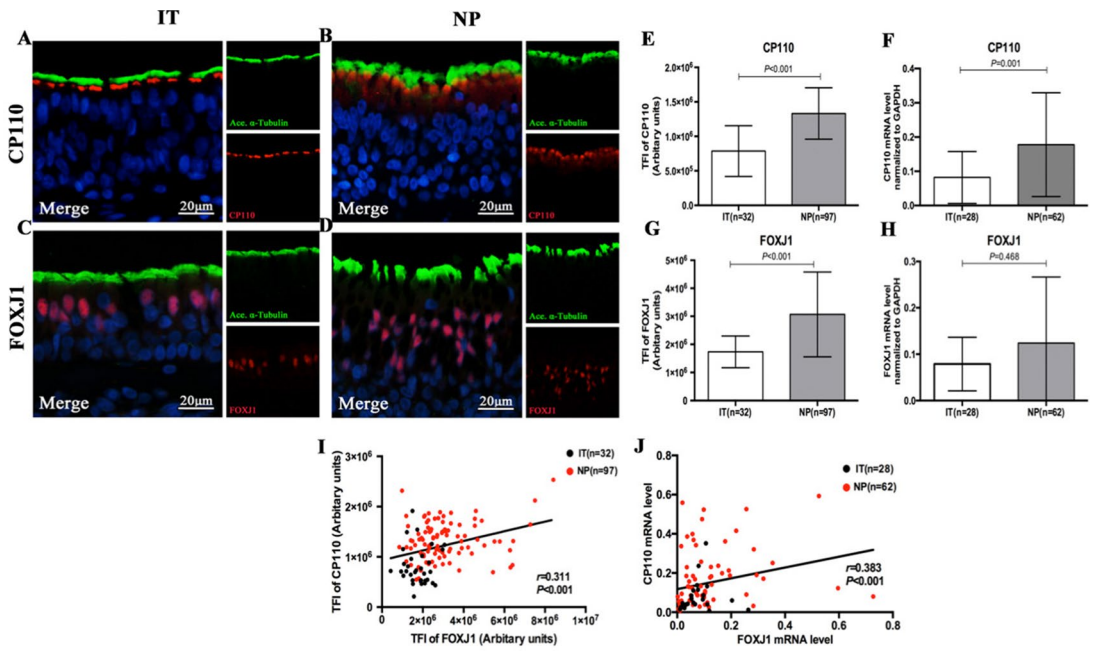

FIGURE 3 | Comparison of the expression levels of *CP110* and *FOXJ1* in patients with nasal polyps and healthy controls and their correlation. Shown in the figure are the expression levels of CP110 **(A–B, E–F)** and FOXJ1 **(C–D, G–H)** in patients with nasal polyps and healthy controls. CP110 staining showed a localized and thin pattern in control subjects, while a diffuse and thick pattern was seen in NP. FOXJ1 was stained within the nucleus of ciliated and non-ciliated epithelial cells. The correlation between FOXJ1 and CP110 expression levels is demonstrated in **Figure 3I**–**J**. *CP110* and *FOXJ, Red*; *alpha-tubulin*, Green; DAPI, Blue. *CP110*, Centrosomal protein 110; *FOXJ*, Fork-head box protein J1, DAPI, 4',6-diamidino-2-phenylindole.

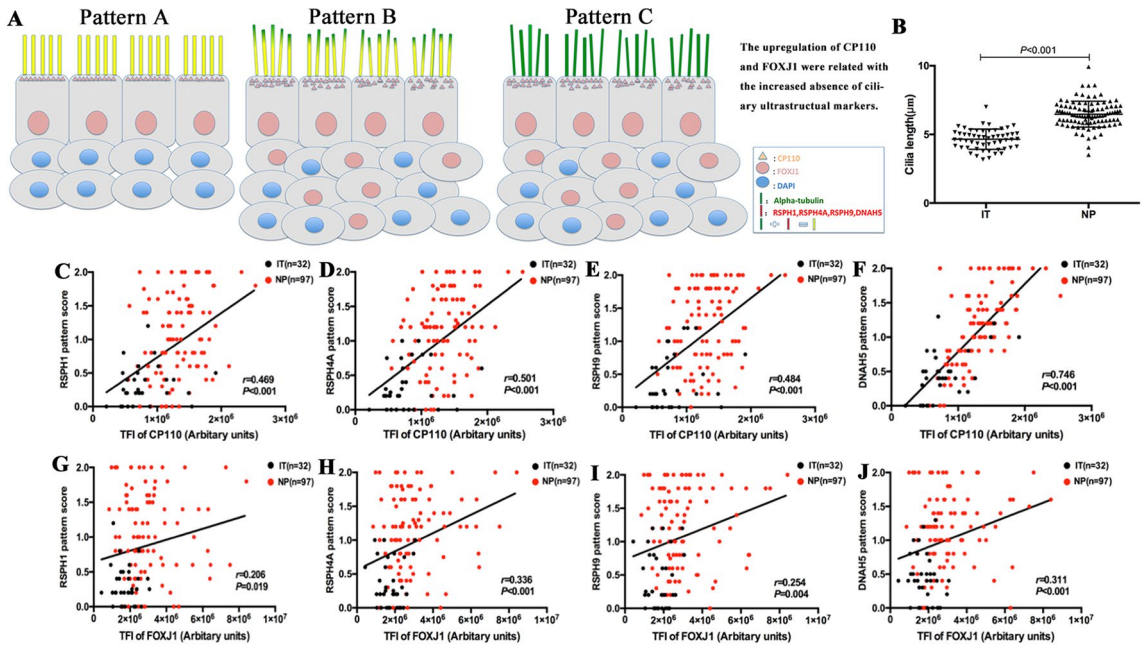

FIGURE 4 | A schematic diagram demonstrating the different patterns of ciliary disorders, the difference of length between NPs and ITs, and the correlation between ciliary ultrastructural markers and ciliogenesis markers. Shown in the figure is a schematic diagram demonstrating the different expression patterns of ciliary disorders and the relevant changes in the expression of ciliogenesis markers and ultrastructural markers **(A)**. Pattern A is the normal baseline. Up-regulation of *CP110* and *FOXJ1* are associated with the greater cilia length and increased absence of ciliary ultrastructural markers in Pattern B and Pattern C. Linear mixed models were employed to compare between healthy controls (n = 13) and patients with NPs (n = 20) **(B)**. The correlation between the expression of *CP110* and ciliary ultrastructural markers **(C–F)**. Data from IT tissues and NP tissues appeared in black and red dots, respectively. The correlation between the expression of *FOXJ1* and ciliary ultrastructural markers **(G–J)**. Data from IT tissues and NP tissues appeared in black and red dots, respectively. *RSPH*, Radial spoke head protein; *DNAH5*, Dynein arm heavy chain 5; *CP110*, Centrosomal protein 110; *FOXJ*, Fork-head box protein J1, DAPI, 4',6-diamidino-2-phenylindole.

while abnormal cilia ultrastructure was observed in NP samples, including the outer dynein arm defects and central pair defects (**Figure 7**). These findings reaffirmed that the ultrastructural defects which are verified by TEM can be detected with immunofluorescence staining.

Increased Abnormal Expressions of Ciliary Ultrastructural and Ciliogenesis Markers in Eosinophilic NP

We further stratified NP into eosinophilic and non-eosinophilic NP. In eosinophilic NP, the median pattern scores of *RSPH1*, *RSPH4A,* and *RSPH9* were significant higher than non-eosinophilic NP [1.3 (0.7, 1.7) vs. 0.8 (0.4, 1.4), 1.3 (1.0, 1.7) vs. 1.0 (0.6, 1.4), and 1.6 (1.0, 2.0) vs. 1.0 (0.6, 1.7), all $P < 0.05$]. However, the pattern score of *DNAH5* was non-significantly higher in eosinophilic NP [1.2 (1.0, 1.6) vs. 1.2 (0.6, 1.4), $P = 0.115$] (**Figure 5**). In light of the positive relationships among these ultrastructural markers and the limited single-cell slide samples, we only further analyzed the subgroups of *DNAH5* staining. The percentage of pattern A, B, and C of *DNAH5* single-cell staining was 43.3%, 15.6%, and 41.1% in eosinophilic NP. Correspondingly, the figures in non-eosinophilic NP were 58.2%, 11.8%, and 30.0% ($P = 0.112$), respectively (**Table S2**).

Compared with non-eosinophilic NP, eosinophilic NP yielded non-significantly higher TFI of *CP110* [1.4 (1.2, 1.6) vs. 1.2 (1.0, 1.5) $\times 10^6$ arbitrary units, $P = 0.100$]. The median TIF of *FOXJ1* was significantly higher in eosinophilic NP [3.1 (2.2, 4.6) vs. 2.6 (2.1, 3.0) $\times 10^6$ arbitrary units, $P < 0.01$] (**Figure 5**).

DISCUSSION

The human nasal epithelium constitutes the first-line defense against pathogens and has self-repairing capabilities that are critical for maintaining homeostasis of mucosal microenvironment (Duan et al., 2016). However, in NP there may be the interplay between the chronic airway inflammation and motile ciliary disorders (Al-Rawi et al., 1998; Gudis et al., 2012). Our study has reaffirmed the intimate association between defective ciliogenesis and abnormal expression of ciliary ultrastructural marker, and highlighted the roles of chronic inflammation in driving abnormal ciliary ultrastructural marker expression and defective ciliogenesis in NP that is not associated with congenital disorders such as PCD. Eosinophilic inflammation might have a role in dampening mucociliary clearance.

In healthy subjects, 4–10% of respiratory cilia reportedly demonstrated ultrastructural abnormalities (Smallman and Gregory 1986; de Iongh and Rutland, 1995; Bush et al., 1998).

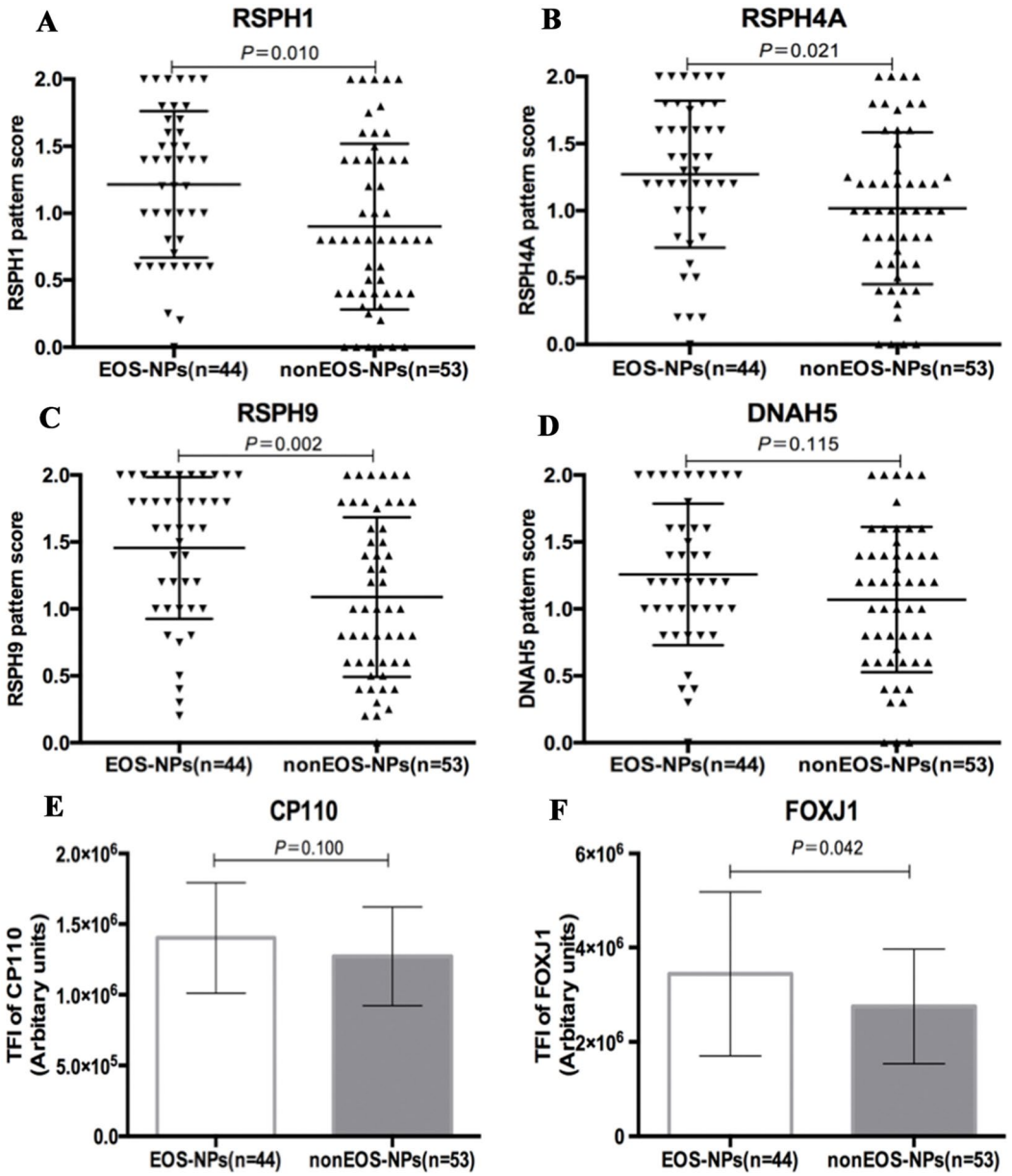

FIGURE 5 | Comparison of the expression levels of *RSPH1*, *RSPH4A*, *RSPH9*, *DNAH5*, *CP110,* and *FOXJ1* based on the airway inflammatory phenotypes. **(A–D)** The different expression pattern scores of ciliary ultrastructure markers (*RSPH1*, *RSPH4A*, *RSPH9,* and *DNAH5*) in eosinophilic and non-eosinophilic nasal polyps. **(E–F)** The different expression levels of ciliogenesis markers in eosinophilic and non-eosinophilic nasal polyps. *RSPH*, Radial spoke head protein; *DNAH5*, Dynein arm heavy chain 5; *CP110*, Centrosomal protein 110; *FOXJ*, Fork-head box protein J1, DAPI, 4',6-diamidino-2-phenylindole. The values are expressed as Mean and standard deviation.

Nonetheless, abnormal cilia can be found in ~20% of patients with chronic inflammatory airway diseases such as chronic rhinosinusitis (CRS) (Al-Rawi et al., 1998; Plesec et al., 2008). Intriguingly, 87% of patients with severe CRS reportedly had compound cilia and microtubule and dynein arm defects (Al-Rawi et al., 1998). Truncation or absence of inner or outer dynein arms were the most common pattern (~71%) in respiratory cilia with abnormal ciliary ultrastructure, and 19% of these patients may have exhibited RS defects (only one patient reportedly had PCD) (Plesec et al., 2008). Consequently, outer dynein arm and RS protein markers might be useful for assessment of ciliary ultrastructural abnormalities in chronic inflammatory airway diseases. In our study, the prevalence of abnormal expression of all ciliary ultrastructural markers (*RSPH1*, *RSPH4A*, *RSPH9,* and *DNAH5*) was markedly higher and highly correlated. The significant correlation between ultrastructural markers suggested that ultrastructural marker assemblies might be affected to a similar magnitude. Therefore, cilia length was significantly greater in NP than in IT (particularly in eosinophilic NP), suggesting that prolongation of the axoneme and assembly of ultrastructural markers was simultaneously affected, thus contributing to abnormal ciliary

function. These findings have expanded our understanding that absence and/or mislocalization of ciliary ultrastructural markers is common in NP (Qiu et al., 2018). Interestingly, despite the greater prevalence of absence of axonemal proteins, the mRNA expression levels of most ultrastructural markers we investigated in this study (*RSPH4A, RSPH9* and *DNAH5*) were significantly higher in NPs. Consistent with the current findings, in light of the longer and denser cilia in NP, we hypothesized that the abnormal up-regulated ciliogenesis (possibly because of chronic airway inflammation) might have contributed to the abnormal expression patterns of ultrastructural markers and that these might be associated with eosinophilic inflammation.

CP110 is localized to the cilia-forming basal bodies and is indispensable to the formation and proper functioning of respiratory cilia. Thus, *CP110* may have contributed to the modulation of cilia length (Walentek et al., 2016). Inflammation-mediated up-regulation of CP110 expression, which correlated with poor ciliogenesis, was reportedly common in NP (Lai et al., 2011; Li et al., 2014). Consistently, our study revealed that the protein and mRNA expression levels of *CP110* in NPs were increased, which was more prominent in eosinophilic NP. The increased *CP110* expression correlated with the abnormal expression patterns of all ultrastructural markers and *FOXJ1*. Greater cilia length reportedly correlated with the up-regulated *CP110* levels in both upper and lower airway diseases (Li et al., 2014; Chen et al., 2018). Therefore, the abnormal expression of ciliogenesis markers (i.e. *CP110*) might drive motile ciliary disorders in chronic airway inflammatory diseases due to abnormal cilia length that affects assembly of ciliary ultrastructural proteins.

FOXJ1 is highly expressed in ciliated cells and is prerequisite for cilia formation (Blatt et al., 1999; You et al., 2004). Decreased *FOXJ1* expression correlated with loss of respiratory cilia, whereas up-regulated *FOXJ1* expression correlated with ultrastructural marker abnormality (Look et al., 2001). *FOXJ1* reportedly activated the gene expression encoding motile ciliary markers, including heavy chain subunits and RS proteins (Stubbs et al., 2008). Additionally, increased expression of *FOXJ1* in NP resulted in lengthened or overly dense cilia, leading to impaired ciliary motility (Li et al., 2014; Jiao et al., 2016). In our study, the heightened *FOXJ1* expression levels correlated with a greater prevalence of absence of ciliary ultrastructural markers in Nasal specimens. In contrast to previous reports (Li et al., 2014; Jiao et al., 2016), *FOXJ1* mRNA levels were non-significantly greater and the correlation between *FOXJ1* and ciliary ultrastructure markers were non-significant in the NP-only group. Nonetheless, the aberrant localization rather than the non-significant increase of *FOXJ1* would be of greater clinical relevance to the pathogenesis of NPs. Recently, we have identified four distinct *FOXJ1* localization patterns in allergic nasal mucosa that partially correlated with allergic airway inflammation (Peng et al., 2018). Further investigation exploring how mislocalization of *FOXJ1* contributes to the abnormal expression patterns of ciliary ultrastructural markers is warranted.

Collectively, in the milieu of the chronic inflammation, both abnormal ciliogenesis and ciliary ultrastructure (i.e., *DNAH5* defects) are responsible for the manifestation of impaired MCC in NP (particularly eosinophilic NP). Upon stimulation of the chronic inflammation, up-regulated *CP110,* and *FOXJ1* expression may contribute to the overly dense and increased cilia length, and the abnormal expression and localization of ciliary ultrastructural markers, resulting in disrupted cilia assembly and affecting ciliary motility (**Figure 6**).

Although in the present study the ciliary ultrastructural defects could be detected with TEM (**Figure 7**), it should be stressed that TEM is not the 'gold standard' for the diagnosis of ciliary disorders, which may be particularly true when the outer or inner dynein arm defects could not be displayed clearly. Some ultrastructural protein mutations might have resulted in a completely normal ciliary ultrastructure. For instance, mutations of RSPH9 might have resulted in completely normal ciliary ultrastructure, RSPH4A mutations might have resulted in approximately 50% of the cilia with normal ultrastructure, and RSPH1 mutation might have led to an overall normal TEM image. Because TEM may be laborious and technically challenging as a diagnostic tool, we have now resorted to immunofluorescence staining that has been increasingly validated as the practical surrogate for assessment of ciliary disorders for the diagnosis.

The study is not without limitations. First, we did not sample nasal mucosa of the middle turbinate or ethmoid mucosa from control subjects for comparison. Ideally, sampling the tissues from the uncinate process as the control would be preferred. Nonetheless, this approach for the healthy controls appeared to be unethical, according to the feedback from our ethics review board. In fact, the turbinate tissue has already been commonly used as the control tissue to represent healthy controls in assessing tissue histology in literature reports, which partially validated our sampling approaches. Contrarily, sampling IT tissues is practical and significantly less invasive. The samples from the nasal cavity are lined with, or covered by, the same type of pseudostratified columnar respiratory epithelium, including ciliated cells, non-ciliated cells, goblet cells, and basal cells. Additionally, we also showed that IT tissues provides comparable readouts as the middle turbinate and uncinate process in cilia architecture in one of our previous publication; thus rendering it particularly suitable for translational cilia research (Li et al., 2014; Duan et al., 2016; Zhao et al., 2017; Qiu et al., 2018). Second, the cilia length in paraffin-embedded tissues was not measured. However, the bending or distortion during sample processing could have confounded our measurement. Third, we did not provide a more direct evidence to confirm the relationships between the chronic airway inflammation and ciliary ultrastructural abnormality and genetic (primary) defects, which warranted further investigations. Fourth, we noted a discordant trend of changes in IF and qPCR finding. Nonetheless, the significantly greater ciliary length and ciliated area in NP (Li et al., 2014) might be responsible for the increase in mRNA expression levels of ciliary markers. Despite the development of semi-quantitative scoring system that helped evaluate the correlation between ultrastructural defects and ciliogenesis, the current classification scheme remains arbitrary. Further investigation of the clinical relevance is warranted. Fifth, multicenter studies with larger sample sizes are needed. Moreover, we did not employ enzyme-linked immunosorbent assay or western blotting for analysis of protein expression. However, immunofluorescence imaging may

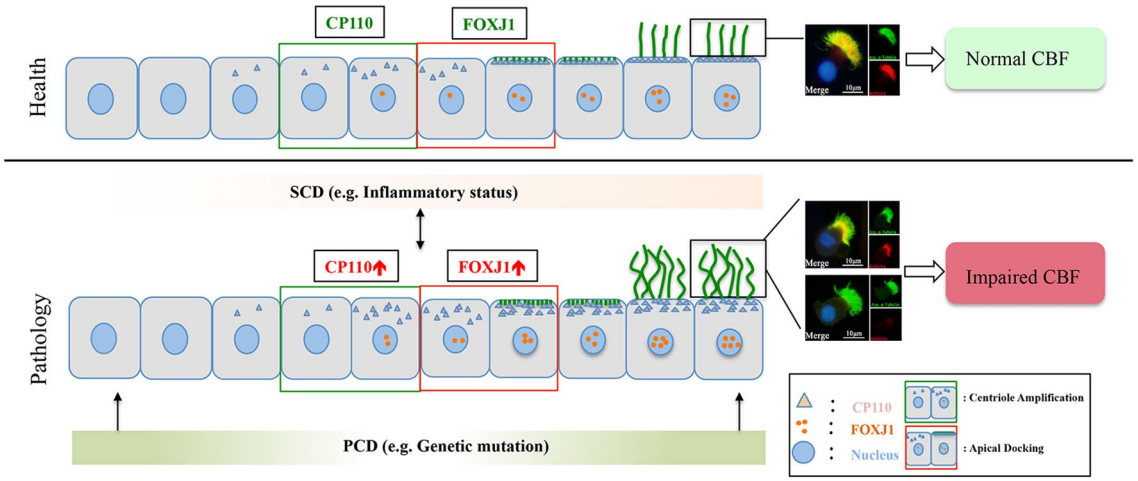

FIGURE 6 | A schematic diagram demonstrating the roles of chronic airway inflammation in driving aberrant ciliogenesis and ultrastructural markers. In health, the differentiation of ciliated cells is under delicate regulation of *CP110* and *FOXJ1* which are responsible for normal assembly of ultrastructural markers. Upon chronic inflammation, up-regulated *CP110* and *FOXJ1* expression contributes to the overly dense and lengthened cilia, which correlates with abnormal expressions and localization of ciliary ultrastructural markers, leading to SCD. Conversely, SCD may disrupt ciliogenesis and result in abnormal expression of ciliary ultrastructural markers (i.e., *RSPH4A*). Contrarily, PCD mainly stems from genetic defects that disrupt cilia assembly at early stages of cell differentiation. For the purpose of illustrating the expression patterns of ciliary markers (i.e., *FOXJ1*), we have only demonstrated the ciliated cells in this schematic diagram. PCD, primary ciliary dyskinesia; SCD, secondary ciliary dyskinesia.

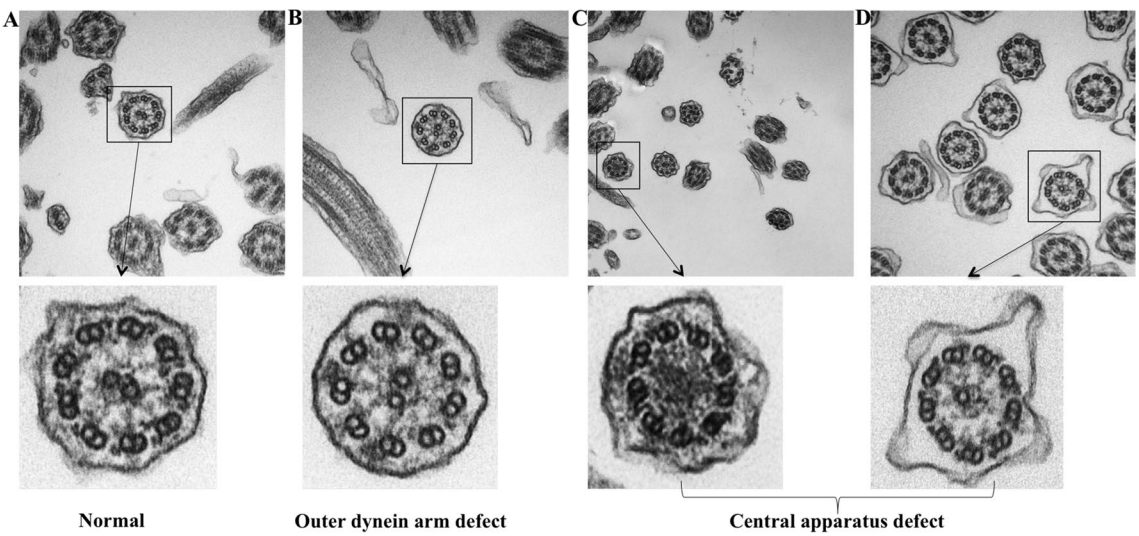

FIGURE 7 | TEM demonstrating the ultrastructural findings in control and NP subject. **(A)** Normal cilia ultrastructure from control subject (original magnification 100,000). **(B)** ODA defect from NP subject (original magnification 100,000). **(C–D)** Miss central pair from NP subject (original magnification 50,000 and 100,000). TEM: Transmission electron microscope; ODA, Outer dynein arms.

not only provide relative quantitative measure (i.e. the TFI) but can also reveal mislocalization of ciliogenesis or partial absence of ciliary ultrastructural markers. Finally, *in vitro* investigation is merited to determine the mechanisms underlying the correlation between expression levels of ultrastructural markers and ciliogenesis markers. Overall, the present study has extended our previous publications in that we have now focused on the defective expression patterns of individual cilia ultrastructural markers, including outer dynein arms and radial spoke head defects (which have been rarely reported) and mislocalization. Furthermore, we have now offered further evidence that insults of airway inflammation could have predisposed to secondary ciliary disorders that could be assessed with IF staining.

In conclusion, a greater prevalence of absence of *RSPH1*, *RSPH4A*, *RSPH9,* and *DNAH5* expressions is observed in NP, which is associated with the up-regulation of ciliogenesis markers (*CP110* and *FOXJ1*) and greater cilia length in the chronic inflammatory milieu. Our integrated findings may help elucidate

the roles and events leading to the manifestation of impaired ciliogenesis that may lead to cilia ultrastructural abnormalities in driving NP formation. Given the chronic inflammation and significant tendency of recurrence even after surgery, impaired ciliary-mediated MCC should be comprehensively appraised and managed as an important therapeutic strategy to restore ciliary functions for patients with NP.

ETHICS STATEMENT

Our study was carried out in accordance with The Declaration of Helsinki. Ethics approval was obtained from the institutional review boards of the two participating hospitals. All participants signed written informed consent.

AUTHOR CONTRIBUTIONS

Conception and design: LS, D-y W, X-x Z, W-j G. Analysis and interpretation: X-x Z, KS T, W-j G, JL, YP. Collection of the samples: X-x Z, YP, JL, Y-k O, MT. Conducting immunofluorescence and immunohistochemistry experiments: X-x Z, W-j G. TEM experiment: T-t H. Drafting the manuscript for important intellectual content: all authors.

FUNDING

This study was supported by grants from the National Medical Research Council No. NMRC/CIRG/1458/2016 (to D-YW), The Major Research Development Program of Shandong Province No. 2016GSF201084 (to LS), National Nature Science Foundation of China No. 81670909 and NO.81873692 (to LS), The Key Research Development Program of Shandong Province No. 2018CXGC1214 (to LS), and Pearl River S&T Nova Program of Guangzhou No. 201710010097 and Guangdong Province Universities and Colleges Pearl River Scholar Funded Scheme 2017 (to W-JG). Dr Kai Sen Tan is a recipient of fellowship support from the EAACI Research Fellowship 2019 (to KST).

ACKNOWLEDGMENTS

We wish to thank Dr. Ying Ying Li (Yong Loo Lin School of Medicine, National University of Singapore, Singapore) for sharing her research experiences in the measurement of cilia length in this study.

SUPPLEMENTARY MATERIAL

The Supplementary Material for this article can be found online at: https://www.frontiersin.org/articles/10.3389/fgene.2019.01083/full#supplementary-material

FIGURE S1 | Expression patterns of RSPH1 and RSPH4A in primary single-cell cytospin slides and paraffin slides. RSPH1and RSPH4A shared three patterns, which were defined as Pattern A, markers located throughout the entire axoneme (A1-A2, D1-D2); Pattern B, markers partly missing at the distal parts of the axoneme (B1-B2, E1-E2). Pattern C, markers completely missing throughout the entire axoneme (C1-C2, F1-F2). RSPH1 and RSPH4A: Red; alpha-tubulin: Green; DAPI: Blue; Co-localization of RSPH1 and RSPH4A with alpha-tubulin: Yellow. RSPH = Radial spoke head protein, DAPI = 4',6-diamidino-2-phenylindole.

FIGURE S2 | Correlation between ciliary ultrastructural and ciliogenesis markers in mRNA level. Correlations between the mRNA expression of RSPH1, RSPH4A, RSPH9 and DNAH5 are shown in panel A and B. The correlation between the expression of ciliagenesis markers (CP110 and FOXJ1) and ciliary ultrastructual markers are demonstrated in panel C and D. RSPH = Radial spoke head protein; DNAH5 = Dynein arm heavy chain 5; CP110 = Centrosomal protein 110; FOXJ = Fork-head box protein J1, DAPI = 4',6-diamidino-2-phenylindole.

FIGURE S3 | The abnormal expressions of ciliary ultrastructural markers and their relationships in nasal specimens. (A, B) Corerlation between the pattern socres of RSPH1, RSPH4A, RSPH9 and DNAH5 in NP. (C, D) Corerlation between the pattern socres of RSPH1, RSPH4A, RSPH9 and DNAH5 in IT. RSPH = Radial spoke head protein; DNAH5= Dynein arm heavy chain 5; CP110 = Centrosomal protein 110; FOXJ = Fork-head box protein J1, DAPI = 4',6-diamidino-2-phenylindole.

FIGURE S4 | The correlation between ciliary ultrastructual markers and ciliogenesis markers in nasal specimens (A, B) Corerlation between the TFI of ciliogenesis markers (CP110 and FOXJ1) and ciliary ultrastructual markers (RSPH1, RSPH4A, RSPH9 and DNAH5) in NP. (C, D) Corerlation between the TFI of ciliogenesis markers (CP110 and FOXJ1) and ciliary ultrastructual markers (RSPH1, RSPH4A, RSPH9 and DNAH5) in IT. RSPH = Radial spoke head protein; DNAH5 = Dynein arm heavy chain 5; CP110 = Centrosomal protein 110; FOXJ = Fork-head box protein J1, DAPI = 4',6-diamidino-2-phenylindole.

FIGURE S5 | Comparison of the expression levels of RSPH1, RSPH4A, RSPH9, DNAH5, CP110 and FOXJ1 based on the neutrophilic status. (A-D) The different expression pattern scores of ciliary ultrastructure markers (RSPH1, RSPH4A, RSPH9 and DNAH5) in neutrophilic and non-neutrophilic NP. (E-F) The different expression levels of ciliogenesis markers in neutrophilic and non-neutrophilic NP. RSPH = Radial spoke head protein; DNAH5= Dynein arm heavy chain 5; CP110 = Centrosomal protein 110; FOXJ = Fork-head box protein J1, DAPI = 4',6-diamidino-2-phenylindole.

FIGURE S6 | Comparison of the single cilia cell length based on the inflammatory phenotypes. (A) Single cilia cell length was compared in patients with eosinophilic and non-eosinophilic NP (B) Single cilia cell length was compared in patients with neutrophilic and non-neutrophilic NP.

REFERENCES

Al-Rawi, M. M., Edelstein, D. R., and Erlandson, R. A. (1998). Changes in nasal epithelium in patients with severe chronic sinusitis: a clinicopathologic and electron microscopic study. *Laryngoscope* 108, 1816–1823. doi: 10.1097/00005537-199812000-00010

Blatt, E. N., Yan, X. H., Wuerffel, M. K., Hamilos, D. L., and Brody, S. L. (1999). Forkhead transcription factor HFH-4 expression is temporally related to ciliogenesis. *Am. J. Respir. Cell Mol. Biol.* 21, 168–176. doi: 10.1165/ajrcmb.21.2.3691

Bush, A., Cole, P., Hariri, M., Mackay, I., Phillips, G., O'Callaghan, C., et al. (1998). Primary ciliary dyskinesia: diagnosis and standards of care. *Eur. Respir. J.* 12, 982–988. doi: 10.1183/09031936.98.12040982

Chen, Z., Indjeian, V. B., McManus, M., Wang, L., and Dynlacht, B. D. (2002). CP110, a cell cycle-dependent CDK substrate, regulates centrosome duplication in human cells. *Develop. Cell* 3, 339–350. doi: 10.1016/S1534-5807(02)00258-7

Chen, Z. G., Li, Y. Y., Wang, Z. N., Li, M., Lim, H. F., Zhou, Y. Q., et al. (2018). Aberrant epithelial remodeling with impairment of cilia architecture in non-cystic fibrosis bronchiectasis. *J. Thorac. Dis.* 10, 1753–1764. doi: 10.21037/jtd.2018.02.13

de Iongh, R. U., and Rutland, J. (1995). Ciliary defects in healthy subjects, bronchiectasis, and primary ciliary dyskinesia. *Am. J. Respir. Crit. Care Med.* 151, 1559–1567. doi: 10.1164/ajrccm.151.5.7735615

Duan, C., Li, C. W., Zhao, L., Subramaniam, S., Yu, X. M., Li, Y. Y., et al. (2016). Differential Expression Patterns of EGF, EGFR, and ERBB4 in Nasal Polyp Epithelium. *PloS One* 11, e0156949. doi: 10.1371/journal.pone.0156949

Failly, M., Bartoloni, L., Letourneau, A., Munoz, A., Falconnet, E., Rossier, C., et al. (2009). Mutations in DNAH5 account for only 15% of a non-preselected cohort of patients with primary ciliary dyskinesia. *J. Med. Gen.* 46, 281–286. doi: 10.1136/jmg.2008.061176

Fokkens, W. J., Lund, V. J., Mullol, J., Bachert, C., Alobid, I., Baroody, F., et al. (2012). European Position Paper on Rhinosinusitis and Nasal Polyps 2012. *Rhinol. Suppl.* 23, 3.

Frommer, A., Hjeij, R., Loges, N. T., Edelbusch, C., Jahnke, C., Raidt, J., et al. (2015). Immunofluorescence analysis and diagnosis of primary ciliary dyskinesia with radial spoke defects. *Am. J. Respir. Cell Mol. Biol.* 53, 563–573. doi: 10.1165/rcmb.2014-0483OC

Gao, T., Ng, C. L., Li, C., et al. (2016). Smoking is an independent association of squamous metaplasia in Chinese nasal polyps. *Int. Forum Allergy Rhinol* 6, 66–74. doi: 10.1002/alr.21631

Gudis, D., Zhao, K. Q., and Cohen, N. A. (2012). Acquired cilia dysfunction in chronic rhinosinusitis. *Am. J. Rhinol. Allergy* 26, 1–6. doi: 10.2500/ajra.2012.26.3716

Hao, J., Pang, Y. T., and Wang, D. Y. (2006). Diffuse mucosal inflammation in nasal polyps and adjacent middle turbinate. *Otolaryngology Head Neck Surg.* 134, 267–275. doi: 10.1016/j.otohns.2005.09.026

Hornef, N., Olbrich, H., Horvath, J., Zariwala, M.A., Fliegauf, M., Loges, N.T., et al. (2006). DNAH5 mutations are a common cause of primary ciliary dyskinesia with outer dynein arm defects. *Am. J. Respir. Crit. Care Med.* 174, 120–126. doi: 10.1164/rccm.200601-084OC

Ibanez-Tallon, I., Heintz, N., and Omran, H. (2003). To beat or not to beat: roles of cilia in development and disease. *Hum. Mol. Gen.* 12, R27–R35. doi: 10.1093/hmg/ddg061

Jiao, J., Duan, S., Meng, N., Li, Y., Fan, E., and Zhang, L. (2016). Role of IFN-gamma, IL-13, and IL-17 on mucociliary differentiation of nasal epithelial cells in chronic rhinosinusitis with nasal polyps. *Clin. Exp. Allergy* 46, 449–460. doi: 10.1111/cea.12644

Lai, Y., Chen, B., Shi, J., Palmer, J. N., Kennedy, D. W., and Cohen, N. A. (2011). Inflammation-mediated upregulation of centrosomal protein 110, a negative modulator of ciliogenesis, in patients with chronic rhinosinusitis. *J. Allergy Clin. Immunol.* 128, 1207–15.e1. doi: 10.1016/j.jaci.2011.09.001

Lee, J. H., McDonald, M. L., Cho, M. H., Wan, E. S., Castaldi, P. J., Hunninghake, G. M., et al. (2014). DNAH5 is associated with total lung capacity in chronic obstructive pulmonary disease. *Respir. Res.* 15, 97. doi: 10.1186/s12931-014-0097-y

Leigh, M. W., Pittman, J. E., Carson, J. L., Ferkol, T. W., Dell, S. D., Davis, S. D., et al. (2009). Clinical and genetic aspects of primary ciliary dyskinesia/Kartagener syndrome. *Gen. Med.* 11, 473–487. doi: 10.1097/GIM.0b013e3181a53562

Li, C. W., Zhang, K. K., Li, T. Y., Lin, Z. B., Li, Y. Y., Curotto de Lafaille, M. A., et al. (2012). Expression profiles of regulatory and helper T-cell-associated genes in nasal polyposis. *Allergy* 67, 732–740. doi: 10.1111/j.1398-9995.2012.02811.x

Li, Y. Y., Li, C. W., Chao, S. S., Yu, F. G., Yu, X. M., Liu, J., et al. (2014). Impairment of cilia architecture and ciliogenesis in hyperplastic nasal epithelium from nasal polyps. *J. Allergy Clin. Immunol.* 134, 1282–1292. doi: 10.1016/j.jaci.2014.07.038

Look, D. C., Walter, M. J., Williamson, M. R., Pang, L., You, Y., Sreshta, J. N., et al. (2001). Effects of paramyxoviral infection on airway epithelial cell Foxj1 expression, ciliogenesis, and mucociliary function. *Am. J. Pathol.* 159, 2055–2069. doi: 10.1016/S0002-9440(10)63057-X

Peng, Y., Chen, Z., Guan, W. J., Zhu, Z., Tan, K. S., Hong, H., et al. (2018). Downregulation and aberrant localization of forkhead box j1 in allergic nasal mucosa. *Int. Arch. Allergy Immunol.* 176, 115–123. doi: 10.1159/000488014

Plesec, T. P., Ruiz, A., McMahon, J. T., and Prayson, R. A. (2008). Ultrastructural abnormalities of respiratory cilia: a 25-year experience. *Arch. Pathol. Lab. Med.* 132, 1786–1791. doi: 10.1043/1543-2165-132.11.1786

Qiu, Q., Peng, Y., Zhu, Z., Chen, Z., Zhang, C., Ong, H. H., et al. (2018). Absence or mislocalization of DNAH5 is a characteristic marker for motile ciliary abnormality in nasal polyps. *Laryngoscope* 128, E97–E104. doi: 10.1002/lary.26983

Shinohara, K., Chen, D., Nishida, T., Misaki, K., Yonemura, S., and Hamada, H. (2015). Absence of radial spokes in mouse node cilia is required for rotational movement but confers ultrastructural instability as a trade-off. *Develop Cell.* 35, 236–246. doi: 10.1016/j.devcel.2015.10.001

Shoemark, A., Frost, E., Dixon, M., Ollosson, S., Kilpin, K., Patel, M., et al. (2017). Accuracy of Immunofluorescence in the Diagnosis of Primary Ciliary Dyskinesia. *Am. J. Respir Crit. Care Med.* 196, 94–101. doi: 10.1164/rccm.201607-1351OC

Smallman, L. A., and Gregory, J. (1986). Ultrastructural abnormalities of cilia in the human respiratory tract. *Hum. Pathol.* 17, 848–855. doi: 10.1016/S0046-8177(86)80206-4

Smith, E. F., and Yang, P. (2004). The radial spokes and central apparatus: mechano-chemical transducers that regulate flagellar motility. *Cell Motil. Cytoskeleton.* 57, 8–17. doi: 10.1002/cm.10155

Stubbs, J. L., Oishi, I., Izpisua Belmonte, J. C., and Kintner, C. (2008). The forkhead protein Foxj1 specifies node-like cilia in Xenopus and zebrafish embryos. *Nat. Gen.* 40, 1454–1460. doi: 10.1038/ng.267

Walentek, P., Quigley, I. K., Sun, D. I., Sajjan, U. K., Kintner, C., and Harland, R. M. (2016). Ciliary transcription factors and miRNAs precisely regulate Cp110 levels required for ciliary adhesions and ciliogenesis. *eLife* 5, e17557. doi: 10.7554/eLife.17557

Yadav, S. P., Sharma, N. K., Liu, C., Dong, L., Li, T., and Swaroop, A. (2016). Centrosomal protein CP110 controls maturation of the mother centriole during cilia biogenesis. *Development* 143, 1491–1501. doi: 10.1242/dev.130120

You, Y., Huang, T., Richer, E. J., Schmidt, J. E., Zabner, J., Borok, Z., et al. (2004). Role of f-box factor foxj1 in differentiation of ciliated airway epithelial cells. *Am. J. Physiol. Lung Cell Mol. Physiol.* 286, L650–L657. doi: 10.1152/ajplung.00170.2003

Zhao, L., Li, Y. Y., Li, C. W., Chao, S. S., Liu, J., Nam, H. N., et al. (2017). Increase of poorly proliferated p63(+) /Ki67(+) basal cells forming multiple layers in the aberrant remodeled epithelium in nasal polyps. *Allergy* 72, 975–984. doi: 10.1111/all.13074

Conflict of Interest: The authors declare that the research was conducted in the absence of any commercial or financial relationships that could be construed as a potential conflict of interest.

Advantages of publishing in Frontiers

OPEN ACCESS
Articles are free to read for greatest visibility and readership

FAST PUBLICATION
Around 90 days from submission to decision

HIGH QUALITY PEER-REVIEW
Rigorous, collaborative, and constructive peer-review

TRANSPARENT PEER-REVIEW
Editors and reviewers acknowledged by name on published articles

Frontiers
Avenue du Tribunal-Fédéral 34
1005 Lausanne | Switzerland

Visit us: www.frontiersin.org
Contact us: info@frontiersin.org | +41 21 510 17 00

REPRODUCIBILITY OF RESEARCH
Support open data and methods to enhance research reproducibility

DIGITAL PUBLISHING
Articles designed for optimal readership across devices

FOLLOW US
@frontiersin

IMPACT METRICS
Advanced article metrics track visibility across digital media

EXTENSIVE PROMOTION
Marketing and promotion of impactful research

LOOP RESEARCH NETWORK
Our network increases your article's readership